INFORMATION TO USERS

This manuscript has been reproduced from the microfilm master. UMI films the text directly from the original or copy submitted. Thus, some thesis and dissertation copies are in typewriter face, while others may be from any type of computer printer.

The quality of this reproduction is dependent upon the quality of the copy submitted. Broken or indistinct print, colored or poor quality illustrations and photographs, print bleedthrough, substandard margins, and improper alignment can adversely affect reproduction.

In the unlikely event that the author did not send UMI a complete manuscript and there are missing pages, these will be noted. Also, if unauthorized copyright material had to be removed, a note will indicate the deletion.

Oversize materials (e.g., maps, drawings, charts) are reproduced by sectioning the original, beginning at the upper left-hand corner and continuing from left to right in equal sections with small overlaps.

Photographs included in the original manuscript have been reproduced xerographically in this copy. Higher quality 6" x 9" black and white photographic prints are available for any photographs or illustrations appearing in this copy for an additional charge. Contact UMI directly to order.

Bell & Howell Information and Learning
300 North Zeeb Road, Ann Arbor, MI 48106-1346 USA

UMI®
800-521-0600

DISSERTATION

INVESTIGATION OF THE REACTIVITY OF 5,6-DIHYDROTHYMIDIN-5-YL AND ITS INVOLVEMENT IN DNA DAMAGE AMPLIFICATION

Submitted by

Keri Ann Tallman

Department of Chemistry

In partial fulfillment of the requirements

for the Degree of

Doctor of Philosophy

Colorado State University

Fort Collins, Colorado

Spring 2000

COLORADO STATE UNIVERSITY

February 9, 2000

WE HEREBY RECOMMEND THAT THE DISSERTATION PREPARED UNDER OUR SUPERVISION BY KERI ANN TALLMAN ENTITLED INVESTIGATION OF THE REACTIVITY OF 5,6-DIHYDROTHYMIDIN-5-YL AND ITS INVOLVEMENT IN DNA DAMAGE AMPLIFICATION BE ACCEPTED AS FULFILLING IN PART REQUIREMENTS FOR THE DEGREE OF DOCTOR OF PHILOSOPHY.

Committee on Graduate Work

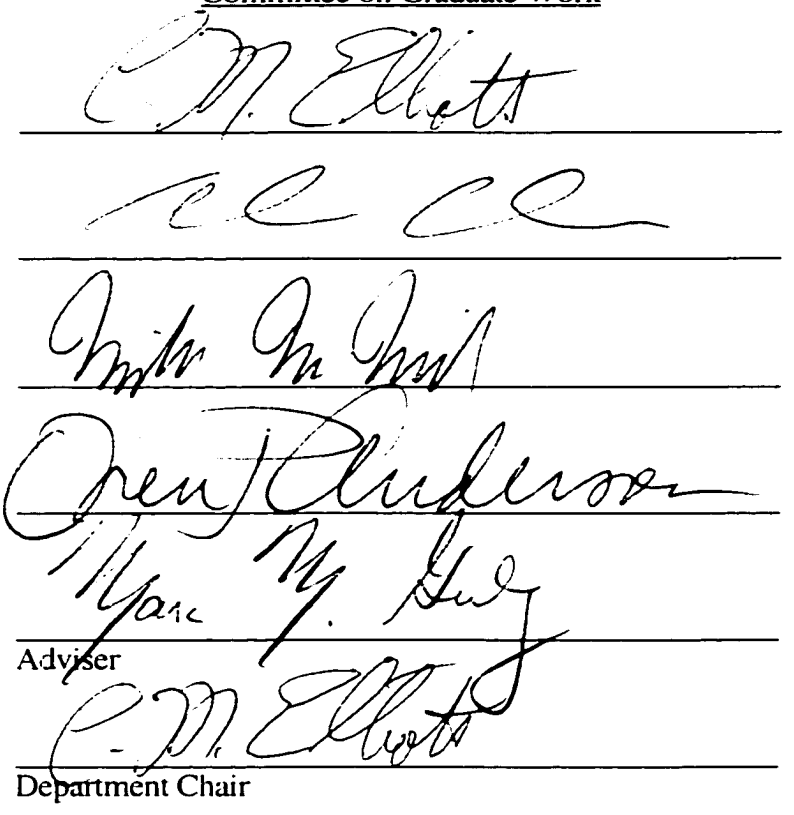

Adviser

Department Chair

Abstract of Dissertation

INVESTIGATION OF THE REACTIVITY OF 5,6-DIHYDROTHYMIDIN-5-YL AND ITS INVOLVEMENT IN DNA DAMAGE AMPLIFICATION

The reactivity of 5,6-dihydrothymidin-5-yl (**4** and **120**) was investigated at the monomeric level and in a dinucleotide using the phenyl selenide (**96** and **121**) as the thermal and photochemical precursor. By studying the reactivity of **4** (and **120**) at the monomeric level and in a dinucleotide, insight into the mechanism by which 5,6-dihydrothymidin-5-yl is involved in DNA damage amplification was attained. The nucleobase radical (**4** and **120**) was studied in the absence and presence of O_2, as well as in the presence of radiosensitizers.

By using anomerization and tetranitromethane as mechanistic probes, we have shown that **120** does not participate in internucleotidyl hydrogen atom abstraction, but is reduced to form the nonmutagenic lesion, 5,6-dihydrothymidine (**128**). The generation of the radical (**4**) in the presence of O_2 resulted in the formation of the peroxyl radical (**7**), which we have shown undergoes superoxide ($O_2^{\bullet-}$) elimination to restore the native nucleobase, thymidine (**3**). Evidence for this mechanism was attained by spectrophotometric assays involving the oxidation of epinephrine and reduction of cytochrome *c* for the detection of $O_2^{\bullet-}$. Competitive kinetics was used to estimate the rate constant for $O_2^{\bullet-}$ elimination as 21 s^{-1}.

Direct evidence for internucleotidyl hydrogen atom abstraction by the peroxyl radical (**163**) was gained by the formation of the 2-deoxyribonolactone lesion (**132**), which occurs preferentially from *5S*-**163**. The transfer of spin from the nucleobase to the sugar occurs in competition with $O_2^{\bullet-}$ elimination and intermolecular hydrogen atom abstraction with a rate constant of 0.1 s^{-1}.

5,6-Dihydrothymidin-5-yl (**4** and **120**) also reacts with the metabolite of tirapazamine (**11**), the 1-*N*-oxide (**12**), and results in the formation of 2-deoxyribonolactone (**132**). The mechanism by which the nucleobase radical is trapped by **12** is unclear, but evidence suggests that regioisomeric trapping of the radical (**4** and **120**) on the nitrogen and oxygen occurs to form a mixture of covalent adducts. Although the nature of the reactive species responsible for internucleotidyl hydrogen atom abstraction is unknown, it is clear that the 1-*N*-oxide (**12**) can serve as a surrogate for O_2 and produce tandem lesions.

Keri Ann Tallman
Chemistry Department
Colorado State University
Fort Collins, CO 80523
Spring 2000

Dedication

The completion of this dissertation would not have been possible without the support and encouragement of a very special group of people. Their presence in my life during my graduate career will not be forgotten and I wish to express my gratitude to all of them. I especially wish to thank my parents, Don and Cathy Tallman, for the encouragement to set my goals high and the love and support to pursue them, and my sister, Teri, and brother, Donald, for always believing in me. I also would like to thank Lisa Kelly and Tami Mangum for the friendship they provided on a daily basis and for sharing in the highs and lows along the way.

I especially wish to express my gratitude to my mentor, Professor Marc M. Greenberg, with whom it has been a pleasure and privilege to have had the opportunity to work. I hope to pursue the standard of excellence that he has set forth as a chemist, educator, and member of the scientific community. I wish to thank Dr. Gary Cook and Dr. Dustin McMinn, whom I respect as chemists and cherish as friends, Dr. Tracy Matray, Dr. Hari Venkatesan, Dr. Tongqian Chen, Dr. Christopher Tronche, Dr. Aruna Sambandam, Dr. Jae-Taeg Hwang, Aaron Anderson, Nolan Carter, Brian Bales, Mike Delaney, and Dr. Zsolt Hantosi for their patience and friendship.

Table of Contents

List of Figures

List of Tables[a]

[a] The data presented in tables is the average of at least two data points and the calculated standard deviation. The reported data with a standard deviation of zero indicates that there was no deviation in the data for the given number of significant figures.

1 Introduction

The deleterious effects of ionizing radiation on biological systems has been known for over a hundred years. Grubbé observed in 1896 that exposure of the skin to X-rays caused lesions to appear.[1] In that same year, ionizing radiation was first used in the treatment of cancer. Since that time, scientists have sought evidence for the mode of action of ionizing radiation to gain a better understanding of its effects on biological systems. The importance in understanding the mechanisms by which ionizing radiation induces oxidative damage is two-fold. Greater mechanistic understanding may provide us with valuable information for developing better therapeutic agents for the treatment of cancer and other degenerative diseases. In addition, the chemistry observed during oxidative damage induced by ionizing radiation may provide insight into the processes that occur during cellular damage associated with many diseases.

Ionizing radiation induces damage in biological systems via free radical mediated reactions. Due to the highly reactive nature of free radicals, damage may occur to all cellular constituents, such as RNA, DNA, proteins, and lipid bilayers. Oxidative damage to lipid bilayers results in the formation of lipid hydroperoxides, which may disrupt the function of the cell membrane.[2-4] Alternatively, lipid hydroperoxides may degrade to products able to induce further damage within the cell.[5-7]

In addition to damaging the cell membrane, ionizing radiation leads to oxidative damage to RNA and DNA through the generation of radical intermediates on the sugar moieties, nucleobases, or phosphodiester linkages present in these biopolymers.[8-11] Ionizing radiation is unique in its ability to produce radical and radical ion intermediates in the nucleobases, whereas other DNA damaging agents used in cancer therapy, such as bleomycin (**1**) or neocarzinostatin (**2**, NCS), target the sugar backbone (Figure 1).[12-14] For

this reason, the damage initiated by nucleobase radicals is of particular interest with respect to ionizing radiation.

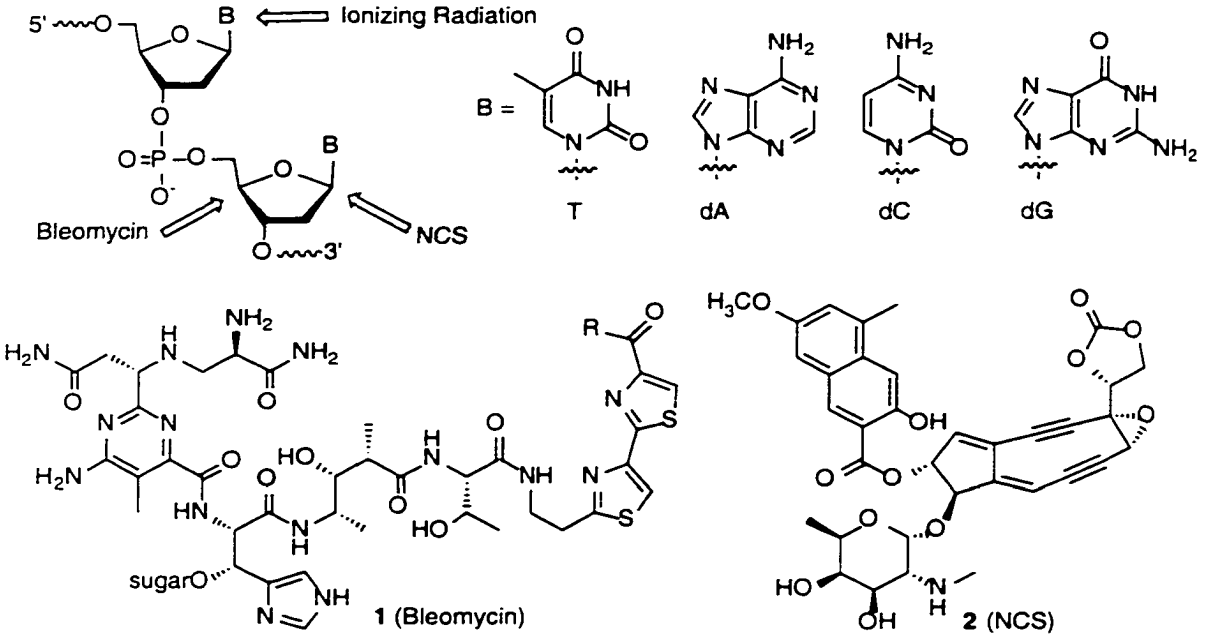

Figure 1. Sites of DNA damage induced by **1**, **2**, and ionizing radiation.

1.1 Formation of 5,6-Dihydrothymidin-5-yl (4) During Ionizing Radiation

Ionizing radiation induces damage by the direct and indirect effects. The direct effect refers to the absorption of energy by the DNA, whereas the latter involves the generation of reactive species produced upon the ionization of H_2O. Nucleobase radicals are believed to account for ≈90% of the reactive intermediates formed during ionizing radiation.[1] One of the major reactive intermediates generated due to the indirect effect is 5,6-dihydrothymidin-5-yl (**4**).[1]

Upon the ionization of H_2O, the H•, e^-_{aq}, and HO• are generated.[1] The H• and e^-_{aq} react with thymidine (**3**) to generate **4** as the major product (Figure 2). The H•

preferentially adds to the C6-position of the double bond to directly generate **4**, whereas the e_{aq}^- generates the radical anion.[1] Protonation at the C6-position ultimately leads to **4**.

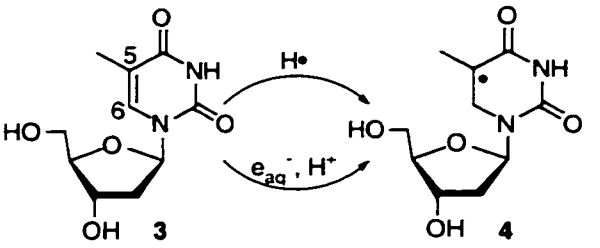

Figure 2. Formation of **4** via the indirect effect of ionizing radiation.

Like the H•, HO• adds to the double bond of thymidine (**3**, Figure 3). Although the major pathway is addition to the C5-position, approximately 30% of the reactivity is accounted for by addition to the C6-position to generate 5,6-dihydro-6-hydroxythymidin-5-yl (**5**).[1] This nucleobase radical (**5**) is also believed to be produced upon the direct effect of ionizing radiation. It is believed that the direct effect leads to the ionization of the nucleobase to generate the radical cation (**6**, Figure 3).[15-17] Hydration of **6** generates the same radical (**5**) observed upon HO• addition to thymidine (**3**). Given the similarities between **4** and **5**, one might expect that these nucleobase radicals may exhibit similar reactivity.

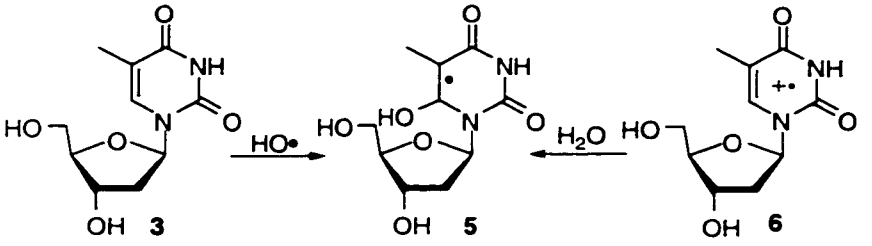

Figure 3. Formation of **5** via the indirect and direct effects of ionizing radiation.

In addition to being produced via ionizing radiation, HO• is also generated during other forms of oxidative stress, which occur when the delicate balance between pro-oxidants and antioxidants is disrupted.[18,19] This can occur by exposure to ionizing radiation, near-UV radiation, redox-cycling drugs, or during normal aerobic metabolism. For example, mitochondria, some enzymes, and leukocytes at sites of inflammation release $O_2^{\bullet}$ and H_2O_2 during normal cell processes.[9] These species are converted into the highly reactive HO•, which is known to react with DNA. The result is an increase in oxidative damage to the cell. Cells have defense mechanisms in the form of antioxidants, such as superoxide dismutase and catalase, which scavenge $O_2^{\bullet}$ and H_2O_2, respectively. Despite these defense mechanisms, the rate of formation of oxidized DNA bases is estimated at several thousands of events per cell, per day.[19] In addition, degenerative processes and diseases, such as cancer, Alzheimer's, ischemic heart disease, and aging have been associated with an increase in DNA damage resulting from oxidative stress.[20-23]

There are clearly several pathways which lead to the generation of **4** and its related radical intermediate **5**. Based upon the expected similarity in reactivity between **4** and **5**, these radicals may also exhibit similar reactivity with respect to DNA damage. Given that **4** and **5** constitute a major portion of the reactive intermediates formed in DNA upon interaction with ionizing radiation and other oxidizing agents, investigation of the chemistry of **4** may provide significant insight into the oxidative damage of DNA induced by both ionizing radiation and other forms of oxidative stress.

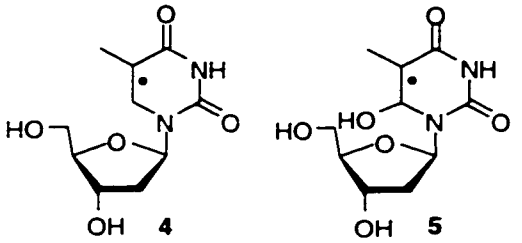

1.2 Potential Reactivity of 4 and its Related Radical 5

There are several interesting and unique reaction pathways potentially available to **4** and its related radical **5**. These pathways will be discussed with respect to **4**, but they may also be applicable to **5**. This nucleobase radical (**4**) has been proposed to be involved in DNA damage via internucleotidyl hydrogen atom abstraction.[24,25] In addition, since alkyl radicals are trapped by O_2 at near diffusion-controlled rates (2×10^9 M^{-1} s^{-1}) and normal cells exist in an O_2 rich environment, formation of the peroxyl radical (**7**) is expected to be one of the major pathways involved in oxidative damage (Figure 4).[26]

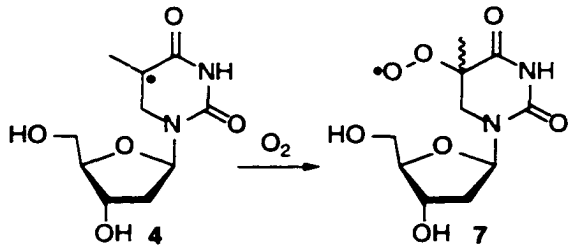

Figure 4. Formation of **7** upon generation of **4** in the presence of O_2.

The peroxyl radical (**7**) may participate in several intranucleotidyl or internucleotidyl reactions. The intranucleotidyl chemistry may be observed in the monomer (**7**, Figure 5) or upon formation of **7** in DNA (**9**, Figure 6). In the presence of hydrogen atom donors, **7** may be converted into 5,6-dihydro-5-hydroperoxythymidine and 5,6-dihydro-5-hydroxythymidine (**8**, Figure 5). The *5R*-diastereomer of the latter (**8**) has been incorporated into DNA and shown to inhibit DNA polymerase and destabilize duplex DNA.[27,28]

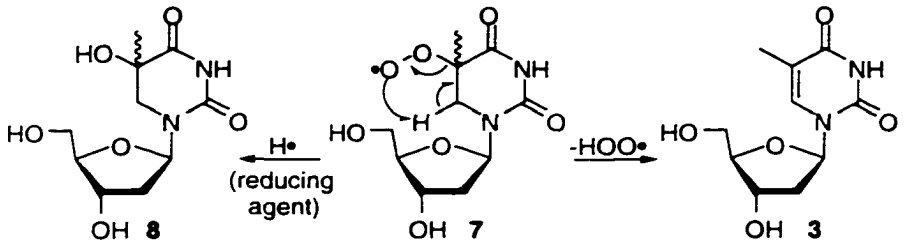

Figure 5. Potential intranucleotidyl chemistry of **7**.

In addition to the formation of **8**, the peroxyl radical (**7**) may undergo intranucleotidyl hydrogen atom abstraction from the C6-position to regenerate thymidine (**3**) with concomitant release of HOO• (Figure 5). Since trapping of alkyl radicals by O_2 is referred to as a damage-fixing event, this pathway is interesting in that it represents a detoxification pathway available to **7**. However, although the elimination of HOO• reconstitutes the native nucleobase, the release of diffusible HOO• in the vicinity of the DNA has the potential of inducing oxidative damage. Since HOO• has a pKa of 4.8, under biological conditions it will dissociate to superoxide ($O_2^{-\bullet}$).[29] Although $O_2^{-\bullet}$ is not deleterious to DNA, it is known to generate reactive oxygen species, such as HO• and peroxynitrite, which do damage DNA.[1,18,19,30-34] The participation of $O_2^{-\bullet}$ in DNA damage processes makes its elimination from **7** a potential double-edged sword.

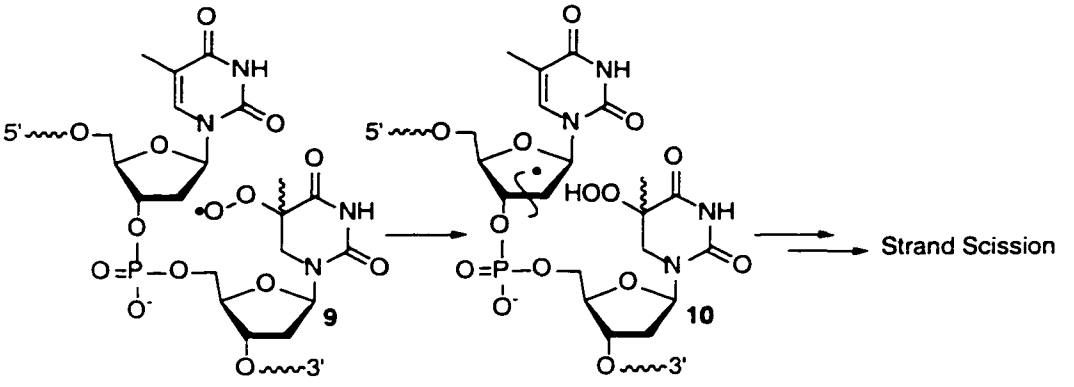

Figure 6. Potential internucleotidyl chemistry of **9**.

Another pathway available to **7** is the possibility that it will participate in internucleotidyl hydrogen atom abstraction when it is formed in DNA (**9**, Figure 6).[35-39] This pathway is interesting in that it provides an explanation for the unusual proposal involving the transfer of spin from the nucleobase to the sugar (**10**).[35-39] Strand scission necessitates the generation of a radical on the sugar backbone. However, ionizing radiation

predominantly targets the nucleobase. The effectiveness of ionizing radiation therapy may in part be due to the transfer of spin from the nucleobase to the sugar via internucleotidyl hydrogen atom abstraction. This cascade of damage events produced upon the initial formation of a single reactive intermediate in DNA is referred to as DNA damage amplification.

5,6-Dihydrothymidin-5-yl (**4**) may also participate in DNA damage amplification in the presence of radiosensitizing agents. Since tumors tend to be hypoxic (oxygen-deficient), oxidative damage to DNA is less efficient in many tumor cells than in O_2 rich cells. Consequently, various small molecules have been used in conjunction with ionizing radiation in order to increase the cytotoxicity of the latter in tumor cells. However, the mechanism of action of these compounds is uncertain.

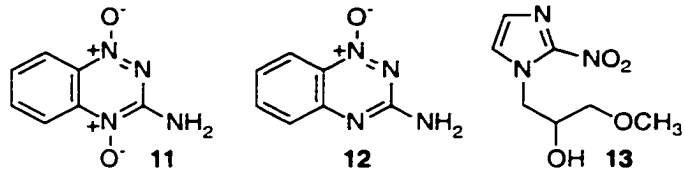

Recently, tirapazamine (**11**) has been shown to act as a bimodal agent in DNA damage *in vitro*. The bis-*N*-oxide (**11**) initiates DNA damage upon one-electron reduction of the drug, and may also act as an O_2 surrogate.[40-45] Although the mode of action is unclear, it is believed that reduction of **11** generates HO• and the reduced drug (**12**).[41-43] As previously discussed, the HO• may subsequently react with thymidine (**3**) to generate **5**, which may exhibit reactivity similar to **4** (Figure 7). Misonidazole (**13**) is another small molecule that has been used in conjunction with ionizing radiation therapy to increase the yields of single strand breaks in DNA.[46] The damage observed in the presence of **13** is similar to the damage observed when DNA is exposed to ionizing radiation in the presence of O_2.[47,48] In this respect, misonidazole is believed to act as a surrogate for O_2 and increases the observed DNA damage under anaerobic conditions.[47,48]

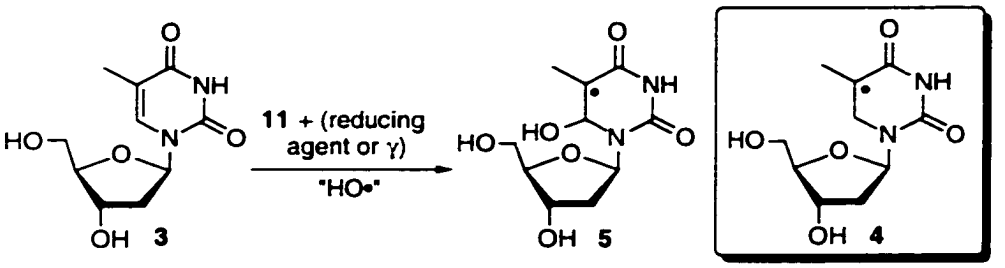

Figure 7. Interaction of thymidine (**3**) with ionizing radiation or tirapazamine (**11**).

It is likely that both tirapazamine (**11**) and misonidazole (**13**), in conjunction with ionizing radiation, induce damage in DNA via generation of the HO•. However, the HO• reacts predominantly with the nucleobases (Figure 7) and strand scission necessitates that the spin be transferred to the sugar moiety. The O_2 deficiency in tumor cells precludes the formation of the peroxyl radical (**9**) and proposed subsequent hydrogen atom abstraction from the adjacent sugar (Figure 6). Therefore, either the nucleobase radical (**14**) or a reactive species generated from the radiosensitizer must be responsible for the transfer of spin to the sugar.[24,25]

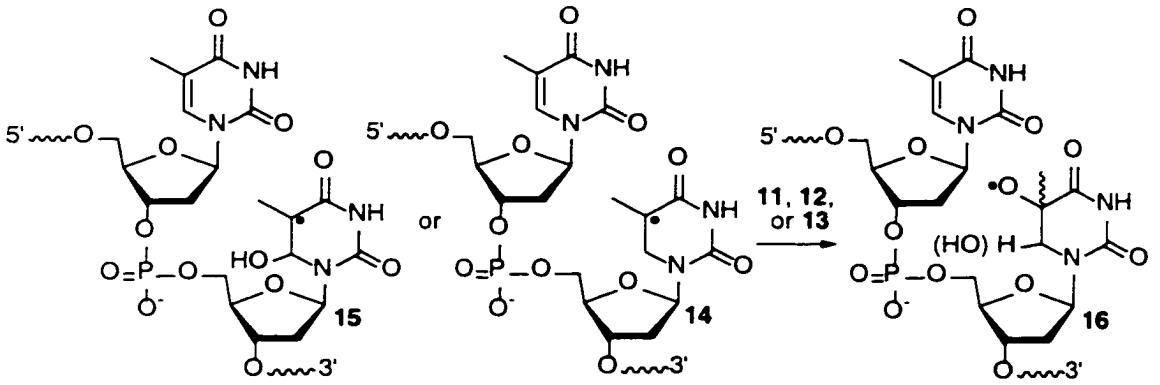

Figure 8. Potential reactivity of **14** (and **15**) in the presence of radiosensitizers.

It has been shown that alkyl radicals are trapped by **11**, **12** (which would be present upon activation of **11**), and **13**.[44,45] The mechanism by which **11**, **12**, and **13** react with alkyl radicals is uncertain, but evidence suggests that the alkoxyl radical (e.g. **16**) may ultimately be produced.[44,45,47,48] Therefore, it is possible that the damage induced by these species during DNA damage is at least partially attributable to initial trapping of the nucleobase radicals (**14** or **15**), which subsequently generate the alkoxyl radical (**16**, Figure 8). The alkoxyl radical (**16**) may participate in internucleotidyl hydrogen atom abstraction and lead to DNA damage amplification as proposed for the peroxyl radical (**9**, Figure 6).

Many of the above studies have been carried out using γ-radiolysis and DNA or model compounds. These studies have provided a wealth of information regarding the generation of reactive intermediates that lead to DNA damage. However, a shortcoming of this experimental approach is that several radical species are formed simultaneously. The generation of more than one reactive intermediate complicates mechanistic analysis since one cannot attribute a given reaction pathway to a discrete radical intermediate. However, independent generation of a discrete radical intermediate would facilitate examination of its reactivity.[49] The focus of this research project is to utilize the tools of organic chemistry to gain a better understanding of the chemistry that occurs upon independent generation of **4**, and consequently the related nucleobase radical **5**.

2 Background

Exposure of DNA to ionizing radiation results in the formation of a myriad of reactive radical intermediates, two of the most abundant being **4** and the related radical **5** (Equation 1). In addition, these radicals may play a role in the damage induced during other forms of oxidative stress. The focus of this research is the study of the formation and subsequent reactivity of **4** with respect to the possible reaction pathways that are described below.

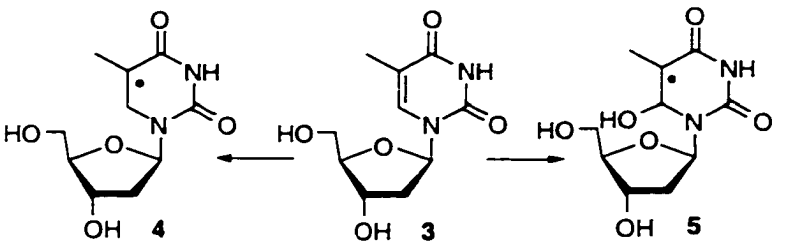

(1)

2.1 Formation of Nucleobase Radicals

2.1.1 Direct Effect of Ionizing Radiation

Ionizing radiation is known to induce damage in DNA via free radical mediated reactions by the direct and indirect effects. The direct effect refers to damage induced by the absorption of energy by DNA, whereas the latter involves the generation of reactive species during the ionization of H_2O, which subsequently react with DNA. It is believed that the direct effect of ionizing radiation results in the ionization of the DNA. The damage may be initiated by the formation of a radical cation in the nucleobase or sugar moiety, or a radical in the phosphodiester linkage, with the former having the most favorable oxidation potentials.[15-17,50-52]

The direct effect of ionizing radiation has been investigated using laser flash photoionization experiments, which minimize the formation of the reactive species attributable to the indirect effect (i.e. HO•, H•, and e_{aq}^-).[15,17] Photoionization studies indicate that there are two pathways which lead to DNA damage.[15,17] One pathway is believed to be formation of the nucleobase radical cation (**18**) via ionization of the nucleobase. The rate-limiting step in strand scission is believed to be hydrogen atom abstraction from the adjacent sugar by the nucleobase-centered radical (or radical cation).[15,17] It is uncertain whether the H• is abstracted directly by the nucleobase radical cation (**18**), or by one of the subsequently formed nucleobase radicals (Figure 9). Deprotonation of **18** leads to the nitrogen-centered radical (**17**), whereas hydration at the C6-position yields **15**.[15,17]

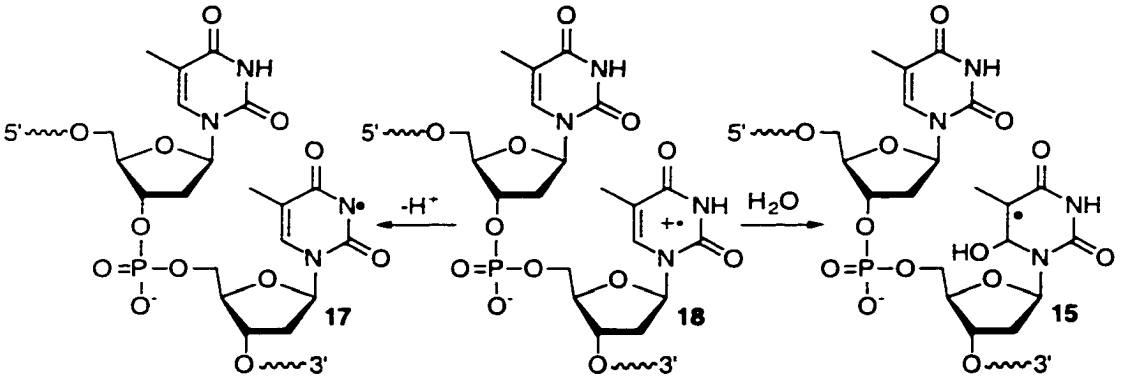

Figure 9. Fate of the nucleobase radical cation (**18**) formed during the direct effect of ionizing radiation.

The second pathway observed upon the ionization of DNA leads to direct strand breaks and is believed to involve ionization of the phosphodiester linkages or the sugar.[17,52] Ionization of the phosphate moiety generates the radical (**20**, Figure 10). In contrast, EPR studies suggest that the C1'-radical (**21**) is most likely formed upon deprotonation of the

nucleobase radical cation (**18**).[17,52] One of these species (**20** or **21**) is believed to be responsible for the observed direct strand breaks upon the ionization of DNA.

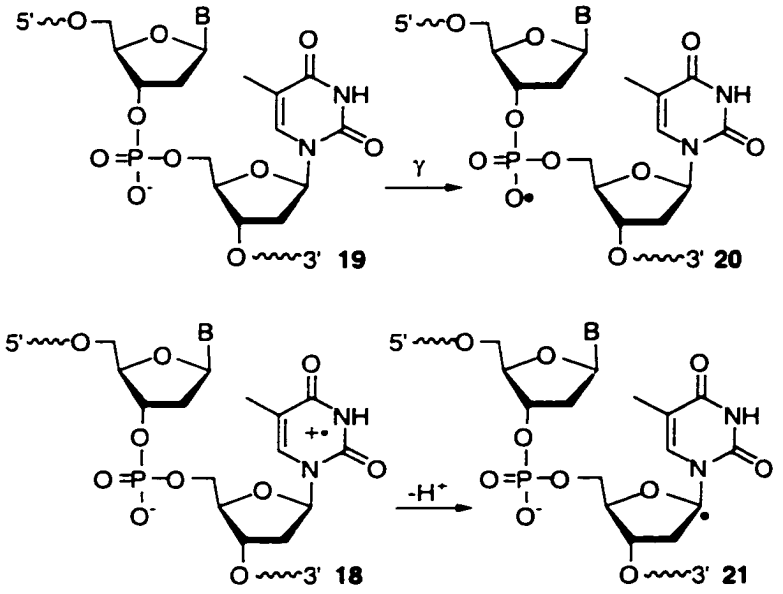

Figure 10. Ionization of the phosphodiester linkage and sugar moiety.

The more plausible explanation for the direct strand breaks is the ionization of the phosphate linkages since the C1'-radical (**21**) is not known to lead to significant amounts of direct strand breaks, but rather to alkaline labile lesions.[53] Although the pathway by which **20** leads to direct strand breaks is unknown, it has been suggested that it may undergo direct cleavage of the phosphodiester bond or participate in hydrogen atom abstraction from the sugar.[17,52] It has been suggested that **20** may abstract a hydrogen atom from one of the C4'-positions of the adjacent sugars to which it is bonded to generate the C4'-radical (**22** or **23**), which leads to direct strand breaks (Figure 11).[52] Alternatively, electron transfer may occur from one of the nucleobases to the phosphate radical, generating a nucleobase radical cation. Literature precedence supports the latter mechanism of electron transfer through DNA.[54-56]

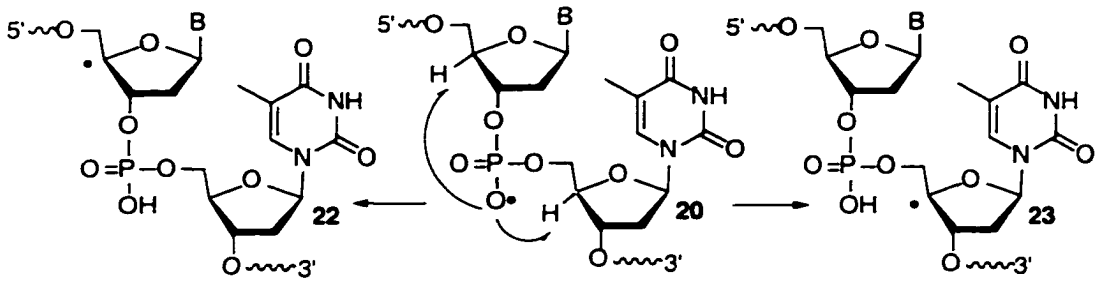

Figure 11. Hydrogen atom abstraction from the sugar by the phosphate radical (**20**).

2.1.2 Indirect Effect of Ionizing Radiation

Although the direct effect of ionizing radiation leads to DNA strand scission, the mechanism by which this occurs is poorly understood. In contrast, the indirect effect of ionizing radiation has received much more attention. The oxidative damage induced in DNA from the indirect effect has been attributed to the formation of reactive species from the ionization of H_2O. The ionization of H_2O is a complex process resulting in the formation of solvated electrons (e_{aq}^-), the hydrogen atom (H•), and the highly reactive hydroxyl radical (HO•).[1]

One of the major reactive species generated during ionizing radiation and many forms of oxidative stress is the hydroxyl radical (HO•). The HO• reacts with DNA via two pathways, hydrogen atom abstraction from the sugar (or methyl group of thymidine) or addition to the nucleobase double bonds, both pathways resulting in the generation of a free radical in the biopolymer.[1] Although generation of the radical on the carbohydrate backbone of DNA is a necessary requirement for strand scission, this pathway comprises only ≈10% of the reactivity of HO•. The remainder of the reactivity is mostly accounted for by the addition to the double bonds of the nucleobases.

It is known that HO• reacts with the purines, for example dG (**25**), at the C4-, C5-, and C8-positions (Figure 12).[11] The radical adducts resulting from addition to the C4- (**24**) and C5- (**26**) positions are suspected to revert back to **25** upon trapping of the radical

by a hydrogen atom donor, followed by dehydration.[11] However, addition to the C8-position results in the formation of 7,8-dihydro-8-oxoguanine (**27**, 8-oxo-dG) and the formamidopyrimidine (FAPy) lesion (**28**) under oxidative and reductive conditions, respectively. The addition of HO• to dA occurs in a similar fashion as to **25** and results in the formation of the analogous lesions 8-oxo-dA (**29**) and FAPy-dA (**30**). 8-Oxo-dG (**27**) has been shown to be a mutagenic lesion *in vivo* and *in vitro*, while 8-oxo-dA (**29**) is at least an order of magnitude less mutagenic.[57,58] Much less is known about the potential mutagenicity of the FAPy lesions (**28** and **30**). However, they are suspected to be mutagenic since there are enzymes that efficiently excise these lesions from DNA.[59,60]

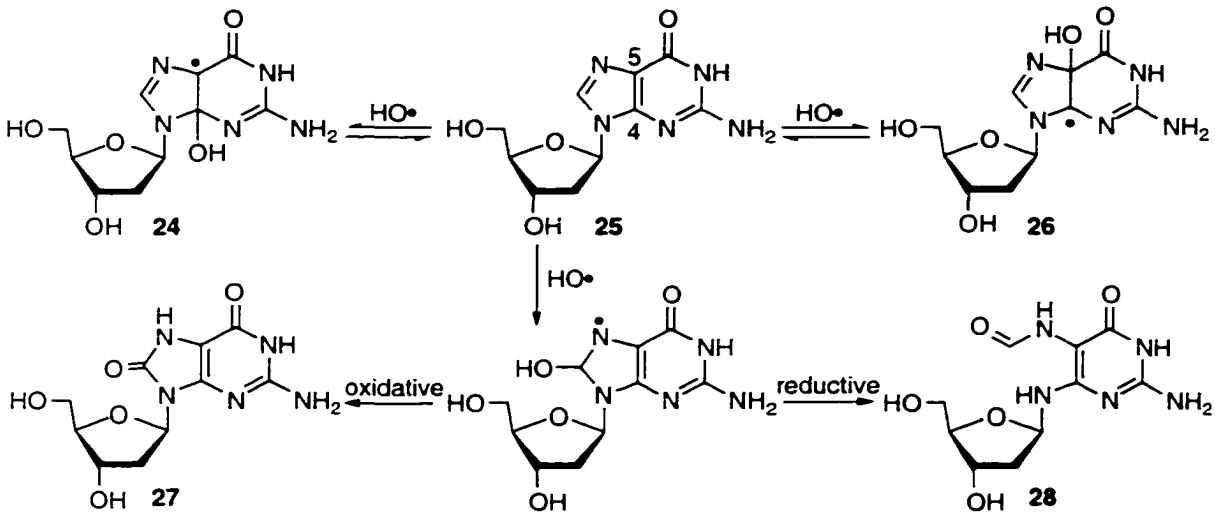

Figure 12. The formation of **27** and **28** from the addition of HO• to dG (**25**).

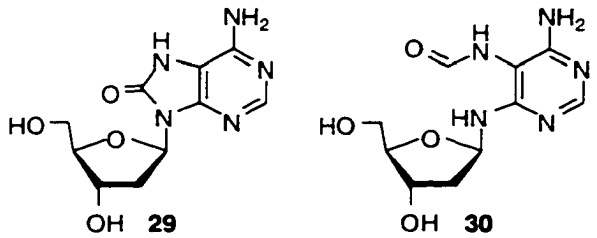

In addition to the purines, HO• also induces damage to the pyrimidines (Figure 13). A minor amount of the damage is a consequence of hydrogen atom abstraction from the methyl group of thymidine to generate the allylic radical (**32**). The major reaction pathway followed by HO• is addition to the double bond. Pulse radiolysis studies involving **3** indicate that the electrophilic HO• reacts predominantly at the more electron rich C5-position of the double bond, generating 5,6-dihydro-5-hydroxythymidin-6-yl (**31**).[1] In addition, approximately 30% of the reactivity of HO• is accounted for by addition to the C6-position to generate **5**.[1]

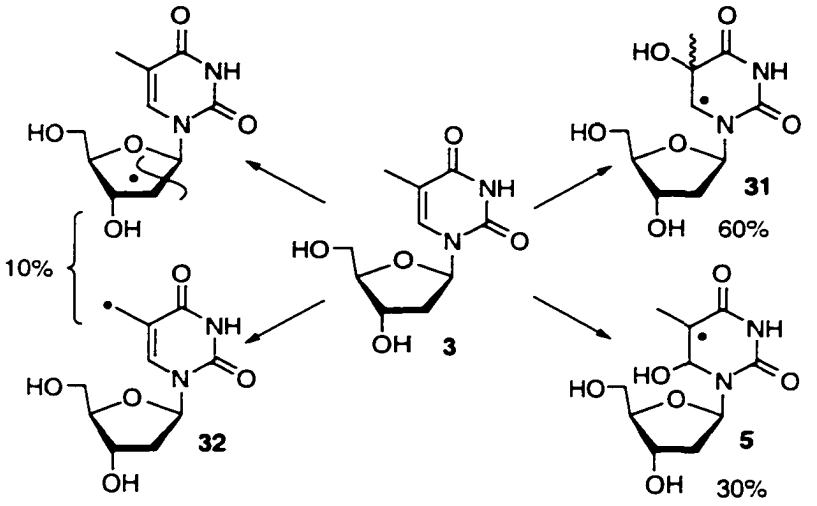

Figure 13. The reaction of HO• with thymidine (**3**).

The reactivity of H• is similar to that of HO•, undergoing a small amount of hydrogen atom abstraction from the sugar, but predominantly undergoing addition to the double bond of thymidine (**3**, Figure 14). In contrast to HO•, however, H• is relatively nucleophilic and preferentially adds to the C6-position of thymidine (**3**), generating **4** in about 60% yield.[1] Like HO•, approximately 30% of H• also adds to the opposite end of

the double bond. 5,6-Dihydrothymidin-5-yl (**4**) is also the major product resulting from the reaction of thymidine (**3**) with the solvated electron (e_{aq}^-).[1] Addition of the e_{aq}^- to the nucleobase results in the formation of the radical anion (**33**), which upon protonation generates **4**.

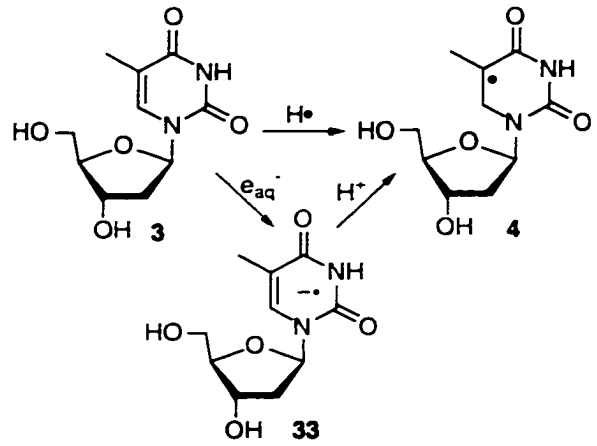

Figure 14. Formation of **4** via H• and e_{aq}^- addition.

If one takes into account the G values (number of product molecules/amount of radiation) for the three reactive species produced from the ionization of H_2O and the rate constants for reaction with the four nucleosides, one would predict that **4** will be one of the most abundant radicals formed upon exposure of DNA to ionizing radiation (Table 1).[1] The G value is analogous to the quantum yield for a photochemical reaction in that it provides information on the efficiency of the reaction. The G values indicate that H• is least abundant and e_{aq}^- and HO• are produced in approximately equal amounts (Table 1). Although HO• is relatively abundant, its reactivity is dispersed almost equally among the four nucleobases. Likewise, the e_{aq}^- reacts with each of the nucleobases with approximately the same rate constant. The H•, on the other hand, reacts five times faster with thymine than with the other nucleobases measured. From this data, one can assume that **4** is one of the radicals generated during ionizing radiation in the greatest amount.

Table 1. Rate constants for addition of HO•, H•, and e_{aq}^- to the nucleobases and G values for their generation upon ionizing radiation.[a]

Nucleobase	k ($M^{-1} s^{-1}$) e_{aq}^-	HO•	H•
Adenine	9×10^9	5×10^9	1×10^8
Cytosine	1.3×10^{10}	4.5×10^9	1×10^8
Guanine	1.3×10^{10}	9×10^9	nd
Thymine	1.7×10^{10}	5×10^9	5×10^8
G value	0.27	0.28	0.057

[a] The G value is the number of product molecules/amount of radiation. The values were obtained by ^{60}Co γ-irradiation of N_2 purged H_2O and are given in μmol J^{-1} (data taken from reference 1).

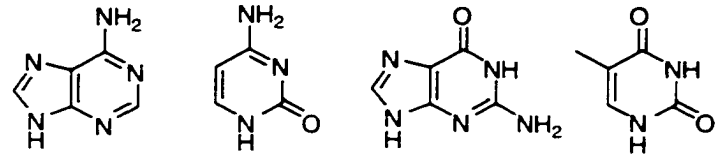

Adenine Cytosine Guanine Thymine

During ionizing radiation, the generation of H• and e_{aq}^- result in the formation of **4** as one of the major sites of damage. However, during oxidative stress the major reactive species generated is HO•. Although HO• preferentially adds to thymidine (**3**) to generate 5,6-dihydro-5-hydroxythymidin-6-yl (**22**), recall that ≈30% of the reactivity is accounted for by the formation of 5,6-dihydro-6-hydroxythymidin-5-yl (**5**). Therefore, although not the major product arising from reaction with HO•, **5** may still play a role in the free radical mediated damage induced during oxidative stress. The similarity between **4** and **5** suggests that they may participate in the same types of reactions. Hence, examination of the reactivity of **4** should have direct bearing on the chemistry of **5**.

2.2 Intranucleotidyl Reactions of Nucleobase Radicals

Upon generation of **4**, there are many possible reaction pathways available, depending on the presence or absence of O_2. One may argue that the proposed anaerobic

pathways for **4** are not biologically relevant since cells exist in such an oxygen rich environment. In normal cells, reaction pathways involving O_2 would be expected to dominate over those that would occur under anaerobic conditions. However, tumor cells are often hypoxic (oxygen-deficient). Therefore, the proposed reaction pathways that occur under anaerobic conditions may be biologically relevant.

2.2.1 Anaerobic Conditions

Upon generation of **4** in the presence of a suitable hydrogen atom donor, such as a thiol, trapping of the radical generates 5,6-dihydrothymidine (**34**, Figure 15).[61] Alternatively, since **4** is an oxidizing radical, it can undergo reaction with redox active metals to generate the carbanion (**35**).[62,63] Evidence for this pathway is gleaned from experiments involving thymine (**36**, Figure 16).

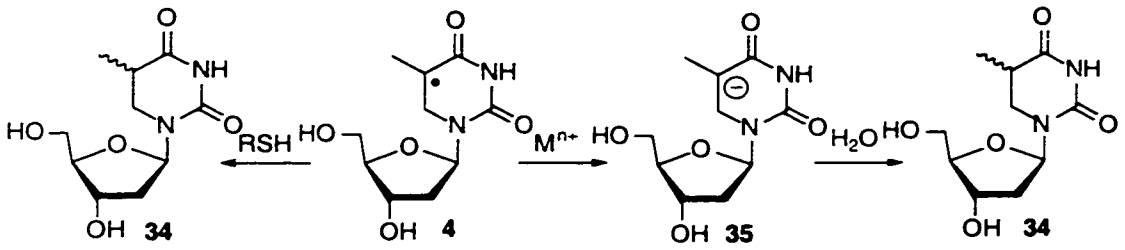

Figure 15. Potential intranucleotidyl reactivity of **4** under anaerobic conditions.

When thymine (**36**) was irradiated in the presence of redox active metals (Fe^{3+}) and absence of trap, two of the products observed were 5,6-dihydrothymine (**38**) and 5,6-dihydro-6-hydroxythymine (**40**, Figure 16).[63] The formation of these products was rationalized by the formation of H• and HO• and subsequent addition to the C6-position of thymine (**36**) to generate **37** and **39**, respectively. Reduction of the radical intermediates by Fe^{2+}, formed as a consequence of the high dose rate, followed by protonation yielded

the observed products. This observation supports the proposal that **4** may be subject to reduction in the presence of redox active metals.

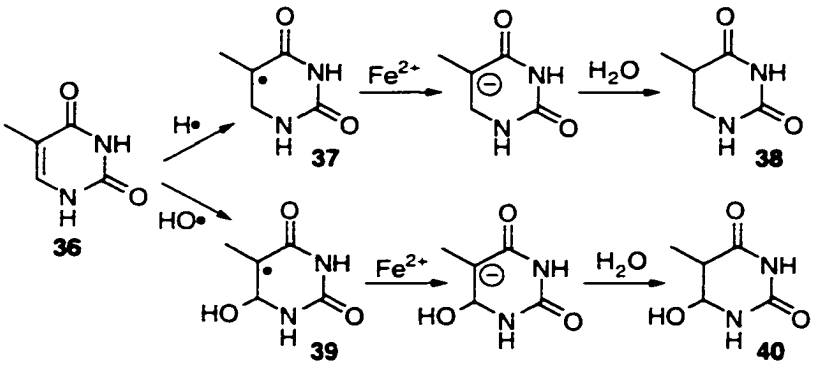

Figure 16. Reduction of nucleobase radicals by metal ions.

The isolable product resulting from the reduction of **4**, 5,6-dihydrothymidine (**34**), does not inhibit DNA polymerase *in vitro* and is a nonlethal lesion *in vivo*.[64] The formation of **34** has therefore been referred to as a protective pathway available to **4**. However, **34** is more susceptible to hydrolysis of the glycosidic bond than the native nucleobases. Therefore, accumulation of a large number of these lesions *in vivo* may result in the formation of abasic sites. The formation of abasic sites is potentially mutagenic due to misincorporation of nucleotides. It may be for these reasons that cells possess enzymes, such as endonuclease III, that recognize and excise 5,6-dihydrothymidine (**34**).[65]

2.2.2. Aerobic Conditions

The aforementioned reaction pathways are expected to predominate in hypoxic cells. However, normal cells exist in an O_2 rich environment. Since alkyl radicals are trapped by O_2 at near diffusion controlled rates (2×10^9 M^{-1} s^{-1}), one would expect trapping of **4** by O_2 to generate the peroxyl radical (**7**, Figure 17) to be one of the major pathways involved in oxidative damage to DNA in normal cells.[26] Upon trapping by O_2, **7** has

several potential pathways available to it. Peroxyl radicals in DNA have been shown to react with *tert*-BuSH and glutathione at 5 x 10^3 and <2 x 10^2 M^{-1} s^{-1}, respectively.[66,67] In the presence of a hydrogen atom donor, **7** is trapped to generate the respective hydroperoxide, which is readily reduced to 5,6-dihydro-5-hydroxythymidine(**8**, Figure 17).

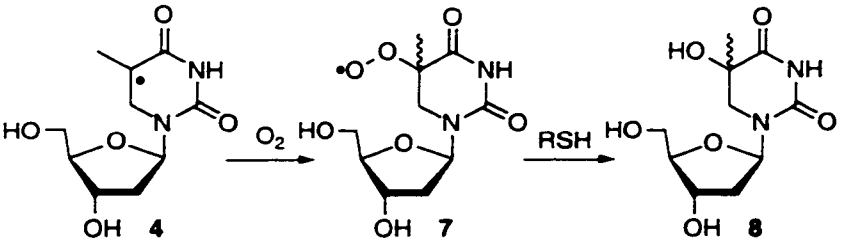

Figure 17. Potential reactivity of **4** under aerobic conditions.

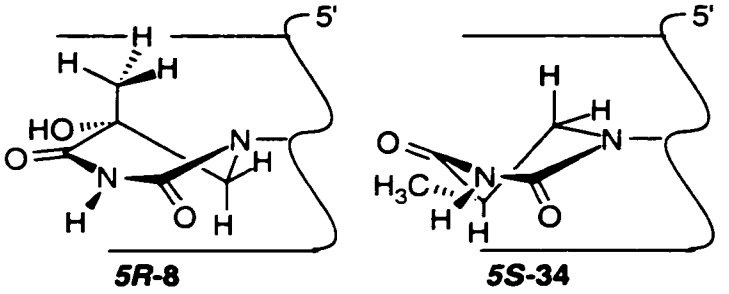

Figure 18. Half chair conformations of (*5R*)-**8** and (*5S*)-**34**.

The introduction of **8** into DNA is potentially a cytotoxic lesion. Incorporation of *5R*-**8** into duplex DNA results in destabilization of the helix.[27] In addition, *5R*-**8** moderately inhibits DNA polymerase in translesional synthesis, i.e. incorporation of a nucleotide across from the damage site, and serves as a significant block for the extension of primers.[28] The inhibition of DNA polymerase and destabilization of duplex DNA is believed to be attributable to the nonplanarity of **8**.[28] The methyl group of *5R*-**8** adopts a

pseudoaxial position, which disrupts base stacking in the 5'-direction (Figure 18). The related lesion, *5S*-5,6-dihydrothymidine (*5S*-**34**), however, is not expected to inhibit DNA polymerase nearly as strongly, possibly due to its ability to adopt a conformation that places the methyl group in the pseudoequatorial position such that base stacking is not disrupted (Figure 18).[68,69]

In addition to intermolecular trapping of **7** to generate **8**, the peroxyl radical (**7**) may undergo intramolecular reactions.[70] One can envision intramolecular hydrogen atom abstraction from the C6-position by **7** resulting in the elimination of HOO• and restoration of the native nucleobase (Figure 19). Literature precedence lends credence to this pathway. The elimination of superoxide has been observed for the C6-peroxyl radical of uracil (**41**), regenerating the native nucleobase (**42**), although under basic conditions.[71] In addition, intramolecular hydrogen atom abstraction can occur at rates greater than 10^5 s^{-1} if a suitable driving force exists, such as rearomatization of phenol (Figure 19).[70]

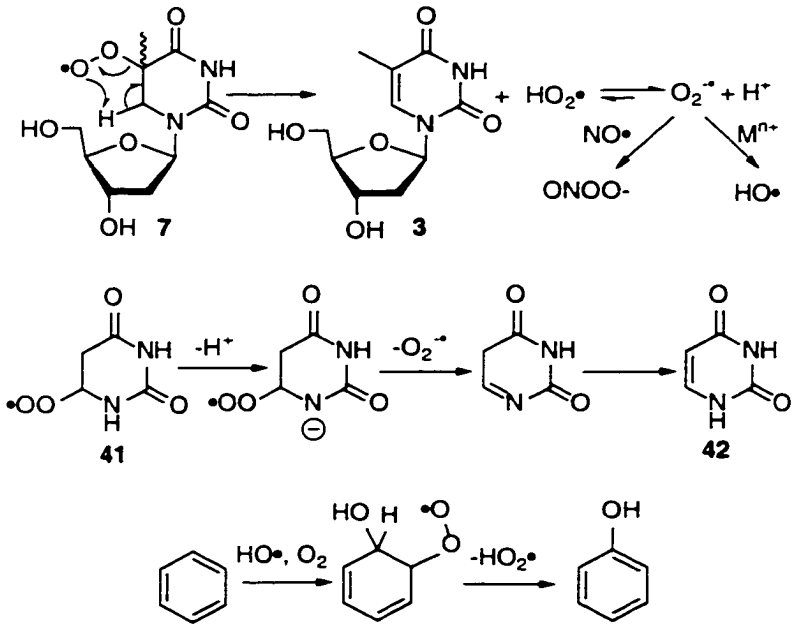

Figure 19. Potential reactivity of **4** under aerobic conditions, superoxide elimination.

Superoxide elimination from **7** would result in regeneration of the native nucleobase and the formation of HOO•. Since the pKa of HOO• is 4.8, under biological conditions it will dissociate to $O_2^{-\bullet}$.[29] Although the elimination of $O_2^{-\bullet}$ from **7** is itself not deleterious to DNA, the subsequent generation of reactive species, such as HO• and peroxynitrite, from it can potentially induce oxidative damage.[1,18,19,30-34]

Superoxide participates in a number of reactions that ultimately lead to the formation of HO•. For example, enzymatic dismutation of $O_2^{-\bullet}$ by superoxide dismutase (SOD) yields H_2O_2, which may be reduced to HO•. Superoxide ($O_2^{-\bullet}$) may also generate HO• in nonenzymatic processes when it is formed in the presence of redox active metals, such as Fe^{3+} or Cu^{2+}.[1] Haber-Weiss chemistry results in the reduction of Fe^{3+} by $O_2^{-\bullet}$ (Equation 3). The Fe^{2+} may subsequently reduce another molecule of $O_2^{-\bullet}$, which upon protonation generates H_2O_2 (Equation 4). The reduced metal (Fe^{2+}) may also reduce H_2O_2 to generate HO•, referred to as the Fenton reaction (Equation 5).[1]

$$O_2^{-\bullet} + Fe^{3+} \longrightarrow O_2 + Fe^{2+} \qquad (3)$$

$$Fe^{2+} + O_2^{-\bullet} \xrightarrow{2H^+} Fe^{3+} + H_2O_2 \qquad (4)$$

$$H_2O_2 + Fe^{2+} \longrightarrow HO\bullet + HO^- + Fe^{3+} \qquad (5)$$

Superoxide also reacts with nitric oxide (•NO) with a rate constant of 4-20 x 10^9 M^{-1} s^{-1} to generate peroxynitrite ($ONOO^-$, Figure 20).[30] Under physiological conditions, peroxynitrite is in equilibrium with the acid (ONOOH), both compounds leading to highly reactive species. The nature of the reactive species has been controversial, but it is generally accepted that ONOOH homolytically decays to generate the HO• and NO_2•.[31] Peroxynitrite also reacts with CO_2 at 5.8 x 10^4 M^{-1} s^{-1} to generate **43**, which is believed to decay to species capable of inducing oxidation and nitration.[30]

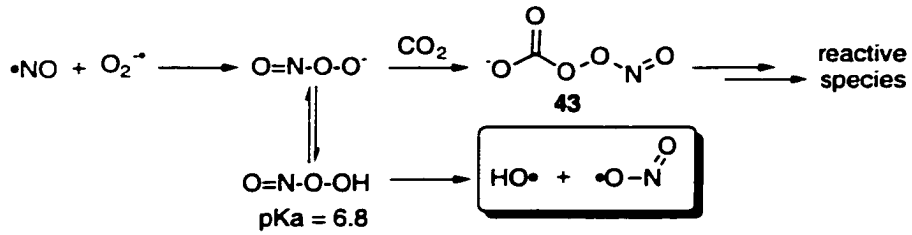

Figure 20. Reactive species generated from the reaction of $O_2^{\bullet-}$ with •NO.

As already mentioned, HO• can abstract a hydrogen atom from the sugar or methyl group of thymidine, or add to the double bond of thymidine.[1] Hence, this pathway contributes to DNA damage amplification through the formation of $O_2^{\bullet-}$-derived reactive species that may further damage the biopolymer. Peroxynitrous acid, or its decomposition products, react predominantly with the purines to generate modified nucleosides, such as 8-nitroguanosine (**44**). 8-Nitroguanosine (**44**) readily depurinates and thus represents a potentially mutagenic lesion.[32-34] In addition to the nitrated compound, the generation of peroxynitrous acid results in the formation of increased levels of modified nucleobases, such as the FAPy lesion (**28**), 8-oxo-dG (**27**), thymidine glycol (**45**), and 5-hydroxymethyl-2'-deoxyuridine (**46**), which are also observed in HO• mediated damage to DNA.[34]

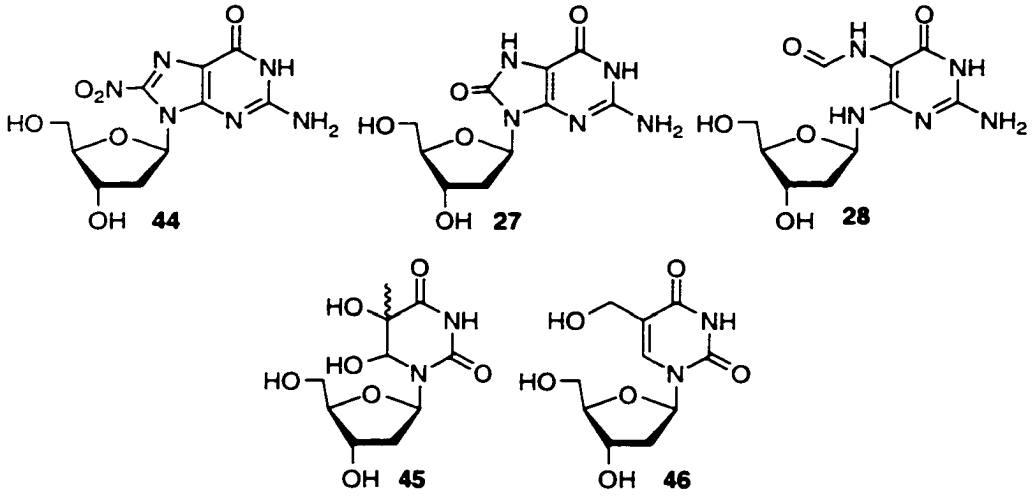

From the above discussion, it is clear that a variety of lesions (e.g. **34** and **8**) may be formed upon generation of **4**, even when only considering the chemistry that occurs within a single nucleotide (Equation 6). In addition, the superoxide elimination pathway may lead to the generation of $O_2^{\cdot-}$-derived reactive species, which have the potential to form additional lesions. Depending on the fate of **4** in these instances, the formation of these other lesions may simply transfer damage to another site in the biopolymer or result in amplification of the initial damage.

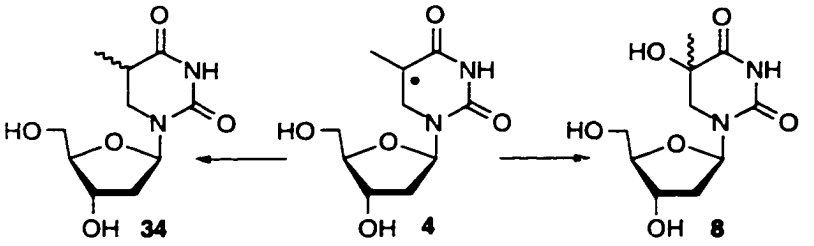

(6)

2.3 Internucleotidyl Reactions of Nucleobase Radicals

2.3.1. Theoretical Studies

The reaction pathway that has received the most attention is the propensity for **4**, or its respective peroxyl radical (**7**), to abstract a hydrogen atom from the adjacent sugar. Models of DNA reveal that **4** resides in the major groove of dsDNA, whereas the C1'-, C4'-, and C5'-hydrogen atoms, which are predicted to be the most likely abstracted on thermodynamic grounds, lie in the minor groove (Figure 21). Although one of the C2'-hydrogen atoms lies in the major groove, this hydrogen is the least likely to be abstracted in DNA since the C-H bond is predicted to have the greatest BDE (Table 2).[72] Although **4** and the hydrogen atoms of the adjacent nucleotide lie in different grooves of the DNA, there are examples of hydrogen atom abstraction occurring from one groove to the other.[73-75] Therefore, it is possible that **4** may participate in hydrogen atom abstraction from the sugar of the nucleotide bonded to its 5'-phosphate.

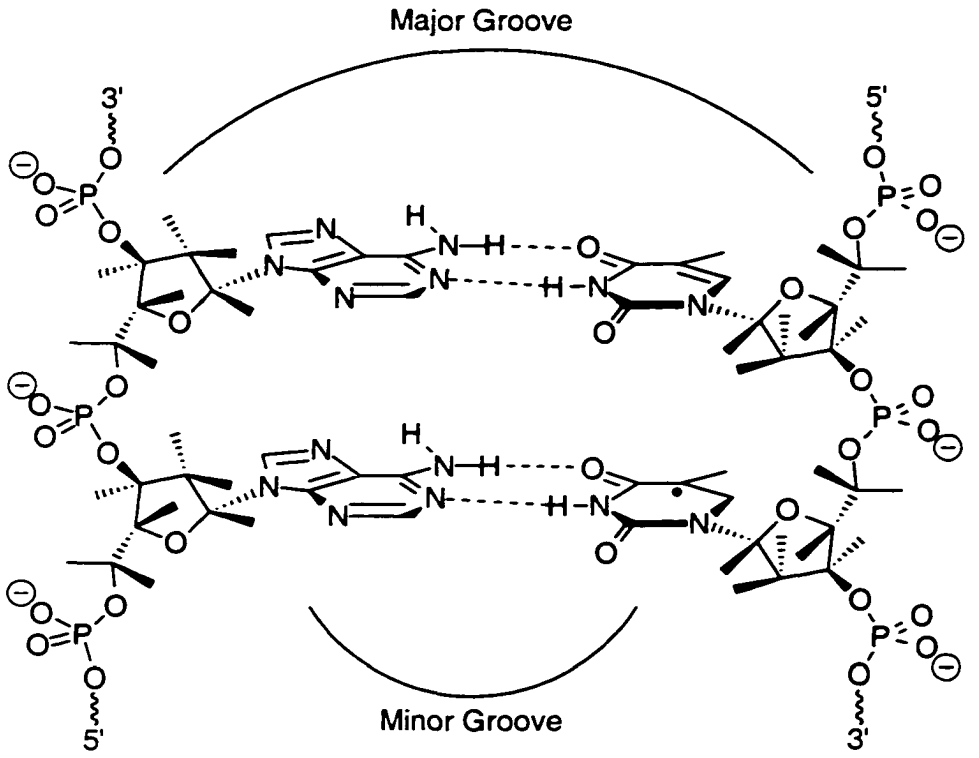

Figure 21. DNA secondary structure with incorporated **4**. The wedge-shaped bonds represent hydrogen atoms that point into the minor groove; the dashed bonds indicate hydrogen atoms that point into the major groove.

Table 2. BDE, relative rate constants for hydrogen atom abstraction, and relative accessibility of hydrogen atoms of deoxyribose.

Hydrogen	BDE (kcal/mol)[a]	k_{rel}[b]	A_{rel}[c]
C1'	87.33	1.85	0.00
C2'	91.20	0.26	0.24
C3'	87.49	1.70	0.43
C4'	88.57	1.00	1.00

[a] Calculated using MP2/6-31G* and may be underestimated; [b] k_{rel} = relative rate constants for hydrogen atom abstraction in isolated deoxyribose estimated from the BDE; [c] A_{rel} = relative accessibilities of hydrogens in B-DNA (data taken from reference 66).

Theoretical studies carried out on deoxyribose indicate that not surprisingly the probability of abstracting a hydrogen atom is related to its bond strength.[72] Accordingly, the bond strength of the C2'-hydrogen of deoxyribose is considerably higher and thus expected to be least likely abstracted (Table 2). Although the bond strength of the C5'-hydrogen was not measured in these studies, it is expected to have a bond strength similar to the C3'- and C4'-hydrogens. Abstraction of the C1'-hydrogen was found to be most energetically favorable (k_{rel}, Table 2), but the C4'-hydrogen (and most likely the C5'-hydrogen although not measured) was found to be most accessible to solvent-borne radicals, such as HO•, that was used in these calculations (A_{rel}, Table 2).[72,76] Experimental observations support this prediction. When the KIE for the rate of cleavage of dsDNA by HO• was measured, the reactivity was determined to be 5' > 4' > 3' ≈ 2' ≈ 1'.[77] However, in the case of **4**, the issue of solvent accessibility addressed in these calculations and experiments may be less important since the radical is already imbedded in the helix, not a freely diffusing solvent-borne radical.

2.3.2 Pulse Radiolysis Studies

Pulse radiolysis[35-37,78,79], in conjunction with EPR spectroscopy[80-82], has been utilized to provide evidence for the transfer of spin from the nucleobase to the sugar, ultimately giving rise to DNA strand breaks via elimination of the phosphate group(s). In radiolysis studies on polyuridylic acid (poly (U)), ≈10% of HO• and <5% of H• directly react with the sugar moiety to generate a radical, but the observed strand scission efficiency under these conditions was 41% and 19%, respectively.[78] The observation that ionizing radiation results predominantly in modification of the nucleobase, but that strand scission results from a sugar radical, led researchers to propose that there must exist a pathway for transfer of the radical from the nucleobase to the sugar.

When pulse radiolysis studies were carried out under conditions in which the yield of HO• was enhanced, the major radical intermediate formed was predicted to be **47** (Figure 22). The decay of the nucleobase radical (**47**) occurred at approximately the same

rate as strand scission.[15,17,81] This observation supports the contention that the rate determining step is hydrogen atom abstraction by **47** and is consistent with the observations made in studies of the direct effect of ionizing radiation.[15,17,81]

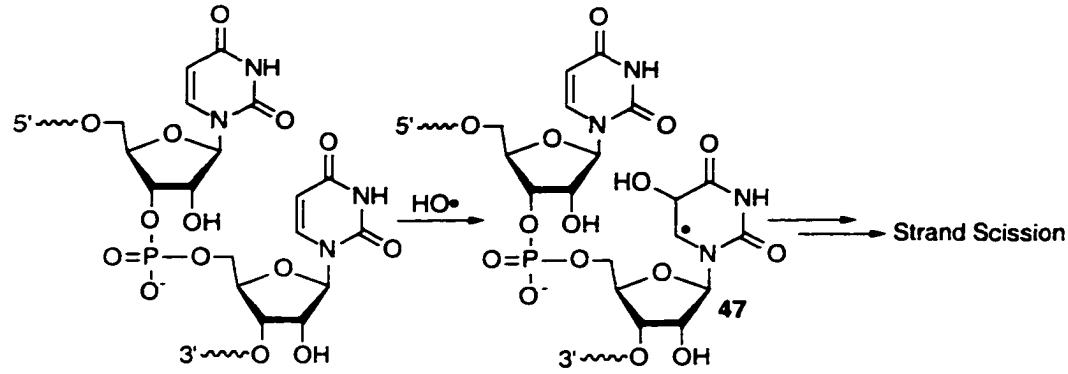

Figure 22. Pulse radiolysis studies of poly (U) suggest the transfer of spin from the nucleobase to the sugar.

When pulse radiolysis studies were carried out in the presence of O_2, an increase in strand scission was observed.[35,37] It is assumed that since O_2 traps alkyl radicals at diffusion-controlled rates, the formation of a nucleobase peroxyl radical was responsible for the strand scission via hydrogen atom abstraction from a nearby sugar. Like the nucleobase radical (**47**), the peroxyl radical also decays with a rate similar to the rate of strand scission, indicating that hydrogen atom abstraction by the peroxyl radical is the rate determining step during strand scission.[37]

Although the pulse radiolysis studies provide evidence that spin is transferred from the nucleobase to the sugar moiety, it is difficult to determine which nucleobase radical is involved in this process. Recall that although HO• preferentially reacts with **3** (and in the above experiments with uridine) by addition to the C5-position to generate **31**, approximately 30% of the reactivity of HO• is accounted for by formation of **5** (Figure 23).[1] From the pulse radiolysis experiments, it is unclear whether hydrogen atom abstraction is due to **31** and/or **5**.

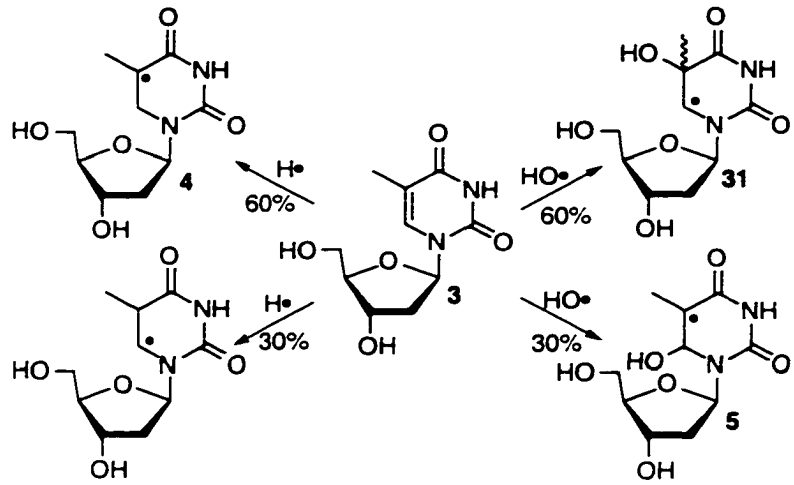

Figure 23. Nucleobase radical intermediates generated upon radiolysis of **3.**

In addition to the potential of generating more than one nucleobase radical simultaneously, distinguishing between internucleotidyl or intranucleotidyl hydrogen atom abstraction is difficult (Figure 24). Internucleotidyl refers to hydrogen atom abstraction from an adjacent or nearby nucleotide, whereas intranucleotidyl hydrogen atom abstraction occurs within the same nucleotide in which the nucleobase radical is generated. However, pulse radiolysis studies carried out with poly T suggest that hydrogen atom abstraction occurs in an internucleotidyl fashion.[36]

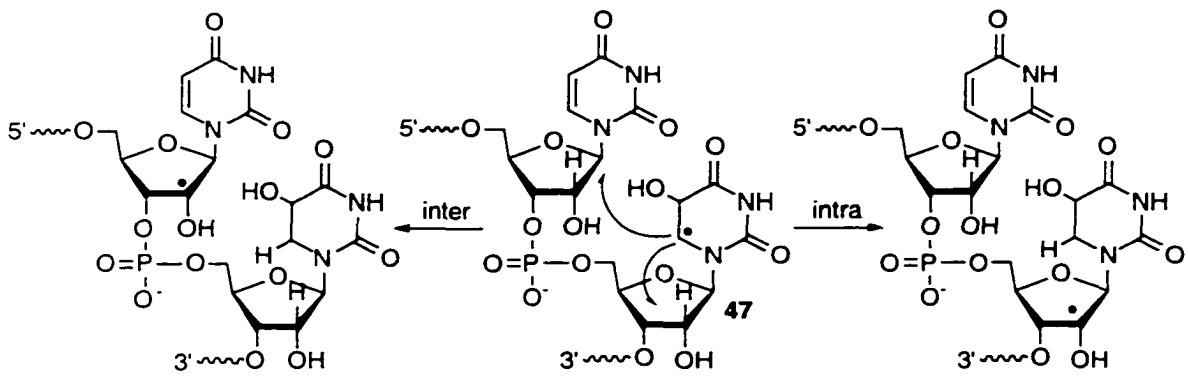

Figure 24. Internucleotidyl *versus* intranucleotidyl hydrogen atom abstraction.

2.3.3 Independent Generation of Reactive Intermediates

To circumvent the problem of simultaneous generation of more than one radical intermediate and address the issues raised in the pulse radiolysis experiments, the nucleobase radicals were independently generated from photolabile free radical precursors. The advantage of using a synthetic precursor is two-fold; 1) one can generate a discrete radical intermediate and study its subsequent reactivity and 2) the precursor can potentially be site-specifically incorporated into a biopolymer.[49] While ionizing radiation generates radical intermediates throughout the biopolymer, this latter method allows one to observe the chemistry resulting from a radical generated at a defined position in the DNA. This is beneficial for not only determining if hydrogen atom abstraction occurs at the adjacent sugar, but also if damage is propagated along the same strand or transferred to the opposite strand.

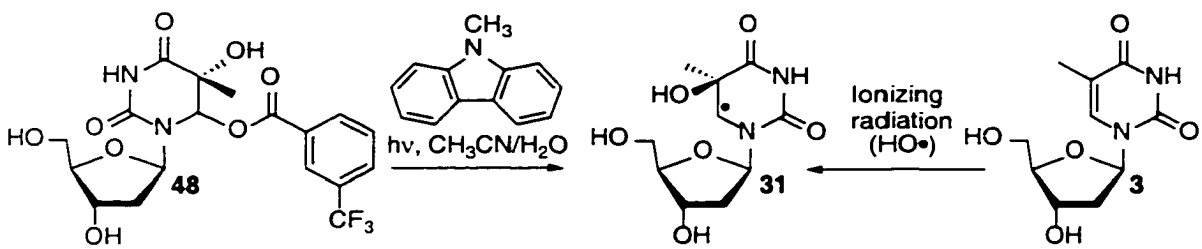

Figure 25. Independent generation of **31** to probe intranucleotidyl hydrogen atom abstraction.

It was assumed in the pulse radiolysis studies that the major radical intermediate formed was **47** (or the analogous **31**, Figure 25). Pulse radiolysis studies suggest that the nucleobase radicals formed abstract a hydrogen atom from a sugar in an internucleotidyl fashion.[36] The ability for **31** to undergo intranucleotidyl hydrogen atom transfer was further investigated by independent generation from **48**.[83,84] Photolysis of **48** in the presence of deuteurium atom donors, followed by analysis of the ^{2}H-incorporation in the product (5,6-dihydro-5-hydroxythymidine, **8**), indicated that intramolecular hydrogen atom

abstraction within **31** does not occur at a rate sufficiently fast to be relevant to DNA strand scission (Figure 25). Therefore, if hydrogen atom abstraction occurs, it must occur in an internucleotidyl fashion, which is consistent with the pulse radiolysis studies carried out with poly T.[36]

Since pulse radiolysis studies lend credence to the ability of some nucleobase radicals (e.g. **31**) to participate in hydrogen atom abstraction, the involvement of **4** in DNA damage amplification was investigated.[36,38,39,61] The feasibility of hydrogen atom abstraction by **4** from a nearby sugar was investigated via Norrish Type I photocleavage of the isopropyl ketone **49** in the presence of either 2-propanol or the dimethyl acetal of glycoaldehyde (**50**), models for the C4'- and C1'-positions, respectively (Figure 26).[61] When the photolysis of **49** was carried out in the presence of D_2O and 5 M hydrogen atom donor, to mimic the effective molarity of an adjacent sugar, the significant amount of ^2H-incorporation in 5,6-dihydrothymidine (**34**) suggested that **4** was not efficiently trapped. These experiments suggest that **4** is unlikely to participate in hydrogen atom abstraction in DNA.

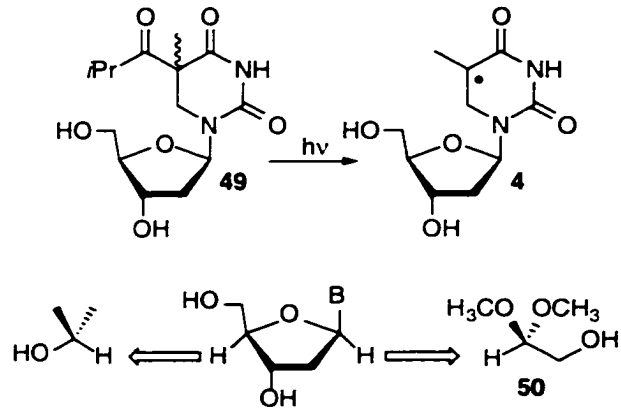

Figure 26. Independent generation of **4** from **49**.

The ability for **4** to participate in hydrogen atom abstraction was further investigated in single-stranded DNA (ssDNA), utilizing the photolabile isopropyl ketone (**49**), which

had been incorporated into oligonucleotides at defined sites (**51**, Figure 27).[38,39] When the radical (**14**) was generated in ssDNA under anaerobic conditions, no direct strand breaks or alkaline labile lesions were observed.[39] This is consistent with the monomer studies, in which it was shown that **4** was unable to participate in hydrogen atom abstraction from models representative of the C1'- and C4'-positions, and refutes previous proposals in the literature concerning the reactivity of 5,6-dihydrothymidin-5-yl (**14**).[24,25]

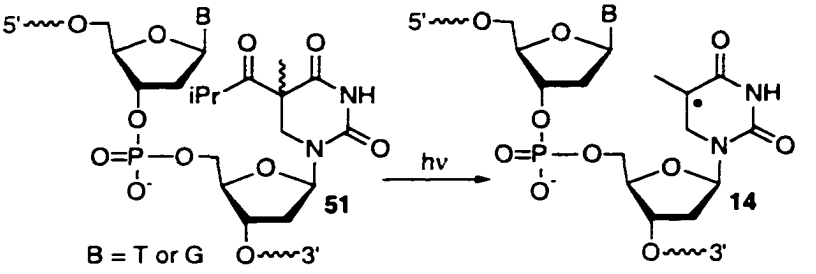

Figure 27. Independent generation of **14** from **51** in ssDNA.

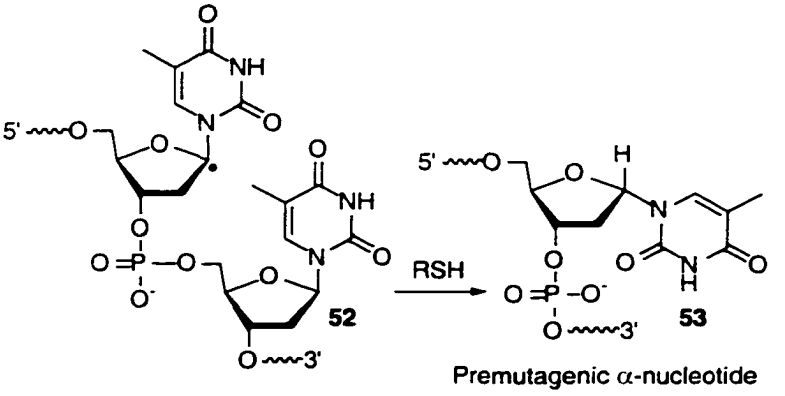

Figure 28. Formation of premutagenic **53** upon trapping of **52**.

Although strand scission was not observed under anaerobic conditions, one cannot ignore the possibility that the nucleobase radical may abstract a hydrogen atom from the adjacent sugar, but that strand scission or alkaline labile lesion formation does not occur under these conditions. For instance, it has been shown that upon generation of the C1'-

radical (**52**) in ssDNA, subsequent trapping by thiol results in ≈20% of the unnatural α-anomer (**53**), which does not present itself as a direct strand break or alkaline labile lesion (Figure 28).[85]

Although no evidence was obtained for internucleotidyl hydrogen atom abstraction by **14**, direct strand breaks and alkaline labile lesions were observed when the radical was generated in the presence of O_2.[38] Since alkyl radicals are trapped by O_2 at diffusion controlled rates, it is assumed that upon generation of **14**, reaction with O_2 yields the peroxyl radical (**9**, Figure 29).[26] The requirement for O_2 in DNA damage suggests that **9** is involved in hydrogen atom abstraction and this is in agreement with the pulse radiolysis experiments which demonstrate that damage is enhanced in the presence of O_2.[35,37]

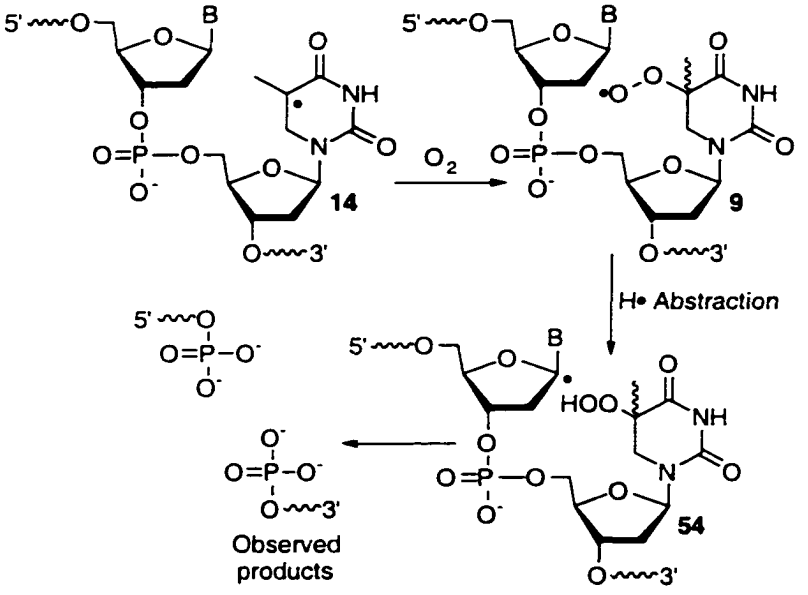

Figure 29. Internucleotidyl hydrogen atom abstraction from the C1'-position by **9** leading to direct strand breaks and alkaline labile lesions.

The observed strand scission implies transfer of spin from the nucleobase to the sugar as predicted by pulse radiolysis studies. In order to determine which hydrogen atom was abstracted by **9**, the kinetic isotope effect (KIE) was measured.[39] The sugar bonded to

the 5'-phosphate of the peroxyl radical (**9**) was enriched with deuterium either at the C1'-, C2'-, or C4'-position. The KIE for the C1'-position was ≈4, whereas no KIE was observed upon substitution at the other positions.[39] This is indicative of **9** selectively abstracting a hydrogen atom from the C1'-position of the adjacent sugar (Figure 29). This result supports the proposal that spin is transferred from the nucleobase to the sugar by hydrogen atom abstraction. In addition, these experiments indicate that the formation of a single lesion on the nucleobase results in a cascade of damaging events that ultimately leads to the formation of direct strand breaks and alkaline labile lesions and constitutes a rare example of DNA damage amplification.

2.4 Other Systems that Induce Damage via the C1'-Radical

Neocarzinostatin (**56**, NCS), manganese porphyrins (**57**), and copper phenanthroline (**55**, Cu(*o*P)$_2$) also induce damage via hydrogen atom abstraction from the C1'-position of the sugar backbone of DNA.

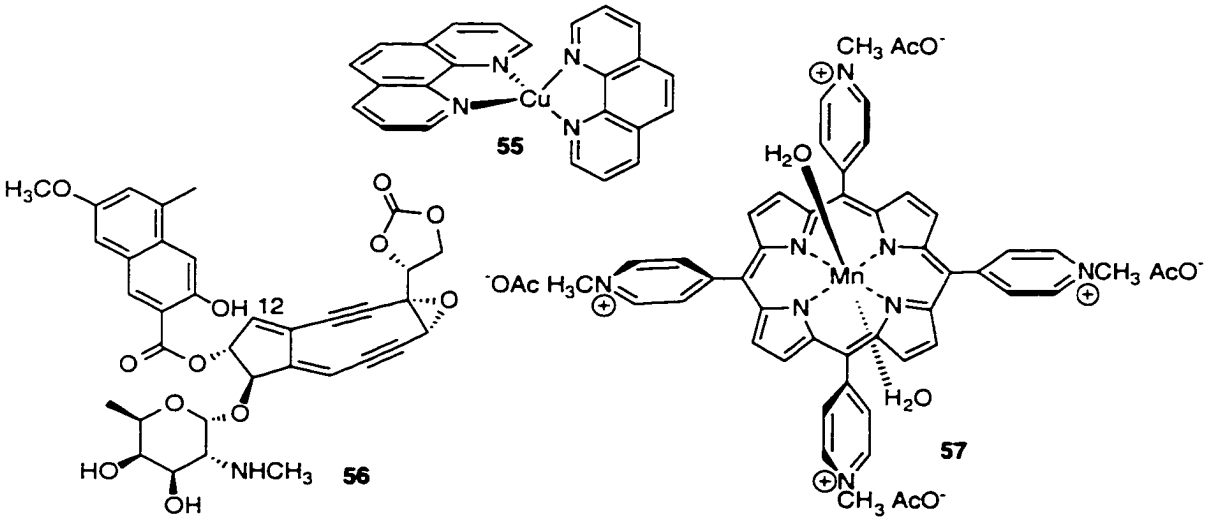

These damaging agents noncovalently bind to the minor groove where the C1'-, C4'- and C5'-hydrogens of the sugar are accessible. Hence it is not surprising that these agents are capable of inducing damage at the C4'- and C5'-positions in addition to the C1'-

position.[9] The manganese porphyrins and NCS result in the formation of alkaline labile lesions, consistent with the chemistry observed for **7** (and **9**), whereas Cu(*o*P)$_2$ results in direct strand breaks.[9]

Neocarzinostatin (**56**) belongs to a class of enediyne antitumor antibiotics that bind in the minor groove of DNA with its chromophore intercalated between the base pairs.[13,14,86,87] NCS is activated by thiol activation at C12 and epoxide opening to form the cumulene intermediate (**58**), which undergoes a Bergman-type rearrangement to generate the biradical (**59**, Figure 30).[13]

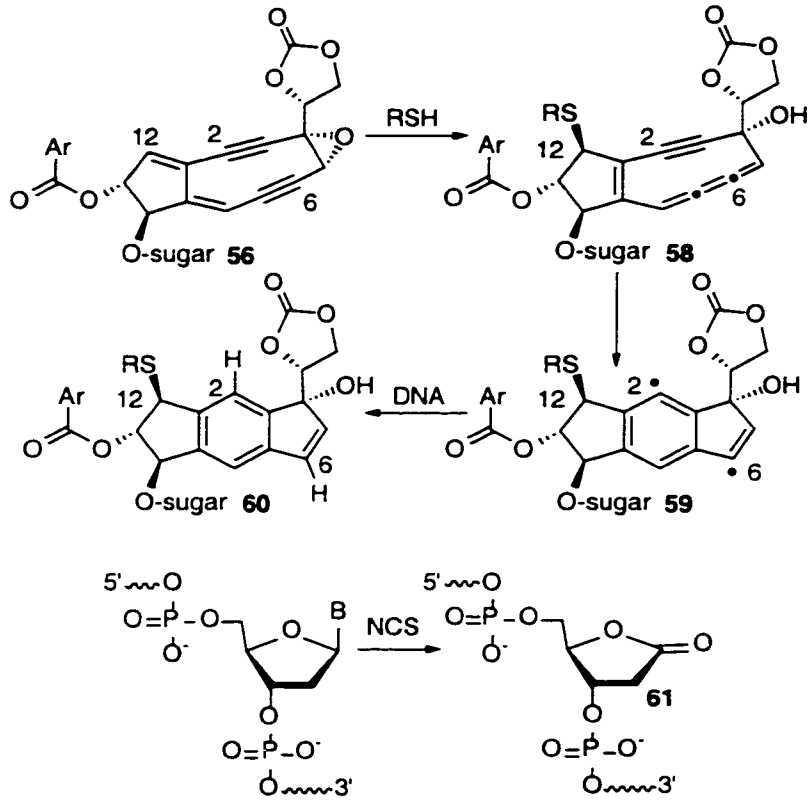

Figure 30. Mechanism of NCS activation and action.

When DNA was exposed to NCS, 2-deoxyribonolactone (**61**) was observed, which is consistent with C1'-hydrogen atom abstraction.[87] It has been postulated that the

biradical effects double strand cleavage via hydrogen atom abstraction from the C5'- and C1'- (or C4'-) positions of sugars on opposite strands by the C6 and C2 radicals, respectively.[9] It was also postulated that formation of the C1'-radical ultimately leads to **61**. Although there was no direct evidence for its formation, **61** was also suggested to be involved in the DNA damage amplification observed in studies on the peroxyl radical (**9**, Figure 29).

Like NCS, Cu(*o*P)$_2$ (**55**) binds to the minor groove of DNA where it is able to generate radicals at the C1'- and C4'-positions.[9] However, Cu(*o*P)$_2$ leads to direct strand breaks, presumably via hydrogen atom abstraction from the C1'-position.[88] The mode of action of Cu(*o*P)$_2$ is unclear, but it is possible that the Cu(*o*P)$_2$ binds to the DNA and subsequently reduces H_2O_2 to generate HO• in the immediate vicinity of the DNA.[89,90] The discovery that the nucleobases are also damaged in the presence of Cu(*o*P)$_2$, in a manner similar to exposure to the HO•, supports the hypothesis that HO• production is the source of damage induced by Cu(*o*P)$_2$.[91] EPR studies of Cu(*o*P)$_2$ also indicate that HO• is generated upon activation.[92]

Sigman has proposed that Cu(*o*P)$_2$ abstracts a hydrogen from the C1'-position and the radical is subsequently oxidized to the carbocation (**62**, Figure 31).[93,94] Upon deprotonation of the carbocation (**62**) to yield the 1',2'-didehydro sugar (**63**), hydrolysis results in elimination of the 3'-phosphate to generate the α,β-unsaturated lactone (**64**) after trapping with H_2O.[94] This mechanism was investigated by independent generation of **66**, a model for **63**, from the selenoxide (**65**, Equation 7).[95] The 1',2'-didehydro sugar (**66**), generated in this manner, was shown to be stable in the presence or absence of Cu(*o*P)$_2$ for 48 h. This suggests that **66** (and **63**) is not an intermediate in the mechanism for the conversion of the C1'-radical (**52**) to **64**.[95]

An alternative mechanism has been proposed for the formation of direct strand breaks in the presence of Cu(*o*P)$_2$ and involves the intermediacy of **61**, which was observed in the NCS mediated strand damage (Figure 31).[95] It was shown that a model of

61 was not stable in the presence of Cu(*o*P)$_2$ and readily undergoes elimination to **64**. Therefore, like NCS, Cu(*o*P)$_2$ mediated damage to DNA most likely results in the formation of **61**, which readily undergoes elimination in the presence of Cu(*o*P)$_2$.[95]

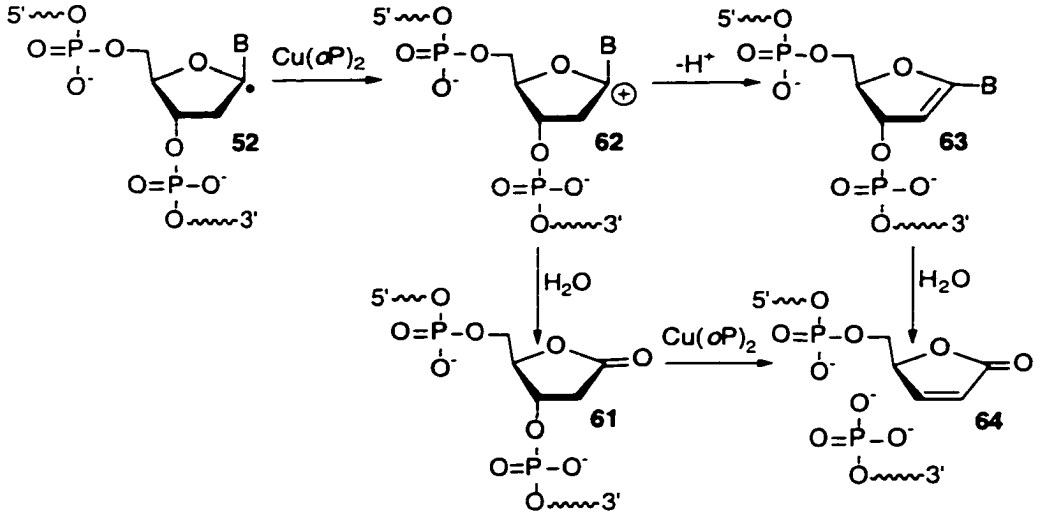

Figure 31. Mechanism of Cu(*o*P)$_2$ mediated direct strand breaks.

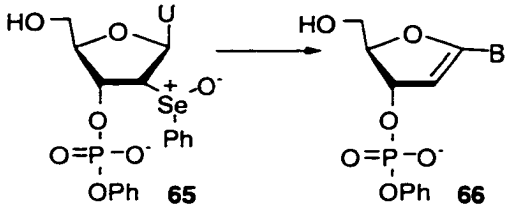

(7)

The metalloporphyrins (**57**) are DNA-damaging agents which also bind in the minor groove of DNA and are activated in the presence of an oxygen atom donor, such as H_2O_2, $KHSO_5$, or O_2 and an electron source (as in cytochrome P450).[9] Upon activation of the metalloporphyrin to Mn^V, strand cleavage is observed with the concominant production of the methylene furanone (**67**) and release of free base (Figure 32).[96] The methylene furanone (**67**) is consistent with hydrogen atom abstraction from the C1'-position. The

C1'-radical is believed to either be oxidized to the carbocation and subsequently trapped by H_2O or directly hydroxylated by the Mn^{IV}-OH species via an oxygen-rebound mechanism. Both pathways ultimately gives rise to the alkaline labile **61**, which undergoes β,γ-elimination to effect strand scission and release of **67**.

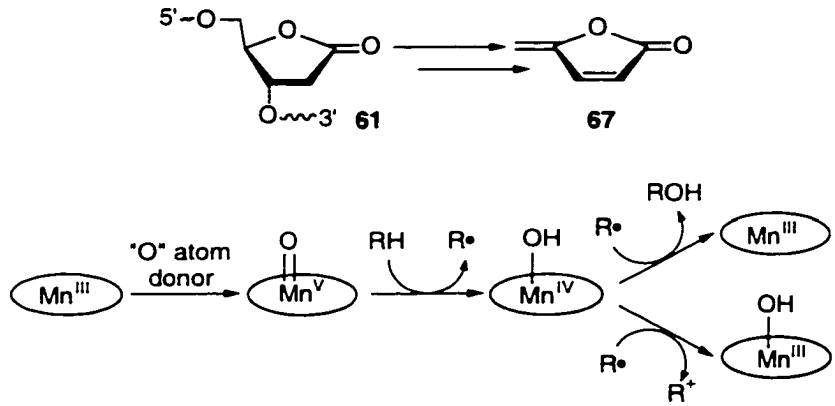

Figure 32. Mechanism of metalloporphyrin mediated DNA damage.

2.5 Reactivity of the C1'-Radical

The generation of the C1'-radical is prevalent in DNA damaging systems, both naturally occurring and unnatural. In the absence of potential acid-base catalysts (e.g. $Cu(oP)_2$), it has been postulated that upon formation of the C1'-radical under aerobic conditions, the ultimate product is **61**. Although **61** had been invoked in mechanisms to account for the observed alkaline labile lesion formation, isolation and characterization of biopolymers containing this lesion is difficult due to its lability. Consequently, the mechanism for its formation has only recently been elucidated. Evidence for the formation of **61** from the C1'-radical (**52**) has been gained through independent generation of the monomeric C1'-radical (**69**) under mild conditions from the *tert*-butyl ketone (**68**, Figure 33).[97,98] When the photolysis of **68** was carried out in the presence of O_2, the 2-deoxyribonolactone (**70**) proposed in the DNA damage processes described above was

observed.[99] These experiments provide direct evidence that **70** is formed via the intermediacy of **69**.

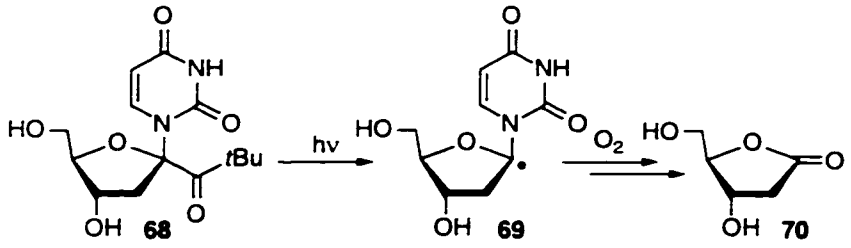

Figure 33. Independent generation of **69** from **68**.

Studies utilizing epinephrine (**73**), an assay to detect $O_2^{\cdot-}$, isotopic incorporation in the presence of $H_2{}^{18}O$, and competitive kinetics indicate that **69** is trapped by O_2 to generate the peroxyl radical (**71**), which undergoes $O_2^{\cdot-}$ elimination to generate the carbocation (**72**, Figure 34).[99] Trapping of **72** by H_2O and subsequent loss of the nucleobase results in the formation of **70**.

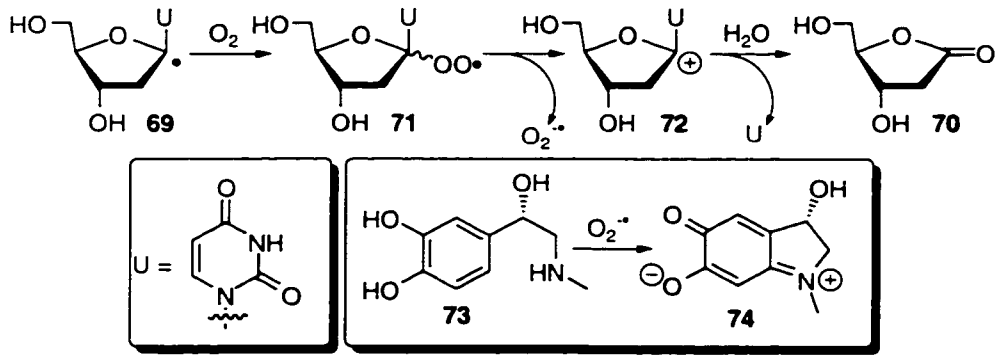

Figure 34. Mechanism for the formation of **70** via $O_2^{\cdot-}$ elimination.

These observations were supported by laser flash photolysis (LFP) experiments.[100] However, there is some discrepancy involving the rate constant for $O_2^{\bullet}$ elimination. The LFP studies indicate that the rate constant for $O_2^{\bullet}$ elimination is 2 x 10^4 s^{-1}, whereas the experiments using competitive kinetics estimated the rate of $O_2^{\bullet}$ elimination to be ≈1 s^{-1}.[99,100] Regardless of which rate constant is correct, pulse radiolysis studies on DNA using glutathione suggest that the elimination of $O_2^{\bullet}$ is a biologically relevant mechanism for the formation of **70**.[67]

2.6 Reactivity of 2-Deoxyribonolactone (70)

Given the prevalence of DNA damage at the C1'-position and the subsequent formation of 2-deoxyribonolactone (**70**), the reactivity of this lesion in DNA is an interesting and important issue with respect to DNA damage amplification. Incorporation of **70** into a biopolymer to study its effect on DNA is difficult due to its labile nature. To avoid this problem, precursors to 2-deoxyribonolactone (**70**) have been incorporated into DNA and subsequently photolyzed to generate **70**. The 2-deoxyribonolactone lesion (**70**) has been successfully incorporated into DNA (**61**) from the stable *tert*-butyl ketone (**75**) and nitroindole (**76**) precursors and subsequent photolysis (Figure 35).[53,101-103]

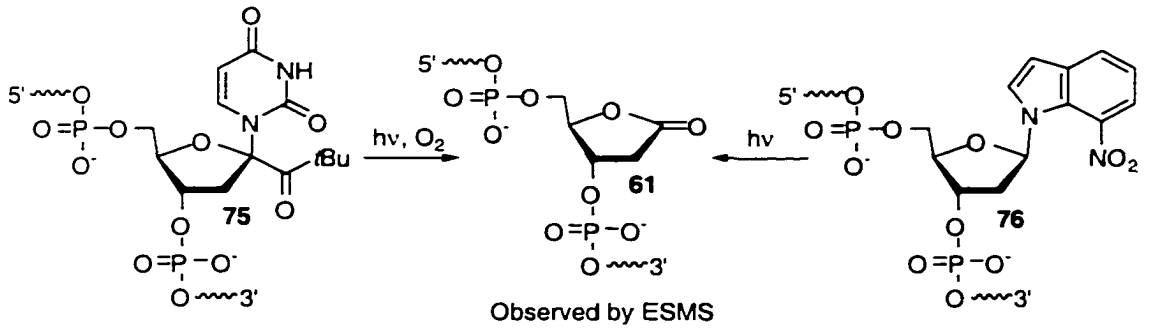

Figure 35. Photochemical precursors to 2-deoxyribonolactone (**70**).

Upon irradiation of **75**, intact **61** was observed by ESMS.[101] Treatment of the DNA with *N,N'*-dimethylethylenediamine (DMEDA) or piperidine resulted in strand scission, consistent with elimination of the 3'- and 5'-phosphates from **61**.[53] The expected product upon elimination of the 3'-phosphate is the α,β-unsaturated lactone (**64**, Figure 36). However, due to the instability of **64**, it could not be isolated and characterized.

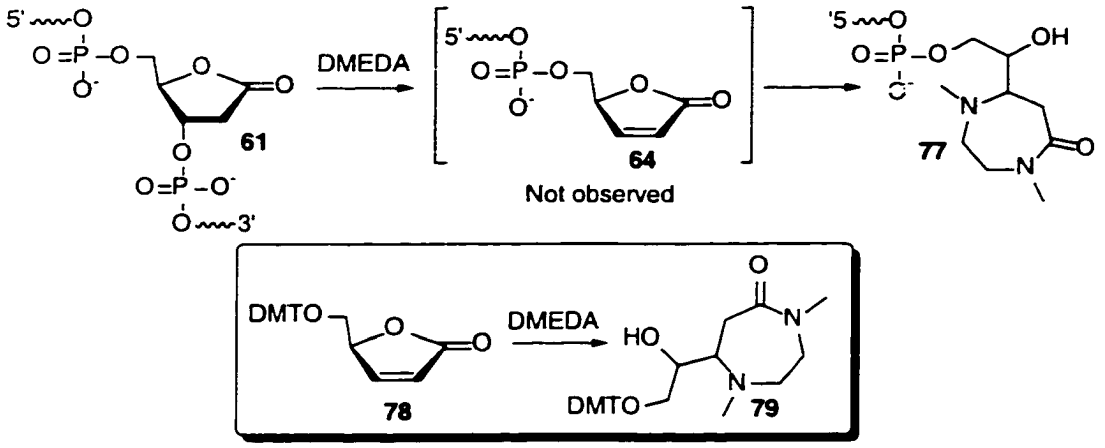

Figure 36. Observed product upon treatment of 2-deoxyribonolactone (**61**) with DMEDA.

Model studies indicate that **78**, representative of the lesion **64**, undergoes a Michael addition, followed by cyclization to afford the lactam (**79**) upon reaction with DMEDA (Figure 36).[101] Therefore, indirect evidence for the intermediacy of **64** was obtained by trapping it with DMEDA. When the DNA product mixtures were analyzed by MALDI-TOF, the 1,4- and 1,2-adducts (**77**) were observed, providing indirect evidence for the formation of **64** in a biopolymer.[101]

2.7 Radiosensitizers as Oxygen Surrogates

The DNA damage amplification described thus far relies on the presence of O_2 in the system. However, cancer cells tend to be hypoxic (i.e. oxygen-deficient) and are expected to be less susceptible to the observed reaction pathways. A variety of small

molecules have been used to sensitize hypoxic cells to ionizing radiation. One potential mechanism of action for these molecules is that they serve as surrogates for O_2 in reactions with DNA radicals. Tirapazamine (**11**) and misonidazole (**13**) are two such compounds that have been utilized as oxygen surrogates.

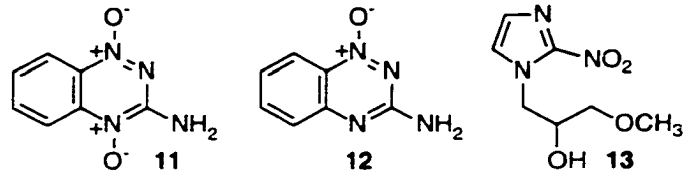

Tirapazamine (**11**) is a bimodal agent that has been used in cancer therapy to induce DNA strand scission.[40-45] Tirapazamine is unique in that it is activated by one-electron reduction in hypoxic cells to initiate DNA damage, possibly through the generation of HO•.[41-43] Upon reduction of **11**, the 1-*N*-oxide (**12**) is generated. In addition, **11** and **12** have been shown to efficiently trap free radicals. For example, **11** and **12** react with the C1'-radical (**52**) in ssDNA at 2.5 x 10^8 and 4.6 x 10^8 M^{-1} s^{-1}, respectively, converting it into an alkaline labile lesion (**61**), presumably via the intermediacy of the alkoxyl radical (**80**, Figure 37).[44,45] In this respect, **11** acts as an oxygen surrogate and ultimately leads to the same product observed upon reaction of **52** with O_2 (Figures 33, 34).

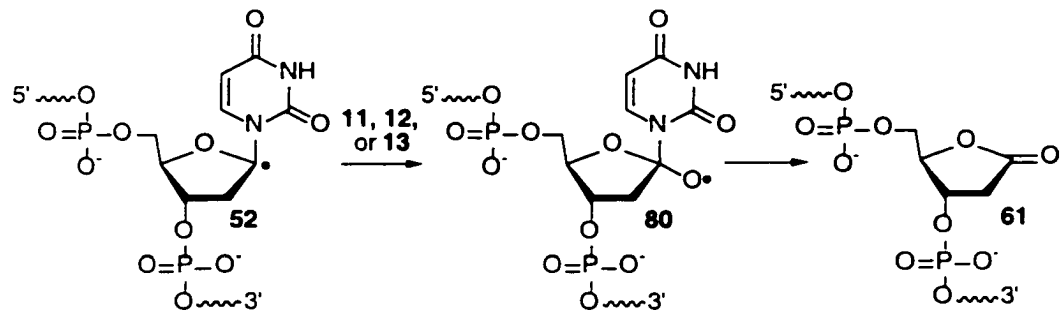

Figure 37. Trapping of the C1'-radical (**52**) by radiosensitizers (**11**, **12**, or **13**) to generate 2-deoxyribonolactone (**61**).

Misonidazole (**13**) is an "oxygen mimetic" that has been used in conjunction with ionizing radiation therapy to increase the yields of single strand breaks in DNA.[46] For example, although the product ratios vary, the damage observed upon generation of the C4'-radical in DNA in the presence of misonidazole (**13**) is similar to the damage observed in the presence of O_2.[48,49] In this respect, misonidazole acts as a surrogate for O_2. Trapping of the radical by **13** and subsequent cleavage to the alkoxyl radical has been invoked to explain the observed damage.[48,49] Like tirapazamine (**11**) and its reduced 1-*N*-oxide (**12**), misonidazole (**13**) has been shown to effectively trap **52** in ssDNA with a rate constant of 6.9×10^8 M^{-1} s^{-1}.[44]

It is likely that both **11** and **13**, in conjunction with ionizing radiation, initially induce damage in DNA via generation of HO•. As previously discussed, HO• preferentially reacts with the nucleobase to generate **15** as one of the products. In order to effect strand scission, it has been shown that spin must be transferred from the nucleobase to the sugar. The corresponding radical (**14**) has been shown not to lead to strand scission in DNA, but the peroxyl radical (**9**) does through hydrogen atom abstraction from the C1'-position of the adjacent sugar.[38,39] However, the O_2 deficiency in tumor cells precludes the formation of **9** and subsequent hydrogen atom abstraction from the adjacent sugar.

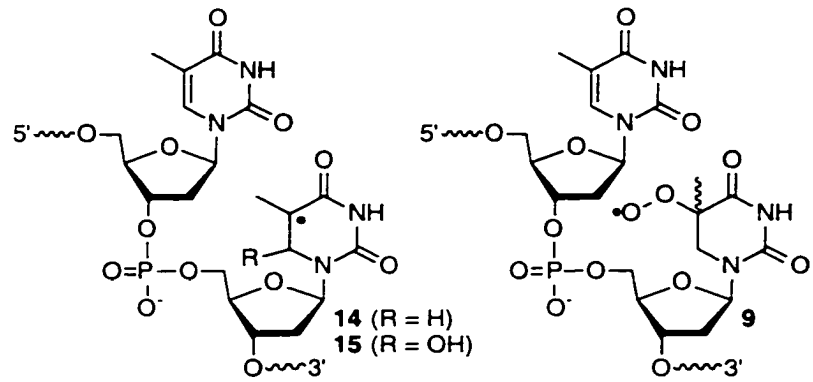

Therefore, since **11**, **12**, and **13** have been shown to trap alkyl radicals, and the resulting adducts are believed to cleave to the alkoxyl radical, it is possible that some of the DNA damage induced by these species is attributable to initial trapping of the nucleobase radical.[44,45] The formation of the nucleobase alkoxyl radical is expected to undergo similar chemistry as the respective peroxyl radical (**9**). Therefore, it is possible that **14** may also undergo reaction with **11**, **12**, or **13** to lead to DNA damage amplification, as proposed in experiments involving **14** and O_2.

2.8 Related Examples of Internucleotidyl Reactions

In addition to formation of the C1'-radical via hydrogen atom abstraction by **9**, other agents have been shown to induce DNA damage by a similar pathway. The radiosensitizing agent, 5-bromo-2'-deoxyuridine (**81**, Figure 38), has been shown to increase strand scission in DNA upon γ-radiolysis and UV-irradiation.[104,105]

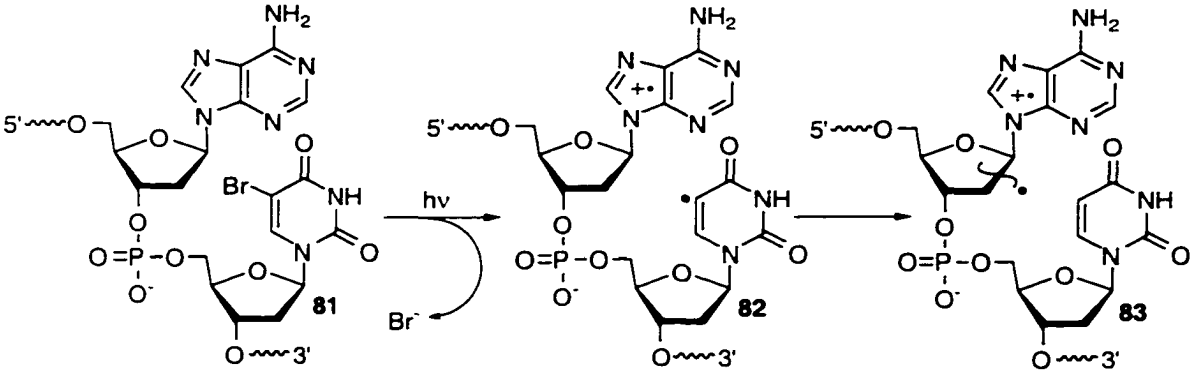

Figure 38. Generation of the σ radical (**82**) via photoinduced single electron transfer.

Excitation of the base adjacent to **81** induces single electron transfer to the latter, generating the radical anion, which undergoes heterolytic cleavage to yield the σ radical (**82**, Figure 38).[106] The generation of the σ radical (**82**) subsequently leads to direct strand

breaks and alkaline labile lesions.[73,74] A combination of KIE and ^{3}H studies indicate that the C1'- and C2'-positions of the adjacent sugar are involved in the observed DNA damage amplification pathways for **81**, and the related compound 5-iodo-2'-deoxyuridine (Figure 38).[73,75,107]

It has been proposed that generation of the radical at the C1'-position gives rise to 2-deoxyribonolactone (**61**), which accounts for the alkali-lability of the DNA.[97-100] However, in the case of **84**, it was proposed that electron transfer occurs from the C1'-radical (**84**) to the nucleobase to quench the radical cation and generate the sugar-centered carbocation (**85**). Subsequent trapping of **85** by H_2O and elimination of the nucleobase generates **61** (Figure 39).

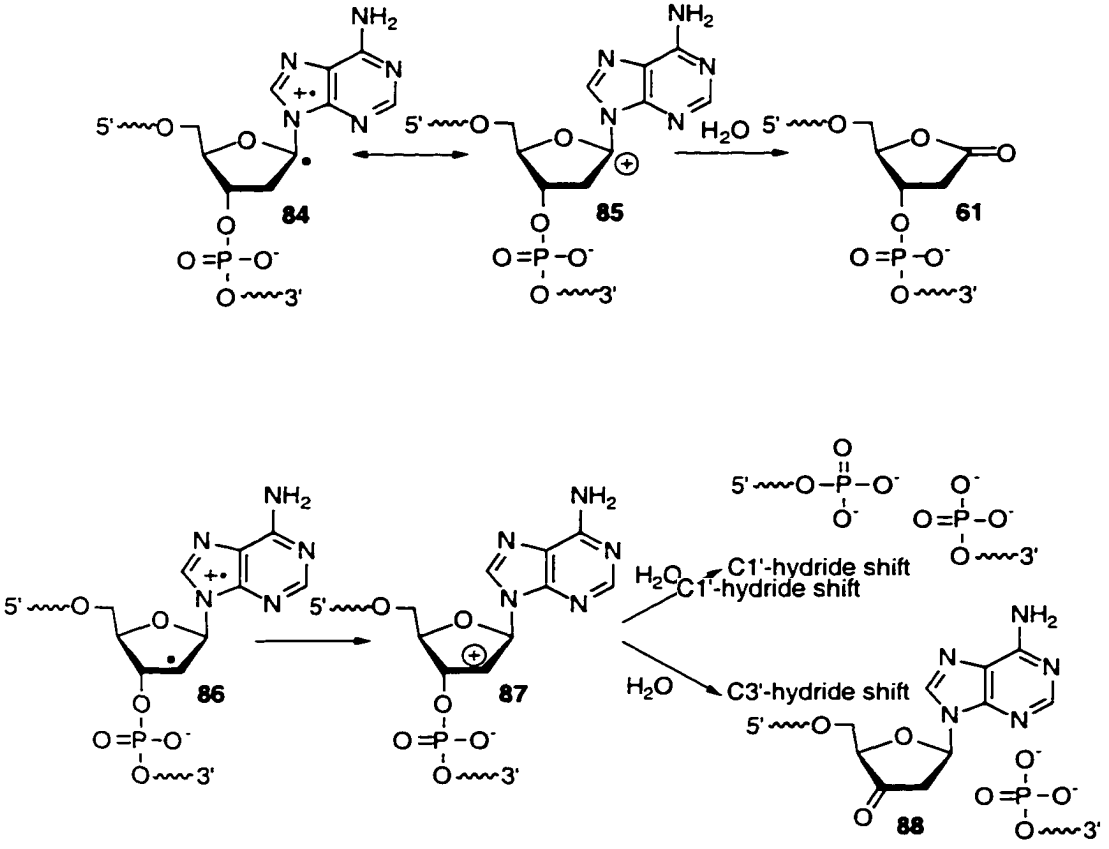

Figure 39. Reactivity of C1'- and C2'-radicals in 5-BrdU system.

Alternatively, electron transfer from the C2'-radical (**86**) to the nucleobase generates **87**. Subsequent 1,2-hydride shift from either the C1'- or C3'-position was invoked to explain the observed products (Figure 39).[73,74] Model studies involving generation of the C2'-carbocation from 2'-iododeoxyuridine supports the mechanism involving 1,2-hydride shifts.[108]

Investigation of the reactivity of **82** under aerobic conditions, in which the peroxyl radical (**89**) was expected to be generated, indicated that **89** selectively abstracts the C1'-hydrogen atom from the adjacent sugar in both ssDNA and dsDNA.[74] Although the sum of direct strand breaks and alkaline labile lesions remained constant, the efficiency of direct strand breaks decreased in dsDNA compared to reactions conducted under anaerobic conditions. This is presumably due to partitioning of the reactivity of the σ radical (**82**) between trapping by O_2 to generate **89** and hydrogen atom abstraction (Figure 40).[74]

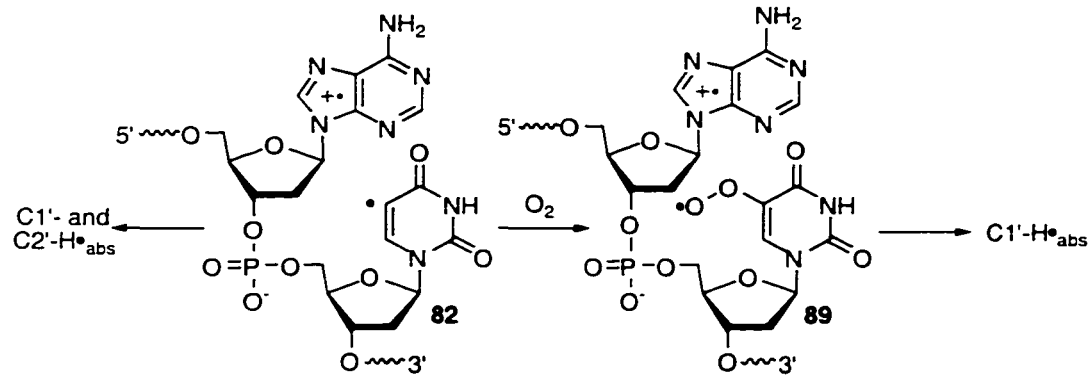

Figure 40. Competitive hydrogen atom abstraction by the σ radical (**82**) and peroxyl radical (**89**).

The DNA damage amplification observed in experiments with **81** are interesting and novel in their own right. However, it is pertinent to note that the reactivity of **89** is analogous to the reactivity observed with **9**, both peroxyl radicals selectively abstracting a

hydrogen atom from the C1'-position of an adjacent sugar. In addition, although the nucleobase radical (**89**) lies in the major groove of duplex DNA, it is able to abstract a hydrogen atom from the minor groove. Although the reactivity of **9** has not been examined in dsDNA, it is expected to be able to undergo hydrogen atom abstraction from the C1'-position, as observed in ssDNA, given the results of experiments involving **81**.

2.9 Shortcomings of Utilizing the Isopropyl Ketone (49) as a Precursor to 5,6-Dihydrothymidin-5-yl (4)

Although the studies utilizing **49** suggest that the peroxyl radical (**9**) is capable of abstracting a hydrogen atom from an adjacent sugar to effect strand scission, the results are compromised by the production of singlet oxygen ($^1O_2$) during the reaction.[39] Singlet oxygen ($^1O_2$) is generated upon quenching of the excited state of the ketone by O_2. When the reactions were carried out in the presence of NaN_3, a $^1O_2$ scavenger, a diminution of overall strand damage was observed. However, the decrease of strand damage may be due to quenching of $^1O_2$ or the excited state of the ketone (**49**) by NaN_3. The presence of $^1O_2$ was therefore confirmed using a trap (**90**, Figure 41), which reacts in a [4+2] fashion to generate the endoperoxide (**91**) or via an ene reaction to generate **92**.

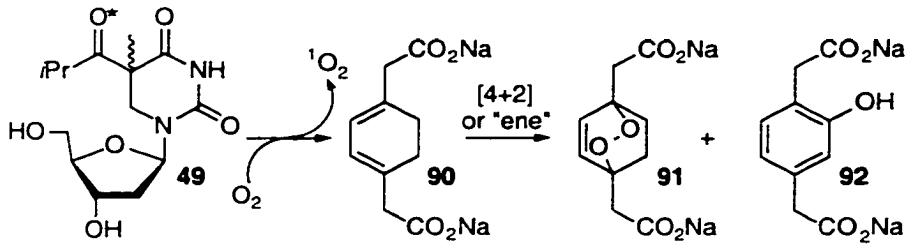

Figure 41. Generation and trapping of $^1O_2$.

Singlet oxygen ($^1O_2$) is known to react with DNA to generate modified nucleobases.[109-111] For example, the formation of endoperoxides in **25** via a [4+2] cyclization ultimately gives rise to **27**, which leads to strand breaks (Figure 42).[110]

Although the [4+2] is more favorable with **25**, $^1O_2$ has also been shown to undergo [2+2] cyclizations with the appropriate substrate.[109] Therefore, the generation of $^1O_2$ in the studies on **4** may compromise the results. Although $^1O_2$ has been shown to preferentially react with **25**, thymidine (**3**) may also undergo reaction with $^1O_2$.[111] One may recall that **4** was generated in biopolymers containing an adjacent dG (**25**), as well as polythymidylate. Conducting the studies on **4** with a more efficient precursor may circumvent the problem of $^1O_2$ and give rise to cleaner, less ambiguous analyses.

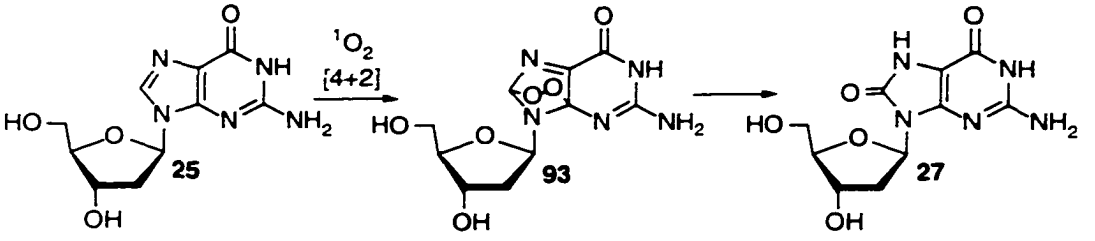

Figure 42. Reaction of $^1O_2$ with **25**.

2.10 Statement of Research Objectives

From the mechanistic studies outlined above, there are several suggestions one can make about the role of **14** in DNA damage amplification:

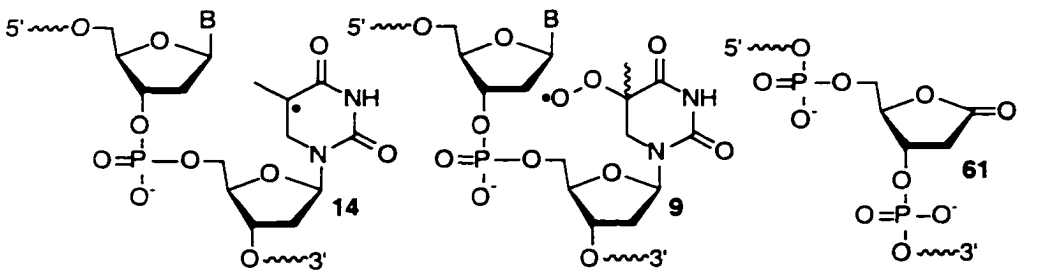

1. Strand scission induced by **14** is an O_2 dependent process involving the peroxyl radical (**9**).
2. The peroxyl radical (**9**) selectively abstracts the C1'-hydrogen atom from the adjacent sugar generating the C1'-radical, which results in the formation of 3'- and 5'-phosphate end groups upon treatment with base.
3. The formation of the C1'-radical in monomeric and biopolymer studies results in the formation of 2-deoxyribonolactone (**61**).
4. Indirect evidence for the intermediacy of the α,β-unsaturated ribonolactone (**64**) in a biopolymer is gleaned from the MALDI-TOF analysis, which suggests the formation of 1,4- and 1,2-adducts of the lesion.

Although these studies support the formation of **61** from the C1'-radical in a biopolymer, direct evidence for its formation during DNA damage amplification initiated by **14** has never been attained. In addition, the results obtained from the experiments involving the generation of **14** from the isopropyl ketone (**49**) are skewed by the generation of $^1O_2$ during the photolysis. Furthermore, product analysis, a hallmark of organic chemistry, was severely lacking in these previous studies.

The goal of this research project was to design a system with a more efficient radical precursor to **4** (**14**), circumventing the problem of $^1O_2$ production, to better investigate the reactivity of **4** and address the following questions:

1. Can we provide further evidence that internucleotidyl hydrogen atom transfer does not occur under anaerobic conditions?
2. Does the peroxyl radical (**9**) transfer spin from the nucleobase to the adjacent sugar as suggested in previous studies? If so, does this process compete with bimolecular reactions available to **9** (e.g. trapping by thiols)? What is the stereoselectivity of this process?
3. Does the peroxyl radical (**9**) protect itself by eliminating superoxide in competition with internucleotidyl hydrogen atom abstraction?
4. If hydrogen atom abstraction by **9** occurs from the C1'-position, is the 2-deoxyribonolactone lesion (**61**) produced?
5. Can a radiosensitizing agent participate in DNA damage amplification involving 5,6-dihydrothymidin-5-yl (**4**) by acting as a surrogate for O_2?

3 Results and Discussion

3.1 Monomer Studies

The chemistry of 5,6-dihydrothymidin-5-yl (**4**) was previously studied utilizing the isopropyl ketone (**49**) as the photochemical precursor.[38,39,61] However, the chemistry was complicated by the inefficiency of the Norrish Type I photocleavage from **48**, which resulted in the competitive generation of $^1O_2$. The presence of $^1O_2$, which is known to damage DNA, complicated interpretation of the chemistry of **4**. The studies described herein were aimed at designing a precursor to **4** that would be more efficient than **49**.

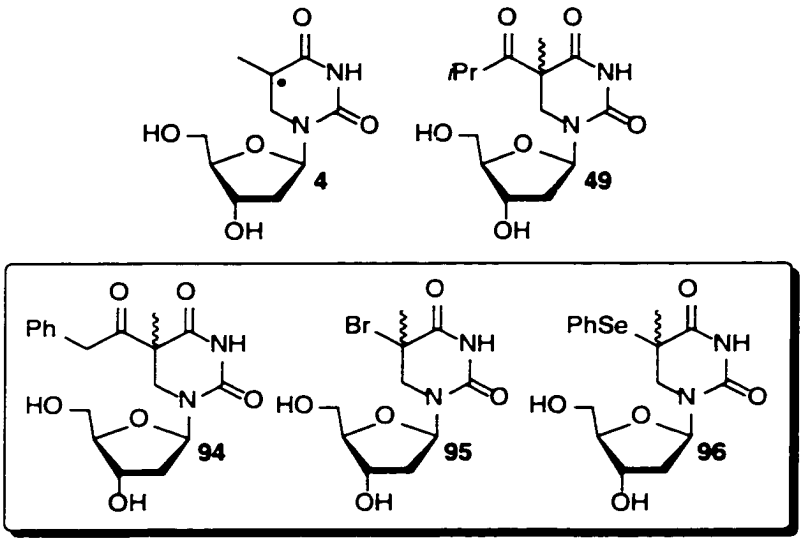

The benzyl ketone (**94**), bromide (**95**), and phenyl selenide (**96**) were investigated as potential precursors to **4**. The quantum yield for the ketone (**94**) was anticipated to be higher than **49** used in previous. The increase in efficiency in cleavage was expected to reduce the generation of $^1O_2$. In addition to photochemical generation, **95** and **96** were also anticipated to be candidates for generation of the radical under thermal conditions since

these compounds are commonly used in conjunction with Bu_3SnH and an initiator in free radical chain chemistry.

The monomer studies were carried out to investigate the reactivity of **4** under aerobic conditions. It has already been shown that **4** is trapped under anaerobic conditions in the presence of an efficient hydrogen atom donor to generate 5,6-dihydrothymidine (**34**).[38,39,61] In the presence of O_2, however, the radical (**4**) is expected to be trapped by O_2 to generate the peroxyl radical (**7**, Equation 8).

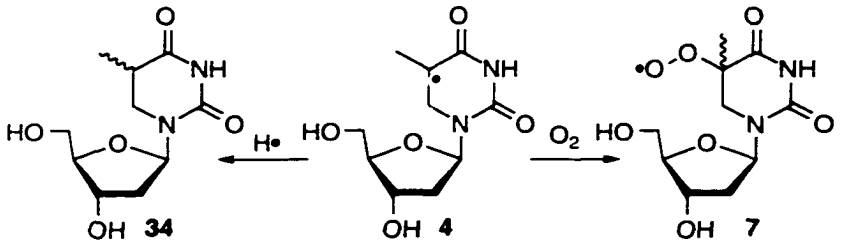

(8)

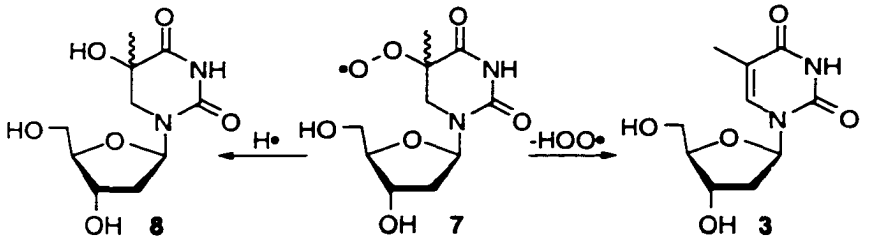

(9)

We proposed that, in addition to trapping and reduction to 5,6-dihydro-5-hydroxythymidine (**8**), the peroxyl radical (**7**) may undergo intranucleotidyl hydrogen atom abstraction to regenerate thymidine (**3**) with release of HOO• (Equation 9). This pathway is interesting in that it represents a detoxification pathway available to **4** in the presence of O_2. However, the release of HOO• may ultimately lead to superoxide ($O_2^{\bullet}$)-derived products that are able to damage DNA.[1,18,19,30-34] The involvement of $O_2^{\bullet}$ in DNA damage processes makes this pathway a potential double-edged sword. The possibility that superoxide elimination occurs upon generation of **4** in the presence of O_2 was investigated

at the monomeric level where product analysis could easily be carried out to determine if superoxide elimination was a kinetically viable pathway.

3.1.1 Synthesis of Radical Precursors

A procedure for the synthesis of **94** had been previously developed (Scheme 1).[112] Hydrogenation of commercially available thymidine (**3**) yielded 5,6-dihydrothymidine (**34**), which was subsequently protected with TBDMSCl to yield **97**. The lithium enolate, generated upon treatment of **97** with *sec*-BuLi, was trapped with diphenyl sulfide and subsequently oxidized to yield the sulfone (**98**). Treatment of **98** with samarium iodide generated the samarium enolate, which was trapped with phenylacetaldehyde to generate the alcohol (**99**) as a mixture of four diastereomers. Dess-Martin oxidation of **99** yielded the silylated ketone (**100**) as a mixture of diastereomers.

Scheme 1[a]

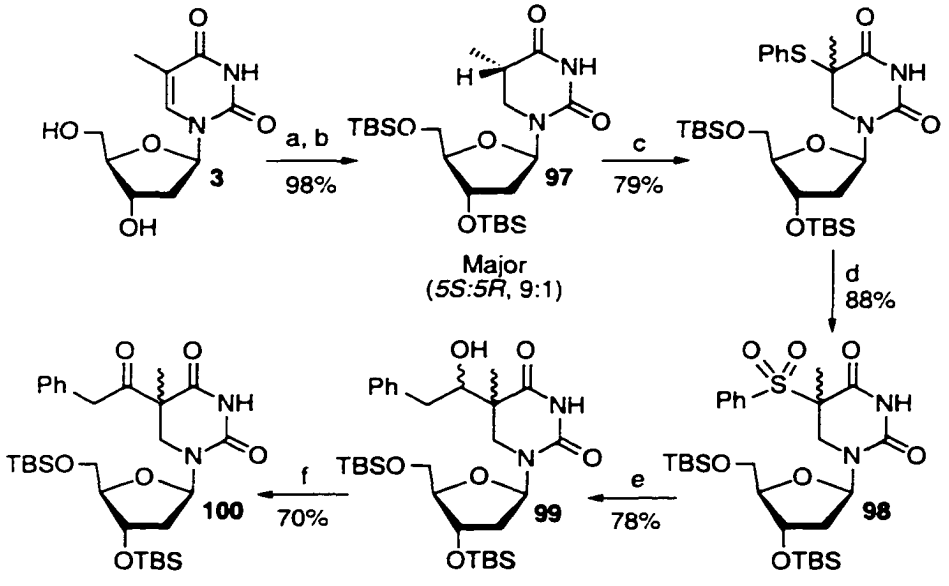

[a]Reagents: a) H_2, Rh/alumina, MeOH:H_2O (1:1 by volume); b) TBDMSCl, imidazole, pyridine, 40 °C; c) *sec*-BuLi, PhSSPh, THF, -78 °C; d) *m*-CPBA, CH_2Cl_2; e) SmI_2, phenylacetaldehyde, THF, -78 °C; f) Dess-Martin periodinane, CH_2Cl_2.

A more straightforward route was developed for the synthesis of **94** for the studies described herein (Scheme 2). Generation of the enolate of **97** with *sec*-BuLi and subsequent addition of phenylacetaldehyde in the presence of DMPU afforded the alcohol (**99**) as a mixture of four diastereomers. The addition of DMPU presumably increases the reactivity of the enolate and eliminates the necessity of forming the samarium enolate (Scheme 1). The four diastereomers of **99** were inseparable from unreacted starting material (**97**) and were immediately oxidized with Dess-Martin periodinane to yield the ketone (**100**) in 61% from **97**. If **99** was not immediately oxidized, it underwent a retro-aldol to regenerate **97**.

Scheme 2[a]

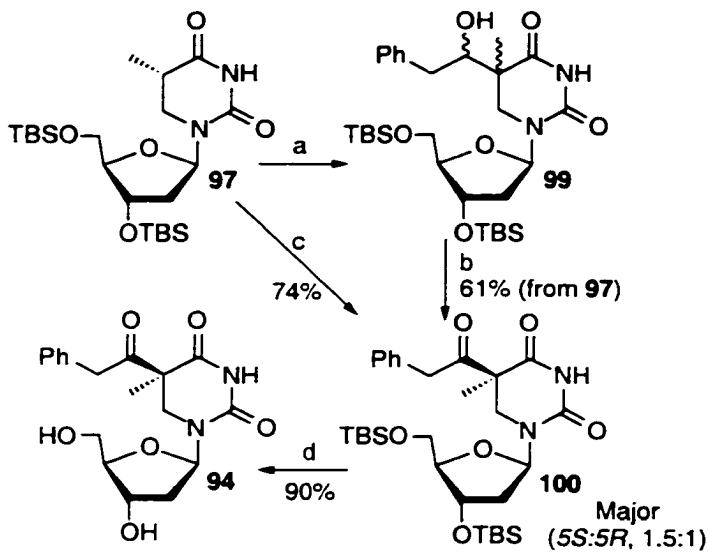

Route	Steps from **97**	Overall Yield
Samarium iodide	4	38%
Phenylacetaldehyde	2	61%
Phenylacetyl chloride	1	74%

[a]Reagents: a) *sec*-BuLi, DMPU, phenylacetaldehyde, THF, -78 °C; b) Dess-Martin periodinane, CH_2Cl_2; c) *sec*-BuLi, DMPU, phenylacetyl chloride, THF, -78 °C; d) $Et_3N{\bullet}3HF$, THF.

The synthesis was further improved by reacting the lithium enolate of **97** with phenylacetyl chloride in the presence of DMPU to directly afford **100** as a mixture of

diastereomers (1.5:1, *5S*:*5R*, Scheme 2). This route affords the ketone (**100**) in one step from **97** in 74% overall yield, whereas the samarium route requires four steps in 38% overall yield. Mild deprotection of **100** with Et_3N•3HF yielded **94** in 90% yield.

The selenide (**96**) and bromide (**95**) radical precursors were synthesized using a similar route as **94** (Scheme 3). The lithium enolate of **97** was trapped in the presence of DMPU with either PhSeBr or *N*-bromosuccinamide (NBS) to generate **101** and **102**, respectively. The low yield (39%) for **102** is due to the basic conditions of the reaction, which results in elimination to generate thymidine (**3**). Deprotection of **101** was effected with Et_3N•3HF to afford **96** in 83% yield. The susceptibility to elimination of **102** precluded the use of Et_3N•3HF, so the TBS ethers were removed with aqueous trifluoroacetic acid to generate **95** in 73% yield.

Scheme 3[a]

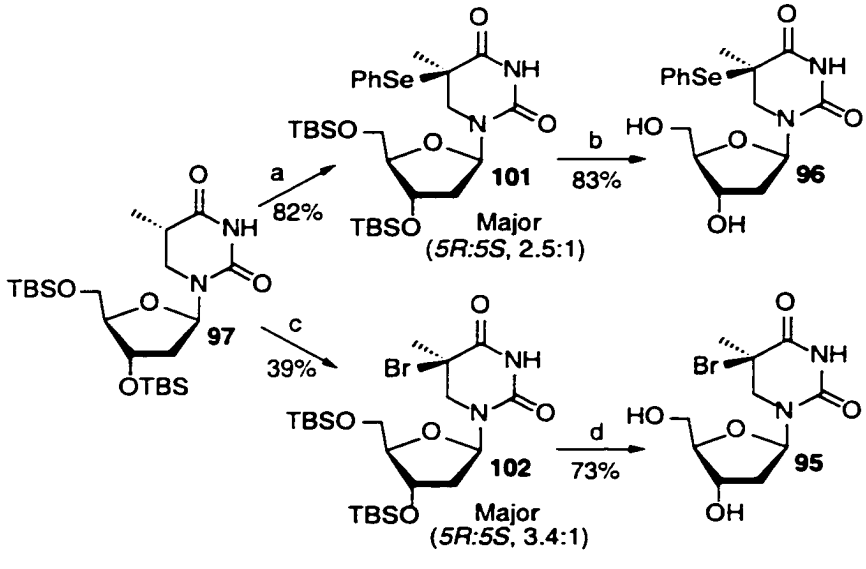

[a]Reagents: a) *sec*-BuLi, DMPU.PhSeBr, THF, -78°C; b) Et_3N•3HF, THF; c) *sec*-BuLi, DMPU, NBS, THF, -78°C; d) 5% TFA/THF:H_2O (1:1 by volume).

The configuration of the products was assigned based on the characterization data for *5S*-**49**, for which a crystal structure was obtained.[39] This diastereomer corresponds to

the product obtained by quenching of the enolate from the *re* face (Figure 43). Comparison of the ^{1}H NMR data of each diastereomer of **94**, **95**, and **96** to the analogous diastereomer of **49** allowed us to assign the absolute configuration of these molecules. One of the C2'-hydrogens of the major diastereomer is shifted downfield relative to the minor diastereomer. The major diastereomers of the benzyl ketone (**94**), bromide (**95**), and selenide (**96**) were assigned an absolute configuration of *5S*, *5R*, and *5R*, respectively.

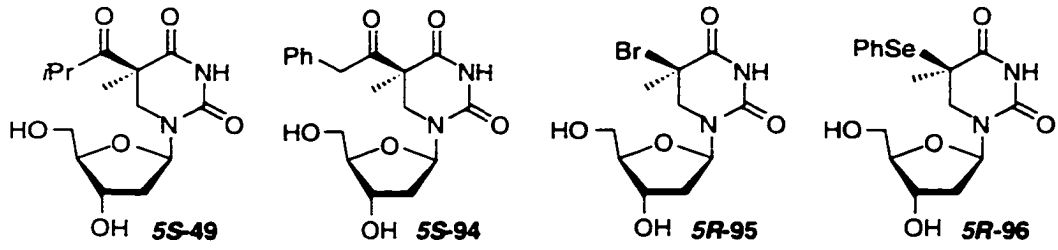

The diastereoselectivity observed in the formation of the three precursors was consistent with the model of the enolate (Figure 43). The bulky TBS group at the 5'-end of the nucleoside partially blocks the *si* face of the enolate. Thus, trapping of the enolate by the electrophile occurs preferentially from the *re* face, opposite the protecting group.

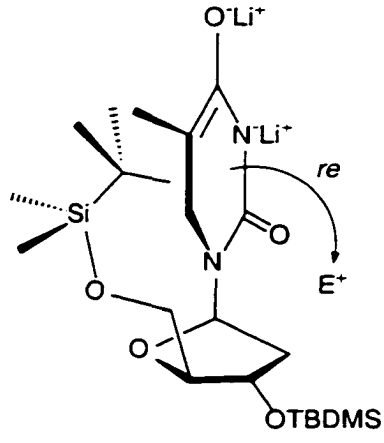

Figure 43. Model invoked to explain observed diastereoselectivity in synthesis of precursors.

3.1.2 Anaerobic Photolysis of the Ketone (94), Bromide (95), and Selenide (96) at 300 nm

The photolyses of the precursors were carried out under anaerobic conditions to gain evidence for the formation of **4** and qualitatively determine the efficiency of the photochemisty. The photolyses were carried out at 300 nm in the presence of Bu_3SnH in THF:H_2O (1:1 by volume) and the products analyzed by reverse-phase HPLC. Complete conversion of **95** and **96** was observed within 45 min, whereas conversion of **94** required 4 h (Table 3).

Table 3. Anaerobic photolysis of **94**, **95**, and **96** at 300 nm.[a]

Precursor	Time	% Yield 3	% Yield 8	% Yield 34	% Conversion	% Mass Balance
94	4 h	0.9 ± 0.1	7 ± 3	64 ± 2	93 ± 2	79 ± 4
95	45 min	1 ± 1	0	65 ± 4	100 ± 0	66 ± 4
96	45 min	17 ± 3	2 ± 1	51 ± 4	96 ± 2	74 ± 6

[a] Photolyses carried out at 300 nm (λ_{max} = 300 nm, 84 watts) with [**94**, **95**, **96**] = 0.1 mM and [Bu_3SnH] = 1.7 mM in THF:H_2O (1:1 by volume).

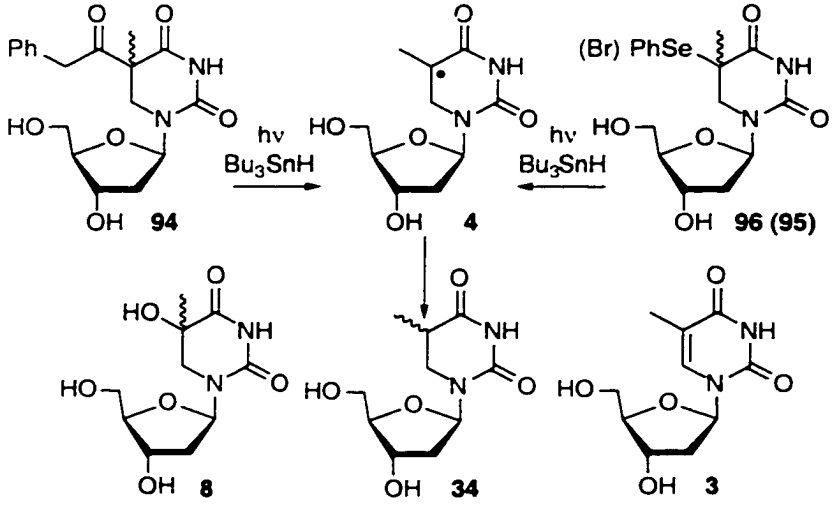

Figure 44. Products observed during anaerobic photolysis.

In all cases, the major product observed upon anaerobic photolysis was **34** as a mixture of diastereomers (≈1:1), which is indicative of the intermediacy of the radical (**4**, Table 3, Figure 44). Photolysis of the ketone (**94**) also resulted in minor amounts of **8** and **3**, which are presumably due to trace amounts of O_2 not removed during degassing and will be described in detail later (Section 3.1.13). Thymidine (**3**) may also be formed via radical-radical disproportionation. A significant amount of this product (**3**) was produced from the phenyl selenide (**96**).

The varying efficiency of the precursors and the formation of thymidine (**3**) during the photolysis of **96** can be explained if one invokes competing pathways for the generation of **4**. The ketone (**94**) does not undergo radical chain chemistry. Therefore, conversion depends only on the efficiency of the photochemistry. The bromide (**95**) and selenide (**96**), however, are classic precursors known to undergo radical chain reactions with Bu_3SnH. The radical (**4**) can either be generated via photoinduced homolysis (path a) or radical chain chemistry (path b) with the $Bu_3Sn^{\bullet}$ acting as the chain carrier (Figure 45). Furthermore, since the selenide (**96**) possesses a better chromophore than the bromide (**95**), it is expected to undergo photoinduced bond homolysis in competition with chain chemistry.

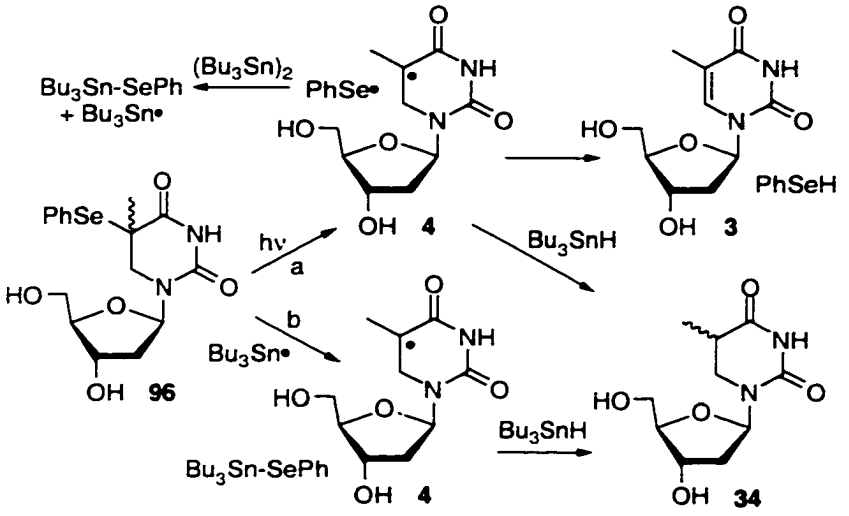

Figure 45. Competitive pathways for generation of **4** during photolysis.

If **96** undergoes photoinduced bond homolysis, a radical pair consisting of PhSe• and **4** is generated (path a, Figure 45). Disproportionation between these radicals generates thymidine (**3**) and PhSeH. The ketone (**94**) is not expected to undergo disproportionation as efficiently as **96** since the radicals generated in the photolysis are separated by a molecule of CO and therefore do not exist in a radical cage. Support for the photoinduced homolysis of **96** is attained from photolyses carried out in the absence of trap or in the presence of traps present at pseudo-first order conditions that are known to be inefficient chain carriers (Table 4).

Table 4. Photolysis of **96** at 300 nm in the presence of alternate hydrogen atom donors.[a]

Trap (mM)	% Yield **3**	% Yield **34**	% Conversion	% Mass Balance
CHD (26)[b]	34 ± 1	17 ± 4	94 ± 1	57 ± 5
βME (34)[c]	13 ± 1	71 ± 4	98 ± 1	83 ± 2
PhSeH (60)[d]	2 ± 1	75 ± 1	98 ± 1	79 ± 1
-	58 ± 3	10 ± 1	100 ± 0	67 ± 1

[a] Photolysis carried out at 300 nm (λ_{max} = 300 nm, 84 watts) for 45 min with [**96**] = [b]2.1, [c]3.2, and [d]6.0 mM.

When the photolyses were carried out in the presence of 2-mercaptoethanol (βME), PhSeH, or 1,4-cyclohexadiene (CHD), complete conversion of **96** was observed (Table 4). The identifiable products consisted of **3** and **34**. In the absence of trap, the selenide (**96**) underwent complete conversion to **3** and **34**, with the latter being produced in a much lower yield. The nonstoichiometric yield of **34** relative to **3** suggests that thymidine (**3**) arises predominantly from disproportionation between the PhSe• and **4**. The dependency of the amount of **3** on the proficiency of the hydrogen atom donor is also consistent with

this interpretation.[113] However, due to the presence of **34** in the product mixture, a minor pathway available to **4** may be disproportionation between two molecules of **4** (Figure 46). Alternatively, 5,6-dihydrothymidine (**34**) may arise via trapping of the radical (**4**) by the PhSeH generated *in situ*. From this data, one can conclude that competing pathways for the generation of **4** may exist under the photolysis conditions.

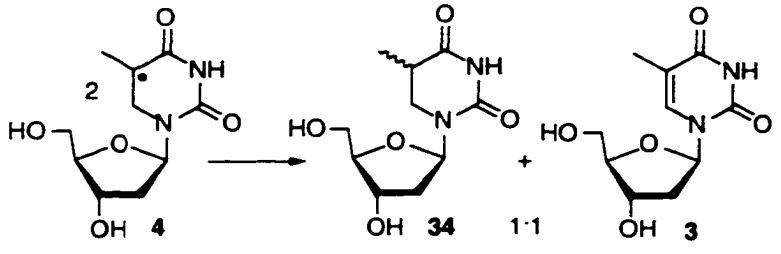

Figure 46. Disproportionation of **4**.

The disproportionation reaction between PhSe• and **4** was eliminated under anaerobic conditions by carrying out the reaction in the presence of $(Bu_3Sn)_2$, which presumably scavenges PhSe• or undergoes photocleavage competitively to yield Bu_3Sn•. The Bu_3Sn• radical acts as the chain transfer agent (Table 5). The $(Bu_3Sn)_2$ provides a pathway for the PhSe• to react in competition with disproportionation (Figure 45). Furthermore, upon reaction of PhSe• with $(Bu_3Sn)_2$, Bu_3Sn• is generated, which results in more efficient chain chemistry. As expected, the addition of $(Bu_3Sn)_2$ to the photolysis samples containing the bromide (**95**) had no effect on the product distribution. The lack of thymidine (**3**) upon photolysis of the bromide (**95**) in the absence of $(Bu_3Sn)_2$ suggests that conversion is due mainly to radical chain chemistry rather than direct homolysis. This is not surprising since the bromide (**95**) absorbs much less efficiently at 300 nm.

Table 5. Anaerobic photolysis of **95** and **96** at 300 nm in the presence of $(Bu_3Sn)_2$.[a]

Precursor	% Yield 3	% Yield 8	% Yield 34	% Conversion	% Mass Balance
96	1 ± 0.1	3 ± 0	78 ± 4	100 ± 0	81 ± 4
95	0	0	73 ± 1	100 ± 0	73 ± 0

[a] Photolyses carried out at 300 nm (λ_{max} = 300 nm, 84 watts) for 45 min with [**96**, **95**] = 0.1 mM, $[Bu_3SnH]$ = 1.7 mM, and $[(Bu_3Sn)_2]$ = 0.2 mM in THF:D_2O (1:1 by volume).

The photolyses of the precursors were also carried out in D_2O to gain evidence for the mechanism by which the precursors are converted to **34**. Carrying out the reaction in D_2O allows one to determine if the product is generated by a radical or ionic pathway (Figure 47). If the product is generated via radical chemisty, the product should arise via trapping by Bu_3SnH and contain no deuterium (^{1}H-**34**). However, if an ionic mechanism is occurring, trapping of the carbanion (**35**) intermediate by D_2O would generate the deuterated product (^{2}H-**34**).

Photolysis of the precursors in the presence of D_2O and Bu_3SnH and subsequent analysis of the persilylated cleaved nucleobases by GC/MS indicated that there was negligible ^{2}H-incorporation in **34** produced from the photolysis of **95** (0.9 ± 0.3%). Analysis of **34** generated during the photolysis of the selenide (**96**) in the absence of $(Bu_3Sn)_2$ contained 8.0 ± 7.3% deuterium. When the photolysis was carried out in the presence of $(Bu_3Sn)_2$, the deuterium content was 12.1 ± 3.4%. The deuterium observed in 5,6-dihydrothymidine (**34**) upon photolysis of **96** may arise via trapping of **4** by PhSeD generated *in situ*. One might have expected that the deuterium content should have been significantly lower when the photolysis of the selenide (**96**) was carried out in the presence of $(Bu_3Sn)_2$ since it presumably scavenges the PhSe•. However, if Bu_3Sn-SePh undergoes hydrolysis, PhSeD will be generated. Alternatively, if PhSeSePh is generated during the reaction, it is known to react with Bu_3SnH to generate Bu_3Sn-SePh and PhSeH.[114]

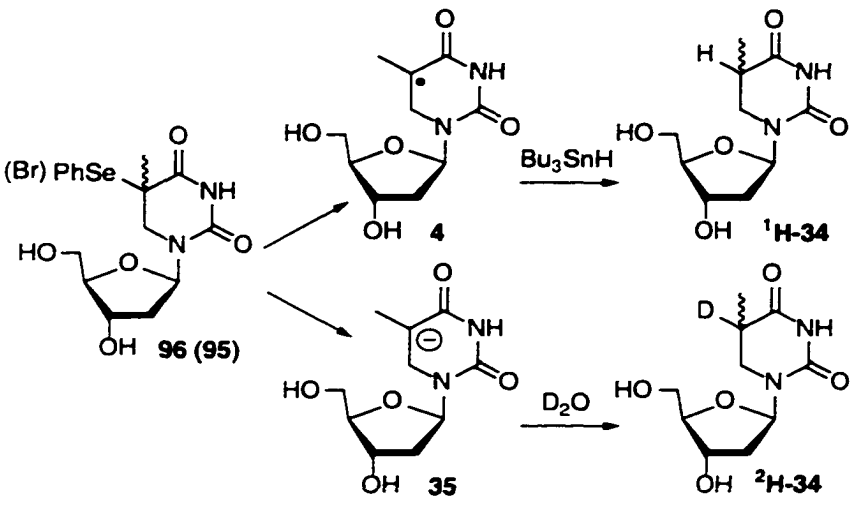

Figure 47. Radical *versus* ionic pathways for the formation of **34**.

3.1.3 Anaerobic Thermolysis of the Bromide (95) and Selenide (96)

The bromide (**95**) and selenide (**96**) are also candidates for thermal generation of **4** under radical chain conditions. The thermolyses were carried out in the presence of Bu_3SnH and VA-044 (**103**), a water-soluble initiator, at 37 °C. The water-soluble initiator (**103**, $t_{1/2}$ = 10 h at 37 °C) is significantly more reactive under biologically relevant conditions than the more commonly used AIBN ($t_{1/2}$ = 2 h at 80 °C, >1000 h at 37 °C).[115]

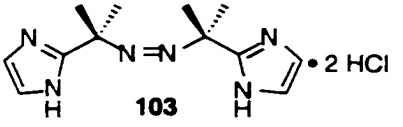

103

After 1.5 h, complete conversion of **96** was observed with the only product being 5,6-dihydrothymidine (**34**, Table 6). Thymidine (**3**) was essentially absent from the reaction mixture, consistent with efficient chain chemistry propagated by $Bu_3Sn•$. The major product upon thermolysis of the bromide (**95**) was also **34**, with a minor amount of thymidine (**3**) and 5,6-dihydro-5-hydroxythymidine (**8**). In all cases, the deuterium

content in **34** was negligible, indicating that the product is generated via a radical pathway (Table 6).

Table 6. Anaerobic thermolysis of **95** and **96**.[a]

Precursor	% Yield 3	% Yield 8	% Yield 34	% Conversion	% Mass Balance	% ^{2}H-**34**
95	2 ± 1	9 ± 7	69 ± 18	100 ± 0	78 ± 14	1.1 ± 0.1
96	0.5 ± 0.1	1 ± 1	86 ± 5	100 ± 0	88 ± 6	6.6 ± 0.4
96[b]	0.7 ± 0.1	1 ± 1	93 ± 0	100 ± 0	94 ± 1	4.4 ± 0.6

[a] Thermolyses carried out at 37 °C for 1.5 h with [**96**, **95**] = 0.1 mM, [Bu_3SnH] = 1.7 mM, and [VA-044] = 0.01 mM in THF:D_2O (1:1 by volume); [b] Thermolysis carried out in the presence of $(Bu_3Sn)_2$ (0.2 mM).

3.1.4 Laser Flash Photolysis under Anaerobic Conditions

In addition to chemical verification for the formation of **4**, spectrophotometric evidence for the radical was gained by laser flash photolysis (LFP) experiments carried out under anaerobic conditions.[116] The selenide (**96**) and ketone (**94**) were subjected to photolysis and data collected to construct the UV spectra for the proposed radical intermediate (Figure 48). Photolysis of **94** produced a spectrum with a strong absorbance at 320 nm and a broad weaker signal at 370-410 nm. The former signal is attributed to the benzyl radical, supported by photolysis of dibenzyl ketone. The latter signal was attributed to the formation of **4**.

The spectrum is consistent with theoretical and experimental data for simple 3° radicals, as well as 1,3-dimethylthymin-5-yl and thymin-5-yl, which have a λ_{max} of 430 and 380 nm, respectively.[117-119] The observed absorbance at 370 nm for **4** is slightly red-shifted relative to a simple 3° radical, but is consistent with the observed trends in the absorbance spectra of radicals. As the stability of the radical increases, the absorbance

becomes red-shifted. One would expect, therefore, that **4** should be more red-shifted than *tert*-Bu• due to its increased stability.

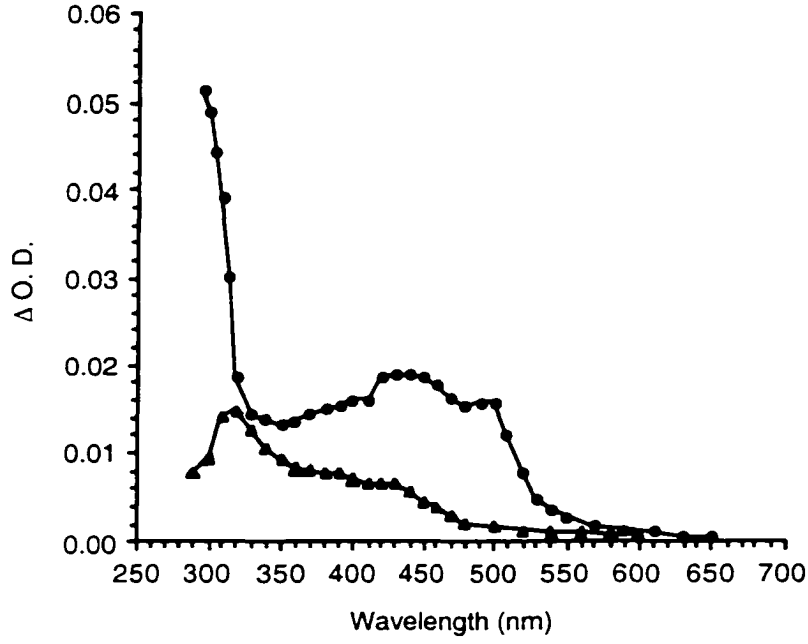

Figure 48. UV spectra obtained in LFP studies of **94** (▲) and **96** (●).

Photolysis of the selenide (**96**) also produces a spectrum with an absorbance at 370-410 nm (Figure 48). In addition, there is a strong signal at 430 nm, which has been assigned to the PhSe•. The spectrum for PhS•, produced by photolysis of PhSSPh, is known and is similar to the observed signal seen upon photolysis of **96**.[120]

The kinetics for the decay of **4** at 370 nm was measured in the presence of various hydrogen atom donors, such as glutathione (**104**) and cysteamine (**105**), to determine the rate constant for trapping of **4**. However, when the photolyses were carried out with **96** and **94**, the kinetics were complicated and the rate constants could not be extrapolated. In

the case of **96**, the strong signal generated by the PhSe• may have interfered with the kinetics for the radical species at 370 nm since there is some overlap in the spectrum. Although the rate constant for trapping of the radical (**4**) by various traps could not be extrapolated from the data, the LFP studies provided additional evidence for the formation of **4** upon photolysis of **96** and **94**.

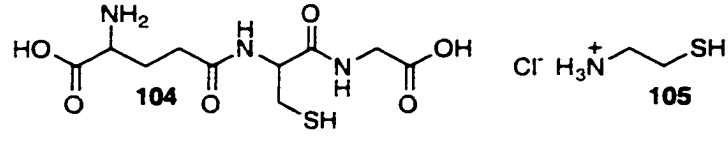

3.1.5 Aerobic Photolysis of the Ketone (94), Bromide (95), and Selenide (96) at 300 nm

The photolyses of the radical precursors were carried out in the presence of O_2 to provide additional evidence for the formation of the radical (**4**). Upon generation of an alkyl radical in the presence of O_2, the radical is trapped at $\approx 2 \times 10^9$ M^{-1} s^{-1} to generate the peroxyl radical (e.g. **7**, Figure 49).[26] Trapping of **7** generates the hydroperoxide, which is known to readily undergo reduction to the alcohol in the presence of reducing agents (e.g. Bu_3SnH, βME). Hence, detection of 5,6-dihydro-5-hydroxythymidine (**8**) would provide further confirmation for the generation of the radical (**4**, Figure 49).

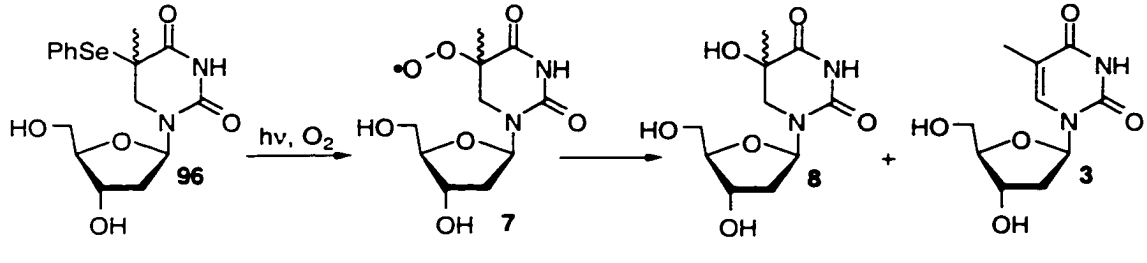

Figure 49. Products observed upon aerobic photolysis of **96**.

The photolysis of the selenide (**96**) was carried out in the presence of Bu_3SnH and $(Bu_3Sn)_2$ to prevent disproportionation between the radical pair and effect more efficient chain chemistry. Photolysis of **96** in the presence of O_2 resulted in the production of **8** as a mixture of diastereomers (≈1:1), but the major product was **3** (Figure 49, Table 7). Recall that one of the potential pathways available to the peroxyl radical (**7**) that we had proposed was the elimination of superoxide, which would result in the formation of thymidine (**3**).

Table 7. Aerobic photolysis of **96** at 300 nm.

	% Yield				
$(Bu_3Sn)_2$	**3**	**8**	**34**	% Conversion	% Mass Balance
-	48 ± 8	8 ± 1	0	95 ± 7	62 ± 5
+	51 ± 1	12 ± 1	0	100 ± 0	64 ± 3

[a] Photolyses carried out at 300 nm (λ_{max} = 300 nm, 84 watts) for 45 min with [**96**] = 0.1 mM, $[Bu_3SnH]$ = 1.7 mM, and $[(Bu_3Sn)_2]$ = 0.2 mM in $THF:H_2O$ (1:1 by volume).

The aerobic photolysis of the bromide (**95**) was also carried out at 300 nm in the presence of Bu_3SnH (Table 8). The conversion was considerably lower compared to the anaerobic photolysis, presumably resulting from quenching of the radical chain chemistry by the presence of O_2. Consequently, longer reaction times were required to attain complete conversion of **95**. Complete conversion was observed after 8 h. However, the mass balance begins to drop after 4 h, suggesting that decomposition may be occurring. Nonetheless, **8** (≈1:1 mixture of diastereomers) was observed upon photolysis of **95**. However, a significant amount of thymidine (**3**) was also observed and was the major product at low conversion. As the conversion increased, however, **8** became the major product. The decrease in the yield of **3** relative to **8** and the decrease in mass balance

suggest that decomposition of **95** and/or the products may be occurring during the course of the photolysis.

Although thymidine (**3**) was observed upon photolysis of both **96** and **95**, the ratio of **3**:**8** obtained upon photolysis of the two precursors was not comparable. This is not what one would expect if the products arise solely from a radical pathway. The observed inconsistencies indicate that there must be some reaction pathway other than the generation of **4** occurring that contributes to the observed products. The discrepancy between the product ratios observed upon photolysis of **95** and **96** will be addressed in detail later (Section 3.1.8).

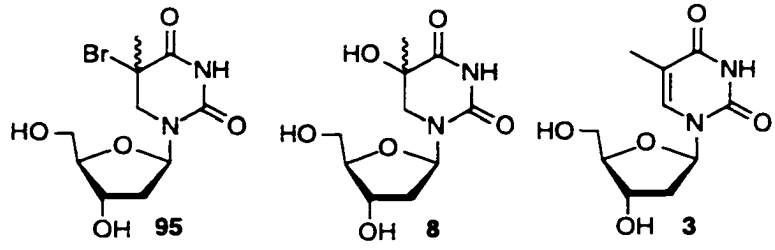

Table 8. Aerobic photolysis of **95** at 300 nm over 8 h.[a]

Time (h)	% Yield **3**	% Yield **8**	% Yield **3**:**4**	% Conversion	% Mass Balance
1	13 ± 1	4 ± 1	0	25 ± 3	92 ± 2
2	20 ± 2	5 ± 1	0	47 ± 2	78 ± 1
3	25 ± 1	16 ± 4	0	59 ± 6	81 ± 10
4	28 ± 1	20 ± 2	0	60 ± 2	87 ± 6
6	23 ± 1	29 ± 6	0	95 ± 1	56 ± 3
8	19 ± 6	29 ± 5	0	100 ± 0	47 ± 11

[a] Photolyses carried out at 300 nm (λ_{max} = 300 nm, 84 watts) with [**95**] = 0.1 mM and [Bu_3SnH] = 1.7 mM in THF:H_2O (1:1 by volume).

When the ketone (**94**) was photolyzed in the presence of O_2 and Bu_3SnH, the major product was a ≈1:1 mixture of diastereomers of **8** as expected (Figure 50, Table 9). However, a significant amount of 5,6-dihydrothymidine (**34**) was also detected in the reaction mixture. Trapping of the radical (**4**) by Bu_3SnH is not expected to efficiently compete with trapping by O_2. At a concentration of 1.7 mM and rate constant of 4×10^6 M^{-1} s^{-1}, the rate of trapping of **4** by Bu_3SnH is 6.8×10^3 s^{-1}.[113] Although the concentration of O_2 (0.2 mM) is much lower than the Bu_3SnH, the rate of trapping of **4** by O_2 is 4×10^5 s^{-1}. It is therefore surprising that such a significant amount of **34** was detected. In addition, only a trace amount of thymidine (**3**) was observed upon photolysis of the ketone (**94**), whereas a significant amount was observed upon photolysis of the bromide (**95**, Table 8) and selenide (**96**, Table 7).

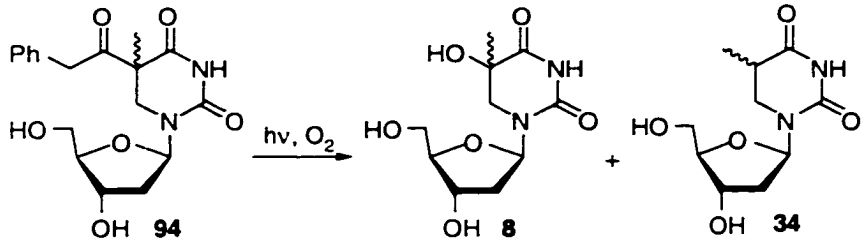

Figure 50. Products observed upon aerobic photolysis of **94**.

Table 9. Aerobic photolysis of **94** at 300 nm.[a]

Trap	% Yield 3	8	34	% Conversion	% Mass Balance
Bu_3SnH	0.7 ± 0.1	54 ± 1	16 ± 1	100 ± 0	70 ± 2
βME	1 ± 0	59 ± 0	0	100 ± 0	61 ± 1
-	1 ± 0	51 ± 1	0	99 ± 1	55 ± 1

[a] Photolyses carried out at 300 nm (λ_{max} = 300 nm, 315 watts) for 3 h with [**94**] = 0.1 mM, [Bu_3SnH] = 1.7 mM, and [βMe] = 0.3 mM in THF:H_2O (1:1 by volume).

It is known that ketones undergo photoreduction to generate the alcohol upon quenching of the excited state by a hydrogen atom donor.[121-125] If the ketone (**94**) undergoes photoreduction in the presence of Bu_3SnH to generate the alcohol (**106**), a retroaldol reaction results in the generation of 5,6-dihydrothymidine (**34**, Figure 51). The rate constant for the Norrish Type I photocleavage of **94** is not known, but the related ketone, $Ph(CO)CH_2Ph$, undergoes cleavage with a first-order rate constant of 2×10^6 s^{-1}.[126] The rate constant for reduction of ketones by Bu_3SnH varies depending on the structure, but is approximately 10^9 M^{-1} s^{-1}. For example, the rate constant varies from 2.9 x 10^8 M^{-1} s^{-1} for benzophenone to 1.3 x 10^9 M^{-1} s^{-1} for acetophenone.[122,123] At the concentration of Bu_3SnH (1.7 mM) in which the photolysis of the ketone (**94**) was carried out and using an average rate constant for photoreduction of 1 x 10^9 M^{-1} s^{-1}, the rate for quenching the triplet state of **94** is estimated at 1.7 x 10^7 s^{-1}. Therefore, it is possible that photoreduction of the ketone (**94**) may occur in competition with Norrish Type I photocleavage (2 x 10^6 s^{-1}).[126]

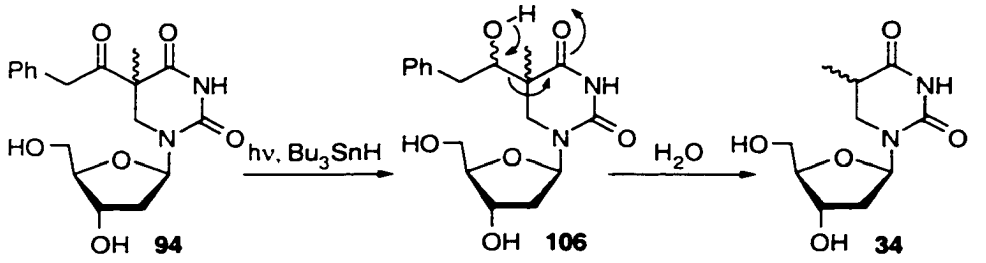

Figure 51. Photoreduction of the ketone (**94**) to generate **34**.

In order to prevent the photoreduction of the ketone (**94**), the photolyses were carried out using βME as the hydrogen atom donor. The rate constant for the quenching of the triplet state of ketones is slower for thiols than Bu_3SnH. For example, *n*-BuSH quenches the excited state of acetophenone with a rate constant of 1.4 x 10^7 M^{-1} s^{-1}, which

is significantly less efficient than Bu_3SnH (1.3×10^9 M^{-1} s^{-1}).[123,125] Indeed, when the photolysis of **94** was carried out in the presence of βME, the only observed product was 5,6-dihydro-5-hydroxythymidine (**8**). This is consistent with photoreduction not competing with Norrish Type I photocleavage of **94**.

In the absence of any trap, the yield of 5,6-dihydro-5-hydroxythymidine (**8**) remained unchanged and no thymidine (**3**) was observed (Table 9). This is quite surprising since a hydrogen atom donor was expected to be required to trap **7** and subsequently reduce the hydroperoxide to **8**. The observation of **8** in the absence of trap may indicate that another reaction pathway occurs in competition with trapping of the peroxyl radical (**7**) that coincidentally leads to the same product. In addition, the absence of thymidine (**3**), which was observed upon photolysis of **95** and **96** and believed to arise via superoxide elimination from the peroxyl radical (**7**), suggests that the chemistry of the ketone (**94**) is more complicated than expected.

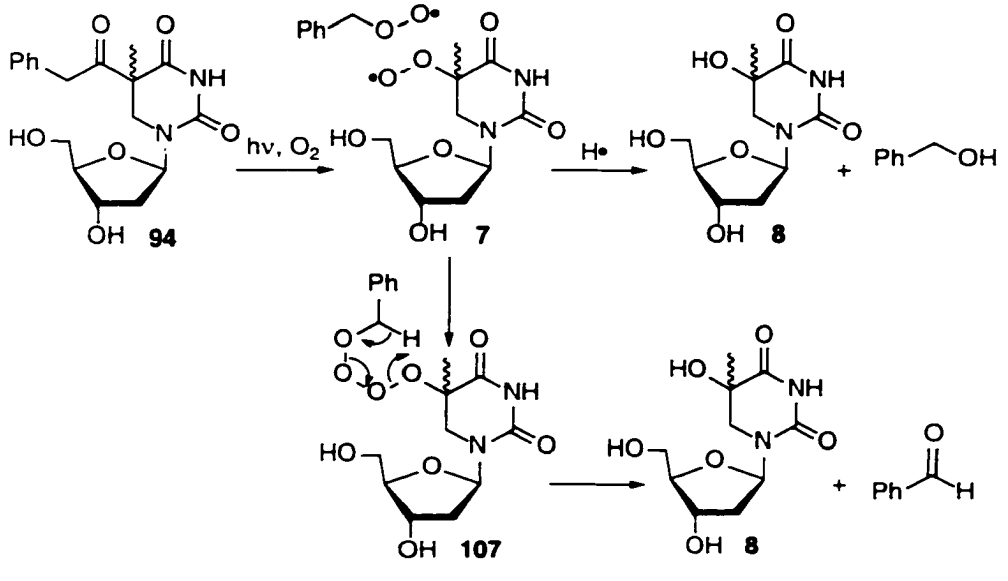

Figure 52. Proposed mechanism for the formation of **8** upon photolysis of **94**, Russell fragmentation.

Upon photolysis of **94**, the radicals are trapped at diffusion-controlled rates to generate the respective peroxyl radicals.[26] Trapping of the peroxyl radicals by Bu_3SnH results in the formation of **8** and benzyl alcohol. Alternatively, if recombination of the peroxyl radicals occurs to generate the tetraoxide (**107**), a Russell fragmentation can occur to also generate **8**, but in this case the by-product is benzaldehyde, which was observed in the product mixture (Figure 52). One can argue that benzaldehyde can also arise via recombination of two molecules of the benzyl peroxyl radical. However, it is erroneous to assume that the benzyl peroxyl radicals would preferentially react with one another, rather than with the nucleoside peroxyl radical (**7**).

It is unlikely that the nucleoside peroxyl radicals (**7**) undergo radical-radical recombination to form a tetraoxide since the recombination of 3° peroxyl radicals is known to be relatively slow (k = 2 x 10^4 M^{-1} s^{-1}).[70] The recombination of 1° and 2° peroxyl radicals is considerably faster, having a rate constant >10^9 M^{-1} s^{-1}.[70] Although recombination of two 3° peroxyl radicals is unlikely, the reaction between **7** and the 1° benzyl peroxyl radical may be sufficiently fast.[70] The pseudo-first order rate for the recombination of the nucleoside peroxyl radical (**7**) and the benzyl peroxyl radical was estimated to be 5.2 s^{-1}. This is based on the following assumptions: 1) the rate constant for the recombination of the peroxyl radicals is 10^9 M^{-1} s^{-1}, and 2) the steady state concentration of the peroxyl radicals is 2.6 x 10^{-9} M. Since 75% of the ketone (**94**, 0.1 mM) was converted in 8 h, the velocity of the reaction was 2.6 x 10^{-9} M s^{-1}, which we can use to make the assumption that the steady state concentration of peroxyl radicals was 2.6 x 10^{-9} M. We believe that the thymidine (**3**) observed under aerobic conditions upon photolysis of the selenide (**96**) occurs via superoxide elimination and we have measured the rate constant as 21 s^{-1} (Section 3.1.14.3). From the above argument concerning the rate of recombination of the peroxyl radicals, it seems unlikely that a Russell fragmentation would account for the absence of thymidine (**3**).

An alternative explanation for the formation of **8** at the expense of thymidine (**3**) involves recombination of the benzyl radical on the oxygen of **4** to generate **108**. Similar enol ethers have been shown to be unstable and readily decompose to the enolate (**35**, Figure 53).[39] Tertiary carbanions that are resonance stabilized (e.g. **35**) are known to react with O_2 to ultimately lead to the alcohol (e.g. **8**).[127] It has been proposed that the enolate (**35**) reduces O_2 to generate the stabilized radical (**4**) and superoxide ($O_2^{-\bullet}$).[127] The radical is subsequently trapped by O_2 to generate the peroxyl radical (**7**), which undergoes reduction by $O_2^{-\bullet}$ or the carbanion (**35**) to ultimately lead to **8**.

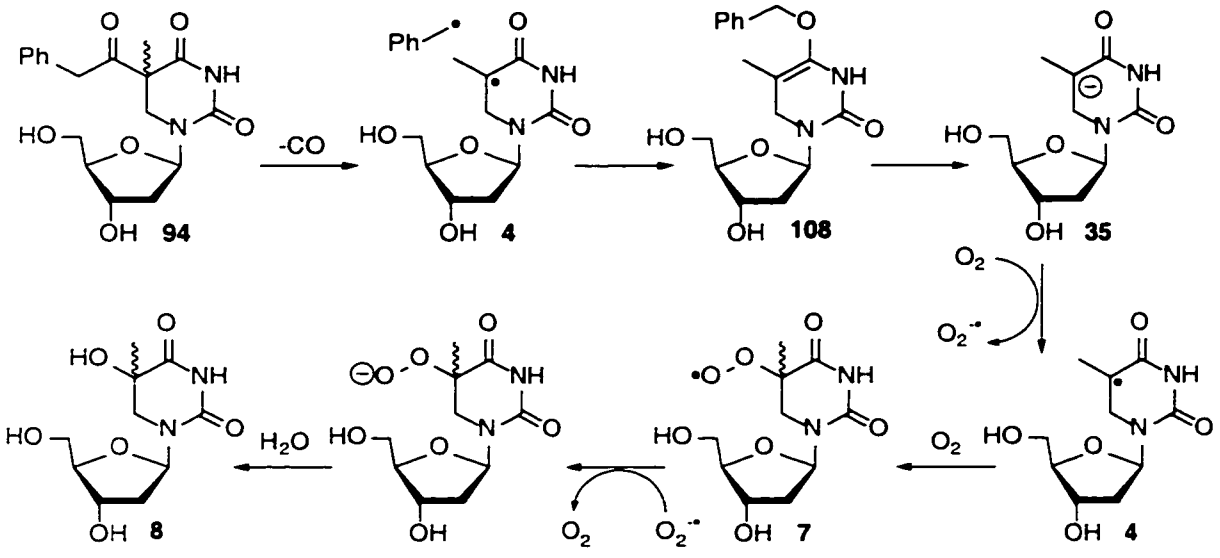

Figure 53. Proposed mechanism for the formation of **8** upon photolysis of **94**, oxidation by O_2.

This mechanism also involves the intermediacy of **7**, which we assumed the steady state concentration was 2.6×10^{-9} M and would be too low for the Russell fragmentation to be operative, despite the fact that the recombination is diffusion-controlled. However, in this mechanism, the recombination adduct (**108**) may build up during the course of the

reaction, resulting in a significantly higher steady state concentration of radicals. Hence, this reaction pathway available to the peroxyl radical (**7**) may be able to compete with superoxide elimination. Since the chemistry of the ketone (**94**) was more complicated than expected, it was not further investigated as a precursor to 5,6-dihydrothymidin-5-yl (**4**).

3.1.6 Aerobic Thermolysis of the Bromide (95) and Selenide (96)

The thermolyses of **95** and **96** were carried out to confirm the observations made during the photolysis (Tables 10, 11). The thermolysis was carried out in the presence of Bu_3SnH and VA-044 in THF:H_2O (1:1 by volume). The conversion was much lower in the aerobic studies, presumably due to quenching of the radical chain chemistry by the presence of O_2. Thermolysis of **96** resulted in the generation of thymidine (**3**) as the major product (Table 10). When the reaction was carried out in the presence of $(Bu_3Sn)_2$, the amount of thymidine (**3**) did not change. Since thymidine (**3**) was not observed under anaerobic conditions, generation of **3** in the aerobic experiments must be dependent on the presence of O_2.

Table 10. Aerobic thermolysis of **96**.

$(Bu_3Sn)_2$	% Yield **3**	% Yield **8**	**3**:**4**	% Conversion	% Mass Balance
-	28 ± 3	4 ± 1	0	28 ± 7	103 ± 6
+	34 ± 7	4 ± 1	0	30 ± 16	108 ± 7

[a] Thermolyses carried out at 37 °C for 24 h with [**96**] = 0.1 mM, [Bu_3SnH] = 1.7 mM, and [$(Bu_3Sn)_2$] = 0.2 mM in THF:H_2O (1:1 by volume).

The thermolysis of the bromide (**95**) under conditions identical to the selenide (**96**) resulted in much higher conversion (Table 11). In addition, the major product generated upon thermolysis of **95** for 19 h was 5,6-dihydro-5-hydroxythymidine (**8**), with a minor amount of thymidine (**3**). When **95** was heated for a shorter amount of time (15 h), the

conversion was lower, as expected, and the major product was **3**. However, as the reaction time was increased, **8** became the major product. This is consistent with the trend observed upon aerobic photolysis of **95** and suggests that the higher conversion may not be due to radical chemistry, but rather to decomposition of **95** at longer reaction times.

Table 11. Aerobic thermolysis of **95**.[a]

$[Bu_3SnH]$ (mM)	Time (h)	% Yield 3	% Yield 8	% Yield 34	% Conversion	% Mass Balance
1.0	15	16 ± 6	3 ± 0	0	24 ± 8	95 ± 3
5.1	15	22 ± 5	5 ± 0	5 ± 1	34 ± 4	97 ± 3
10.2	15	20 ± 1	4 ± 0	6 ± 1	34 ± 1	95 ± 0
1.7	19	8 ± 1	49 ± 1	4 ± 1	84 ± 1	77 ± 2

[a] Thermolyses carried out at 37 °C with [**95**] = 0.1 mM and [VA-044] = 0.1 mM in THF:H_2O (1:1 by volume).

The results of the experiments involving the selenide (**96**) suggest that it is an efficient radical precursor under both thermal and photochemical conditions. Under anaerobic conditions, the expected product arising via the intermediacy of **4** was observed. One would expect the formation of **8** in the presence of O_2, but the major product was thymidine (**3**). The bromide (**95**) appears to be an efficient precursor at short reaction times. However, as the reaction time increases, there is evidence for decomposition of the precursor. Interestingly, though, thymidine (**3**) was also observed upon aerobic thermolysis and photolysis of **95**. This issue involving the formation of thymidine (**3**) in the presence of O_2 is consistent with our proposed pathway involving superoxide elimination and will be addressed in greater detail in Section 3.1.13.

3.1.7 Effect of Bu_3SnH Concentration on Product Distribution

The photolysis and thermolysis of **95** and **96**, respectively, was carried out over a range of Bu_3SnH concentrations. The effect of Bu_3SnH concentration on the product distribution may provide insight into their mechanism of formation. For example, if the proposed mechanism involving superoxide elimination from the peroxyl radical (**7**) is operative, then **8** and thymidine (**3**) arise via a common intermediate (**7**) and the ratio of the products depends on the concentration of trap.

Table 12. Aerobic photolysis of **95** at 300 nm over range of $[Bu_3SnH]$.[a]

$[Bu_3SnH]$ (mM)	% Yield **3**	% Yield **8**	% Yield **34**	% Conversion	% Mass Balance	**8**:**3**
1.0	15 ± 0	18 ± 0	27 ± 0	93 ± 1	68 ± 0	1.2 ± 0.0
2.0	15 ± 1	20 ± 1	24 ± 3	91 ± 4	68 ± 2	1.3 ± 0.1
3.1	15 ± 1	25 ± 0	24 ± 2	94 ± 1	70 ± 0	1.7 ± 0.2
5.1	13 ± 1	28 ± 4	25 ± 1	96 ± 1	70 ± 2	2.2 ± 0.2
7.1	11 ± 0	30 ± 3	22 ± 0	95 ± 1	67 ± 4	2.7 ± 0.3

[a] Photolyses carried out at 300 nm (λ_{max} = 300 nm, 84 watts) for 3 h with [**95**] = 0.1 mM in $THF:H_2O$ (19:1 by volume).

Since the data suggests that the bromide (**95**) decomposes over the course of the reaction, evident by the decrease in mass balance, **95** was photolyzed for a short period of time (3 h). In addition, in order to ensure complete solubility of the Bu_3SnH, the reactions were carried out in $THF:H_2O$ (19:1 by volume). As the concentration of Bu_3SnH was increased, the ratio of **8**:**3** also increased (Table 12). This is indicative of competing pathways involving **7** in which the pathway leading to **8** depends on the presence of Bu_3SnH. However, a significant amount of **34** was produced in the reaction that did not change with increasing Bu_3SnH concentration. One would expect some 5,6-

dihydrothymidine (**34**) at high concentrations of Bu_3SnH. However, the yield of **34** remains constant over the entire concentration range.

The effect of Bu_3SnH concentration on product distribution was also investigated upon thermolysis of the selenide (**96**). When the concentration of Bu_3SnH was increased from ≈2 to ≈22 mM, the yield of **8** increased and **3** decreased (Table 13). Although the ratio of products differed significantly from the results of the bromide (**95**), it is important to note that the ratio of products is dependent on the concentration of Bu_3SnH. This result suggests that **8** and **3** arise via a common intermediate and the generation of **8** is dependent on the presence of Bu_3SnH.

Table 13. Aerobic thermolysis of **96** over range of $[Bu_3SnH]$.[a]

$[Bu_3SnH]$ (mM)	% Yield 3	% Yield 8	% Yield 34	% Conversion	% Mass Balance	8:3
2.4[b]	40 ± 6	15 ± 1	11 ± 3	87 ± 3	79 ± 4	0.38 ± 0.07
21.8[c]	6 ± 1	54 ± 2	5 ± 2	72 ± 3	93 ± 4	8.8 ± 0.5

[a] Thermolyses carried out at 55 °C; [b] [**96**] = 0.29 mM and [AIBN] = 0.20 mM; [c] [**96**] = 2.9 mM and [AIBN] = 2.2 mM in THF:H_2O (19:1 by volume).

3.1.8 Source of 5,6-Dihydrothymidine (34) upon Aerobic Photolysis of the Bromide (95)

The presence of **34** in the aerobic photolysis experiments of the bromide (**95**) suggests that radical chemistry does not account for all of the observed products. Interestingly, a significant amount of **34** was not observed upon photolysis of the selenide (**96**). One potential source for the significant amount of **34** in the photolysis is trapping of the radical (**4**) by THF in competition with O_2. This pathway is not likely to be responsible for the formation of **34** upon photolysis of the bromide (**95**) since **34** was not observed upon photolysis of **96**, which was also carried out in THF. However, this possibility was

addressed by carrying out the photolyses in THF-d_8. Incorporation of deuterium in the product would indicate that the THF was acting as a hydrogen atom donor.

The photolysis of **95** was carried out at 300 nm in the presence of Bu_3SnH and THF-d_8. The major product was **34** with minor amounts of **8** and **3** (Table 14). The lack of ^{2}H-incorporation in the product (**34**) indicated that the THF was not acting as a hydrogen atom donor. It had already been shown that photolysis of **95** in the presence of D_2O also did not lead to ^{2}H-incorporation in the product (Table 14). Therefore, **34** is not obtained by trapping the radical by THF or from an ionic intermediate.

Table 14. Aerobic photolysis of **95** in THF-d_8 or D_2O.[a]

Solvent	% Yield			%	% Mass	
	3	**8**	**34**	Conversion	Balance	% ^{2}H-**34**
D_2O	13 ± 1	21 ± 4	35 ± 3	92 ± 0	81 ± 8	1.3 ± 0.3
THF-d_8	11 ± 0	7 ± 1	26 ± 3	93 ± 2	53 ± 5	2 ± 1

[a] Photolyses carried out at 300 nm (λ_{max} = 300 nm, 84 watts) for 3 h with [**95**] = 0.1 mM and [Bu_3SnH] = 1.7 mM in THF-d_8:H_2O (19:1 by volume) or THF:D_2O (19:1 by volume).

Another possibility for the generation of **34** during the photolyses is the decomposition of either the radical precursor or products. It has been shown that thymidine (**3**) is not stable at 300 nm in the presence of βME under anaerobic conditions.[128] Therefore, the stability of **3** was investigated under the conditions used in these experiments. When thymidine (**3**) was photolyzed at 300 nm for 3 h, the reaction time used in the photolysis of **95**, complete recovery of the thymidine was observed (Table 15). However, when the photolysis was carried out in the presence of Bu_3SnH, more than half of the thymidine was converted to **8** and **34**.

Since photolysis at 300 nm resulted in degradation of **3**, the stability was investigated at 350 nm. Regardless of the presence of Bu_3SnH, **3** was stable at 350 nm for up to 6 h (Table 15). The presence of **34** upon photolysis of the bromide (**95**) is attributed to decomposition of **3** at long reaction times. Since the photolysis of **96** is complete in a much shorter time (45 min), degradation of **3** is much less of a problem. Given these observations, the photochemical efficiency of the radical precursors was investigated at 350 nm.

Table 15. Photolysis of **3** at 300 and 350 nm.[a]

Bu_3SnH	Wavelength	% Yield **8**	% Yield **34**	% Conversion	% Mass Balance
-	300 nm	0	0.1 ± 0	0	100 ± 0
+	300 nm	13 ± 1	16 ± 4	59 ± 1	48 ± 7
-	350 nm	0	0	6 ± 0	94 ± 0
+	350 nm	0	0	9 ± 4	91 ± 4

[a] Photolyses carried out at 300 nm (λ_{max} = 300 nm, 84 watts) for 3 h or 350 nm (λ_{max} = 350 nm, 192 watts) for 6 h with [thymidine (**3**)] = 0.033 mM and [Bu_3SnH] = 10.2 mM in THF:H_2O (19:1 by volume).

3.1.9 Anaerobic and Aerobic Photolysis of the Bromide (95) and Selenide (96) at 350 nm

The photolysis of the selenide (**96**) was carried out at 350 nm and proved to be as efficient at this wavelength as it was at 300 nm, undergoing complete conversion within 45 min (Table 16). Moreover, the results of the photolysis of the selenide (**96**) at this wavelength are comparable to the results obtained when **96** was photolyzed at 300 nm (Tables 3 and 7). When the photolysis was carried out in the presence of Bu_3SnH and $(Bu_3Sn)_2$ under anaerobic conditions, the major product was 5,6-dihydrothymidine (**34**). The minor amounts of thymidine (**3**) and 5,6-dihydro-5-hydroxythymidine (**8**) are

attributed to the presence of O_2 not removed during degassing. A significant amount of thymidine (**3**) was observed when the photolysis of **96** was carried out with βME as the hydrogen atom donor. This is consistent with inefficient radical chain propagation, in which disproportionation between the radical (**4**) and PhSe• becomes more competitive. Finally, when the photolysis was carried out in the presence of O_2, the major products were **3** and **8**.

Table 16. Anaerobic and aerobic photolysis of **96** at 350 nm.[a]

Trap	O_2	% Yield **3**	% Yield **8**	% Yield **34**	% Conversion	% Mass Balance
Bu_3SnH[b]	-	12 ± 0	7 ± 1	46 ± 1	100 ± 0	64 ± 1
βME[b]	-	38 ± 1	4 ± 1	7 ± 1	100 ± 0	48 ± 2
Bu_3SnH[c]	+	41 ± 2	9 ± 0	0	100 ± 0	50 ± 2

[a] Photolyses were carried out at 350 nm (λ_{max} = 350 nm, 96 watts) for 45 min with [**96**] = 0.1 mM in THF:H_2O (1:1 by volume); [b] photolyses carried out with [trap] = 1.0 mM; [c] photolyses carried out with [Bu_3SnH] = 1.7 mM and [$(Bu_3Sn)_2$] = 0.2 mM.

When the bromide (**95**) was photolyzed at 350 nm in the absence of O_2, the major product was 5,6-dihydrothymidine (**34**), as expected. The photolysis of the bromide (**95**) is much less efficient at 350 nm (Table 17) under aerobic conditions than when carried out at 300 nm (Table 8). Although the yield of **34** was greatly diminished under aerobic conditions, the conversion of **95** was only 32% after 6 h (Table 17). In addition, at short reaction times, **3** is the major product. However, as the reaction time increases to 6 h, **8** became the major product . This is consistent with the aerobic thermolysis experiments and indicates that **95** is not stable on the timescale of the experiment.

Table 17. Anaerobic and aerobic photolysis of **95** at 350 nm.[a]

O_2	Time (h)	% Yield **3**	% Yield **8**	% Yield **34**	% Conversion	% Mass Balance
-	1	4 ± 0	2 ± 2	79 ± 8	100 ± 0	84 ± 6
+	1	3 ± 1	2 ± 1	2 ± 2	1 ± 1	106 ± 1
+	3	6 ± 3	4 ± 1	3 ± 4	18 ± 5	94 ± 2
+	6	6	14	0	32	87

[a] Photolyses carried out at 350 nm (λ_{max} = 350 nm, 96 watts) with [**95**] = 0.1 mM and [Bu_3SnH] = 1.7 mM. Anaerobic photolyses carried out in THF:H_2O (1:1 by volume) and aerobic photolyses carried out in THF:H_2O (19:1 by volume).

3.1.10 Stability Studies Involving 95

The bromide (**95**) may be inherently unstable, or it may be unstable to the reaction conditions. Upon reaction of **96**, the by-product is Bu_3Sn-SePh. However, in the case of **95**, the by-product of the reaction is Bu_3Sn-Br. Since the Sn-Br (47 kcal/mol) bond is so weak, relative to the Sn-Se bond (96 kcal/mol) it may hydrolyze under the reaction conditions to Bu_3SnOH and HBr.[129] The presence of HBr in the reaction may either contribute to the instability of **95** or affect the product distribution. To determine if HBr had an effect on product distribution, several experiments were carried out. First, attempts to scavenge the HBr with Et_3N were investigated.

The thermolysis of **95** was carried out under aerobic conditions in the presence of stoichiometric Et_3N (Table 18). Although **95** was not stable to excess base, it was unknown whether stoichiometric Et_3N would result in decomposition under the dilute conditions at which analytical experiments were carried out. The product distribution was the same regardless of the presence or absence of Bu_3SnH and initiator. These results indicate that **95** is not stable in the presence of Et_3N. Interestingly, though, the bromide

(**95**) did not undergo elimination to generate thymidine (**3**) as expected, based upon the observations made during the synthesis of **95** (Section 3.1.1).

Table 18. Thermolysis of **95** in the presence of Et_3N.[a]

Bu_3SnH	VA-044	% Yield **3**	% Yield **8**	% Yield **34**	% Conversion	% Mass Balance
-	-	0	37 ± 1	34 ± 2	100 ± 0	70 ± 1
+	-	0	24 ± 0	15 ± 0	67 ± 1	72 ± 1
+	+	0	26 ± 0	16 ± 1	69 ± 1	73 ± 1

[a] Thermolyses carried out at 55 °C for 7 h with [**95**] = 0.1 mM, [Bu_3SnH] = 5.1 mM, [VA-044] = 0.1 mM, and [Et_3N] = 0.1 mM in THF.

Since HBr, if produced during the reaction, could not be scavenged, its effect on the product distribution was investigated with the selenide (**96**, Table 19). The photolysis of **96** was carried out in the presence of Bu_3SnH at pH ranging from 4 to 6.8. The change in pH had no effect on the product distribution.

Table 19. Effect of pH on product distribution in aerobic photolysis of **96**.[a]

pH	% Yield **3**	% Yield **8**	% Yield **34**	% Conversion	% Mass Balance
6.8	42 ± 1	9 ± 0	0	100 ± 0	51 ± 1
5.3	43 ± 1	9 ± 0	0	100 ± 0	51 ± 1
4.0	40 ± 4	9 ± 0	0	100 ± 0	49 ± 4

[a] Photolyses carried out at 350 nm (λ_{max} = 350 nm, 96 watts) for 45 min with [**96**] = 0.1 mM, [Bu_3SnH] = 1.7 mM, and [$(Bu_3Sn)_2$] = 0.2 mM in THF:H_2O (1:1 by volume).

In addition to the effect of pH on the reactivity of **96**, the effect of Bu_3SnI and HBr on the product distribution was investigated (Table 20). Thermolysis of **96** for 6 h resulted

in **3** as the major product and a small amount of **8**. Upon addition of Bu_3SnI or HBr, the product distribution did not vary. Therefore, the presence of Bu_3SnBr or HBr should have no effect on the products generated upon reaction of **95** if 5,6-dihydrothymidin-5-yl (**4**) is being produced. The evidence suggests that **95** is inherently unstable over the reaction times required for moderate conversion under aerobic conditions.

Table 20. Effect of Bu_3SnI and HBr on product distribution in aerobic thermolysis of **96**.[a]

		% Yield				
Bu_3SnI	HBr	**3**	**8**	**34**	% Conversion	% Mass Balance
-	-	23 ± 8	6 ± 1	14 ± 9	93 ± 4	49 ± 2
-	+	30 ± 0	10 ± 1	0	94 ± 0	46 ± 1
+	-	24 ± 1	6 ± 1	7 ± 2	86 ± 2	49 ± 2

[a] Thermolyses carried out at 55 °C for 6 h with [**96**] = 0.1 mM, $[Bu_3SnH]$ = 5.1 mM, [Vazo 52] = 0.1 mM, $[Bu_3SnI]$ = 0.1 mM, and [HBr] = 0.1 mM in THF:H_2O (1:1 by volume).

3.1.11 First-Order Rate Constant for Disappearance of the Selenide (96)

From the photochemical and thermal investigations of the radical precursors, the selenide (**96**) appears to be the most versatile and reliable precursor for studies on **4**. Although **94** and **95** are efficient precursors under anaerobic conditions, the chemistry under aerobic conditions was complicated by either inefficient conversion or competing side reactions. The efficiency of the thermolysis of the selenide (**96**) in the presence of Bu_3SnH and VA-044 (**103**) was gauged by determining the kinetics for the conversion. The conversion of **96** was determined in intervals over 1 h and a plot of the conversion *versus* the time was constructed (Figure 54). The slope of the line was 5.13×10^{-2}, which corresponds to a first-order rate constant of 8.6×10^{-4} s^{-1} for the disappearance of **96**, and a $t_{1/2}$ of 13.5 min at 37 °C.

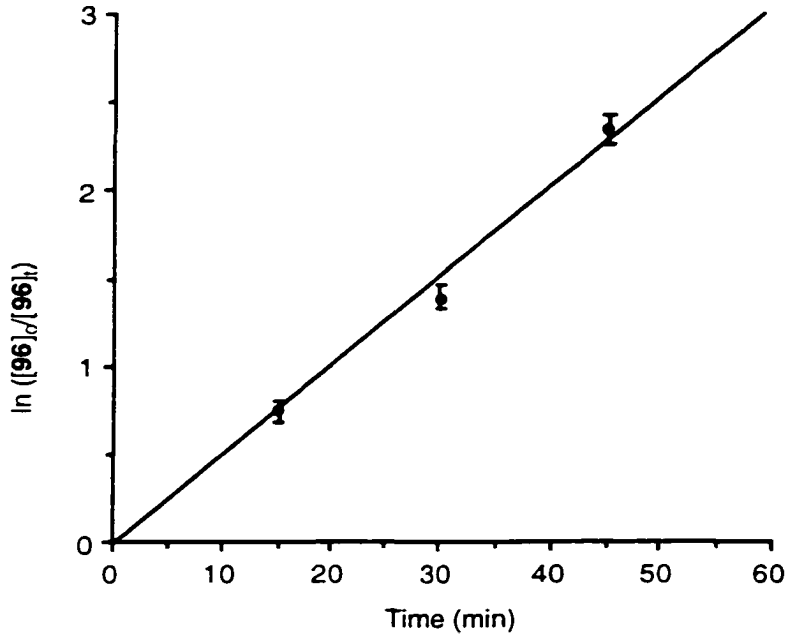

Figure 54. Plot of $\ln[\mathbf{96}]_0/[\mathbf{96}]_t$ *versus* time.

3.1.12 Thermolysis of the Selenide (96) in the Presence of a Water-Soluble Tin Hydride (109)

Since the selenide (**96**) proved to be an efficient precursor in which to study **4** under aerobic and anaerobic thermal and photolytic conditions, we wished to extend the studies to more biologically relevant conditions. In order to mimic biological conditions as closely as possible, we wished to carry out the photolysis and thermolysis of **96** in the presence of a water-soluble tin hydride, which are typically used in radical chain reactions. This would enable us to eliminate the need for organic cosolvents.

A water-soluble tin hydride (**109**) has been reported that traps alkyl radicals at 1.2 x 10^6 M^{-1} s^{-1}, comparable to Bu_3SnH.[130-132] However, in the presence of **109**, complete reduction of **96** was observed in the absence of initiator. Although the major product was

34 as expected, a significant amount of deuterium was detected in the product when reactions were carried out in D_2O. The incompatibility of **109** with **96** may be due to one-electron reduction of **96** to generate the radical anion (**110**, Figure 55). Evidence for tin hydrides acting as electron donors and phenyl selenides as electron acceptors (under photolytic conditions) has been reported.[133,134] In addition, ligands on tin, such as the glycol ligands on **109**, reduce the oxidation potential through oxygen stabilization of the resultant cation upon oxidation.[135] Subsequent cleavage of **110** to either the carbanion (**35**) or radical (**4**) will ultimately give rise to the reduced product, **34**.

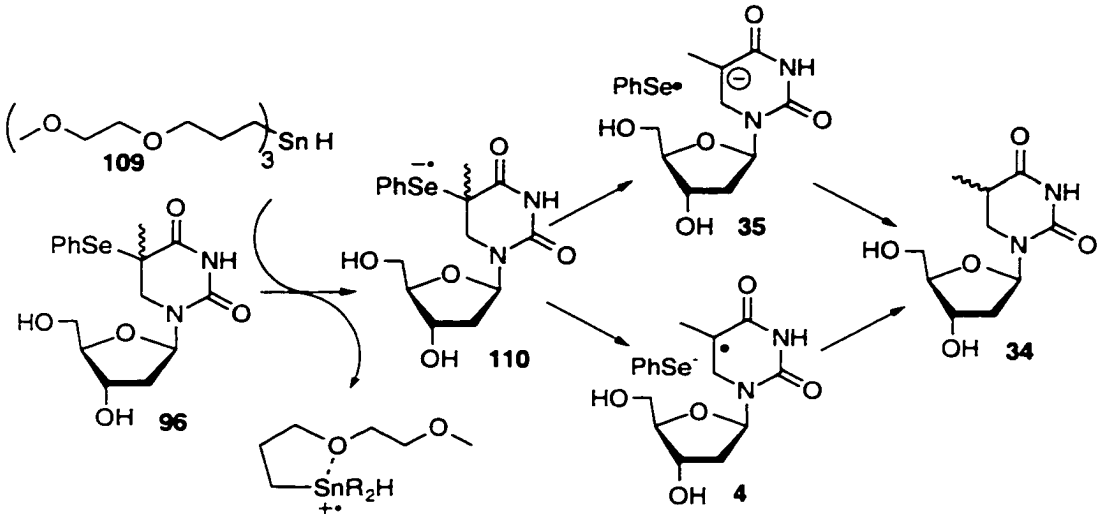

Figure 55. Proposed mechanism for the decomposition of **96** in the presence of **109**.

An alternative explanation for the observed behavior of **109** with **96** requires proposing that there is increased nucleophilicity of the tin hydride (**109**) due to the inductive effect of the oxygen (Equation 10). Ligand to metal complexation may result in a weakening of the tin-hydrogen bond, thus making the tin hydride behave more like a "hydride", which is able to reduce **96** in a bimolecular reaction. The oxygen ligand thus stabilizes the resultant positive charge on the tin upon loss of the hydride. The mechanism by which the reduction of **96** occurs remains to be determined. Due to the complicated

nature of the chemistry observed in the presence of **109**, its use as a hydrogen atom donor was abandoned.

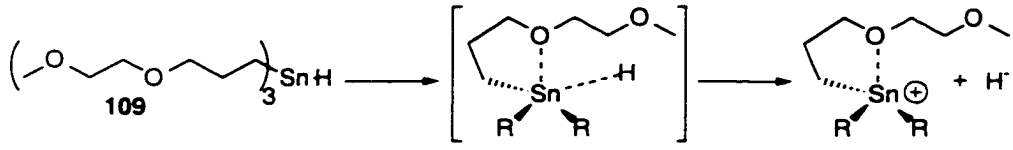

(10)

3.1.13 Mechanism for the Formation of 5,6-Dihydro-5-hydroxythymidine (8) and Thymidine (3)

The studies described thus far have shown that the selenide (**96**) is the most promising radical precursor for studying **4**. During the course of the investigation, one important observation was made that should be stressed. Upon generation of the radical (**4**) in the presence of O_2, the alkyl radical should be trapped to generate the peroxyl radical (**7**). The peroxyl radical (**7**) is expected to generate **8** in the presence of a reducing agent (e.g. Bu_3SnH, βME, Equation 11). However, in the studies described thus far with **96**, the major product was always thymidine (**3**). In addition, it has been shown that the formation of **3** depends on the presence of O_2.

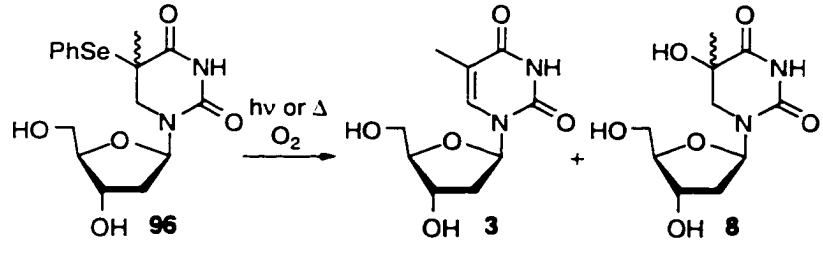

(11)

Furthermore, the results from the photolysis of **95** and **96** over a range of Bu_3SnH concentrations indicated that a common intermediate may be responsible for the formation

of **3** and **8** (Section 3.1.7). The mechanism for the generation of **8** may provide insight into the generation of **3** if they arise via a common intermediate. The source of oxygen in **8** may be molecular O_2 or water (Figure 56). Although thermodynamically unfavorable, formation of the carbocation (**111**) as a common intermediate was investigated. If **111** was formed under the reaction conditions, trapping by H_2O would generate **8**, whereas deprotonation from the C6-position would generate **3**. In order to determine the source of the oxygen in the product (**8**), the thermolysis was carried out in $H_2{}^{18}O$. GC/MS analysis of the persilylated nucleobases indicated no ^{18}O-incorporation in the product (**8**). Therefore, the source of oxygen in **8** is molecular O_2, as expected for a radical process. 5,6-Dihydro-5-hydroxythymidine (**8**) arises via trapping and reduction of the peroxyl radical (**7**).

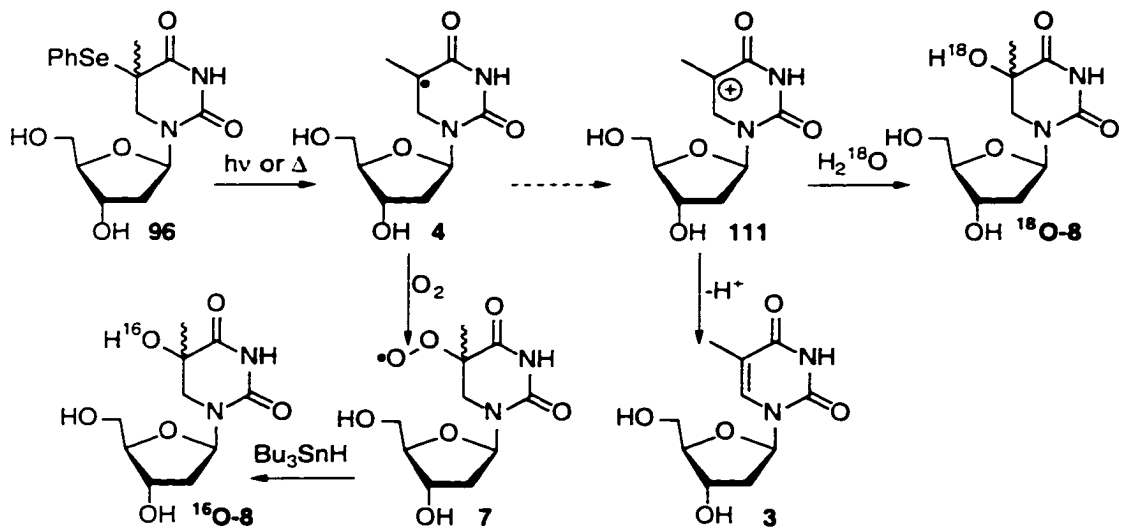

Figure 56. Mechanism for the formation of **8** via peroxyl radical or carbocation.

Another mechanism to explain the formation of **3** in the presence of O_2 is a selenoxide elimination of **112** (Equation 12). It has been observed that subjection of α-

selenoketones to radical chemistry in the presence of O_2 results in the formation of the α, β-unsaturated ketone.[136] Although the mechanism by which this occurs in unknown, the product was rationalized by invoking a selenoxide elimination.[136] Bear in mind that the formation of **3** via this route dictates that there is no common intermediate in the generation of **8** and **3**.

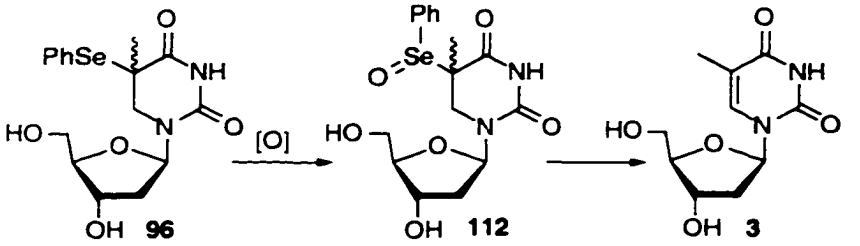

(12)

There are two possible oxidants in the system that could generate the selenoxide (**112**), peroxides from the THF or O_2. If **96** was oxidized by peroxides in the THF, one would expect to observe **3** under aerobic as well as anaerobic conditions. Recall that thymidine (**3**) is not observed under anaerobic conditions (Tables 5, 6). Nonetheless, the THF used in the reactions was distilled from $LiAlH_4$ and passed through alumina to remove trace amounts of peroxides. In addition, the reaction was carried out in CH_3CN in which peroxide formation is not expected. Regardless of the solvent used in the reaction, **3** was still produced in the same O_2 dependent manner.

The other oxidant present in the system is O_2. When the selenide (**96**) was subjected to thermolysis conditions in the presence of Bu_3SnH and absence of initiator, there was no conversion of **96**. Likewise, exposure of **96** to initiator in the absence of Bu_3SnH also did not result in generation of **3**. This suggests that a selenoxide elimination is not responsible for the generation of **3** since **96** is stable to the reaction conditions.

Conversion of **96** to **3** is only observed under free radical conditions, indicating that formation of **4** is a prerequisite for the formation of **3**.

Evidence for a common intermediate in the formation of **8** and **3** was obtained from experiments in which the effect of Bu_3SnH concentration on the product distribution was investigated. As the concentration of Bu_3SnH is increased, the yield of **3** decreased and **8** increased (Table 13). The dependence of product distribution on the concentration of trap present indicates that a common intermediate exists in which reactivity is partitioned between two competing pathways. Although the ratio is not the same, the trend is consistent with the photolysis experiments of the bromide (**95**, Table 12). The evidence for a common intermediate, prerequisite for a radical intermediate, and the dependence on the presence of O_2 led to the proposed mechanism outlined below for the generation of **3** (Figure 57).

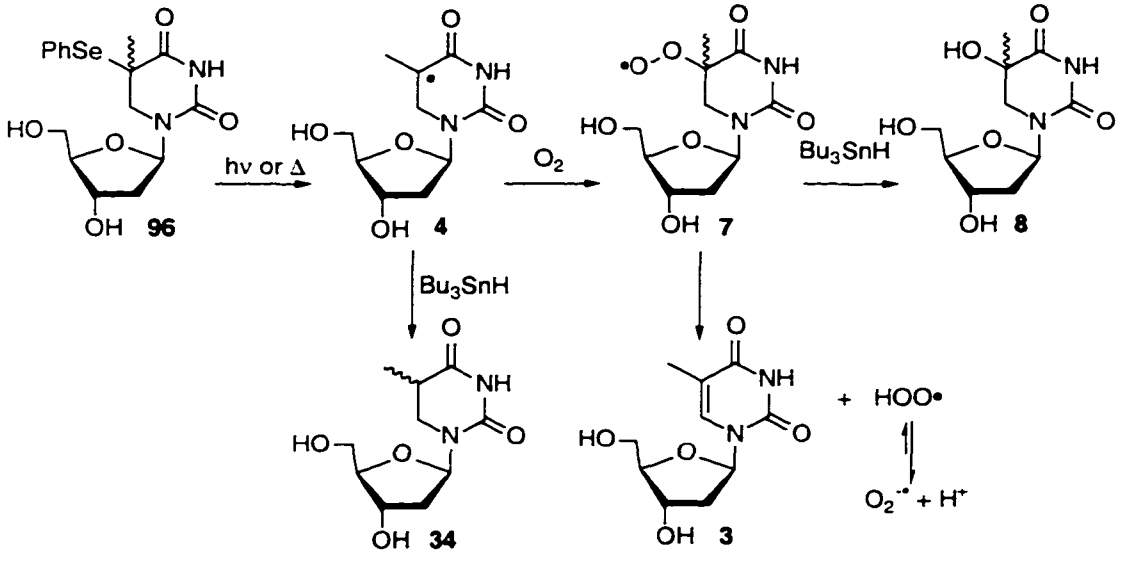

Figure 57. Mechanism for the formation of **8** and **3** via peroxyl radical intermediate.

Upon generation of the radical (**4**) in the absence of O_2, hydrogen atom abstraction from the Bu_3SnH generates **34**. However, in the presence of O_2, the radical is trapped to

generate **7** at diffusion-controlled rates.[26] The peroxyl radical (**7**) has two reaction pathways available to it. Trapping by Bu_3SnH yields the hydroperoxide, which is known to be readily reduced to **8**. An alternative pathway is available to **7** if there is a hydrogen atom in the β-position of the molecule, as is the case for **7**. Intramolecular hydrogen atom abstraction from the C6-position by **7** generates the native nucleobase and HOO•. Recall that this elimination reaction has been observed for compounds such as phenol (Equation 13).[70] If a peroxyl radical is generated with a hydrogen atom in the β-position, intramolecular hydrogen atom abstraction occurs. If a suitable driving force exists, such as the rearomatization in the case of phenol, the rate constant can be $>10^5\ s^{-1}$.[70]

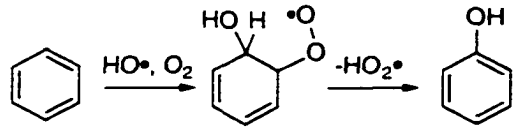

(13)

The proposed mechanism for the fate of **7** is important for several reasons. To our knowledge, this general reaction pathway available to **7** has never been observed for a DNA based peroxyl radical. Since the effects of ionizing radiation have been studied on the native nucleosides, the regeneration of thymidine (**3**) could not have been detected because the product of such a process is the initial substrate. Second, this pathway provides the peroxyl radical (**7**) with a naturally occurring repair mechanism in addition to the enzymatic repair processes available to metastable lesions. Trapping of an alkyl radical by O_2 is usually referred to as a damage fixing process, with the result usually a modified nucleobase or strand scission in extreme cases. This pathway is an exception to this rule, since **7** is able to repair itself and regenerate the nucleobase.

Although this mechanism provides a pathway in which the nucleobase can be repaired, the by-product in the reaction is HOO•. Since the pKa of HOO• is 4.8, under

physiological conditions it will dissociate to $O_2^{\bullet}$. Although $O_2^{\bullet}$ is not deleterious to DNA, it is known to generate the very reactive HO• and peroxynitrite which are known to damage DNA.[1,18,19,30-34] Therefore, while the proposed reaction would restore thymidine (**3**) in DNA, it has the potential to lead to DNA damage and the overall process could be considered a double-edged sword.

3.1.14 Superoxide Elimination

Given the importance and novelty of the proposed superoxide elimination to generate **3**, experiments were conducted to gain evidence for the proposed mechanism and determine the rate constant for the elimination. Two complimentary spectrophotometric assays were utilized to gain evidence for the release of $O_2^{\bullet}$ during the formation of **3**. One assay involves the oxidation of epinephrine (**73**) to adrenochrome (**74**, Equation 14) while the other relies on reduction of cytochrome *c* (Equation 15).[137-139] In the presence of $O_2^{\bullet}$, **73** is oxidized to **74** through a four-electron process. An increase in the absorbance at 480 nm due to the formation of adrenochrome (**74**) is indicative of the formation of $O_2^{\bullet}$. Alternatively, one-electron reduction of cytochrome *c* results in an increase in absorbance at 550 nm. The advantage of the latter is the ability to quantitate the amount of cytochrome *c* reduced and thus correlate the amount of superoxide generated to the yield of **3**.

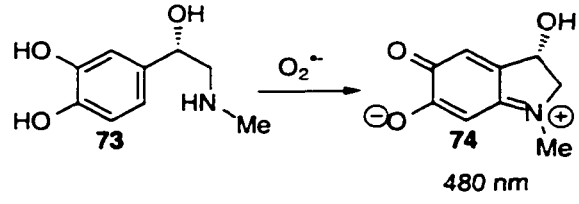

(14)

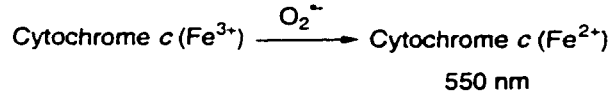

(15)

3.1.14.1 Epinephrine Assay for Superoxide

The photolysis of **96** was carried out in the presence of epinephrine (**73**) and the absorbance measured at 480 nm over a period of time. The absorbance increased relative to the background (**96** not present), in which the epinephrine (**73**) undergoes a small amount of oxidation during the photolysis (Figure 58). To show that the increase in absorbance was due to the formation of $O_2^{\cdot}$, the photolysis was carried out in the presence of superoxide dismutase (SOD) and catalase. The SOD and catalase scavenge $O_2^{\cdot}$ and H_2O_2, respectively. In the presence of SOD (100 units), the absorbance was significantly diminished (Figure 59). When the SOD was increased to 200 units, the absorbance was completely quenched, indicating that $O_2^{\cdot}$ was responsible for the oxidation of **73**.

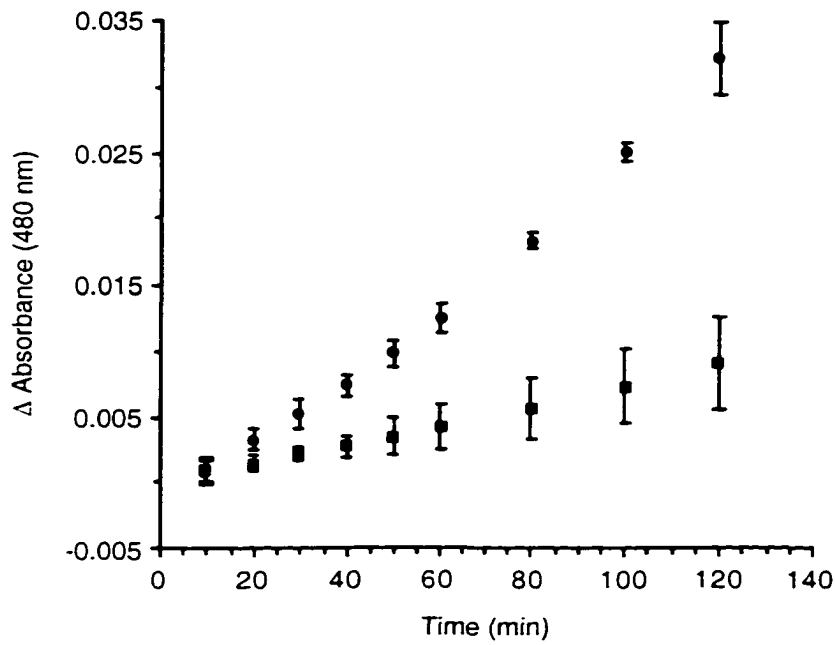

Figure 58. Photolysis of: (●) **96** (0.1 mM) and epinephrine (0.1 mM); (■) epinephrine (0.1 mM).

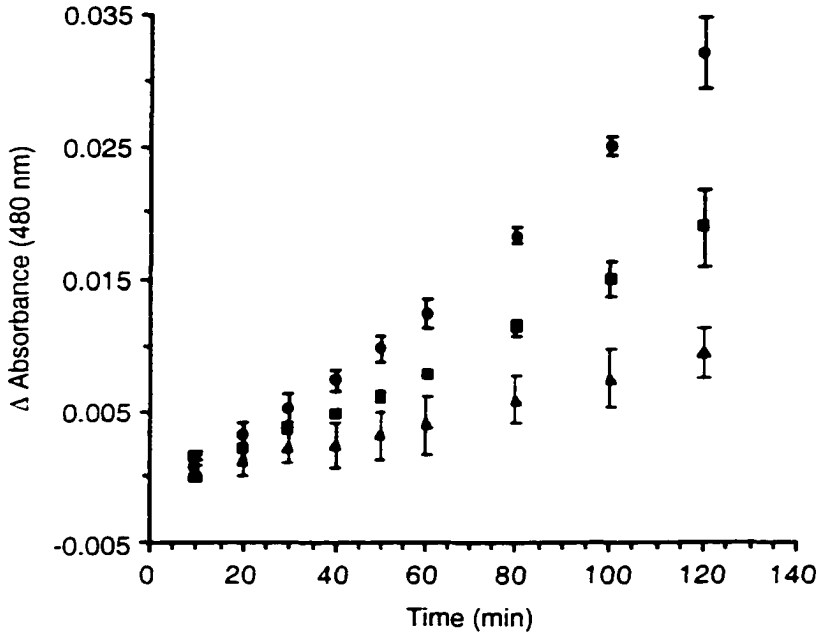

Figure 59. Photolysis of: (●) **96** (0.1 mM) and epinephrine (0.1 mM); (■) **96** (0.1 mM), epinephrine (0.1 mM), and SOD (100 units); (▲) **96** (0.1 mM), epinephrine (0.1 mM), and SOD (200 units).

It was observed that increasing the concentration of Bu_3SnH results in a decrease in the amount of **3** generated, thus a decrease in the amount of $O_2^{\cdot}$. Photolysis of **96** in the presence of Bu_3SnH should therefore result in a decrease in the observed absorbance in the epinephrine assay. When the photolysis of **96** was carried out in the presence of **73** and Bu_3SnH, the absorbance was completely quenched. Although the conditions used in the photolysis resulted in **3**, it appeared that $O_2^{\cdot}$ was not being generated. It is possible that the Bu_3SnH quenches the $O_2^{\cdot}$ or one of the radical intermediates generated during the formation of **74** (Figure 60).

To address this issue, $O_2^{\cdot}$ was independently generated from KO_2. When the $O_2^{\cdot}$ was generated in the presence of epinephrine (**73**) , the observed absorbance was 0.022 at 480 nm. However, when the $O_2^{\cdot}$ was generated in the presence of Bu_3SnH, the absorbance decreased to 0.007, supporting the above hypothesis.

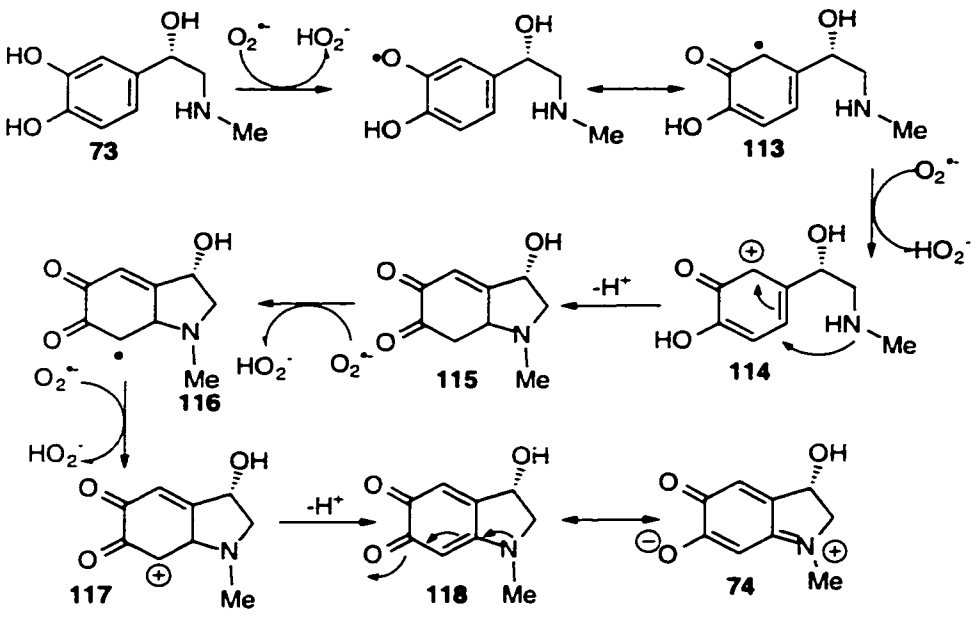

Figure 60. Mechanism for oxidation of **73** to **74** by $O_2^{\cdot-}$.[137]

3.1.14.2 Cytochrome *c* Assay for Superoxide

Although the epinephrine assay verified that $O_2^{\cdot-}$ was being generated during the photolysis of **96**, quantitation was difficult since adrenochrome formation is not a stoichiometric process and may involve radical chain chemistry. An alternative spectrophotometric assay for the detection of $O_2^{\cdot-}$ involves cytochrome *c*. In this assay, the Fe^{3+} of the cytochrome *c* is reduced by $O_2^{\cdot-}$, the absorbance of which can be measured. The Fe^{2+} species exhibits a characteristic absorbance at 550 nm and can be quantitated, thus allowing one to determine the amount of $O_2^{\cdot-}$ generated during the course of the reaction. This assumes that all of the superoxide generated reduces the cytochrome *c*, and no other species is able to reduce the cytochrome *c*. The photolysis of **96** was carried out in the presence of cytochrome *c* and the absorbance monitored at 550 nm at defined time intervals. The absorbance increased at 550 nm, indicating that the cytochrome *c* was being reduced (Figure 61).

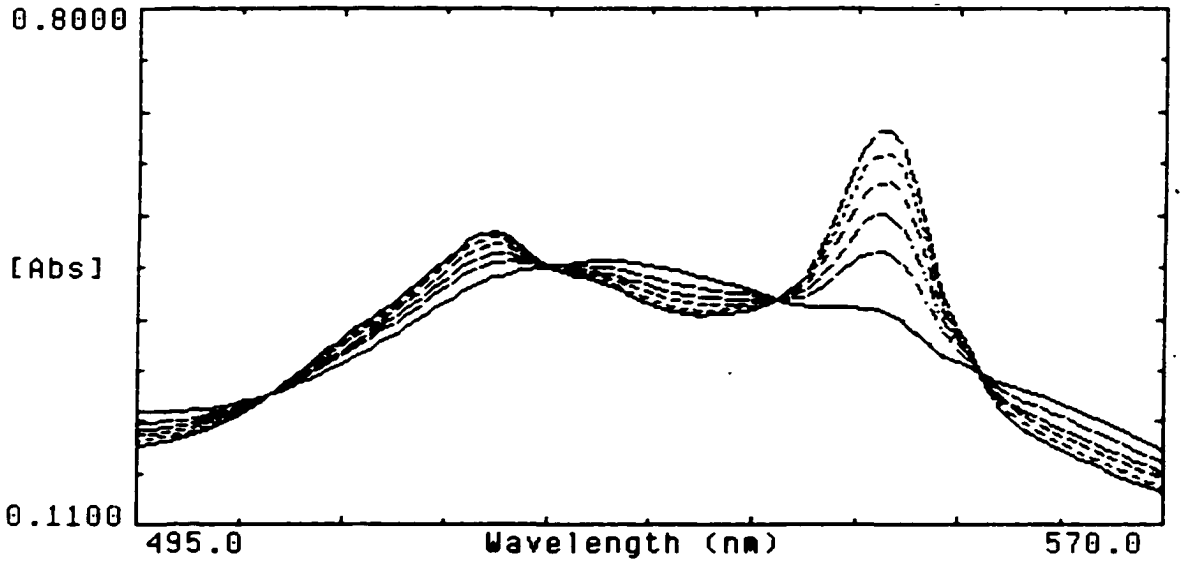

Figure 61. Photolysis of **96** in the presence of cytochrome *c*, t=0 (bottom) to 100 min (top) in 20 min intervals.

The photolysis of **96** was carried out out at 350 nm in PE buffer (EDTA and phosphate buffer). A significant increase in the absorbance was detected for samples containing **96** relative to the control, which only contained cytochrome *c* (Figure 62). The amount of cytochrome *c* reduced corresponds to the amount of $O_2^{\bullet-}$ generated during the photolysis. Photolysis of **96** in the presence of SOD (5 units) quenched 74% of the amount of cytochrome *c* reduction, supporting the contention that $O_2^{\bullet-}$ is responsible for the reduction of cytochrome *c*. Additional SOD (100 units) resulted in no further reduction in the amount of reduced cytochrome *c*. We suggest that the cytochrome *c* reduction that could not be suppressed was due to a superoxide-independent process involving PhSe• released upon photolysis.

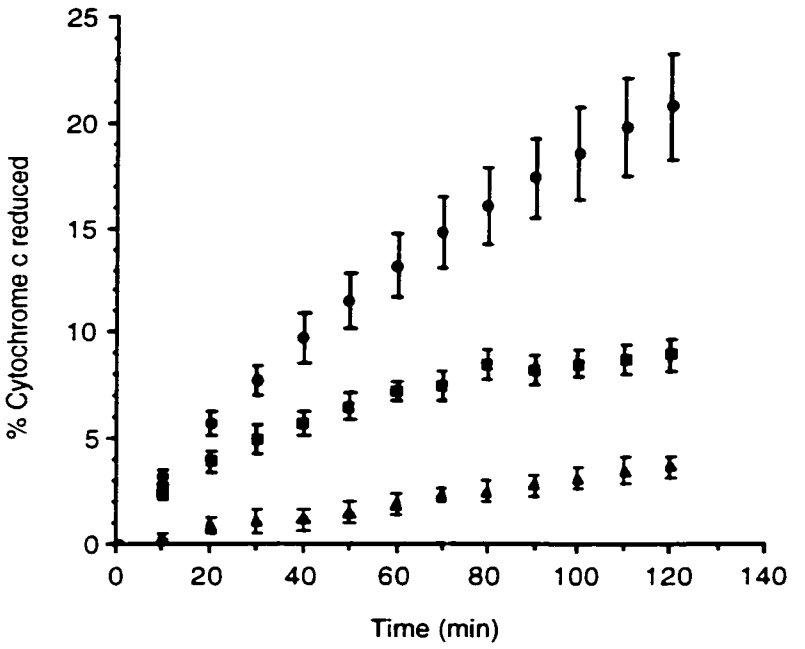

Figure 62. Photolysis of: (●) **96** (50 μM) in the presence of cyt *c* (50 μM), EDTA (0.1 mM), and catalase (252 units); (■) **96** (50 μM), cyt *c* (50 μM), EDTA (0.1 mM), catalase (252 units); and superoxide dismutase (5 units); (▲) cyt *c* (50 μM), EDTA (0.1 mM), and catalase (252 units).

The samples containing the selenide (**96**) that were photolyzed in the presence of cytochrome *c* were analyzed by reverse-phase HPLC in order to correlate the yield of thymidine (**3**) to the amount of cytochrome *c* reduced (Table 21). In the absence of SOD, the amount of cytochrome *c* reduced corresponds to ≈62% of the observed thymidine (**3**), which is formed as a result of superoxide elimination. However, one should note that the standard deviations measured in the experiments are significantly large such that the two are within experimental error of one another. Given this caveat, the remainder of the thymidine (**3**) generated upon the photolysis of **96** could be attributable to disproportionation between **4** and PhSe•. When the photolysis was carried out in the presence of SOD, in which the

$O_2^{\bullet}$ should have been scavenged, a small amount of cytochrome *c* reduction was observed. The observed cytochrome *c* reduction is believed to be due to reduction by PhSe•.

Table 21. HPLC analysis of samples containing **96** photolyzed in the presence of cytochrome *c*.[a]

SOD	% Yield **3**	% Conversion	% Cyt *c* reduced
-	29 ± 8	49 ± 0	18 ± 7
+	25 ± 1	64 ± 0	9 ± 1

[a] Photolyses carried out as described in Figure 62.

Photolysis of $(PhSe)_2$ in the presence of cytochrome *c* would provide evidence that PhSe• was partially responsible for the reduction of cytochrome *c*. Unfortunately, solubility problems prevented us from carrying out this experiment. The cytochrome *c* and/or $(PhSe)_2$ were insoluble in CH_3CN, THF, MeOH, and DMSO mixtures (1:1 by volume with PE buffer).

Although the above experiment could not be carried out, photolysis of **96** under anaerobic conditions would provide the same information we hoped to gain from the photolysis of $(PhSe)_2$. Upon photolysis of **96**, the radical pair, **4** and PhSe•, is generated. Since **4** is an oxidizing radical, it is not expected to be involved in the reduction of cytochrome *c*. Therefore, any observed cytochrome *c* reduction can be attributed to PhSe•. Photolysis of **96** under anaerobic conditions resulted in a significant increase in absorbance (Figure 63). As expected, the cytochrome *c* reduction under anaerobic conditions could not be quenched by SOD. This is consistent with reduction of the cytochrome *c* by the PhSe•. Therefore, the reduced cytochrome *c* produced in the presence of the phenyl selenide (**96**) that could not be quenched by SOD under aerobic conditions is believed to be attributable to PhSe•.

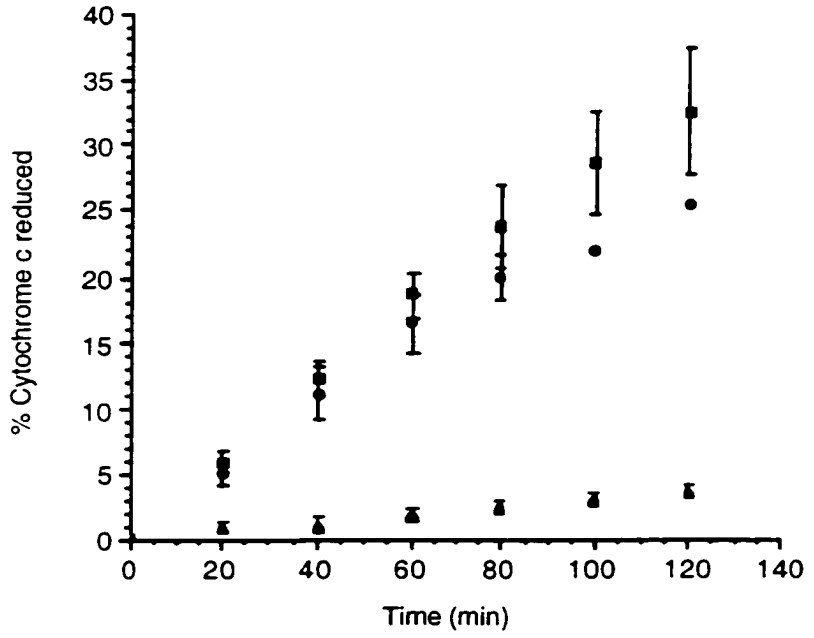

Figure 63. Anaerobic photolysis of: (●) **96** (50 μM), cyt *c* (50 μM), and catalase (252 units); (■) **96** (50 μM), cyt *c* (50 μM), catalase (252 units), and SOD (100 units); (▲) cyt *c* (50 μM) and catalase (252 units).

3.1.14.3 Rate Constant for Superoxide Elimination

The cytochrome *c* and epinephrine assays provide evidence for the formation of $O_2^{\bullet}$ upon photolysis of **96**. The cytochrome *c* assay relies on the reduction of Fe^{3+}, whereas the epinephrine involves an oxidative process. The complimentary nature of the two assays provides a stronger case for the presence of $O_2^{\bullet}$, rather than an artifact of the photolysis. Given the significance and novelty of the observed reaction, the facility of superoxide elimination was gauged by estimating the rate constant for this process using competitive kinetics.

Upon photolysis or thermolysis of **96**, a mixture of **3** and **8** were observed. Both of these products are generated from **7**, which partitions itself between two pathways in a

manner that is dependent on the concentration of Bu_3SnH (Equation 16). The rate constant for trapping a peroxyl radical (k_{Red}) by Bu_3SnH is $\approx 1.6 \times 10^3$ M^{-1} s^{-1}.[140] By varying the concentration of Bu_3SnH, the dependency of the ratio of products on the trap can be measured and the rate constant, k_{Elim}, estimated using k_{Red} as a comparison.

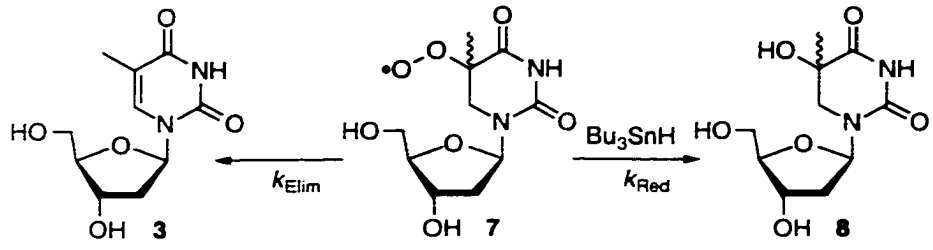

(16)

Competitive kinetics experiments were carried out under thermal conditions to generate **4** from **96**. In contrast to earlier studies on **96**, the thermolyses were carried out at 55 °C in THF:H_2O (19:1 by volume) to ensure complete reduction of the hydroperoxide to **8** and complete solubility of the Bu_3SnH over its entire concentration range. As expected, the yield of **8** increased, and that of **3** generally decreased when the concentration of Bu_3SnH increased (Table 22). This is consistent with more efficient trapping of **7** as the concentration of Bu_3SnH increases. The photolysis of the selenide (**96**) was also carried out in aqueous CH_3CN. The product ratios were consistent with the results of the photolyses carried out in aqueous THF (Table 22) and indicate that hydrogen atom abstraction from the THF by the peroxyl radical (**7**) does not occur to give rise to **8**. Since trapping of **4** by Bu_3SnH also becomes more competitive as the concentration increases, the relationship between absolute yields of oxygenated products (**3** and **8**) and [Bu_3SnH] is not necessarily linear. Therefore, the ratio of **3**:**8** was plotted against [Bu_3SnH]$^{-1}$ rather than absolute yields (Figure 64).

Table 22. Aerobic thermolysis of **96** with varying $[Bu_3SnH]$.[a]

$[Bu_3SnH]$ mM	% Yield 3	% Yield 8	% Yield 3+4	% Conversion	% Mass Balance	3:8
1.0	51 ± 1	4 ± 1	7 ± 1	99 ± 1	63 ± 1	12.0 ± 2.1
3.0	23 ± 9	7 ± 5	13 ± 9	71 ± 27	71 ± 23	4.0 ± 1.6
8.0	13 ± 0	7 ± 1	36 ± 5	83 ± 11	73 ± 5	1.8 ± 0.2
10.0	20 ± 2	19 ± 6	19 ± 3	86 ± 7	72 ± 2	1.1 ± 0.2

[a] Thermolyses carried out at 55 °C for 24 h with [**96**] = 0.05 mM and [VA-044] = 0.05 mM in THF:H_2O (19:1 by volume).

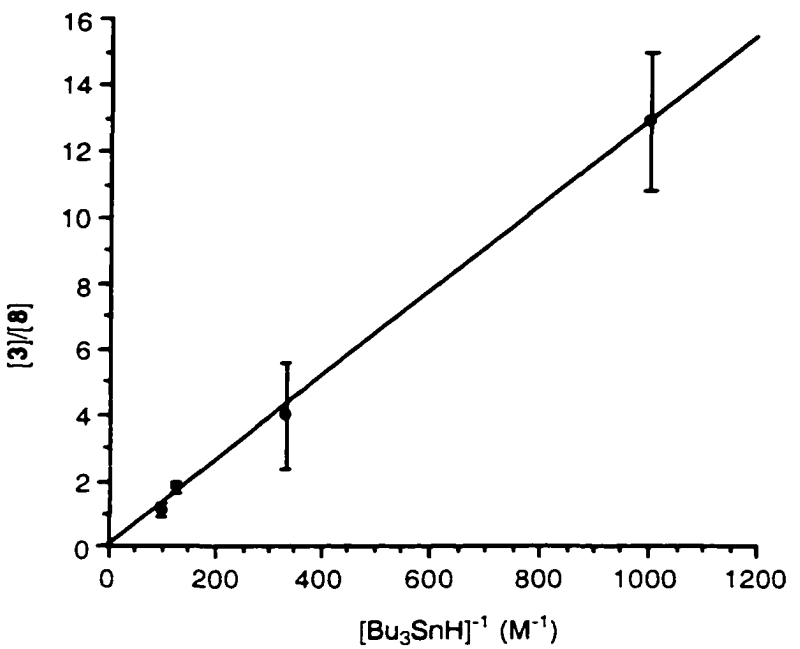

Figure 64. Plot of [**3**]/[**8**] *versus* $[Bu_3SnH]^{-1}$.

Using Equation 17, where k_{Elim} and k_{Red} are the rate constants for superoxide elimination and trapping of **7** by Bu_3SnH, respectively, k_{Elim} was determined. The slope of the line, 1.3×10^{-2}, represents k_{Elim}/k_{Red}. Given that the rate constant for k_{Red} is $\approx 1.6 \times 10^3$ M^{-1} s^{-1}, the rate constant for superoxide elimination is estimated as 21 s^{-1}.[140]

$$\frac{[3]}{[8]} = \frac{k_{Elim}}{k_{Red}\,[Bu_3SnH]} \qquad (17)$$

During the course of the investigations on the reactivity of **4**, a novel pathway available to the peroxyl radical (**7**) was discovered. The peroxyl radical (**7**) was shown to undergo intranucleotidyl hydrogen atom abstraction from the adjacent carbon to restore the native nucleobase (**3**) with release of HOO•. Restoration of thymidine (**3**) represents a naturally occurring detoxification pathway available to the peroxyl radical (**7**), whereas trapping of alkyl radicals in DNA by O_2 has been referred to as a damage-fixing event. Interestingly, superoxide elimination was the major pathway observed for **7** in the presence of Bu_3SnH at concentrations as high as 10 mM. Therefore, superoxide elimination may be a biologically relevant process. Although the elimination of superoxide restores the nucleobase, the generation of HOO• may ultimately give rise to superoxide-derived products that are able to induce damage in DNA. The involvement of superoxide in DNA damage makes this pathway a potential double-edged sword.

3.2 Dinucleotide Studies

One of the most abundant nucleobase radicals generated during ionizing radiation and other forms of oxidative stress is 5,6-dihydrothymidin-5-yl (**14**).[1] The generation of **14** in ssDNA under aerobic conditions has been shown to lead to direct strand breaks and alkaline labile lesions, whereas no damage was observed in the absence of O_2.[38,39] A novel mechanism involving internucleotidyl hydrogen atom abstraction by the peroxyl radical (**9**, Equation 18) was invoked to rationalize the transfer of spin from the nucleobase to the adjacent sugar, a necessary requirement for direct strand breaks.[38,39] Pulse radiolysis studies on poly T support this mechanism of internucleotidyl hydrogen atom abstraction by nucleobase radicals, such as **14**.[36]

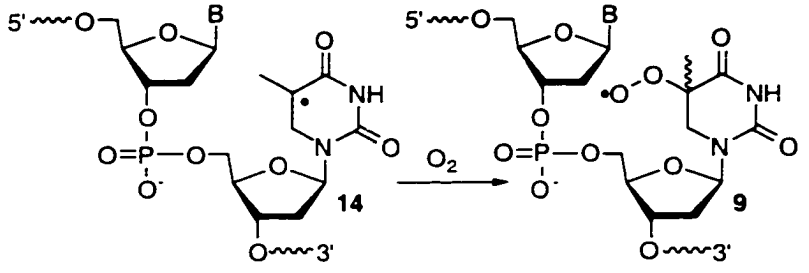

(18)

Although evidence suggests that spin is transferred from the nucleobase radical (**9**) to the sugar via internucleotidyl hydrogen atom abstraction, this novel DNA damage amplification process has not been rigorously characterized at the molecular level. In addition, investigation of 5,6-dihydrothymidin-5-yl (**4**) at the monomeric level suggests that a novel pathway involving superoxide elimination (Section 3.1.14) from its respective peroxyl radical (**7**) may be a biologically relevant process. This pathway available to **7** may compete with the proposed internucleotidyl hydrogen atom abstraction pathway.

Consequently, there are several questions we wished to address regarding the chemistry of 5,6-dihydrothymidin-5-yl (**14**) and its involvement in DNA damage amplification:

1. Can we provide further evidence that internucleotidyl hydrogen atom transfer does not occur under anaerobic conditions?
2. Does the peroxyl radical (**9**) transfer spin from the nucleobase to the adjacent sugar as suggested in previous studies? If so, does this process compete with bimolecular reactions available to **9** (e.g. trapping by thiols)? What is the stereoselectivity of this process?
3. Does the peroxyl radical (**9**) protect itself by eliminating superoxide in competition with internucleotidyl hydrogen atom abstraction?
4. If hydrogen atom abstraction by **9** occurs from the C1'-position, is the 2-deoxyribonolactone lesion (**61**) produced?
5. Can a radiosensitizing agent participate in DNA damage amplification involving 5,6-dihydrothymidin-5-yl (monomer **4** or dinucleotide **120**) by acting as a surrogate for O_2?

These questions regarding the involvement of 5,6-dihydrothymidin-5-yl (**4**) in DNA damage amplification were addressed through incorporation of the ketone (**94**) and selenide (**96**) into dinucleotides **119** and **121** (Figure 65). The dinucleotide is the minimal system in which to study the chemistry of 5,6-dihydrothymidin-5-yl (**120**). In addition, it would be amenable to conventional organic product analysis because the dinucleotide allows one to synthesize the expected products so that the observed products can be confirmed using an authentic sample.

3.2.1 Design of the Dinucleotide

The dinucleotides were designed with several important features. The incorporation of the phenyl selenide into its respective dinucleotide (**121**) is expected to provide an

efficient source of **120** via thermolysis or photolysis. Likewise, the ketone containing dinucleotide (**119**) provides an alternative photolabile precursor to the same radical. Although the chemistry of the ketone monomer (**94**) was not as clean as studies carried out using the phenyl selenide (**96**), it was utilized to a limited extent in those involving the dinucleotide. Furthermore, while the photochemistry of the ketone (**94**) was more complicated than expected, the rate constant for internucleotidyl hydrogen atom abstraction is not known. Hence, in the event that the latter process had a rate constant fast enough to compete with the reactions occurring upon photolysis of the ketone (**119**), it would be a useful substitute.

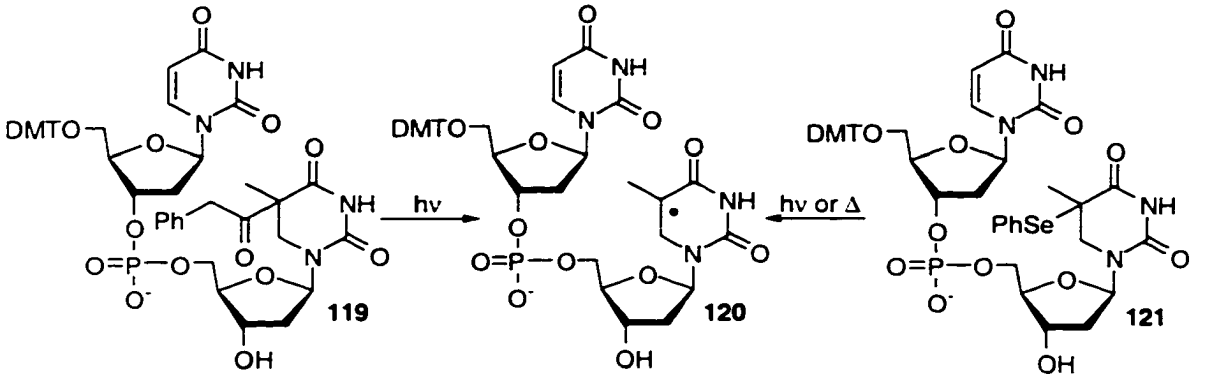

Figure 65. Alternate precursors to 5,6-dihydrothymidin-5-yl (**120**).

The dinucleotide was designed with a dimethoxytrityl (DMT) ether at the 5'-end, which provides a chromophore for convenient HPLC analysis. Most importantly, the competition between $O_2^{-\bullet}$ elimination from the peroxyl radical (**9**) and hydrogen atom abstraction from the adjacent sugar can be determined by product analysis since each chemical process results in distinguishable products detectable by HPLC analysis.

3.2.2 Synthesis of Dinucleotide Precursors and Expected Products

The dinucleotide precursors (**119**, **121**) were synthesized via a coupling reaction of single diastereomers of the free monomers (**94** and **96**), for which the syntheses have already been described (Section 3.1.1), and the appropriate phosphoramidite. Although mechanistic studies can be carried out with **119** and **121** as a mixture of diastereomers, the syntheses of **119** and **121** were carried out using the individual diastereomers of the radical precursors (**94** and **96**) in order to simplify the synthesis and purification of synthetic intermediates, as well as **119** and **121**. The diastereomers of the protected and free monomers were inseparable, but the 3'-protected monomers could be easily separated. Selective deprotection of the ketone (**100**) and the selenide (**101**) was effected with 10% TFA/H_2O in THF to yield **122** and **123**, respectively (Scheme 4). The diastereomers were separated by column chromatography and subsequently deprotected with Et_3N•3HF to yield *5R*-**94**, *5S*-**94**, *5R*-**96**, and *5S*-**96** for the synthesis of **119** and **121**.

Scheme 4[a]

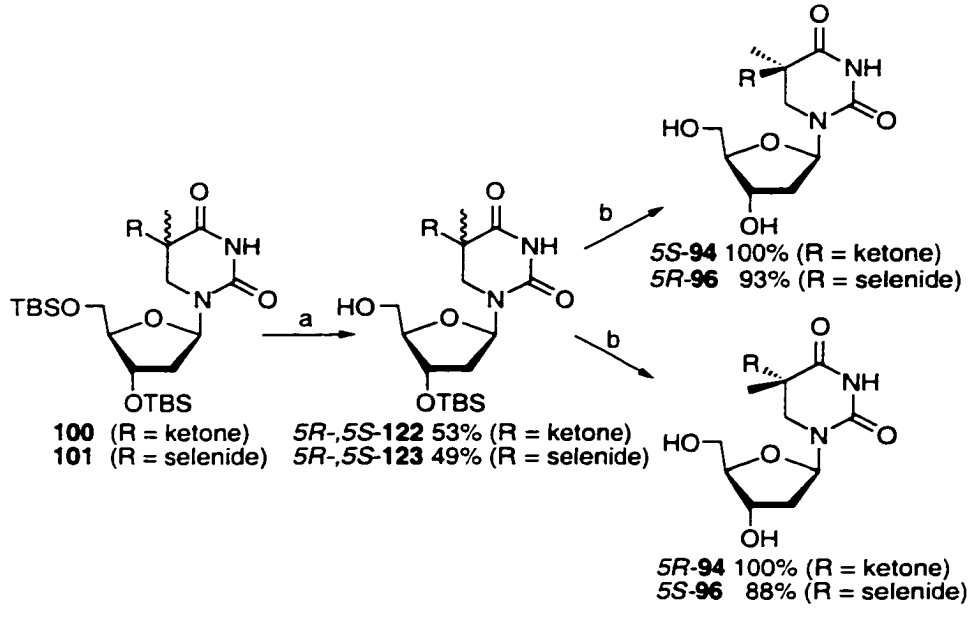

[a]Reagents: a) 10% TFA/H_2O, THF, 0 °C; b) Et_3N•3HF, THF.

Scheme 5[a]

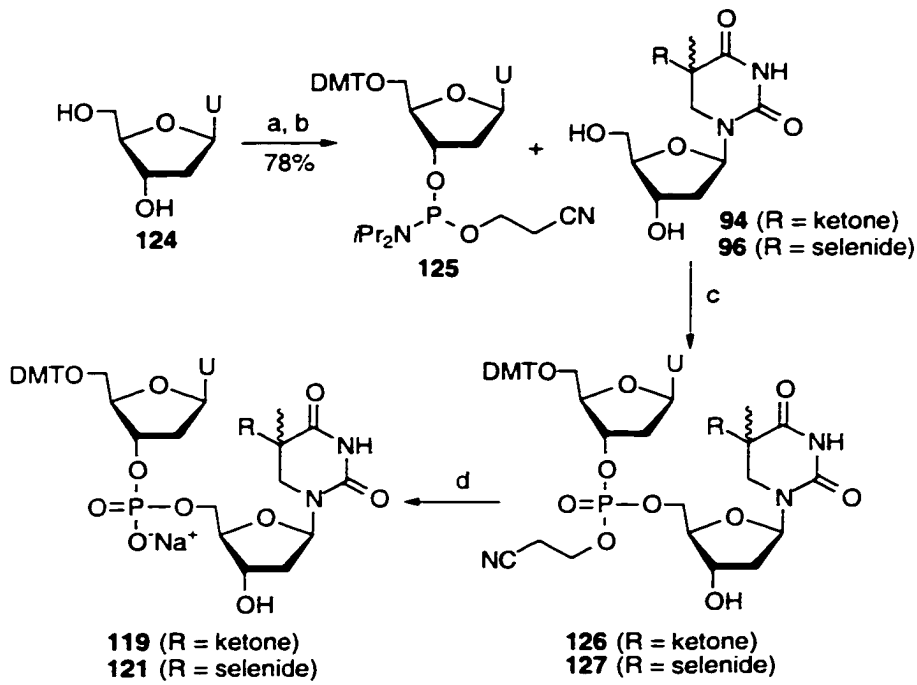

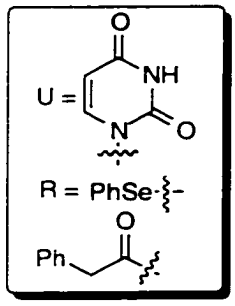

Monomer	Coupling (c)	Deprotection (d)
5R-**94**	42% (*5R*-**126**)	53% (*5R*-**119**)
5S-**94**	43% (*5S*-**126**)	64% (*5S*-**119**)
5R-**96**	51% (*5R*-**127**)	72% (*5R*-**121**)
5S-**96**	58% (*5S*-**127**)	59% (*5S*-**121**)

[a]Reagents: a) DMTCl, pyridine; b) β-cyanoethyl diisopropylchlorophosphoramidite, CH_2Cl_2; c) tetrazole/ CH_3CN (0.5 M), THF, 0 °C; 1.0 M I_2/THF:2,6-lutidine:H_2O (2:2:1 by volume); d) 50% Et_3N/THF, reflux.

The dinucleotides **119** and **121** were synthesized by coupling **94** and **96**, respectively, to the dU phosphoramidite (**125**, Scheme 5). The phosphoramidite (**125**) was synthesized by protecting the 5'-alcohol of 2'-deoxyuridine (**124**) as the 4,4'-dimethoxytrityl (DMT) ether, followed by phosphitylation of the free alcohol. The coupling of **125** to the monomers (**94** and **96**) was initially carried out on the mono-protected compounds (**122** and **123**) to prevent the formation of regioisomers as a result

of coupling to both the C3'- and C5'-alcohols. However, deprotection of the TBS protecting groups resulted in decomposition of the ketone (**119**) and/or detritylation. Therefore, the coupling reaction was carried out on the free monomers (**94** and **96**) under carefully controlled conditions to minimize the formation of regioisomers.

A solution of **125** in CH_3CN was activated with tetrazole and added slowly to a solution of the free monomer (**94** or **96**) in THF at 0 °C, and subsequently oxidized to yield **126** and **127** (Scheme 5). Following deprotection of the phosphate with refluxing Et_3N, the compound was isolated as a mixture of Et_3NH^+ and Na^+ salts, the latter presumably resulting from work-up and purification. The products (**119**, **121**) could be isolated solely as the Na^+ salt by passing the compound through a Dowex column that had been treated with NaOH and neutralized.

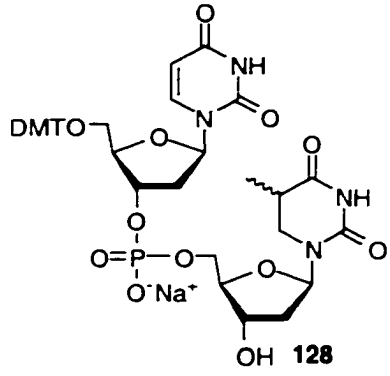

128

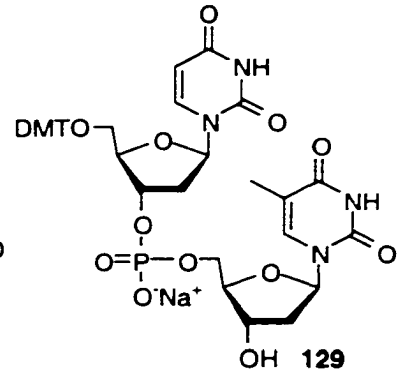

129

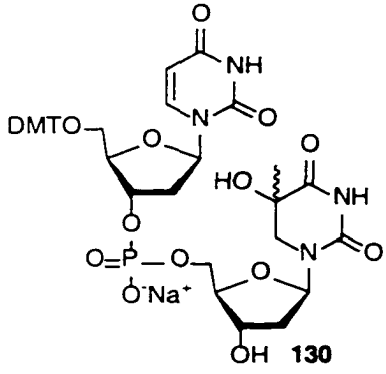

130

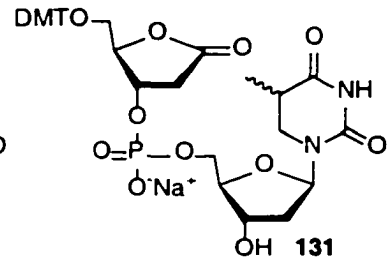

131

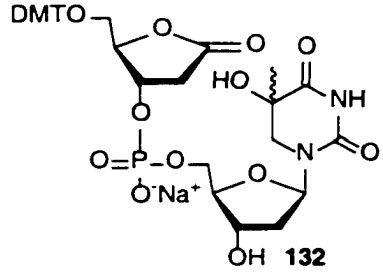

132

In addition to the precursors, the expected products (**128-132**) from the reaction of 5,6-dihydrothymidin-5-yl (**120**) in the dinucleotide were independently synthesized. The dU/5,6-dihydrothymidine dinucleotide (**128**) arises from trapping of **120** by hydrogen atom donation, and was to be used to determine that the radical (**120**) was being efficiently generated in the dinucleotide, as well as a tool for estimating the rate constant for internucleotidyl hydrogen atom abstraction by **120**. The dU/thymidine dinucleotide (**129**) and dU/5,6-dihydro-5-hydroxythymidine dinucleotide (**130**) are expected to be generated under aerobic conditions, as in the monomer (Section 3.1.5), via superoxide elimination and reduction of the peroxyl radical, respectively. The 2-deoxyribonolactone/5,6-dihydrothymidine dinucleotide (**131**) was one of the expected products if the C1'-radical was generated in the presence of TNM under anaerobic conditions. Finally, one of the most important anticipated products was **132**, which is the proposed product in the DNA damage amplification pathway put forth upon internucleotidyl hydrogen atom abstraction by the peroxyl radical.

The synthesis of the product dinucleotides was conducted in an analogous fashion as the synthesis of the radical precursors. However, the monomers (e.g. thymidine (**3**) and 5,6-dihydro-5-hydroxythymidine (**8**)) required for the synthesis of **128-132** were not sufficiently soluble in the THF solvent employed in the coupling of the monomeric radical precursors (**94** and **96**, Scheme 5) to the dU phosphoramidite (**125**). Attempts to carry out the coupling reaction in pyridine, a non-nucleophilic solvent commonly used in nucleoside chemistry, were unsuccessful. It is possible that the pyridine may compete with the diisopropylamine on the phosphoramidite (**125**) for the proton from the tetrazole. Protonation of the phosphoramidite (**125**) by the tetrazole is necessary for activation. Therefore, the coupling reactions were carried out on the 3'-protected compounds to increase the solubility of the monomers in organic solvent that are compatible with the coupling method, despite the aforementioned difficulties of removing the 3'-silyl protecting group from the dinucleotides.

Prior to carrying out the coupling reactions, the requisite monomers were synthesized. Thymidine is commercially available. 5,6-Dihydrothymidine is generated upon hydrogenation of thymidine. Thymidine and 5,6-dihydrothymidine were protected as their bis(TBS) ethers (Section 3.1.1). The hydrogenation of thymidine is very selective (*5S*:*5R*, 9:1). However, for these experiments a mixture of diastereomers was desired since the photolysis would most likely generate a mixture of diastereomers (**128**) as observed in the monomer studies (Section 3.1.2, 3.1.5). This was accomplished by epimerizing the C5-center of the protected 5,6-dihydrothymidine with *sec*-BuLi, followed by quenching with H_2O to yield a ratio of 1.5:1 (*5S*:*5R*).

Scheme 6[a]

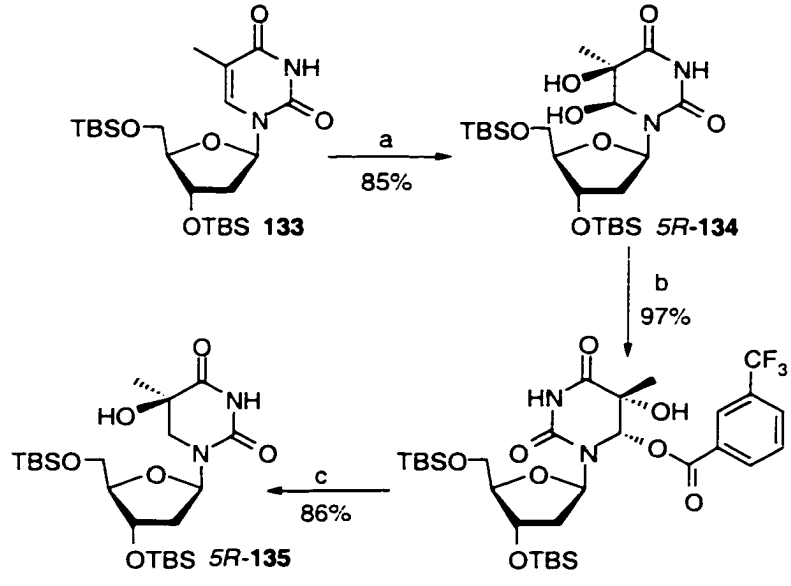

[a]Reagents: a) OsO_4, NMO, THF, *tert*-BuOH, H_2O; b) *m*-(Trifluoromethyl)-benzoyl chloride, DMAP, THF, -10 °C; c) *N*-methylcarbazole, hv, THF, H_2O.

A diastereoselective synthesis of **135** required for the syntheses of **130** and **132** has been reported (Scheme 6).[141] This approach involves controlling the stereoselectivity at

C5 during preparation of the diol, followed by deoxygenation at the C6-position. In the dinucleotide studies, separation of the diastereomers was not crucial, and both diastereomers of **130** and **132** were needed. The reported synthesis of the major diastereomer (*5R*-**135**) involves synthesis of the glycol (**134**) via OsO4, which results in only a minor amount of *5S*-**134**.[141] Attempts to increase the yield of *5S*-**134** by heating the reaction mixture resulted in a 3:1 mixture of diastereomers. However, the minor diastereomer could not be purified. Purification was probably further complicated by epimerization of the C6-position under these conditions. Alternatively, *5S*-**134** could be selectively synthesized utilizing AD-mix α (asymmetric dihydroxylation reagent generated *in situ*), but the reaction times were long, often taking as long as a week.[142]

Scheme 7[a]

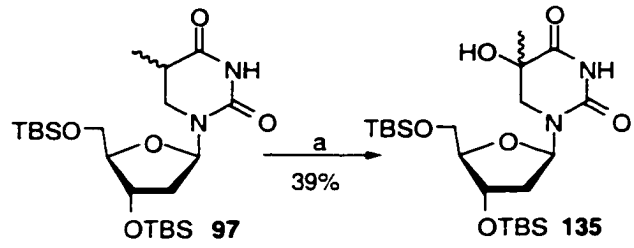

[a]Reagents: a) *sec*-BuLi, DMPU, O_2, ether/THF.

Since both diastereomers of the thymidine C5-hydrate (**135**) were needed for the dinucleotide studies and separation of the diastereomers was not crucial, a more direct route was utilized in the synthesis of **135** (Scheme 7). It has been reported that O_2 is an adequate electrophile for the synthesis of α-hydroxy carbonyl compounds.[143] Therefore, **135** was synthesized as a mixture of diastereomers by quenching of the lithium enolate of **97** with O_2 in the presence of DMPU (Scheme 7). Upon quenching and reduction of the peroxide with aqueous Na_2SO_3, **135** was isolated in 39% yield as a mixture of

diastereomers (*5R*:*5S*, 3:1). Although the yield was only modest, this route for the synthesis of **135** has the advantage that fewer steps are required than the previously reported method.[141] Moreover, the *5S*-diastereomer is obtainable in greater quantities more easily.

The lactone moiety of **132** is very labile and would not be stable to the reaction conditions for the synthesis of the dinucleotide. Therefore, a precursor to **132** was employed (**146**, Scheme 8) that would be stable to the reaction conditions required for the dinucleotide synthesis from which the lactone could be revealed in the last step of the synthesis. The *tert*-butyl ketone (**68**) was used in the studies on the C1'-radical and has been shown to be a very efficient precursor to **70** (Equation 19).[97,98]

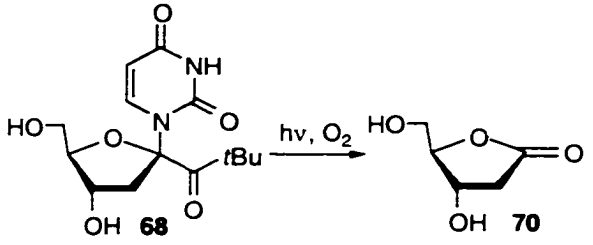

(19)

The ketone (**68**) was synthesized utilizing the intermediate bromonitrile (**142**), for which the synthesis has been reported (Scheme 8).[144,145] Uridine (**136**) was converted to the cyclouridine and subsequently protected as the bis(TBS) ether (**137**).[146] The cyclouridine (**137**) was ring-opened by the addition of PhSe· generated *in situ* to yield the α-selenide (**138**) exclusively in quantitative yield.[146] Oxidation of **138**, followed by a selenoxide elimination, yielded the 1',2'-didehydro nucleoside (**140**).[146] The 1',2'-didehydro nucleoside (**140**) was subjected to pivalic acid, followed by NBS, to yield the bromopivaloate (**141**) as a mixture of diastereomers.[144,145] The desired β-bromo-α-pivaloate (**141**) was obtained by recrystallization of the chromatographed product from hexanes. The bromopivaloate (**141**) was converted to the nitrile (**142**) with TMSCN in

the presence of a Lewis acid, and the bromide subsequently reduced under radical conditions to yield **143**. The nitrile (**143**) was treated with 3 equivalents of *tert*-BuLi and subsequently hydrolyzed to yield **144**. The silylated ketone (**144**) could not be purified. However, deprotection of **144** under mild conditions with $Et_3N{\bullet}3HF$, followed by recrystallization from CH_3CN, afforded **68** as a pure compound in 34% yield from **143**. The ketone (**68**) was converted to the phosphoramidite (**146**) by protecting the primary alcohol as the DMT ether and phosphitylating the 3'-alcohol.

Scheme 8[a]

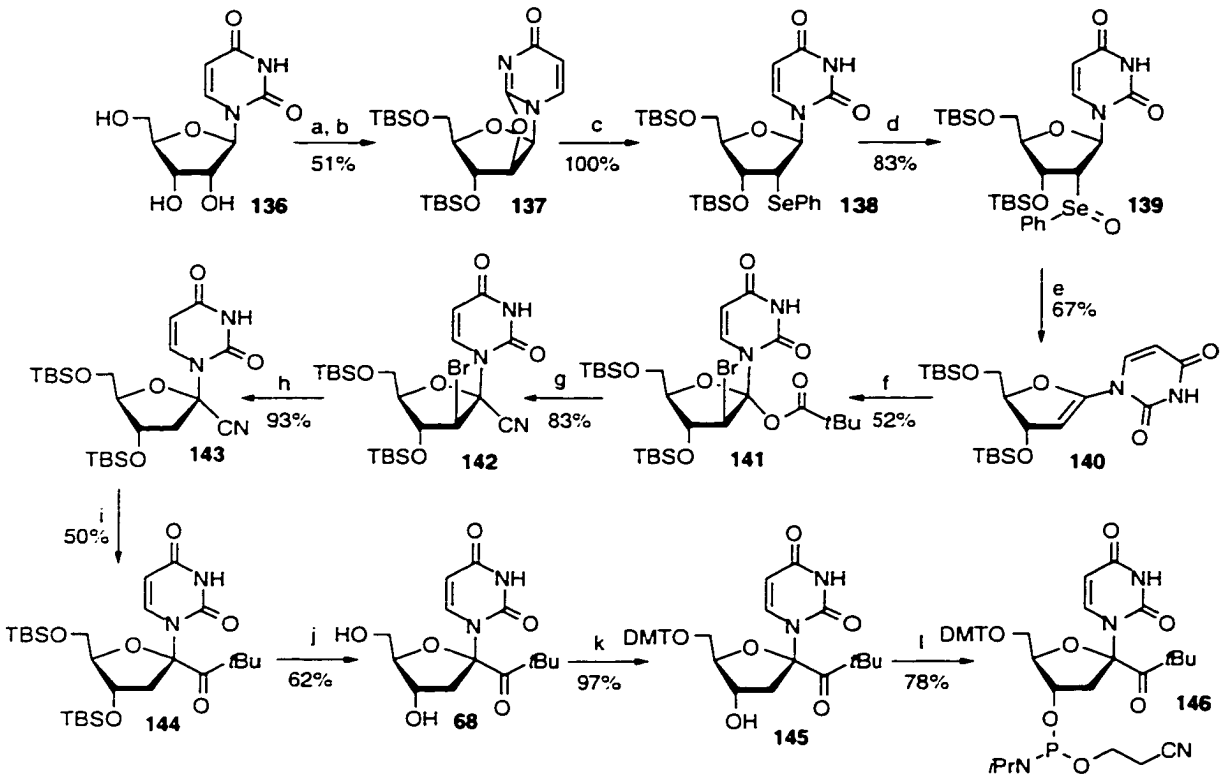

[a]Reagents: a) diphenyl carbonate, $NaHCO_3$, DMF, reflux; b) TBDMSCl, pyridine, 40 °C; c) $(PhSe)_2$, $LiAlH_4$, THF, reflux; d) *m*-CPBA, CH_2Cl_2, e) Et_3N, CH_2Cl_2; f) pivalic acid, Et_3N, NBS, ether; g) TMSCN, $SnCl_4$; h) Bu_3SnH, AIBN, benzene, reflux; i) *tert*-BuLi, THF, -78 °C, $HOAc/H_2O$; j) $Et_3N{\bullet}3HF$, THF; k) DMTCl, pyridine; l) β-cyanoethyl diisopropylchlorophosphoramidite, CH_2Cl_2.

In order to couple the various monomers to **125**, the 5'-TBS protecting group was selectively removed (Scheme 9). Robins reported a method for the quantitative selective deprotection of 5'-TBS groups for the ribonucleosides using 90% TFA/H_2O.[147] However, these conditions resulted in complete deprotection of the 2'-deoxyribonucleosides within 20 min. Consequently, alternative deprotection methods were explored. When the bis(TBS)monomer was subjected to 10% TFA in aqueous THF, the 5'-protecting group was removed on average to yield the desired compound in 50% yield. Despite the modest yields, since the deprotection was early in the synthesis, the TFA method was employed for the deprotection (Scheme 9). The monomers **147**, **148**, and **149** were synthesized from their respective bis(TBS) precursors in 58, 35, and 52% yield, respectively.

Scheme 9[a]

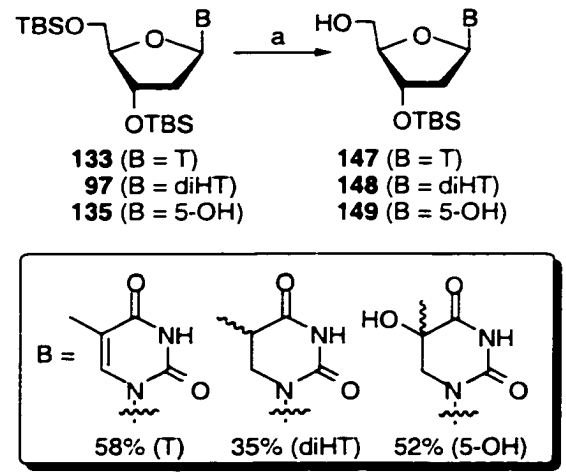

[a]Reagents: a) 10% TFA/H_2O, THF, 0 °C.

The 3'-protected monomers (**147**, **148**, and **149**) were coupled to **125** (Scheme 10) as described above (Scheme 5). The phosphate was deprotected with refluxing Et_3N,

purified by column chromatography, and passed through Dowex cation exchange resin to isolate its sodium salt.

Scheme 10[a]

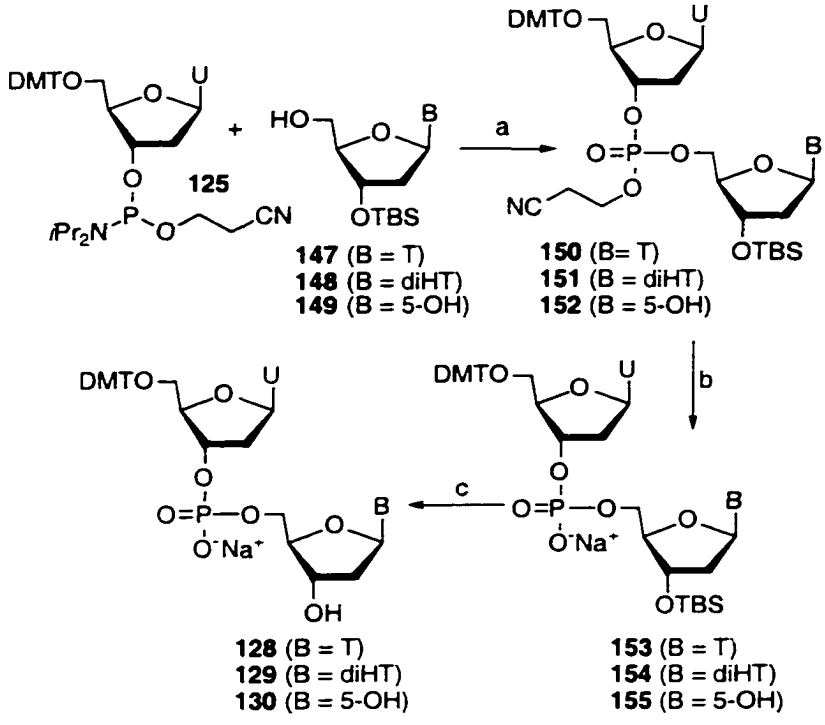

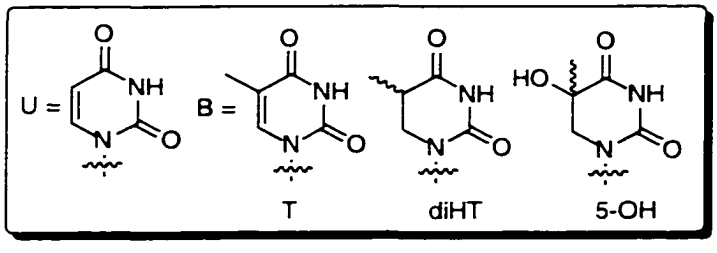

Substrate	Coupling (a)	βCE[a] Deprotection (b)	TBS[b] Deprotection (c)
147	80%	68%	51%
148	82%	70%	48%
149	74%	77%	54%

[a]βCE = β-cyanoethyl; [b]TBS = *tert*-butyldimethylsilyl

[a]Reagents: a) 0.5 M tetrazole/CH_3CN; 1.0 M I_2/2, 6-lutidine:THF:H_2O (2:2:1); b) 50% Et_3N, THF, reflux; c) Et_3N•3HF, Et_3N, THF.

As expected, desilylation of the dinucleotides was difficult. A variety of reagents (e.g. TAS-F, NH_4F, $Et_3N{\bullet}3HF$) were attempted to deprotect the 3'-alcohol. TAS-F ($[(CH_3)_2N]_3S^+$ $[(CH_3)_3F_2]Si^-$) is a neutral reagent that is compatible with acid and/or base sensitive compounds. Hence, the dinucleotides were stable to these deprotection conditions. However, contaminants from the reagent could not be removed from the product. As expected, the other reagents proved too acidic for the extremely acid labile DMT-moiety.

The most mild reagent employed was $Et_3N{\bullet}3HF$. In the presence of excess Et_3N, the substrate was stable on the timescale of the deprotection. However, work-up of the reaction proved problematic. The reaction mixture became too acidic upon concentration and resulted in detritylation. Alternatively, quenching the $Et_3N{\bullet}3HF$ with $NaHCO_3$ resulted in a poor yield, presumably due to the product being trapped in the salts. Ultimately, the $Et_3N{\bullet}3HF$ was neutralized by passing the crude reaction mixture through an anion exchange column (Amberlite). The resin contains polyamine groups which neutralize the HF without contaminating the product with salt. The products were subsequently chromatographed and passed through a cation exchange column (Dowex) to isolate them as their sodium salts.

The lactone dinucleotides (**131** and **132**) were synthesized in a similar manner as described above (Scheme 11). The ketone phosphoramidite (**146**) was coupled to a diastereomeric mixture of the 3'-protected 5,6-dihydro-5-hydroxythymidine (**149**) or 5,6-dihydrothymidine (**148**) in 63% and 71% yield, respectively. The dinucleotides (**156** and **157**) were deprotected with refluxing Et_3N to remove the β-cyanoethyl group, followed by deprotection of the TBS protecting groups with $Et_3N{\bullet}3HF$ to yield **160** and **161**. The ketone dinucleotides (**160** and **161**) were subsequently photolyzed at 350 nm in the presence of O_2 to generate **132** (3:1, *5R*:*5S*) and **131** (1.5:1, *5S*:*5R*) as a mixture of diastereomers, which proved to be stable to purification by column chromatography.

Scheme 11[a]

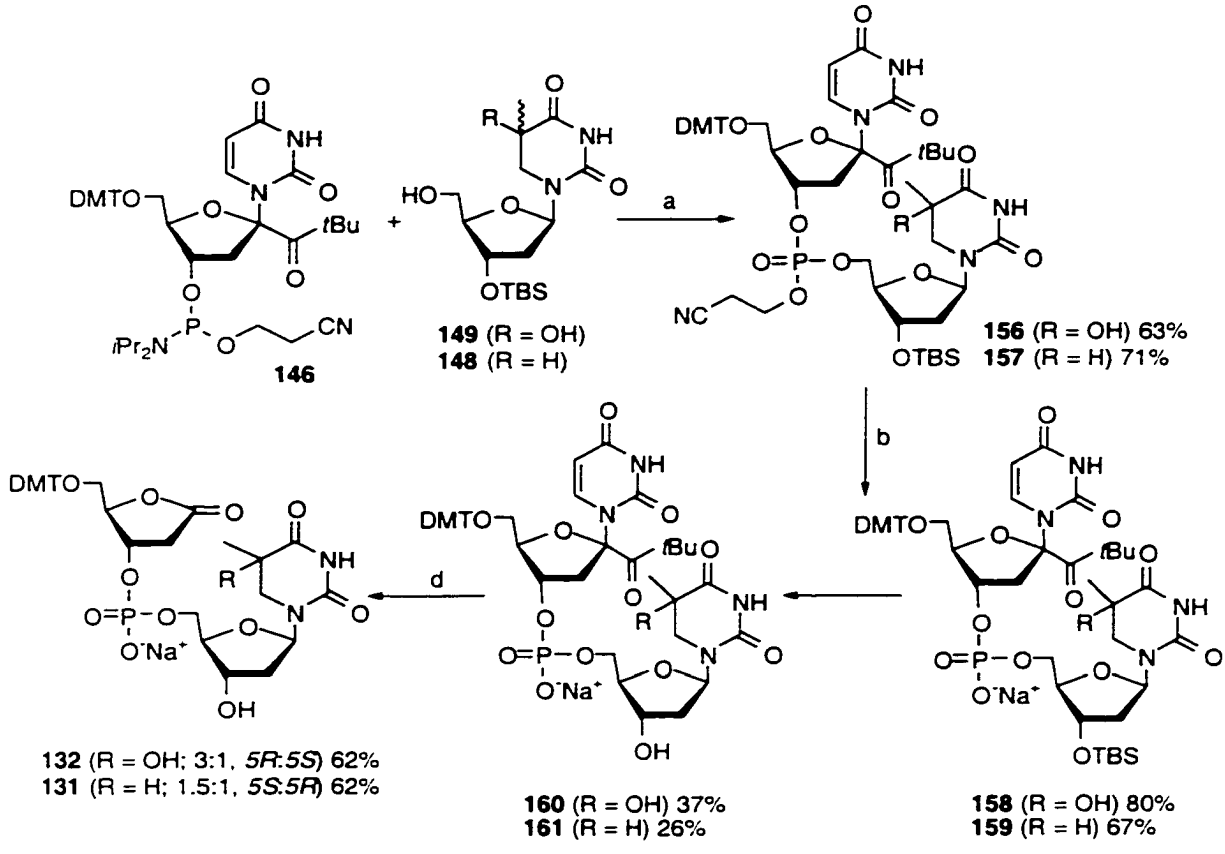

[a]Reagents: a) 0.5 M tetrazole/CH_3CN; 1.0 M I_2/2, 6-lutidine:THF:H_2O (2:2:1); b) 50% Et_3N, THF, reflux; c) $Et_3N{\cdot}3HF$, Et_3N, THF; d) hv, O_2, CH_3CN:H_2O (1:1).

3.2.3 HPLC Analysis of Product Mixtures

The product mixtures were analyzed by C8 reverse-phase HPLC to identify and quantitate the products formed upon the photolysis of the dinucleotides (**119** and **121**). In particular, since one of the issues we wished to address was the diastereoselectivity of the observed chemistry of 5,6-dihydrothymidin-5-yl (**120**), it was crucial to separate the diastereomers of each of the expected products. All of the authentic compounds could not be separated under a single set of HPLC conditions. However, by analyzing the samples

under two sets of conditions, all of the products (including their diastereomers) could be quantitated.

The samples were analyzed using a solvent gradient of NH_4HCO_2 buffer (0.2 M, pH 6.2) and MeOH or CH_3CN. The samples were first analyzed using CH_3CN as the organic solvent (Figure 66). These conditions allowed separation of *5R*-**130**, *5R*- and *5S*-**128**, **131**, and *5R*- and *5S*-**132**. However, *5S*-**130** and **129** coeluted under these conditions. In order to determine the yield of *5S*-**130** and **129**, which is the product expected if superoxide elimination occurs, the samples were analyzed with a second gradient program using MeOH as the organic cosolvent (Figure 67). These conditions resulted in coelution of *5R*- and *5S*-**130**, which were resolved from **129**. Although *5S*-**130** was now separable from **129**, both diastereomers of **128** and **132** coeluted with **129**.

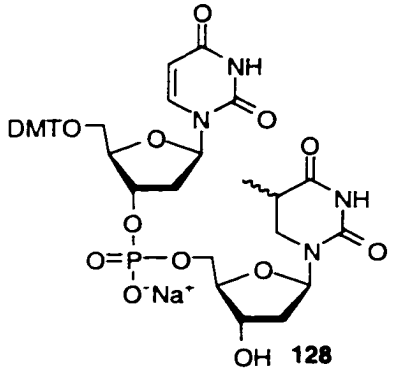

128

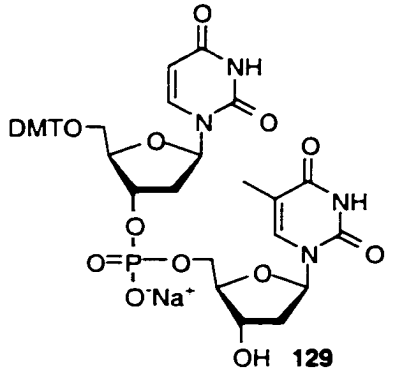

129

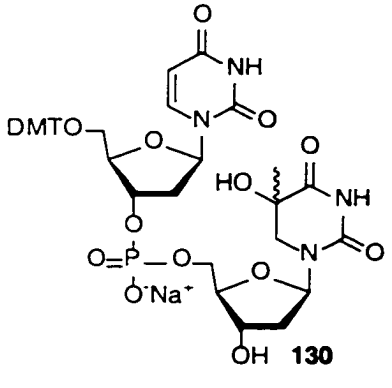

130

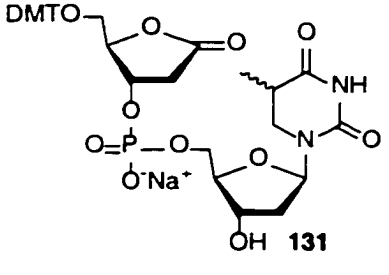

131

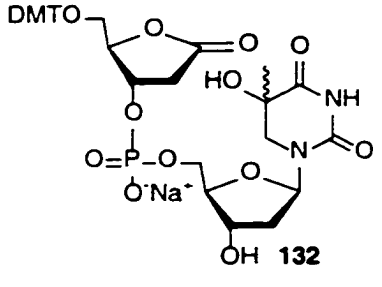

132

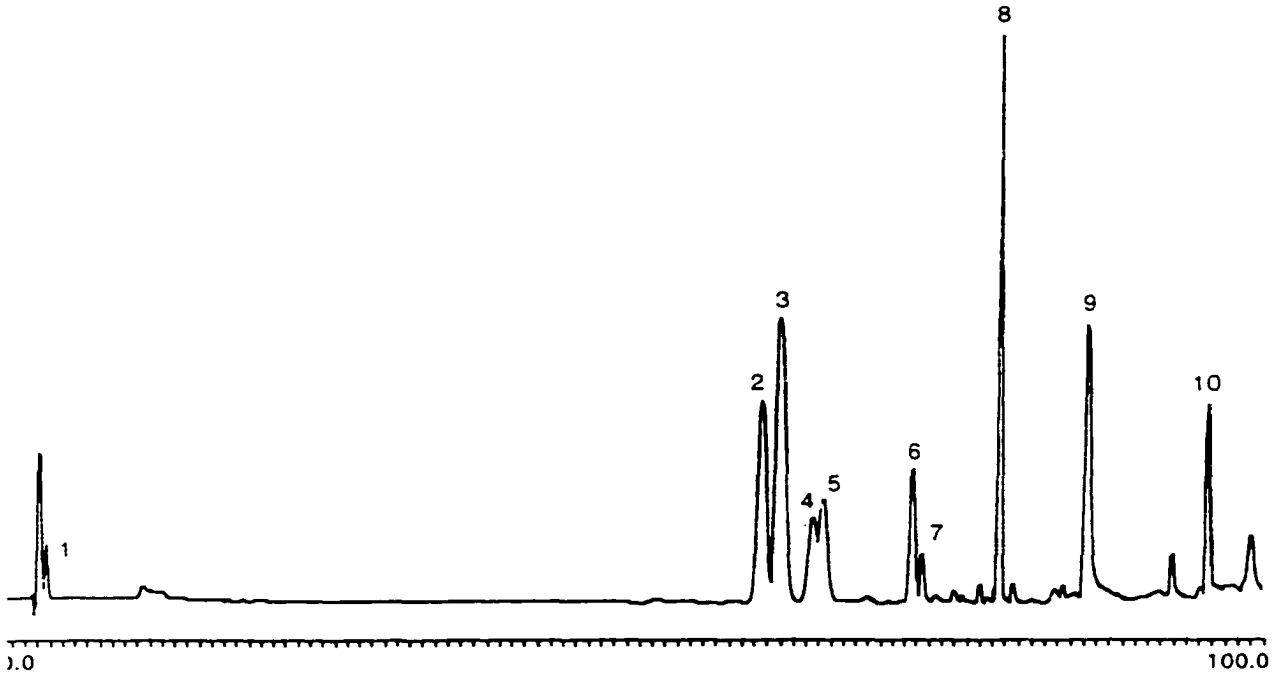

Figure 66. Sample HPLC chromatogram using a solvent gradient of NH_4HCO_2 and CH_3CN; Peaks: 1. uracil; 2. *5R*-**130**; 3. *5S*-**130**, **129**; 4. *5S*-**128**; 5. *5R*-**128**; 6. *5R*-**132**; 7. *5S*-**132**; 8. (*5R*, *5S*-**121**); 9. benzophenone; 10. **78**.

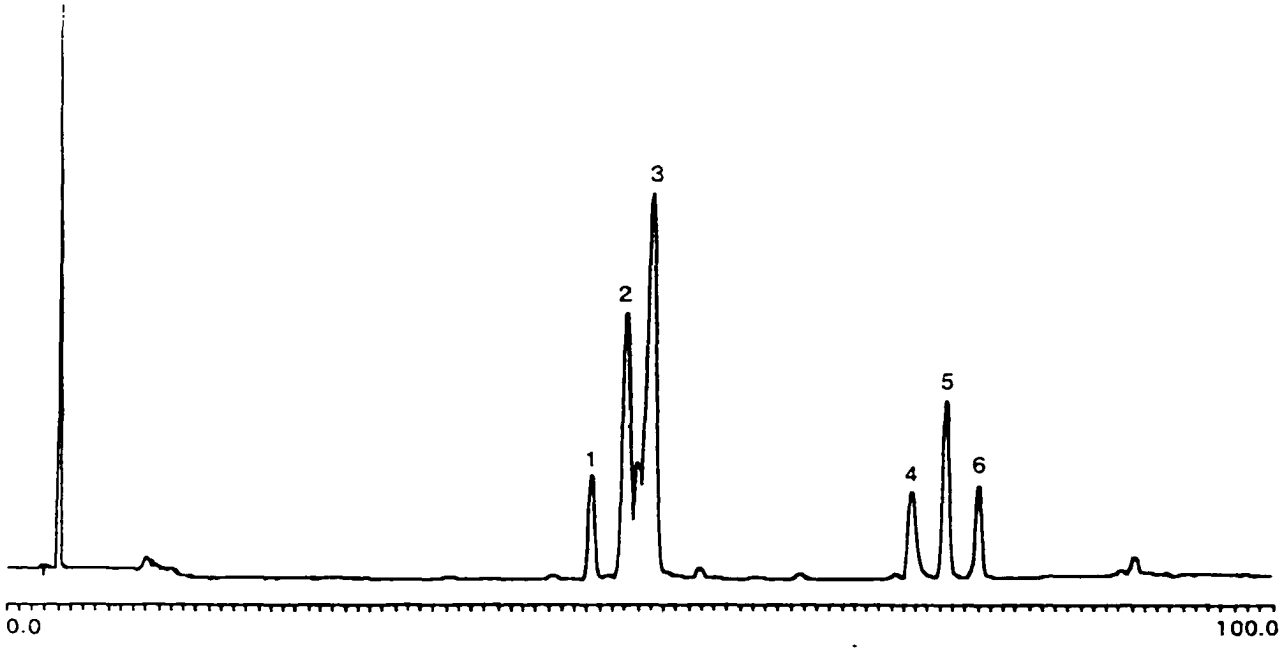

Figure 67. Sample HPLC chromatogram using a solvent gradient of NH_4HCO_2 and MeOH; Peaks: 1. benzophenone; 2. (*5R*, *5S*-**130**); 3. **129**, (*5R*, *5S*-**128**), (*5R*, *5S*-**132**); 4. **79**; 5. (*5R*, *5S*-**121**); 6. **78**.

The yields of each diastereomer of **128** and **132** were determined using the CH_3CN gradient (Figure 66). The total yield of **130** was determined from the MeOH gradient (Figure 67), whereas the yield of *5R*-**130** was obtained from analysis under the CH_3CN conditions. The amount of *5S*-**130** formed was determined by subtracting the amount of *5R*-**130** from the total yield of **130**. Once the yield of *5S*-**130** was known, it could be subtracted from the total yield of *5S*-**130** and **129** that was obtained during the analysis of the samples under the CH_3CN conditions, providing the yield of the latter dinucleotide. In addition, conversion of **121** and **119** (t_R = 78.7, 79.7 min, data not shown) and the yield of **78**, which is the product that arises from elimination of **132** (Section 3.2.7), were determined by CH_3CN analysis. The yield of **79**, the formation of which will be described later (Section 3.2.7), was obtained from the analysis under MeOH conditions.

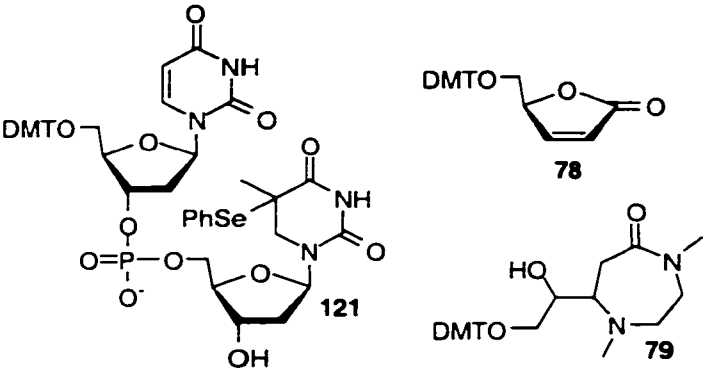

3.2.4 Photolysis of the Ketone Dinucleotide (119)

Although the photochemistry of the ketone (**94**) was complicated compared to studies utilizing the selenide (**96**) in the monomer studies (Section 3.1.5), **94** was incorporated into a dinucleotide (**119**). Since the rate constant for the proposed internucleotidyl hydrogen atom abstraction (k_{inter}) by the peroxyl radical (**163**) is unknown, the possibility that it may be fast enough to compete with the proposed intermolecular

recombination pathway (k_{rec}) was considered (Figure 68). Therefore, **119** was investigated as a potential precursor for 5,6-dihydrothymidin-5-yl (**120**).

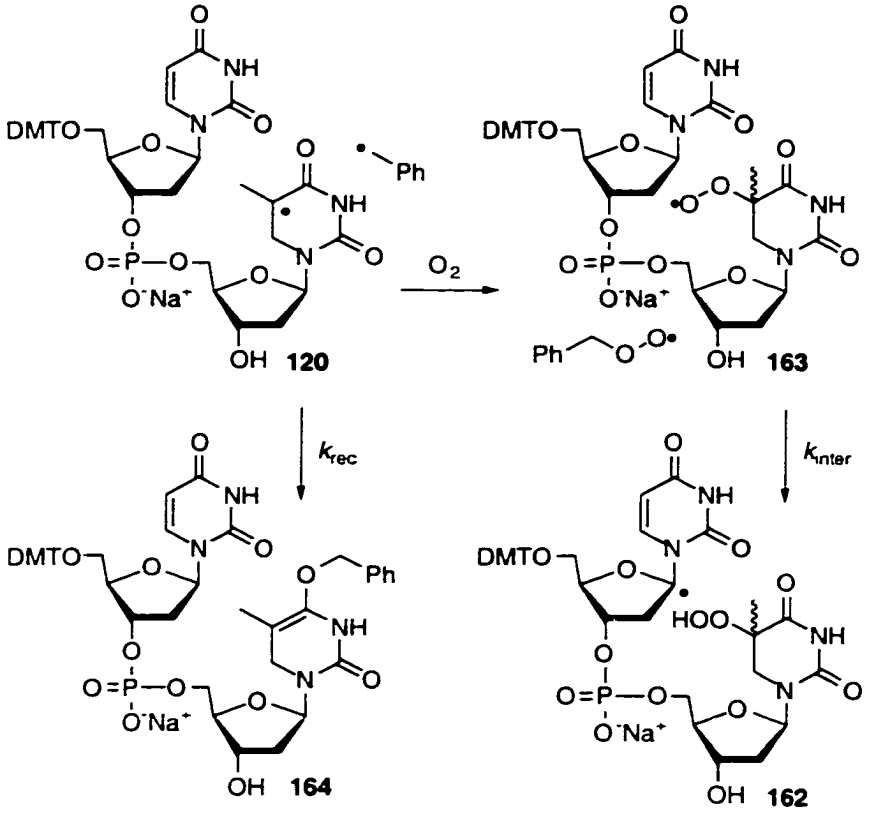

Figure 68. Internucleotidyl hydrogen atom abstraction (k_{inter}) *versus* recombination (k_{rec}).

The ketone dinucleotide (**119**) was photolyzed (λ_{max} = 350 nm) under anaerobic conditions in the presence of Bu_3SnH or βME in aqueous THF. Complete conversion of **119** was observed after 8 h and the only product formed was **128**. Given the results of the aerobic photolysis of the monomeric ketone (**94**) in the presence of Bu_3SnH (Section 3.1.5), the formation of **128** is not necessarily indicative of the intermediacy of the radical (**120**, Figure 69). The ketone dinucleotide (**119**) may undergo photoreduction in the

presence of Bu_3SnH to generate the alcohol (**165**), which may undergo a subsequent retro-aldol to generate the dU/5,6-dihydrothymidine dinucleotide (**128**).

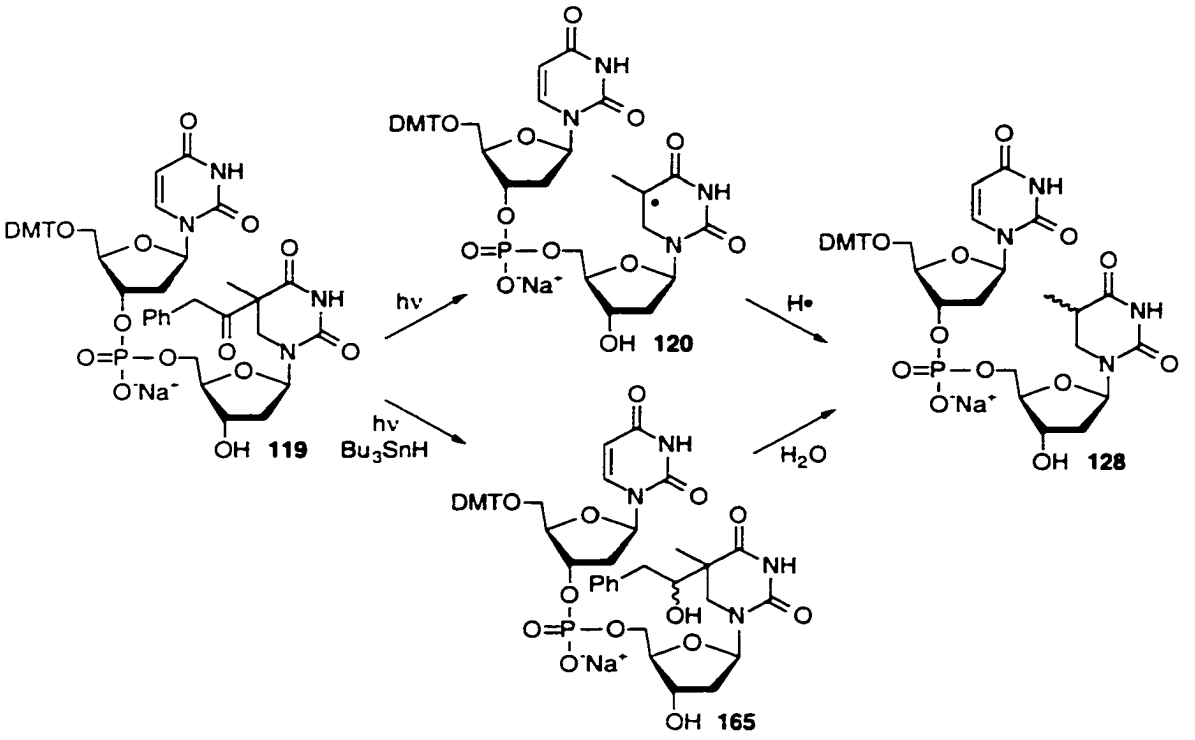

Figure 69. Photolysis of **119** under anaerobic conditions.

When **119** was photolyzed under aerobic conditions in aqueous THF in the presence of Bu_3SnH or βME, the only observed product was **130**, which can arise by reduction of the peroxyl radical (**163**) or recombination of the alkyl radicals (**164**, Figure 70). Photolysis of **119** in the absence of trap also resulted in the formation of **130**, consistent with the results obtained in the monomer studies (Section 3.1.5). The ketone dinucleotide (**119**) was also photolyzed in aqueous CH_3CN, and again the only product observed was **130**, suggesting that **130** does not arise by trapping of the peroxyl radical (**163**) by THF. Regardless of the solvent or trap used in the photolysis of the ketone

(**119**), the 2-deoxyribonolactone (**132**) was not observed. These results indicate that if internucleotidyl hydrogen atom abstraction results in the formation of 2-deoxyribonolactone (**132**), this pathway cannot compete with recombination.

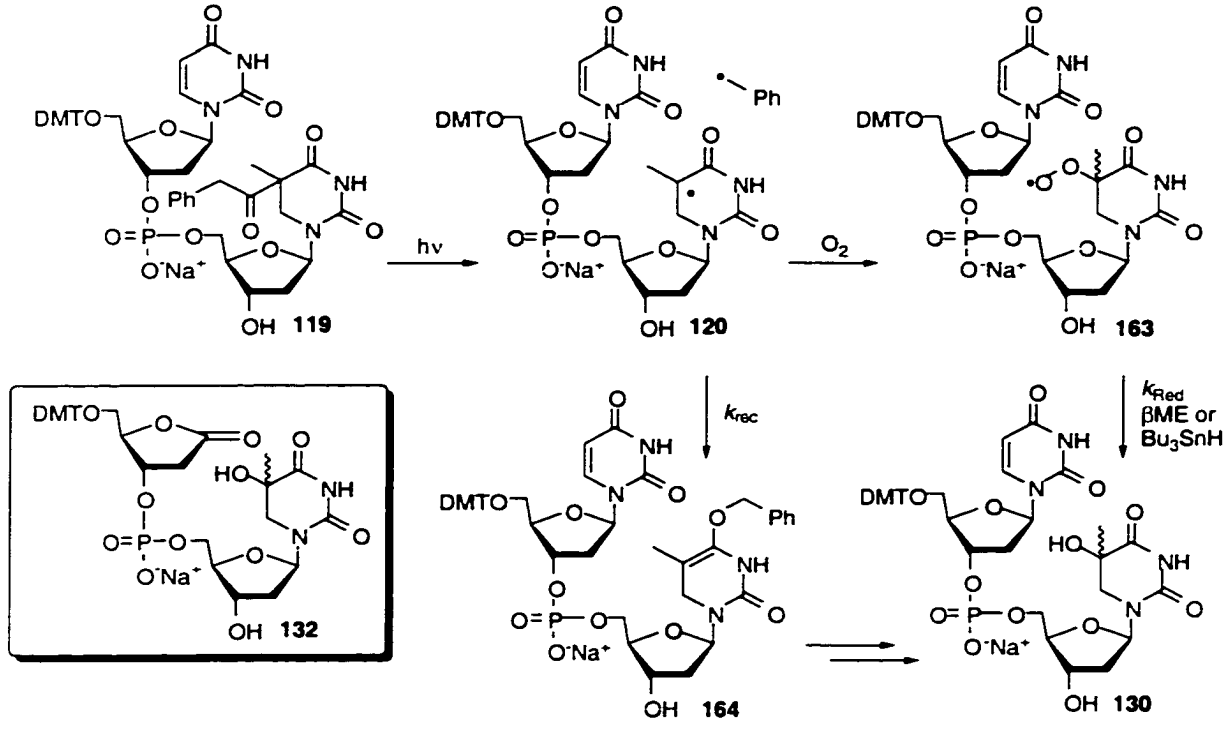

Figure 70. Formation of **130** via reduction of the peroxyl radical (**163**) or recombination.

If recombination of the peroxyl radicals is significantly faster than internucleotidyl hydrogen atom abstraction, the yield of **132**, the proposed product formed during the latter pathway, may be too low to detect by HPLC analysis. Consequently, the samples from the aerobic and anaerobic photolyses of the **119** were analyzed by ESMS. A significant amount of **130** was detected under aerobic conditions, consistent with HPLC analysis. Also, the 2-deoxyribonolactone (**132**) was not detected in the reaction mixture by this method of analysis. However, the phosphate (**166**), which could result from elimination

from **132**, was observed in the samples that were photolyzed in the presence of O_2 (Figure 71). This is not surprising given the lability of **132** to base and/or heat, and the formation of **166** was considered to be consistent with the intermediacy of **132**.

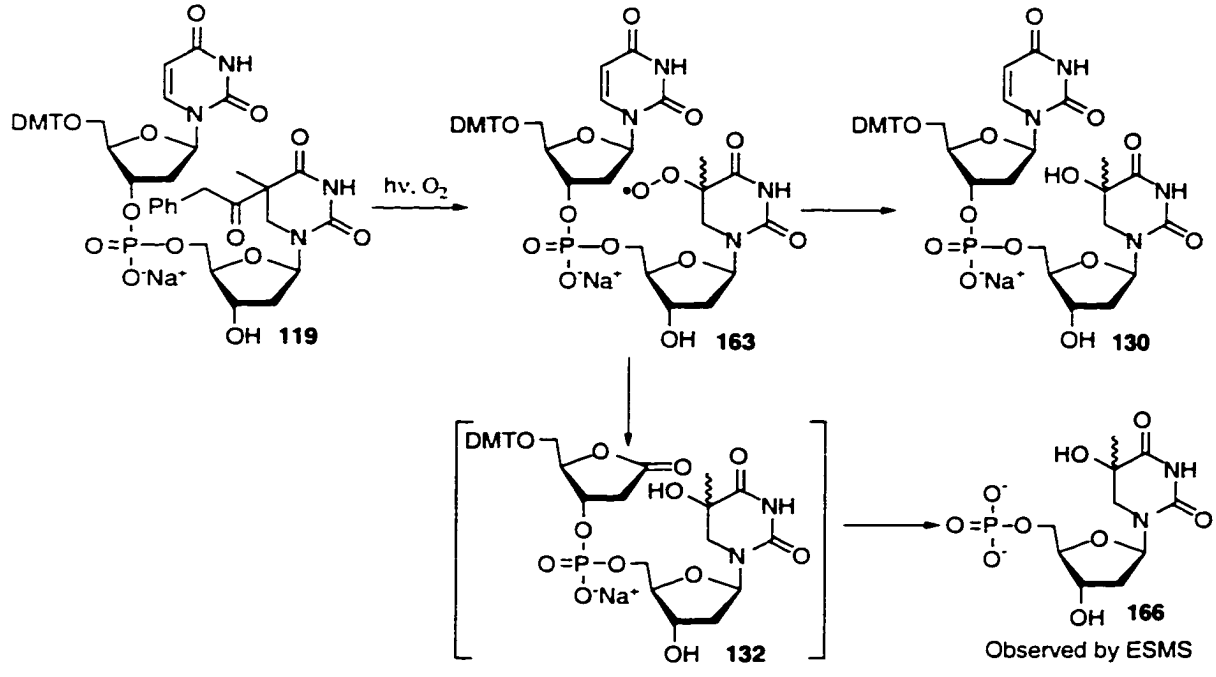

Figure 71. Products observed upon aerobic photolysis of **119**.

Although indirect evidence was obtained for the formation of **132**, which could arise via internucleotidyl hydrogen atom abstraction from the C1'-position in **163**, the Norrish Type I photocleavage of **119** produces an additional peroxyl radical that may be responsible for the hydrogen atom abstraction. To determine which peroxyl radical (**163** or the benzyl peroxyl radical) is responsible for the hydrogen atom abstraction, the aerobic photolysis of **119** was conducted under low concentrations of βME. It was anticipated that intermolecular hydrogen atom abstraction by the benzyl peroxyl radical will become less competitive in the presence of a trap, whereas the intramolecular reaction by **163** will

be affected less by the presence of βME due to the high effective molarity of the adjacent sugar. Therefore, the addition of βME should prohibit the formation of **166** if the benzyl peroxyl radical is responsible for the observed reaction. In the presence of βME, **166** was still observed, suggesting that **163** is responsible for internucleotidyl hydrogen atom abstraction from the adjacent sugar.

3.2.5 Anaerobic Photolysis of the Selenide Dinucleotide (121)

Investigation of the reactivity of 5,6-dihydrothymidin-5-yl (**4**, **120**) in ssDNA indicated that strand scission and alkaline labile lesion formation was an oxygen-dependent process.[38,39] Although strand damage was not detected under anaerobic conditions, this does not prove that hydrogen atom abstraction does not occur. It is possible that internucleotidyl hydrogen atom abstraction occurs (e.g. from the C1'-position), but that subsequent strand scission and alkaline labile lesion formation are dependent on O_2. The dinucleotide offers the possibility of probing this reaction pathway further to verify the observations made in the studies on ssDNA.

The dinucleotide (**121**) was photolyzed in the presence of Bu_3SnH under degassed conditions. Complete conversion of **121** was attained after 1 h and the only observed product was **128**, expected upon trapping of **120** by Bu_3SnH (Figure 72, Table 23). Interestingly, the dU/thymidine dinucleotide (**129**) was not observed upon photolysis of **121**. Recall that a significant amount of the analogous product, thymidine (**3**), was observed during the photolysis of the selenide monomer (**94**), and was attributed to radical cage chemistry. Only in the presence of $(Bu_3Sn)_2$ was the formation of **3** inhibited in the monomer (Section 3.1.2). In contrast, when the photolysis of **121** was carried out in the presence of βME, a significant amount of **129** was observed (Table 23). The formation of **129** in the presence of βME is consistent with inefficient radical chain propagation that results in a significant amount of disproportionation between **120** and PhSe•.

Table 23. Anaerobic photolysis of **121**.[a]

Solvent	Trap	% Yield **128**	% Yield **129**	*5S*:*5R* **128**	% Mass Balance
THF	Bu_3SnH	30 ± 5	0	2.2 ± 0.2	30 ± 5
CH_3CN	Bu_3SnH	66 ± 11	0	1.2 ± 0.1	66 ± 11
THF	βME	9 ± 1	46 ± 4	0.6 ± 0	55 ± 5
CH_3CN	βME	28 ± 3	42 ± 2	0.6 ± 0	70 ± 1

[a]The photolyses were carried out at 350 nm (λ_{max} = 350 nm, 96 watts) for 1 h with [**121**] = 0.1 mM and [trap] = 1.1 mM in THF (or CH_3CN):H_2O (1:1 by volume).

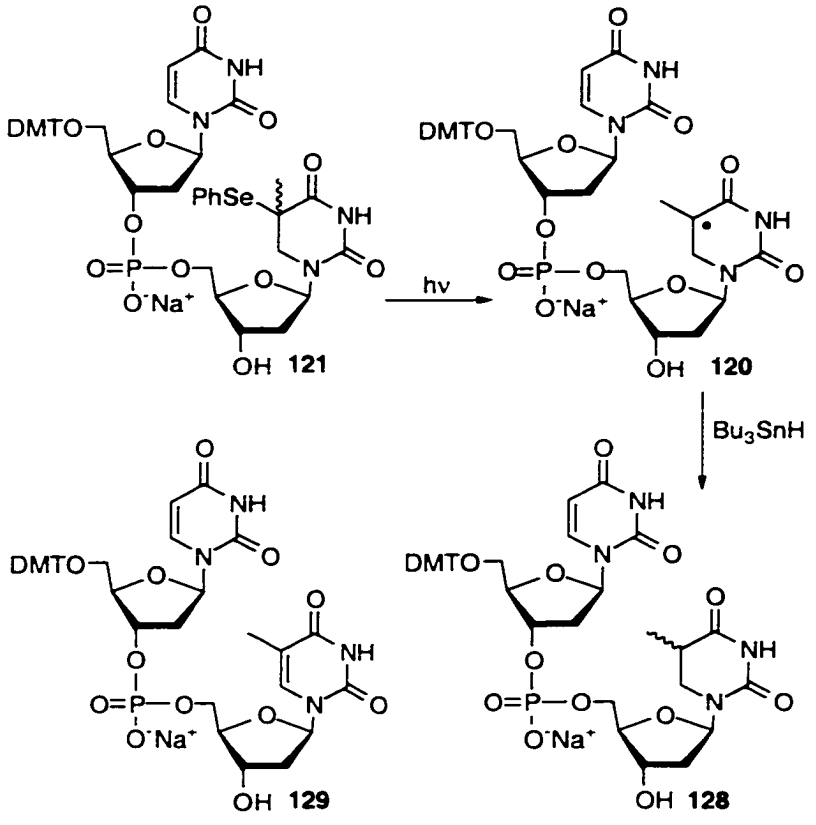

Figure 72. Products observed upon anaerobic photolysis of **121**.

The absence of **129** in the photolyses of **121** in the presence of Bu_3SnH can be explained if one assumes that the radical (**120**) is generated either by free radical chain chemistry or direct bond homolysis. In the case of the dinucleotide, the DMT moiety may compete with the phenyl selenide moiety for the light. This is evident by the longer reaction times required to achieve complete conversion of the phenyl selenide dinucleotide (**121**) than when using the monomer (**96**). Consequently, the bond homolysis pathway may become less efficient and fewer chains are initiated per given period of time, resulting in a greater proportion of the radical being generated via free radical chain chemistry in which radical cage chemistry is not an issue. The significance of this observation will become more apparent when analyzing the results from the aerobic photolysis of **121** with respect to the origin of **129** (Section 3.2.6).

Another interesting observation made upon anaerobic photolysis of **121** is the diastereoselectivity exhibited upon trapping of **120**. Recall that in the monomer studies, the photolysis of **96** under anaerobic conditions resulted in a 1:1 mixture of diastereomers of 5,6-dihydrothymidine (**34**, Section 3.1.2). However, in the dinucleotide, the ratio of diastereomers of **128** depended on the trap. When the photolysis of **121** was carried out in the presence of Bu_3SnH, the major diastereomer was *5S*-**128**, which results from trapping of the radical (**120**) from the *re* face. In the dinucleotide, one would expect that the 5'-dU moiety would partially block the *si* face of the radical (Figure 73). In order to explain the observed diastereoselectivity in the presence of βME, we suggest that this hydrogen atom donor hydrogen bonds to the nucleobases. When the βME is hydrogen bonded to the nucleobase containing the radical (**120**), the diastereotopic faces of the radical are equally accessible. However, when the βME hydrogen bonds to the uracil moiety, the hydrogen atom is delivered preferentially from the *si* face, resulting in *5R*-**128** as the major diastereomer.

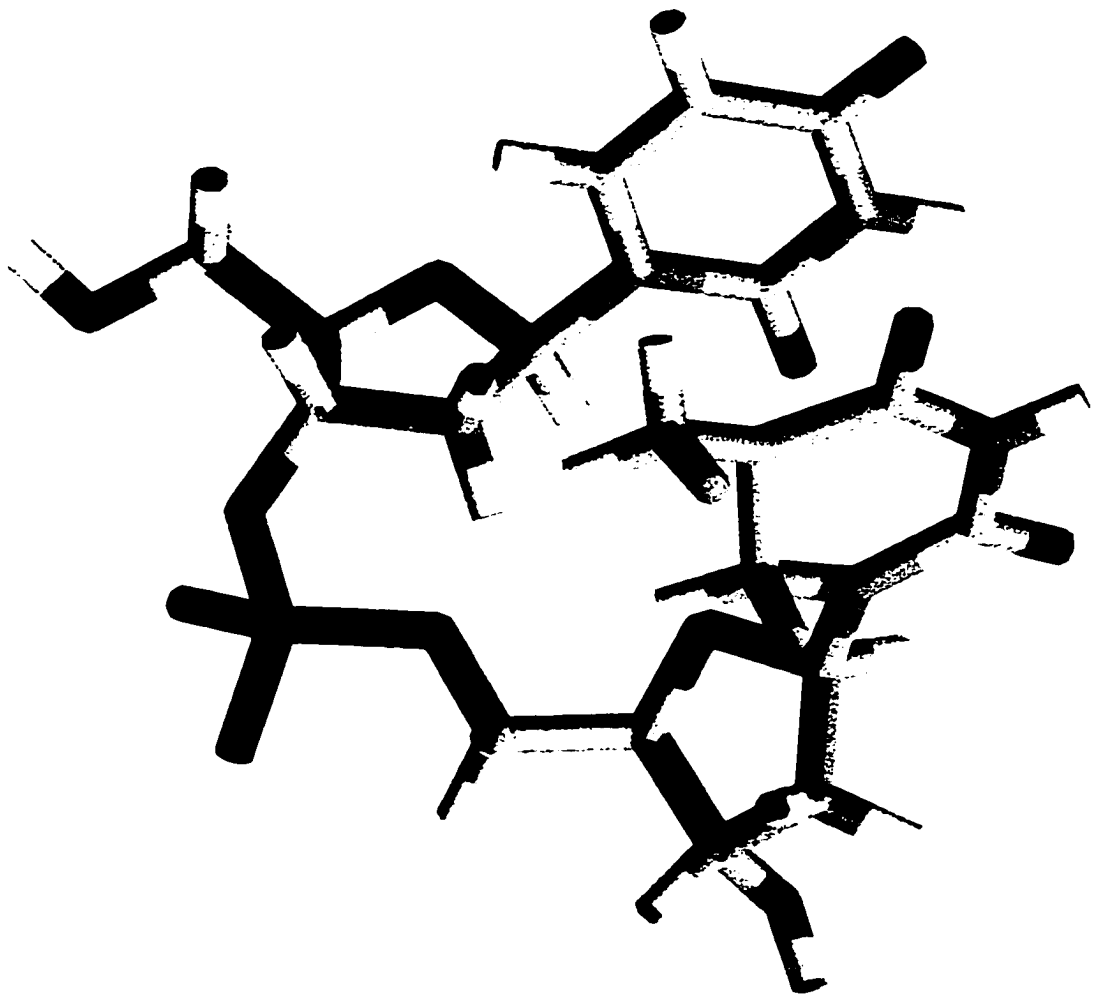

Figure 73. Model of dU/5,6-dihydrothymidin-5-yl dinucleotide (**120**).

3.2.5.1 Internucleotidyl Hydrogen Atom Abstraction by 120? Anomerization as a Mechanistic Probe.

With confirmation that the radical (**120**) is efficiently generated in the dinucleotide, the question of internucleotidyl hydrogen atom abstraction was addressed (Equation 20). The possibility exists that hydrogen atom abstraction may occur from the C1'-position, as had been proposed.[24,25] This was observed in the studies on 5-BrdU (**81**), in which it was observed that the more reactive σ radical abstracts a hydrogen atom from both the C1'- and C2'-positions, resulting in the formation of alkaline labile lesions and direct strand breaks.[73,74] Studies involving **120** in ssDNA indicated that no direct strand breaks or alkaline labile lesions are formed.[38,39] However, one cannot ignore the possibility that hydrogen atom abstraction may occur from the C1'-position, the most easily abstracted Table 2), but that subsequent strand scission and alkaline labile lesion formation is an O_2 dependent process.

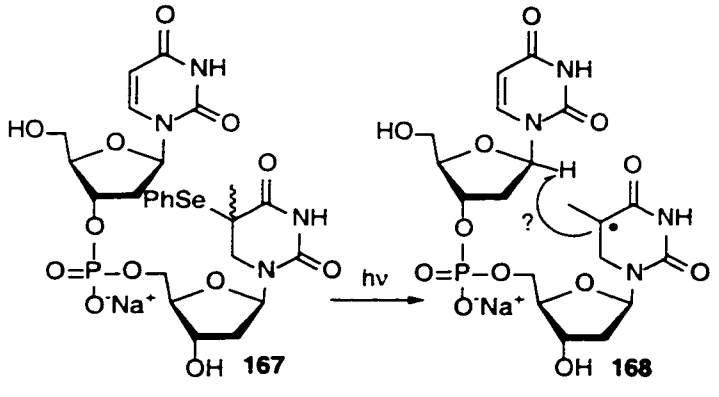

(20)

This possibility was investigated in the deprotected dinucleotide (**167**, Equation 20), which was prepared by detritylation of **121**. It has been shown that generation of the C1'-radical (**169**) results in generation of the α-anomer following reaction with thiols.[85] Therefore, if **168** participates in internucleotidyl hydrogen atom abstraction from the C1'-

position in the presence of an exogenous hydrogen atom donor (e.g. Bu_3SnH), the α-anomer should be detected (Figure 74).

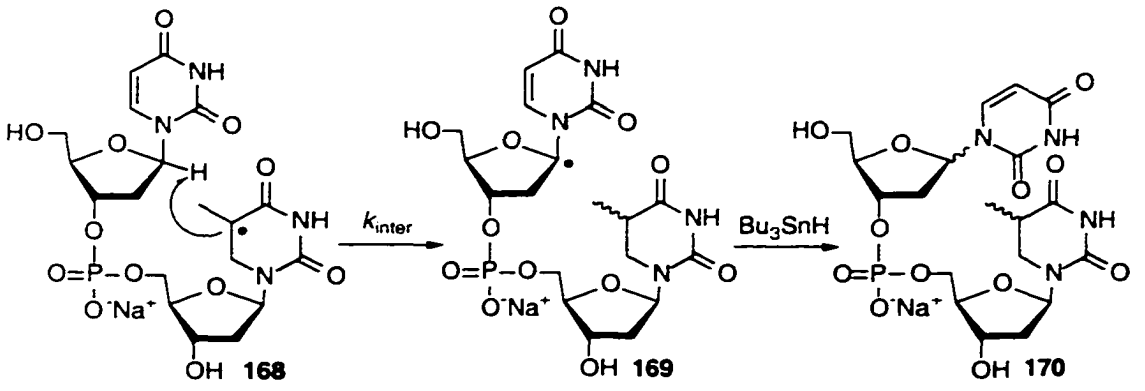

Figure 74. Anaerobic photolysis of **168** to probe for internucleotidyl hydrogen atom abstraction by **169** and subsequent anomerization.

Table 24. Anaerobic photolysis of **167**, followed by digestion, to investigate anomerization.[a]

		% Yield		%	% Mass
Bu_3SnH	dU	**3**	**34**	Conversion	Balance
-	95 ± 4	50 ± 3	18 ± 1	100 ± 0	82 ± 4
+	88 ± 6	19 ± 2	50 ± 11	100 ± 0	79 ± 8

[a] The photolyses were carried out at 350 nm (λ_{max} = 350 nm, 96 watts) for 1 h with [**167**] = 0.1 mM and [Bu_3SnH] = 1.1 mM in THF:H_2O (1:1 by volume). Upon digestion, the theoretical yield for dU and (**3** + **34**) was 0.1 mM. Therefore, the theoretical percent yield for dU and (**3** + **34**) was 100%; **3** = thymidine, **34** = 5,6-dihydrothymidine.

The photolysis of **167** was carried out in the presence and absence of Bu_3SnH under anaerobic conditions and the samples subjected to enzymatic digestion to release the nucleosides (Table 24). Analysis of the intact dinucleotides indicates that <3% of the dU/thymidine dinucleotide (**129**) was formed in the presence of Bu_3SnH. The significant

amount of thymidine (**3**) observed in the digested samples may be due to decomposition of unreacted selenide (**121**) during the digestion. Analysis of the cleaved dinucleotides indicated that only the β-anomer of dU was released during the digestion. There was no evidence for hydrogen atom abstraction from the C1'-position in the form of α-dU by the nucleobase radical (**168**). Therefore, the rate constant for internucleotidyl hydrogen atom abstraction by **168** must be < 220 s^{-1}. This is based on the following using the given rate expression (Equation 21): 1) the rate constant for trapping of the alkyl radical (**168**) by Bu_3SnH is 4 x 10^6 M^{-1} s^{-1}, 2) the ratio of β-dU:α-dU observed upon independent generation of the C1'-radical in a monomer is 3:2, and 3) the detection limit for α-dU is 2%.[85,113]

$$\frac{[\alpha\text{-dU}]}{[\beta\text{-dU}]} = \left(\frac{k_\alpha}{k_\alpha + k_\beta}\right) \frac{k_{\text{Inter}}}{k_H\,[Bu_3SnH]}$$

$$0.02 = \left(\frac{2}{5}\right) \frac{k_{\text{inter}}}{(4 \times 10^6\ M^{-1}\ s^{-1})(1.1 \times 10^{-3}\ M)} \qquad (21)$$

$$k_{\text{inter}} = 220\ s^{-1}$$

3.2.5.2 Internucleotidyl Hydrogen Atom Abstraction by 120? The Use of Tetranitromethane (TNM) as a Mechanistic Probe.

The results obtained above argue against internucleotidyl hydrogen atom abstraction by **168** (or the analogous **120**). Further evidence for this proposal was obtained by carrying out the photolysis of **121** in the presence of tetranitromethane (TNM, Figure 75). Tetranitromethane (TNM) has been utilized as an oxidant in pulse radiolysis studies.[148,149]

Since **120** is an oxidizing radical, it is not expected to undergo oxidation by TNM. However, if **171** is generated in the presence of TNM, oxidation should occur to generate the carbocation (**172**). Upon trapping by H_2O, **131** would be formed. Hence, TNM could provide an approach complementary to that using anomerization for probing internucleotidyl hydrogen atom abstraction. Although it is not expected that **120** will be oxidized by TNM, one cannot ignore the possibility of trapping the radical by TNM since alkyl radicals are known to readily react with this compound.[100,150]

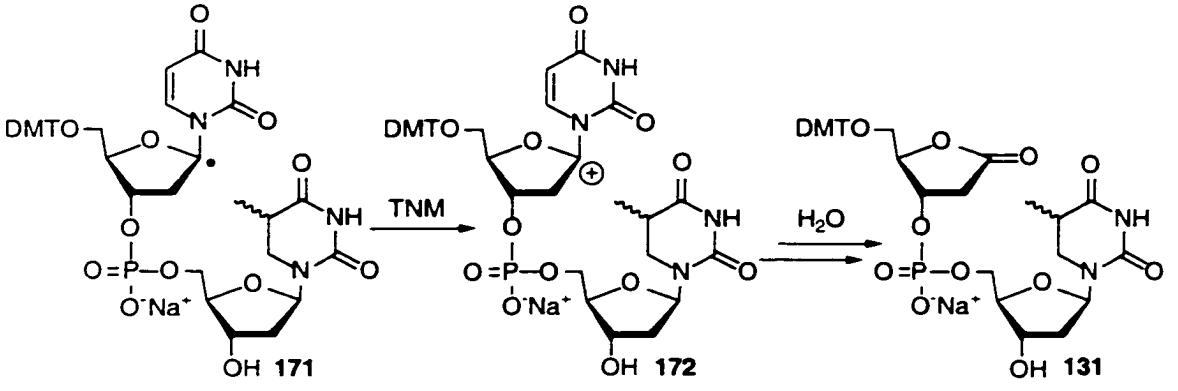

Figure 75. Oxidation of C1'-radical (**171**) by TNM.

When **121** was photolyzed in the presence of TNM, the observed products were **129** and **130** in the absence of βME (Figure 76, Table 25). The dU/5,6-dihydrothymidine dinucleotide (**128**) was also detected when the photolyses were carried out in the presence of a hydrogen atom donor. The lactone (**131**) was not observed, which is consistent with the observations of the anomerization experiment (Figure 74, Table 24). The absence of **131** in the product mixture again suggests that **120** does not participate in internucleotidyl hydrogen atom abstraction to generate the C1'-radical (**171**).

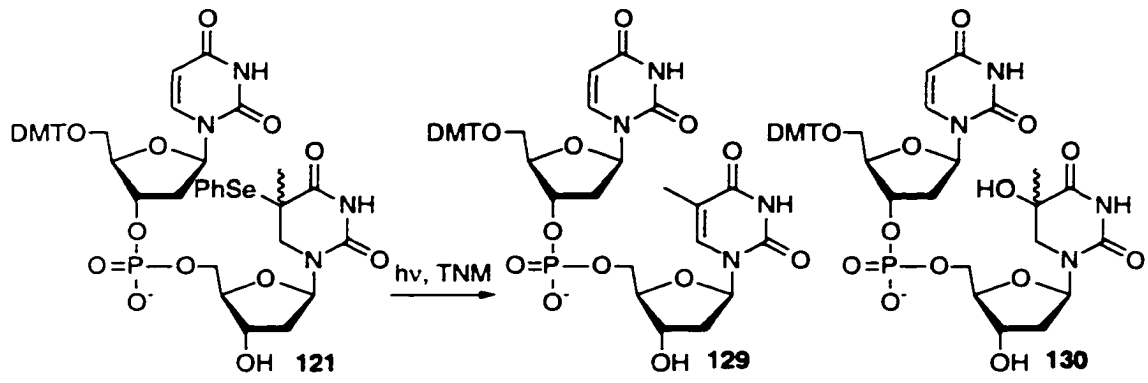

Figure 76. Observed products upon photolysis of **121** in the presence of TNM.

Table 25. Anaerobic photolysis of **121** in the presence of TNM.[a]

βME	% Yield **128**	**129**	**130**	% Conversion	% Mass Balance
-	0	30 ± 6	5 ± 0	79 ± 3	44 ± 6
+	6 ± 1	29 ± 0	6 ± 0	76 ± 4	54 ± 1

[a] The photolyses were carried out at 350 nm (λ_{max} = 350 nm, 96 watts) for 1 h with [**121**] = 0.1 mM and [βME] = 1.1 mM in CH_3CN:NH_4HCO_2 buffer (25 mM, pH 6.8; 1:1 by volume).

The dU/thymidine dinucleotide (**129**) presumably arises via disproportion between **120** and PhSe•, generated upon direct photocleavage of the C-Se bond. The presence of **130** under anaerobic conditions is an interesting result. To gain insight into the origin of **130**, the photolysis of **121** was carried out in $H_2{}^{18}O$, which showed that the ^{18}O-incorporation in **130** was 3.1 ± 2.8%. The lack of ^{18}O-incorporation in **130** indicates that **120** may be trapped by TNM (Figure 77). The covalent adduct (**172**) then decomposes to generate **130**. This experiment presents a shortcoming of using TNM in pulse radiolysis studies as an oxidant for reducing radicals due to the fact that the radical(s) may be trapped by the TNM in addition to undergoing oxidation.[148-150]

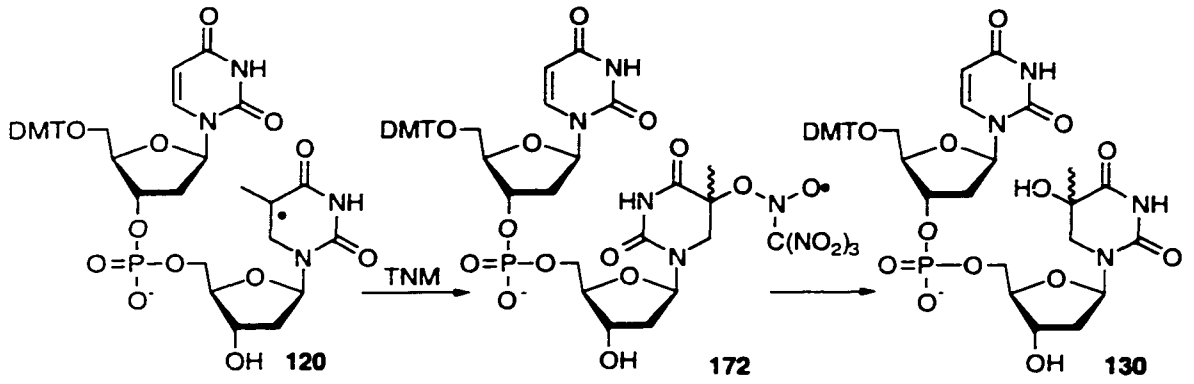

Figure 77. *Proposed reactivity between* **120** *and* TNM.

3.2.6 Aerobic Photolysis of the Selenide Dinucleotide (121)

The photolysis of the dinucleotide was carried out under aerobic conditions to verify the reported oxygen-dependent DNA damage amplification process, gain evidence for the intermediacy of the 2-deoxyribonolactone (**132**), and to determine if superoxide elimination is a competitive pathway.[38,39] As mentioned previously (Section 3.2.4), the first issue was supported by ESMS analysis of photolysates of **119** (Figure 78).

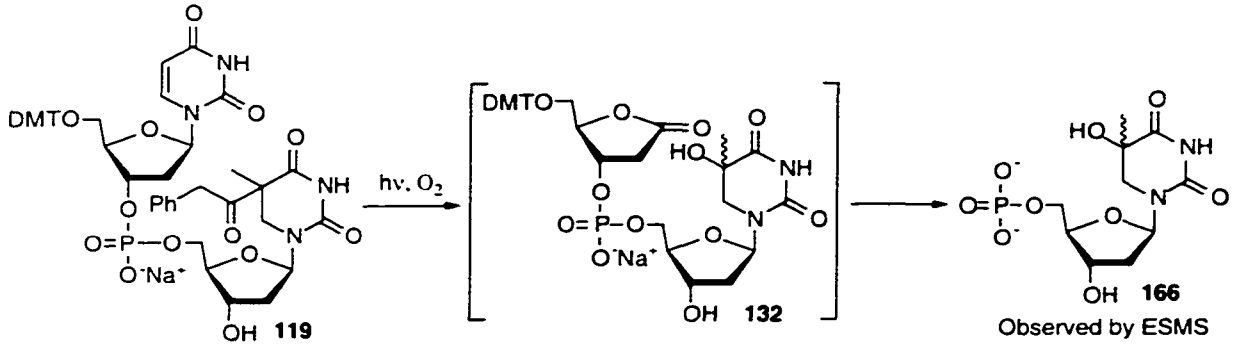

Figure 78. Formation of phosphate (**166**) upon aerobic photolysis of **119**.

Although the detection of **166** suggests that the 2-deoxyribonolactone (**132**) is formed upon the photolysis of **119**, direct evidence for this diagnostic product was

desired. The possibility of internucleotidyl hydrogen atom abstraction under aerobic conditions was further investigated utilizing the phenyl selenide dinucleotide (**121**). The photolysis of **121** was carried out under aerobic conditions in aqueous THF or CH_3CN in the presence of Bu_3SnH or βME as a hydrogen atom donor. Complete conversion of **121** upon photolysis at 350 nm was observed after 1 h (Table 26).

Table 26. Aerobic photolysis of **121**, observed products.[a]

Solvent	Trap	% Yield **128**	% Yield **129**	% Yield **130**	% Yield **132**	% Mass Balance
THF	Bu_3SnH	0	34 ± 10	26 ± 16	0.16 ± 0.01	60 ± 6
CH_3CN	Bu_3SnH	0	62 ± 4	27 ± 3	0.27 ± 0.09	87 ± 7
THF	βME	18 ± 3	22 ± 4	24 ± 12	0	63 ± 18
CH_3CN	βME	4 ± 2	28 ± 17	33 ± 3	0.1 ± 0.1	65 ± 22
THF	-	0	43 ± 6	17 ± 3	0.25 ± 0.01	60 ± 4
CH_3CN	-	0	41 ± 14	36 ± 8	0.29 ± 0.1	77 ± 8

[a] The photolyses were carried out at 350 nm (λ_{max} = 350 nm, 96 watts) for 1 h with [**121**] = 0.1 mM and [trap] = 1.1 mM in THF (or CH_3CN):H_2O (1:1 by volume).

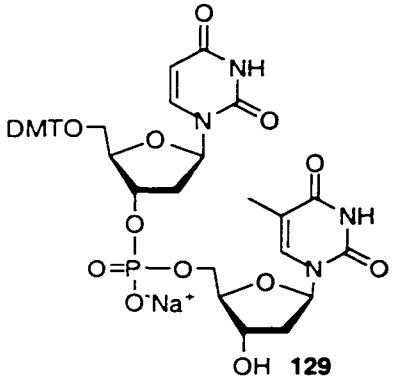

129

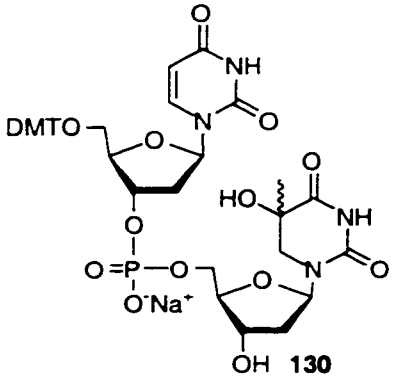

130

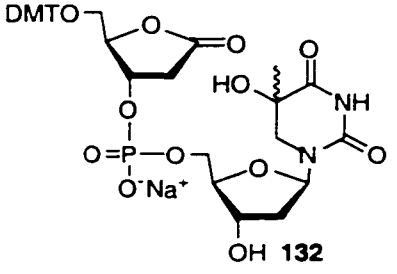

132

The major products formed upon photolysis of the phenyl selenide dinucleotide (**121**) are **129** and **130**, which arise from the intermediate peroxyl radical (**163**, Figure

79). The ratio of **129**:**130** in the photolyses carried out in the presence of Bu_3SnH in aqueous THF was ≈1.3, which is considerably lower than the ratio of the analogous products observed in the monomer studies (≈12, Section 3.1.14.3). Although the dinucleotide and monomer studies were both carried out in aqueous THF, the dinucleotide was photolyzed in 1:1 THF:H_2O, whereas the monomer studies were carried out in 19:1 THF:H_2O. The higher yield of **130** in the dinucleotide studies may be a reflection of the increased rates of hydrogen atom donation in more polar solvents.[151] We also cannot rule out a solvent effect of the elimination reaction (k_{Elim}).

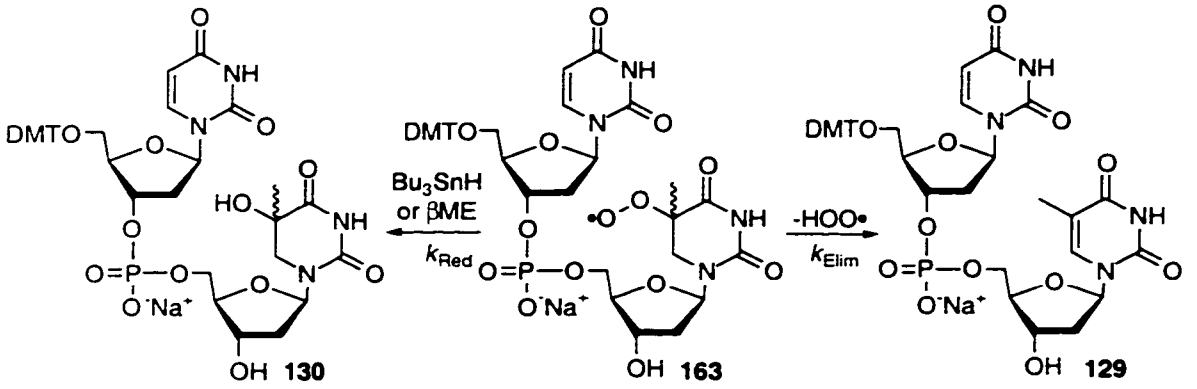

Figure 79. Intranucleotidyl pathways available to the peroxyl radical (**163**).

The dU/5,6-dihydro-5-hydroxythymidine (**130**) is generated upon reduction of **163**, whereas **129** arises from elimination of superoxide. Recall that under anaerobic conditions in the presence of Bu_3SnH, **129** was not observed upon photolysis of **121** (Section 3.2.5), suggesting that this product arises solely from superoxide elimination. One may argue that the presence of O_2 inhibits free radical chain chemistry, resulting in more disproportionation between **120** and PhSe• to generate **129**. However, when the photolyses of **121** were carried out in the presence of Bu_3SnH and $(Bu_3Sn)_2$ (0.2 mM) to ensure efficient chain propagation, the yield of **129** did not change. This supports the

proposal that **129** arises solely from superoxide elimination. The formation of **129** and **130** enabled us to estimate the rate constant for internucleotidyl hydrogen atom abstraction by competitive kinetics. If the assumption that **129** arises solely from superoxide elimination is inaccurate, then the rate constant based on the formation of **130** can be used for comparison purposes. The rate constant for superoxide elimination was estimated in the monomer studies (Section 3.1.14.3), and the rate constant for trapping of the peroxyl radical (**163**) by Bu_3SnH is known.[140]

The formation of **130** is useful for estimating the rate constant for internucleotidyl hydrogen atom abstraction, but more interesting is the dependence of the ratio of diastereomers on the trap present during the photolysis (Table 27). When the photolysis was carried out in the presence of Bu_3SnH, the major diastereomer was *5R*-**130**, as expected for trapping of the peroxyl radical (**163**) from the *re* face. This is consistent with the observations made for the anaerobic photolysis of the dinucleotide, in which the radical (**120**) was also trapped from the *re* face (Section 3.2.5) in the presence of Bu_3SnH.

Table 27. Aerobic photolysis of **121**, observed diastereoselectivity of **130** and **132**.[a]

Solvent	Trap	*5S:5R*-**130**	*5S:5R*-**132**
THF	Bu_3SnH	0.48 ± 0.40	nd
CH_3CN	Bu_3SnH	0.63 ± 0.04	6.3 ± 1.8
THF	βME	3.5 ± 2.7	nd
CH_3CN	βME	2.4 ± 1.3	6.4
THF	-	0.57 ± 0.20	1.7 ± 0.1
CH_3CN	-	1.3 ± 0.6	4.9 ± 1.2

[a]The photolyses were carried out at 350 nm (λ_{max} = 350 nm, 84 watts) for 1 h with [**121**] = 0.1 mM and [trap] = 1.1 mM in THF (or CH_3CN):H_2O (1:1 by volume).

The observed preference for formation of the *5R*-diastereomer of **130** may arise from selective O_2 trapping of the radical (**120**) or selective trapping of the resultant peroxyl radical (**163**) by Bu_3SnH. Given the higher reactivity of O_2 with alkyl radicals (2×10^9 M^{-1} s^{-1}), it is not likely that the formation of **163** proceeds with high diastereoselectivity.[26] We propose that the 5'-moiety of the dinucleotide partially blocks the *si* face, resulting in preferential trapping of the peroxyl radical (**163**) by Bu_3SnH from the *re* face. This explanation is consistent with the results of the monomer studies, in which either face of the peroxyl radical (**7**) is readily accessible and the diastereomeric ratio of the analogous product (**8**) was ≈1:1 (Section 3.1.5).

When the photolysis of the dinucleotide was carried out in the presence of βME, the major product was *5S*-**130**, which is consistent with trapping of the peroxyl radical (**163**) from the *si* face. This observation is consistent with the diastereoselectivity observed for trapping of the nucleobase radical (**120**) by βME (Section 3.2.5). Recall that this observation was explained by hydrogen bonding of the βME to the nucleobase (Figure 80).

When the βME is hydrogen bonded to the nucleobase containing the peroxyl radical (**163**), the diastereotopic faces are equally accessible. However, when the βME is hydrogen bonded to the uracil moiety, the hydrogen atom is delivered preferentially from the *si* face, resulting in *5S*-**130** as the major diastereomer (Figure 80). The observed diastereomeric ratio of **130** (0.9 ± 0.1) in aqueous CH_3CN when *tert*-BuSH, which is not expected to hydrogen bond to the dinucleotide, was used as the hydrogen atom donor supports this explanation. The presence of **128** in the aerobic photolyses is also consistent with the ability of βME to hydrogen bond to the dinucleotide, in which trapping of the nucleobase radical (**120**) by βME becomes competitive with trapping by O_2 due to its higher effective concentration.

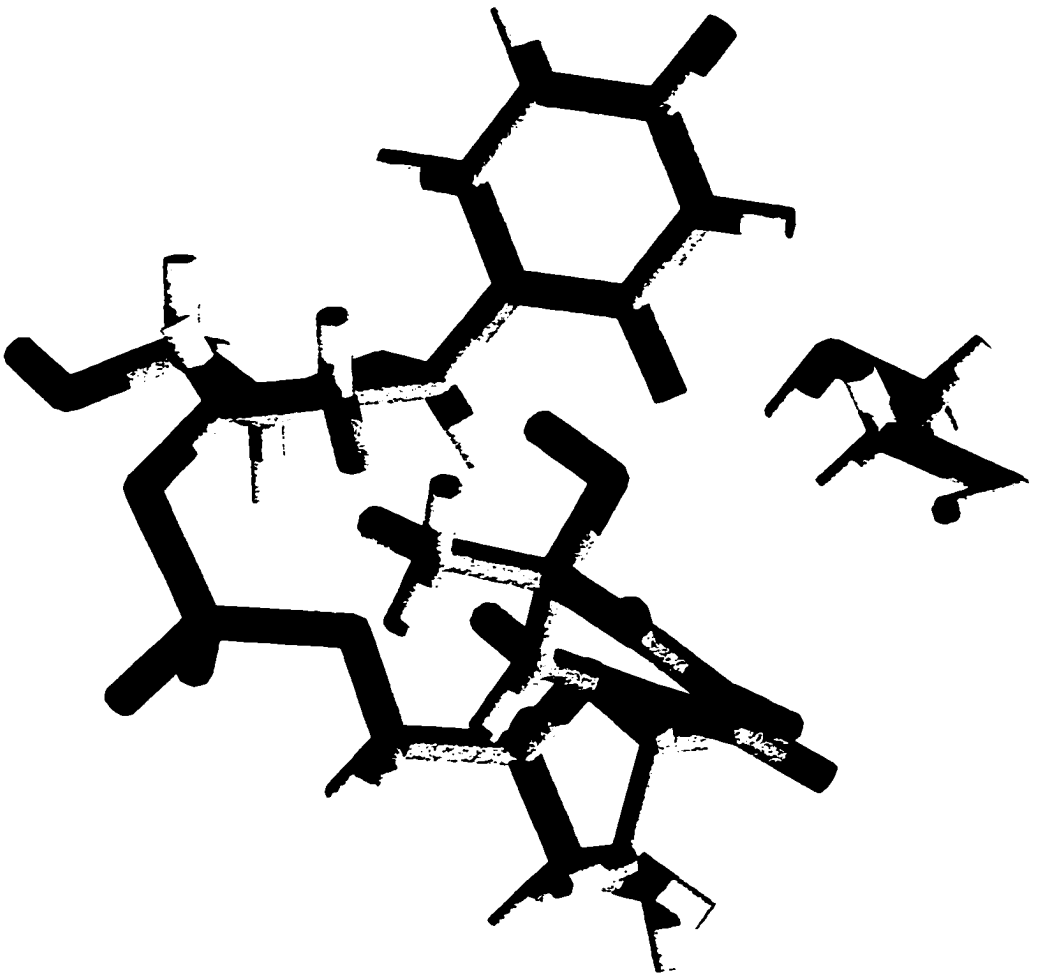

Figure 80. Model of the peroxyl radical (**163**) with βME hydrogen bonded to the nucleobase.

The most interesting product observed upon photolysis of **121** was the 2-deoxyribonolactone lesion (**132**), which was proposed to be involved in DNA damage amplification involving the peroxyl radical (**163**, Figure 81).[38,39] This is the first direct evidence for the formation of **132** upon internucleotidyl hydrogen atom abstraction by the peroxyl radical (**163**).

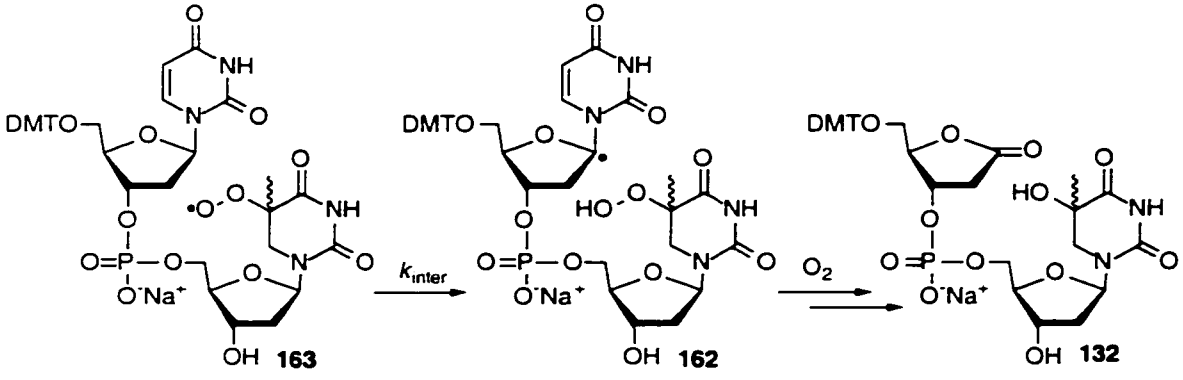

Figure 81. Formation of 2-deoxyribonolactone (**132**) upon internucleotidyl hydrogen atom abstraction by the peroxyl radical (**163**).

Since the yield of **132** was so low, the possibility that its formation was an artifact and was attributable to another reactive species (e.g. HO•-mediated generation of the C1'-radical) was investigated. Recall that the formation of the dU/thymidine dinucleotide (**129**) was a result of superoxide elimination. Under the reaction conditions, the HOO• release from the nucleobase will dissociate to $O_2^{\bullet-}$. Although precautions were taken to eliminate metal ions in the reaction, one cannot rule out the presence of trace metals. Therefore, it is possible that the HO• is generated in the photolysis of the dinucleotides. The HO• has been shown to preferentially react with the nucleobase, but a small amount does react with the sugar by hydrogen atom abstraction.[1]

Carbohydrates, such as mannitol, are commonly used to scavenge HO•.[1] If the photolysis of the dinucleotide was carried out in the presence of mannitol, any damage induced by the presence of HO• will be diminished. However, the yield of **132** (0.16 ± 0.01%, see Table 26 for conditions) was independent of mannitol (1.1 mM), indicating that the formation of the C1'-radical is not due to hydrogen atom abstraction by HO•.

Interestingly, the internucleotidyl hydrogen atom abstraction by **163** is a diastereoselective process. The *5S*-2-deoxyribonolactone dinucleotide (*5S*-**132**) was generated preferentially over *5R*-**132** (Figure 82). This is in agreement with models of the peroxyl radical (**163**) that suggest *5S*-**163** (Figure 83) is better positioned to reach the C1'-hydrogen atom of the adjacent sugar, whereas *5R*-**132** (Figure 84) is directed away from the sugar.

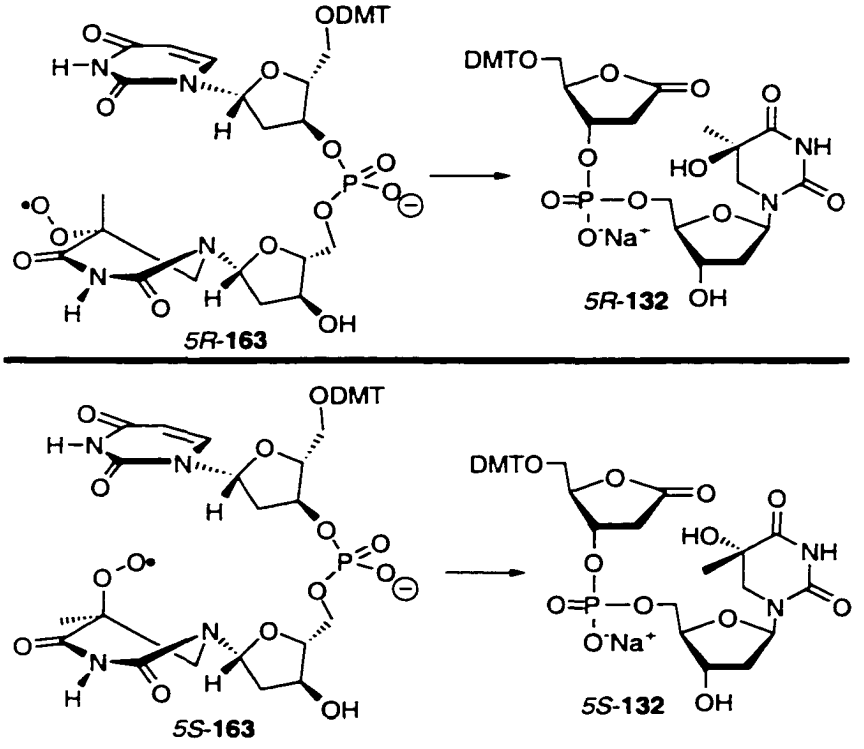

Figure 82. Diastereoselective internucleotidyl hydrogen atom abstraction by **163**.

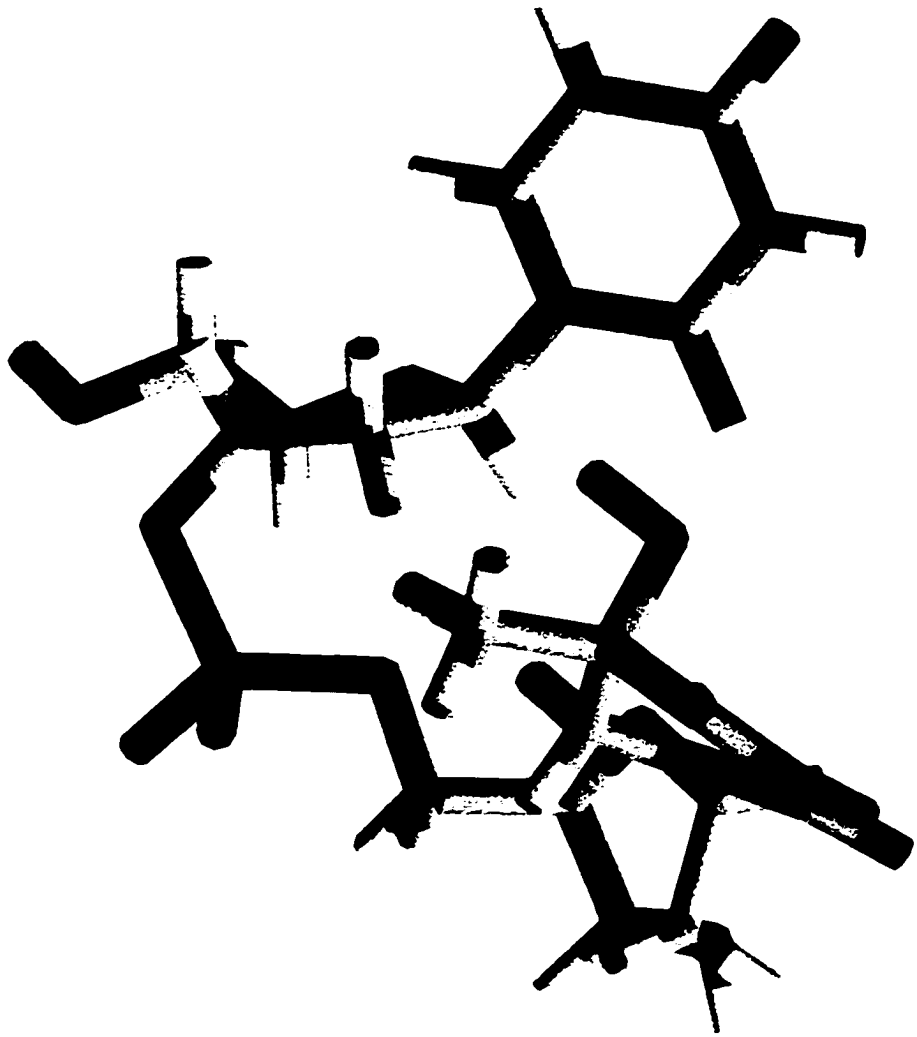

Figure 83. Model of *5S*-**163.**

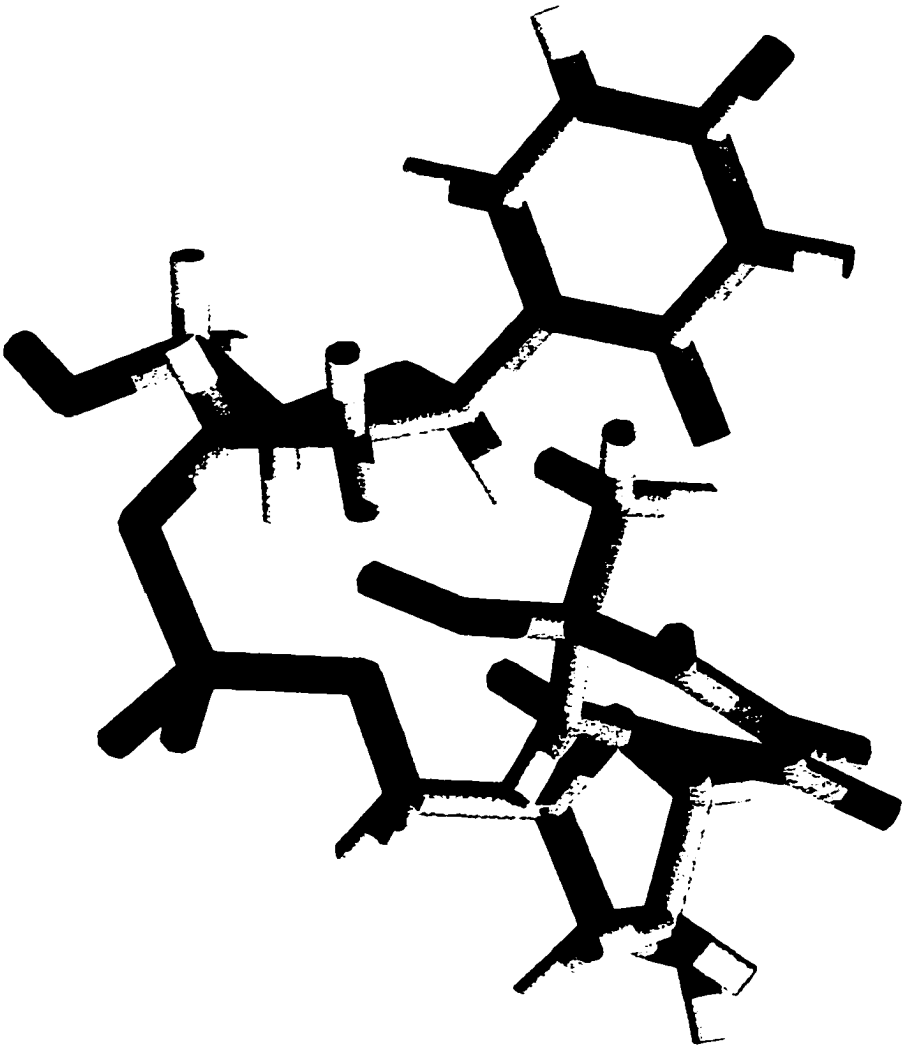

Figure 84. Model of *5R*-**163**.

The peroxyl radical (**163**) partitions itself among internucleotidyl hydrogen atom abstraction (k_{inter}), intermolecular hydrogen atom abstraction (k_{Red}), and superoxide elimination (k_{Elim}, Figure 85). The rate constant for internucleotidyl hydrogen atom abstraction (k_{inter}) was calculated using either the ratio of **129**:**132** or **130**:**132**, which correlate to k_{Elim}/k_{inter} and k_{Red}/k_{inter}, respectively (Table 26). Since the rate constant for superoxide elimination (k_{Elim}) is known from the monomer studies (21 s^{-1}, Section 3.1.14.3) and the formation of **129** in the presence of Bu_3SnH is believed to be due solely to superoxide elimination, the rate constant for internucleotidyl hydrogen atom abstraction (k_{inter}) was estimated at 0.1 s^{-1}.

In addition, the rate constant (k_{inter}) was calculated using the ratio of **130**:**132** since the rate constants for the trapping of peroxyl radicals by Bu_3SnH and βME are known ($k_{Red(Bu_3SnH)}$ = 1.6 x 10^3 M^{-1} s^{-1}, $k_{Red(\beta ME)}$ = 5 x 10^3 M^{-1} s^{-1}).[67,140] The rate constant for internucleotidyl hydrogen atom abstraction (k_{inter}) was estimated as 0.018 s^{-1} using the ratio of **130**:**132** observed in photolyses carried out in CH_3CN in the presence of Bu_3SnH (Table 26). The calculated rate constant (k_{inter} = 0.017 s^{-1}) using the data from the photolyses carried out in βME is in close agreement.

The rate constant calculated for internucleotidyl hydrogen atom abstraction by the peroxyl radical (**163**) is reasonable based on literature values for the analogous reaction. For example, *tert*-BuOO• abstracts a hydrogen atom from THF, which may be a simple model for deoxyribose, with a rate constant of 0.085 M^{-1} s^{-1}.[152] In addition, hydrogen atom abstraction by *tert*-BuOO• from cumene has recently been measured and has a rate constant of 0.74 M^{-1} s^{-1}.[153] Comparison of the first-order rate constant obtained in the dinucleotide studies (k_{inter}) to the bimolecular rate constant for the reaction of *tert*-BuOO• with THF suggests that the effective molarity of the sugar in the dinucleotide is 0.2-1.2 M. Since one would anticipate that the bimolecular rate constant (0.085 M^{-1} s^{-1}) is a lower limit for the analogous reaction with the sugar moiety, the effective molarity of the sugar in the

dinucleotide may be overestimated. On the other hand, since the dinucleotide is less ordered than DNA, the effective molarity of the sugar in DNA may be higher.

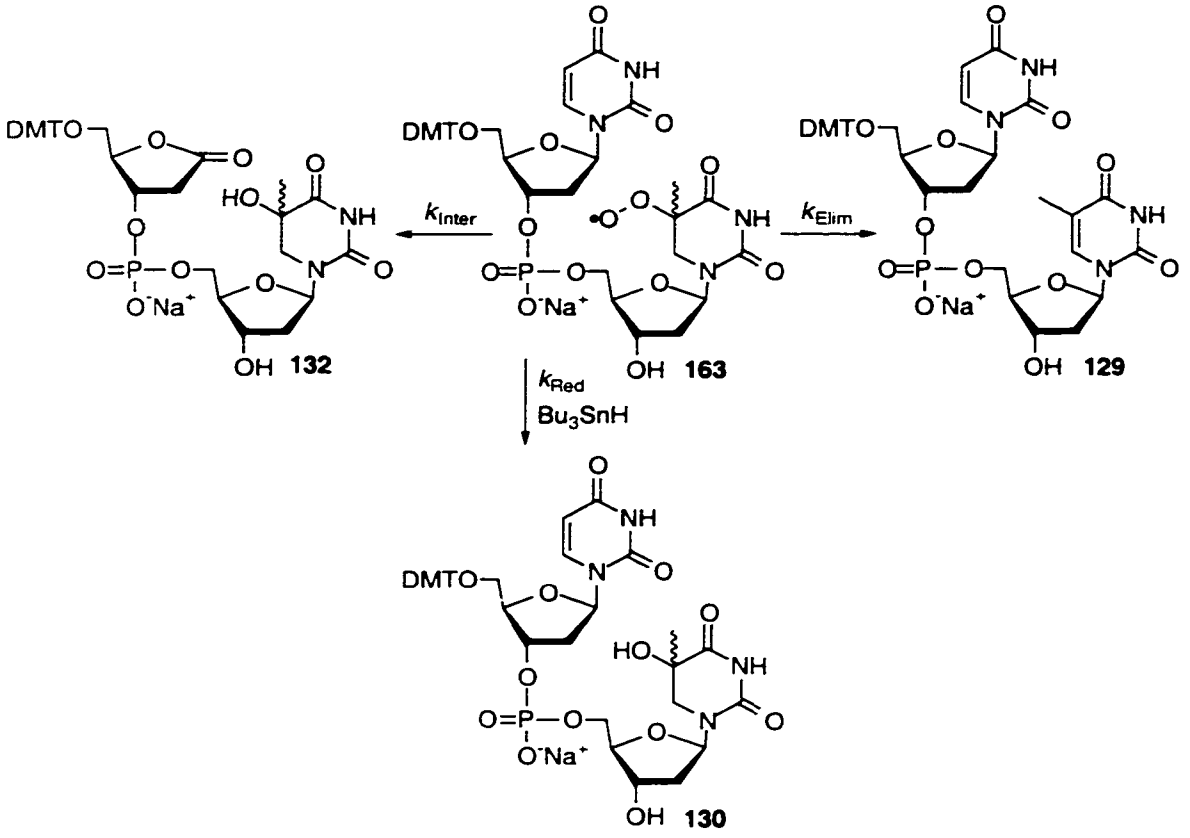

Figure 85. Internucleotidyl *versus* intranucleotidyl chemistry available to the peroxyl radical (**163**).

3.2.7 Reactivity of 2-Deoxyribonolactone

In addition to the importance of obtaining direct evidence for the formation of **61**, its subsequent reactivity is of interest. It is known that the 2-deoxyribonolactone lesioin (**61**) is extremely labile, and is suspected to undergo elimination to yield the the α,β-unsaturated lactone (**64**, Figure 86).[101] The lability of this compound (**64**) has made it

difficult to isolate in DNA since it readily undergoes a second elimination to liberate the methylenefuranone (**67**). In the dinucleotide (**132**), however, elimination of the DMT-moiety is not likely to occur. Therefore, the stability of **64** (and the analogous **78**) could be investigated, which may provide insight into its reactivity in DNA.

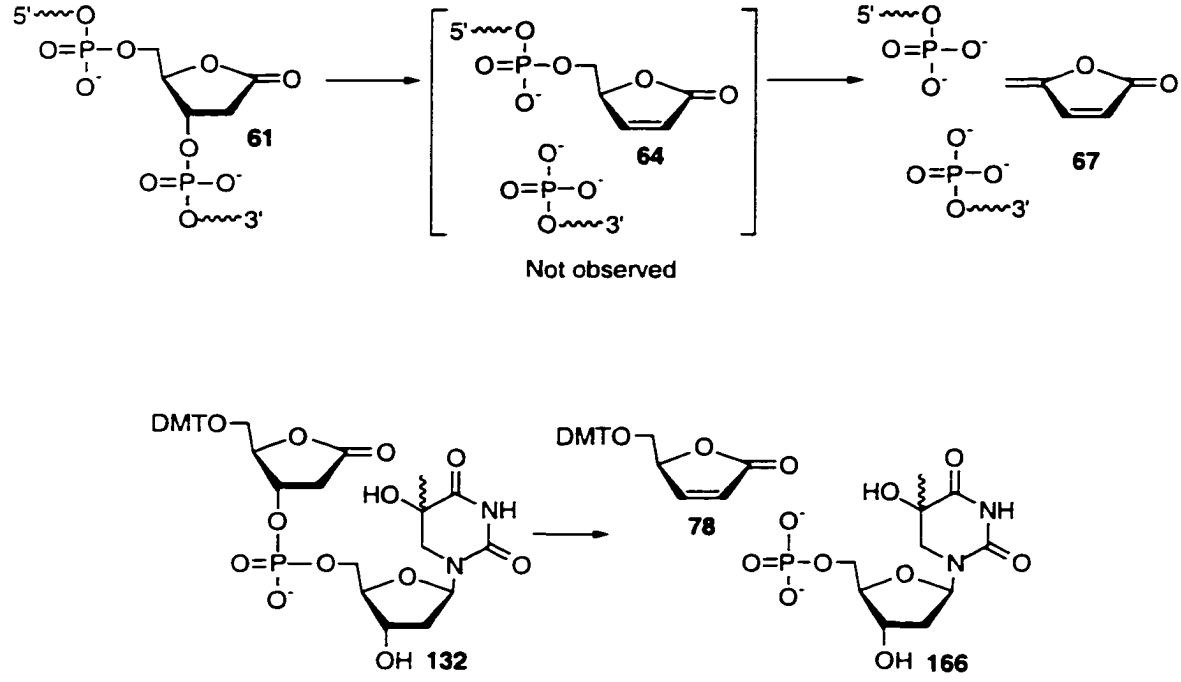

Figure 86. Expected reactivity of 2-deoxyribonolactone (**132**) under basic conditions.

The expected product upon elimination of **132** is **78**. An authentic sample of **78** was subjected to the *N*, *N'*-dimethylethylenediamine (DMEDA) conditions that have been used to induce the elimination.[93] When **78** was heated at 37 °C in the presence of DMEDA, complete conversion was observed after 1 h. The major product was characterized and identified as the seven-membered lactam (**79**, Figure 87). This product arises via a Michael addition to **78**, followed by an intramolecular cyclization and concomitant ring

opening of the sugar. NMR, IR, and exact mass are consistent with this product. The furanone (**78**) also proved to be unstable in the presence of nonnucleophilic bases, such as Et_3N, and H_2O upon heating at 37 °C.

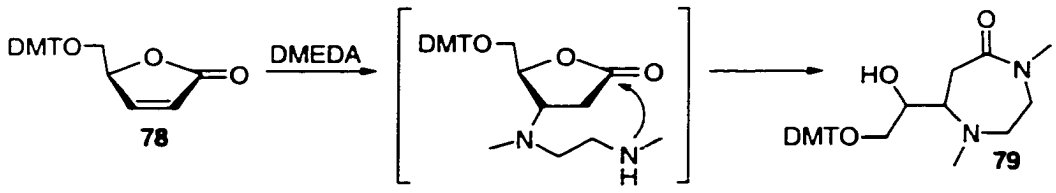

Figure 87. Reactivity of the furanone (**78**) in the presence of DMEDA.

When an authentic sample of **132** was subjected to DMEDA and heated at 37 °C, only the lactam (**79**) was detected (Figure 88). Although **78** cannot be observed directly upon elimination of **132**, formation of **79** is indicative of its intermediacy. With **79** characterized, an aerobic photolysis sample of **121** was subjected to DMEDA conditions and analyzed by HPLC. The yield of **79** (0.41 ± 0.2%) was comparable to that measured for **132** (0.29 ± 0.1%). This result confirms the formation of **132** upon generation of the peroxyl radical (**163**) in the dinucleotide, its subsequent elimimation to **78**, and trapping by DMEDA.

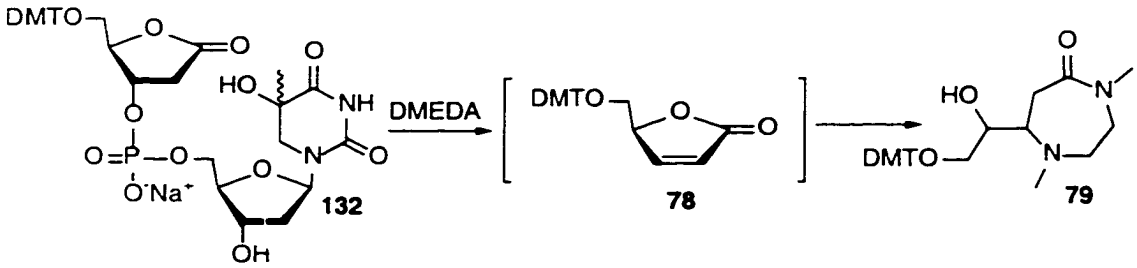

Figure 88. Reactivity of 2-deoxyribonolactone dinucleotide (**132**) with DMEDA.

The results of the photolysis of the phenyl selenide dinucleotide (**121**) under both anaerobic and aerobic conditions provides valuable information in understanding the role of 5,6-dihydrothymidin-5-yl (**120**) in DNA damage amplification. The anaerobic photolysis reveals that **120** is unable to participate in internucleotidyl hydrogen atom abstraction, consistent with previous experiments on the reactivity of **120** in ssDNA.[38,39] The aerobic experiments also confirm the proposal that strand scission is an O_2-dependent process involving the peroxyl radical (**163**). Although it had been shown that the formation of **163** leads to alkaline labile lesions via hydrogen atom abstraction from the C1'-position, direct evidence for the formation of the 2-deoxyribonolactone (**132**) had not been attained until now. The studies involving the dinucleotide (**121**) provide direct evidence for the formation of **132** in DNA damage amplification involving **4** in the presence of O_2.

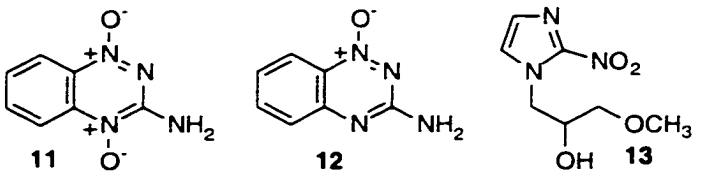

3.2.8 DNA Damage Amplification in the Presence of Radiosensitizers

Although DNA damage amplification has been observed upon generation of 5,6-dihydrothymidin-5-yl (**120**) in the presence of O_2, tumor cells are often hypoxic. Consequently, small molecules, such as tirapazamine (**11**) and misonidazole (**13**), have been used in conjunction with ionizing radiation to increase DNA damage.[40-46] The former has been investigated as a bimodal agent to initiate and propagate DNA damage.[40-45] Evidence suggests that tirapazamine (**11**) is activated by one-electron reduction to release HO• and generate the 1-*N*-oxide (**12**).[41-43] The bis-*N*-oxide (**11**) has been suggested to react with alkyl radicals, but its metabolite (**12**) also has the potential of undergoing the same types of reactions. Therefore, the 1-*N*-oxide (**12**) may also play a role in the propagation of DNA damage. The mode of action of these compounds is unknown, but it

has been suggested that they act as surrogates for oxygen in their reactions with radicals.[40-48] Since **120** is one of the major reactive species generated during ionizing radiation, the possibility that this radical (**120**) may react with tirapazamine (**11**), the 1-*N*-oxide (**12**), or misonidazole (**13**) to propagate DNA damage led us to investigate this reaction pathway.

3.2.8.1 Attempted Investigation of Misonidazole (13) as an Oxygen Surrogate

The potential for misonidazole (**13**) to act as an oxygen surrogate in the presence of 5,6-dihydrothymidin-5-yl (**4**) was investigated at the monomeric level. Investigation of the reactivity of **13** with **4** at the monomeric level simplifies product analysis and allows one to determine the rate constant (k_{MISO}) for trapping of the nucleobase radical (**4**) by **13** via competitive kinetics (Figure 89). Since the rate constant for trapping of alkyl radicals (e.g. **4**) by thiols in aqueous CH_3CN is known ($k_H = 1.1 \times 10^7\ M^{-1}\ s^{-1}$) and the expected product upon reaction of **4** with **13** is 5,6-dihydro-5-hydroxythymidine (**8**), the ratio of **8**:**34** can be used to determine the rate constant for trapping of **4** by misonidazole (**13**, k_{MISO}).[113,151]

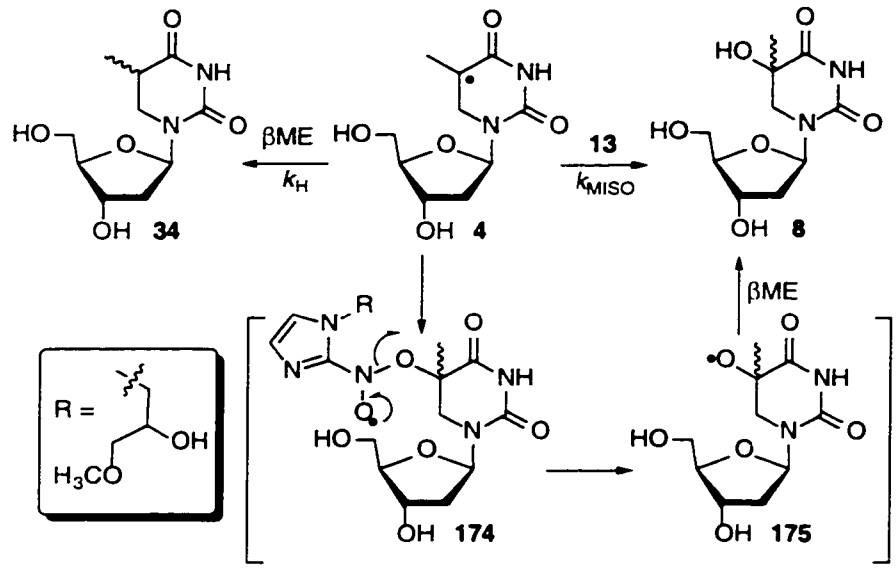

Figure 89. Potential reactivity of **4** with misonidazole (**13**).

Since the phenyl selenide (**96**) proved to be the most versatile and reliable precursor to **4**, it was utilized in the studies of the reactivity of misonidazole (**13**) with the radical (**4**). The phenyl selenide (**96**) was photolyzed at 350 nm in the presence of βME and misonidazole (**13**) under anaerobic conditions (Table 28). In the absence of **13**, the observed products were 5,6-dihydrothymidine (**34**) and thymidine (**3**) as expected (Section 3.1.2). When **13** was present in the photolysis reaction, a minor amount of **8** was detected in addition to **34** and **3**, presumably arising from trapping of **4** by misonidazole (**13**, Figure 89). However, the yield of **8** was low and did not increase upon increasing the concentration of misonidazole (**13**), which would be expected if formation of **34** and **8** are competing pathways (Figure 89). In addition, the mass balances for the photolyses were low.

Table 28. Anaerobic photolysis of **96** in the presence of misonidazole (**13**).[a]

	% Yield				
[**13**] mM	**3**	**8**	**34**[b]	% Conversion	% Mass Balance
-	20 ± 1	0	≈25 ± 1	100 ± 0	45 ± 1
2.0	9 ± 0	2 ± 0	≈31 ± 1	91 ± 0	51 ± 0
5.0[c]	nd	3 ± 1	≈37 ± 1	91 ± 1	39 ± 11

[a] The photolyses were carried out at 350 nm (λ_{max} = 350 nm, 96 watts) for 45 min with [**96**] = 0.1 mM and [βME] = 1.1 mM in CH_3CN:H_2O (1:1 by volume); [b] the yield of **34** was estimated assuming the diastereomeric ratio was 1:1 since only one diastereomer could be quantitated; [c] the yield of **3** could not be determined due to a coeluting peak.

If one uses the data from Table 28 and a rate constant for trapping of **4** by βME (k_H) of 1.1 x 10^7 M^{-1} s^{-1}, the rate constant for trapping by **13** (k_{MISO}) is estimated at 2.0-3.9 x 10^5 M^{-1} s^{-1}.[113,151] This is considerably lower than expected based on literature values for the rate constants for trapping of alkyl radicals by misonidazole (**13**) and other nitro-

containing compounds. For example, the C1'-radical in ssDNA is trapped by **13** with a rate constant of 6.9 x 10^8 M^{-1} s^{-1}.[44] In addition, rate constants for trapping of 5,6-dihydro-5-hydroxy-thymin-6-yl (**176**, Equation 22) by nitrobenzenes range from 3.1 x 10^7 - 1.2 x 10^9 M^{-1} s^{-1}, depending on the nucleobase and substituent on the nitrobenzene.[154,155] The low yield of **8**, moderate mass balances, and surprisingly low rate constant (k_{MISO}) suggest that perhaps the covalent adduct (**174**) does not readily undergo decomposition to generate the alkoxyl radical (**175**). Hence, an accurate rate constant for reaction of **4** with misonidazole (**13**) could not be determined. Consequently, the potential reactivity of nucleobase radicals (e.g. **4**) with radiosensitizing agents was investigated using the mono-*N*-oxide (**12**).

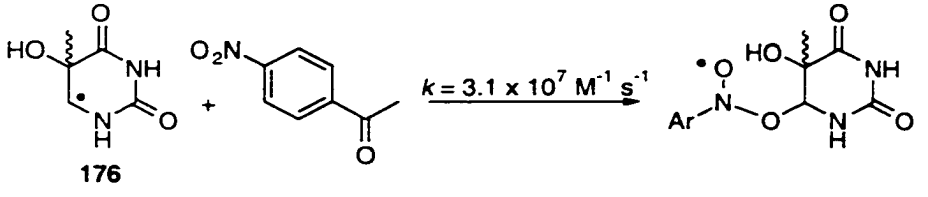

176 (22)

3.2.8.2 Metabolite (12) of Tirapazamine (11) as an Oxygen Surrogate, Monomer Studies

The reactivity of 5,6-dihydrothymidin-5-yl (**4**) with tirapazamine (**11**) could not be investigated due to the instability of the latter to the photolysis conditions. The 1-*N*-oxide (**12**) of tirapazamine (**11**), however, was stable. The 1-*N*-oxide (**12**) is the metabolite of **11** and therefore its subsequent reactivity is of interest.

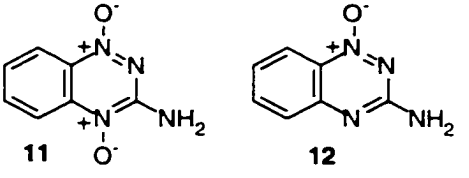

The photolysis of the phenyl selenide (**96**) was carried out in the presence of the 1-*N*-oxide (**12**) and βME (Figure 90, Table 29). A significant amount of thymidine (**3**) was observed, as expected, due to disproportionation of **4** and PhSe• under the inefficient radical chain conditions of the photolysis. In addition, 5,6-dihydrothymidine (**34**, *5S*:*5R*, 0.8 ± 0.1) and 5,6-dihydro-5-hydroxythymidine (**8**, *5R*:*5S*, 1.0 ± 0.1) were observed. The latter is the expected product upon trapping of **4** by **12**, following decomposition of the initial covalent adduct. As the concentration of βME increased, the yield of **8** decreased, but **34** remained constant. The decrease in the yield of **8** was expected due to more efficient trapping of **4** by βME in competition with **12** as the concentration of hydrogen atom donor increased. However, the relationship between the ratio of products (**34**:**8**) and the concentration of βME was not linear as expected.

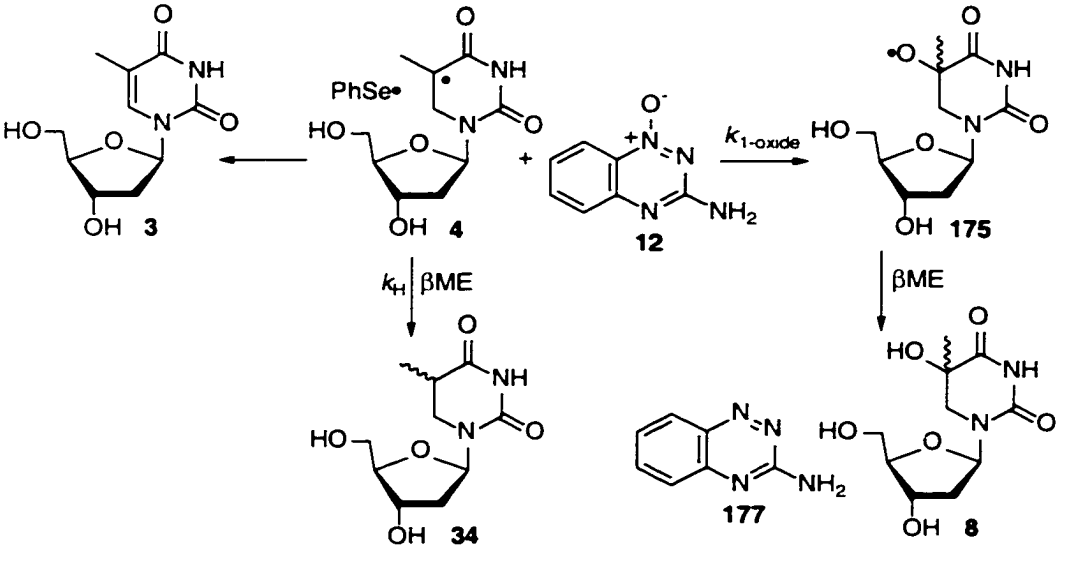

Figure 90. Observed products upon photolysis of **96** in the presence of the 1-*N*-oxide (**12**).

Table 29. Anaerobic photolysis of **96** in the presence of 1-*N*-oxide (**12**) and βME.[a]

[βME] mM	% Yield 3	% Yield 8	% Yield 34	% Conversion	% Mass Balance	34:8
0.14	27 ± 1	20 ± 3	34 ± 3	100 ± 0	81 ± 4	1.7 ± 0.1
0.51	21 ± 4	17 ± 8	42 ± 3	100 ± 0	80 ± 9	2.9 ± 1.5
1.03	18 ± 1	11 ± 3	51 ± 13	100 ± 0	80 ± 8	4.8 ± 2.3
2.06	15 ± 1	10 ± 0	52 ± 11	100 ± 0	77 ± 10	5.2 ± 1.4
3.15	15 ± 1	9 ± 1	48 ± 3	100 ± 0	71 ± 1	5.6 ± 1.0

[a] Photolyses carried out at 350 nm (λ_{max} = 350 nm, 96 watts) for 45 min with [**96**] = 0.01 mM and [**12**] = 2.5 mM in CH_3CN:H_2O (1:1 by volume).

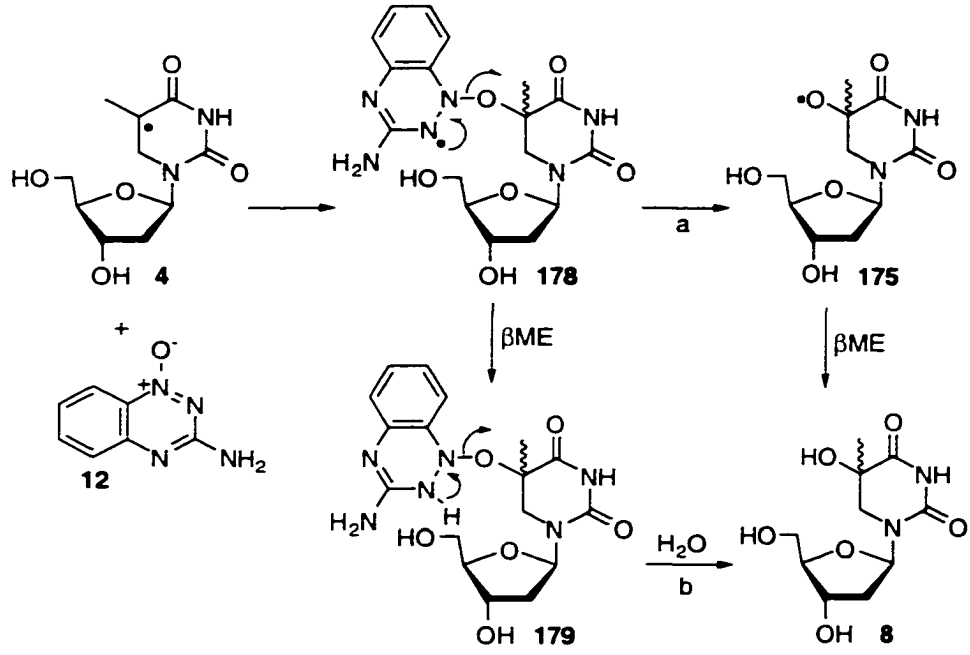

Figure 91. Proposed mechanism for the trapping of **4** by 1-*N*-oxide (**12**).

The mechanism by which the 1-*N*-oxide (**12**) reacts with alkyl radicals is not known, but it has been suggested that alkyl radicals (e.g. **4**) are trapped on the oxygen of **12** to form the covalent adduct (e.g. **178**, Figure 91).[44] This reaction pathway is analogous to the reactivity observed for TEMPO (**180**, Equation 23), a radical trap

commonly used in ESR studies.[156,157] The covalent adduct of **12** (**178**) may cleave homolytically (path a) or heterolytically (path b) to generate the alkoxyl radical (**175**) or alkoxide, respectively, both intermediates leading to the formation of **8**. Alternatively, the radical could be trapped on the nitrogen (N2) of **12**. Although, to our knowledge, this reaction pathway has not been proposed to account for the reactivity of **12**, similar compounds, such as DMPO (**181**, Equation 24) are known to undergo an analogous reaction with alkyl radicals.[158-160]

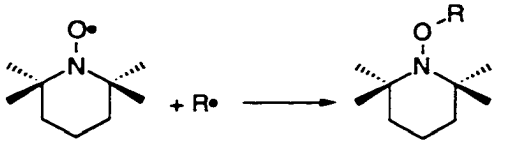

180 (23)

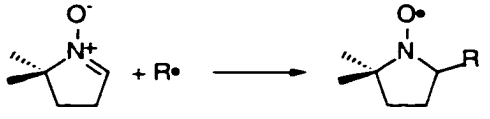

181 (24)

If the 1-*N*-oxide (**12**) reacts with alkyl radicals exclusively on the oxygen as suggested, then the ratio of products (**34**:**8**) is representative of the ratio of the rate constants, k_H:$k_{1\text{-oxide}}$ (Figure 90). However, the covalent adduct must completely break down to product (**8**) in order for the rate constant to be accurately determined. The nonlinear relationship observed above (Table 29) led us to consider that the covalent adduct (**178**) was not completely cleaved under the reaction conditions and thus the yield of **8** was not entirely representative of the initial trapping reaction, or that the reactivity of **12** with alkyl radicals is more complicated than previously thought.

The photolysis of **96** was carried out as described above, then heated at 55 °C in the presence of excess βME (2 mM) to ensure that the covalent adduct (**178** or **179**) had completely cleaved to product (**8**). Heating the reaction mixture had no effect on the yield

of **34** (Table 30). Interestingly, the yield of **8** increased significantly, especially in the samples that contained a high concentration of βME. The more significant effect of heating the samples at high βME concentration is unknown. However, at high βME concentrations, one would expect that the initial covalent adduct (**178**) would be more efficiently trapped to generate **179**, which may cleave at a different rate than the former. Finally, although the yield of **8** increased upon heating, there was very little change in the ratio of **34**:**8** upon varying the concentration of βME.

Table 30. Anaerobic photolysis of **96** in the presence of 1-*N*-oxide (**12**) and βME with subsequent heating.[a]

[βME] mM	% Yield **3**	% Yield **8**	% Yield **34**	% Yield **177**	% Mass Balance	**34**:**8**
0.14	38 ± 3	19 ± 1	27 ± 4	20 ± 6	84 ± 1	1.5 ± 0.3
0.51	31 ± 1	19 ± 2	32 ± 0	40 ± 8	82 ± 4	1.7 ± 0.1
1.03	29 ± 1	19 ± 0	33 ± 4	27 ± 3	81 ± 6	1.7 ± 0.2
2.06	35 ± 10	19 ± 1	40 ± 0	38 ± 10	94 ± 8	2.1 ± 0.1
3.15	24 ± 0	21 ± 2	45 ± 1	42 ± 3	90 ± 4	2.2 ± 0.1

[a] Photolyses carried out at 350 nm (λ_{max} = 350 nm, 96 watts) for 45 min with [**96**] = 0.01 mM and [**12**] = 2.5 mM in CH_3CN:H_2O (1:1 by volume).

The photolysis of the selenide (**96**) was also carried out in the presence of the 1-*N*-oxide (**12**) and *tert*-BuSH as a hydrogen atom donor (Table 31). The photolyses were carried out as described above for βME and the samples subsequently heated at 55 °C in the presence of excess thiol to ensure complete cleavage of the covalent adduct (**178** or **179**). As expected, thymidine (**3**), 5,6-dihydrothymidine (**34**), and 5,6-dihydro-5-hydroxythymidine (**8**) were observed in the product mixture. The yield of **8** and **34** was

fairly constant, resulting in no significant change in the ratio of products (**34**:**8**) upon varying the concentration of *tert*-BuSH, as was observed for the photolyses carried out in the presence of βME. The mass balances for the photolyses carried out in the presence *tert*-BuSH were considerably lower than the photolyses carried out with βME. The reason for this is not understood at this time.

Table 31. Anaerobic photolysis of **96** in the presence of 1-*N*-oxide (**12**) and *tert*-BuSH with subsequent heating.[a]

[*tert*-BuSH] mM	% Yield **3**	**8**	**34**	% Conversion	% Mass Balance	**34**:**8**
0.17	9 ± 0	7 ± 1	29 ± 1	100 ± 0	45 ± 1	4.3 ± 0.7
1.14	5 ± 1	8 ± 4	35 ± 1	100 ± 0	48 ± 5	5.4 ± 3.0
2.27	4 ± 0	7 ± 4	30 ± 10	100 ± 0	41 ± 14	4.5 ± 1.1
3.20	5 ± 1	9 ± 1	36 ± 7	100 ± 0	50 ± 8	4.2 ± 0.1
5.33	2	10	41	100 ± 0	53	4.1

[a] Photolyses carried out at 350 nm (λ_{max} = 350 nm, 96 watts) for 45 min with [**96**] = 0.01 mM and [**12**] = 1.7 mM in CH_3CN:H_2O (1:1 by volume).

An attempt was made to determine the rate constant for trapping of the alkyl radical (**4**) by the 1-*N*-oxide (**12**) using the data in Table 30. Since the reactivity of **4** is partitioned between trapping by a hydrogen atom donor (k_H), for which the rate constant is known (k_H = 1.1 x 10^7 M^{-1} s^{-1} for thiols), and trapping by **12** ($k_{1\text{-oxide}}$), the ratio of products (**34**:**8**) was used to estimate the rate constant $k_{1\text{-oxide}}$ (Equation 25).[113,151] The data from the photolysis of **96** in the presence of βME (Table 30) was used to construct a plot of the ratio of **34**:**8** *versus* the concentration of βME (**12**, Figure 92), which resulted in a straight line with a slope of 248.9 and y-intercept of 1.51.

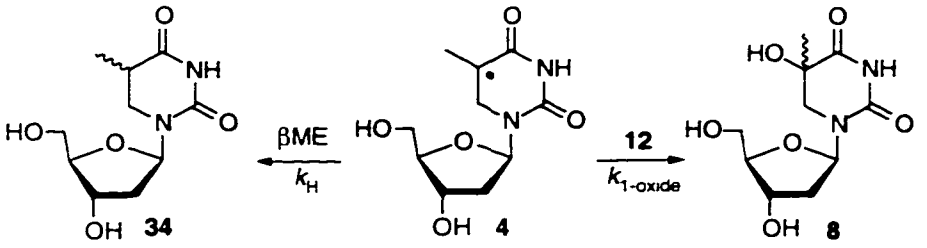

(25)

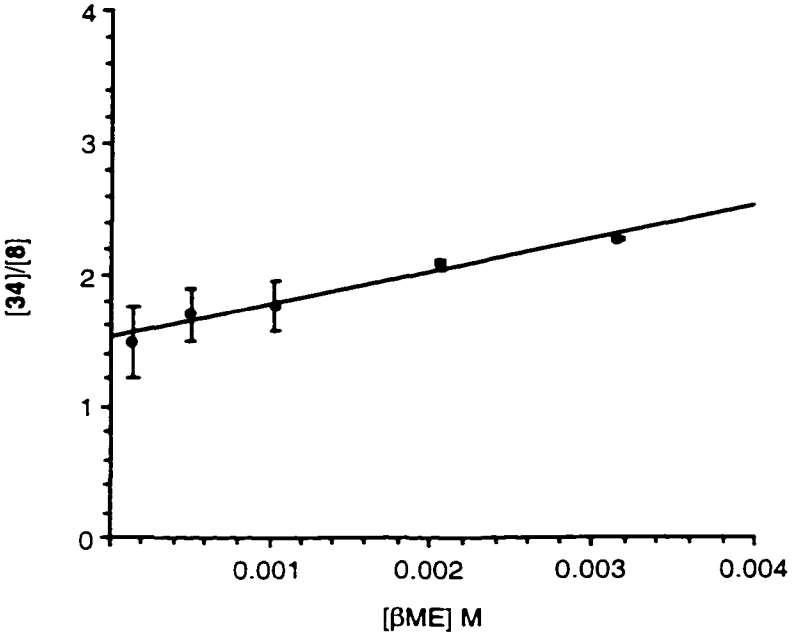

Figure 92. Plot of [**34**]/[**8**] *versus* [βME].

Although a linear relationship was observed for the plot, the non-zero y-intercept and relatively constant ratio of products over the entire range of βME concentration suggest that another reaction pathway exists that contributes to the formation of the products (Figure 92). One possibility is an increased yield of **34** due to the presence of PhSeH

generated *in situ*, which is known to trap alkyl radicals with a rate constant of 2 x 10^9 M^{-1} s^{-1}.[113] If the presence of PhSeH contributes to the yield of **34**, the rate expression for the ratio of **34**:**8** includes a term that takes into account trapping of **4** by PhSeH (Equation 26).

$$\frac{[\mathbf{34}]}{[\mathbf{8}]} = \frac{[\beta ME]\, k_H + [PhSeH]\, k_{PhSeH}}{[\mathbf{12}]\, k_{1\text{-oxide}}} \qquad (26)$$

$$\text{slope} = \frac{k_H}{[\mathbf{12}]\, k_{1\text{-oxide}}} \qquad \text{y-intercept} = \frac{[PhSeH]\, k_{PhSeH}}{[\mathbf{12}]\, k_{1\text{-oxide}}}$$

Using the slope of the line and a rate constant for k_H of 1.1 x 10^7 M^{-1} s^{-1}, the rate constant for $k_{1\text{-oxide}}$ was estimated as 1.8 x 10^7 M^{-1} s^{-1}.[113,151] The rate constant for $k_{1\text{-oxide}}$ was also estimated using the y-intercept. If one assumes a maximum concentration of PhSeH of 0.01 mM, the concentration of the selenide (**96**) used in the reaction, and a rate constant for PhSeH of 2 x 10^9 M^{-1} s^{-1}, $k_{1\text{-oxide}}$ is estimated as 5.3 x 10^6 M^{-1} s^{-1}.[113] The rate constant using the latter method, however, must be considered as an upper limit since the average concentration of PhSeH must be less than 0.01 M. This analysis leads to the suggestion that the rate constant for trapping of the nucleobase radical (**4**) by the 1-*N*-oxide (**12**) is considerably slower than other measured rate constants for this same compound (**12**). For example, the rate constant for trapping of the C1'-radical in ssDNA by **12** was estimated at 4.6 x 10^8 M^{-1} s^{-1}.[44] The rate constant ($k_{1\text{-oxide}}$) is also slower than the analogous reaction of 3° radicals with TEMPO (**180**), which occurs at 6.8-8.0 x 10^8 M^{-1} s^{-1}.[113,157] Interestingly, the rate constant for the 1-*N*-oxide is closer to the rate constant measured for a 3° radical reacting with DMPO (**181**, k = 6.8 x 10^7 M^{-1} s^{-1}).[158]

Based on the results above, we believe the products (**34** and **8**) are due to the regioisomeric trapping of the radical (**4**) by **12** to generate the covalent adduct on the nitrogen (**182**) or oxygen (**178**, Figure 93). Although it has been assumed that the alkyl radical (e.g. **4**) reacts at the oxygen of **12**, there is no evidence that this is the only reaction pathway available to **4**.[44] If the covalent adduct (**182**) is trapped and subsequently reduced by βME, the observed product would be **34**. Therefore, it is possible that the formation of **34** and **8** depends on which covalent adduct (**178** or **182**) is formed, in which the concentration of hydrogen atom donor would have no effect on the product distribution. The yield of reduced **12** (**177**) is consistent with this proposal (Table 30). In most instances, the yield of **177** exceeds the yield of **8**, indicating that the 1-*N*-oxide (**12**) was consumed by another pathway. The observation, though, that the combined yields of **34** and **8** is not completely accounted for the the amount of reduced **12** (**177**) suggests that the former arises from more than one reaction pathway.

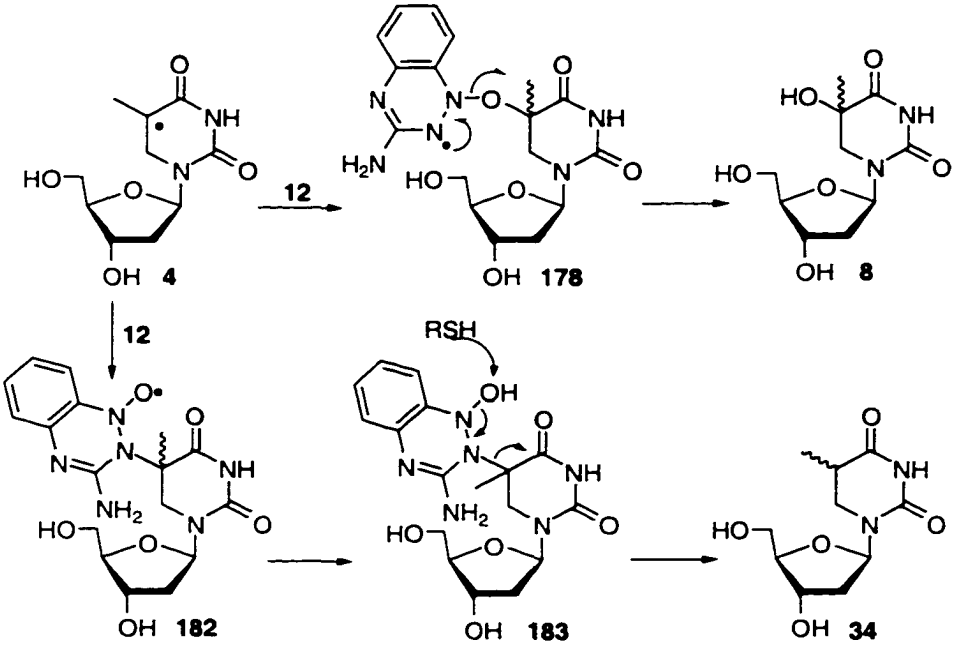

Figure 93. Competitive trapping of **4** on oxygen *versus* nitrogen of the 1-*N*-oxide (**12**).

3.2.8.3 1-*N*-Oxide (12) of Tirapazamine (11) as an Oxygen Surrogate, Dinucleotide Studies

Although it is uncertain if the rate constant for $k_{1\text{-oxide}}$ obtained from the studies involving the monomer is accurate or if a regioisomeric mixture of covalent adducts are generated, it is clear that 5,6-dihydrothymidin-5-yl (**4**) is trapped by the 1-*N*-oxide (**12**). The ability for **12** to serve as a surrogate for O_2 and its involvement in DNA damage amplification was further investigated utilizing the phenyl selenide dinucleotide (**121**).

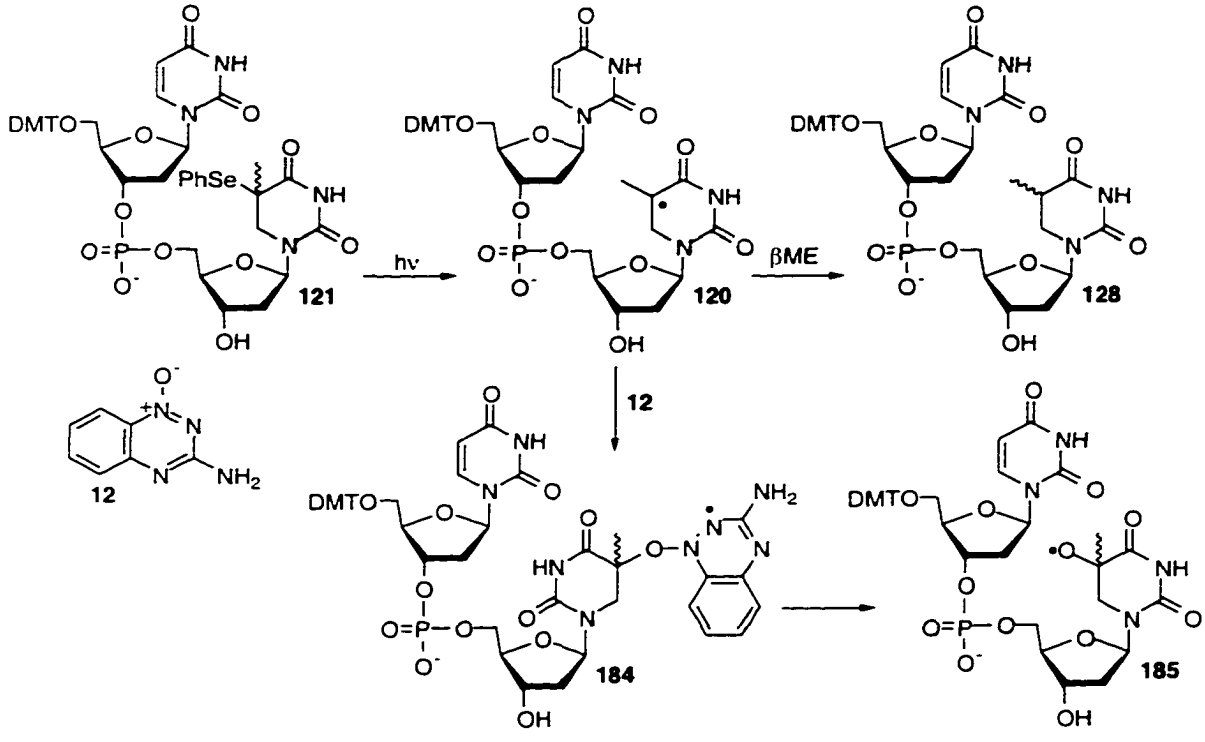

Figure 94. Potential reactivity of **120** with the 1-*N*-oxide (**12**).

The dinucleotide (**121**) was photolyzed in the presence of **12** and βME, the hydrogen atom donor that produced the most reliable data in the monomer studies (Section 3.2.8.3). Unlike the monomer studies, the photolysis samples containing the dinucleotide (**121**) were not subsequently heated in the presence of excess βME. If the covalent adduct

(**184**) was cleaved in the presence of excess βME during the post-treatment, an inaccurate yield of the dU/5,6-dihydro-5-hydroxythymidine (**130**) may be detected. Incomplete cleavage of the covalent adduct (**184**) is not as critical in the dinucleotide studies since we were interested in the partitioning of the reactivity of the alkoxyl radical (**185**) that arises from **184**, rather than the reactivity of the alkyl radical (**120**, Figure 94).

Upon photolysis of **121**, the dU/thymidine dinucleotide (**129**) was detected, consistent with the monomer studies and believed to be generated via disproportionation of **120** and PhSe• under the inefficient radical chain conditions (Table 32). In addition, **128** and **130** were detected, also consistent with the monomer studies. When the photolyses were carried out in $H_2{}^{18}O$ and the persilylated nucleobases analyzed by GC/MS, a negligible amount of ^{18}O-incorporation was detected in **130** (3.1 ± 1.9%). The lack of ^{18}O-incorporation indicates that **130** arises from the covalent adduct (**184**) of **120** with the 1-*N*-oxide (**12**). The amount of reduced drug (**177**), however, ranged from 2 ± 0 to 5 ± 1% upon increasing concentration of βME, which is inconsistent with the monomer studies (Section 3.2.8.2) and does not account for the yield of **130**. This discrepancy is unclear at this time.

Table 32. Anaerobic photolysis of **121** in the presence of the 1-*N*-oxide (**12**).[a]

[βME] mM	% Yield **128**	% Yield **129**	% Yield **130**	% Yield **132**	% Conversion	% Mass Balance
0.14	44 ± 4	18 ± 2	20 ± 3	1.9 ± 0.4	94 ± 5	89 ± 0
0.51	49 ± 6	13 ± 4	21 ± 0	2.9 ± 0	97 ± 4	89 ± 13
1.03	58 ± 6	10 ± 4	29 ± 7	3.9 ± 0.8	94 ± 6	106 ± 4
2.06	61 ± 3	13 ± 4	24 ± 0	4.6 ± 0.7	98 ± 3	90 ± 16
3.15	66 ± 4	13 ± 4	29 ± 0	4.4 ± 0.8	94 ± 7	97 ± 41

[a] Photolyses carried out at 350 nm (λ_{max} = 350 nm, 96 watts) for 1 h with [**121**] = 0.017 mM and [**12**] = 2.5 mM in CH_3CN:H_2O (1:1 by volume).

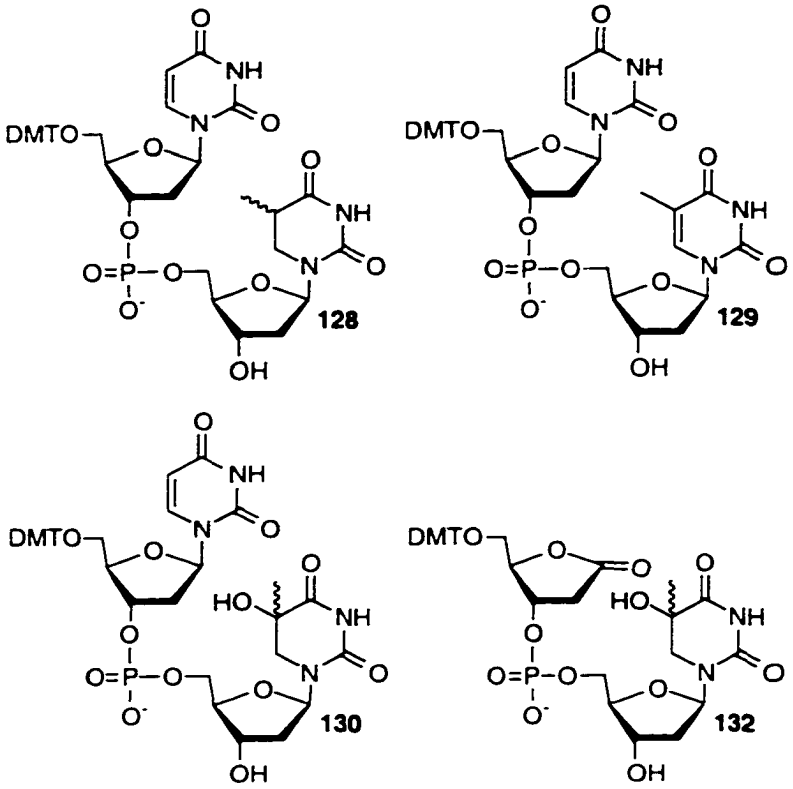

The diastereomeric ratio observed for **128** (2.0 ± 0.4, *5R*:*5S*) and **130** (1.6 ± 0.2, *5S*:*5R*), was consistent with the diastereoselectivity observed in the aerobic photolyses of **121** carried out in the presence of βME (Section 3.2.6, Table 27). Recall that the observed diastereoselectivity was explained by invoking hydrogen bonding of the βME to the uracil moiety of the dinucleotide, with delivery of the hydrogen atom from the *si* face (Figure 73). This argument is consistent with the diastereomeric ratio of the dU/5,6-dihydrothymidine dinucleotide (**128**) observed in the studies involving **12** (Figure 95).

Likewise, the diastereoselectivity observed in the formation of *5S*-**130** as the major product from the peroxyl radical (**9**) in the presence of βME was explained by a similar argument (Figure 80). However, in the case of the peroxyl radical (**9**), the *5R*-diastereomer had an alternative pathway available to it (i.e. superoxide elimination). In the case of the alkoxyl radical (**185**), a comparable pathway is unlikely. Although it may

undergo fragmentation, this is at most a minor pathway since the mass balances were high. Another explanation for the observed diastereomeric ratio observed for **130** is selective trapping of the nucleobase radical (**120**) by the 1-*N*-oxide (**12**) from the *si* face (Figure 95). Subsequent cleavage of the covalent adduct (**184**) would result in the major diastereomer being *5S*-**130**.

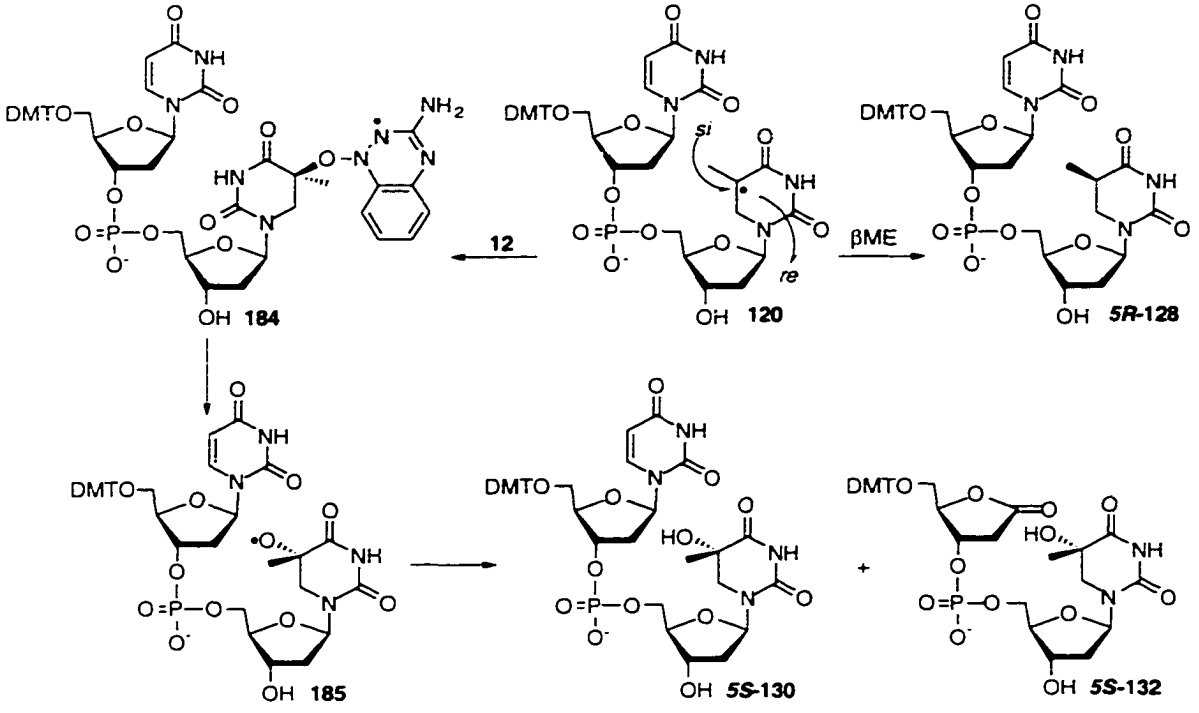

Figure 95. Diastereoselective trapping of **120** by βME and 1-*N*-oxide (**12**).

One of the most important products observed upon the photolysis of **121** in the presence of **12** was the alkaline labile lesion (**132**), which arises via hydrogen atom abstraction from the C1'-position and was also directly observed upon photolysis of **121** in the presence of O_2 (Section 3.2.6). The formation of this product (**132**) indicates that reaction of the nucleobase radical (**120**) with the 1-*N*-oxide (**12**) may be involved in the DNA damage induced by tirapazamine (**11**). If the nucleobase radical (**120**) is trapped by

12 and subsequently cleaved to generate the alkoxyl radical (**183**), there are two pathways potentially available to the latter (Figure 95). The alkoxyl radical (**183**) may be trapped by βME to generate **130**. Alternatively, **183** may abstract a hydrogen atom from the C1'-position of the adjacent sugar giving rise to the 2-deoxyribonolactone (**132**), as observed for the peroxyl radical (**9**).

As observed in the studies of the peroxyl radical (**9**), the internucleotidyl hydrogen atom abstraction by the alkoxyl radical is a diastereoselective process. The diastereomeric ratio observed in the reaction was 33 ± 14:1 (*5S*:*5R*-**132**), considerably higher than the ratio observed for the peroxyl radical (**9**). This is surprising given the higher reactivity of alkoxyl radicals and expected lower selectivity. The proposal that the nucleobase radical (**120**) may be trapped by the 1-*N*-oxide (**12**) preferentially from the *si* face is consistent with the diastereomeric ratio observed for **132** (Figure 95).

Since the rate constant for trapping of an alkoxyl radical by thiols (k_H = 2 x 10^8 M^{-1} s^{-1}) is known, the ratio of products (**130**:**132**) was used to estimate the rate constant for internucleotidyl hydrogen atom abstraction by the alkoxyl radical (**183**).[160] However, upon increasing the concentration of βME, the ratio of **130**:**132** did not increase as expected due to more efficient trapping of the alkoxyl radical (**183**) at higher concentrations of hydrogen atom donor (Table 33). Consequently, a linear relationship was not observed when the ratio of **130**:**132** was plotted *versus* the concentration of βME.

Using the data from Table 33 and a rate constant for k_H of 2 x 10^8 M^{-1} s^{-1}, the rate constant for k_{inter} was estimated at 1.3 x 10^3-4.8 x 10^4 s^{-1}.[161] Although this rate constant is a very rough estimate, it is clearly significantly faster than the rate constant for the peroxyl radical (**9**, 0.1 s^{-1}), as expected due to the higher reactivity of alkoxyl radicals than peroxyl radicals. For example, using THF as a comparison of the reactivity, *tert*-BuOO• and *tert*-BuO• abstract a hydrogen atom from THF with rate constants of 0.085 M^{-1} s^{-1} and 8.3 x10^6 M^{-1} s^{-1}.[152,162] Although this data indicates that internucleotidyl hydrogen atom abstraction in

the presence of the 1-*N*-oxide (**12**) is significantly more efficient than in the presence of O_2, the effective molarity calculated for the former reaction is 0.16-5.8 mM, considerably lower than that calculated for the analogous reaction of the peroxyl radical (1.2 M, Section 3.2.6). This discrepancy may be due to the participation of other reactive species, in addition to the alkoxyl radical, in internucleotidyl hydrogen atom abstraction that is not represented by the yield of **132**.

Table 33. Product ratios upon photolysis of **121** in the presence of **12** over a range of βME concentrations.[a]

[βME] mM	**130**:**132**	**128**:(**130** + **132**)
0.14	10.9 ± 0.6	2.0 ± 0.1
0.51	7.2 ± 0	2.1 ± 0.2
1.03	7.5 ± 0.3	1.8 ± 0.3
2.06	5.2	2.1
3.15	6.6	2.0

[a] Photolyses carried out at 350 nm (λ_{max} = 350 nm, 96 watts) for 1 h with [**121**] = 0.017 mM and [**12**] = 2.5 mM in CH_3CN:H_2O (1:1 by volume).

Interestingly, the ratio of **128**:(**130** + **132**) was also constant over the range of βME concentrations used in the photolyses (Table 33). The ratio of **128**:(**130** + **132**) in the dinucleotide studies was ≈2, consistent with the monomer studies (Table 30). Recall that in the monomer studies, it was suggested that the formation of the analogous products (**34** and **8**) may arise via regioisomeric trapping of the nucleobase radical by the 1-*N*-oxide (**12**). Hence, the concentration of βME would have no effect on the product ratio. The same explanation may be used here to explain the inability of increasing the concentration of hydrogen atom donor to affect the product distribution.

Since the mechanism by which alkyl radicals are trapped by the 1-*N*-oxide (**12**) is unknown and given the results described above, the intermediate responsible for the internucleotidyl hydrogen atom abstraction is unclear. It is possible that the alkyl radical (**120**) may be trapped on the oxygen (**184**) or nitrogen (**186**) of **12**. Hence, there are several radical intermediates (e.g. **184-186**) that may be able to participate in hydrogen atom abstraction (Figure 96). The covalent adduct on oxygen (**184**) ultimately gives rise to **132**. Alternatively, the regioisomeric adduct (**186**) was anticipated to yield **131** upon hydrogen atom abstraction from the adjacent sugar. The presence of **131** (2.4 ± 0.1%) and **132** (2.0 ± 0.2%) supports the contention that regioisomeric trapping of **120** by **12** generates a mixture of covalent adducts able to participate in internucleotidyl hydrogen atom abstraction.

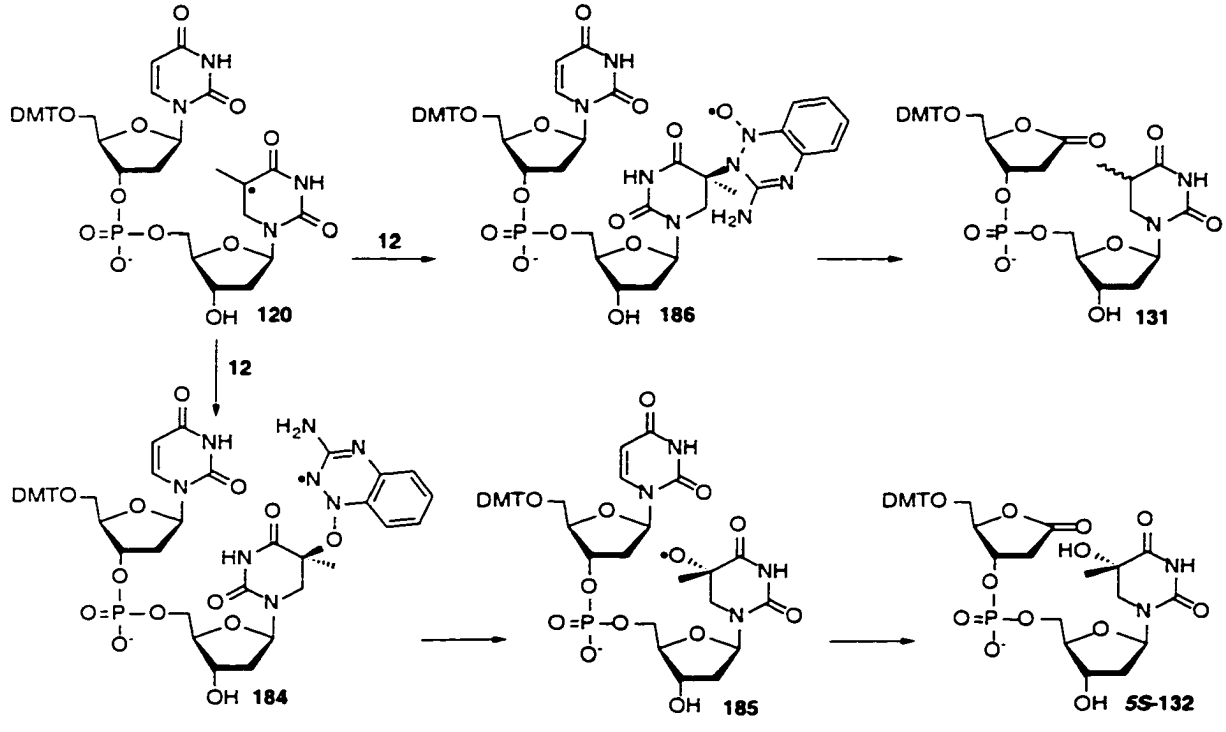

Figure 96. Potential intermediates derived from the reaction of **120** with the 1-*N*-oxide (**12**) able to undergo internucleotidyl hydrogen atom abstraction.

Although the intermediate responsible for internucleotidyl hydrogen atom abstraction is uncertain, it is clear that the 1-*N*-oxide (**12**) is involved in DNA damage amplification via transfer of the radical from the nucleobase to the sugar, as observed for the peroxyl radical (**9**). In addition, the 2-deoxyribonolactone (**132**) was directly observed upon reaction of the nucleobase radical (**120**) with **12** in a much higher yield than observed in the peroxyl radical (**9**). In this respect, the 1-*N*-oxide (**12**) does act as a surrogate for O_2 and results in the formation of the same alkaline labile lesion (**132**) observed upon generation of the nucleobase radical under aerobic conditions.

4 Conclusion

Generation of 5,6-dihydrothymidin-5-yl (**4** and **120**) from the phenyl selenide radical precursor in the monomer and dinucleotide has enabled us to study the reactivity of this nucleobase radical in greater chemical detail than when it was studied in oligonucleotides. The monomer studies allowed us to investigate the chemistry of **4** at the most basic level to design an efficient thermal and photochemical precursor to the radical and study its subsequent chemistry. The dinucleotide is the minimal model in which to study the unusual proposed mechanism for the transfer of spin from the nucleobase to the sugar via internucleotidyl hydrogen atom abstraction.

Investigation of the reactivity of the nucleobase radical (**120**) in the dinucleotide provided direct evidence that internucleotidyl hydrogen atom abstraction does not occur in the absence of O_2. Through the use of anomerization and tetranitromethane as mechanistic probes, we have shown that **120** is reduced to the nonmutagenic lesion, 5,6-dihydrothymidine (**128**). Interestingly, the diastereomeric ratio of the reduced product (**128**) was dependent on the hydrogen atom donor. Bu_3SnH resulted in preferential trapping of the radical from the less hindered *re* face, whereas βME trapped the radical from the *si* face. We propose that the βME undergoes hydrogen bonding to the nucleobase, which results in delivery of the hydrogen atom preferentially from the *si* face.

When **4** was generated in the presence of O_2, the peroxyl radical (**7**) was generated, as expected. By studying its reactivity in the monomer, we discovered a novel pathway available to **7** that has not been previously observed for this particular radical. Intranucleotidyl hydrogen atom abstraction from the the adjacent carbon resulted in restoration of the native nucleobase with concomitant release of HOO•, which dissociates to

superoxide ($O_2^{\bullet}$) under biological conditions, with a rate constant of 21 s^{-1}. Although $O_2^{\bullet}$ is not deleterious to DNA, it is converted into reactive species, such as HO•, that are able to damage DNA. Moreover, $O_2^{\bullet}$ elimination presents a detoxification pathway available to the peroxyl radical (**7**). The additional involvement of $O_2^{\bullet}$-derived products in DNA damage makes this pathway a potential double-edged sword.

The reactivity of the peroxyl radical (**163**) was further investigated in the dinucleotide. Trapping of **163** by Bu_3SnH and βME occurred in the same diastereoselective fashion as observed for the alkyl radical (**120**). More importantly, direct evidence was obtained for the formation of 2-deoxyribonolactone (**132**), which was generated from the C1'-radical. This result confirmed the unusual mechanism involving the transfer of spin from the nucleobase to the sugar by internucleotidyl hydrogen atom abstraction by the peroxyl radical (**163**). Investigation of this mechanism in the dinucleotide also allowed us to determine that *5S*-**163** preferentially abstracts a hydrogen atom from the adjacent sugar. The diastereoselective nature of this reaction could not be observed when the radical was generated in oligonucleotides.

Internucleotidyl hydrogen atom abstraction by **163** occurs in competition with $O_2^{\bullet}$ elimination and intermolecular hydrogen atom abstraction. Since the rate constant for $O_2^{\bullet}$ elimination was determined from the monomer studies, competitive kinetics was used to estimate the rate constant for internucleotidyl hydrogen atom abstraction as 0.1 s^{-1}.

The potential for radiosensitizers, such as tirapazamine (**11**) and its metabolite (**12**), to react with the nucleobase radical (**4** and **120**) and propagate DNA damage was also investigated. Based on the results of the monomer and dinucleotide studies, the mechanism for the reactivity of the 1-*N*-oxide (**12**) is more complicated that previously thought. The evidence suggests that the nucleobase radical undergoes trapping on either the oxygen or nitrogen of **12**, generating a regioisomeric mixture of covalent adducts. Nonetheless, the reaction of **12** with the dinucleotide radical resulted in the formation of 2-deoxyribonolactone (**132**), the same lesion observed when the damage was propagated by

the peroxyl radical (**163**). Although the nature of the reactive species is unknown, it is clear that internucleotidyl hydrogen atom abstraction also occurs when the nucleobase radical was generated in the presence of **12**. Hence, the 1-*N*-oxide (**12**) can serve as a surrogate for O_2 in the propagation of DNA damage.

Investigation of the reactivity of 5,6-dihydrothymidin-5-yl (**4** and **120**) at the monomeric level and in the dinucleotide has provided us with a better understanding of its involvement in DNA damage amplification. The propagation of damage is dependent on the presence of O_2 or a radiosensitizer and is a consequence of internucleotidyl hydrogen atom abstraction and formation of 2-deoxyribonolactone (**132**). In addition, the peroxyl radical may protect itself through the elimination of superoxide. Although the dinucleotide is a simple model for ssDNA, investigation of the nucleobase radical (**120**) at this level has allowed us to more completely characterize that chemistry that occurs with respect to DNA damage which could not be done with oligonucleotides.

5 Experimental Procedures

General Methods. ^{1}H, ^{13}C, and ^{31}P NMR spectra were collected at 300, 75, and 109 MHz, respectively, using Varian software. HPLC analyses were carried out with a Waters 501 or 515 liquid chromatograph equipped with a Microsorb-MV C18 or C8 5 μm column (Rainin) interfaced to a Waters 490E or 2487 Multiwavelength detector. GC/MS analyses were carried out with a Hewlett-Packard 5970 mass spectrometer interfaced to a Hewlett-Packard 5890A gas chromatograph equipped with a DB-1 (30 m) fused silica column from J&W Scientific. Photolyses were carried out in pyrex tubes (0.25 in i.d.) in a Rayonet photoreactor (RPR-100) equipped with lamps having a maximum output of 300 (21 watts per lamp) or 350 (24 watts per lamp) nm. Samples were lyophilized on a Savant speed-vac.

All reactions were carried out in oven-dried glassware under an atmosphere of nitrogen unless otherwise specified. THF used in synthesis was dried with Na°/benzophenone ketyl. Pyridine, CH_2Cl_2, DMF, DMSO, ether, benzene, Et_3N, and Hünig's base were distilled from CaH_2. THF for mechanistic studies was distilled from $LiAlH_4$ and passed through alumina to remove trace amounts of peroxides. HPLC grade CH_3CN used in mechanistic studies was passed through anhydrous $CuSO_4$ and distilled from CaH_2 to remove amine impurities. Water (dd H_2O) for HPLC analysis and mechanistic studies was obtained from a Barnstead Nanopure still. All DMT-protected dinucleotides were chromatographed with anhydrous CH_2Cl_2 and MeOH.

Materials. All reagents were purchased from Aldrich unless otherwise specified. TBDMSCl was purchased from GFS Chemicals. Thymidine, 2'-deoxyuridine, 2'-deoxycytidine, DMTCl, uridine, and β-cyanoethyl diisopropylchlorophosphoramidite were

purchased from ChemGenes. NBS was purchased from Acros and was recrystallized from H_2O and dried over P_2O_5. Dowex (50W-X8, H^+ form) strongly acidic cation exchange resin was from Baker and Amberlite (IRA-93) weakly basic anion exchange resin was purchased from Sigma. BSTFA, superoxide dismutase (from bovine erythrocytes; 4400 units per mg, 1 unit inhibits cytochrome c reduction by 50%), catalase (21000 units per mg, 1 unit quenches 1 μmol of H_2O_2), and cytochrome *c* (from horse heart) were obtained from Sigma. The tetrazole/CH_3CN solution used in the coupling reactions of the dinucleotides was from Glen Research. Isotopically enriched solvents (D_2O, $H_2{}^{18}O$) were from Cambridge Isotope Laboratories. The water-soluble initiator, 2,2'-azobis[2-(2-imidazolin-2-yl)propane]-dihydrochloride (**103**, VA-044), was obtained from Wako. Tetranitromethane was washed with dilute NaOH, H_2O, and distilled from NaOH. PhSeH was prepared by $NaBH_4$ reduction of $(PhSe)_2$, followed by distillation. Bu_3SnH, *tert*-BuSH, and βME were distilled from themselves. Misonidazole (**13**) was obtained from Hoffmann-LaRoche. Tirapazamine (**11**), 1-*N*-oxide (**12**), and benzotriazine (**177**) were obtained from Professor Kent Gates (University of Missouri-Columbia).

General Procedure for the Photolysis and Thermolysis of 94, 95, and 96. Stock solutions of the radical precursors and hydrogen atom donors were prepared in THF or CH_3CN. Samples were prepared in duplicate with the appropriate reagents having a final volume of 100-500 μL (1:1 or 19:1; THF or CH_3CN:H_2O). Isotopic studies were carried out in D_2O or $H_2{}^{18}O$. Reactions were carried out with 0.01-0.1 mM of the radical precursor under pseudo-first order conditions. Samples for anaerobic studies were degassed using four freeze-pump-(3 min)-thaw cycles. Aerobic experiments were conducted so that O_2 was not the limiting reagent and the reaction vessels were left open to the atmosphere. Photolyses were carried out at either 300 or 350 nm in a Rayonet photoreactor with an internal temperature of 25 °C. Aerobic thermolyses were carried out at

37 °C (water bath) or 55 °C (heat block) for 24 h. Anaerobic thermolyses were carried out at 37 °C for 1.5 h.

Upon completion of the reaction, the samples were transferred to 1.5 mL eppendorf tubes and lyophilized. The residue was taken up in dd H_2O (95 μL), the internal standard (dU, 5 μL) was added, and the samples containing tin were extracted with hexanes (3 x 200 μL). The samples were analyzed by reverse-phase (C18) HPLC using a linear gradient of H_2O and MeOH at a flow rate of 1.0 mL/min (Method A, Table 34). Typically, 50 μL of the sample was injected using an AUFS of 1.0 and monitored at 205 nm. The products were quantitated using the calculated response factors listed below (Table 35).

Table 34. HPLC Method A: Solvent A: H_2O, Solvent B: MeOH.

Time (min)	% H_2O (A)	% MeOH (B)	Gradient Curve
0	95	5	-
5	95	5	6
35	0	100	6
40	95	5	6

The response factors were calculated using Equation 27, where X is the compound of interest and dU is the internal standard. Samples containing a range a concentrations of X and a constant concentration of dU were analyzed by HPLC. A plot of the ratio of the known concentrations was plotted against the ratio of the areas determined by HPLC. The slope of the line represencts the response factor.

$$\frac{[X]}{[dU]} = \frac{\text{Area (X)}}{\text{Area (dU)}} \bullet \text{response factor} \qquad (27)$$

Table 35. Retention times and response factors *versus* dU for monomers using Method A (Table 34).

Compound	Retention Time (min)	Response Factor
5R-**8**	5.1	1.2
5S-**8**	6.4	1.2
dU	9.4	-
5S-**34**	11.2	1.2
5R-**34**	13.5	1.2
3	18.0	0.8
5S-**95**	18.4	1.2
5R-**95**	22.2	1.2
5R-**94**	27.4	0.6
5S-**94**	28.7	0.6
5S-**96**	30.0	0.6
5R-**96**	31.1	0.6

Mass Spectral Analysis of Persilylated Derivatives in Monomer and Dinucleotide Studies. An aliquot of the HPLC sample (50 μL) was transferred to a 1 mL Kontes conical reaction vial fitted with a teflon septa. The sample was treated with 96% formic acid (450 μL) and heated at 100°C for 1 h. The formic acid was removed *in vacuo* and the samples lyophilized from absolute ethanol (3 x 50 μL). The residue was dissolved in BSTFA (50 μL). The solution was heated at 100 °C for 2 h. GC/MS analysis was carried out immediately. Samples were reheated for 1 h if analysis was not completed within 3 h of silylation.

GC/MS analysis was carried out directly on the BSTFA solution containing the persilylated nucleosides. Data was collected in the SIM mode for isotopic studies with a dwell time of 100 ms. Injections were made in the split mode with an injection port temperature of 250 °C, detector temperature of 285 °C, and solvent delay of 2.5 min.

Analysis of cleaved nucleosides was carried out using a temperature program of 150 °C (2 min) to 190 °C at 10 °C/min. Ions monitored for the detection of the persilylated nucleobases were 241.1 (uracil), 255.1 (thymine), 257.1 (5,6-dihydrothymine), 258.1, 345.1 (5,6-dihydro-5-hydroxythymine), and 347.1. Ions 258.1 and 347.1 were detected to determine ^{2}H and ^{18}O incorporation, respectively.

Kinetics for First-Order Rate Constant of Phenyl Selenide (96) Disappearance. Thermolysis samples for kinetic experiments were prepared with **96** (1.0 eq) and Bu_3SnH (10 eq) as described above and carried out under anaerobic conditions. After the samples had reacted for the designated time, they were immediately frozen and worked up as described in the general procedure. The samples were analyzed by reverse-phase HPLC using Method A. A plot was constructed of $\ln[\mathbf{96}]_o/[\mathbf{96}]_t$ versus time, and the rate constant determined from the slope.

Detection of Superoxide using Epinephrine Assay. A solution of **96** (0.1 mM) and (*R*)-(-)-epinephrine was prepared in phosphate buffer (50 mM) and desferal (1 mM). The epinephrine was prepared in HCl (10 mM, pH 2) and SOD was prepared in phosphate buffer. The samples were prepared in eppendorf tubes (1 mL total volume), vortexed, and transferred to a UV cell. The initial absorbance was measured (480 nm) and the sample photolyzed at 350 nm (1 lamp). The UV absorbance was measured at 480 nm at the specified time intervals.

When experiments were conducted with KO_2, a sample of epinephrine (0.1 mM) and/or Bu_3SnH (0.17 or 1.7 mM) was prepared in 1:1 THF:H_2O (1 mM desferal) and transferred to a UV cell. The initial absorbance was measured at 480 nm. A solution of KO_2 (0.1 mM) in anhydrous DMSO was added dropwise at 0.06 mL/h over 2 h and the final absorbance at 480 nm was measured.

Detection of Superoxide using Cytochrome *c* Assay. A solution of **96** (50 μM), cytochrome *c* (50 μM), and catalase (12 μg) was prepared in phosphate buffer (50 mM, pH 8, 0.1 mM EDTA). SOD was prepared in phosphate buffer (50 mM, pH 8, 0.1 mM EDTA). The samples were prepared in eppendorf tubes (1 mL total volume), vortexed, and transferred to a UV cell. The initial absorbance was measured at 550 nm. The samples were photolyzed at 350 nm (4 lamps) for 2h, measuring the absorbance in 10 min intervals. Aliquots of the sample were analyzed by reverse-phase HPLC (C18) as described above (Method A, Table 34) to determine the extent of conversion of **96** and the yield of **3**.

Samples for anaerobic experiments were prepared as described above and transferred to modified UV cells (equipped for degassing) and degassed using the freeze-pump-thaw method (4 x 3 min cycles). The initial absorbance was measured at 550 nm. The samples were photolyzed at 350 nm (4 lamps) and the absorbance measured at 550 nm in 20 min intervals.

The amount of cytochrome *c* reduced was calculated using Equation 28:

$$\% \text{ cyt } c_{red} = 100 \times \left[\frac{A(550)_t - A(550)_o}{A(550)_o \times \left(\frac{e(550)_{red}}{e(550)_{ox}} - A(550)_o \right)} \right] \qquad (28)$$

where A_t is the absorbance at 550 nm after t min, A_o is the initial absorbance, $e(550)_{red}$ is the extinction coefficient of cyt c (Fe^{2+}) at 550 nm (29500 M^{-1} cm^{-1}), and $e(550)_{ox}$ is the extinction coefficient of cyt c (Fe^{3+}) at 550 nm (8900 M^{-1} cm^{-1}).

Cyclic Voltammetry to Determine O_2 Concentration. Cyclic voltammetry was employed to determine the concentration of O_2 in aqueous THF mixtures. The reduction of

O_2 (Equation 29) was followed in both 100% H_2O and 1:1 THF:H_2O and the concentration of O_2 calculated using Equation 30:

$$O_2 + 2e^- + 2H^+ \rightleftharpoons H_2O_2 \quad (29)$$

$$i_p = (2.69 \times 10^5)\, n^{3/2}\, A\, D_o^{1/2}\, v^{1/2}\, C_o \quad (30)$$

where i_p is the peak current (amps), n the number of electrons transferred in the reaction, A the area of the electrode (cm^2), D_o the diffusion coefficient ($cm^2\ s^{-1}$), v the scan rate ($V\ s^{-1}$), and C_o the concentration of O_2 ($mol\ cm^{-3}$). The diffusion coefficient of O_2 in each solvent mixture was calculated using Equation 31 (Table 36):

$$D = \frac{k\,T}{6\pi\,\eta\,r} \quad (31)$$

where k is Boltzmann's constant ($kg\ m^2\ s^{-1}\ k^{-1}$), T the temperature (K), η the viscosity of the solvent ($kg\ m^{-1}\ s^{-1}$), and r the radius of an O_2 molecule (m).

Table 36. Diffusion coefficients of O_2.

Solvent	Viscosity ($kg\ m^{-1}\ s^{-1}$)	Diffusion Coefficient ($m^2\ s^{-1}$)
100% H_2O	0.89×10^{-3}	4.3×10^{-9}
1:1 THF:H_2O	0.72×10^{-3}	5.3×10^{-9}
19:1 THF:H_2O	0.57×10^{-3}	6.7×10^{-9}

The peak currents for the reduction of O_2 measured from the cyclic voltammograms were 12.6 μA and 19.6 μA in 100% H_2O and 1:1 THF:H_2O, respectively. Using Equation 30, the concentration of O_2 was 0.14 mM and 0.20 mM in 100% H_2O and 1:1 THF:H_2O, respectively. Although the concentration of O_2 in 19:1 THF:H_2O could not be measured, we assume that since the concentration of O_2 increased in 1:1 THF:H_2O, it will at least be comparable in 19:1 THF:H_2O. Therefore, the thermolyses and photolyses of the selenide to probe the effect of the concentration of Bu_3SnH were carried out in 19:1 THF:H_2O.

Kinetics of Superoxide Elimination. Samples containing **96** (0.1 mM), VA-044 (0.1 mM), and varying concentrations of Bu_3SnH (1.0-7.1 mM) were prepared in THF:H_2O (19:1 by volume) and heated at 55 °C for 24 h to ensure complete solubility of the Bu_3SnH and reduction of the hydroperoxide. The samples were worked up as described above and analyzed by reverse-phase HPLC (C18) using Method A (Table 34). The ratio of **3**:**8** was plotted against $[Bu_3SnH]^{-1}$ and the slope of the line used to determine the rate constant for superoxide elimination.

Anaerobic Photolysis of 96 in the Presence of 1-*N*-Oxide (12). Samples containing **96** (0.01 mM), **12** (2.0 mM), and βME (0.14-3.15 mM) or *tert*-BuSH (0.17-5.33 mM) were degassed and photolyzed at 350 nm (4 lamps) for 1h. After the photolysis, the samples were treated with excess βME (2 mM) and heated at 55 °C for 30 min to ensure cleavage of the covalent adduct. The samples were transferred the eppendorf tubes and lyophilized. The residue was taken up in H_2O (80 μL), benzophenone (10 μL), and dU (10 μL) and analyzed by reverse-phase (C18) HPLC using Method A (Table 34). The formation of nucleosides was monitored at 205 nm as described above. The conversion of **12** and yield of reduced benzotriazine (**176**) was monitored at 240 nm at an AUFS of 3.0 and benzophenone as the internal standard using the response factors below (Table 37).

The rate constant for trapping of **4** by **12** was calculated by plotting the ratio of **34**:**8** against the concentration of βME.

Table 37. Retention times and response factors for **11**, **12**, and **177** *versus* benzophenone.

Compound	Retention Time (min)	Response Factor
SR4233 (**11**)	21.1	1.8
1-*N*-oxide (**12**)	28.2	0.4
Benzotriazine (**177**)	26.8	0.3
Benzophenone	37.3	-

General Procedure for the Photolysis of 119 and 121. Samples containing **119** or **121** (0.1 mM) and the appropriate trap (1 mM) were prepared in THF (or CH_3CN):H_2O (1:1 by volume) having a final volume of 500 μL. Anaerobic samples were degassed using the freeze-pump-thaw method (4 x 3 min cycles) and aerobic samples were left open to the atmosphere. The samples were photolyzed at 350 nm for the appropriate time.

Upon completion of the reaction, the samples were transferred to eppendorf tubes (1.5 mL) and lyophilized. The residue was taken up in benzophenone (10 μL) and CH_3CN:NH_4HCO_2 buffer (90 μL, 25 mM, pH 6.8, 1:1 by volume). Samples containing tin were extracted with hexanes (3 x 200 μL). The samples were analyzed by reverse-phase (C8) HPLC using a gradient of NH_4HCO_2 (0.2 M, pH 6.2) and either CH_3CN or MeOH at a flow rate of 1.0 mL/min. Complete resolution was not obtained under a single gradient program. Therefore, the samples were analyzed using both Methods B (Table 38) and C (Table 39). Typically, 50 μL of the sample was injected using an AUFS of 1.0 and monitored at 240 nm.

The products were quantitated using the calculated response factors listed below with benzophenone as the internal standard (Table 40). The yields of *5R*-**130**, *5R*-, *5S*-**128**, *5R*-, *5S*-**132** and conversion of **119** or **121** was determined using Method B (Table 38). Under these conditions, *5S*-**130** and **129** coelute. Therefore, the samples were also analyzed by Method C (Table 39), in which *5R*-, *5S*-**130** coelute, but are separable from **129**. The yield of *5S*-**130** was obtained by subtracting the *5R*-**130** determined using Method B from the total yield found in Method C. The yield of **129** was determined by subsequently substracting the *5S*-**130** from the total **129** + *5S*-**130** determined in Method B.

Table 38. HPLC Method B: Solvent A: 0.2 M NH_4HCO_2, pH 6.2, Solvent B: CH_3CN.

Time (min)	% NH_4HCO_2 (A)	% CH_3CN (B)	Gradient Curve
0	95	5	-
5	95	5	6
65	70	30	2
95	30	70	6
100	95	5	6

Table 39. HPLC Method C: Solvent A: 0.2 M NH_4HCO_2, pH 6.2, Solvent B: MeOH.

Time (min)	% NH_4HCO_2 (A)	% MeOH (B)	Gradient Curve
0	95	5	-
5	95	5	6
65	35	65	2
85	20	80	6
90	0	100	6
95	0	100	6
100	95	5	6

Table 40. Retention times and response factors *versus* benzophenone for the dinucleotides.

Compound	Retention Time (min) Method A	Retention Time (min) Method B	Response Factor
Uracil	3.8	4.0	3.7
11	12.2	12.2	1.8
176	16.6	17.4	0.3
12	17.5	17.4	0.4
5R-**130**	60.5	49.1	0.8
5S-**130**	61.9	49.1	0.8
129	61.9	51.0	0.5
5S-**128**	64.4	51.0	0.9
5R-**128**	65.3	51.0	0.9
5R-**132**	72.6	51.0	1.2
5S-**132**	73.3	51.0	1.2
5R + *5S*-**131**	74.2	51.6	1.2
79	-	71.6	0.8
5R + *5S*-**121**	79.4	74.4	0.5
5R-**119**	78.7	66.5	0.6
5S-**119**	79.7	72.2	0.6
Benzophenone	86.2	46.3	-
78	95.6	77.0	0.6

Anaerobic Photolysis of 121 and Subsequent Enzymatic Digestion. Samples containing **121** (0.1 mM) and Bu_3SnH (1.1 mM) in CH_3CN:H_2O (500 μL, 1:1 by volume) were degassed and photolyzed at 350 nm (4 lamps) for 1 h. The samples were transferred to eppendorf tubes and lyophilized. One set of samples was taken up in dC (10 μL) and H_2O (90 μL) and analyzed directly by reverse-phase (C18) HPLC. The second set was subjected to enzymatic digest. The residue was taken up in buffer (86 μL, Tris-HCl, pH

7.9, 50 mM; NaCl, 100 mM; DTT, 1 mM) and $MgCl_2$ (100 mM). Nuclease P1 (10 μL, 0.3 units/μL), snake venom phosphodiesterase (2 μL, 0.003 units/μL), and calf intestine alkaline phosphatase (2 μL, 10 units/μL) were added to the sample and incubated at 37 °C for 12 h. dC (10 μL) was added to the sample and analyzed by reverse-phase (C18) HPLC using Method D (Table 41). The sample was analyzed at 205 nm at an AUFS of 1.0 with dC as the internal standard. The response factors listed below were estimated based on the extinction coefficients of dU and dC at 205 nm (Table 42).

Table 41. HPLC Method D: Solvent A: 10 mM KH_2PO_4, pH 6.8, Solvent B: MeOH.

Time (min)	% KH_2PO_4 (A)	% MeOH (B)	Gradient Curve
0	99	1	-
20	99	1	6
40	20	80	6
55	20	80	6
60	99	1	6

Table 42. Retention times and response factors *versus* dC for products of enzymatic digestion.

Compound	Retention Time (min)	Response Factor
dC	13.7	-
α-dU	21.0	2.2
β-dU	21.9	2.2
5S-**34**	27.3	2.6
5R-**34**	28.3	2.6
3	29.8	1.8
128	30.6	2.6
129	31.4	1.8

Anaerobic Photolysis of 121 in the Presence of Tetranitromethane. Samples containing **121** (0.15 mM), tetranitromethane (1.04 mM), and βME (1.4 mM) were prepared in CH_3CN:NH_4HCO_2 buffer (25 mM, pH 6.8, 1:1 by volume) with a final volume of 500 μL. The samples were degassed using the freeze-pump-thaw method (4 x 3 min cycles) and photolyzed at 350 nm (4 lamps) for 1 h. The samples were transferred to eppendorf tubes and lyophilized. The residue was taken up in benzophenone (10 μL) and CH_3CN:NH_4HCO_2 buffer (90 μL, 25 mM, pH 6.8, 1:1 by volume) and analyzed by reverse-phase (C8) HPLC using Methods B and C (Tables 38 and 39).

Aerobic Photolysis of 121 in the Presence of Mannitol. Samples containing **121** (0.10 mM) and mannitol (1.1 mM) were prepared in CH_3CN:H_2O (500 μL, 1:1 by volume) and photolyzed at 350 nm (4 lamps) for 1 h. The samples were worked up as above and analyzed by reverse-phase (C8) HPLC using Method B (Table 38) for formation of **132**.

Anaerobic Photolysis of 121 in the Presence of the 1-*N*-Oxide (12). A solution of the dinucleotide **121** (0.011 mM) in CH_3CN:H_2O (500 μL, 1:1 by volume) was photolyzed in the presence of the 1-*N*-oxide (**12**, 2.0 mM) and βME (0.14-3.15 mM) at 350 nm (4 lamps) for 1 h . The samples were worked up and analyzed by reverse-phase (C8) HPLC using Methods B and C as described above (Tables 38 and 39). The ratio of **130**:**132** was plotted against the concentration of βME.

Titration of Lithium and Grignard Reagents. A 15 mL flask equipped with a stir bar was heated while under vacuum to remove residual acetone and/or water. A few crystals of 1,10-phenanthroline were dissolved in benzene (3 mL) and the base was added

until a persistent violet color appeared. The solution was titrated with 2-butanol (1.0 M) in xylenes until a yellow endpoint was reached.

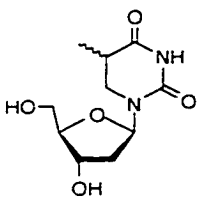

Preparation of 5,6-Dihydrothymidine (34). 5% Rhodium on alumina (0.31 g, 10%/wt) was added to a solution of thymidine (3.08 g, 0.013 mol) in MeOH:H_2O (200 mL, 1:1 by volume) and the reaction mixture pressurized with H_2 (50 psi). After 8 h, the reaction mixture was filtered through Celite and concentrated to yield a white solid (3.10 g,100%). ^{1}H NMR (MeOH-d_4) δ 6.26 (t, 1H, J = 6 Hz), 4.28 (quintet, 1H, J = 3 Hz), 3.79-3.74 (m, 1H), 3.70-3.59 (m, 2H), 3.51 (dd, 1H, J = 5.4, 12.9 Hz), 3.21 (dd, 1H, J = 9.6, 12.6 Hz), 2.71-2.64 (m, 1H), 2.27-2.17 (m, 1H), 2.03-1.96 (m, 1H), 1.20 (d, 3H, J = 12 Hz).

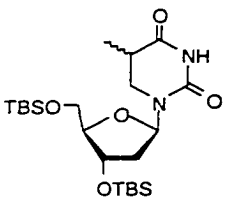

Preparation of 97. TBDMSCl (4.70 g, 0.031 mol), imidazole (4.58 g, 0.067 mol), and **34** (3.10 g, 0.013 mol) were dissolved in pyridine (30 mL) and stirred at 40 °C for 5 h. The reaction mixture was diluted with saturated $NaHCO_3$ (50 mL) and H_2O (25 mL) and extracted with ether (3 x 100 mL). The organics were washed with brine and dried over $MgSO_4$. The product was purified by flash chromatography (hexanes:EtOAc, 3:1to 1:1) and isolated as a white solid (5.26 g, 88%). ^{1}H NMR ($CDCl_3$) δ 7.66 (br s, 1H), 6.32 (t, 1H, J = 7.2 Hz), 4.38-4.34 (m, 1H), 3.80 (q, 1H, J = 2.7 Hz), 3.71 (t, 2H, J = 2.7 Hz), 3.41-3.23 (m, 2H), 2.64-2.57 (m, 1H), 2.01-1.96 (m, 2H), 1.26 (d, 3H, J = 7.2 Hz), 0.90 (s, 9H), 0.89 (s, 9H), 0.08 (s, 6H), 0.07 (s, 3H), 0.06 (s, 3H).

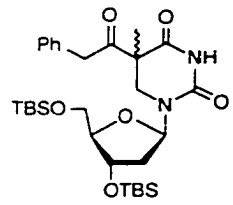

Preparation of 100. *sec*-BuLi (0.68 mL, 1.3 M, 0.88 mmol) was added to a solution of **97** (0.17 g, 0.35 mmol) in THF (3.5 mL) at -78 °C. After 1 h, DMPU (0.21 g, 1.65 mmol) was added. A solution of phenylacetyl chloride (0.082 g, 0.53 mmol) in THF (0.5 mL) was added after 30 min at -78 °C and allowed to warm to room temperature. After 2 h, the reaction mixture was diluted with saturated NH_4Cl (50 mL) and extracted with EtOAc (3 x 70 mL). The organic layer was washed with brine and dried over $MgSO_4$. Column chromatography (hexanes:EtOAc, 2:1) yielded the product (0.15 g, 74%) as a mixture of diastereomers (1.5:1, 5*S*:5*R*). m.p. 41-46 °C; ^{1}H NMR ($CDCl_3$) δ 7.86 (s, 0.6 H), 7.83 (s, 0.4H), 7.35-7.25 (m, 3H), 7.19-7.11 (m, 2H), 6.26-6.19 (m, 1H), 4.41-4.35 (m, 1H), 4.19 (d, 0.4H, J = 13.2 Hz), 4.04 (d, 0.4H, J = 16.5 Hz), 3.99 (d, 0.6 H, J = 15.9 Hz), 3.89 (d, 1H, J = 2.4 Hz), 3.85 (s, 1H), 3.79-3.73 (m, 1.6H), 3.70 (d, 1H, J = 3.3 Hz), 3.16 (d, 1H, J = 13.2 Hz), 2.25 (ddd, 0.6H, J = 6.0, 7.8, 13.5 Hz) apparent quintet, 2.00-1.94 (m, 0.8H), 1.85 (ddd, 0.6H, J = 3.3, 6.0, 13.5 Hz), 1.47 (s, 1.2H), 1.45 (s, 1.8H), 0.92 (s, 3H), 0.90 (s, 15H), 0.09 (s, 3H), 0.084 (s, 3H), 0.079 (s, 4H), 0.06 (s, 2H); ^{13}C NMR ($CDCl_3$) δ 202.9, 202.4, 170.8, 170.6, 152.2, 151.6, 133.0, 132.6, 130.0, 129.7, 128.9, 128.7, 127.6, 127.3, 87.2, 86.6, 84.7, 83.7, 73.1, 72.1, 63.8, 63.1, 55.5, 45.3, 44.6, 44.5, 43.9, 37.7, 37.3, 26.1, 26.0, 19.2, 18.6, 18.2, 18.1, -4.4, -4.6, -5.2, -5.3; IR (film) 3214 (br), 3090, 3033, 2955, 2930, 2897, 2858, 1714, 1698, 1472, 1429, 1383, 1361, 1254, 1225, 1096, 1032, 971, 836, 778 cm^{-1}.

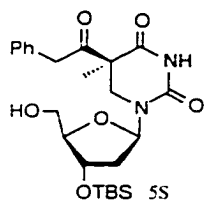

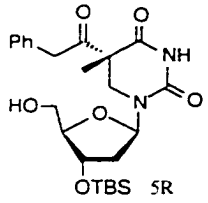

Preparation of *5S*-and *5R*-122. A solution of TFA/H_2O (8 mL, 10% by volume) was added to a solution of **100** (0.96 g, 1.62 mmol) in THF (8 mL) at 0 °C. After 3 h, the reaction mixture was quenched with saturated $NaHCO_3$, diluted with H_2O (20 mL), and extracted with CH_2Cl_2 (3 x 30 mL). The organic layer was dried over $MgSO_4$ and concentrated *in vacuo*. Column chromatography (EtOAc:CH_2Cl_2, 1:9 to EtOAc) yielded 0.13 g of ***5R*-122** as a white powder and 0.28 g of ***5S*-122** as a white foam in 53% total yield. ***5S*-122**: m.p. 49-54 °C; ^{1}H NMR ($CDCl_3$) δ 7.52 (s, 1H), 7.32-7.27 (m, 3H), 7.13 (dd, 2H, J = 1.5, 7.5 Hz), 6.12 (t, 1H, J = 7.2 Hz), 4.32 (dt, 1H, J = 4.2, 6.9 Hz), 3.99 (d, 1H, J = 16.2 Hz), 3.88-3.75 (m, 4H), 3.68-3.62 (m, 1H), 3.16 (d, 1H, J = 12.6 Hz), 2.34 (ddd, 1H, J = 7.2, 13.8, 7.2 Hz) apparent quintet, 2.00-1.90 (m, 1H), 1.92 (m, 1H), 1.46 (s, 3H), 0.90 (s, 9H), 0.10 (s, 3H), 0.09 (s, 3H); ^{13}C NMR ($CDCl_3$) δ 202.4, 170.3, 151.9, 132.4, 129.7, 128.9, 127.7, 86.0, 84.5, 71.6, 62.6, 55.7, 45.2, 44.7, 37.7, 25.9, 19.2, 18.2, -4.4, -4.7; IR (film) 3460 (br), 3217, 3089, 2929, 2857, 1710, 1474, 1430, 1384, 1360, 1252, 1224, 1096, 1036, 836, 778 cm^{-1}. ***5R*-122**: m.p. 144-152 °C; ^{1}H NMR ($CDCl_3$) δ 7.50 (s, 1H), 7.32-7.27 (m, 3H), 7.14 (dd, 2H, J = 2.4, 8.1 Hz), 6.01 (t, 1H, J = 6.9 Hz), 4.45 (dt, 1H, J = 4.2, 6.9 Hz), 4.00 (d, 1H, J = 12.9 Hz), 3.97 (d, 1H, J = 15.6 Hz), 3.90-3.81 (m, 2H), 3.76 (dt, 1H, J = 2.7, 4.2 Hz), 3.66-3.58 (m, 1H), 3.30 (dd, 1H, J = 4.2, 9.3 Hz), 3.20 (d, 1H, J = 12.6 Hz), 2.19 (ddd, 1H, J = 6.9, 13.5, 6.9 Hz) apparent quintet, 2.03 (ddd, 1H, J = 4.2, 6.9, 13.5 Hz), 1.43 (s, 3H), 0.90 (s, 9H), 0.09 (s, 6H); ^{13}C NMR ($CDCl_3$) δ 203.4, 170.7, 151.3, 132.0, 129.8, 129.0, 127.7, 86.5, 85.3, 71.4, 61.9, 55.6, 46.5, 45.8, 38.0, 26.0, 19.3, 18.2, -4.5, -4.6; IR (film) 3417 (br), 3211, 3059, 2928, 2855, 1716, 1698, 1470, 1388, 1372, 1304, 1249, 1096, 1038, 835, 784, 721 cm^{-1}.

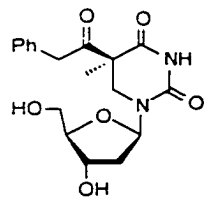

Preparation of *5S*-94. Et_3N•3HF (0.38 g, 0.23 mmol) was added to a solution of ***5S*-122** (0.28 g, 0.47 mmol) in THF (5 mL). After 15 h, the reaction mixture was concentrated *in vacuo* and purified by column chromatography (CH_2Cl_2:MeOH, 9:1). The product was isolated in quantitative yield (0.20 g) as a white foam. m.p. 51-59 °C; ^{1}H NMR (MeOH-d_4) δ 7.30-7.22 (m, 3H), 7.13 (dd, 2H, J = 1.8, 8.1 Hz); 6.18 (dd, 1H, J = 6.6, 7.5 Hz); 4.29 (dt, 1H, J = 3.3, 6.6 Hz), 3.93 (s, 2H), 3.91 (d, 1H, J = 13.2 Hz), 3.76-3.69 (m, 1H), 3.67-3.59 (m, 2H), 3.26 (d, 1H, J = 13.5 Hz), 2.30 (ddd, 1H, J = 6.9, 14.1, 6.9 Hz) apparent quintet, 1.87 (ddd, 1H, J = 3.3, 6.3, 13.5 Hz), 1.44 (s, 3H); ^{13}C NMR (MeOH-d_4) δ 204.8, 172.7, 154.5, 134.6, 130.8, 129.5, 128.1, 87.3, 84.9, 72.4, 63.4, 56.7, 45.6, 45.0, 37.6, 18.9; IR (film) 3398 (br), 3240, 3085, 2938, 2874, 1704, 1479, 1454, 1432, 1385, 1360, 1300, 1226, 1090, 1038, 724 cm^{-1}.

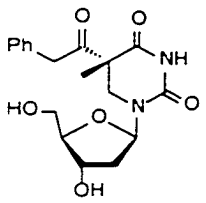

Preparation of *5R*-94. Et_3N•3HF (0.18 g, 1.10 mmol) was added to a solution of ***5R*-122** (0.13 g, 0.23 mmol) in THF (3 mL). After 14 h, the reaction mixture was concentrated *in vacuo* and purified by column chromatography (CH_2Cl_2:MeOH, 9:1). The product (0.091 g) was isolated as a white powder in quantitative yield. m.p. 208-213 °C; ^{1}H NMR (MeOH-d_4) δ 7.30-7.17 (m, 5H), 6.19 (dd, 1H, J = 6.0, 8.4 Hz), 4.35 (dt, 1H, J = 3.0, 6.3 Hz), 4.28 (d, 1H, J = 13.2 Hz), 4.12 (d, 1H, J = 17.4 Hz), 4.00 (d, 1H, J = 17.7 Hz), 3.85 (q, 1H, J = 3.3 Hz), 3.72 (d, 1H, J = 3.3 Hz), 3.72 (d, 1H, J = 4.8 Hz), 3.38 (d, 1H, J = 13.2 Hz), 2.19 (ddd, 1H, J = 6.3, 8.7, 13.8 Hz), 1.97 (ddd, 1H, J = 2.7, 6.0, 13.5 Hz), 1.48 (s, 3H); ^{13}C NMR (MeOH-d_4) δ 207.7, 173.3, 154.2, 134.5, 131.0, 129.5, 128.1, 87.3, 85.4, 72.6, 63.2, 57.0, 45.4, 44.5, 37.2, 17.7; IR (film) 3410 (br), 3219, 3088, 2933, 2878, 1698, 1474, 1456, 1388, 1363, 1306, 1233, 1036, 724 cm^{-1}.

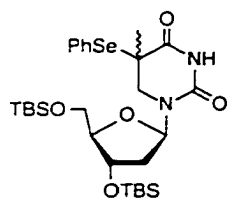

Preparation of 101. *sec*-BuLi (2.2 mL, 1.3 M, 2.86 mmol) was added to a solution of **97** (0.55 g, 1.16 mmol) in THF (10 mL) at -78 °C. After 1.5 h, DMPU (0.74 g, 5.79 mmol) was added, followed by a solution of PhSeBr (0.43 g, 1.84 mmol) in THF (5 mL). After 12 h, allowing to warm to room temperature, the reaction mixture was diluted with NH_4Cl (50 mL), H_2O (50 mL), and extracted with EtOAc (3 x 70 mL). The organic layer was washed with brine and dried over $MgSO_4$. Column chromatography (CH_2Cl_2:EtOAc, 19:1) yielded 0.60 g (82%) of the product as a mixture of diastereomers (≈2.5:1, 5*R*:5*S*). m.p. 44-49 °C; ^1H NMR ($CDCl_3$) δ 7.63-7.56 (m, 2H), 7.47-7.31 (m, 4H), 6.38 (dd, 0.7H, J = 5.7, 7.8 Hz), 6.29 (t, 0.3H, J = 7.2 Hz), 4.43-4.37 (m, 1H), 3.95-3.77 (m, 1.5H), 3.73-3.72 (m, 1.5H) apparent t, 3.64-3.51 (m, 1.7H) apparent q, 3.35 (d, 0.3H, J = 13.2 Hz), 2.23 (ddd, 0.7H, J = 6.3, 8.7 Hz), 2.06 (ddd, 0.7H, J = 2.7, 6.0, 12.6 Hz), 1.97 (dd, 0.6H, J = 4.2, 7.5 Hz), 1.48 (s, 0.9H), 1.44 (s, 2.1H), 0.95-0.91 (m, 18H), 0.14-0.08 (m, 12H); ^{13}C NMR ($CDCl_3$) δ 170.8, 152.3, 138.3, 138.1, 130.0, 129.9, 129.2, 129.1, 125.3, 87.0, 86.7, 84.3, 83.8, 72.8, 72.2, 63.6, 48.8, 47.7, 44.2, 38.3, 37.8, 26.3, 26.1, 21.2, 21.0, 18.7, 18.3, -4.3, -4.5, -5.0, -5.1; IR (film) 3207, 3076, 2952, 2931, 2858, 1709, 1472, 1433, 1363, 1253, 1218, 1094, 1029, 836, 779, 740 cm^{-1}.

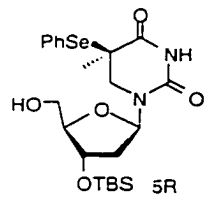

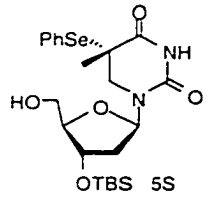

Preparation of *5R*- and *5S*-123. A solution of TFA/H_2O (7 mL, 10% by volume) was added to a solution of **101** (0.91 g, 1.45 mmol) in THF (7 mL) at 0 °C. After 4 h, the reaction mixture was quenched with saturated $NaHCO_3$ (50 mL) and extracted with EtOAc (3 x 50 mL). The organic layer was washed with brine and dried over $MgSO_4$. Column chromatography (CH_2Cl_2:MeOH, 19:1 to 4:1) yielded 0.29 g of ***5R*-123** and 0.081 g of ***5S*-123** in 49% total yield. ***5R*-123**: m.p. 196-199 °C;

^{1}H NMR ($CDCl_3$) δ 7.60-7.57 (m, 2H), 7.47-7.32 (m, 4H), 6.25 (t, 1H, J = 6.9 Hz), 4.37 (dt, 1H, J = 3.9, 6.6 Hz), 3.87-3.79 (m, 2H), 3.70-3.64 (m, 1H), 3.61-3.49 (m, 2H), 2.34 (ddd, 1H, J = 7.2, 13.8, 7.2 Hz) apparent quintet, 2.12 (ddd, 1H, J = 4.2, 6.6, 13.2 HZ), 1.99 (m, 1H), 1.48 (s, 3H), 0.92 (s, 9H), 0.13 (s, 3H), 0.12 (s, 3H); ^{13}C NMR ($CDCl_3$) δ 170.7, 152.4, 138.1, 130.1, 129.3, 125.2, 86.0, 84.5, 71.6, 62.4, 49.9, 44.2, 38.3, 26.0, 21.1, 18.3, -4.3, -4.5; IR (film) 3421 (br), 3215, 3073, 2950, 2930, 2891, 2857, 1698, 1474, 1434, 1364, 1253, 1216, 1093, 1048, 1026, 835, 778, 740 cm^{-1}. ***5S*-123**: m.p. 145-149 °C; ^{1}H NMR ($CDCl_3$) δ 7.73 (s, 1H), 7.60 (dd, 2H, J = 1.2, 8.1 Hz), 7.45-7.31 (m, 3H), 6.04 (t, 1H, J = 7.2 Hz), 4.44 (dt, 1H, J = 4.5, 6.9 Hz), 3.96-3.91 (m, 1H), 3.85-3.82 (m, 1H), 3.73-3.64 (m, 1H), 3.63 (s, 2H), 2.80-2.76 (m, 1H), 2.30 (ddd, 1H, J = 6.9, 13.5, 6.9 Hz) apparent quintet, 2.10 (ddd, 1H, J = 4.2, 6.9, 13.2 Hz), 1.47 (s, 3H), 0.91 (s, 9H), 0.10 (s, 6H); ^{13}C NMR ($CDCl_3$) δ 170.7, 151.8, 138.1, 130.1, 129.2, 125.2, 86.3, 86.0, 71.5, 62.2, 51.3, 44.1, 38.1, 26.0, 21.0, 18.2, -4.4, -4.5; IR (film) 3418 (br), 3202, 3074, 2951, 2931, 2890, 2857, 1698, 1473, 1379, 1249, 1220, 1094, 1052, 1025, 836, 779, 737 cm^{-1}.

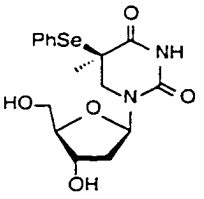

Preparation of *5R*-96. Et_3N•3HF (0.40 g, 2.45 mmol) was added to a solution of ***5R*-123** (0.25 g, 0.48 mmol) in THF (5 mL). After 12 h, the reaction mixture was concentrated *in vacuo* and purified by column chromatography (CH_2Cl_2:MeOH, 9:1). The product was isolated in 93% yield (0.18 g) as a white powder. m.p. 179-182 °C; ^{1}H NMR (MeOH-d_4) δ 7.58 (dd, 2H, J = 1.2, 8.4 Hz), 7.46-7.40 (m, 1H), 7.37-7.31 (m, 2H), 6.31 (dd, 1H, J = 6.6, 7.8 Hz), 4.32 (ddd, 1H, J = 3.3, 6.6, 3.3 Hz), 3.78 (dt, 1H, J = 3.6, 4.5 Hz) apparent q, 3.70 (d, 1H, J = 14.4 Hz), 3.70-3.63 (m, 2H), 3.57 (d, 1H, J = 14.4 Hz), 2.35 (ddd, 1H, J = 6.6, 7.8, 13.5 Hz), 2.07 (ddd, 1H, J = 3.3, 6.6, 13.5 Hz), 1.44 (s, 3H); ^{13}C NMR

(MeOH-d_4) δ 173.1, 154.9, 139.2, 130.9, 130.2, 126.8, 87.5, 84.9, 72.4, 63.4, 49.8, 45.8, 38.2, 21.2; IR (film) 3389 (br), 3075, 2925, 2869, 1693, 1477, 1434, 1366, 1285, 1219, 1088, 1047, 745 cm^{-1}.

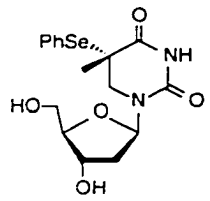

Preparation of *5S*-96. Et_3N•3HF (0.12 g, 0.74 mmol) was added to a solution of ***5S*-123** (0.074 g, 0.14 mmol) in THF (2 mL). After 12 h, the reaction mixture was concentrated *in vacuo* and purified by column chromatography (CH_2Cl_2:MeOH, 9:1). The product was isolated in 88% yield (51 mg) as a white foam. m.p. 46-53 °C; ^1H NMR (MeOH-d_4) δ 7.61 (dd, 2H, J = 1.2, 8.1 Hz), 7.45-7.39 (m, 1H), 7.35-7.30 (m, 2H), 6.20 (dd, 1H, J = 5.7, 8.1 Hz), 4.32 (dt, 1H, J = 2.7, 5.7 Hz), 3.89 (d, 1H, J = 13.5 Hz), 3.88-3.84 (m, 1H), 3.73 (d, 2H, J = 4.5 Hz), 3.50 (d, 1H, J = 13.5 Hz), 2.16 (ddd, 1H, J = 6.0, 8.4, 13.5 Hz), 1.98 (ddd, 1H, J = 2.4, 5.7, 13.5 Hz), 1.44 (s, 3H); ^{13}C NMR (MeOH-d_4) δ 173.2, 154.0, 139.4, 130.8, 130.0, 127.1, 87.8, 85.6, 73.0, 63.7, 49.1, 45.4, 37.6, 21.3; IR (film) 3399 (br), 3074, 2925, 2870, 1692, 1475, 1437, 1376, 1221, 1088, 1048, 745 cm^{-1}.

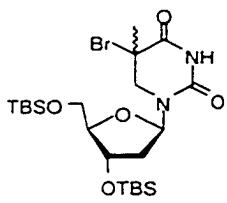

Preparation of 102. *sec*-BuLi (15.0 mL, 1.3 M, 18.8 mmol) was added to a solution of **97** (3.47 g, 7.34 mmol) in THF (35 mL) at -78 °C. After 1.5 h, DMPU (4.66 g, 36.4 mmol) was added and stirred for 30 min. A solution of NBS (2.09 g, 11.7 mmol) in THF (20 mL) was added dropwise at -78 °C. After 10 min, the reaction mixture was poured into saturated NH_4Cl (100 mL) and extracted with EtOAc (3 x 100 mL). The organic layer was washed with brine and dried over $MgSO_4$. Column chromatography (hexanes:EtOAc, 3:1) yielded 1.56 g (39%) of **103** as a mixture of diastereomers (3.4:1, *5R*:*5S*). m.p. 50-59 °C; ^1H NMR ($CDCl_3$) δ 7.60 (br s, 0.77H), 7.56 (br s, 0.23H), 6.40 (dd, 0.77H, J = 6.0, 7.8

Hz), 6.30 (dd, 0.23H, J = 6.0, 8.4 Hz), 4.37 (ddd, 1H, J = 2.7, 5.7, 2.7H) apparent quintet, 3.99 (d, 0.23H, J = 14.1 Hz), 3.88 (m, 0.23H), 3.83-3.77 (m, 1H), 3.75-3.68 (m, 1.77H), 3.69 (d, 0.77H, J = 15.3 Hz), 3.40 (d, 0.77H, J = 15.3 Hz), 3.28 (d, 0.23H, J = 14.4 Hz), 2.16 (ddd, 1H, J = 6.0, 7.8, 12.9 Hz), 2.04 (ddd, 0.23H, J = 3.0, 5.7, 13.2 Hz), 1.95 (s, 2.3H), 1.94 (s, 0.7H), 0.93 (s, 8H), 0.91 (s, 7H), 0.90 (s, 3H), 0.11 (s, 3H), 0.09 (s, 4H), 0.08 (s, 3H), 0.07 (s, 2H); ^{13}C NMR ($CDCl_3$) δ 167.6, 151.7, 151.1, 87.0, 86.8, 84.4, 83.9, 72.5, 72.1, 63.4, 63.2, 52.7, 50.2, 49.5, 38.4, 38.2, 26.2, 26.0, 24.5, 18.6, 18.2, -4.4, -4.6, -5.18, -5.21; IR (film) 3203, 3086, 2954, 2929, 2885, 2857, 1714, 1698, 1472, 1433, 1381, 1255, 1222, 1119, 1095, 1029, 835, 777 cm^{-1}; LRMS (FAB) calcd for $C_{22}H_{43}N_2O_5BrSi_2$: 551.2 (M+H), found 551.2.

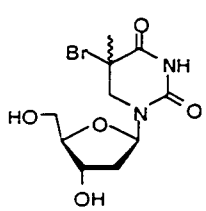

Preparation of 95. A solution of TFA/H_2O (2 mL, 10% by volume) was added to a solution of **102** (0.22 g, 0.39 mmol) in THF (2 mL) at room temperature. After 4 h, the reaction was quenched with $NaHCO_3$ and concentrated *in vacuo*, avoiding excessive heating. Column chromatography (CH_2Cl_2:MeOH, 9:1 to 4:1) yielded 0.093 g (73%) of **95** as a mixture of diastereomers. m.p. 43-57 °C; ^1H NMR (MeOH-d_4) δ 6.35 (dd, 0.8H, J = 6.0, 7.5 Hz), 6.21 (dd, 0.2H, J = 5.7, 8.1 Hz), 4.30 (ddd, 1H, J = 3.0, 6.3, 3.0 Hz), 3.98 (d, 0.2H, J = 14.4 Hz), 3.84-3.78 (m, 1H), 3.79 (d, 0.8H, J = 15.3 Hz), 3.72-3.60 (m, 2H), 3.50 (d, 0.2H, J = 14.7 Hz), 3.49 (d, 0.8H, J = 15.3 Hz), 2.31 (ddd, 0.8H, J = 6.6, 7.8, 13.8 Hz), 2.16 (ddd, 0.2H, J = 6.3, 8.4, 13.5 Hz), 2.04 (ddd, 1H, J = 3.3, 6.6, 13.8 Hz), 1.92 (s, 2.4H), 1.90 (s, 0.6H); ^{13}C NMR (MeOH-d_4) δ 169.7, 154.1, 87.8, 87.5, 85.7, 85.0, 72.7, 72.3, 63.5, 63.3, 55.1, 54.1, 50.9, 38.2, 37.9, 24.5, 24.4; IR (film) 3390 (br), 2930, 2873, 1698, 1478, 1434, 1384, 1294, 1224, 1088, 1049 cm^{-1}; Exact mass (FAB) calcd for $C_{10}H_{15}N_2O_5Br$: 323.0243 (M+H), found 323.0248.

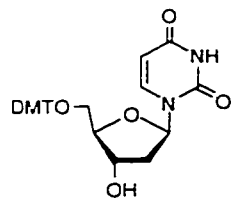

Preparation of DMT-dU. A solution of DMTCl (3.60 g, 10.6 mmol) in pyridine (15 mL) was slowly added dropwise to a solution of 2'-deoxyuridine (2.02 g, 8.85 mmol) in pyridine (20 mL). After stirring overnight, the reaction was quenched with MeOH (2 mL), diluted with saturated $NaHCO_3$ (100 mL), and extracted with EtOAc (3 x 100 mL). The organics were washed with brine and dried over $MgSO_4$. Column chromatography (EtOAc:hexanes, 2:1 to 3:1) yielded the product (4.36 g) as a white foam in 93% yield. ^1H NMR ($CDCl_3$) δ 8.68 (br s, 1H), 7.80 (d, 1H, J = 8.4 Hz), 7.40-7.25 (m, 9H), 6.88-6.83 (m, 4H), 6.32 (dd, 1H, J = 6.3, 6.3 Hz), 5.41 (d, 1H, J = 8.1 Hz), 4.58-4.55 (m, 1H), 4.02 (m, 1H), 3.81 (s, 3H), 3.79 (s, 3H), 3.52-3.42 (m, 2H), 2.46 (ddd, 1H, J = 4.5, 6.3, 13.8 Hz), 2.28 (ddd, 1H, J = 6.3, 12.9, 6.3 Hz) apparent quintet, 2.15 (m, 1H) apparent d.

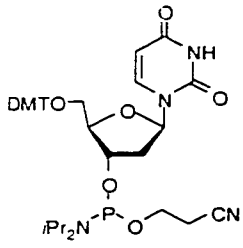

Preparation of 125. β-Cyanoethyl diisopropylchlorophosphoramidite (2.23 g, 9.41 mmol) was added dropwise to a solution of DMT-dU (4.15 g, 7.82 mmol) and Hünig's base (4.01 g, 9.41 mmol) in CH_2Cl_2 (40 mL). After stirring overnight, the reaction mixture was diluted with EtOAc (120 mL) and washed quickly with 10% Na_2CO_3 (50 mL) and brine (50 mL). The organic layer was dried over Na_2SO_4 and concentrated to yield an off-white foam. The product was purified by column chromatography (hexanes:EtOAc, 1:1 to 1:2) and isolated as a white foam (4.79 g, 84%). ^1H NMR ($CDCl_3$) δ 8.72 (br s, 1H), 7.86 (d, 0.5H, J = 8.4 Hz), 7.80 (d, 0.5H, J = 8.1 Hz), 7.40-7.37 (m, 2H), 7.32-7.24 (m, 7H), 6.87-6.83 (m, 4H) apparent dd, 3.33 (dd, 1H, J = 6.0, 12.0 Hz), 5.36 (d, 0.5H, J = 8.1 Hz), 5.36 (d, 0.5H, J = 8.1 Hz), 4.69 (m, 1H), 4.17-4.12 (m, 1H), 3.90-3.70 (m, 1H), 3.81 (s, 3H), 3.80 (s, 3H), 3.68-3.51 (m, 3H), 3.49-3.38 (m, 2H), 2.64 (t, 1H, J = 6.3

Hz), 2.59-2.50 (m, 1H), 2.47 (t, 1H, J = 6.3 Hz), 2.35-2.26 (m, 1H) apparent quintet, 1.21-1.17 (m, 9H), 1.09 (d, 3H, J = 6.9 Hz).

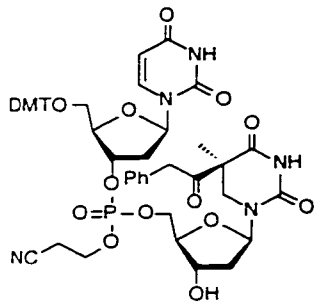

General Procedure for Coupling Reaction: Preparation of *5S*-126. A solution of **125** (0.29 g, 0.39 mmol) in CH_3CN (3 mL, 0.5 M tetrazole) was added dropwise to a solution of ***5S*-94** (0.12 g, 0.32 mmol) in THF (3 mL). After 1 h, a solution of I_2 (1.0 M/THF:2,6-lutidine:H_2O, 2:2:1 by volume) was added until the orange color did not dissipate. After 30 min, the excess I_2 was quenched with 10% $Na_2S_2O_3$/saturated $NaHCO_3$, diluted with $NaHCO_3$ (40 mL), and extracted with CH_2Cl_2 (3 x 50 mL). The organic layer was dried over Na_2SO_4 and concentrated *in vacuo* to yield a yellow foam. Column chromatography (CH_2Cl_2:MeOH, 19:1 to 9:1) yielded 0.14 g (43%) of product as a mixture of diastereomers. m.p. 121 °C (color change from white to pink), 113-125 °C (phase change); ^{1}H NMR ($CDCl_3$) δ 9.94 (br s, 0.5H), 9.79 (br s, 0.5H), 8.77 (br s, 0.5H), 8.71 (br s, 0.5H), 7.64 (d, 1H, J = 8.1 Hz), 7.36-7.23 (m, 12H), 7.08 (d, 2H, J = 6.6 Hz), 6.84 (d, 4H, J = 8.7 Hz), 6.31-6.23 (m, 2H), 5.40 (dd, 1H, J = 3.3, 8.1 Hz), 5.14 (m, 1H), 4.32-4.11 (m, 6H), 4.02-3.92 (m, 2H), 3.80 (m, 2H), 3.782 (s, 3H), 3.777 (s, 3H), 3.45 (m, 2H), 3.15 (dd, 1H, J = 4.2, 12.6 Hz), 2.74-2.57 (m, 1H), 2.67 (t, 2H, J = 6.0 Hz), 2.34 (m, 2H), 2.05 (m, 1H), 1.43 (s, 3H); ^{13}C NMR ($CDCl_3$) δ 203.1, 203.0, 170.7, 170.6, 163.6, 158.9, 152.6, 150.9, 150.8, 144.2, 139.9, 135.2, 135.1, 132.9, 132.8, 130.4, 130.3, 129.8, 128.8, 128.3, 127.5, 117.0, 116.8, 113.6, 102.9, 87.5, 85.1, 84.7 (t), 83.9 (d), 83.3 (d), 79.3 (t), 71.4, 71.3, 68.2, 63.1, 62.8, 62.7, 62.6, 62.5, 55.5, 55.4, 45.1, 43.8, 39.5, 39.4, 36.6, 19.8, 19.7, 19.1; ^{31}P NMR ($CDCl_3$) H_3PO_4 reference δ -2.88, -3.12; IR (film) 3401 (br), 3194, 3064, 2935, 2839, 2253,

1714, 1694, 1682, 1608, 1510, 1463, 1384, 1275, 1252, 1226, 1178, 1034, 911, 830, 730 cm^{-1}.

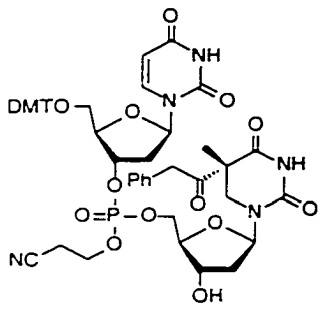

Preparation of *5R*-126. A solution of **125** (0.15 g, 0.20 mmol) in CH_3CN (2 mL, 0.5 M tetrazole) was added dropwise to a solution of ***5R*-94** (0.058 g, 0.16 mmol) in THF (2 mL). After stirring overnight, the phosphite was oxidized with I_2 as described above, diluted with saturated $NaHCO_3$ (30 mL), and extracted with CH_2Cl_2 (3 x 40 mL). The organic layer was dried over Na_2SO_4 and concentrated *in vacuo*. The product was purified by column chromatography (CH_2Cl_2:MeOH, 19:1 to 9:1) and isolated as a mixture of diastereomers (0.068 g, 42%). m.p. 110 °C (color change from white to pink), 110-121 °C (phase change): ^1H NMR ($CDCl_3$) δ 10.07 (br s, 0.5H), 9.92 (br s, 0.5H), 9.00 (br s, 0.5H), 8.92 (br s, 0.5H), 7.64 (t, 1H, J = 6.3 Hz), 7.33-7.22 (m, 12H), 7.11 (m, 2H), 6.84 (d, 4H, J = 8.4 Hz), 6.28 (m, 1H), 6.10 (m, 1H), 5.39 (d, 1H, J = 7.5 Hz), 5.16-5.11 (m, 1H), 4.39 (m, 1H), 4.24-4.22 (m, 2H), 4.12 (m, 2H), 4.02-3.87 (m, 5H), 3.78 (s, 6H), 3.42 (br s, 2H), 3.21 (dd, 1H, J = 12.6, 25.5 Hz), 2.63 (m, 1H), 2.49 (m, 2H), 2.32 (m, 1H), 2.12 (m, 2H), 1.44 (s, 3H); ^{13}C NMR ($CDCl_3$) δ 203.7, 203.4, 171.0, 163.6, 158.9, 152.3, 152.2, 151.0, 150.9, 144.2, 140.0, 139.9, 135.1, 135.0, 133.3, 133.2, 130.3, 130.2, 130.0, 128.7, 128.3, 127.5, 127.3, 117.1, 116.9, 113.6, 103.0, 102.9, 87.5, 87.4, 85.1, 85.0, 84.9, 84.7, 84.6, 83.6, 83.5, 83.4, 79.5, 79.3, 71.2, 67.9, 63.2, 62.9, 62.8, 62.7, 62.6, 55.5, 55.4, 45.5, 45.4, 44.7, 44.6, 39.3, 39.2, 36.8, 29.9, 19.7, 19.6, 19.5, 18.3, 18.2; ^{31}P NMR ($CDCl_3$) H_3PO_4 reference δ -2.97, -3.46; IR (film) 3402 (br), 3199, 3064, 2935, 2838, 2253, 1698, 1608, 1509, 1457, 1385, 1251, 1178, 1033, 911, 829, 728 cm^{-1}.

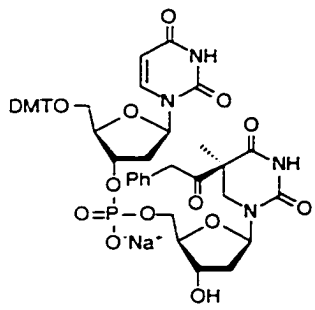

General Procedure for Deprotecting Phosphate and Cation Exchange: Preparation of *5S*-119. Et_3N (1 mL) was added to a solution of ***5S*-126** (0.14 g, 0.14 mmol) in THF (1 mL) and refluxed. After 12 h, the reaction mixture was concentrated *in vacuo* to yield a pale yellow powder. Dowex cation exchange resin (1 g/5 mmol) was washed with MeOH (50 mL) and H_2O (50 mL), then treated with 3.0 N NaOH (50 mL). The resin was subsequently washed with H_2O (100 mL) until the pH of the eluant was neutral, then washed with MeOH (50 mL). The crude product was taken up in MeOH (1 mL) and passed through the Dowex resin and eluted with MeOH (50 mL) to exchange the Et_3NH^+ cation for Na^+. Column chromatography (CH_2Cl_2:MeOH, 4:1) yielded 0.086 g (64%) of product as a white powder. m.p. 142 °C (color change to orange), 158-165 °C (phase change): ^1H NMR (MeOH-d_4) δ 7.77 (d, 1H, J = 8.1 Hz), 7.39 (dd, 2H, J = 1.5, 8.7 Hz), 7.32-7.19 (m, 10H), 7.12 (dd, 2H, J = 1.8, 8.1 Hz), 6.87 (dd, 4H, J = 0.6, 8.7 Hz), 6.26 (t, 1H, J = 6.9 Hz), 6.17 (t, 1H, J = 7.5 Hz), 5.25 (d, 1H, J = 8.1 Hz), 5.01 (m, 1H), 4.33-4.28 (m, 2H), 3.97-3.90 (m, 2H), 3.91 (s, 2H), 3.86 (m, 2H), 3.77 (s, 6H), 3.46 (dd, 1H, J = 3.3, 10.8 Hz), 3.38 (dd, 1H, J = 3.0, 10.5 Hz), 3.16 (d, 1H, J = 14.1 Hz), 2.63 (ddd, 1H, J = 2.7, 6.0, 14.1 Hz), 2.42-2.27 (m, 2H), 1.86 (ddd, 1H, J = 3.3, 6.6, 13.5 Hz), 1.37 (s, 3H); ^{13}C NMR (MeOH-d_4) δ 205.1, 172.8, 166.2, 160.5, 154.7, 152.2, 146.1, 142.5, 136.9, 136.7, 134.9, 131.7, 131.6, 130.9, 129.6, 129.1, 128.3, 128.2, 114.5, 102.7, 88.5, 86.8, 85.9, 85.8, 85.1, 77.3, 72.7, 66.9, 64.9, 56.9, 55.9, 45.4, 45.1, 40.7, 37.4, 18.8; ^{31}P NMR (MeOH-d_4) H_3PO_4 reference δ -1.00; IR (film) 3406 (br), 3207, 3063, 2954, 2875, 1698, 1508, 1463, 1248, 1065, 1036, 830 cm^{-1}; ESMS (ES^-) calcd for $C_{48}H_{50}N_4O_{15}P$: 953.3 ($M\text{-}Na^+$), found 953.3.

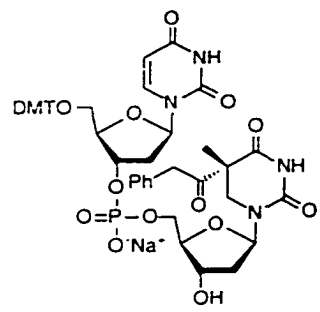

Preparation of *5R*-119. Et_3N (1mL) was added to a solution of ***5R*-126** (0.068 g, 0.067 mmol) in THF (1 mL) and refluxed. After 9 h, the reaction mixture was concentrated *in vacuo*. The crude product was taken up in MeOH (1mL) and passed through a Dowex cation exchange column as described above, eluted with MeOH (50 mL), and purified by column chromatography (CH_2Cl_2:MeOH, 4:1). The product (0.035 g) was isolated as a white powder in 53% yield. m.p. 113 °C (color change to orange), 170-177 °C (phase change); ^{1}H NMR (MeOH-d_4) δ 7.69 (d, 1H, J = 8.1 Hz), 7.39-7.10 (m, 14H), 6.88-6.81 (m, 4H), 6.19 (t, 2H, J = 7.5 Hz), 5.24 (d, 1H, J = 8.1 Hz), 4.92 (m, 1H), 4.42 (m, 1H), 4.22 (d, 1H, J = 13.5 Hz), 4.10-4.06 (m, 2H), 4.03 (d, 2H, J = 8.4 Hz), 3.95-3.90 (m, 2H), 3.78 (s, 6H), 3.78-3.70 (m, 1H), 3.38-3.28 (m, 2H), 2.50-2.44 (m, 1H), 2.27-2.12 (m, 2H), 1.97 (ddd, 1H, J = 3.0, 6.3, 13.5 Hz), 1.48 (s, 3H); ^{13}C NMR (MeOH-d_4) δ 207.1, 173.2, 166.2, 160.5, 154.4, 152.1, 146.1, 142.4, 136.8, 136.7, 135.4, 131.7, 131.6, 131.3, 130.6, 129.6, 129.5, 129.3, 129.1, 128.3, 127.9, 114.4, 114.0, 102.7, 88.4, 86.8, 86.6, 86.1, 85.5, 77.3, 72.7, 66.7, 64.8, 57.2, 55.9, 55.8, 45.7, 44.5, 40.6, 37.6, 17.6; ^{31}P NMR (MeOH-d_4) H_3PO_4 reference δ -0.94; IR (film) 3387 (br), 3249, 3063, 2953, 2876, 1696, 1507, 1460, 1248, 1062, 1036, 828 cm^{-1}; ESMS (ES$^-$) calcd for $C_{48}H_{50}N_4O_{15}P$: 953.3 (M-Na$^+$), found 953.3.

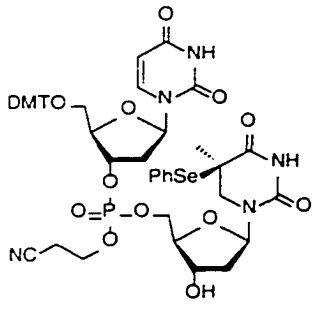

Preparation of *5R*-127. A solution of **125** (0.35 g, 0.48 mmol) in CH_3CN (2 mL, 0.5 M tetrazole) was added dropwise to a solution of ***5R*-96** (0.16 g, 0.40 mmol) in THF (2 mL). After 30 min, the phosphite was oxidized with I_2 as described above, diluted with saturated $NaHCO_3$ (40 mL), and extracted with

CH_2Cl_2 (3 x 50 mL). The organic layer was dried over $MgSO_4$ and concentrated *in vacuo*. The product was purified by column chromatography (CH_2Cl_2:MeOH, 19:1) and isolated as a mixture of diastereomers (0.22 g, 51%). m.p. 112-124 °C; ^1H NMR ($CDCl_3$) δ 9.93 (br s, 0.5H), 9.80 (br s, 0.5H), 8.37 (s, 0.5H), 8.32 (s, 0.5H), 7.66 (d, 1H, J = 8.4 Hz), 7.54 (d, 2H, J = 6.9 Hz), 7.38-7.23 (m, 12H), 6.85 (d, 4H, J = 8.7 Hz), 6.39-6.32 (m, 2H), 5.41 (dd, 1H, J = 3.0, 8.1 Hz), 5.16 (m, 1H), 4.31-4.18 (m, 6H), 4.02-3.72 (m, 2H), 3.78 (s, 6H), 3.59-3.43 (m, 4H), 2.74 (t, 2H, J = 5.4 Hz), 2.71-2.66 (m, 1H), 2.38-2.25 (m, 3H), 1.42 (s, 3H); ^{13}C NMR ($CDCl_3$) δ 171.0, 163.6, 159.0, 153.1, 150.9, 150.8, 144.2, 139.9, 138.1, 135.1, 130.3, 129.3, 128.3, 127.5, 125.3, 117.0, 116.8, 113.6, 103.0, 129.9, 87.5, 84.8 (m), 83.8 (m), 83.2, 79.4 (m), 71.3, 68.3, 63.7, 62.8, 62.7, 55.5, 55.4, 49.1, 44.2, 39.4, 39.3, 37.0, 20.8, 19.8; ^{31}P NMR ($CDCl_3$) H_3PO_4 reference δ -2.00, -2.36; IR (film) 3401, 3198, 3065, 2958, 2932, 2840, 2252, 1695, 1609, 1508, 1467, 1381, 1253, 1181, 1029, 911, 830, 732 cm^{-1}.

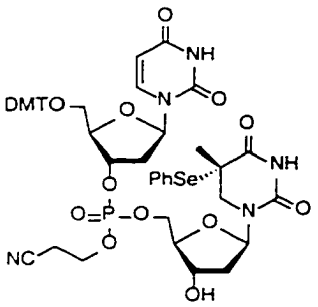

Preparation of *5S*-127. A solution of **125** (0.097 g, 0.13 mmol) in CH_3CN (1 mL, 0.5 M tetrazole) was added dropwise to a solution of ***5S*-96** (0.047 g, 0.12 mmol) in THF (1 mL). After 4 h, the phosphite was oxidized with I_2 as described above, diluted with saturated $NaHCO_3$ (20 mL), and extracted with CH_2Cl_2 (3 x 30 mL). The organic layer was dried over $MgSO_4$ and concentrated *in vacuo*. The product was purified by column chromatography (CH_2Cl_2:MeOH, 19:1) and isolated as a mixture of diastereomers (0.071 g, 58%). m.p. 99-107 °C; ^1H NMR ($CDCl_3$) δ 9.75 (br s, 0.5H), 9.60 (br s, 0.5H), 8.28 (br s, 0.5H), 8.17 (br s, 0.5H), 7.66 (dd, 1H, J = 3.6, 8.1 Hz), 7.56 (d, 2H, J = 8.1 Hz), 7.42-7.23 (m, 12H), 6.85 (d, 4H, J = 8.7 Hz), 6.33 (t, 1H, J = 6.3 Hz), 6.09 (m, 1H), 5.40 (m,

1H), 5.21-5.16 (m, 1H), 4.42-4.31 (m, 6H), 4.05-3.92 (m, 2H), 3.79 (s, 6H), 3.63-3.48 (m, 4H), 2.77-2.72 (m, 3H), 2.38 (m, 1H), 2.18 (m, 2H), 1.47 (s, 1.5H), 1.46 (s, 1.5H); ^{13}C NMR ($CDCl_3$) δ 171.4, 171.1, 170.8, 163.5, 158.9, 152.1, 150.9, 144.2, 139.9, 138.2, 135.1, 130.3, 130.1, 129.3, 128.3, 127.5, 125.5, 116.9, 116.8, 114.4, 113.5, 103.0, 87.5, 84.7 (m), 83.8, 79.3 (m), 71.5, 68.2 (m), 62.9, 62.8, 60.6, 55.5, 55.4, 49.5, 44.1, 39.4, 36.8, 29.9, 20.9, 19.9, 14.4; ^{31}P NMR ($CDCl_3$) H_3PO_4 reference δ -2.02, -2.34; IR (film) 3403, 3199, 3065, 2958, 2931, 2841, 2252, 1694, 1610, 1508, 1468, 1381, 1252, 1181, 1030, 911, 830, 832 cm^{-1}.

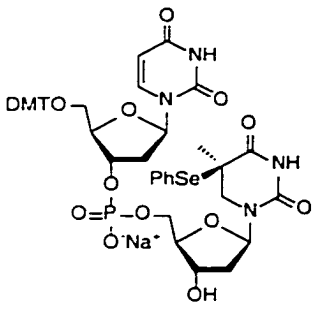

Preparation of *5R*-121. Et_3N (1mL) was added to a solution of ***5R*-127** (0.20 g, 0.19 mmol) in THF (1 mL) and refluxed. After 12 h, the reaction mixture was concentrated *in vacuo*. The crude product was taken up in MeOH (1 mL) and passed through a Dowex cation exchange column as described above, eluted with MeoH (50 mL), and purified by column chromatography (CH_2Cl_2:MeOH, 4:1). The product (0.14 g) was isolated as a white powder in 72% yield. m.p. 160 °C (color change from white to orange), 190-196 °C (phase change); ^{1}H NMR (CD_3CN:D_2O, 1:1 by volume) δ 7.57 (d, 1H, J = 7.8 Hz), 7.47-7.18 (m, 14H), 6.81 (d, 4H, J = 7.5 Hz), 6.17-6.09 (m, 2H), 5.35 (d, 1H, J = 8.1 Hz), 4.84 (m, 1H), 4.27-4.21 (m, 2H), 3.83-3.76 (m, 3H), 3.69 (s, 6H), 3.52-3.29 (m, 2H), 3.22-3.17 (m, 2H), 2.58-2.54 (m, 1H), 2.31-2.18 (m, 2H), 2.02 (ddd, 1H, J = 3.9, 6.6, 14.1 Hz), 1.20 (s, 3H); ^{13}C NMR (CD_3CN:D_2O, 1:1 by volume) δ 172.6, 165.7, 159.4, 154.3, 152.0, 145.4, 142.1, 138.8, 136.6, 136.5, 131.0, 130.1, 129.0, 128.1, 126.0, 114.2, 102.8, 87.6, 86.4, 86.0, 85.2, 85.0, 84.5, 76.6, 71.9, 66.4, 64.4, 56.1, 48.9, 45.4, 39.9, 36.8, 20.7; ^{31}P NMR (CD_3CN:D_2O, 1:1 by volume) H_3PO_4 reference δ -0.09; IR (film) 3314 (br),

2957, 2890, 1682, 1608, 1509, 1462, 1442, 1251, 1180, 1068, 1036, 832 cm^{-1}; ESMS (ES^-) calcd for $C_{46}H_{48}N_4O_{14}PSe$: 991.2 ($M\text{-}Na^+$), found 991.3.

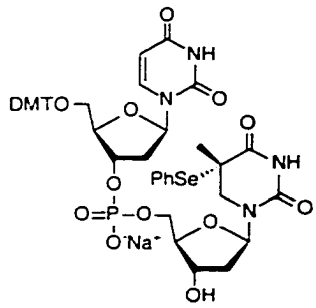

Preparation of *5S*-121. Et_3N (0.5 mL) was added to a solution of ***5S*-127** (30 mg, 0.029 mmol) in THF (0.5 mL) and refluxed. After 12 h, the reaction mixture was concentrated *in vacuo*. The crude product was taken up in MeOH (1 mL) and passed through a Dowex cation exchange column as described above, eluted with MeOH (50 mL), and purified by column chromatography (CH_2Cl_2:MeOH, 4:1 to 3:1). The product (17 mg) was isolated as a white powder in 59% yield. m.p. 159 °C (color change from white to orange), 172-180 °C (phase change); ^1H NMR (CD_3CN:D_2O, 1:1 by volume) δ 7.55 (d, 1H, J = 7.8 Hz), 7.42-7.31 (m, 5H), 7.25-7.17 (m, 9H), 6.78 (dd, 4H, J = 2.1, 9.0 Hz), 6.17 (t, 1H, J = 7.5 Hz), 6.05 (dd, 1H, J = 6.6, 8.7 Hz), 5.35 (d, 1H, J = 8.1 Hz), 4.89 (m, 1H), 4.35-4.30 (m, 2H), 3.90-3.85 (m, 3H), 3.68 (s, 6H), 3.47-3.30 (m, 2H), 3.25-3.15 (m, 2H), 2.63-2.56 (m, 1H), 2.26 (m, 1H) apparent quintet, 2.09 (m, 1H) apparent quintet, 1.91-1.81 (m, 1H), 1.33 (s, 3H); ^{13}C NMR (CD_3CN:D_2O, 1:1 by volume) δ 172.8, 165.8, 159.4, 153.6, 151.9, 145.5, 142.0, 139.1, 136.6, 136.5, 131.0, 130.8, 130.0, 129.0, 128.9, 128.1, 126.3, 114.3, 102.8, 87.6, 86.4, 85.5, 84.7, 76.9, 72.3, 66.6, 64.7, 56.1, 48.6, 47.9, 45.3, 40.0, 36.6, 20.9; ^{31}P NMR (CD_3CN:D_2O, 1:1 by volume) H_3PO_4 reference δ -0.25; IR (film) 3258 (br), 2955, 2926, 1771, 1686, 1608, 1508, 1464, 1250, 1179, 1067, 1035, 829 cm^{-1}; ESMS (ES^-) calcd for $C_{46}H_{48}N_4O_{14}PSe$: 991.2 ($M\text{-}Na^+$), found 991.3.

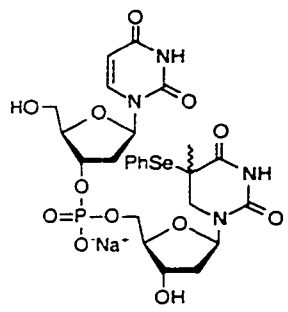

Preparation of 167. A diastereomeric mixture of **121** (0.176 g, 0.174 mmol) was dissolved in 80% HOAc (40 mL) and stirred at room temperature for 3h. The reaction mixture was diluted with H_2O (100 mL) and extracted with ether (3 x 75 mL). The aqueous layer was concentrated *in vacuo*, yielding 0.111 g of **167** (90%). mp 174 °C (color change, white to brown), 191-201 °C (phase change): ^{1}H NMR (300 MHz, D_2O) δ 7.82 (d, 0.9H, J = 8.1 Hz), 7.73 (m, 0.1H), 7.54 (d, 2H, J = 6.9 Hz), 7.46 (t, 1H, J = 7.5 Hz), 7.35 (t, 2H, J = 7.5 Hz), 6.26 (dd, 1H, J = 0.9, 6.6 Hz), 6.14 (t, 1H, J = 7.2 Hz), 5.82 (d, 0.9H, J = 8.1 Hz), 5.69-5.65 (m, 0.1H), 4.78-4.74 (m, 1H), 4.50-4.46 (m, 1H), 4.24-4.20 (m, 1H), 4.03-3.95 (m, 3H), 3.83-3.62 (m, 4H), 2.60-2.53 (m, 1H), 2.47 (m, 1H, apparent quintet), 2.35 (m, 1H, apparent quintet), 2.25-2.17 (m, 1H), 1.50 (s, 2.8H), 1.43 (s, 0.2H); ^{13}C NMR (75 MHz, D_2O) MeOH-d_4 reference δ 173.9, 167.1, 154.9, 152.4, 142.9, 138.7, 131.3, 130.4, 126.2, 103.3, 87.0, 86.9, 85.0, 84.9, 76.4, 72.0, 66.4, 62.2, 49.5, 45.8, 39.1, 36.8, 20.8; ^{31}P NMR (109 MHz, D_2O) H_3PO_4 reference δ -3.99, -4.71; IR (film) 3392 (br), 1694, 1476, 1382, 1223, 1057 cm^{-1}; HRMS (FAB) calcd 713.0739 (M+H), found 713.0754.

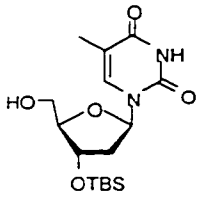

Preparation of 147. A solution of TFA in H_2O (10 mL, 10% by volume) was added to a solution of **133** (1.01 g, 2.15 mmol) in THF (20 mL) at 0 °C. After 8 h, the reaction mixture was poured into saturated $NaHCO_3$ (50 mL) and extracted with EtOAc (3 x 75 mL). The organic layer was washed with brine and dried over $MgSO_4$. Column chromatography (CH_2Cl_2:EtOAc:MeOH, 1:1:0 to 4:1:1) yielded 0.45 g (58%) of the product as a white foam. m.p. 107-110 °C; ^{1}H NMR ($CDCl_3$) δ 8.96 (br s, 1H), 7.38 (s, 1H), 6.15 (t, 1H, J = 6.9 Hz), 4.50 (dt, 1H, J = 3.6, 6.6 Hz), 3.95-3.90 (m, 2H), 3.79-3.73 (m, 1H), 2.76

(br s, 1H), 2.35 (ddd, 1H, J = 6.9, 13.5, 6.9 Hz) apparent quintet, 2.22 (ddd, 1H, J = 4.2, 6.6, 13.5 Hz), 1.91 (s, 3H), 0.90 (s, 9H), 0.09 (s, 6H); ^{13}C NMR ($CDCl_3$) δ 164.0, 150.6, 137.3, 111.2, 87.8, 87.1, 71.8, 62.2, 40.7, 25.9, 18.2, 12.7, -4.5, -4.6; IR (film) 3445 (br), 3192, 3062, 2954, 2930, 2857, 1694, 1682, 1472, 1362, 1275, 1258, 1133, 1102, 1062, 1032, 834, 779 cm^{-1}.

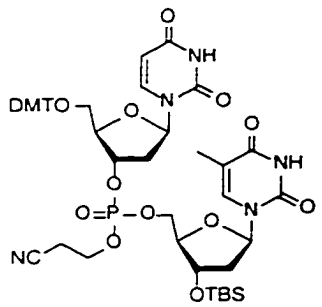

Preparation of 150. The dU phosphoramidite (**125**, 0.76 g, 1.04 mmol) and **147** (0.31 g, 0.86 mmol) were dissolved in CH_3CN (5 mL, 0.5 M tetrazole). After 3 h, the phosphite was oxidized with I_2 as described above. The reaction mixture was diluted with saturated $NaHCO_3$ (50 mL), extracted with CH_2Cl_2 (3 x 50 mL), and dried over $MgSO_4$. Column chromatography (CH_2Cl_2:MeOH, 9:1) yielded 0.69 g (80%) of product as a mixture of diastereomers. m.p. 96-109 °C; ^{1}H NMR ($CDCl_3$) δ 9.52 (br s, 0.5H), 9.42 (br s, 0.5H), 9.30 (br s, 0.5H), 9.14 (br s, 0.5H), 7.66 (d, 0.5H, J = 8.1 Hz), 7.64 (d, 0.5H, J = 8.1 Hz), 7.37-7.21 (m, 10H), 6.83 (d, 4H, J = 8.7 Hz), 6.35-6.29 (m, 1H), 6.17 (q, 1H, J = 6.6 Hz), 5.36 (d, 1H, J = 7.8 Hz), 5.17 (m, 1H), 4.39 (m, 1H), 4.28-4.13 (m, 4H), 4.01-3.97 (m, 1H), 3.85-3.76 (m, 1H), 3.78 (s, 6H), 3.46 (m, 2H), 2.78-2.63 (m, 3H), 2.39-2.14 (m, 3H), 1.89 (s, 1.5H), 1.88 (s, 1.5H), 0.881 (s, 5H), 0.875 (s, 4H), 0.09 (s, 1H), 0.08 (s, 3H), 0.07 (s, 2H); ^{13}C NMR ($CDCl_3$) δ 164.1, 163.3, 159.0, 150.7, 150.6, 144.2, 139.8, 136.2, 136.1, 135.1, 135.0, 130.2, 128.3, 127.5, 116.5, 116.3, 113.6, 111.5, 102.9, 87.6, 86.1, 85.8, 84.9, 84.6, 79.3, 77.4, 71.5, 67.6, 63.1, 62.6, 55.5, 40.4, 39.4, 25.9, 19.8, 18.1, 12.6, -4.5, -4.7; ^{31}P NMR ($CDCl_3$) H_3PO_4 reference δ -1.98; IR (film) 3184, 3060, 2954, 2930, 2856, 2342, 1694, 1608, 1509, 1464, 1275, 1252, 1178, 1033, 834 cm^{-1}.

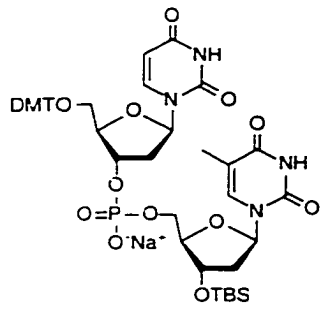

Preparation of 153. Et_3N (4 mL) was added to a solution of **150** (0.60 g, 0.60 mmol) in THF (4 mL) and refluxed. After 12 h, the reaction mixture was concentrated *in vacuo* to yield an off-white foam. The crude product was taken up in MeOH (4 mL) and passed through Dowex resin as described above and chromatographed (CH_2Cl_2:MeOH, 4:1). The product (0.42 g) was isolated in 68% yield as a white powder. m.p. 184-189 °C (phase change, color change to red); ^1H NMR (MeOH-d_4) δ 7.81 (d, 1H, J = 8.1 Hz), 7.70 (s, 1H), 7.40 (d, 2H, J = 7.2 Hz), 7.30-7.22 (m, 7H), 6.87 (d, 4H, J = 8.4 Hz), 6.29 (m, 2H), 5.27 (d, 1H, J = 8.1 Hz), 5.10 (m, 1H), 4.52 (m, 1H), 4.30 (m, 1H), 4.04 (m, 2H), 3.99 (m, 1H), 3.77 (s, 6H), 3.51-3.37 (m, 2H), 2.65 (m, 1H), 2.41 (m, 1H), 2.23 (m, 1H), 2.16 (m, 1H), 1.88 (s, 3H), 0.91 (s, 9H), 0.11 (s, 6H); ^{13}C NMR (MeOH-d_4) δ 166.5, 166.2, 160.4, 152.5, 152.1, 146.0, 142.4, 138.2, 136.8, 136.7, 131.6, 131.5, 129.6, 129.1, 128.2, 114.4, 112.1, 102.7, 88.5, 87.9, 86.7, 86.4, 77.5, 74.3, 66.6, 65.0, 55.9, 47.9, 41.6, 40.8, 26.4, 18.9, 12.8, 9.4, -4.4; ^{31}P NMR (MeOH-d_4) H_3PO_4 reference δ -0.62; IR (film) 3194, 3061, 2952, 2930, 2855, 1693, 1607, 1508, 1470, 1275, 1251, 1178, 1067, 1034, 832 cm^{-1}.

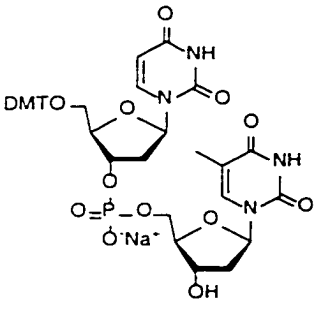

General Procedure for Deprotecting the 3'-Alcohol and Neutralization on Amberlite Resin: Preparation of 129. Et_3N (40.7 mg, 0.40 mmol) and Et_3N•3HF (64.3 mg, 0.40 mmol) were added to a solution of **153** (78.0 mg, 0.080 mmol) in THF (1 mL). After 6 h, the reaction mixture was diluted with MeOH (1 mL) and passed through Amberlite anion exchange resin (1 g/5 mmol of Et_3N•3HF) to neutralize the HF. The product was eluted

with MeOH (50 mL). The Amberlite resin had been washed with MeOH (50 mL) prior to use. After column chromatography (CH_2Cl_2:MeOH, 4:1 to 3:1), the product was taken up in MeOH and passed through Dowex resin as described above. The product must be chromatographed prior to passing it through the Dowex resin in order for the cation exchange to occur. The product (35.0 mg) was isolated as a white powder in 51% yield. m.p. 159-164 °C (phase change, color change to red); ^{1}H NMR (MeOH-d_4) δ 7.80 (d, 1H, J = 8.4 Hz), 7.72 (d, 1H, J = 1.5 Hz), 7.40 (dd, 2H, J = 1.8, 9.0 Hz), 7.32-7.22 (m, 7H), 6.87 (d, 4H, J = 9.0 Hz), 6.30 (t, 2H, J = 6.6 Hz), 5.25 (d, 1H, J = 8.1 Hz), 5.06 (m, 1H), 4.43 (m, 1H), 4.27 (m, 1H), 4.03-4.00 (m, 2H), 3.98-3.97 (m, 1H), 3.78 (s, 6H), 3.49 (dd, 1H, J = 3.3, 10.8 Hz), 3.38 (dd, 1H, J = 2.7, 10.5 Hz), 2.64 (ddd, 1H, J = 3.0, 6.3, 13.8 Hz), 2.40 (ddd, 1H, J = 6.6, 13.8, 6.6 Hz) apparent quintet, 2.29-2.15 (m, 2H), 1.87 (d, 3H, J = 0.6 Hz); ^{13}C NMR (MeOH-d_4) δ 166.9, 166.7, 160.4, 152.6, 146.1, 142.4, 138.2, 136.8, 136.7, 131.64, 131.57, 129.6, 129.1, 128.2, 114.4, 112.1, 102.7, 88.5, 87.5, 87.4, 86.7, 86.2, 77.2, 72.7, 66.6, 64.8, 55.9, 41.0, 40.8, 12.8; ^{31}P NMR (MeOH-d_4) H_3PO_4 reference δ -0.98; IR (film) 3390, 3062, 2953, 1694, 1607, 1506, 1470, 1275, 1250, 1177, 1065, 1034, 828 cm^{-1}; ESMS (ES$^-$) calcd for $C_{40}H_{42}N_4O_{14}P$: 833.2 (M-Na$^+$), found 833.3.

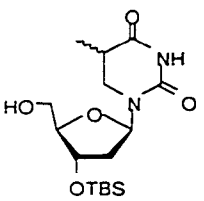

Preparation of 148. The 9:1 mixture of diastereomers obtained from the hydrogenation of thymidine was epimerized to enhance the amount of the minor diastereomer. *sec*-BuLi (1.3 mL, 1.3 M, 1.70 mmol) was added to a solution of **97** (0.32 g, 0.67 mmol) in THF (7 mL) at -78 °C. The reaction mixture was warmed to room temperature over 2 h, quenched with H_2O (40 mL), and extracted with ether (3 x 50 mL). The organic layer was washed with brine and dried over $MgSO_4$. The product (0.31 g) was isolated as a mixture of diastereomers (1.5:1, *5S:5R*) in 98% yield. A solution of TFA/H_2O (3 mL, 10% by volume) was added

to a solution of **97** (0.31 g, 0.65 mmol) in THF (3 mL) at 0 °C. After 1 h, the reaction was quenched with saturated $NaHCO_3$ (20 mL), diluted with H_2O (40 mL), and extracted with CH_2Cl_2 (3 x 50 mL). The organic layer was dried over $MgSO_4$ and concentrated *in vacuo*. Column chromatography (CH_2Cl_2:MeOH, 19:1 to 9:1) yielded 0.082 g (35%) of **148** as a mixture of diastereomers. m.p. 128-130 °C; ^1H NMR ($CDCl_3$) δ 8.28 (s, 0.6H), 8.26 (s, 0.4H), 6.11 (t, 0.6H, J = 6.9 Hz), 6.07 (t, 0.4H, J = 6.9 Hz), 4.33 (m, 1H), 3.82-3.76 (m, 2H), 3.65 (m, 1H), 3.54 (dd, 0.4H, J = 5.7, 12.3 Hz), 3.40 (dd, 0.6H, J = 5.7, 12.6 Hz), 3.19 (dd, 0.6H, J = 9.6, 12.6 Hz), 3.11 (dd, 0.4H, J = 10.8, 12.3 Hz), 2.85 (m, 0.4H), 2.73-2.61 (m, 1.6H), 2.26-2.15 (m, 1H), 2.06-1.95 (m, 1H), 1.24 (d, 1.8H, J = 6.9 Hz), 1.22 (d, 1.2H, J = 6.3 Hz), 0.88 (s, 9H), 0.06 (s, 6H); ^{13}C NMR ($CDCl_3$) δ 172.9, 153.0, 152.8, 86.3, 86.2, 85.7, 85.3, 71.9, 71.8, 62.4, 44.5, 44.1, 38.1, 37.9, 35.5, 35.4, 25.9, 18.1, 13.1, 12.6, -4.5, -4.7; IR (film) 3422, 3221, 3083, 2954, 2930, 2885, 2857, 1694, 1484, 1444, 1387, 1235, 1098, 1050, 1025, 836, 778, 734 cm^{-1}.

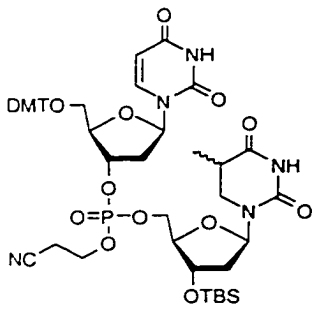

Preparation of 151. The dU phosphoramidite (**125**, 0.19 g, 0.26 mmol) and **148** (0.076 g, 0.21 mmol) were dissolved in CH_3CN (2 mL, 0.5 M tetrazole). After 45 min, the reaction mixture was oxidized as described above, poured into saturated $NaHCO_3$ (20 mL), and extracted with CH_2Cl_2 (3 x 40 mL). The organics were dried over Na_2SO_4 and concentrated to yield an orange oil. Column chromatography (CH_2Cl_2:EtOAc:MeOH, 1:1:0 to 5:5:1) yielded 0.17 g (82%) of **151** as a mixture of diastereomers. m.p. 110-119 °C; ^1H NMR ($CDCl_3$) δ 9.84 (br s, 1H), 8.47 (s, 0.5H), 8.46 (s, 0.5H), 7.62 (d, 1H, J = 8.1 Hz), 7.31-7.19 (m, 9H), 6.80 (d, 4H, J = 8.7 Hz), 6.29 (t, 1H, J = 6.0 Hz), 6.20 (m, 1H), 5.33 (d, 1H, J = 8.4 Hz), 5.13 (m, 1H), 4.23 (m, 3H), 4.13 (m, 3H), 3.84 (m, 1H), 3.75 (s, 6H), 3.43 (m, 2H), 3.14-2.96 (m, 1H), 2.72 (t, 1H, J = 6.0 Hz), 2.63-2.60 (m, 2H), 2.34 (m, 1H),

2.12-1.94 (m, 2H), 1.18 (m, 3H) apparent t, 0.85 (s, 5H), 0.84 (s, 4H), 0.04 (s, 4H), 0.03 (s, 2H); ^{13}C NMR ($CDCl_3$) δ 172.9, 163.5, 158.9, 153.1, 152.7, 150.7, 150.6, 144.1, 139.8, 135.1, 134.9, 130.2, 128.2, 127.4, 116.4, 113.5, 102.8, 87.5, 84.8, 84.7, 84.6, 84.5, 84.3, 84.1, 83.5, 83.4, 79.0, 78.9, 71.7, 67.7, 63.0, 62.7, 62.6, 62.5, 62.4, 55.4, 42.9, 39.4, 37.6, 37.5, 37.2, 35.4, 35.3, 25.8, 19.9, 19.8, 19.7, 18.0, 13.0, 12.6, -4.5, -4.7; ^{31}P NMR ($CDCl_3$) H_3PO_4 reference δ -1.92, -1.95; IR (film) 3201, 3064, 2932, 2857, 2253, 1694, 1682, 1608, 1506, 1456, 1385, 1252, 1178, 1030, 912, 832, 731 cm^{-1}.

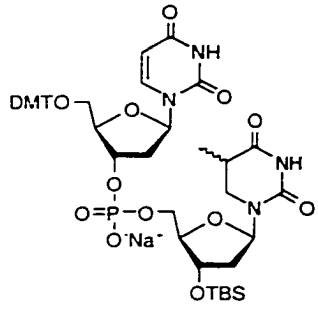

Preparation of 154. Et_3N (1 mL) was added to a solution of **151** (0.17 g, 0.17 mmol) in THF (1 mL) and refluxed. The reaction mixture was concentrated *in vacuo*, the residue taken up in MeOH (1 mL) and passed through Dowex resin as described above. Column chromatography (CH_2Cl_2:MeOH, 4:1) yielded 0.12 g (70%) of product as a white powder. m.p. 169-174 ℃ (phase change, color change to orange); ^{1}H NMR (MeOH-d_4) δ 7.78 (d, 1H, J = 8.1 Hz), 7.37 (d, 2H, J = 7.2 Hz), 7.26-7.18 (m, 7H), 6.83 (d, 4H, J = 8.4 Hz), 6.26-6.22 (m, 2H), 5.22 (d, 1H, J = 7.5 Hz), 5.02 (m, 1H), 4.41 (m, 1H), 4.25 (m, 1H), 3.84 (m, 3H), 3.73 (s, 6H), 3.48-3.45 (m, 2H), 3.36-3.27 (m, 1H), 3.17-3.07 (m, 1H), 2.59 (m, 2H), 2.39-2.35 (m, 1H), 2.19-2.15 (m, 1H), 1.84 (m, 1H), 1.13 (d, 3H, J = 6.0 Hz), 0.86 (s, 9H), 0.06 (s, 6H); ^{13}C NMR (MeOH-d_4) δ 175.8, 175.5, 166.2, 160.4, 155.2, 154.9, 152.1, 146.1, 142.4, 136.8, 136.7, 131.6, 129.6, 129.1, 128.3, 114.4, 102.8, 88.5, 86.8, 85.5, 77.5, 74.4, 74.3, 66.8, 65.0, 56.0, 55.9, 47.9, 43.4, 40.7, 38.2, 37.9, 36.6, 26.5, 18.9, 13.5, 13.0, 9.4, -4.3; ^{31}P NMR (MeOH-d_4) H_3PO_4 reference δ -1.05;

IR (film) 3433, 3189, 3047, 2955, 2925, 2843, 1695, 1609, 1512, 1466, 1441, 1385, 1248, 1177, 1065, 1029, 831 cm^{-1}.

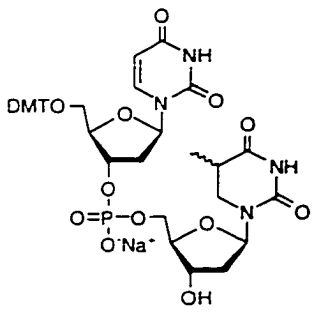

Preparation of 128. Et_3N (39.9 mg, 0.40 mmol) and Et_3N•3HF (62.3 mg, 0.39 mmol) were added to a solution of **154** (75.0 mg, 0.077 mmol) in THF (1 mL). After 6 h, the reaction mixture was diluted with MeOH (1 mL) and passed through Amberlite resin, chromatographed (CH_2Cl_2:MeOH, 4:1 to 3:1), and passed through Dowex resin as described above. The product (32.0 mg) was isolated in 48% yield as a white powder. m.p. 147-153 ℃ (phase change, color change to red); ^1H NMR (MeOH-d_4) δ 7.82 (d, 1H, J = 8.4 Hz), 7.41 (dd, 2H, J = 1.2, 8.7 Hz), 7.33-7.23 (m, 7H), 6.88 (dd, 4H, J = 1.2, 9.3 Hz), 6.32-6.25 (m, 2H), 5.25 (dd, 1H, J = 1.8, 8.1 Hz), 5.04 (m, 1H), 4.37-4.34 (m, 1H), 4.30-4.27 (m, 1H), 3.94-3.86 (m, 3H), 3.78 (s, 6H), 3.65 (dd, 0.5H, J = 5.7, 12.3 Hz), 3.55-3.47 (m, 1.5H), 3.41 (t, 1H, J = 3.0 Hz), 3.37 (t, 1H, J = 3.0 Hz), 3.17 (dd, 0.5H, J = 9.3, 12.9 Hz), 3.06 (dd, 0.5H, J = 11.1, 12.3 Hz), 2.67-2.54 (m, 2H), 2.40 (ddd, 1H, J = 6.9, 13.5, 6.9 Hz) apparent quintet, 2.28-2.14 (m, 1H), 1.98-1.87 (m, 1H), 1.17 (d, 1.5H, J = 7.2 Hz), 1.16 (d, 1.5H, J = 6.9 Hz); ^{13}C NMR (MeOH-d_4) δ 176.0, 175.7, 166.4, 160.4, 155.2, 152.3, 146.1, 142.5, 136.9, 136.7, 131.7, 131.6, 129.6, 129.1, 128.2, 114.4, 102.6, 88.5, 86.7, 86.2, 85.3, 77.0, 73.1, 72.9, 66.8, 64.9, 55.9, 43.3, 40.8, 37.5, 37.2, 36.6, 36.5, 30.9, 13.5, 12.9; ^{31}P NMR (MeOH-d_4) H_3PO_4 reference δ -1.61; IR (film) 3385 (br), 3065, 2939, 1689, 1607, 1510, 1462, 1249, 1060, 1026, 827 cm^{-1}; ESMS (ES^-) calcd for $C_{40}H_{44}N_4O_{14}P$: 835.3 ($M-Na^+$), found 835.3.

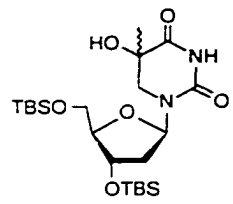

Preparation of 135.[143] *sec*-BuLi (25 mL, 1.3 M, 0.033 mol) was added to a solution of **97** (5.20 g, 0.011 mol) in THF (100 mL) at -78 °C. After 1 h, DMPU (7.10 g, 0.055 mol) was added. The reaction mixture was added to O_2 saturated THF (50 mL) at room temperature via cannula. The O_2 was passed over P_2O_5 and bubbled through the THF during addition of the enolate. After 5 min, the reaction was quenched with aqueous Na_2SO_3 (4.3 g, 0.034 mol in 50 mL H_2O) and stirred for 30 min. The reaction mixture was diluted with saturated NH_4Cl (100 mL), extracted with CH_2Cl_2 (3 x 150 mL), and dried over $MgSO_4$. Column chromatography (hexanes:EtOAc, 2:1) yielded 1.82 g (34%) of product as a mixture of diastereomers (4:1, *5R:5S*). m.p. 121-133 °C; ^{1}H NMR ($CDCl_3$) δ 8.90 (s, 0.8H), 8.84 (s, 0.2H), 6.34 (t, 0.2H, J = 7.5 Hz), 6.28 (t, 0.8H, J = 6.9 Hz), 4.34 (m, 1H), 4.10 (s, 0.8H), 4.06 (s, 0.2H), 3.80 (m, 1H), 3.70-3.67 (m, 2.2H), 3.59 (d, 0.8H, J = 12.0 Hz), 3.44-3.27 (m, 0.2H), 3.20 (d, 0.8H, J = 12.0 Hz), 1.96-1.93 (m, 2H), 1.43 (s, 2.4H), 1.40 (s, 0.6H), 0.90 (s, 9H), 0.88 (s, 9H), 0.08 (s, 6H), 0.06 (s, 6H); ^{13}C NMR ($CDCl_3$) δ 175.2, 174.5, 152.7, 152.0, 86.7, 83.9, 72.5, 72.4, 68.5, 68.4, 63.4, 46.4, 37.5, 26.1, 25.9, 23.8, 23.2, 18.5, 18.2, -4.5, -4.6, -5.2, -5.4; IR (film) 3376, 3215, 3086, 2955, 2930, 2896, 2858, 1722, 1714, 1694, 1682, 1471, 1391, 1255, 1223, 1097, 1030, 836, 777, 669 cm^{-1}.

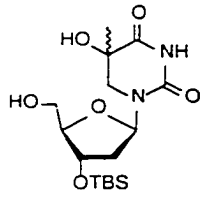

Preparation of 149. A solution of TFA/H_2O (18 mL, 10% by volume) was added to a solution of **135** (1.78 g, 3.64 mmol) in THF (18 mL) at 0 °C. After 1.5 h, the reaction mixture was quenched with saturated $NaHCO_3$ (50 mL), and extracted with EtOAc (3 x 75 mL). The organic layer was washed with brine and dried over $MgSO_4$. Column chromatography (CH_2Cl_2:EtOAc, 1:1 to 1:2) yielded 0.71 g (52%) of **149** as a mixture of diastereomers (*5R:5S*, 3:1). m.p. 57-68 °C; ^{1}H NMR ($CDCl_3$) δ 8.99 (s, 0.2H), 8.90 (s, 0.8H), 6.24 (t,

0.2H, J = 6.6 Hz), 6.14 (t, 0.8H, J = 6.9 Hz), 4.79 (s, 0.2H), 4.65 (s, 0.8H), 4.37-4.34 (m, 1H), 3.85-3.76 (m, 2H), 3.69-3.63 (m, 1H), 3.55-3.23 (m, 2.2H), 3.09 (m, 0.8H), 2.18-2.07 (m, 1H), 2.04-1.95 (m, 1H), 1.45 (s, 2.4H), 1.42 (s, 0.6H), 0.88 (s, 9H), 0.07 (s, 6H); ^{13}C NMR ($CDCl_3$) δ 174.8, 173.9, 152.8, 152.1, 86.4, 86.2, 84.9, 84.1, 72.0, 71.3, 68.7, 68.5, 62.4, 61.9, 48.1, 47.8, 38.1, 37.8, 25.9, 23.4, 22.9, 18.1, -4.5, -4.7; IR (film) 3417 (br), 3242, 3093, 2954, 2930, 2886, 2858, 1722, 1714, 1694, 1682, 1472, 1386, 1297, 1253, 1222, 1139, 1097, 1050, 1026, 835, 778, 734, 669 cm^{-1}.

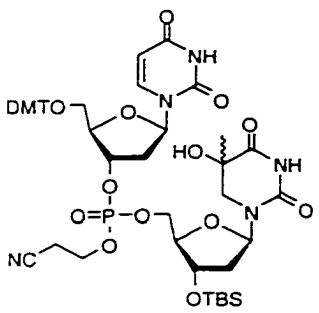

Preparation of 152. The dU phosphoramidite (**125**, 0.24 g, 0.33 mmol) and **149** (0.12 g, 0.33 mmol) were dissolved in CH_3CN (3 mL, 0.5 M tetrazole). After 2 h, the reaction mixture was oxidized as described above, poured into saturated $NaHCO_3$ (50 mL), and extracted with CH_2Cl_2 (3 x 60 mL). The organics were dried over Na_2SO_4 and concentrated *in vacuo*. Column chromatography (CH_2Cl_2:MeOH, 19:1) yielded 0.25 g (74%) of **152** as a mixture of four diastereomers. m.p. 104-128 °C; ^{1}H NMR ($CDCl_3$) δ 9.68 (s, 1H), 8.59 (s, 0.5H), 8.53 (s, 0.5H), 7.67 (dd, 1H, J = 3.9, 7.8 Hz), 7.33-7.23 (m, 9H), 6.85 (d, 4H, J = 8.7 Hz), 6.39-6.33 (m, 1H), 6.26-6.20 (m, 1H), 5.39 (d, 1H, J = 8.1 Hz), 5.18 (m, 1H), 4.36-4.13 (m, 7H), 3.93-3.87 (m, 1H), 3.80 (s, 6H), 3.49 (m, 2H), 3.45-3.27 (m, 2H), 2.81-2.64 (m, 3H), 2.42-2.33 (m, 1H), 2.13-2.06 (m, 2H), 1.45 (s, 3H), 0.89 (s, 5H), 0.88 (s, 4H), 0.08 (s, 4H), 0.07 (s, 2H); ^{13}C NMR ($CDCl_3$) δ 174.7, 174.6, 173.7, 173.6, 163.6, 158.9, 152.7, 151.9, 150.9, 150.8, 144.1, 139.9, 135.1, 135.0, 130.3, 128.2, 127.4, 116.8, 116.5, 113.5, 103.0, 87.4, 86.4, 84.9 (m), 84.4, 84.3, 83.6 (m), 79.3, 79.0, 71.8, 71.6, 71.4, 71.3, 68.5, 68.4, 67.7, 62.8 (m), 62.6 (m), 55.4, 47.9, 47.3, 47.1, 39.3, 37.5 (m), 25.8, 23.5, 23.4, 22.9, 19.7 (t), 18.0, -4.5, -4.7; ^{31}P NMR ($CDCl_3$) H_3PO_4 reference δ -1.74, -1.93, -2.08, -2.17; IR (film) 3265, 3067, 2954, 2931,

2857, 2254, 1704, 1682, 1608, 1509, 1463, 1376, 1252, 1178, 1032, 834, 779, 759 cm^{-1}.

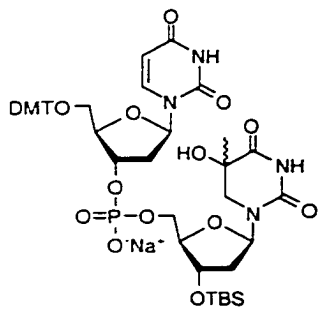

Preparation of 155. Et_3N (1 mL) was added to a solution of **152** (0.24 g, 0.24 mmol) in THF (1 mL) and refluxed. The reaction mixture was concentrated *in vacuo*, the residue taken up in MeOH (1 mL), and passed through Dowex resin as described above. Column chromatography (CH_2Cl_2:MeOH, 4:1) yielded 0.18 g (77%) of product as a mixture of two diastereomers. m.p. 136 °C (color change from white to pink), 156-168 °C (phase change, color change to red); ^1H NMR (MeOH-d_4) δ 7.78 (d, 1H, J = 8.1 Hz), 7.38 (d, 2H, J = 7.5 Hz), 7.30-7.20 (m, 7H), 6.85 (dd, 4H, J = 1.5, 8.7 Hz), 6.31-6.22 (m, 2H), 5.27 (d, 1H, J = 8.1 Hz), 5.02 (m, 1H), 4.37 (m, 1H), 4.30 (m, 1H), 3.95 (m, 2H), 3.88 (m, 1H), 3.75 (s, 6H), 3.50-3.34 (m, 4H), 2.67 (m, 1H), 2.42-2.35 (m, 1H), 2.20-2.11 (m, 1H), 1.94-1.87 (m, 1H), 1.36 (s, 3H), 0.88 (s, 9H), 0.08 (s, 3H), 0.06 (s, 3H); ^{13}C NMR (MeOH-d_4) δ 175.2, 166.1, 160.3, 154.2, 152.1, 146.0, 142.4, 136.7, 136.6, 131.6, 129.5, 129.1, 128.2, 114.4, 102.7, 88.4, 86.7, 86.5, 85.5, 77.5, 74.2, 69.5, 69.4, 66.7, 65.0, 55.9, 47.8, 40.7, 38.1, 26.4, 23.1, 22.9, 18.9, 9.4, -4.3; ^{31}P NMR (MeOH-d_4) H_3PO_4 reference δ -1.37; IR (film) 3206, 3062, 2953, 2931, 2856, 1694, 1608, 1509, 1463, 1384, 1251, 1223, 1178, 1068, 1033, 832, 779 cm^{-1}.

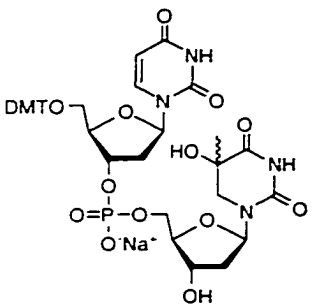

Preparation of 130. Et_3N (0.13 g, 1.29 mmol) and Et_3N•3HF (0.21 g, 1.29 mmol) were added to a solution of **155** (0.13 g, 0.13 mmol) in THF (2 mL). After 12 h, the reaction mixture was diluted with MeOH (2 mL) and passed through Amberlite resin, chromatographed (CH_2Cl_2:MeOH, 4:1), and passed through Dowex resin as described above. The product (0.061 g) was isolated in 54% yield as a white powder. m.p. 181 °C (color change to orange), 188-202 °C (phase change); ^{1}H NMR (MeOH-d_4) δ 7.82 (d, 1H, J = 8.4 Hz), 7.41 (d, 2H, J = 8.7 Hz), 7.33-7.23 (m, 7H), 6.88 (dd, 4H, J = 1.2, 8.7 Hz), 6.32-6.25 (m, 2H), 5.26 (d, 1H, J = 8.1 Hz), 5.06-5.02 (m, 1H), 4.35 (m, 1H), 4.28 (m, 1H), 3.94 (m, 2H), 3.87 (m, 1H), 3.78 (s, 6H), 3.52-3.34 (m, 4H), 2.64 (ddd, 1H, J = 3.3, 6.0, 13.8 Hz), 2.42 (ddd, 1H, J = 6.3, 13.5, 6.3 Hz) apparent quintet, 2.19 (ddd, 1H, J = 6.3, 8.1, 13.5 Hz) apparent quintet, 1.94 (ddd, 1H, J = 3.0, 5.7, 13.5 Hz), 1.39 (s, 0.7H), 1.36 (s, 2.3 H); ^{13}C NMR (MeOH-d_4) δ 175.2, 166.2, 160.4, 154.3, 152.1, 146.1, 142.5, 136.8, 136.7, 131.64, 131.57, 129.6, 129.1, 128.2, 114.4, 102.6, 88.4, 86.8, 86.7, 86.1, 86.0, 85.3, 77.1, 77.0, 72.9, 69.4, 67.0, 66.9, 64.8, 55.9, 47.9, 40.7, 37.5, 23.0, 22.8, 9.3; ^{31}P NMR (MeOH-d_4) H_3PO_4 reference δ 0.44; IR (film) 3196 (br), 2931, 1692, 1606, 1508, 1462, 1248, 1222, 1177, 1062, 1033 cm^{-1}; ESMS (ES$^-$) calcd for $C_{40}H_{44}N_4O_{15}P$: 851.3 (M-Na$^+$), found 851.3.

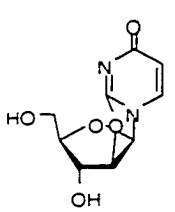

Preparation of Cyclouridine.[146] Diphenyl carbonate (7.00 g, 0.033 mol) and $NaHCO_3$ (0.13 g, 0.002 mol) were added to a solution of uridine (6.09 g, 0.025 mol) in DMF (20 mL) and heated to 150 °C. After 45 min, the reaction mixture was cooled to room temperature and poured into ether. The gummy brown precipitate was recrystallized from MeOH. The filtrate was cooled to generate a second lot of crystals. The product was isolated as an off-white powder (3.73

g, 66%). ^{1}H NMR (MeOH-d_4:D_2O, 1:1 by volume) δ 7.84 (d, 1H, J = 7.5 Hz), 6.43 (d, 1H, J = 5.7 Hz), 6.12 (d, 1H, J = 7.2 Hz), 5.38 (d, 1H, J = 5.4 Hz), 4.58 (d, 1H, J = 1.5 Hz), 4.30 (ddd, 1H, J = 1.8, 4.2, 4.2 Hz), 3.50 (dd, 2H, J = 1.8, 3.9 Hz).

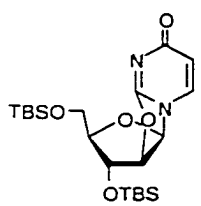

Preparation of 137. The cyclouridine (5.95 g, 0.026 mol), TBDMSCl (9.78 g, 0.065 mol), and imidazole (8.85 g, 0.13 mol) were dissolved in pyridine (30 mL) and heated to 40 °C. After 4 h, the reaction mixture was poured into H_2O (200 mL) and extracted with EtOAc (3 x 250 mL). The organic layer was washed with brine and dried over $MgSO_4$. Column chromatography (CH_2Cl_2:MeOH, 1:0 to 9:1) yielded 9.30 g (78%) of **137** as a white powder. ^{1}H NMR ($CDCl_3$) δ 7.34 (d, 1H, J = 7.2 Hz), 6.19 (d, 1H, J = 5.4 Hz), 6.01 (d, 1H, J = 7.8 Hz), 5.13 (dd, 1H, J = 0.9, 5.7 Hz), 4.60 (d, 1H, J = 1.2 Hz) apparent s, 4.14-4.10 (m, 1H), 3.56 (dd, 1H, J = 4.5, 11.1 Hz), 3.37 (dd, 1H, J = 6.9, 10.8 Hz), 0.90 (s, 9H), 0.82 (s, 9H), 0.16 (s, 3H), 0.13 (s, 3H), 0.00 (s, 3H), -0.02 (s, 3H).

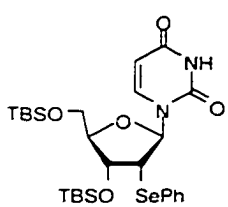

Preparation of 138.[146] $LiAlH_4$ (23 mL, 1.0 M/THF, 0.023 mol) was added to a solution of $(PhSe)_2$ (9.00 g, 0.029 mol) in THF (120 mL). Upon addition of the $LiAlH_4$, the orange solution turned pale yellow. After 20 min, a solution of **137** (8.14 g, 0.018 mol) in THF (20 mL) was added via cannula and the reaction mixture refluxed. After 6.5 h, the reaction mixture was cooled to room temperature and quenched with 5% HOAc/MeOH (16 mL), diluted with saturated $NaHCO_3$ (200 mL), and extracted with EtOAc (3 x 250 mL). The organic layer was washed with brine and dried over $MgSO_4$. Column chromatography (hexanes:EtOAc, 4:1 to 2:1) yielded 11.61 g (100%) of **138** as a white powder. ^{1}H NMR ($CDCl_3$) δ 8.44 (br s, 1H), 7.51 (d, 2H, J = 6.9 Hz), 7.41 (d, 1H, J = 8.1 Hz), 7.29-7.16

(m, 3H), 6.56 (d, 1H, J = 9.0 Hz), 5.38 (d, 1H, J = 8.1 Hz), 4.51 (d, 1H, J = 4.8 Hz), 4.08 (s, 1H), 3.86 (d, 1H, J = 10.2 Hz), 3.76 (d, 1H, J = 10.5 Hz), 3.61 (dd, 1H, J = 4.8, 9.0 Hz), 0.98 (s, 9H), 0.93 (s, 9H), 0.22 (s, 3H), 0.16 (s, 2H), 0.14 (s, 2H), 0.11 (s, 2H), 0.09 (s, 3H).

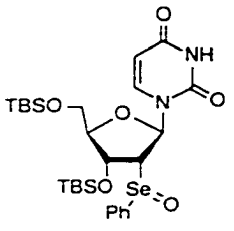

Preparation of 139.[146] *m*CPBA (5.53 g, 0.032 mol) and **138** (9.87 g, 0.016 mol) were dissolved in CH_2Cl_2 (160 mL). After stirring overnight (12 h), the reaction mixture was quenched with Et_3N (4.5 mL), diluted with saturated $NaHCO_3$ (60 mL), and extracted with CH_2Cl_2 (3 x 100 mL). The organic layer was dried over $MgSO_4$ and purified by column chromatography (CH_2Cl_2:MeOH, 19:1). The product was isolated as a mixture of diastereomers as an off-white foam (8.28 g, 83%). ^1H NMR ($CDCl_3$) δ 8.70 (br s, 1H), 7.73 (d, 1H, J = 6.9 Hz), 7.64 (d, 0.6H, J = 7.8 Hz), 7.56-7.34 (m, 4H), 7.14 (d, 0.4H, J = 8.4 Hz), 6.43 (d, 0.6H, J = 8.7 Hz), 6.01 (d, 0.4H, J = 3.9 Hz), 5.46 (d, 0.4H, J = 8.1 Hz), 5.39 (d, 0.6H, J = 8.1 Hz), 4.89-4.85 (m, 1H), 4.10-4.05 (m, 0.4H), 3.98 (m, 0.6H) apparent s, 3.91-3.82 (m, 1H), 3.80-3.70 (m, 2H), 1.02-0.88 (m, 18H), 0.32-0.05 (m, 12H).

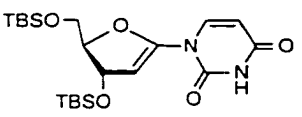

Preparation of 140.[146] Et_3N (3.92 g, 0.039 mol) was added to a solution of **139** (8.28 g, 0.013 mol) in THF (60 mL) and heated to 50 °C. After 12 h, the reaction mixture was concentrated and purified by column chromatography (hexanes:EtOAc, 3:1 to 2:1). The product (3.96 g) was isolated as a white powder in 67% yield. ^1H NMR ($CDCl_3$) δ 8.80 (br s, 1H), 7.76 (d, 1H, J = 8.4 Hz), 5.79 (d, 1H, J = 8.4 Hz), 5.57 (d, 1H, J = 2.7 Hz), 5.03 (t, 1H, J = 3.0 Hz), 4.42 (ddd, 1H, J = 3.0, 5.7, 5.7 Hz), 3.75 (dd, 1H, J = 5.4, 10.8 Hz), 3.66

(dd, 1H, J = 5.7, 11.1 Hz), 0.91 (s, 9H), 0.90 (s, 9H), 0.12 (s, 3H), 0.11 (s, 3H), 0.08 (s, 3H), 0.07 (s, 3H).

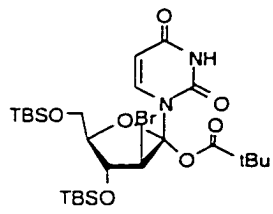

Preparation of 141.[144,145] A solution of Et_3N (0.36 g, 3.52 mmol) and pivalic acid (0.38 g, 3.72 mmol) in ether (12 mL) was added to a solution of **140** (0.32 g, 0.702 mmol) in ether (7 mL), followed by NBS (0.15 g, 0.84 mmol). A white precipitate formed immediately upon addition of the NBS. After 2 h, the reaction mixture was diluted with saturated $NaHCO_3$ (30 mL) and extracted with ether (3 x 40 mL). The organic layer was washed with brine and dried over $MgSO_4$. Column chromatography (hexanes:EtOAc, 2:1) yielded **141** as a mixture of diastereomers. The mixture was recrystallized from hexanes to yield the desired diastereomer (0.231 g, 52%) as a white powder. ^1H NMR ($CDCl_3$) δ 8.48 (br s, 1H), 7.83 (d, 1H, J = 8.4 Hz), 5.69 (d, 1H, J = 8.4 Hz), 4.91 (s, 1H), 4.74 (d, 1H, J = 3.3 Hz), 4.13 (ddd, 1H, J = 2.7, 5.1, 5.1 Hz), 3.90-3.88 (m, 2H), 1.21 (s, 9H), 0.93 (s, 9H), 0.92 (s, 9H), 0.18 (s, 3H), 0.13 (s, 3H), 0.10 (s, 6H).

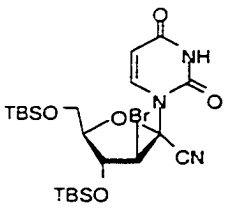

Preparation of 142. TMSCN (1.56 g, 16.0 mmol) was added to a solution of **141** (2.02 g, 3.2 mmol) in CH_2Cl_2 (80 mL), then cooled to -40 °C. $SnCl_4$ (1.11 g, 4.3 mmol) was added to the reaction mixture at -40 °C, then slowly warmed to 10 °C. After stirring overnight, the reaction mixture was warmed to room temperature, poured into saturated $NaHCO_3$ (50 mL), and extracted with CH_2Cl_2 (3 x 100 mL). The organic layer was dried over $MgSO_4$ and purified by column chromatography (hexanes:EtOAc, 3:1) to yield 1.48 g (83%) of **142** as a pale yellow foam. ^1H NMR ($CDCl_3$) δ 8.85 (br s, 1H), 7.59 (d, 1H, J = 8.7 Hz), 5.79 (d, 1H, J = 8.1 Hz), 5.01 (d, 1H, J = 0.9 Hz), 4.71 (dd, 1H, J = 0.6, 2.7 Hz),

4.41 (ddd, 1H, J = 3.0, 6.3, 6.3 Hz), 3.98-3.88 (m, 2H), 0.95 (s, 9H), 0.93 (s, 9H), 0.19 (s, 3H), 0.15 (s, 3H), 0.12 (s, 6H).

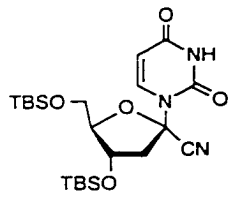

Preparation of 143. A solution of Bu_3SnH (1.04 g, 3.57 mmol) and AIBN (0.027 g, 0.16 mmol) in benzene (10 mL, sparged with N_2 for 20 min) was slowly added to a solution of **142** (1.83 g, 3.26 mmol) in refluxing benzene (160 mL, sparged with N_2 for 20 min) via a syringe pump. After 6.5 h, the reaction mixture was concentrated to yield a white solid. The product was purified by column chromatography (CH_2Cl_2:EtOAc, 19:1 to 4:1) to yield 1.46 g (93%) of **143** as a white powder. ^1H NMR ($CDCl_3$) δ 9.61 (br s, 1H), 7.81 (d, 1H, J = 8.4 Hz), 5.73 (d, 1H, J = 8.4 Hz), 4.41-4.38 (m, 2H), 3.82 (dd, 1H, J = 3.0, 11.7 Hz), 3.72 (dd, 1H, J = 2.1, 11.7 Hz), 3.17 (dd, 1H, J = 3.0, 14.4 Hz), 2.64 (dd, 1H, J = 5.4, 14.1 Hz), 0.93 (s, 9H), 0.86 (s, 9H), 0.13 (s, 3H), 0.10 (s, 3H), 0.06 (s, 3H), 0.05 (s, 3H).

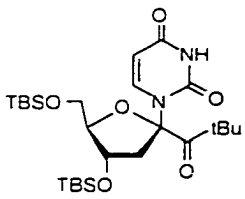

Preparation of 144. *tert*-BuLi (1.5 mL, 1.7M, 2.55 mmol) was added dropwise to a solution of **143** (0.39 g, 0.80 mmol) in THF (16 mL) at -78 °C. After 30 min, HOAc/H_2O (10 mL, 66%) was added and stirred overnight, allowing the reaction mixture to warm to room temperature. The reaction mixture was quenched with portions of saturated $NaHCO_3$ to control foaming and extracted with ether (3 x 50 mL). The organic layer was washed with saturated $NaHCO_3$ and brine, and dried over $MgSO_4$. Column chromatography (hexanes:EtOAc, 3:1 to 1:1) yielded 0.22 g (50%) of **144** as a white foam, which was impure and could not be purified until the compound was deprotected. ^1H NMR ($CDCl_3$) δ 8.45 (br s, 1H), 8.27 (d, 1H, J = 8.1 Hz), 5.73 (d, 1H, J = 8.4 Hz), 4.44-4.36 (m, 1H),

4.09-4.00 (m, 1H), 3.86-3.76 (m, 2H), 3.39 (dd, 1H, J = 9.3, 13.5 Hz), 2.28-2.20 (m, 1H), 1.19 (s, 9H), 0.95-0.88 (m, 18H), 0.14-0.05 (m, 12H).

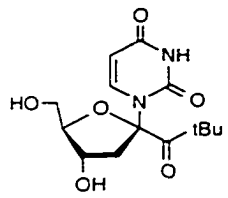

Preparation of 68. $Et_3N•3HF$ (0.71 g, 4.42 mmol) was added to a solution of **144** (0.24 g, 0.442 mmol) in THF (5 mL). After stirring overnight, the reaction mixture was concentrated *in vacuo*. Column chromatography (CH_2Cl_2:MeOH, 19:1 to 9:1), followed by recrystallization from CH_3CN (cooled at -30 °C), yielded 0.086 g of **68** in 62% yield (34% from **143**). ^{1}H NMR (MeOH-d_4) δ 8.33 (d, 1H, J = 8.4 Hz), 5.75 (d, 1H, J = 8.4 Hz), 4.34 (dt, 1H, J = 7.5, 7.8 Hz) apparent q, 3.96-3.90 (m, 1H), 3.82-3.74 (m, 2H), 3.30 (dd, 1H, J = 8.1, 14.4 Hz), 2.31 (dd, 1H, J = 7.8, 14.4 Hz), 1.19 (s, 9H).

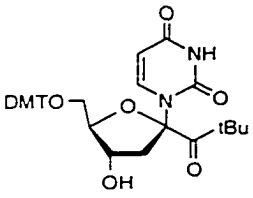

Preparation of 145. The ketone (**68**) was dried by azeotroping with pyridine (2 x 1 mL). A solution of DMTCl (0.19 g, 0.56 mmol) in pyridine (2 mL) was added dropwise to a solution of **68** (0.16 g, 0.51 mmol) in pyridine (2 mL) at 0 °C, then allowed to warm to room temperature. After stirring overnight, the reaction mixture was poured into saturated $NaHCO_3$ (25 mL) and extracted with EtOAc (3 x 40 mL). The organic layer was washed with brine and dried over $MgSO_4$. The product was purified by column chromatography (hexanes:EtOAc, 1:1) to yield 0.30 g (97%) of **145** as a white foam. ^{1}H NMR ($CDCl_3$) δ 8.60 (br s, 1H), 7.88 (d, 1H, J = 8.1 Hz), 7.42-7.25 (m, 9H), 6.88 (d, 4H, J = 8.4 Hz), 5.56 (d, 1H, J = 8.1 Hz), 4.46 (m, 1H), 4.23-4.21 (m, 1H), 3.84 (s, 6H), 3.50-3.39 (m, 3H), 3.28-3.25 (m, 1H), 2.30 (dd, 1H, J = 6.9, 14.7 Hz), 1.23 (s, 9H).

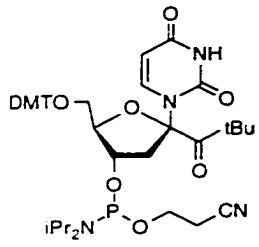

Preparation of 146. β-cyanoethyl diisopropylchlorophosphoramidite (0.14 g, 0.58 mmol) was added dropwise to a solution of **145** (0.30 g, 0.49 mmol) and Hünig's base (0.25 g, 1.95 mmol) in CH_2Cl_2 (5 mL). After 1 h, the reaction mixture was diluted with EtOAc (25 mL) and quickly washed with saturated Na_2CO_3 (10 mL) and brine (10 mL). The organic layer was dried over Na_2SO_4 and concentrated to yield a yellow foam. Column chromatography (CH_2Cl_2:EtOAc, 2:1) with Matrex silica gel (neutral) yielded 0.31 g (78%) of product as a white foam. ^{1}H NMR ($CDCl_3$) δ 8.48 (br s, 1H), 8.21 (d, 0.5H, J = 8.1 Hz), 8.14 (d, 0.5H, J = 8.4 Hz), 7.42 (t, 2H, J = 6.6 Hz), 7.33-7.27 (m, 7H), 6.87-6.82 (m, 4H) apparent dd, 5.37 (d, 0.5H, J = 8.1 Hz), 5.36 (d, 0.5H, J = 8.4 Hz), 4.70 (ddd, 0.5H, J = 8.7, 17.4, 8.7 Hz), 4.58 (ddd, 0.5 H, J = 9.0, 16.8, 9.0 Hz), 3.97 (m, 1H), 3.88-3.72 (m, 1H), 3.82 (s, 3H), 3.81 (s, 3H), 3.61-3.41 (m, 7H), 2.63 (t, 1H, J = 6.3 Hz), 2.46-2.43 (m, 1H), 2.41 (t, 1H, J = 6.0 Hz), 1.19 (s, 9H), 1.19-1.14 (m, 9H), 1.02 (d, 3H, J = 6.6 Hz).

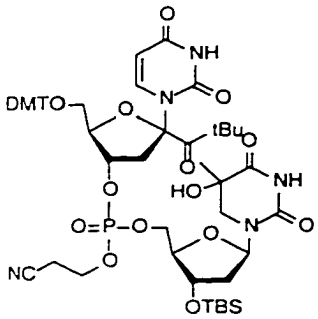

Preparation of 156. The ketone phosphoramidite (**146**, 0.14 g, 0.17 mmol) and **149** (0.064 g, 0.17 mmol) were dissolved in CH_3CN (2 mL, 0.5 M tetrazole). After 2 h, the reaction mixture was oxidized as described above, poured into saturated $NaHCO_3$ (25 mL), and extracted with CH_2Cl_2 (3 x 30 mL). The organics were dried over Na_2SO_4 and concentrated *in vacuo*. Column chromatography (CH_2Cl_2:MeOH, 19:1) yielded 0.12 g (63%) of **156** as a mixture of four diastereomers. m.p. 117-126 °C; ^{1}H NMR ($CDCl_3$) δ 9.71 (br s, 1H), 8.67 (br s, 0.5H), 8.63 (br s, 0.5H), 7.98 (d, 0.5H, J = 8.7 Hz), 7.96 (d, 0.5H, J = 8.1 Hz), 7.39-7.26 (m, 9H), 6.85 (dd, 4H, J = 1.8, 8.4 Hz), 6.35 (t, 0.2H, J = 6.6 Hz), 6.24 (t, 0.7H, J = 6.6 Hz), 6.17 (t, 0.1H, J = 6.9 Hz), 5.45 (d, 0.5H, J = 7.8 Hz), 5.44 (d, 0.5H, J = 7.8 Hz),

5.09 (m, 1H), 4.29 (m, 4H), 4.15 (m, 3H), 3.93-3.71 (m, 2H), 3.80 (s, 6H), 3.61-3.21 (m, 4H), 2.78 (t, 1H, J = 6.0 Hz), 2.64-2.56 (m, 1H), 2.53-2.45 (m, 1H), 2.05-2.01 (m, 2H), 1.42 (m, 3H), 1.16 (s, 9H), 0.884 (s, 5H), 0.877 (s, 4H), 0.07 (s, 6H); ^{13}C NMR ($CDCl_3$) δ 201.9, 201.7, 174.7, 174.6, 163.5, 159.0, 152.6, 151.8, 150.6, 150.5, 144.1, 138.9, 135.1, 135.0, 130.3, 128.3, 127.5, 116.9, 116.5, 113.5, 113.2, 102.8, 102.7, 98.1, 98.0, 87.4, 86.3, 84.9, 84.6, 84.3, 83.9, 75.3, 72.1, 71.9, 68.7, 68.6, 67.8, 62.8, 62.5, 61.2, 55.5, 47.3, 47.2, 43.7, 40.8, 37.4, 29.7, 28.8, 25.9, 23.5, 19.7, 19.6, 18.1, -4.5, -4.7; ^{31}P NMR ($CDCl_3$) H_3PO_4 reference δ -1.78, -1.92, -2.18; IR (film) 3198, 3062, 2957, 2931, 2857, 2253, 1696, 1608, 1509, 1471, 1446, 1386, 1300, 1253, 1223, 1177, 1034, 912, 833, 732 cm^{-1}.

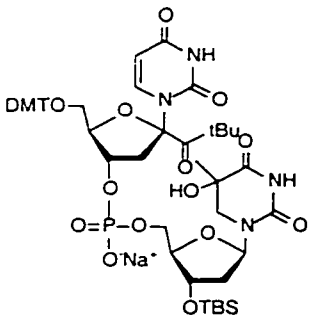

Preparation of 158. Et_3N (1 mL) was added to a solution of **156** (0.11 g, 0.10 mmol) in THF (1 mL) and refluxed. After 12 h, the reaction mixture was concentrated *in vacuo*, the residue taken up in MeOH (1 mL), and passed through Dowex resin as described above. Column chromatography (CH_2Cl_2:MeOH, 4:1) yielded 0.086 g (80%) of product as a mixture of two diastereomers. m.p. 121 °C (color change from white to pink), 185-189 °C (phase change); ^{1}H NMR (MeOH-d_4) δ 8.07 (d, 1H, J = 8.4 Hz), 7.44 (d, 2H, J = 7.5 Hz), 7.33-7.23 (m, 7H), 6.87 (dd, 4H, J = 1.5, 8.7 Hz), 6.26 (dd, 1H, J = 5.7, 7.8 Hz), 5.34 (d, 1H, J = 8.1 Hz), 4.90 (m, 1H), 4.40 (m, 1H), 4.07 (m, 1H), 3.89-3.84 (m, 3H), 3.77 (s, 6H), 3.75-3.74 (m, 1H), 3.56-3.51 (m, 3H), 3.35-3.28 (m, 1H), 2.55-2.48 (m, 1H), 2.21-2.10 (m, 1H), 1.91-1.86 (m, 1H), 1.40 (s, 0.7H), 1.35 (s, 2.3H), 1.17 (s, 9H), 0.89 (s, 9H), 0.10 (s, 3H), 0.07 (s, 3H); ^{13}C NMR (MeOH-d_4) δ 203.8, 175.3, 166.0, 160.4, 154.3, 152.1, 146.1, 141.2, 136.7, 131.7, 131.6, 129.5, 129.1, 128.3,

114.4, 102.8, 99.2, 88.4, 86.4, 85.5, 74.2, 73.6, 69.5, 66.7, 62.9, 55.9, 44.7, 41.9, 37.9, 30.3, 29.4, 26.5, 23.1, 18.9, -4.3; ^{31}P NMR (MeOH-d_4) H_3PO_4 reference δ -1.65; IR (film) 3400 (br), 3247, 3019, 2943, 2890, 1701, 1590, 1497, 1458, 1276, 1235, 1194, 1162, 1044, 797 cm^{-1}; ESMS (ES$^-$) calcd for $C_{51}H_{66}N_4O_{16}PSi$: 1049.4 (M-Na$^+$), found 1049.5.

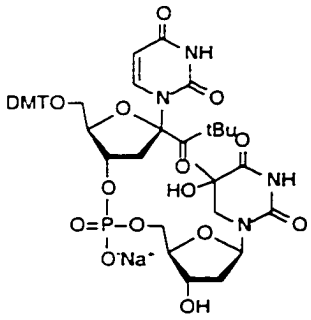

Preparation of 160. Et_3N (0.080 g, 0.79 mmol) and Et_3N•3HF (0.12 g, 0.74 mmol) were added to a solution of **158** (0.078 g, 0.073 mmol) in THF (1 mL). After 12 h, the reaction mixture was diluted with MeOH (1 mL) and passed through Amberlite resin, chromatographed (CH_2Cl_2:MeOH, 4:1), and passed through Dowex resin as described above. The product was isolated in 37% yield (26 mg) as a white powder. m.p. 180-184 °C; ^{1}H NMR (MeOH-d_4) δ 8.15 (d, 0.3H, J = 8.4 Hz), 8.14 (d, 0.7H, J = 7.8 Hz), 7.45 (d, 2H, J = 7.2 Hz), 7.34-7.22 (m, 7H), 6.88 (d, 4H, J = 7.8 Hz), 6.30-6.26 (m, 1H), 5.28 (d, 1H, J = 8.1 Hz), 4.95 (m, 1H), 4.38 (m, 1H), 4.04 (m, 1H), 3.88-3.84 (m, 3H), 3.79 (s, 6H), 3.58 (m, 2H), 3.48-3.39 (m, 2H), 3.34 (m, 1H), 2.56 (dd, 1H, J = 7.8, 14.4 Hz), 2.23-2.14 (m, 1H), 1.97-1.87 (m, 1H), 1.39 (s, 0.7H), 1.35 (s, 2.3H), 1.18 (s, 9H); ^{13}C NMR (MeOH-d_4) δ 203.9, 175.3, 166.2, 160.4, 154.3, 152.2, 146.2, 141.5, 136.7, 131.7, 131.6, 129.6, 129.1, 128.3, 114.4, 102.7, 99.1, 88.4, 86.2, 86.0, 85.4, 73.0, 69.5, 66.8, 62.5, 55.9, 55.0, 47.9, 44.8, 41.6, 37.4, 29.3, 23.0; ^{31}P NMR (MeOH-d_4) H_3PO_4 reference δ 0.50; IR (film) 3374 (br), 2955, 1701, 1686, 1607, 1508, 1458, 1299, 1249, 1223, 1176, 1072, 1035, 827 cm^{-1}.

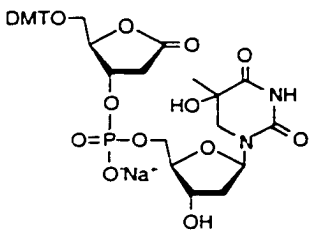

Preparation of 132. A solution of **160** (18 mg, 0.019 mmol) in CH_3CN:H_2O (150 mL, 1:1 by volume) was photolyzed at 350 nm (14 lamps) for 2.5 h. The reaction mixture was concentrated *in vacuo* and purified by column chromatography (CH_2Cl_2:MeOH, 3:1). The product was isolated in 62% yield (9 mg) as a white powder. m.p. 133 °C (color change from white to orange), 192-194 °C (phase change); ^{1}H NMR (MeOH-d_4) δ 7.37-7.19 (m, 9H), 6.88 (d, 4H, J = 8.7 Hz), 6.25 (dd, 1H, J = 7.8, 6.3 Hz), 4.83 (m, 1H), 4.78 (m, 1H), 4.27 (m, 1H), 3.93 (m, 2H), 3.84 (m, 1H), 3.79 (s, 6H), 3.55-3.52 (m, 2H), 3.35-3.15 (m, 3H), 2.73 (d, 1H, J = 18.6 Hz), 2.20-2.10 (m, 1H), 1.98-1.94 (m, 1H), 1.34 (s, 3H); ^{31}P NMR (MeOH-d_4) H_3PO_4 reference δ 1.87, 0.30; IR (film) 3300 (br), 2959, 1702, 1686, 1682, 1608, 1509, 1462, 1300, 1250, 1177, 1073, 1035, 827 cm^{-1}; ESMS (ES$^-$) calcd for $C_{36}H_{40}N_2O_{14}P$: 755.2 (M-Na$^+$), found 755.3.

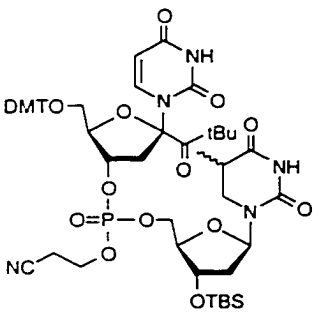

Preparation of 157. The ketone phosphoramidite (**146**, 0.11 g, 0.13 mmol) and **148** (0.064 g, 0.17 mmol) were dissolved in CH_3CN (2 mL, 0.5 M tetrazole). After 2 h, the reaction mixture was oxidized as described above, poured into saturated $NaHCO_3$ (20 mL), and extracted with EtOAc (3 x 30 mL). The organics were washed with brine (20 mL), dried over Na_2SO_4, and concentrated *in vacuo*. Column chromatography (CH_2Cl_2:EtOAc:MeOH, 1:1:0 to 5:5:1) yielded 99 mg (71%) of **157** as a mixture of four diastereomers. m.p. 105-111 °C; ^{1}H NMR ($CDCl_3$) δ 9.51 (br s, 1H), 8.164 (s, 0.5H), 8.155 (s, 0.5H), 7.99 (dd, 1H, J = 3.6, 8.1 Hz), 7.41-7.28 (m, 9H), 6.88 (dd, 4H, J = 0.9, 8.4 Hz), 6.33-6.23 (m, 0.8H), 6.19-6.09 (m, 0.2H), 5.45 (dd, 1H, J = 3.0, 8.1 Hz), 5.12 (m, 1H), 4.35-4.26 (m, 3H), 4.22-4.05 (m, 3H), 3.831 (s, 3H), 3.825 (s, 3H), 3.91-3.71 (, 2H), 3.62-3.38 (m, 3H),

3.18 (m, 1H), 2.79 (t, 1H, J = 6.0 Hz), 2.70-2.59 (m, 2H), 2.49-2.43 (m, 1H), 2.14-2.03 (m, 2H), 1.29-1.25 (m, 3H), 1.19 (s, 9H), 0.92 (s, 3H), 0.91 (s, 6H), 0.11 (s, 2H), 0.10 (s, 2H), 0.09 (s, 2H); ^{13}C NMR ($CDCl_3$) δ 201.8, 201.6, 173.0, 172.9, 163.3, 159.0, 153.0, 152.6, 150.3, 144.1, 138.9, 138.8, 135.0, 134.9, 130.3, 128.3, 128.2, 127.5, 116.7, 116.4, 113.5, 102.6, 98.2, 98.1, 87.4, 86.3, 86.2, 85.8, 85.3, 85.1, 85.0, 84.6, 84.4, 84.1, 83.6, 83.5, 75.4 (m), 71.9, 71.8, 71.7, 67.7 (t), 62.6, 62.5, 62.43, 62.36, 61.2, 60.6, 55.5, 55.4, 43.7, 42.7, 40.9, 37.5, 37.4, 37.2, 35.5, 28.8, 25.9, 21.2, 19.9, 19.8, 19.7, 19.6, 18.1, 14.4, 13.2, 13.1, 12.6, -4.5, -4.7; ^{31}P NMR ($CDCl_3$) H_3PO_4 reference δ -1.78, -1.84; IR (film) 3389, 2956, 2886, 2269, 1716, 1700, 1508, 1446, 1252, 1180, 1063, 1035, 958, 835 cm^{-1}.

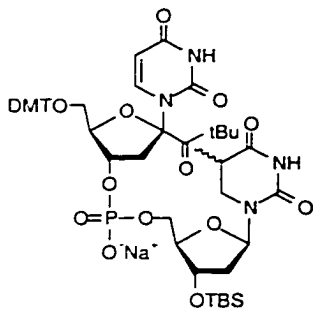

Preparation of 159. Et_3N (1 mL) was added to a solution of **157** (98 mg, 0.10 mmol) in THF (1 mL) and refluxed. After 12 h, the reaction mixture was concentrated *in vacuo*, the residue taken up in MeOH (1 mL), and passed through Dowex resin as described above. Column chromatography (CH_2Cl_2:MeOH, 4:1) yielded 64 mg (67%) of product as a mixture of two diastereomers. m.p. 172 °C (color change from white to orange), 175-182 °C (phase change); ^{1}H NMR (MeOH-d_4) δ 8.11 (d, 1H, J = 8.1 Hz), 4.45 (d, 2H, J = 7.2 Hz), 7.34-7.23 (m, 7H), 6.87 (dd, 4H, J = 1.5, 8.7 Hz), 6.31-6.24 (m, 1H), 5.31 (d, 1H, J = 8.1 Hz), 4.94 (m, 1H), 4.47 (m, 1H), 4.03 (m, 1H), 3.85 (m, 3H), 3.78 (s, 6H), 3.62-3.43 (m, 4H), 3.20-3.04 (m, 1H), 2.70-2.50 (m, 2H), 2.27-2.14 (m, 1H), 1.89-1.83 (m, 1H), 1.18 (s, 9H), 1.16 (m, 3H) apparent s, 0.91 (9H), 0.11 (s, 3H), 0.09 (s, 3H); ^{13}C NMR (MeOH-d_4) δ 203.8, 176.1, 175.8, 166.1, 160.4, 155.3, 155.0, 152.2, 146.2, 141.4, 136.7, 131.7, 131.6, 129.6, 129.1, 128.3, 114.4, 102.6, 99.1, 88.3, 86.7 (m),

86.3 (m), 85.6, 85.5, 74.7, 74.5, 73.2, 66.6, 62.7, 55.9, 44.7, 43.2, 41.8, 38.1, 37.8, 36.6, 36.5, 29.4, 26.5, 18.9, 13.6, 13.1, -4.3; ^{31}P NMR (MeOH-d_4) H_3PO_4 reference δ 0.13; IR (film) 3364, 3094, 2956, 2885, 1704, 1608, 1509, 1446, 1302, 1251, 1188, 1069, 962, 834 cm^{-1}.

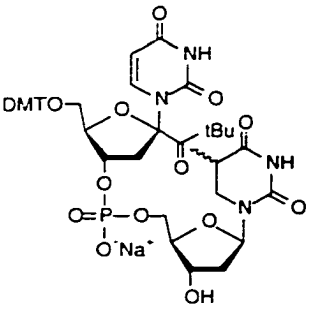

Preparation of 161. Et_3N (36 mg, 0.36 mmol) and Et_3N•3HF (49 mg, 0.31 mmol) were added to a solution of **159** (64 mg, 0.061 mmol) in THF (1 mL). After 8 h, the reaction mixture was diluted with MeOH (10 mL) and passed through Amberlite resin, chromatographed (CH_2Cl_2:MeOH, 3:1), and passed through Dowex resin as described above. The product was isolated in 26% yield (15 mg) as a white powder. m.p. 190 °C (color change from white to brown), 193-209 °C (phase change); ^{1}H NMR (MeOH-d_4) δ 8.14 (d, 1H, J = 8.4 Hz), 7.46 (dd, 2H, J = 2.1, 9.0 Hz), 7.34-7.24 (m, 7H), 6.88 (dd, 4H, J = 1.2, 9.0 Hz), 6.32-6.25 (m, 1H), 5.28 (d, 1H, J = 8.4 Hz), 4.92 (m, 1H), 4.38 (m, 1H), 4.01 (m, 1H), 3.86 (m, 3H) apparent d, 3.79 (s, 6H), 3.68-3.40 (m, 4H), 3.20-3.04 (m, 1H), 2.69-2.51 (m, 2H), 2.28-2.14 (m, 1H), 1.96-1.89 (m, 1H), 1.18 (s, 9H), 1.16 (m, 3H) apparent s; ^{13}C NMR (MeOH-d_4) δ 203.9, 176.2, 160.5, 155.2, 152.4, 146.2, 141.5, 136.8, 131.7, 131.6, 129.6, 129.1, 128.3, 114.4, 102.6, 99.0, 88.4, 86.1, 86.0, 85.4, 85.3, 73.2, 73.0, 66.8, 62.5, 55.9, 44.7, 43.2, 41.7, 37.5, 37.2, 36.6, 29.4, 13.6, 13.1; ^{31}P NMR (MeOH-d_4) H_3PO_4 reference δ 0.49; IR (film) 3358, 2957, 2886, 1714, 1698, 1608, 1510, 1454, 1188, 1066, 1037, 961 cm^{-1}; ESMS (ES$^-$) calcd for $C_{45}H_{52}N_4O_{15}P$: 919.3 (M-Na$^+$), found 919.4.

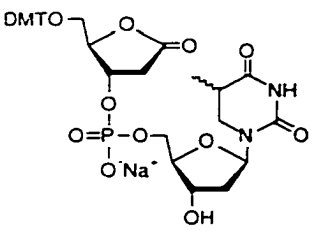

Preparation of 131. A solution of **161** (12 mg, 0.013 mmol) in CH_3CN:H_2O (100 mL, 1:1 by volume) was photolyzed at 350 nm (16 lamps) for 2 h. The reaction mixture was concentrated *in vacuo* and purified by column chromatography (CH_2Cl_2:MeOH, 3:1). The product was isolated in 62% yield (6 mg) as a white powder. m.p. 135 °C (color change to tan), 140-145 °C (phase change); ^{1}H NMR (MeOH-d_4) δ 7.38-7.21 (m, 9H), 6.89-6.84 (m, 4H), 6.29-6.22 (m, 1H), 4.89 (m, 1H), 4.77 (m, 1H), 4.34-4.27 (m, 1H), 3.89 (m, 2H), 3.84 (m, 1H), 3.79 (s, 6H), 3.65-3.47 (m, 2H), 3.24-3.05 (m, 2H), 2.75-2.60 (m, 2H), 2.24-2.11 (m, 1H), 1.96-1.90 (m, 1H), 1.17 (d, 3H, J = 6.9 Hz); ^{31}P NMR (MeOH-d_4) H_3PO_4 reference δ 0.35; IR (film) 3372, 2957, 2887, 1722, 1442, 1367, 1344, 1185, 1062, 1044, 986, 923, 852 cm^{-1}; ESMS (ES$^-$) calcd for $C_{36}H_{40}N_2O_{13}P$: 739.2 (M-Na$^+$), found 739.3.

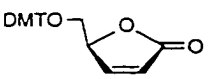

Preparation of 78. Hünig's base (0.096 g, 0.75 mmol) and CH_2Cl_2 (5 mL) were added to the furanone (0.061 g, 0.54 mmol) and DMTCl (0.22 g, 0.67 mmol) at room temperature. After 3 h, the reaction mixture was quenched with MeOH (1 mL), diluted with H_2O (15 mL), and extracted with ether (3 x 20 mL). The organic layer was washed with brine, dried over $MgSO_4$, and concentrated. Column chromatography (hexanes:EtOAc, 2:1) yielded 0.19 g (84%) of **78** as a white powder. m. p. 109 °C (color change to orange), 109-113 °C (phase change); ^{1}H NMR (300 MHz, $CDCl_3$) δ 7.46-7.40 (m, 3H), 7.33-7.20 (m, 7H), 6.87-6.82 (m, 4H) apparent d, 6.19 (dd, 1H, J = 2.4, 6.0 Hz), 5.11-5.07 (m, 1H), 3.80 (s, 6H), 3.40 (d, 2H, J = 5.1 Hz); ^{13}C NMR (75 MHz, $CDCl_3$) δ 158.9, 154.5, 144.5, 135.7, 135.6, 130.2, 128.22, 128.18, 127.2, 122.6, 113.5, 86.7, 82.5, 63.6, 55.4; IR (film) 3002, 2932, 2870, 2837,

1760, 1608, 1582, 1509, 1464, 1446, 1301, 1252, 1177, 1159, 1119, 1095, 1033, 830, 728, 703 cm^{-1}.

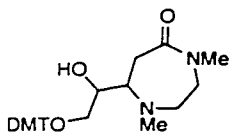

Preparation of 79. *N,N*-dimethylethylenediamine (0.33 g, 3.76 mmol) was added to a solution of **78** in $CH_3CN:H_2O$ (12 mL, 2:1 by volume) at 37 °C. After 1 h, the reaction mixture was concentrated *in vacuo*. Column chromatography (hexanes:EtOAc:MeOH, 2:1:0 to 5:5:1) yielded 0.11 g (56%) of **79** as a white foam. m. p. 57-64 °C; ^1H NMR (300 MHz, $CDCl_3$) δ 7.45 (d, 2H, J = 7.2 Hz), 7.37-7.18 (m, 7H), 6.86-6.81 (m, 4H) apparent d, 3.98-3.87 (m, 1H), 3.80 (s, 6H), 3.50 (dd, 1H, J = 6.9, 15.3 Hz), 3.33-3.20 (m, 3H), 2.96 (s, 3H), 2.97-2.90 (m, 1H), 2.75-2.57 (m, 5H), 2.38 (s, 3H); ^{13}C NMR (75 MHz, $CDCl_3$) δ 174.0, 158.7, 145.2, 136.40, 136.35, 130.3, 128.4, 128.0, 126.9, 113.3, 86.5, 70.3, 65.7, 60.4, 55.4, 52.9, 47.4, 41.5, 35.9, 34.7; IR (film) 3399 (br), 3058, 2932, 2836, 1634, 1608, 1509, 1463, 1445, 1398, 1301, 1250, 1177, 1069, 1034, 911, 829, 728 cm^{-1}; exact mass (FAB) calcd for $C_{30}H_{36}N_2O_5$: 505.2704 (M+H), found 505.2691.

6 References

[1] von Sonntag, C. *The Chemical Basis of Radiation Biology*; Taylor & Francis: London, 1987.

[2] Girotti, A. W. "Lipid Hydroperoxide Generation, Turnover, and Effector Action in Biological Systems." *J. Lipid Res.* **1998**, *39*, 1529.

[3] Porter, N. A.; Lehman, L. S.; Weber, B. A.; Smith, K. J. "Unified Mechanism for Polyunsaturated Fatty Acid Autoxidation." *J. Am. Chem. Soc.* **1981**, *103*, 6447.

[4] Porter, N. A.; Caldwell, S. E.; Mills, K. A. "Mechanisms of Free Radical Oxidation of Unsaturated Lipids." *Lipids* **1995**, *30*, 277.

[5] Comporti, M. "Lipid Peroxidation and Biogenic Aldehydes: From the Identification of 4-Hydroxynonenal to Further Achievements in Biopathology." *Free Rad. Res.* **1998**, *28*, 623.

[6] Esterbauer, H. "Lipid Peroxidation Products: Formation, Chemical Properties and Biological Activities." In: *Free Radicals in Liver Injury*, Proc. Int. Meeting; Poli, G.; Cheeseman, K. H.; Dianzani, M. U., Eds.; IRL: Oxford, 1985, pp 29.

[7] Esterbauer, H. "Aldehydic Products of Lipid Peroxidation." In: *Free Radicals, Lipid Peroxidation and Cancer*; McBrien, D. C. H.; Slater, T. F., Eds.; Academic: London, 1982, pp 101.

[8] Greenberg, M. M. "The Chemistry of DNA Damage." In *Comprehensive Natural Products Chemistry*; Kool, E. T., Ed.; Elsevier: Amsterdam, 1999; Vol. 7, Chapter 11.

[9] Pratviel, G.; Bernadou, J.; Meunier, B. "Carbon-Hydrogen Bonds of DNA Sugar Units as Targets for Chemical Nucleases and Drugs." *Angew. Chem. Int. Ed. Engl.* **1995**, *34*, 746.

[10] Pogozelski, W. K.; Tullius, T. D. "Oxidative Strand Scission of Nucleic Acids: Routes Initiated by Hydrogen Atom Abstraction from the Sugar Moiety." *Chem. Rev.* **1998**, *98*, 1089.

[11] Burrows, C. J.; Muller, J. G. "Oxidative Nucleobase Modifications Leading to Strand Scission." *Chem. Rev.* **1998**, *98*, 1109.

[12] Worth, Jr., L.; Frank, B. L.; Christner, D. F.; Absalon, M. J.; Stubbe, J.; Kozarich, J. W. "Isotope Effects on the Cleavage of DNA by Bleomycin: Mechanism and Modulation." *Biochemistry* **1993**, *32*, 2601.

[13] Myers, A. G.; Cohen, S. B.; Kwon, B.-M. "DNA Cleavage by Neocarzinostatin Chromophore. Establishing the Intermediacy of Chromophore-Derived Cumulene and

Biradical Species and their Role in Sequence-Specific Cleavage." *J. Am. Chem. Soc.* **1994**, *116*, 1670.

[14] Dedon, P. C.; Goldberg, I. H. "Free-Radical Mechanisms Involved in the Formation of Sequence-Dependent Bistranded DNA Lesions by the Antitumor Antibiotics Bleomycin, Neocarzinostatin, and Calicheamicin." *Chem. Res. Toxicol.* **1992**, *5*, 311.

[15] Schulte-Frohlinde, D.; Opitz, J.; Görner, H.; Bothe, E. "Model Studies for the Direct Effect of High-energy Irradiation on DNA. Mechanism of Strand Break Formation Induced by Laser Photoionization of Poly U in Aqueous Solution." *Int. J. Radiat. Biol.* **1985**, *48*, 397.

[16] Shaw, A. A.; Voituriez, L.; Cadet, J.; Gregoli, S.; Symons, M. C. R. "Identification of the Products Resulting from the Direct Effects of γ-Radiation on Thymidine." *J. Chem. Soc. Perkin Tran. 2* **1988**, 1303.

[17] Melvin, T.; Botchway, S. W.; Parker, A. W.; O'Neill, P. "Induction of Strand Breaks in Single-Stranded Polyribonucleotides and DNA by Photoionization: Electron Oxidized Nucleobase Radicals as Precursors." *J. Am. Chem. Soc.* **1996**, *118*, 10031.

[18] Floyd, R. A.; Schneider, J. E. "Hydroxyl Free Radical Damage to DNA." In *Membrane Lipid Oxidation*; Vigo-Pelfrey, C., Ed.; CRC: Boca Raton, 1991; Vol. 3, Chapter 4.

[19] Joenje, H.; Lafleur, V. M.; Retél, J. "Biological Consequences of Oxidative DNA Damage." In *Membrane Lipid Oxidation*; Vigo-Pelfrey, C., Ed.; CRC: Boca Raton, 1991; Vol. 3, Chapter 5.

[20] Wiseman, H.; Halliwell, B. "Damage to DNA by Reactive Oxygen and Nitrogen Species: Role in Inflammatory Disease and Progression to Cancer." *Biochem. J.* **1996**, *313*, 17.

[21] Simonian, N. A.; Coyle, J. T. "Oxidative Stress in Neurodegenerative Diseases." *Annu. Rev. Pharmocol. Toxicol.* **1996**, *36*, 83.

[22] Ferrari, R. "The Role of Mitochondria in Ischemic Heart Disease." *J. Cardiovasc. Pharmacol.* **1996**, *28 (Suppl. 1)*, S1.

[23] Ames, B. N.; Shigenaga, M. K.; Hagen, T. M. "Oxidants, Antioxidants, and the Degenerative Diseases of Aging." *Proc. Natl. Acad. Sci.* **1993**, *90*, 7915.

[24] Cullis, P. M.; Langman, S.; Podmore, I. D.; Symons, M. C. R. "Effects of Ionizing Radiation on Deoxyribonucleic Acid. Part VI. Effects of Hydroxyl Radical Scavengers on Radiation Damage to DNA." *J. Chem. Soc., Faraday Trans.* **1990**, *86*, 3267.

[25] Symons, M. C. R. "Application of Electron Spin Resonance Spectroscopy to the Study of the Effects of Ionizing Radiation on DNA and DNA Complexes." *J. Chem. Soc., Faraday Trans.* **1987**, *83*, 1.

[26] Maillard, B.; Ingold, K. U.; Scaiano, J. C. "Rate Constants for the Reactions of Free Radicals with Oxygen in Solution." *J. Am. Chem. Soc.* **1983**, *105*, 5095.

[27] Sambandam, A.; Greenberg, M. M. "The Effects of *5R*-5,6-Dihydro-5-hydroxythymidine on Duplex DNA Stability and Structure." *Nucleic Acids Res.* **1999**, *27*, 3597.

[28] Greenberg, M. M.; Matray, T. J. "Inhibition of Klenow Fragment (exo$^-$) Catalyzed DNA Polymerization by (*5R*)-5,6-Dihydro-5-hydroxythymidine and Structural Analogue 5,6-Dihydro-5-methylthymidine." *Biochemistry* **1997**, *36*, 14071.

[29] Buxton, G. V.; Malone, T. N.; Salmon, G. A. "Pulse Radiolysis Study of the Reaction of $SO_4^{\bullet-}$ with $HO_2\bullet$." *J. Chem. Soc., Faraday Trans.* **1996**, *92*, 1287.

[30] Ducrocq, C.; Blanchard, B.; Pignatelli, B.; Ohshima, H. "Peroxynitrite: an Endogenous Oxidizing and Nitrating Agent." *Cell. Mol. Life Sci.* **1999**, *55*, 1068.

[31] a) Coddington, J. W.; Hurst, J. K.; Lymar, S. V. "Hydroxyl Radical Formation during Peroxynitrous Acid Decomposition." *J. Am. Chem. Soc.* **1999**, *121*, 2438. b) Squadrito, G. L.; Pryor, W. A. "Oxidative Chemistry of Nitric Oxide: the Role of Superoxide, Peroxynitrite, and Carbon Dioxide." *Free Radical Biol. Med.* **1998**, *25*, 392.

[32] Szabó, C.; Ohshima, H. "DNA Damage Induced by Peroxynitrite: Subsequent Biological Effects." *Nitric Oxide Biol. Chem.* **1997**, *1*, 373.

[33] Douki, T.; Cadet, J. "Peroxynitrite Mediated Oxidation of Purine Bases of Nucleosides and Isolated DNA." *Free Radical Res.* **1996**, *24*, 369.

[34] Inoue, S.; Kawanishi, S. "Oxidative DNA Damage Induced by Simultaneous Generation of Nitric Oxide and Superoxide." *FEBS Lett.* **1995**, *371*, 86.

[35] Deeble, D. J.; von Sonntag, C. "Radiolysis of Poly (U) in Oxygenated Solution." *Int. J. Radiat. Biol.* **1986**, *49*, 927.

[36] Karam, L. R.; Dizdaroglu, M.; Simic, M. G. "Intramolecular H Atom Abstraction from the Sugar Moiety by Thymine Radicals in Oligo- and Polydeoxynucleotides." *Radiat. Res.* **1988**, *116*, 210.

[37] Jones, G. D. D.; O'Neill, P. "The Kinetics of Radiation-Induced Strand Breakage in Polynucleotides in the Presence of Oxygen: a Time-Resolved Light-Scattering Study." *Int. J. Radiat. Biol.* **1990**, *57*, 1123.

[38] Barvian, M. R.; Greenberg, M. M. "Independent Generation of 5,6-Dihydrothymid-5-yl in Single-Stranded Polythymidylate. O_2 is Necessary for Strand Scission." *J. Am. Chem. Soc.* **1995**, *117*, 8291.

[39] Greenberg, M. M.; Barvian, M. R.; Cook, G. P.; Goodman, B. K.; Matray, T. J.; Tronche, C.; Venkatesan, H. "DNA Damage Induced via 5,6-Dihydrothymid-5-yl in Single-Stranded Oligonucleotides." *J. Am. Chem. Soc.* **1997**, *119*, 1828.

[40] Daniels, J. S.; Chatterji, T.; MacGillivray, L. R.; Gates, K. S. "Phototochemical DNA Cleavage by the Antitumor Agent 3-Amino-1,2,4-benzotriazine 1,4-Dioxide (Tirapazamine, WIN 59075, SR4233)." *J. Org. Chem.* **1998**, *63*, 10027.

[41] Brown, J. M.; Wang, L.-H. "Tirapazamine: Laboratory Data Relevant to Clinical Activity." *Anti-Cancer Drug Des.* **1998**, *13*, 529.

[42] Jones, G. D. D.; Weinfeld, M. "Dual Action of Tirapazamine in the Induction of DNA Strand Breaks." *Cancer Res.* **1996**, *56*, 1584.

[43] Daniels, J. S.; Gates, K. S. "DNA Cleavage by the Antitumor Agent 3-Amino-1,2,4-benzotriazine 1,4-Dioxide (SR4233): Evidence for Involvement of Hydroxyl Radical." *J. Am. Chem. Soc.* **1996**, *118*, 3380.

[44] Hwang, J.-T.; Greenberg, M. M.; Fuchs, T.; Gates, K. S. "Reaction of the Hypoxia-Selective Antitumor Agent Tirapazamine with a C1'-Radical in Single-Stranded and Double-Stranded DNA: The Drug and its Metabolites Can Serve as Surrogates for Molecular Oxygen in Radical-Mediated DNA-Damage Reactions." *Biochemistry* **1999**, *38*, 14248.

[45] Daniels, J. S.; Gates, K. S.; Tronche, C.; Greenberg, M. M. "Direct Evidence for Bimodal DNA Damage Induced by Tirapazamine." *Chem. Res. Toxicol.* **1998**, *11*, 1254.

[46] Buchko, G. W.; Weinfeld, M. "Influence of Nitrogen, Oxygen, and Nitroimidazole Radiosensitizers on DNA Damage Induced by Ionizing Radiation." *Biochemistry* **1993**, *32*, 2186.

[47] Dedon, P. C.; Jiang, Z.-W.; Goldberg, I. H. "Neocarzinostatin-Mediated DNA Damage in a Model AGT•ACT Site: Mechanistic Studies of Thiol-Sensitive Partitioning of C4' DNA Damage Products." *Biochemistry* **1992**, *31*, 1917.

[48] Kappen, L. S.; Lee, T. R.; Yang, C.-C.; Goldberg, I. H. "Oxygen Transfer from the Nitro Group of a Nitroaromatic Radiosensitizer to a DNA Sugar Damage Product." *Biochemistry* **1989**, *28*, 4540.

[49] Greenberg, M. M. "Investigating Nucleic Acid Damage Processes via Independent Generation of Reactive Intermediates." *Chem. Res. Toxicol.* **1998**, *11*, 1235.

[50] Candeias, L. P.; O'Neill, P.; Jones, G. D. D.; Steenken, S. "Ionization of Polynucleotides and DNA in Aqueous Solution by 193 nm Pulsed Laser Light: Identification of Base-Derived Radicals." *Int. J. Radiat. Biol.* **1992**, *61*, 15.

[51] Deeble, D. J.; Schuchmann, M. N.; Steenken, S.; von Sonntag, C. "Direct Evidence for the Formation of Thymine Radical Cations from the Reaction of Sulfate ($SO_4^{\bullet-}$) with Thymine Derivatives: A Pulse Radiolysis Study with Optical and Conductance Detection." *J. Phys. Chem.* **1990**, *94*, 8186.

[52] Steenken, S.; Goldbergerova, L. "Photoionization of Organic Phosphates by 193 nm Laser Light in Aqueous Solution: Rapid Intramolecular H-Transfer to the Primarily Formed Phosphate Radical. A Model for Ionization-Induced Chain-Breakage in DNA?" *J. Am. Chem. Soc.* **1998**, *120*, 3928.

[53] Tronche, C.; Goodman, B. K.; Greenberg, M. M. "DNA Damage Induced via Independent Generation of the Radical Resulting from Formal Hydrogen Atom Abstraction from the C1'-Position of a Nucleotide." *Chem. Biol.* **1998**, *5*, 263.

[54] Stemp, E. D. A.; Arkin, M. R.; Barton, J. K. "Oxidation of Guanine in DNA by $Ru(phen)_2(dppz)^{3+}$ Using the Flash-Quench Technique." *J. Am. Chem. Soc.* **1997**, *119*, 2921.

[55] Dandliker, P. J.; Holmlin, R. E.; Barton, J. K. "Oxidative Thymine Dimer Repair in the DNA Helix." *Science* **1997**, *275*, 1465.

[56] Arkin, M. R.; Stemp, E. D. A.; Holmlin, R. E.; Barton, J. K.; Hörmann, A.; Olson, E. J. C.; Barbara, P. F. "Rates of DNA-Mediated Electron Transfer Between Metallointercalators." *Science* **1997**, *273*, 475.

[57] Wood, M.L.; Esteve, A.; Morningstar, M. L.; Kuziemko, G. M.; Essigmann, J. M. "Genetic Effects of Oxidative DNA Damage: Comparative Mutagenesis of 7,8-Dihydro-8-oxoguanine and of 7,8-Dihydro-8-oxoadenine in *Escherichia coli*." *Nucleic Acids Res.* **1992**, *20*, 6023.

[58] Shibutani, S.; Bodepudi, V.; Johnson, F.; Grollman, A. P. "Translesional Synthesis on DNA Templates Containing 8-Oxo-7,8-dihydrodeoxyadenosine." *Biochemistry* **1993**, *32*, 4615.

[59] Tchou, J.; Bodepudi, V.; Shibutani, S.; Antoshechkin, I.; Miller, J.; Grollman, A. P.; Johnson, F. "Substrate Specificity of Fpg Protein." *J. Biol. Chem.* **1994**, *269*, 15318.

[60] Tchou, J.; Grollman, A. P. "The Catalytic Mechanism of Fpg Protein." *J. Biol. Chem.* **1995**, *270*, 11671.

[61] Barvian, M. R.; Greenberg, M. M. "Independent Generation of 5,6-Dihydrothymid-5-yl and Investigation of its Ability to Effect Nucleic Acid Strand Scission via Hydrogen Atom Abstraction." *J. Org. Chem.* **1995**, *60*, 1916.

[62] Nishimoto, S.; Ide, H.; Nakamichi, K.; Otsuki, N.; Kagiya, T. "Radiation-Induced Reductive Conversion of 5-Bromo-6-hydroxythymine to Thymine Promoted by Transition Metal Salts in Deaerated Aqueous Solution." *Chem. Lett.* **1983**, 1441.

[63] Bhattacharyya, S. N.; Mandal, P. C.; Chakrabarti, S. "Effect of Fe(III) on the γ-Radiolysis of Thymine." *Bull. Chem. Soc. Jpn.* **1990**, *63*, 3001.

[64] Ide, H.; Petrullo, L. A.; Hatahet, Z.; Wallace, S. S. "Processing of DNA Base Damage by DNA Polymerases." *J. Biol. Chem.* **1991**, *266*, 1469.

[65] Dizdaroglu, M.; Laval, J.; Boiteux, S. "Substrate Specificity of the *Escherichia coli* Endonuclease III: Excision of Thymine- and Cytosine-Derived Lesions in DNA Produced by Radiation-Generated Free Radicals." *Biochemistry* **1993**, *32*, 12105.

[66] Schulte-Frohlinde, D.; Behrens, G.; Önal, A. "Lifetime of Peroxyl Radicals of Poly (U), Poly (A) and Single- and Double-Stranded DNA and the Rate of their Reaction with Thiols." *Int. J. Radiat. Biol.* **1986**, *50*, 103.

[67] Hildenbrand, K.; Schulte-Frohlinde, D. "Time-Resolved EPR Studies on the Reaction Rates of Peroxyl Radicals of Poly (Acrylic Acid) and of Calf Thymus DNA with Glutathione. Re-Examination of a Rate Constant for DNA." *Int. J. Radiat. Biol.* **1997**, *71*, 377.

[68] Miaskiewicz, K.; Miller, J.; Ornstein, R.; Osman, R. "Molecular Dynamics Simulations of the Effects of Ring-Saturated Thymine Lesions on DNA Structure." *Biopolymers* **1995**, *35*, 113.

[69] Miaskiewicz, K.; Miller, J.; Osman, R. "Energetic Basis for Structural Preferences in 5/6-Hydroxy-5,6-Dihydropyrimidines: Products of Ionizing and Ultraviolet Radiation Action on DNA Bases." *Biochim. Biophys. Acta* **1994**, 1218, 283.

[70] von Sonntag, C.; Schuchmann, H.-P. "The Elucidation of Peroxyl Radical Reactions in Aqueous Solution with the Help of Radiation-Chemical Methods." *Angew. Chem. Int. Ed. Engl.* **1991**, *30*, 1229.

[71] Al-Sheikhly, M. I.; Hissung, A.; Schuchmann, H.-P.; Schuchmann, M. N.; von Sonntag, C.; Garner, A.; Scholes, G. "Radiolysis of Dihydrouracil and Dihydrothymine in Aqueous Solutions Containing Oxygen; First- and Second-Order Reactions of the Organic Peroxyl Radicals; the Role of Isopyrimidines as Intermediates." *J. Chem. Soc. Perkin Trans. II* **1984**, 601.

[72] Miaskiewicz, K.; Osman, R. "Theoretical Study on the Deoxyribose Radicals Formed by Hydrogen Abstraction." *J. Am. Chem. Soc.* **1994**, *116*, 232.

[73] Cook, G. P.; Greenberg, M. M. "A Novel Mechanism for the Formation of Direct Strand Breaks upon Anaerobic Photolysis of Duplex DNA containing 5-Bromodeoxyuridine." *J. Am. Chem. Soc.* **1996**, *118*, 10025.

[74] Cook, G. P.; Chen, T.; Koppisch, A. T.; Greenberg, M. M. "The Effects of Secondary Structure and O_2 on the Formation of Direct Strand Breaks upon UV Irradiation of 5-Bromodeoxyuridine-Containing Oligonucleotides." *Chem. Biol.* **1999**, *6*, 451.

[75] Sugiyama, H.; Fujimoto, K.; Saito, I. "Evidence for Intra-Strand C2' Hydrogen Abstraction in Photo-Irradiation of 5-Halouracil-Containing Oligodeoxyribonucleotides by Using Stereospecifically C2'-Deuterated Deoxyadenosine." *Tetrahedron Lett.* **1996**, *37*, 1805.

[76] Colson, A.-O.; Sevilla, M. D. "Structure and Relative Stability of Deoxyribose Radicals in a Model DNA Backbone: Ab Initio Molecular Orbital Calculations." *J. Phys. Chem.* **1995**, *99*, 3867.

[77] Balasubramanian, B.; Pogozelski, W. K.; Tullius, T. D. "DNA Strand Breaking by the Hydroxyl Radical is Governed by the Accessible Surface Areas of the Hydrogen Atoms of the DNA Backbone." *Proc. Natl. Acad. Sci.* **1998**, *95*, 9738.

[78] Lemaire, D. G. E.; Bothe, E.; Schulte-Frohlinde, D. "Yields of Radiation-Induced Main Chain Scission of Poly U in Aqueous Solution: Strand Break Formation via Base Radicals." *Int. J. Radiat. Biol.* **1984**, *45*, 351.

[79] Deeble, D. J.; von Sonntag, C. "γ-Radiolysis of Poly (U) in Aqueous Solution. The Role of Primary Sugar and Base Radicals in the Release of Undamaged Uracil." *Int. J. Radiat. Biol.* **1984**, *46*, 247.

[80] Catterall, H.; Davies, M. J.; Gilbert, B. C. "An EPR Study of the Transfer of Radical-Induced Damage from the Base to Sugar in Nucleic Acid Components: Relevance to the Occurrence of Stand-Breakage." *J. Chem. Soc. Perkin Trans. 2* **1992**, 1379.

[81] Hildenbrand, K.; Schulte-Frohlinde, D. "E.S.R. Studies on the Mechanism of Hydroxyl Radical-Induced Strand Breakage on Polyuridylic Acid." *Int. J. Radiat. Biol.* **1989**, *55*, 725.

[82] Davies, M. J.; Gilbert, B. C.; Hazlewood, C.; Polack, N. P. "EPR Spin-Trapping Studies of Radical Damage to DNA." *J. Chem. Perkin Trans. 2* **1995**, 13.

[83] Barvian, M. R.; Barkley, R. M.; Greenberg, M. M. "Reactivity of 5,6-Dihydrothymid-6-yl Generated via Photoinduced Single Electron Transfer and the Role of Cyclohexa-1,4-diene in the Photodeoxygenation Process." *J. Am. Chem. Soc.* **1995**, *117*, 4894.

[84] Barvian, M. R.; Greenberg, M. M. "Independent Generation of the Major Adduct of Hydroxyl Radical and Thymidine. Examination of Intramolecular Hydrogen Atom Transfer in Competition with Thiol Trapping." *Tetrahedron Lett.* **1992**, *33*, 6057.

[85] Hwang, J.-T.; Greenberg, M. M. "Kinetics and Stereoselectivity of Thiol Trapping of Deoxyuridin-1'-yl in Biopolymers and their Relationship to the Formation of Premutagenic α-Deoxynucleotides." *J. Am. Chem. Soc.* **1999**, *121*, 4311.

[86] Goldberg, I. H. "Mechanism of Neocarzinostatin Action: Role of DNA Microstructure in Determination of Chemistry of Bistranded Oxidative Damage." *Acc. Chem. Res.* **1991**, *24*, 191.

[87] Kappen, L. S.; Goldberg, I. H. "Identification of 2-Deoxyribonolactone at the Site of Neocarzinostatin-Induced Cytosine Release in the Sequence d(AGC)." *Biochemistry* **1989**, *28*, 1027.

[88] Goyne, T. E.; Sigman, D. S. "Nuclease Acitivity of 1,10-Phenanthroline-copper Ion. Chemistry of Deoxyribose Oxidation." *J. Am. Chem. Soc.* **1987**, *109*, 2846.

[89] Reich, K. A.; Marshall, L. E.; Graham, D. R.; Sigman, D. S. "Cleavage of DNA by the 1,10-Phenanthroline-copper Ion Complex. Superoxide Mediates the Reaction Dependent on NADH and Hydrogen Peroxide." *J. Am. Chem. Soc.* **1981**, *103*, 3582.

[90] Graham, D. R.; Marshall, L. E.; Reich, K. A.; Sigman, D. S. "Cleavage of DNA by Coordination Complexes. Superoxide Formation in the Oxidation of 1,10-Phenanthroline-cuprous Complexes by Oxygen-Relevance to DNA-Cleavage Reaction." *J. Am. Chem. Soc.* **1980**, *102*, 5419.

[91] Dizdaroglu, M.; Aruoma, O. I.; Halliwell, B. "Modification of Bases in DNA by Copper Ion-1,10-phenanthroline Complexes." *Biochemistry* **1990**, *29*, 8447.

[92] Gilbert, B. C.; Silvester, S.; Walton, P. H.; Whitwood, A. C. "DNA Damage via Intercalation of Copper Complexes and Activation by Ascorbate and Peroxides: Direct EPR Evidence for Hydroxyl Radical Formation and Reaction." *J. Chem. Perkin Trans. 2* **1999**, *1891*.

[93] Zelenko, O.; Gallagher, J.; Sigman, D. S. "Scission of DNA with Bis(1,10-phenanthroline)copper without Intramolecular Hydrogen Migration." *Angew. Chem. Int. Ed. Engl.* **1998**, *36*, 2776.

[94] Meijler, M. M.; Zelenko, O.; Sigman, D. S. "Chemical mechanism of DNA Scission by (1,10-Phenanthroline)copper. Carbonyl Oxygen of 5-Methylenefuranone is Derived from Water." *J. Am. Chem. Soc.* **1997**, *119*, 1135.

[95] Chen, T.; Greenberg, M. M. "Model Studies Indicate that Copper Phenanthroline Induces Direct Strand Breaks via β-Elimination of the 2-Deoxyribonolactone Intermediate Observed in Enediyne Mediated DNA Damage." *J. Am. Chem. Soc.* **1998**, *120*, 3815.

[96] Pratviel, G.; Pitie, M.; Bernadou, J.; Meunier, B. "Mechanism of DNA Cleavage by Cationic Manganese Porphyrins: Hydroxyations at the 1'-Carbon and 5'-Carbon Atoms of Deoxyribose as Initial Damages." *Nucleic Acids Res.* **1991**, *19*, 6283.

[97] Chatgilialoglu, C.; Gimisis, T. "Fate of the C1'-Peroxyl Radical in the 2'-Deoxyuridine System." *Chem. Commun.* **1998**, *1249*.

[98] Goodman, B. K.; Greenberg, M. M. "Independent Generation and Reactivity of 2'-Deoxyurid-1'-yl." *J. Org. Chem.* **1996**, *61*, 2.

[99] Tallman, K. A.; Tronche, C.; Yoo, D. J.; Greenberg, M. M. "Release of Superoxide from Nucleoside Peroxyl Radicals, a Double-Edged Sword?" *J. Am. Chem. Soc.* **1998**, *120*, 4903.

[100] Emanuel, C. J.; Newcomb, M.; Ferreri, C.; Chatgilialoglu, C. "Kinetics of 2'-Deoxyuridin-1'-yl Radical Reactions." *J. Am. Chem. Soc.* **1999**, *121*, 2927.

[101] Hwang, J.-T.; Tallman, K. A.; Greenberg, M. M. "The Reactivity of the 2-Deoxyribonolactone Lesion in Single-Stranded DNA and its Implication in Reaction Mechanisms of DNA Damage and Repair." *Nucleic Acids Res.* **1999**, *27*, 3805.

[102] Kotera, M.; Bourdat, A.-G.; Defrancq, E.; Jourdan, M.; Garcia, J.; Coulombeau, C.; Lhomme, J. "Efficient Chemical Synthesis of Oligonucleotides Containing the 2-Deoxyribonolactone Site." *Nucleosides Nucleotides* **1999**, *18*, 1323.

[103] Kotera, M.; Bourdat, A.-G.; Defrancq, E.; Lhomme, J. "A Highly Efficient Synthesis of Oligodeoxyribonucleotides Containing the 2-Deoxyribonolactone Lesion." *J. Am. Chem. Soc.* **1998**, *120*, 11810.

[104] Lawrence, T. S.; Davis, M. A.; Normolle, D. P. "Effect of Bromodeoxyuridine on Radiation-Induced DNA and Repair Based on DNA Fragment Size using Pulsed-Field Gel Electrophoresis." *Radiat. Res.* **1995**, *144*, 282.

[105] Sugiyama, H.; Tsutsumi, Y.; Saito, I. "Highly Sequence-Selective Photoreaction of 5-Bromouracil-Containing Deoxyhexanucleotides." *J. Am. Chem. Soc.* **1990**, *112*, 6720.

[106] Fujimoto, K.; Sugiyama, H.; Saito, I. "Sequence Dependent Photoreduction of 5-Bromouracil-Containing Oligodeoxyribonucleotides via Electron Transfer." *Tetrahedron Lett.* **1998**, *39*, 2137.

[107] Sugiyama, H.; Tsutsumi, Y.; Fujimoto, K.; Saito, I. "Photoinduced Deoxyribose C2' Oxidation in DNA. Alkali-Dependent Cleavage of Erythrose-Containing Sites via a Retroaldol Reaction." *J. Am. Chem. Soc.* **1993**, *115*, 4443.

[108] Sugiyama, H.; Fujimoto, K.; Saito, I. "Stereospecific 1,2-Hydride Shift in Ribonolactone Formation in the Photoreaction of 2'-Iododeoxyuridine." *J. Am. Chem. Soc.* **1995**, *117*, 2945.

[109] Sheu, C.; Foote, C. S. "Photosensitized Oxygenation of a 7,8-Dihydro-8-oxoguanosine Derivative. Formation of Dioxetane and Hydroperoxide Intermediates." *J. Am. Chem. Soc.* **1995**, *117*, 474.

[110] Devasagayam, T. P. A.; Steenken, S.; Obendorf, M. S. W.; Schulz, W. A.; Sies, H. "Formation of 8-Hydroxy(deoxy)guanosine and Generation of Strand Breaks at Guanine Residues in DNA by Singlet Oxygen." *Biochemistry* **1991**, *30*, 6283.

[111] Simon, M. I.; van Vuankis, H. "The Photodynamic Reaction of Methylene Blue with Deoxyribonucleic Acid." *J. Mol. Biol.* **1962**, *4*, 488.

[112] Hwang, J.-T.; Tronche, C.; Greenberg, M. M. Unpublished results.

[113] Newcomb, M. "Competition Methods and Scales for Alkyl Radical Reaction Kinetics." *Tetrahedron* **1993**, *49*, 1151.

[114] Crich, D.; Jiao, X.-Y.; Yao, Q.; Harwood, J. S. "Radical Clock Reactions under Pseudo-First-Order Conditions Using Catalytic Quantities of Diphenyl Diselenide. A ^{77}Se- and ^{119}Sn-NMR Study of the Reaction of Tributylstannane and Diphenyl Diselenide." *J. Org. Chem.* **1996**, *61*, 2368.

[115] Motherwell, W. B.; Crich, D. *Free Radical Chain Reactions in Organic Synthesis*; Academic: London, 1992.

[116] Johnston, L. J.; Lusztyk, J.; Tallman, K. A.; Greenberg, M. M. Unpublished results.

[117] Lengsfield, III, B. H.; Siegbahn, P. E. M.; Liu, B. "*Ab Initio* Assignment of the Ethyl, Isopropyl, and t-Butyl Radicals." *J. Chem. Phys.* **1984**, *81*, 710.

[118] Wendt, H. R.; Hunziker, H. E. "The UV Spectra of Primary, Secondary, and Tertiary Alkyl Radicals." *J. Chem. Phys.* **1984**, *81*, 717.

[119] Deeble, D. J.; Das, S.; von Sonntag, C. "Uracil Derivatives: Sites and Kinetics of Protonation of the Radical Anions and the UV Spectra of the C(5) and C(6) H-Atom Adducts." *J. Phys. Chem.* **1985**, *89*, 5784.

[120] Johnston, L. J.; Lusztyk, J. Unpublished results.

[121] Scaiano, J. C. "Solvent Effects in the Photochemistry of Xanthone." *J. Am. Chem. Soc.* **1980**, *102*, 7747.

[122] Scaiano, J. C. "Detection of Trialkylstannyl Radicals Using Laser Flash Photolysis." *J. Am. Chem. Soc.* **1980**, *102*, 5399.

[123] Wagner, P. J.; Kelso, P. A.; Zepp, R. G. "Type II Photoprocesses of Phenyl Ketones. Evidence for a Biradical Intermediate." *J. Am. Chem. Soc.* **1972**, *94*, 7480.

[124] Wagner, P. J. "Photoreduction of Acetone by Tributylstannane." *J. Am. Chem. Soc.* **1967**, *89*, 2503.

[125] Zepp, R. G.; Wagner, P. J. "Slow Quenching of Triplet Ketones by Alkyl Thiols." *J. Chem. Soc., Chem. Commun.* **1972**, 167.

[126] *Organic Photochemistry and Photobiology;* Horspool, W. M., Ed.; CRC: Boca Raton, 1995, Chapter 34.

[127] Russell, G. A.; Bemis, A. G. "The Oxidation of Carbanions. I. Oxidation of Triaryl Carbanions and Other Tertiary Carbanions." *J. Am. Chem. Soc.* **1966**, *88*, 5491.

[128] Anderson, A. S. Thesis, Spring 2000, Colorado State University.

[129] *Handbook of Chemistry and Physics*; Weast, R. C., Ed.; Chemical Rubber: Cleveland, 1967.

[130] Light, J.; Breslow, R. "A Water-Soluble Tin Hydride: Tris[3-(2-methoxyethoxy)-propyl]stannane." In *Organic Syntheses*; Coffen, D. L., Ed.; Organic Syntheses: USA, 1993; Vol. 72, pp 199.

[131] Light, J.; Breslow, R. "A Water-Soluble Tin Hydride." *Tetrahedron Lett.* **1990**, *31*, 2957.

[132] Lenz, R.; Giese, B. "Studies on the Mechanism of Ribonucleotide Redutases." *J. Am. Chem. Soc.* **1997**, *119*, 2784.

[133] Wong, C. L.; Klingler, R. J.; Kochi, J. K. "Metal Hydrides as Electron Donors. The Mechanism of Oxidative Cleavage with Tris (phenanthroline) Complexes of Iron(III)." *Inorg. Chem.* **1980**, *19*, 423.

[134] Pandey, G.; Sesha Poleswara Rao, K. S.; Soma Sekhar, B. B. V. "Photosensitized One-Electron Reductive Cleavage of a Carbon-Selenium Bond: a Novel Chemoselective Deselenenylation and Phenylselenenyl Group Transfer Radical Chain Reaction." *J. Chem. Soc., Chem. Commun.* **1993**, 1636.

[135] Yoshida, J.; Izawa, M. "Intramolecular Assistance of Electron Transfer. Oxidative Cleavage of the Carbon-Tin Bond of Tetraalkylstannanes." *J. Am. Chem. Soc.* **1997**, *119*, 9361.

[136] Porter, N. A. Personal communication.

[137] Misra, H. P.; Fridovich, I. "Role of Superoxide Anion in the Autoxidation of Epinephrine and a Simple Assay for Superoxide Dismutase." *J. Biol. Chem.* **1972**, *247*, 3170.

[138] Armitage, B.; Yu, C.; Devadoss, C.; Schuster, G. B. "Cationic Athraquinone Derivatives as Catalytic DNA Photonucleases: Mechanisms for DNA Damage and Quinone Recycling." *J. Am. Chem. Soc.* **1994**, *116*, 9847.

[139] McCord, J. M.; Fridovich, I. "Superoxide Dismutase. Enzymatic Function for Erythrocuprein (Hemocuprein)." *J. Biol. Chem.* **1969**, *244*, 6049.

[140] Chatgilialoglu, C.; Timokhin, V. I.; Zaborovskiy, A. B.; Lutsyk, D. S.; Prystansky, R. E. "Rate Constant for the Reaction of Cumylperoxyl Radicals with Bu_3SnH and $(TMS)_3SiH$." *Chem. Commun.* **1999**, 405.

[141] Barvian, M. R.; Greenberg, M. M. "Diastereoselective Synthesis of Hydroxylated Dihydrothymidines Resulting from Oxidative Stress." *J. Org. Chem.* **1993**, *58*, 6151.

[142] Sharpless, K. B.; Amberg, W.; Bennani, Y. L.; Crispino, G. A.; Hartung, J.; Jeong, K.-S.; Kwong, H.-L.; Morikawa, K.; Wang, Z.-M.; Xu, D.; Zhang, X.-L. "The Osmium-Catalyzed Asymmetric Dihydroxylation: A New Ligand Class and a Process Improvement." *J. Org. Chem.* **1992**, *57*, 2768.

[143] Wasserman, H. H.; Lipshutz, B. H. "Reactions of Lithium Enolates with Molecular Oxygen. α-Hydroxylation of Amides and Other Carboxylate Derivates." *Tetrahedron Lett.* **1975**, 1731.

[144] Haraguchi, K.; Itoh, Y.; Tanaka, H.; Yamaguchi, K.; Miyasaka, T. "Anomeric Manipulation of Nucleosides: Stereospecific Entry to 1'-C-Branched Uracil Nucleosides." *Tetrahedron Lett.* **1993**, 6913.

[145] Itoh, Y.; Haraguchi, K.; Tanaka, H.; Gen, E.; Miyasaka, T. "Divergent and Stereocontrolled Approach to the Synthesis of Uracil Nucleosides Branched at the Anomeric Position." *J. Org. Chem.* **1995**, *60*, 656.

[146] Haraguchi, K.; Tanaka, H.; Maeda, H.; Itoh, Y.; Saito, S.; Miyasaka, T. "Selenoxide Elimination for the Synthesis of Unsaturated Sugar Uracil Nucleosides." *J. Org. Chem.* **1991**, *56*, 5401.

[147] Robins, M. J.; Sarker, S.; Samano, V.; Wnuk, S. F. "Nucleic Acid Related Compounds. 94. Remarkably High Stereoselective Reductions of 2'- and 3'-Keto Nucleosides to Give Arabino, Ribo, and Xylofuranosyl Nucleosides with Hydrogen Isotopes at C2' and C3'." *Tetrahedron* **1997**, *53*, 447.

[148] Hiller, K.-O.; Asmus, K.-D. "Formation and Reduction Reactions of α-Amino Radicals Derived from Methionine and its Derivatives in Aqueous Solution." *J. Phys. Chem.* **1983**, *87*, 3682.

[149] Rabani, J.; Mulac, W. A.; Matheson, M. S. "The Pulse Radiolysis of Aqueous Tetranitromethane." *J. Phys. Chem.* **1965**, *69*, 53.

[150] Eibenberger, J.; Schulte-Frohlinde, D.; Steenken, S. "One-Electron Oxidation of α-Monoalkoxyalkyl Radicals by Tetranitromethane via an Intermediate Adduct. Influence of Radical Structure on Rate of Decomposition of the Adduct." *J. Phys. Chem.* **1980**, *84*, 704.

[151] Tronche, C.; Martinez, F. N.; Horner, J. H.; Newcomb, M.; Senn, M.; Giese, B. "Polar Substituent and Solvent Effects on the Kinetics of Radical Reactions with Thiols." *Tetrahedron Lett.* **1996**, *37*, 5845.

[152] Howard, J. A. In *Free Radicals*; Kochi, J. K., Ed.; John Wiley & Sons: New York, 1973; Vol. 2, Chapter 12.

[153] Lucarini, M.; Pedulli, G. F.; Valgimigli, L. "Do Peroxyl Radicals Obey the Principle that Kinetic Solvent Effects on H-Atom Abstraction are Independent of the Nature of the Abstracting Radical?" *J. Org. Chem.* **1998**, *63*, 4497.

[154] Jagannadham, V.; Steenken, S. "Reactivity of α-Heteroatom-Substituted Alkyl Radicals with Nitrobenzenes in Aqueous Solution: An Entropy-Controlled Electron-Transfer/Addition Mechanism." *J. Am. Chem. Soc.* **1988**, *110*, 2188.

[155] Steenken, S.; Jagannadham, V. "Reaction of 6-yl Radicals of Uracil, Thymine, and Cytosine and Their Nucleosides and Nucleotides with Nitrobenzenes via Addition to Give Nitroxide Radicals. OH^--Catalyzed Nitroxide Heterolysis." *J. Am. Chem. Soc.* **1985**, *107*, 6818.

[156] Beckwith, A. L. J.; Bowry, V. W.; Ingold, K. U. "Kinetics of Nitroxide Radical Trapping. 1. Solvent Effects." *J. Am. Chem. Soc.* **1992**, *114*, 4983.

[157] Bowry, V. W.; Ingold, K. U. "Kinetics of Nitroxide Trapping. 2. Structural Effects." *J. Am. Chem. Soc.* **1992**, *114*, 4992.

[158] Taniguchi, H.; Madden, K. P. "An *in Situ* Radiolysis Time-Resolved ESR Study of the Kinetics of Spin Trapping by 5,5-Dimethyl-1-pyrroline-*N*-oxide." *J. Am. Chem. Soc.* **1999**, *121*, 11875.

[159] Janzen, E. G.; Zhang, Y.-K. "Identification of Reactive Free Radicals with a New ^{31}P-Labeled DMPO Spin Trap." *J. Org. Chem.* **1995**, *60*, 5441.

[160] Barker, P.; Beckwith, A. L. J.; Cherry, W. R.; Huie, R. "Characterization of Spin Adducts Obtained with Hydrophobic Nitrone Spin Traps." *J. Chem. Soc., Perkin Trans. 2* **1985**, 1147.

[161] Ingold, K. U. In *Free Radicals*; Kochi, J. K., Ed.; John Wiley & Sons: New York, 1973; Vol. 1, Chapter 2.

[162] Baignée, A.; Howard, J. A.; Scaiano, J. C.; Stewart, L. C. "Absolute Rate Constants for Reactions of Cumyloxy in Solution." *J. Am. Chem. Soc.* **1983**, *105*, 6120.

APPENDIX A

Response Factor Plots

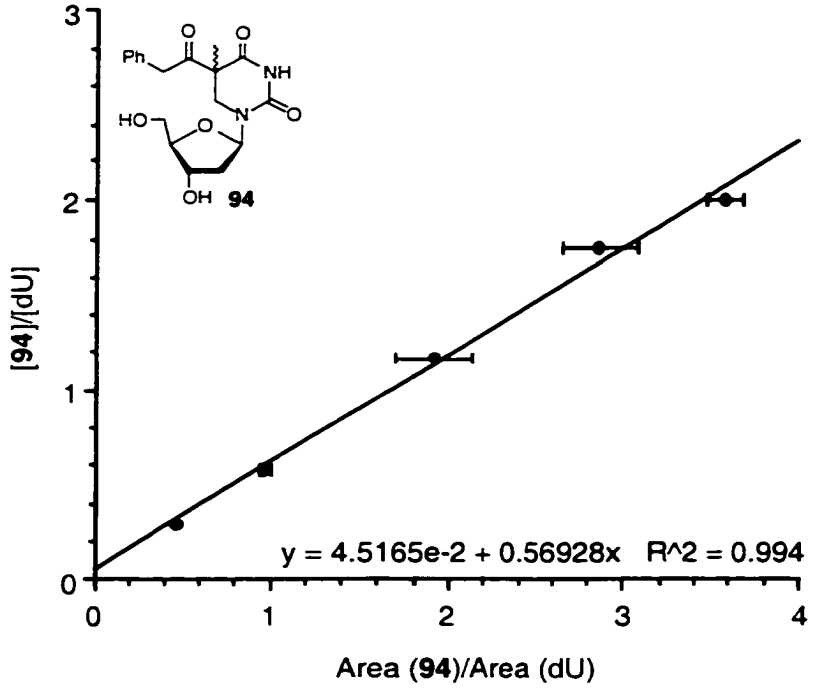

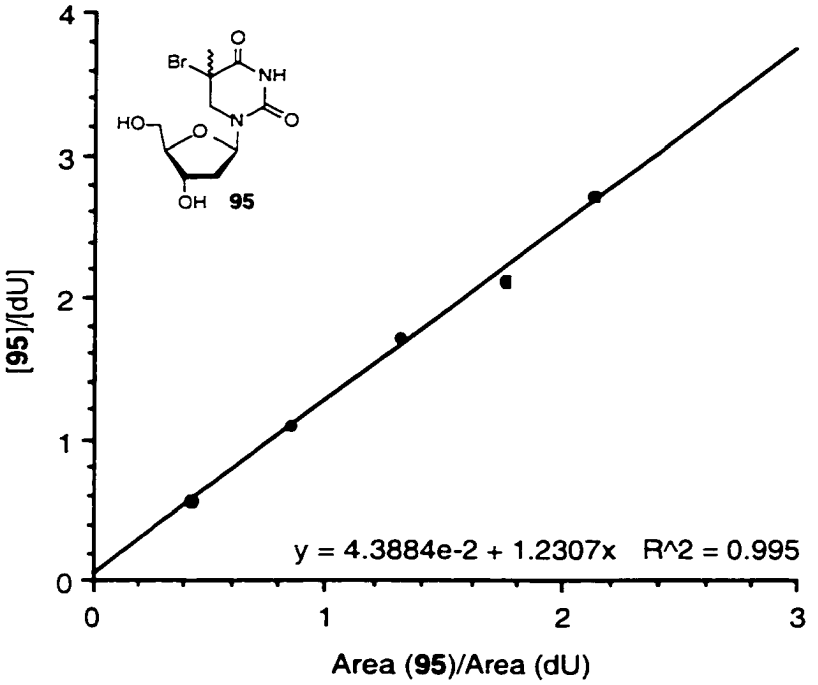

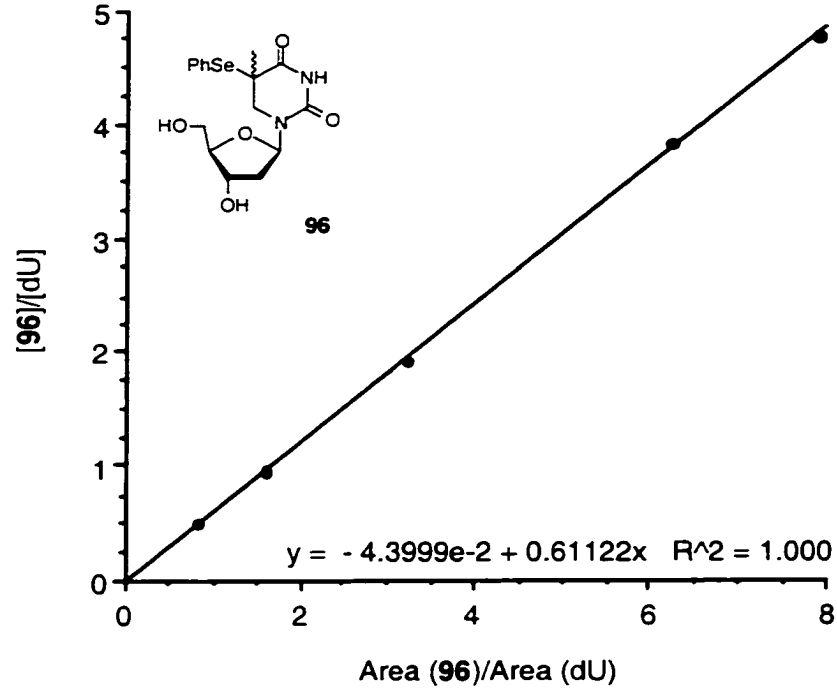

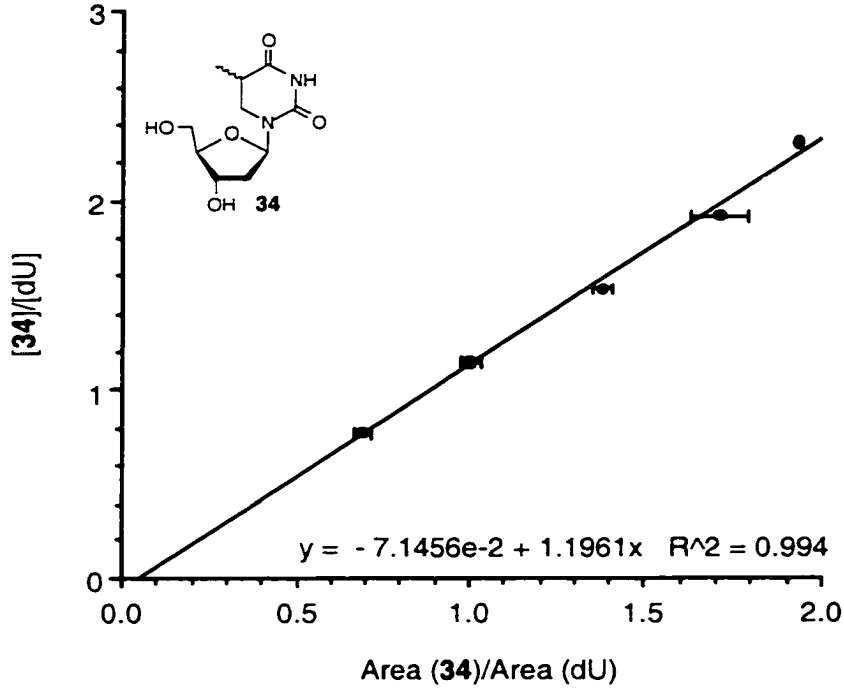

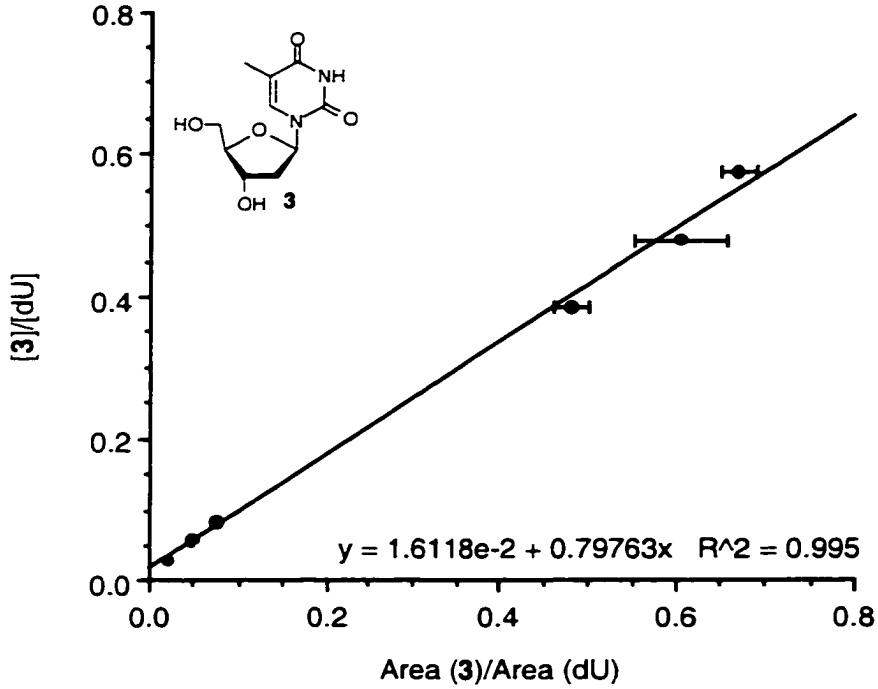

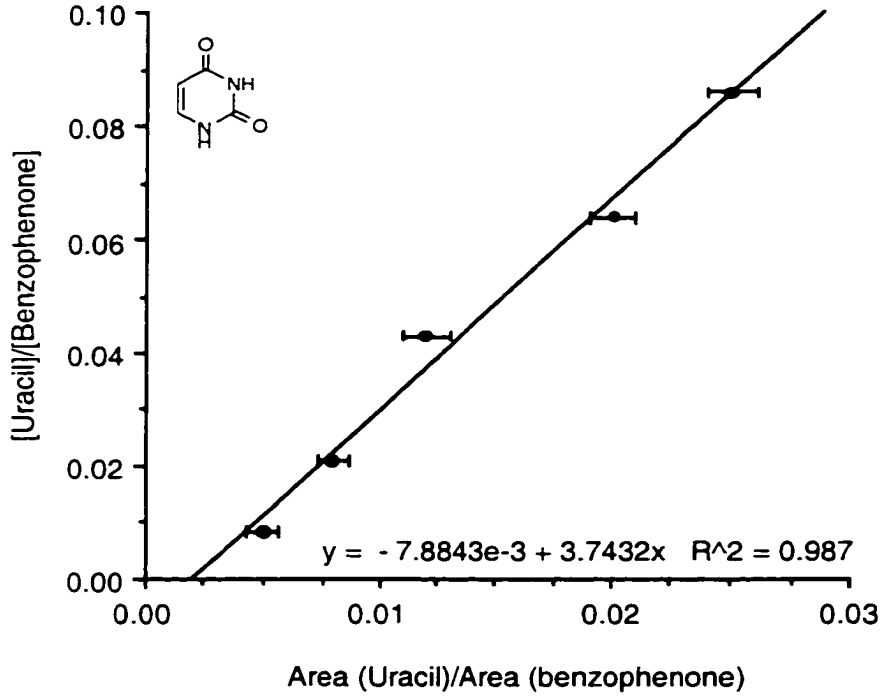

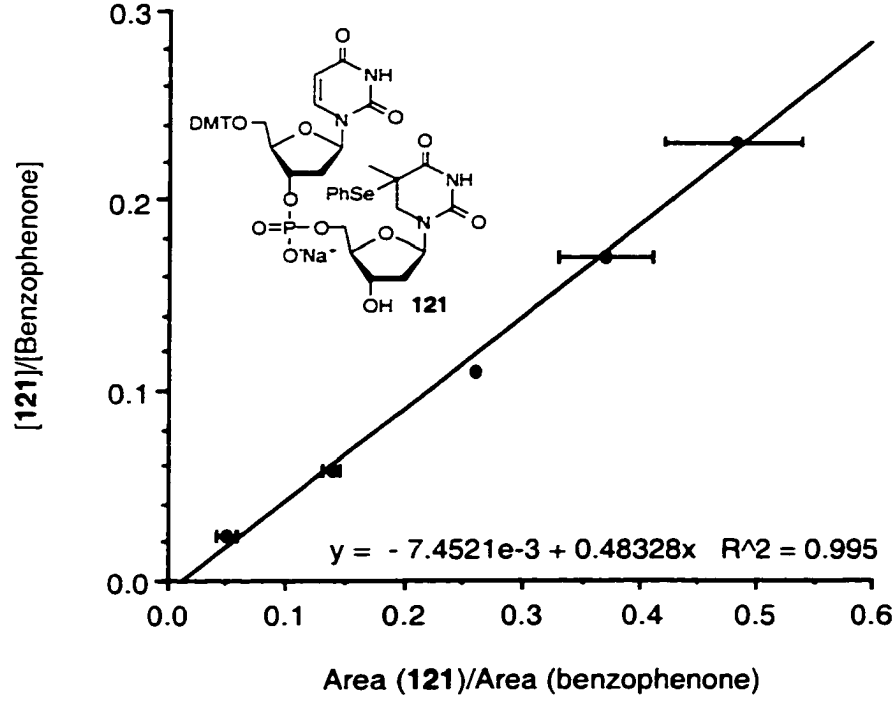

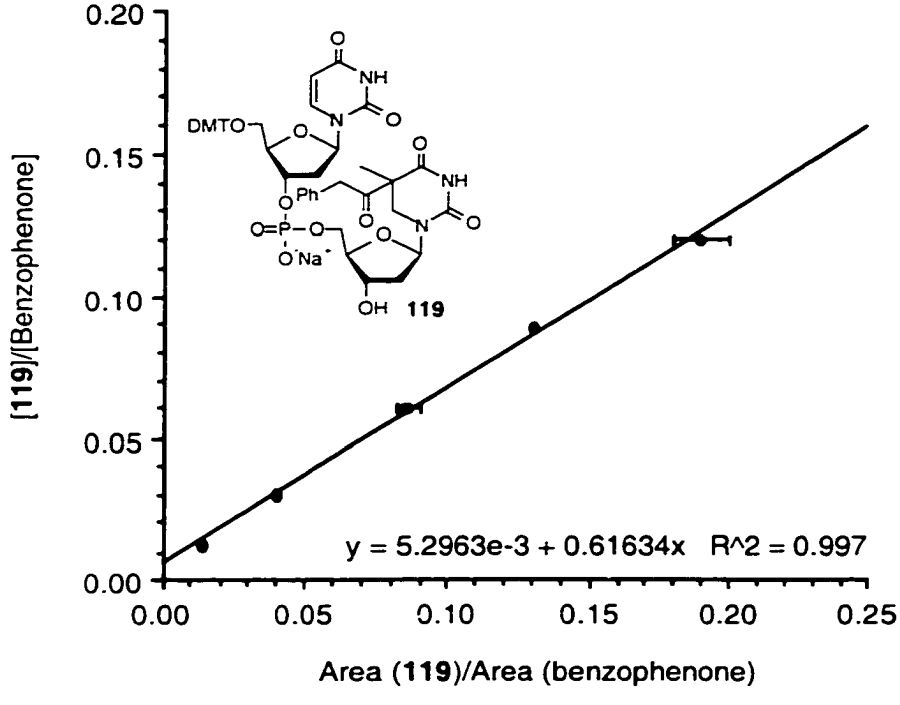

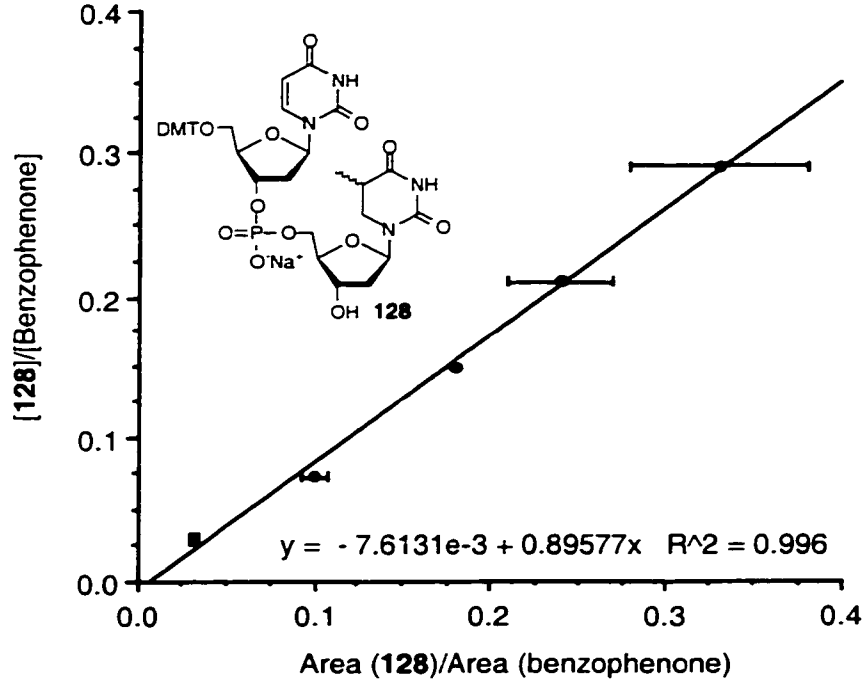

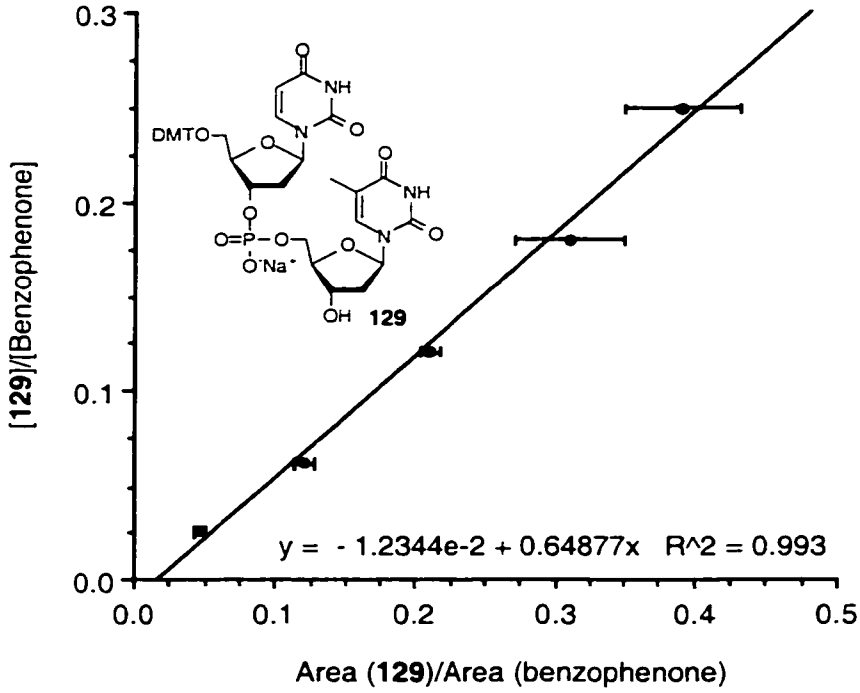

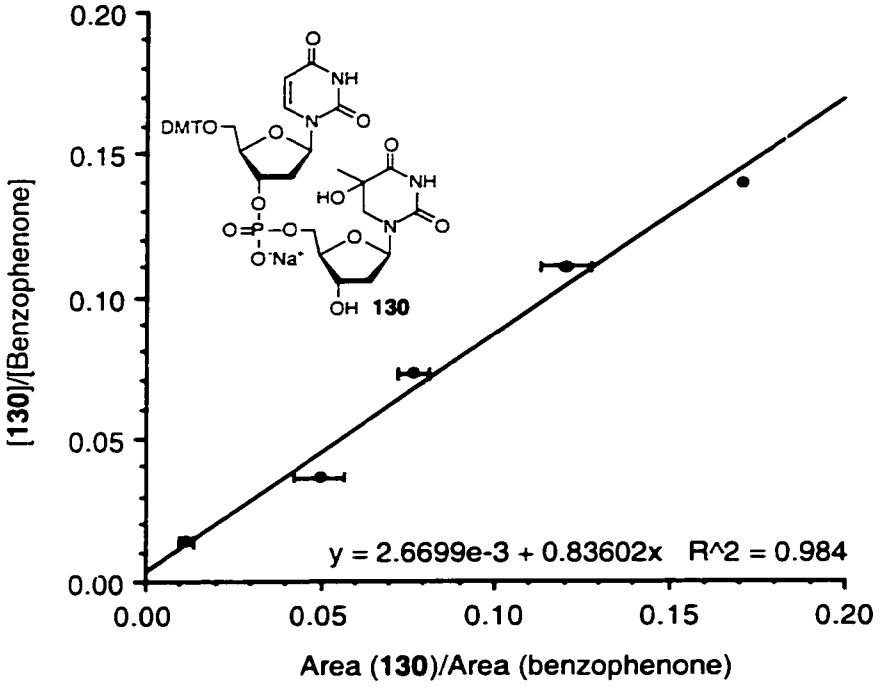

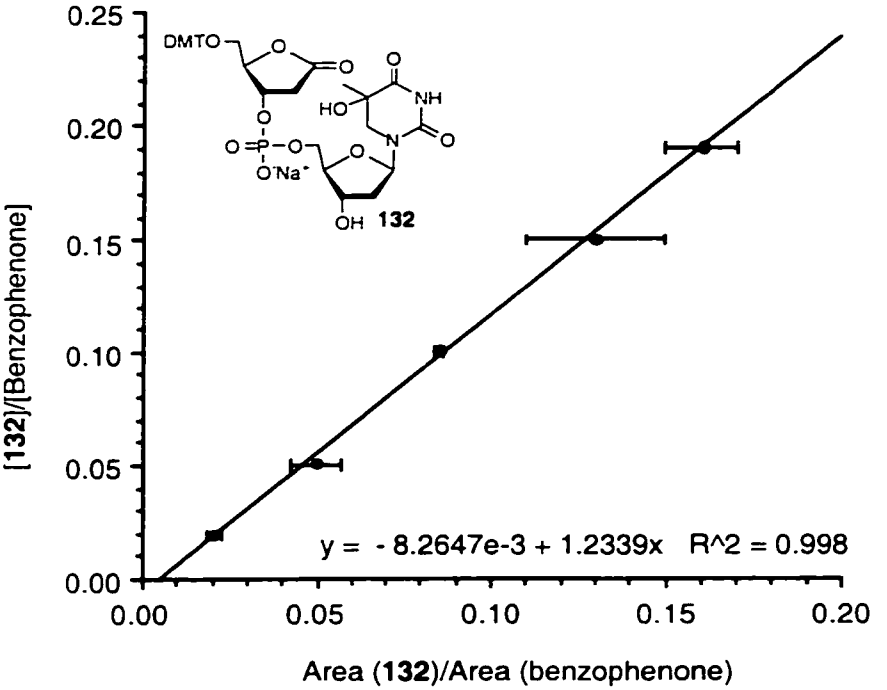

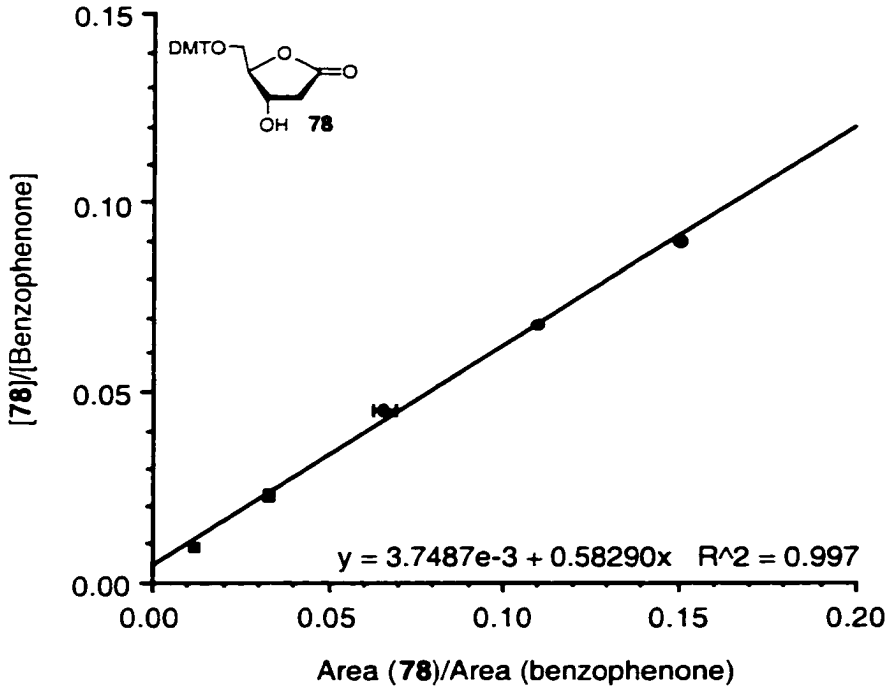

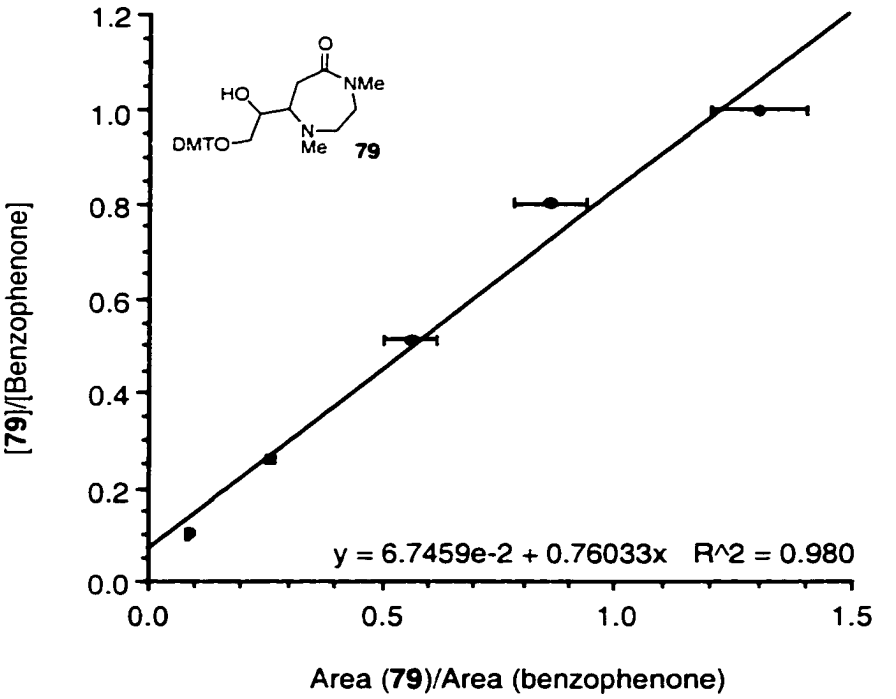

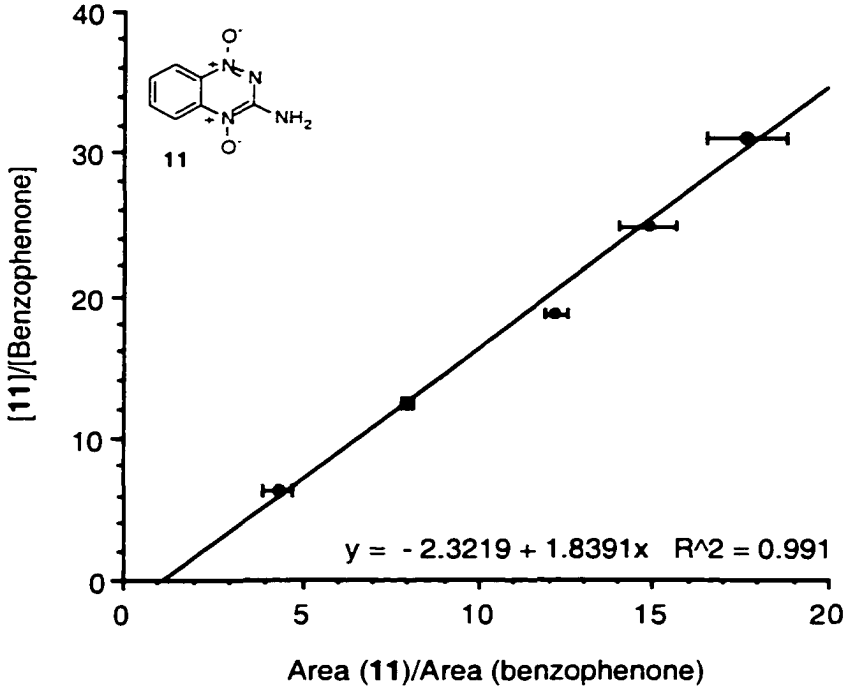

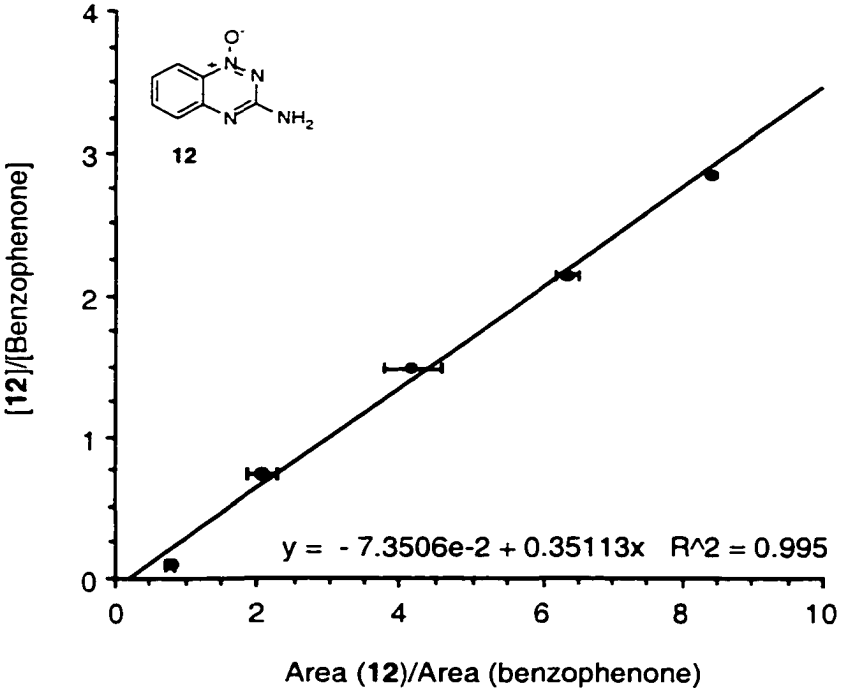

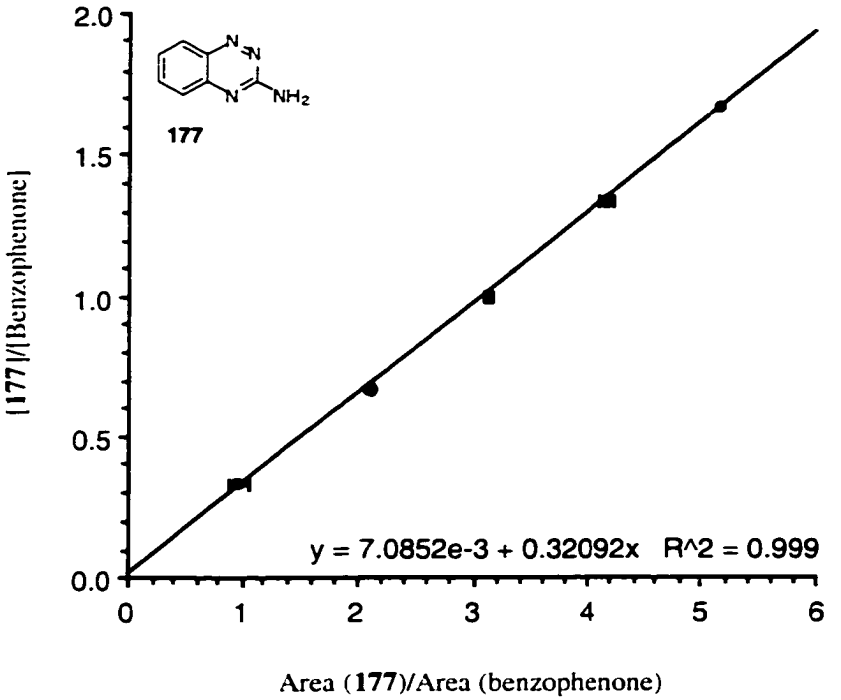

APPENDIX B

ESMS Analyses of Ketone Dinucleotide

Appendix B.1

Anaerobic photolysis of ketone dinucleotide (**119**).

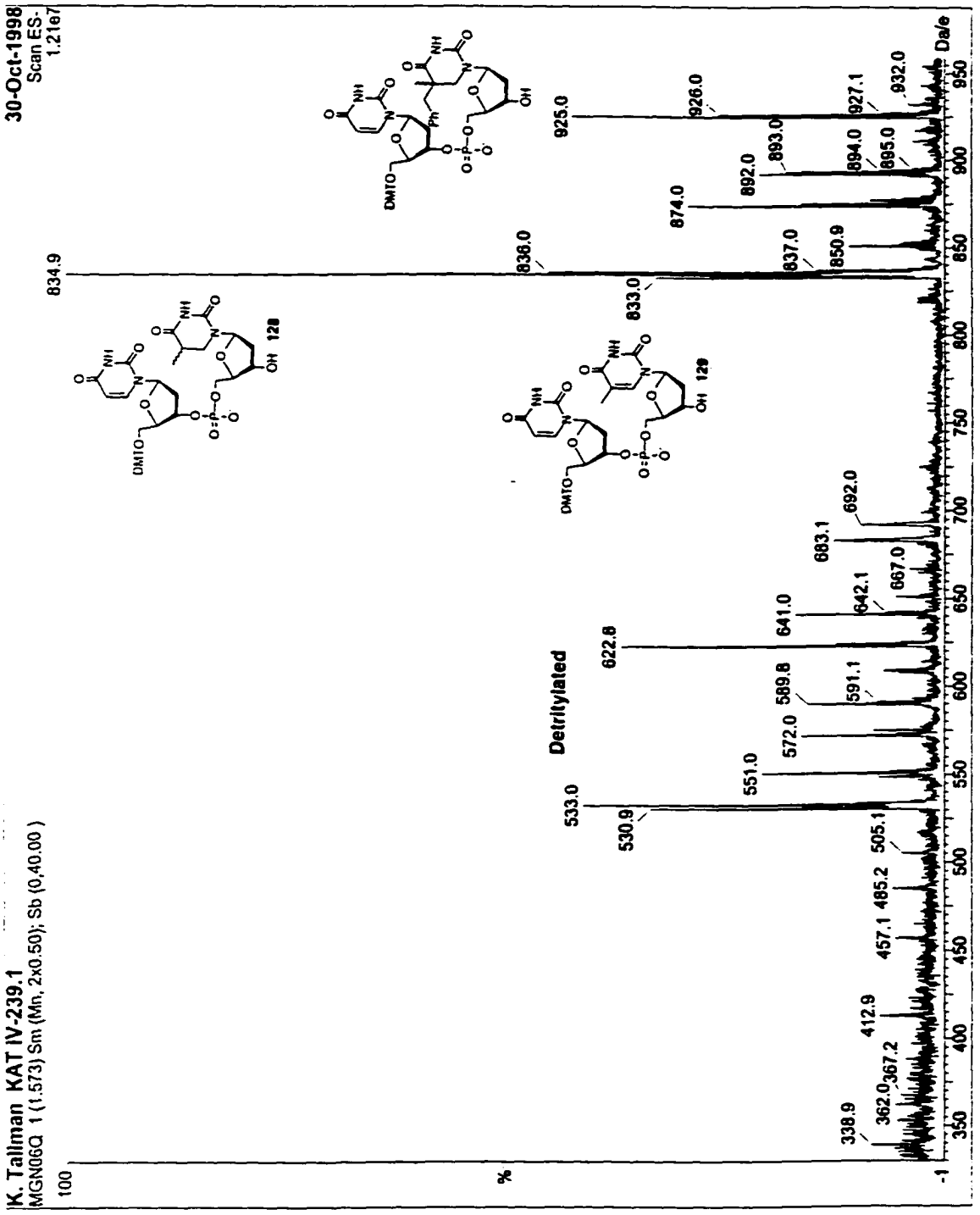

Appendix B.2

Aerobic photolysis of ketone dinucleotide (**119**).

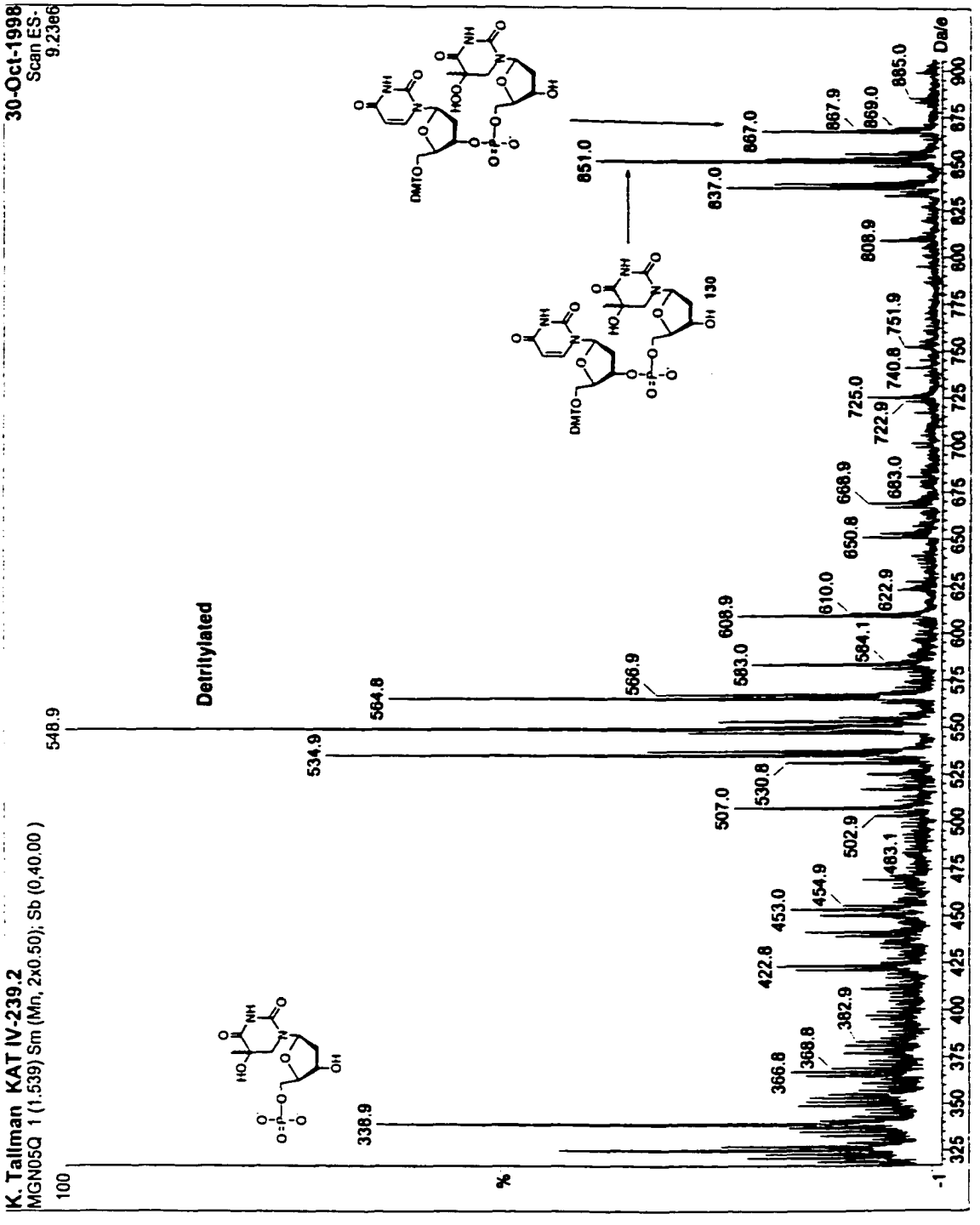

Appendix B.3

Aerobic photolysis of ketone dinucleotide (**119**) in the presence of βME.

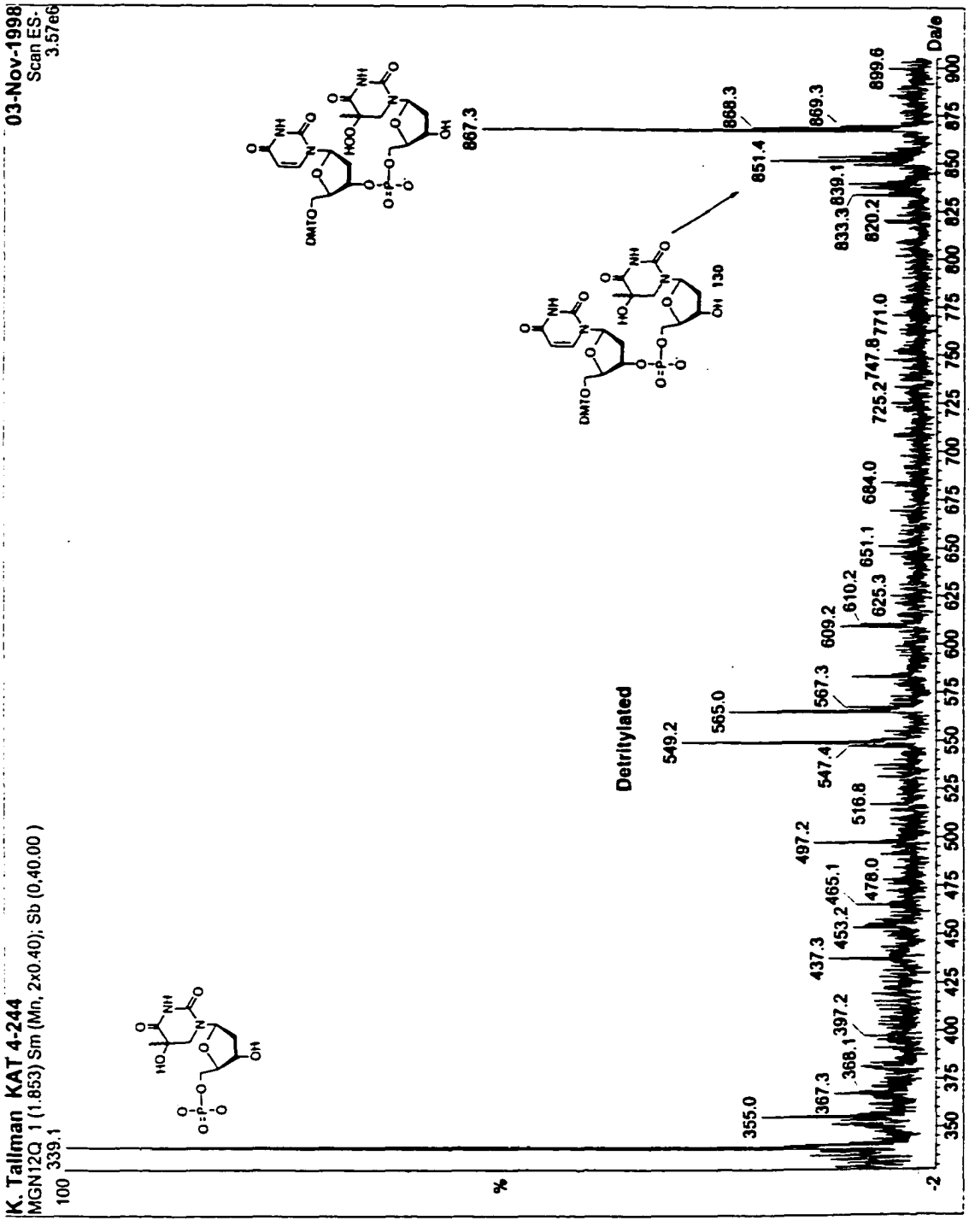

APPENDIX C

NMR, IR, and ESMS Spectra

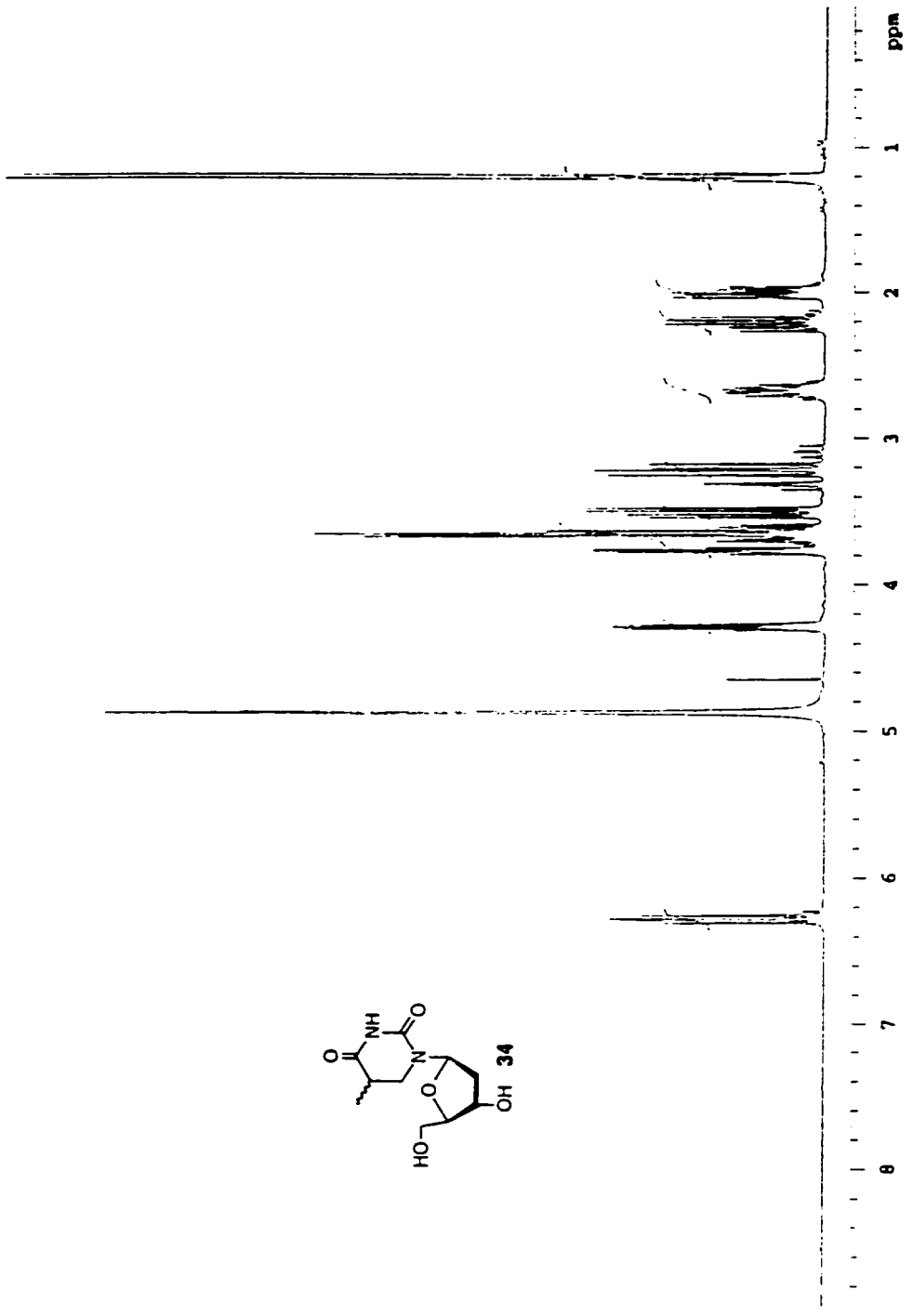

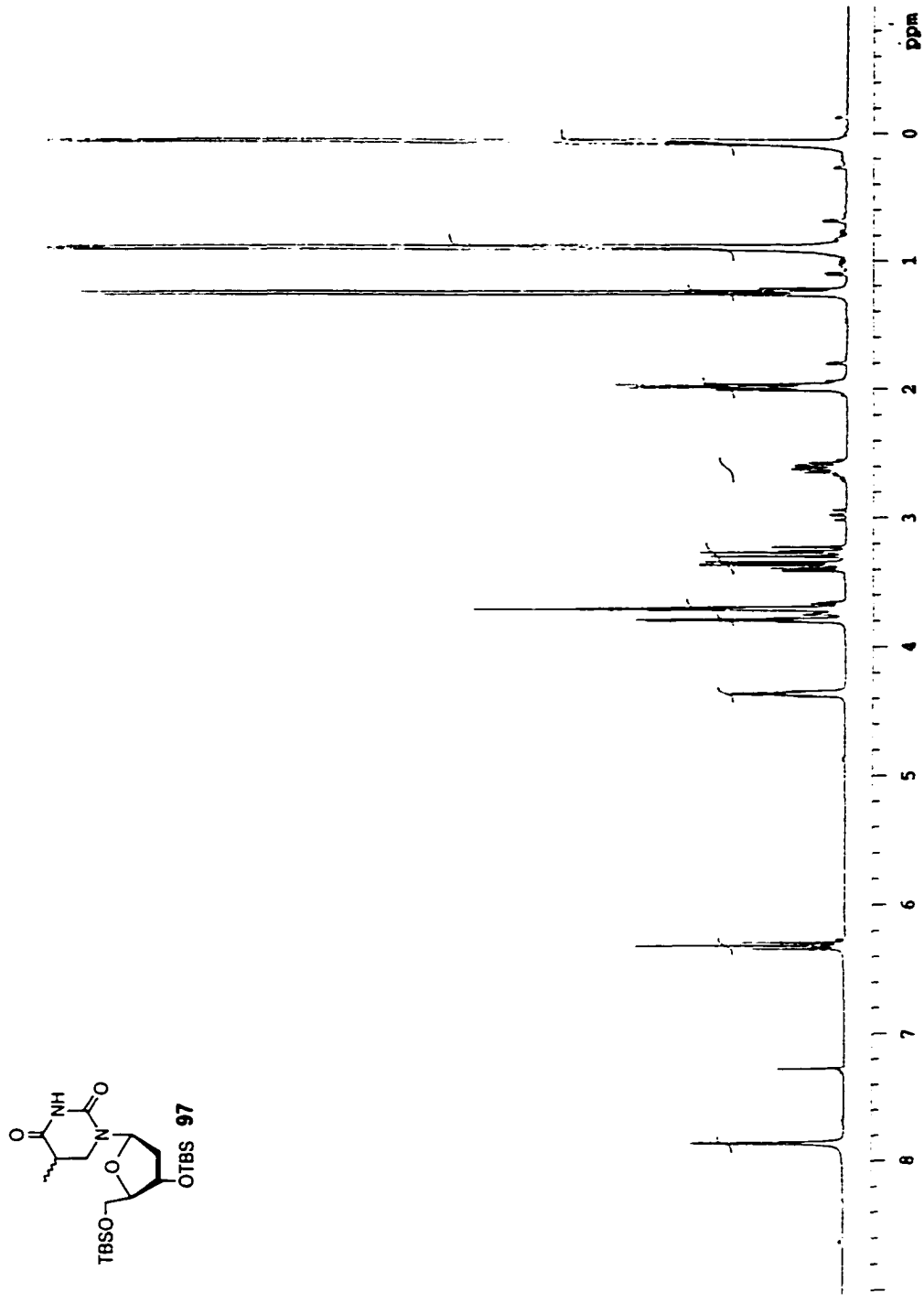

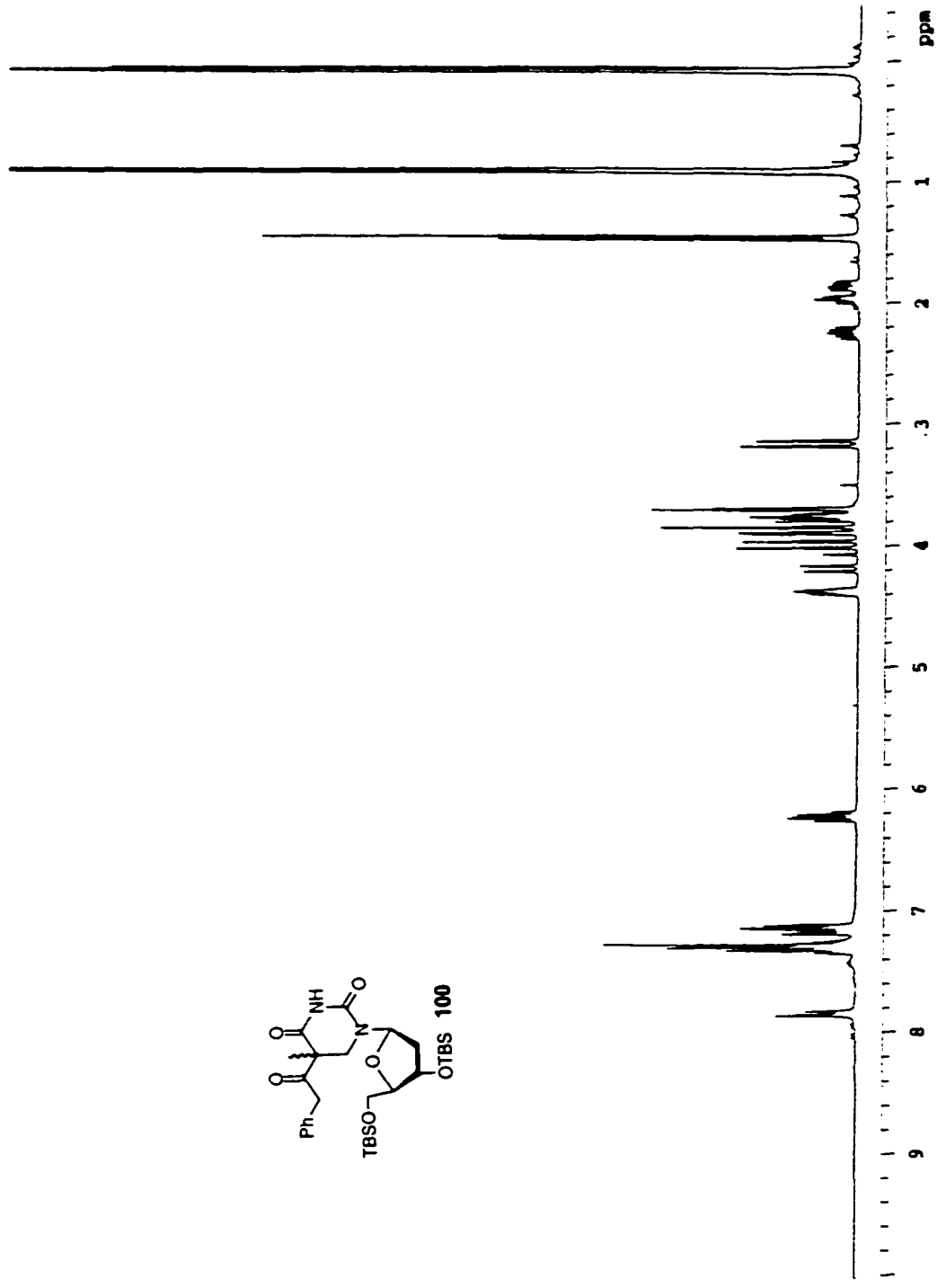

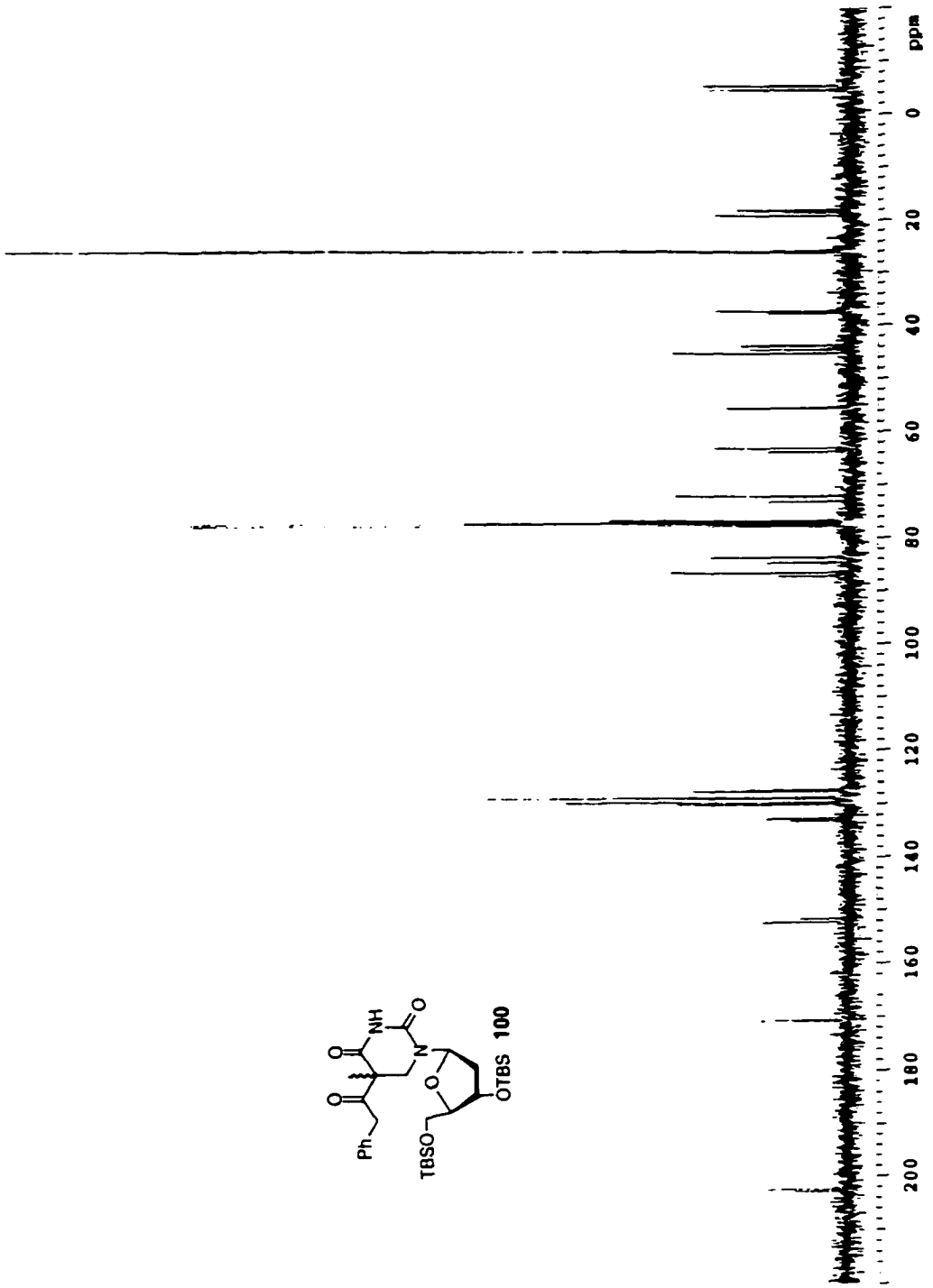

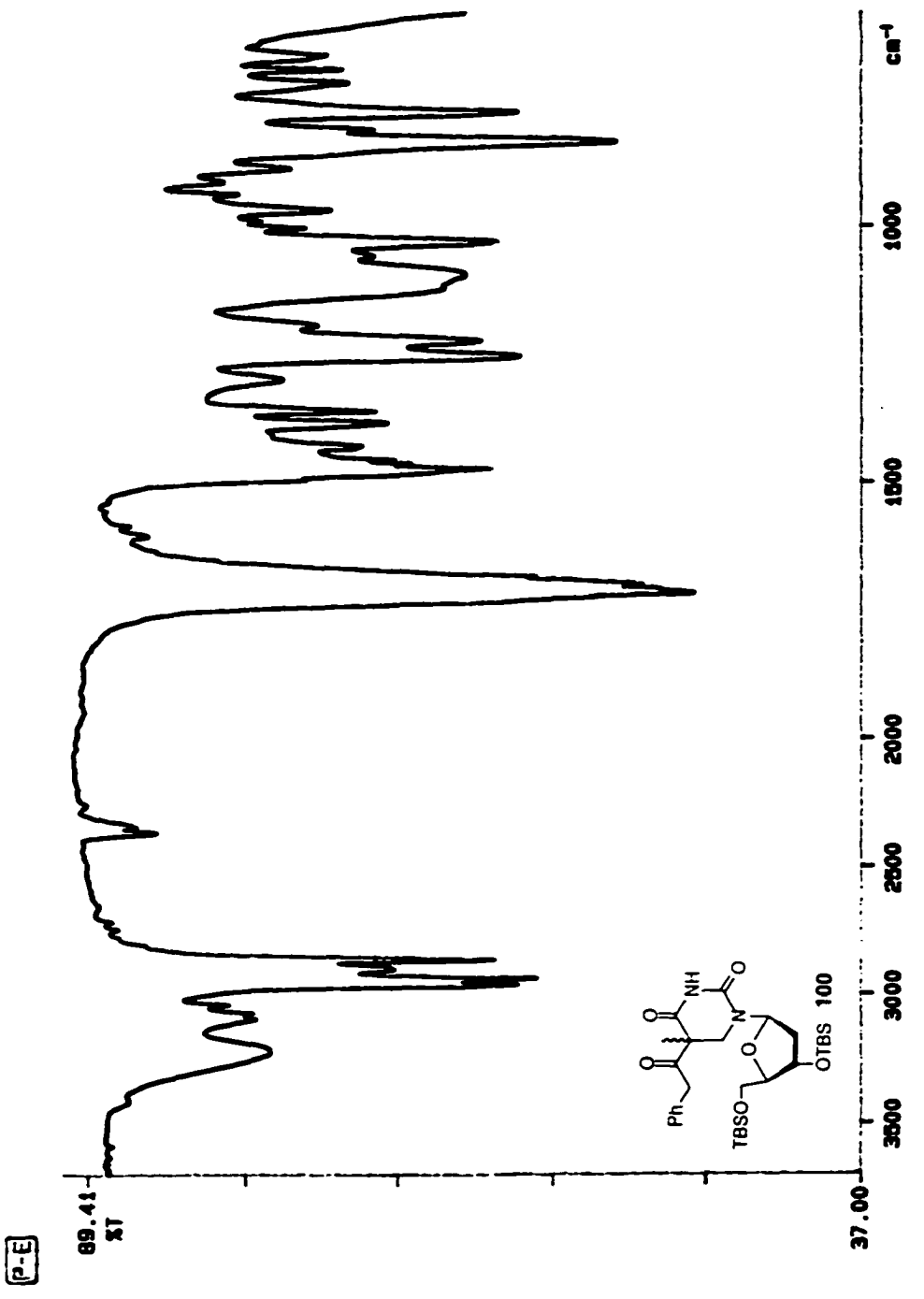

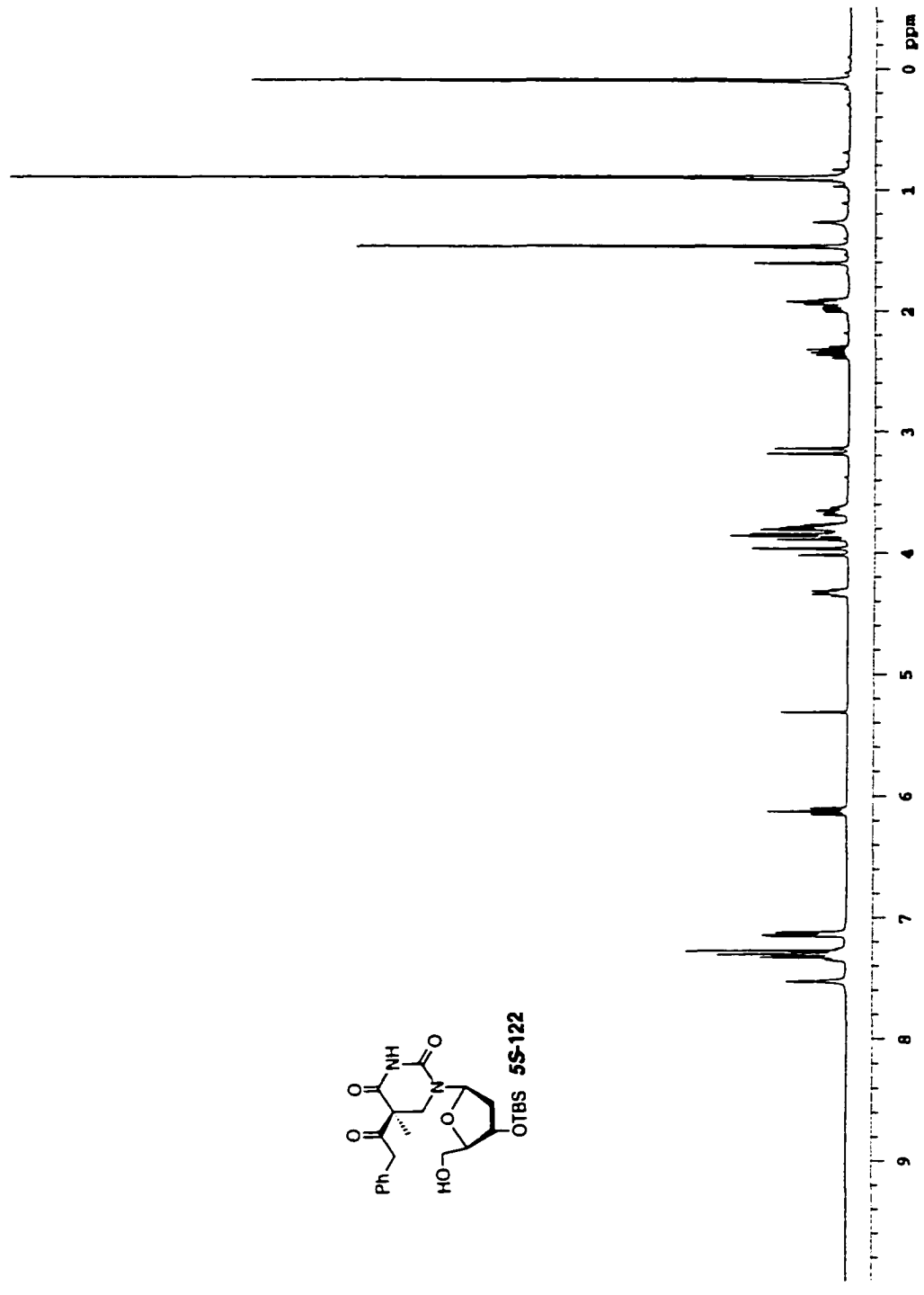

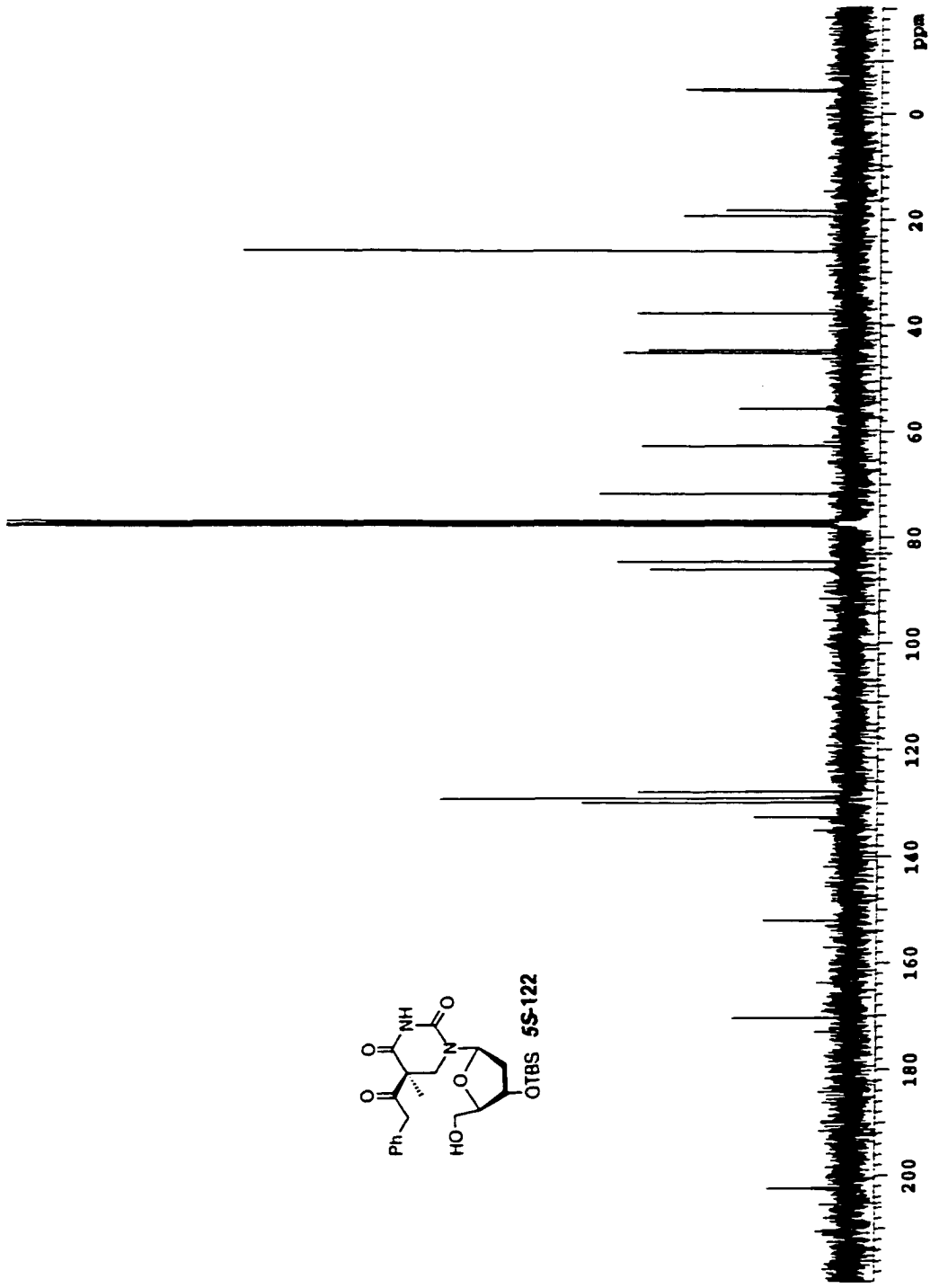

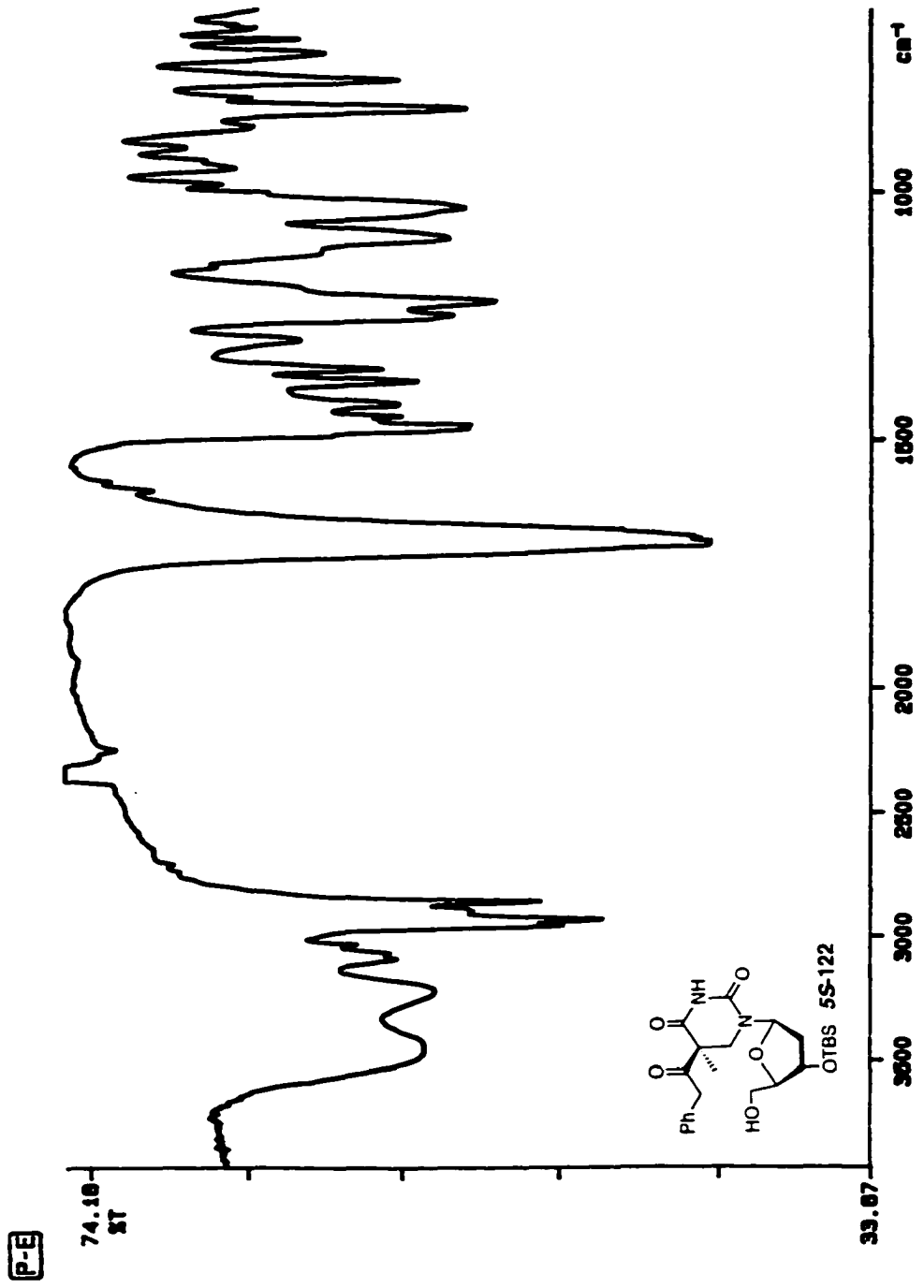

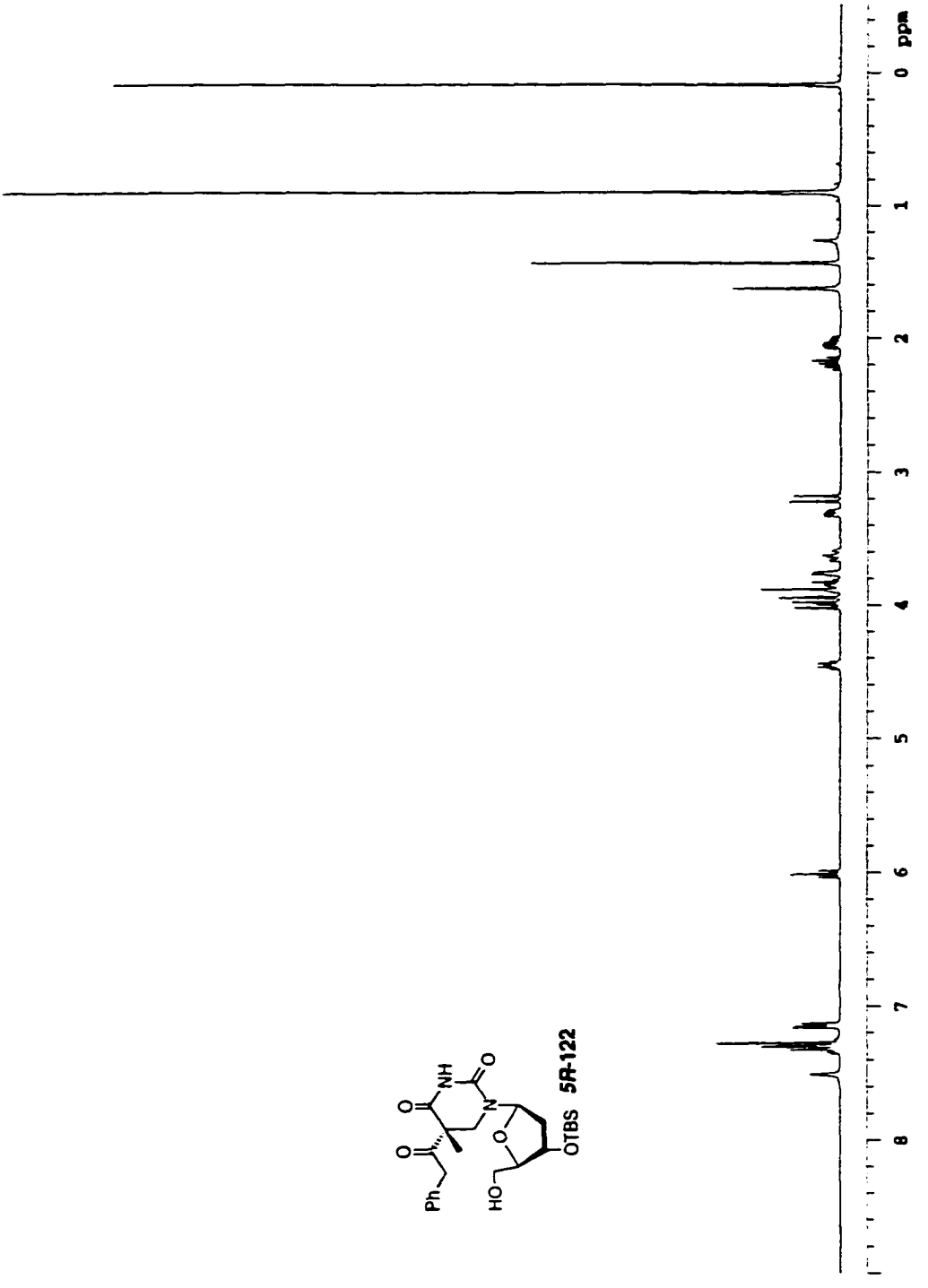

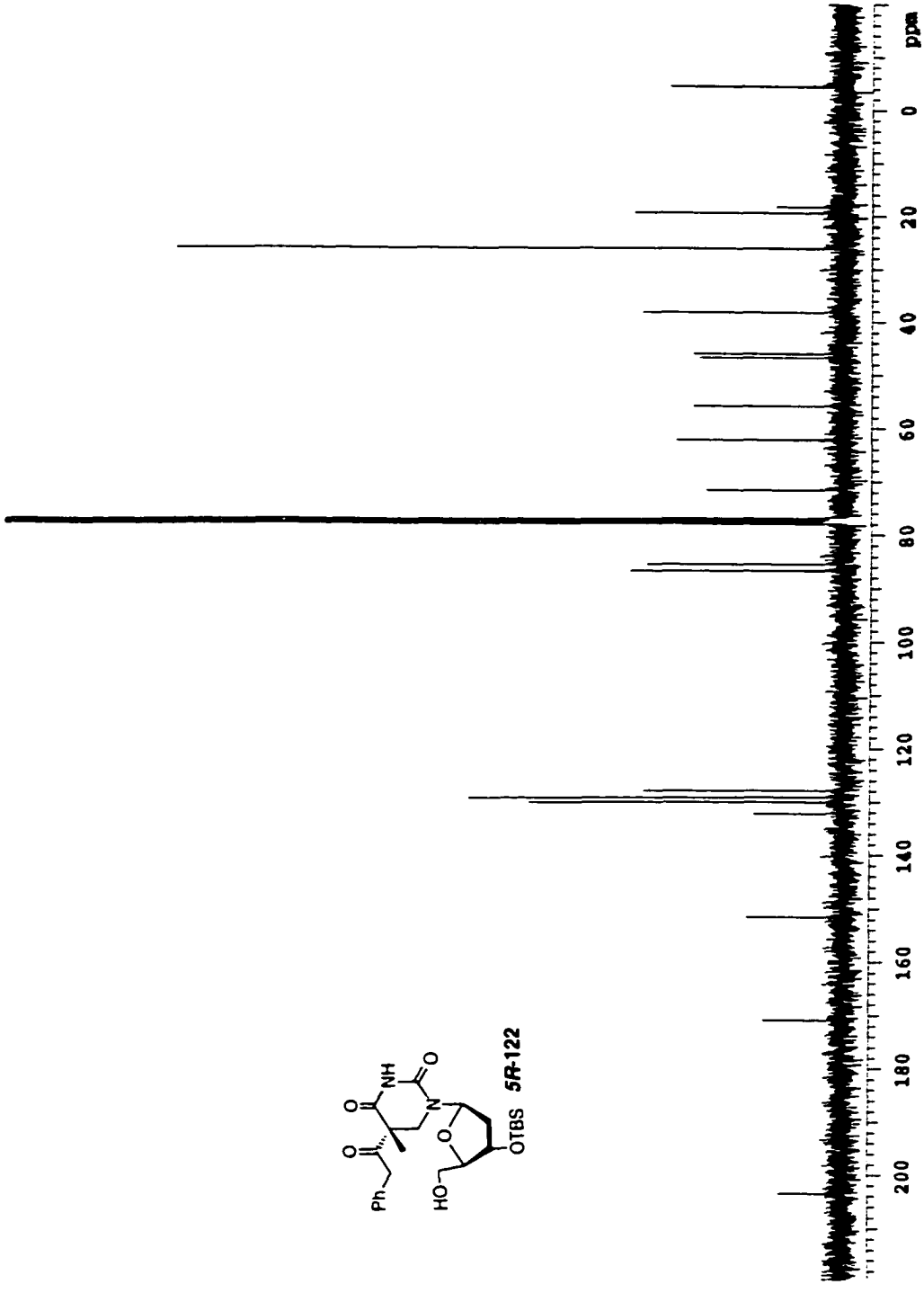

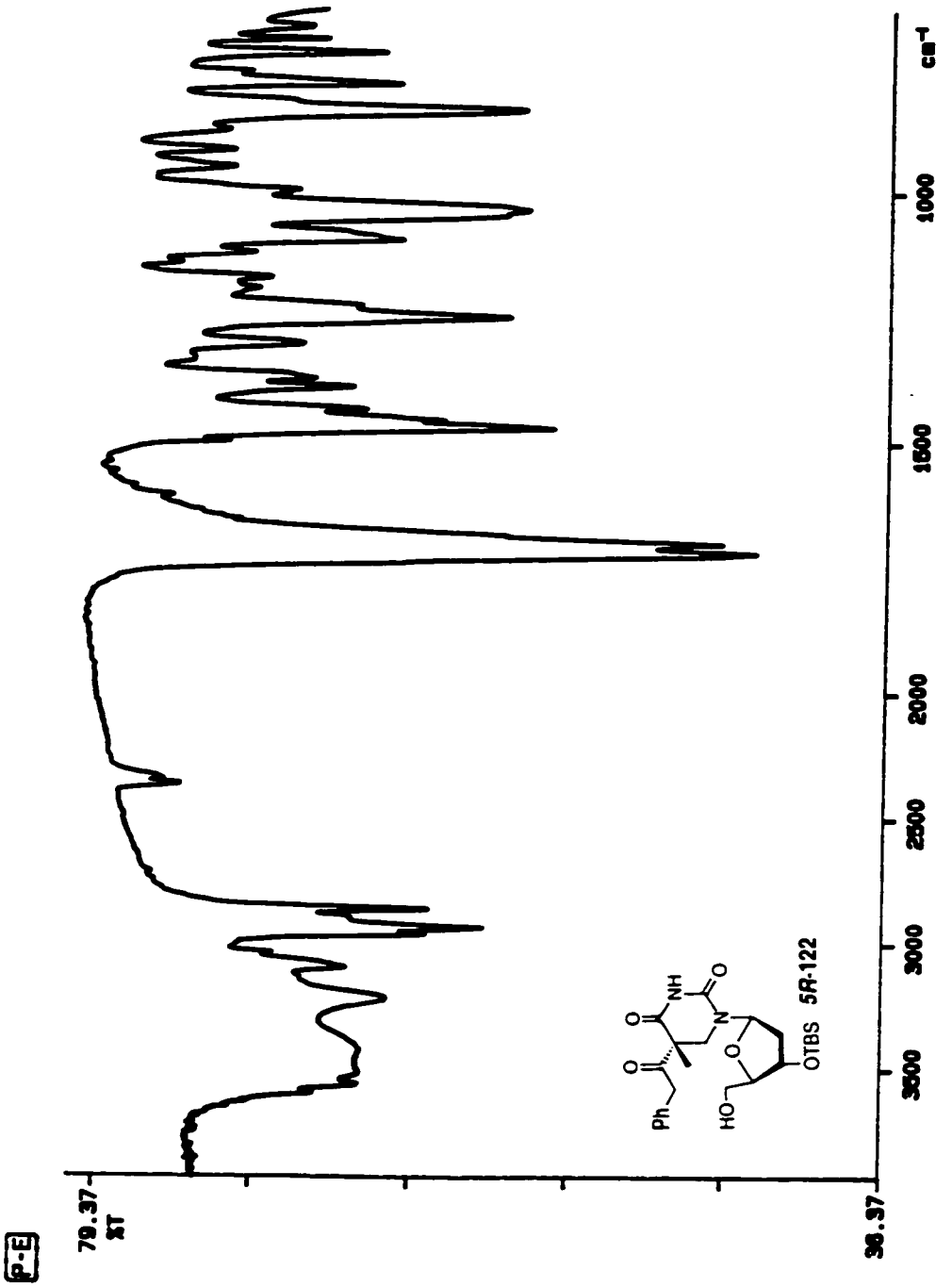

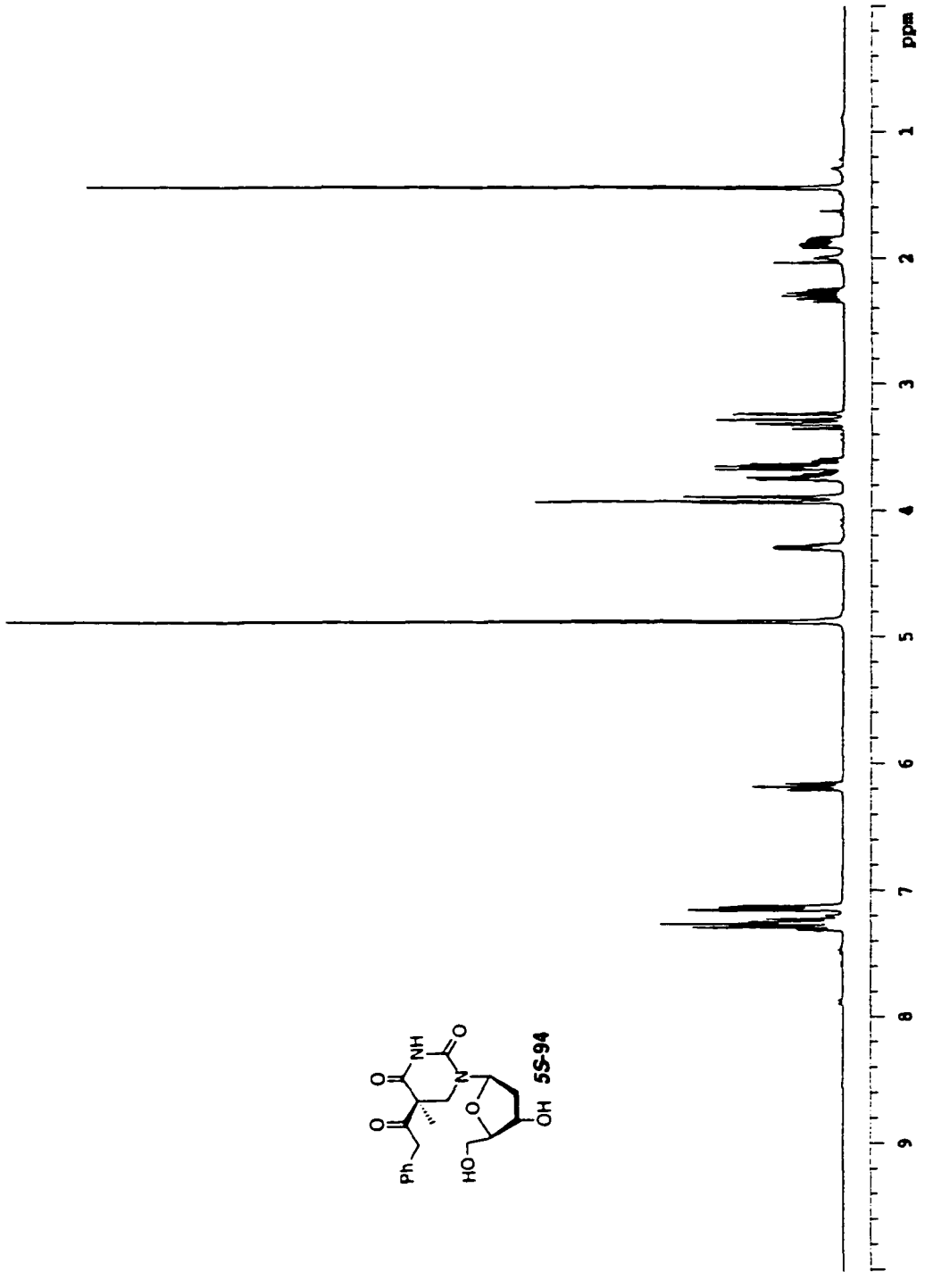

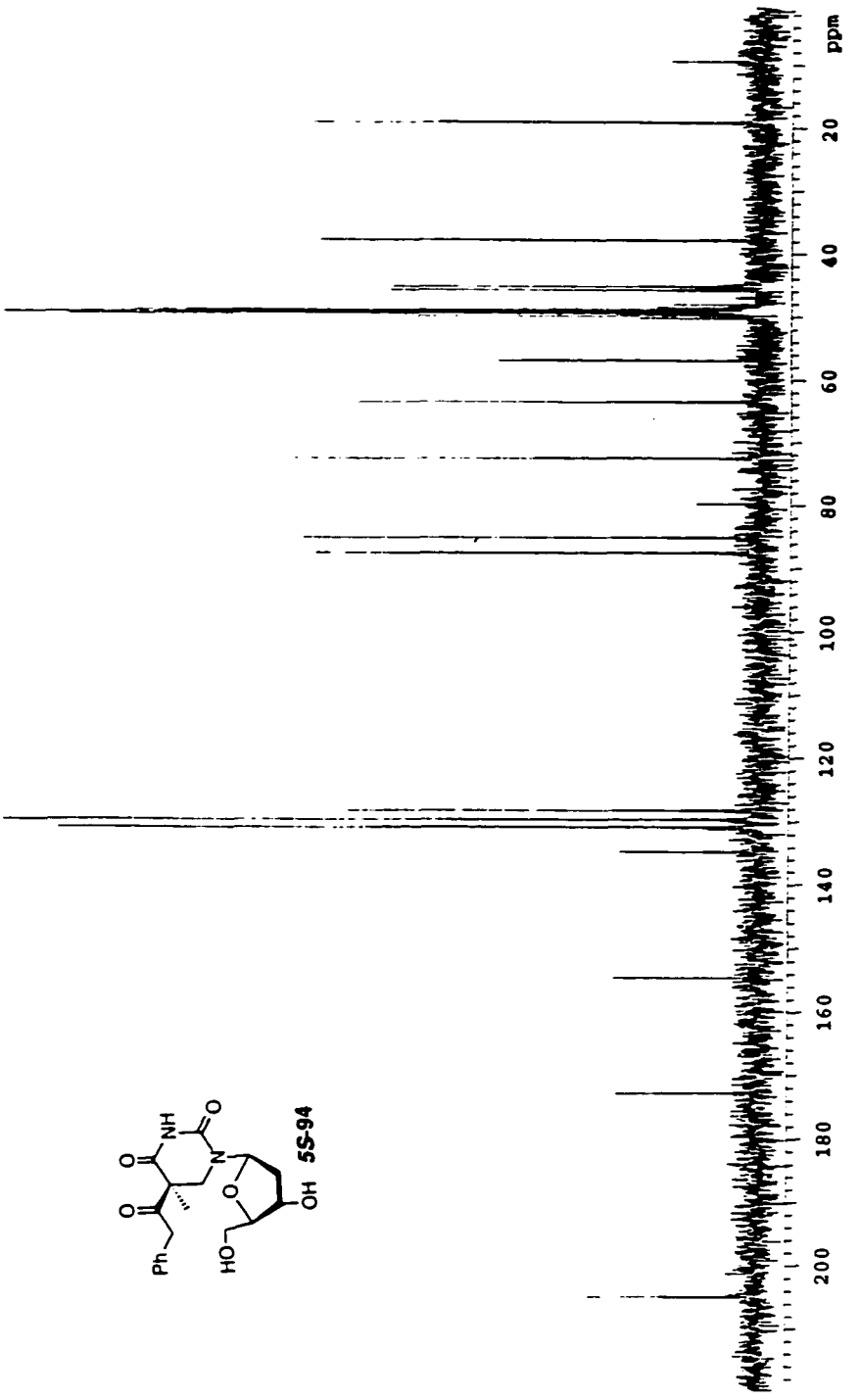

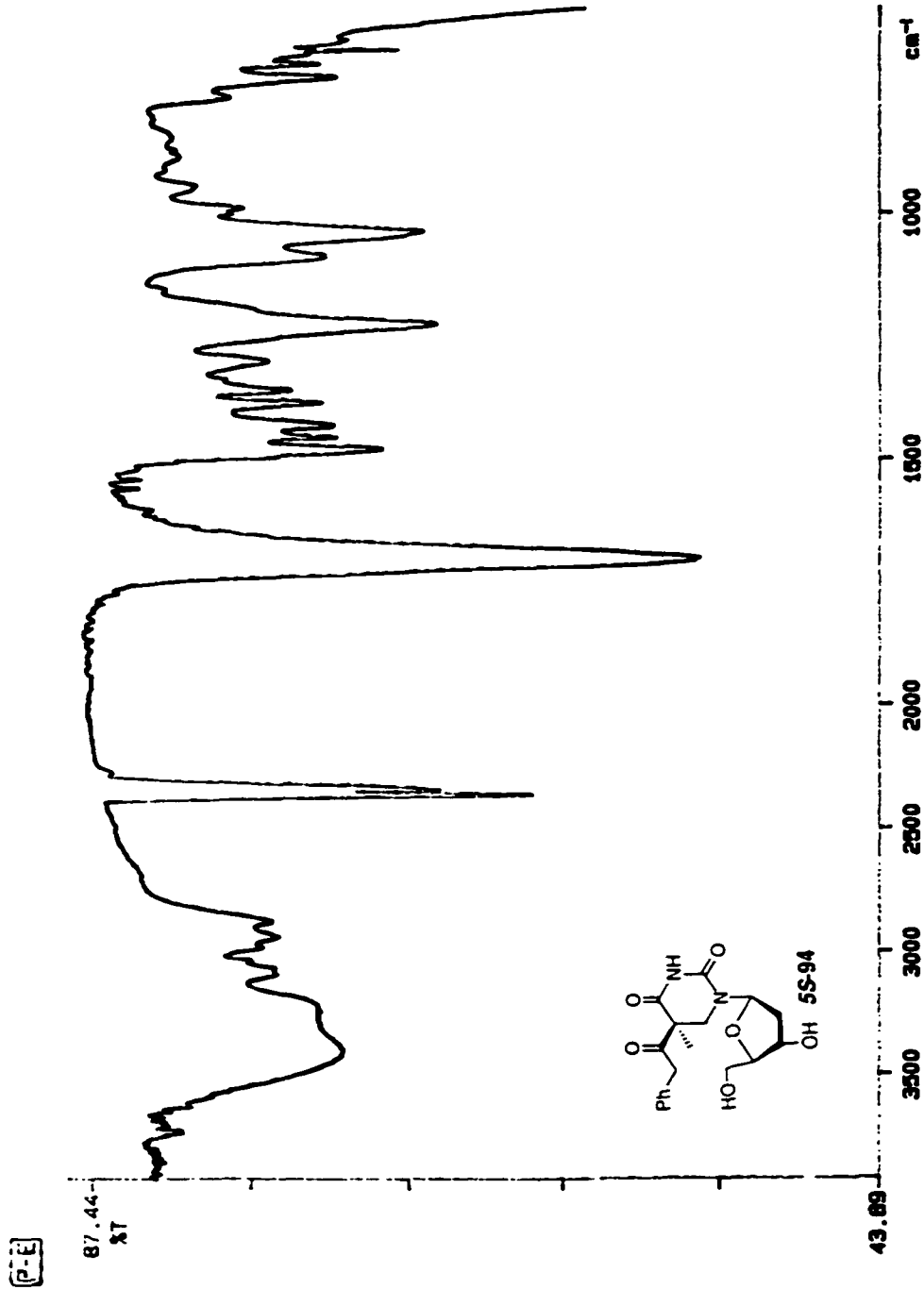

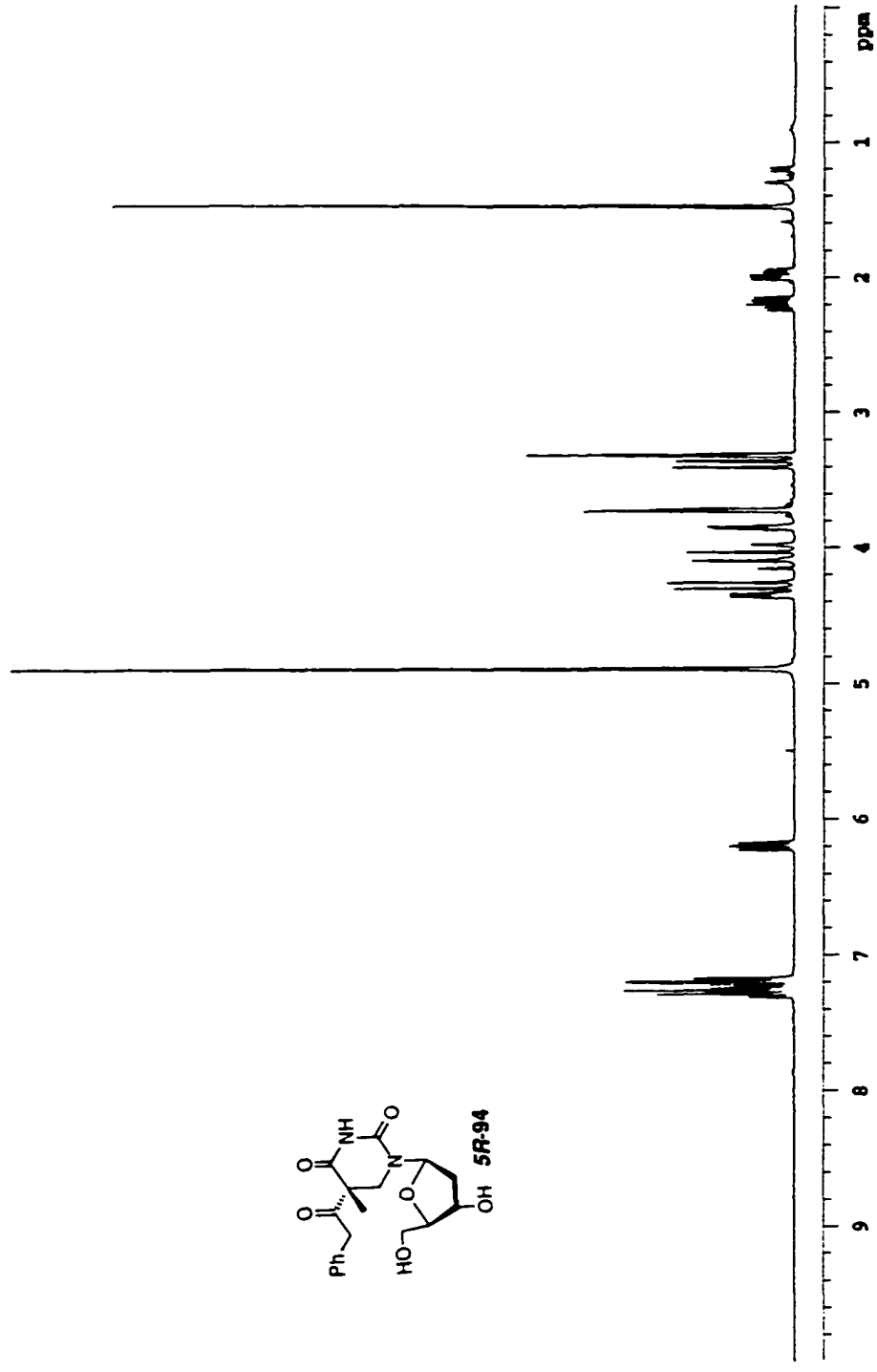

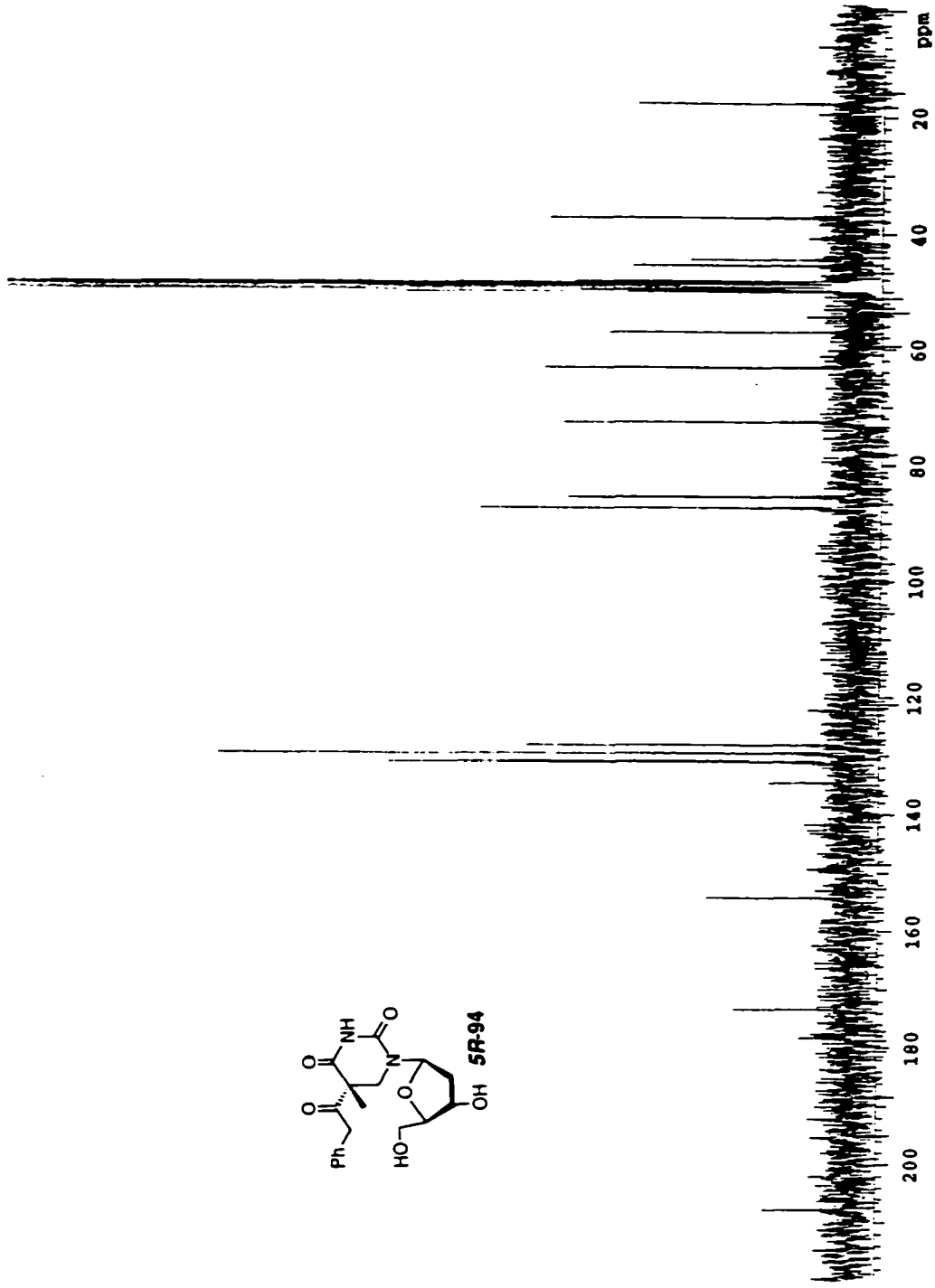

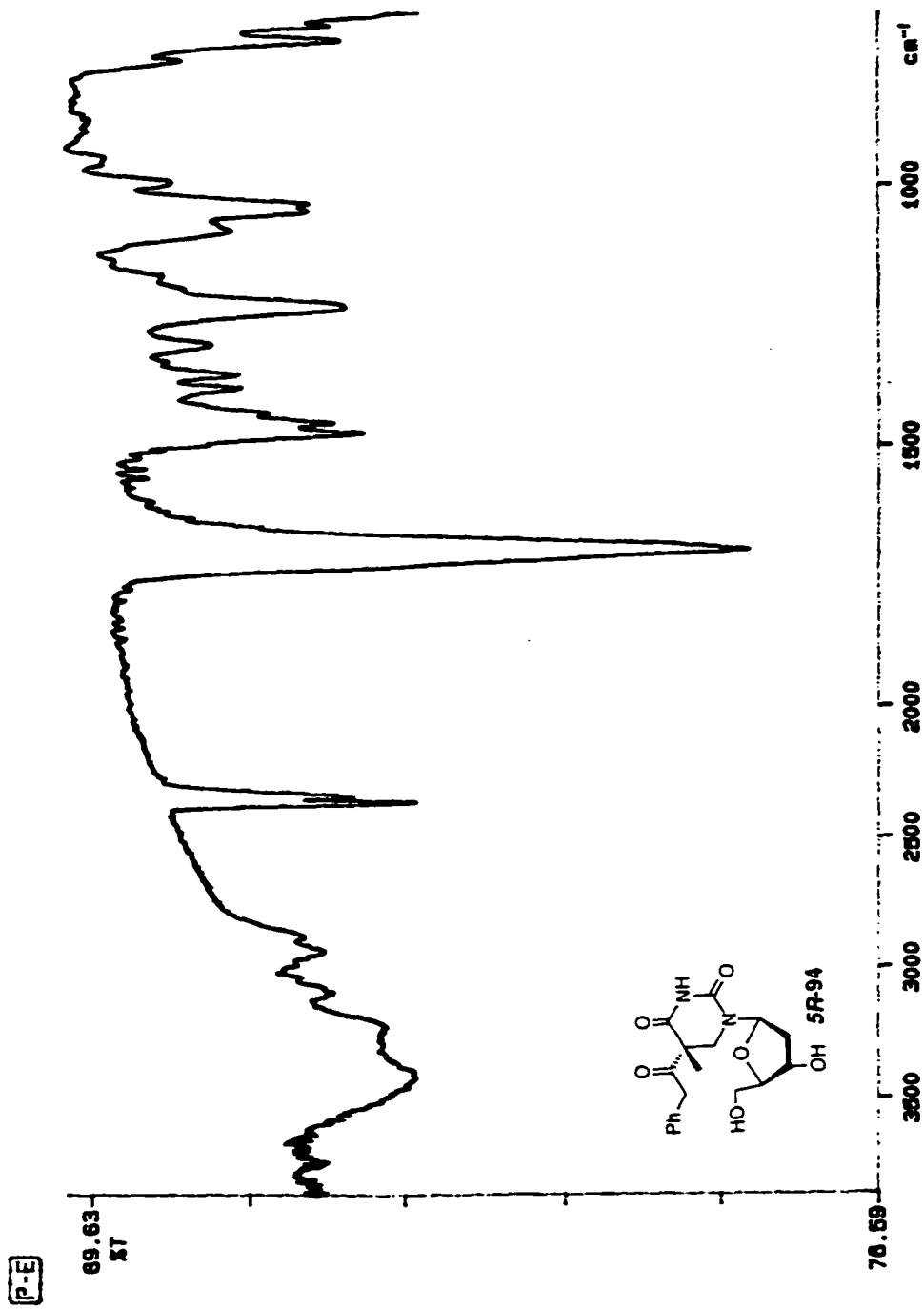

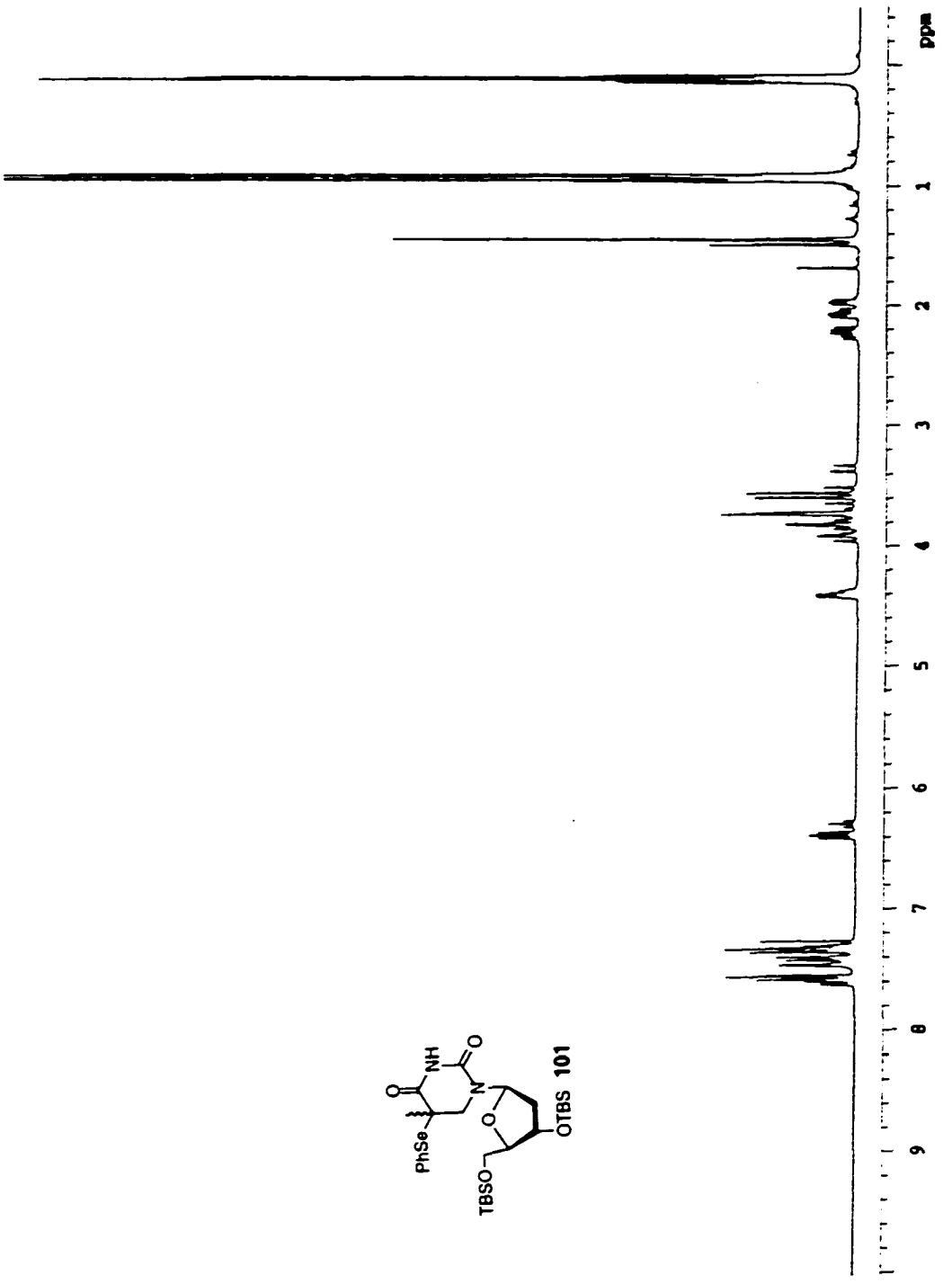

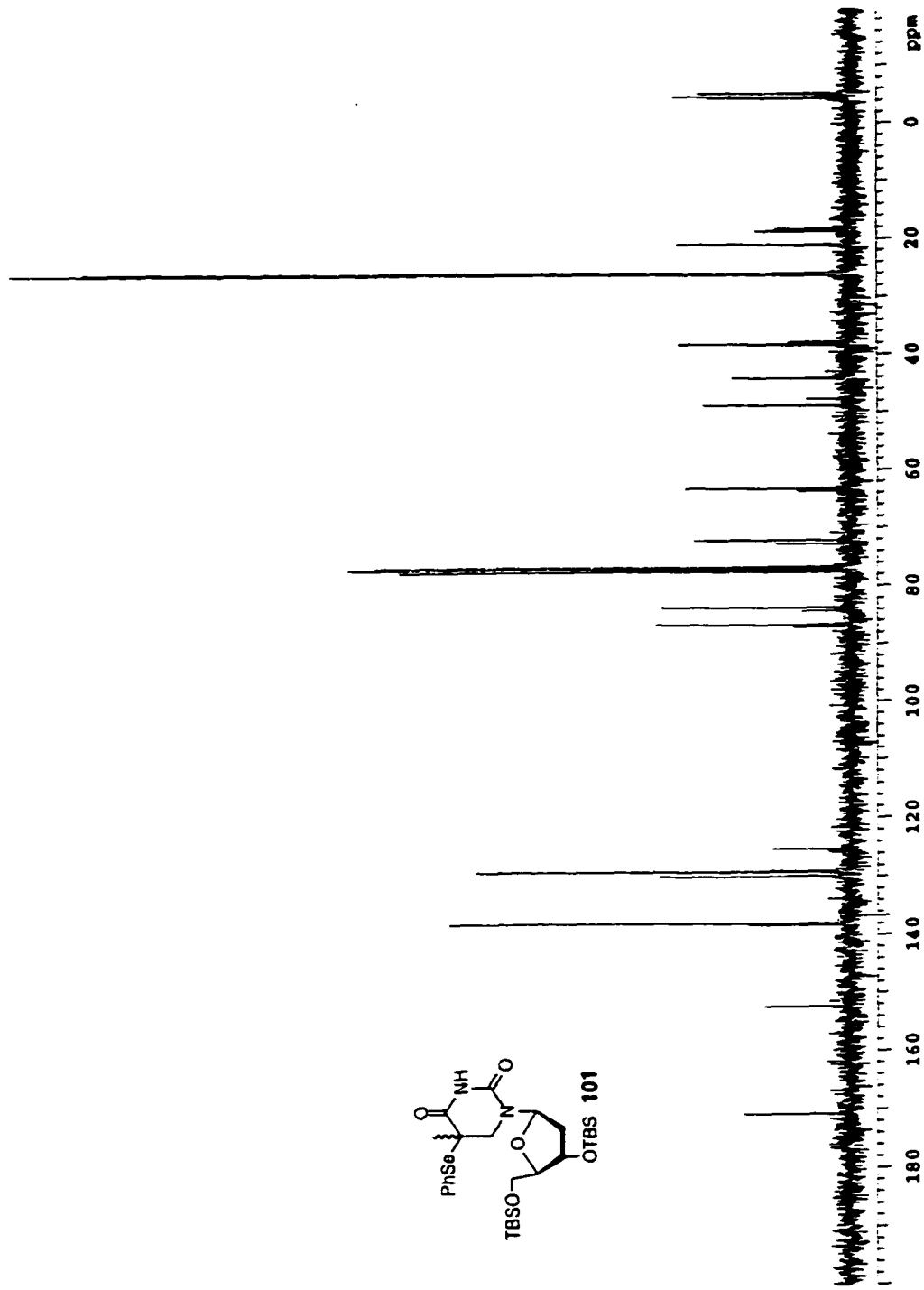

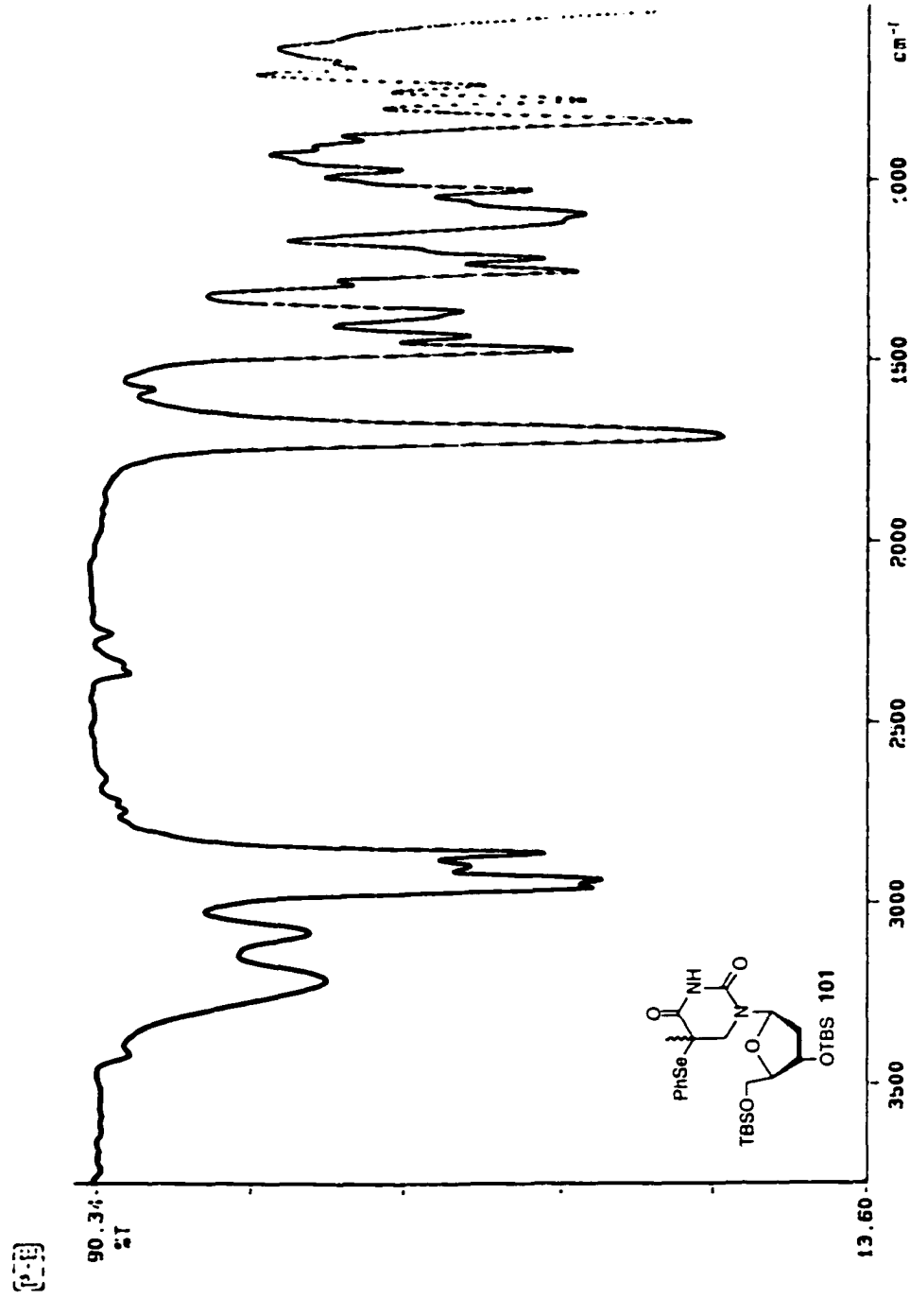

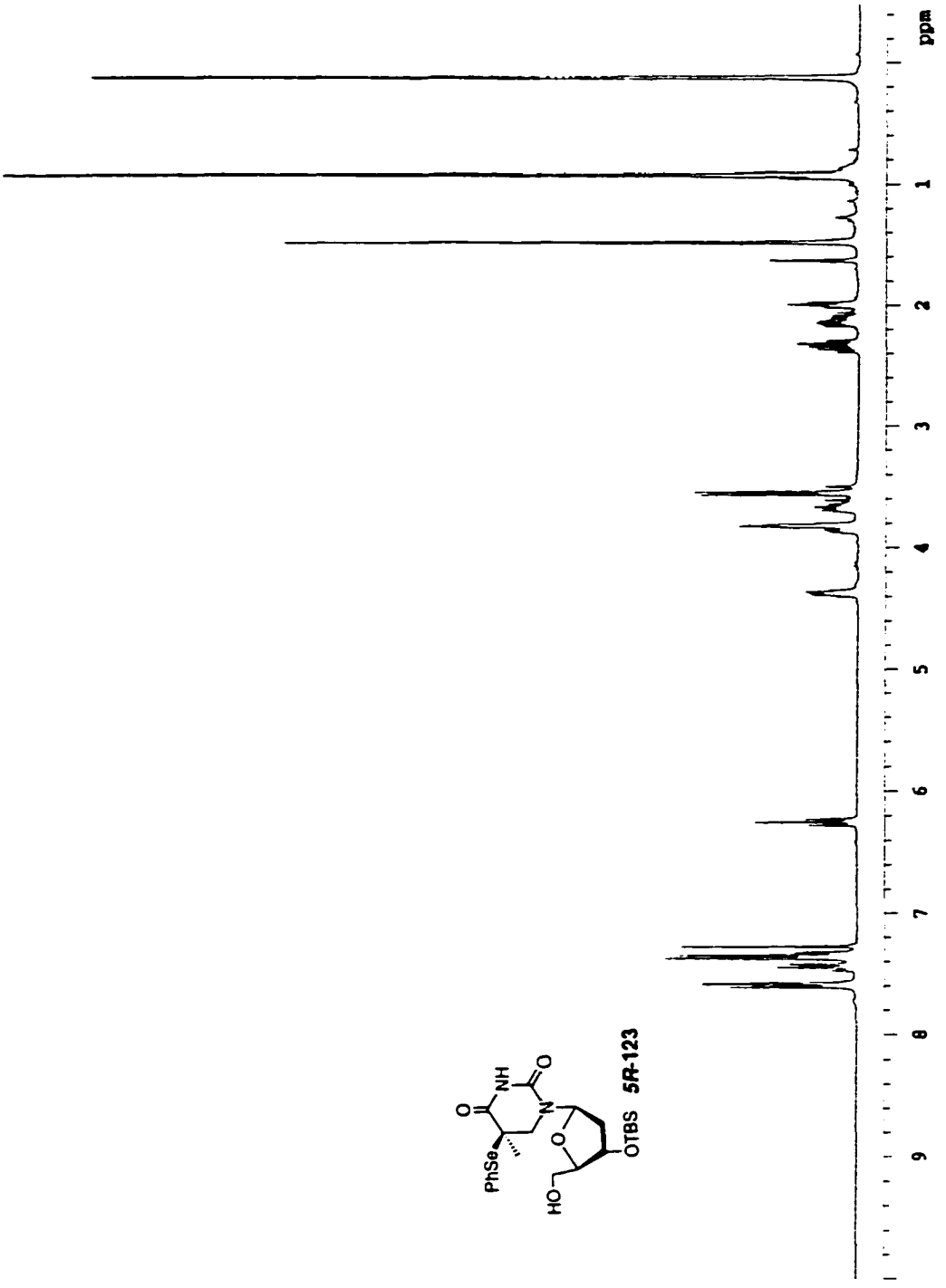

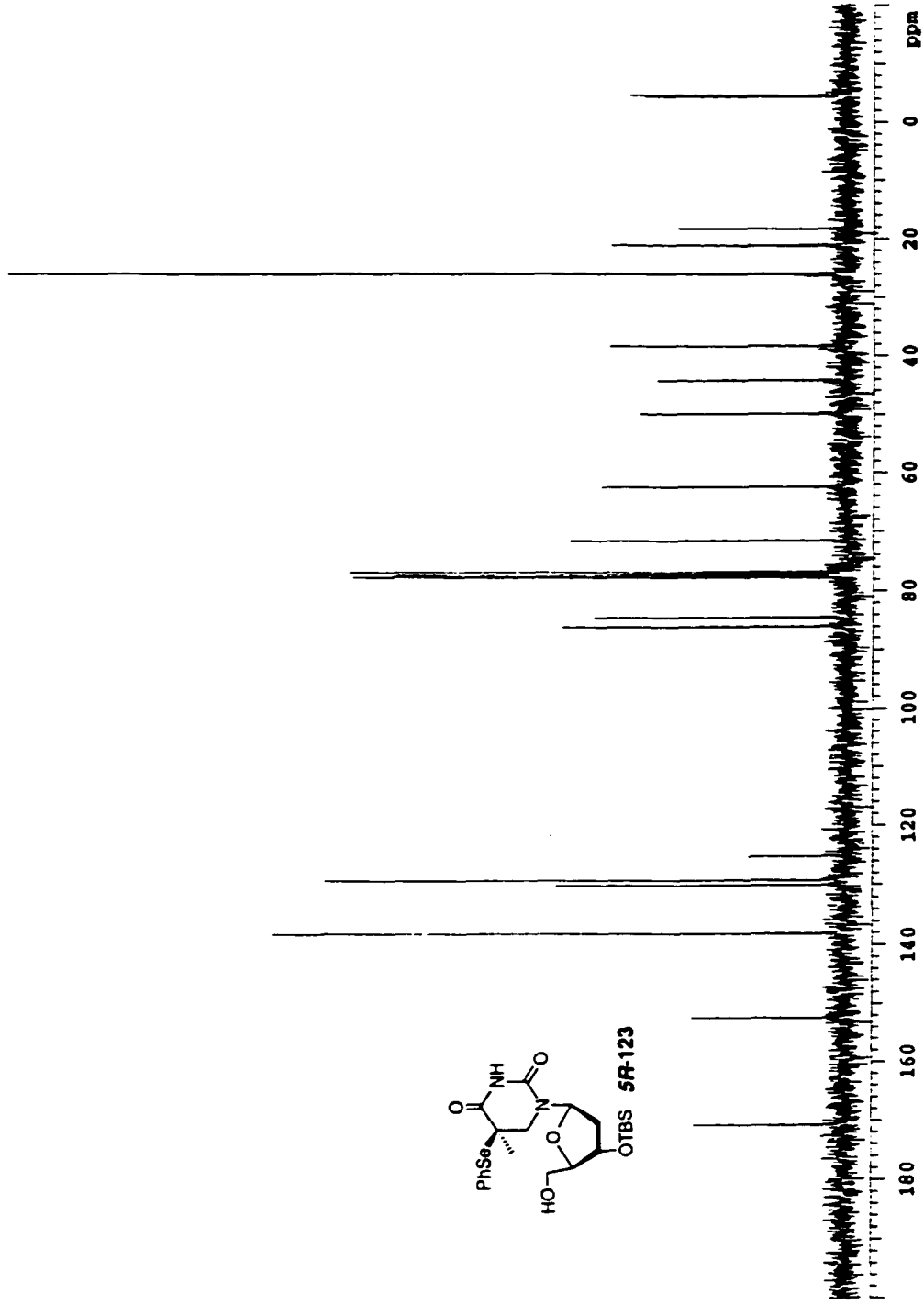

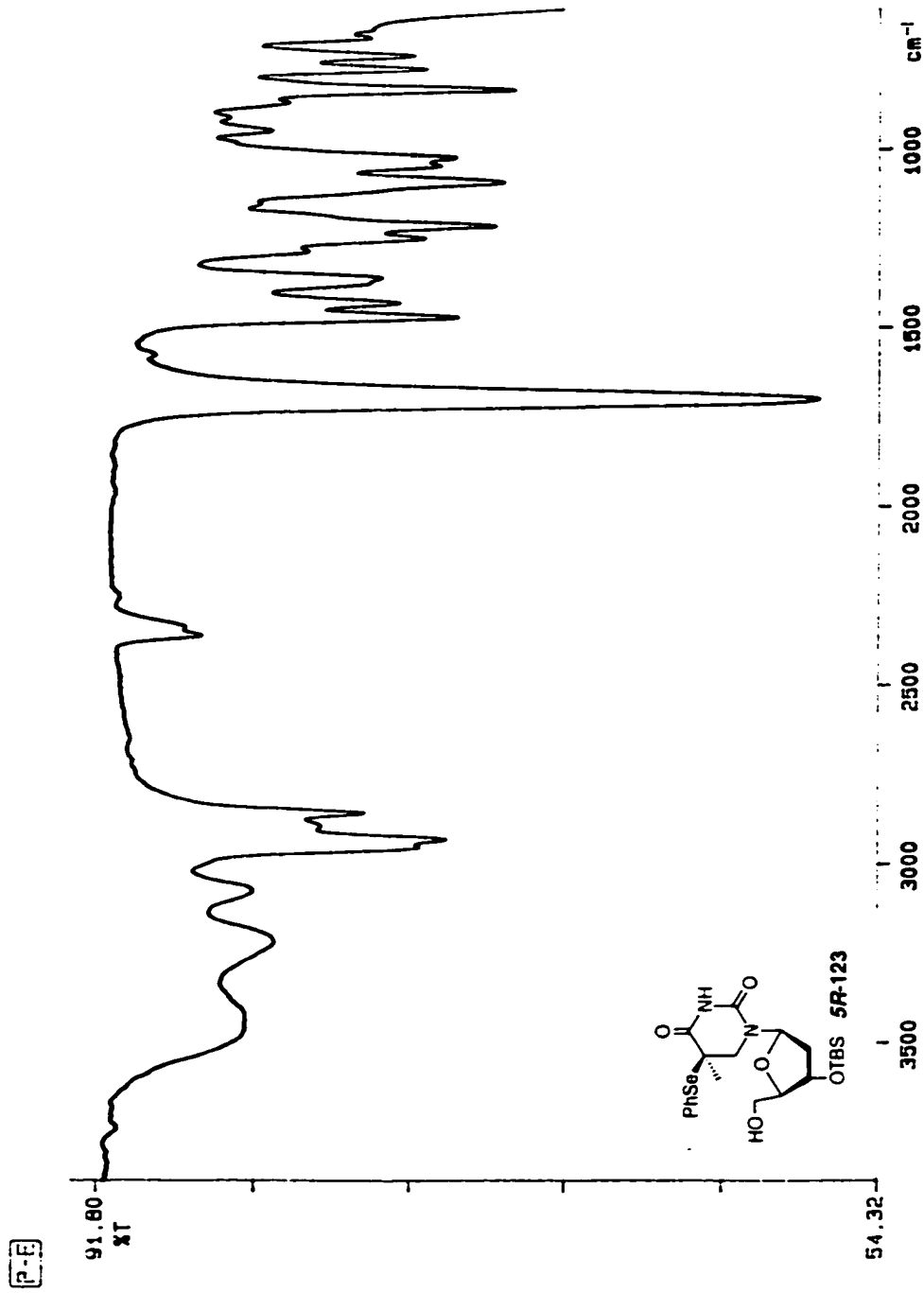

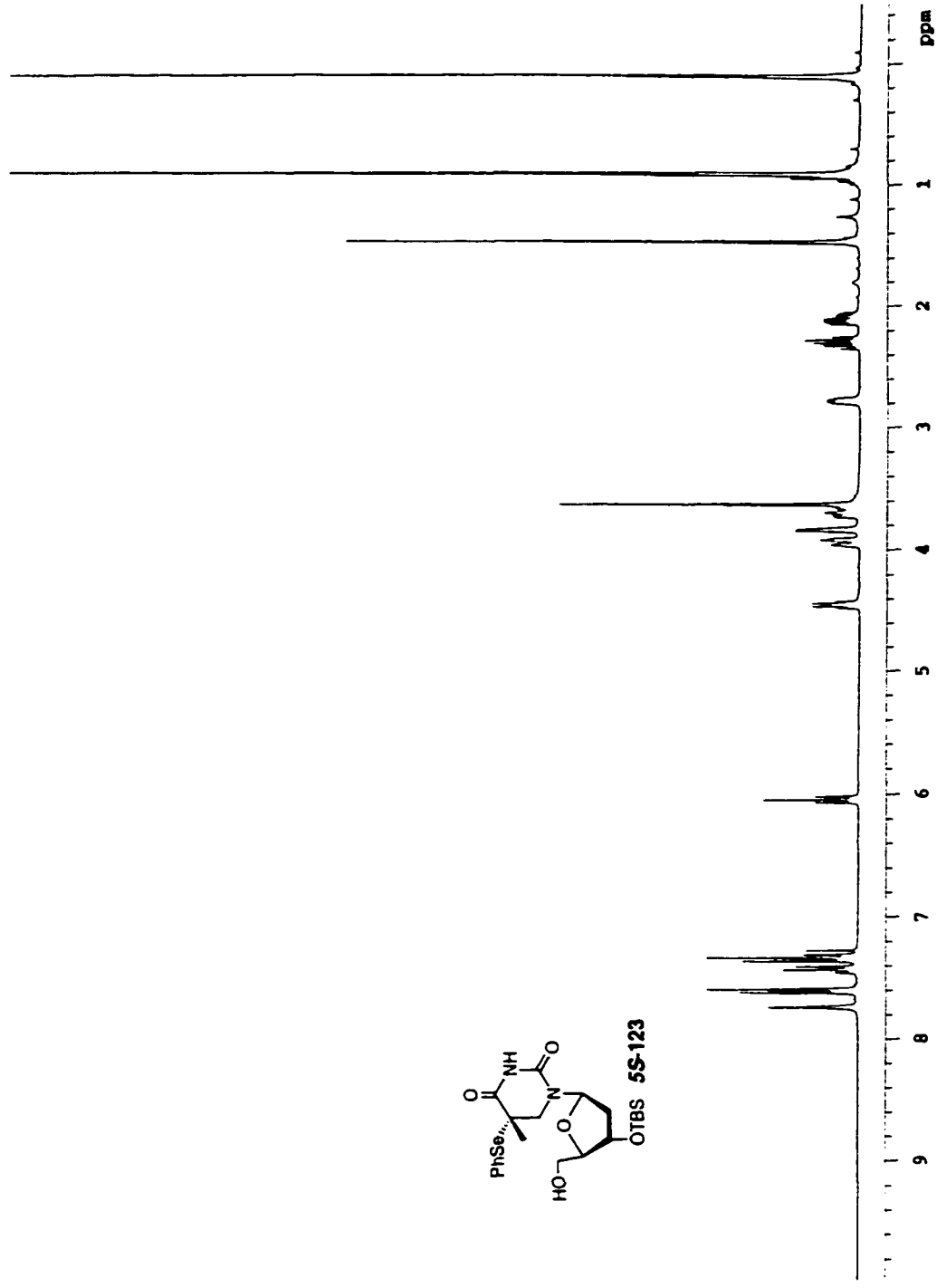

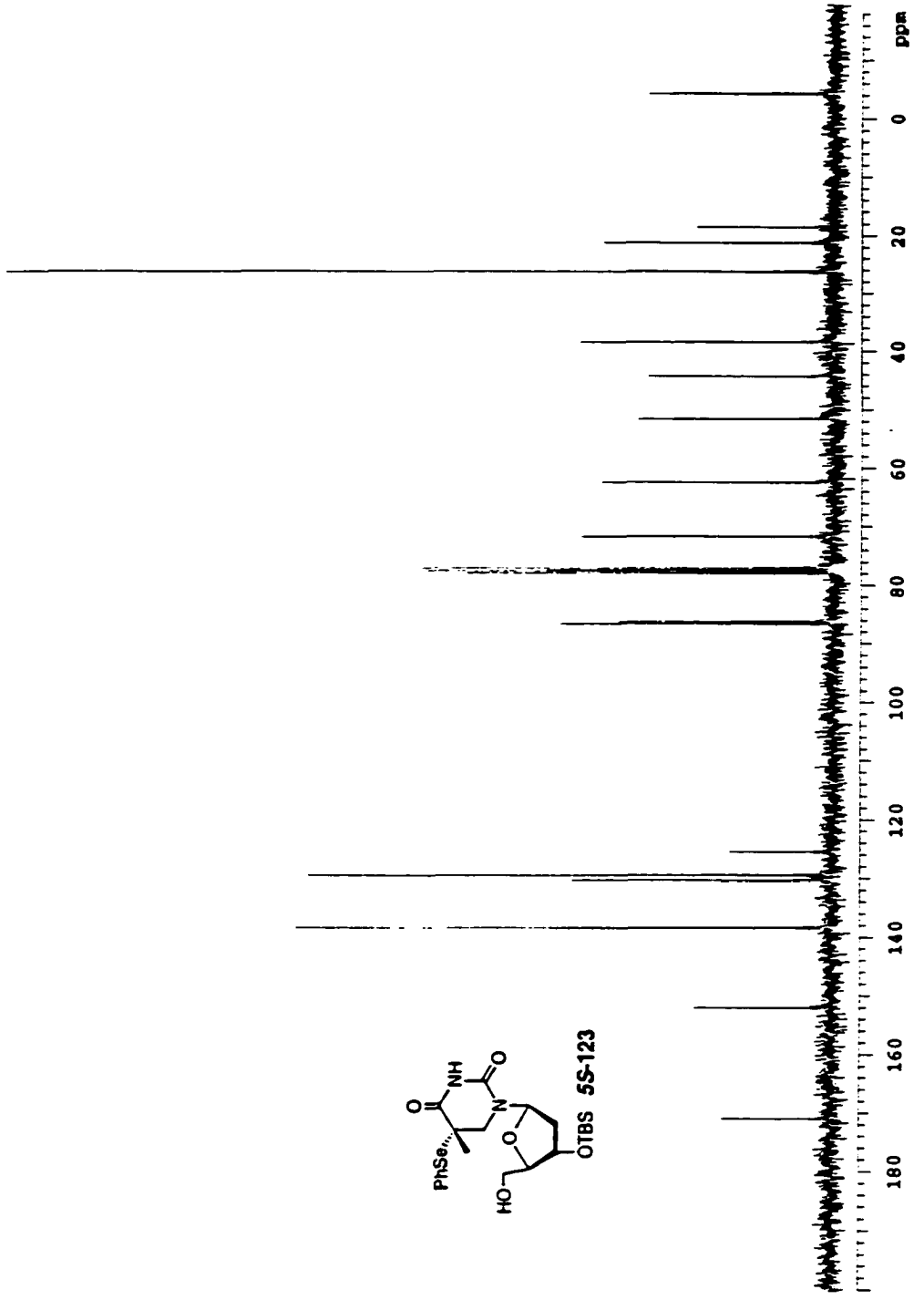

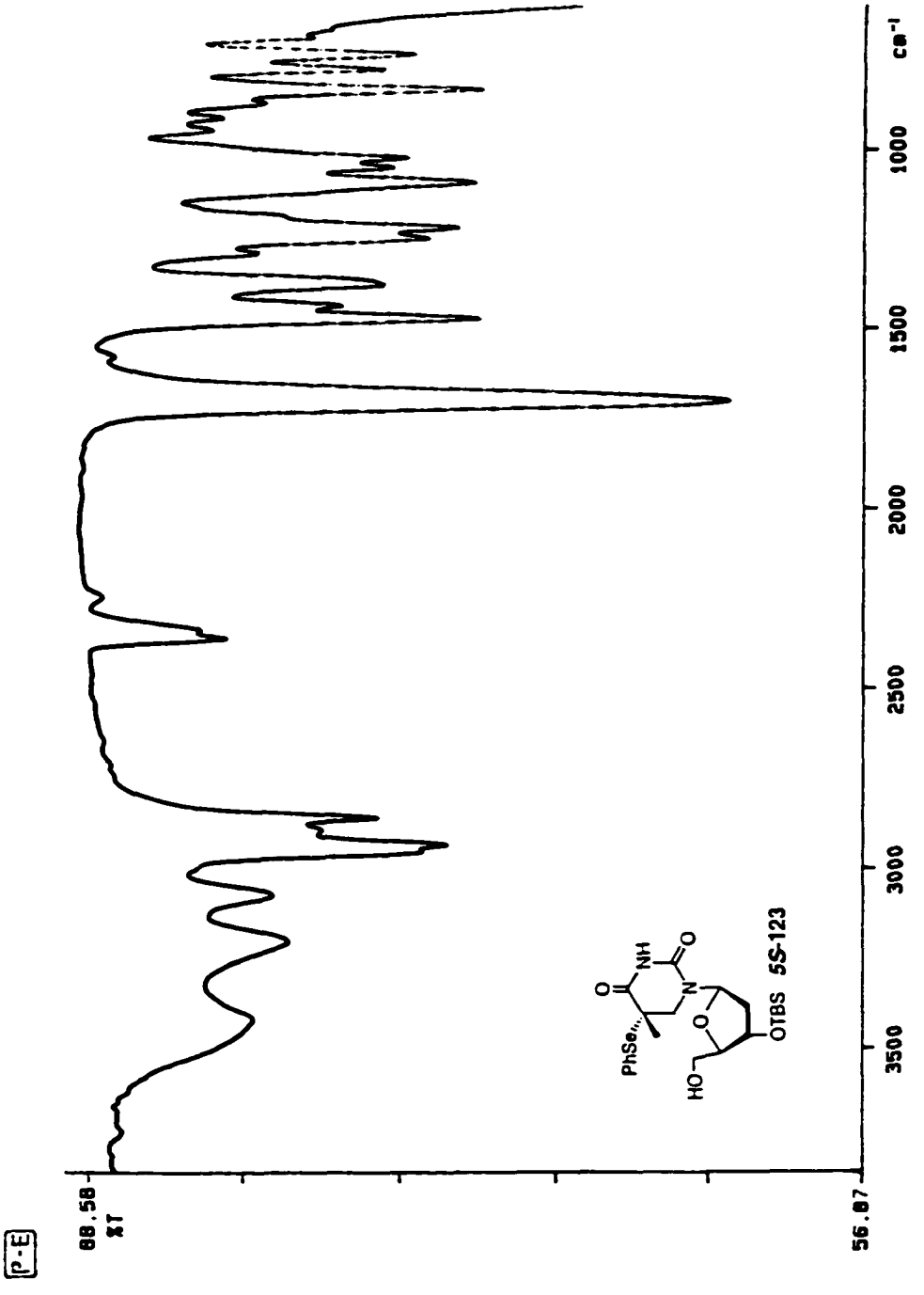

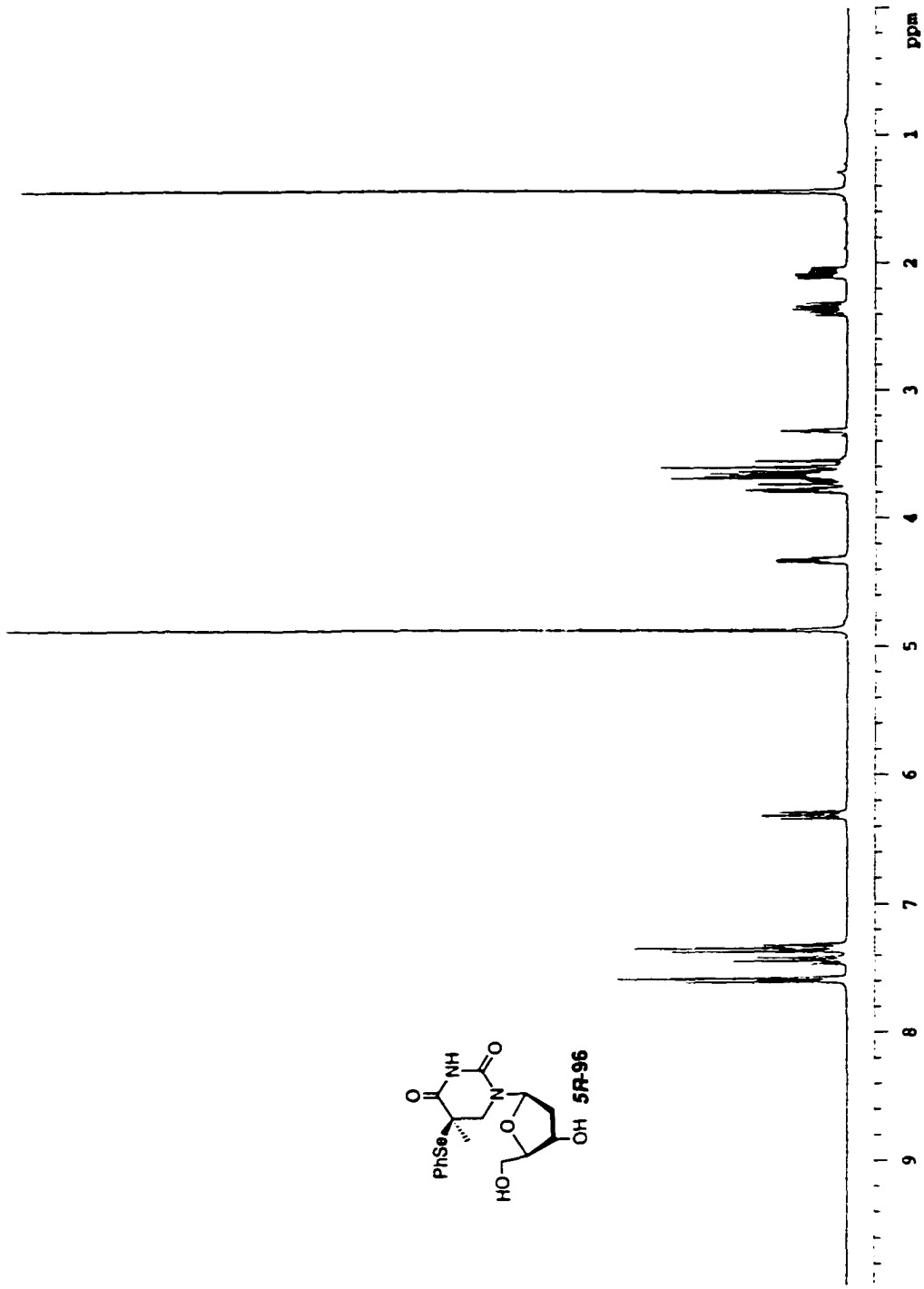

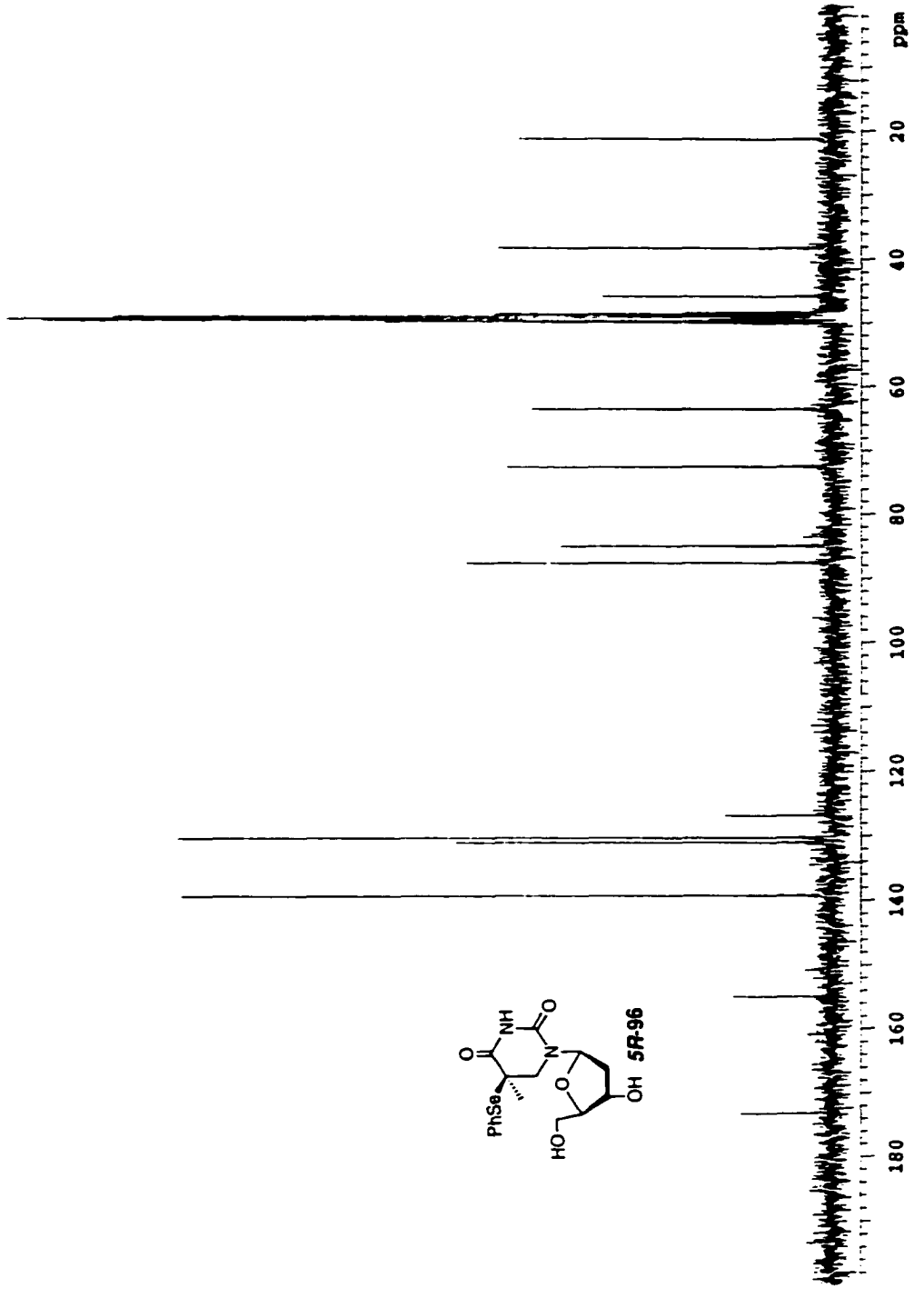

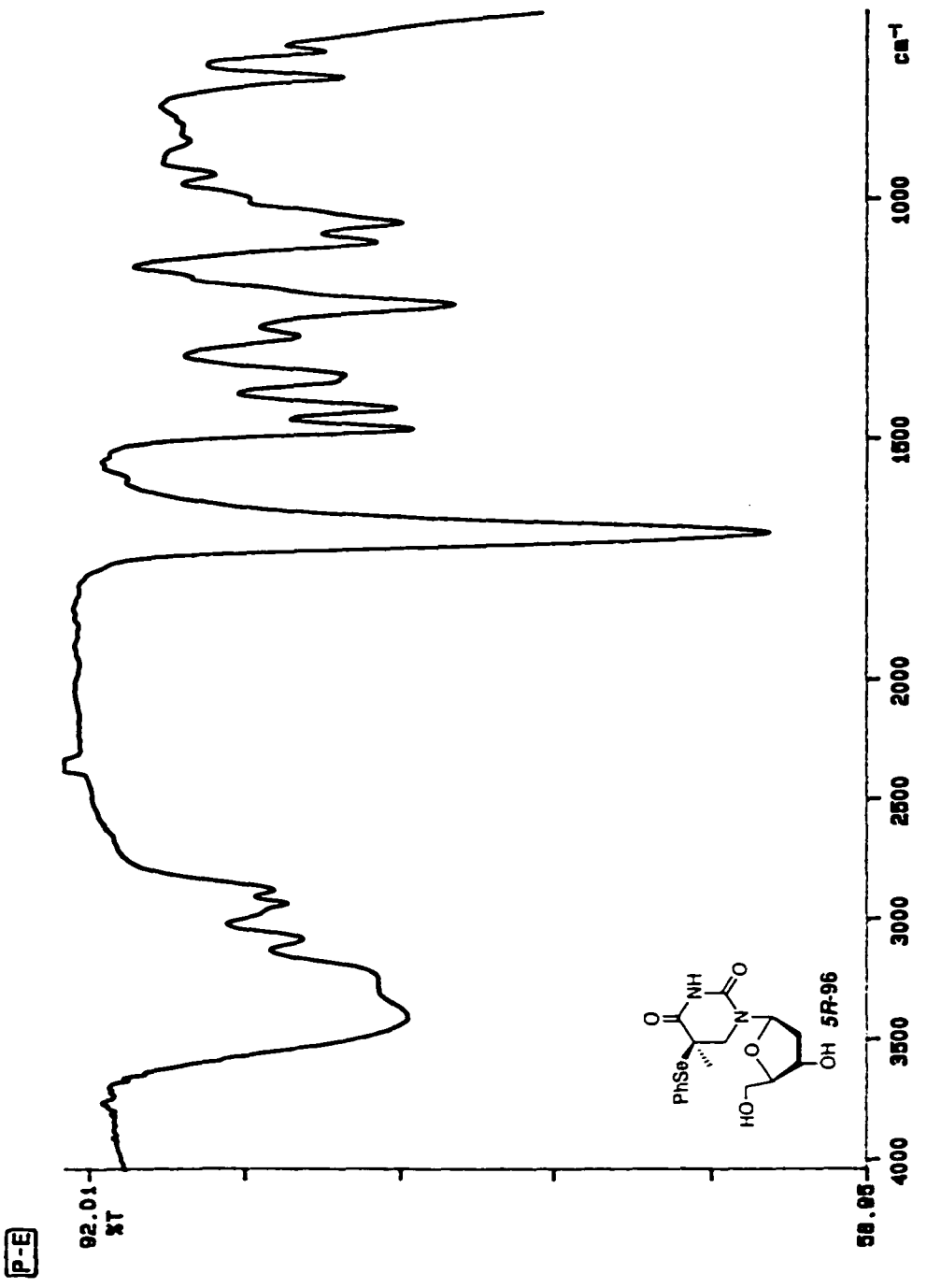

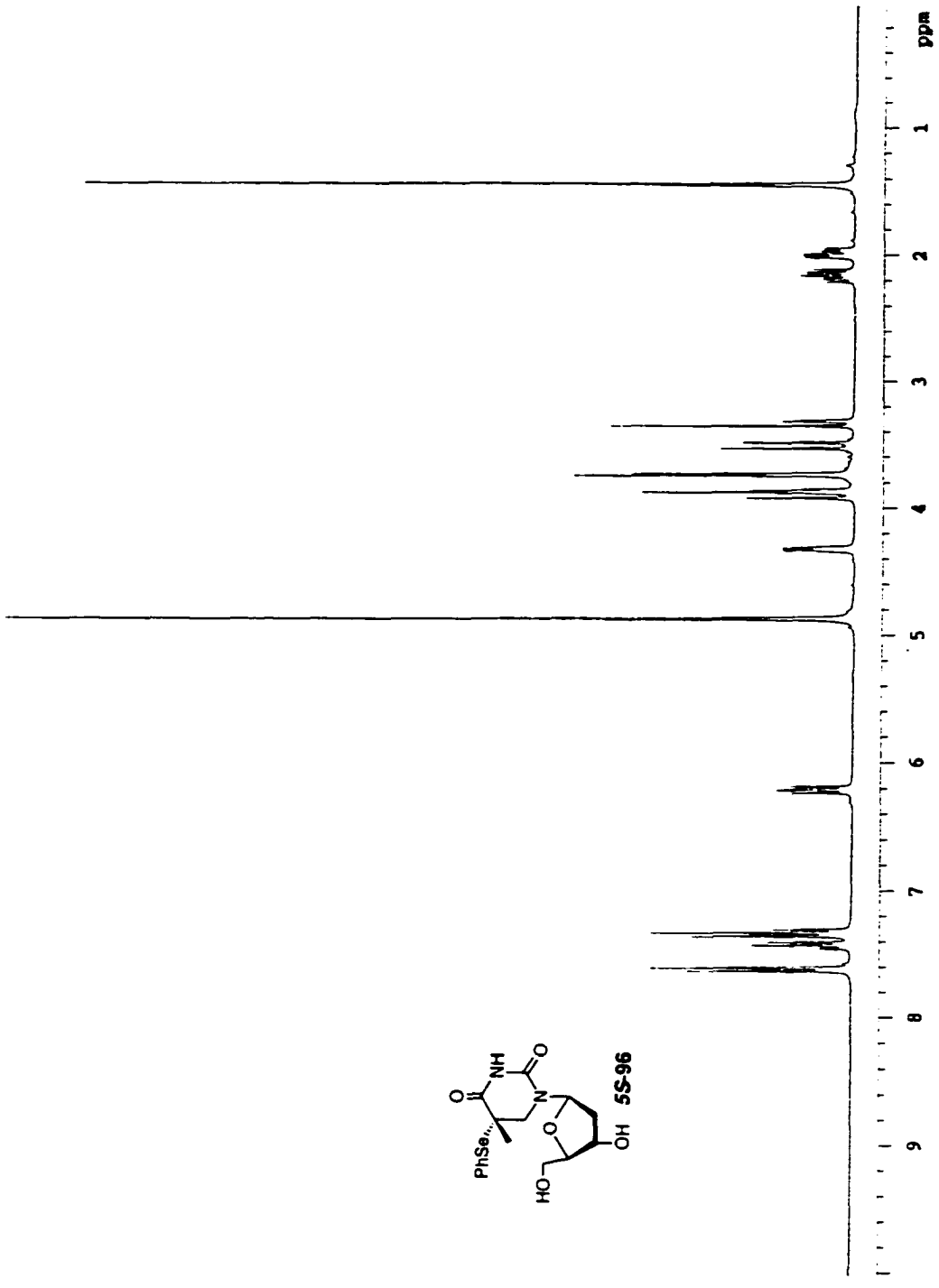

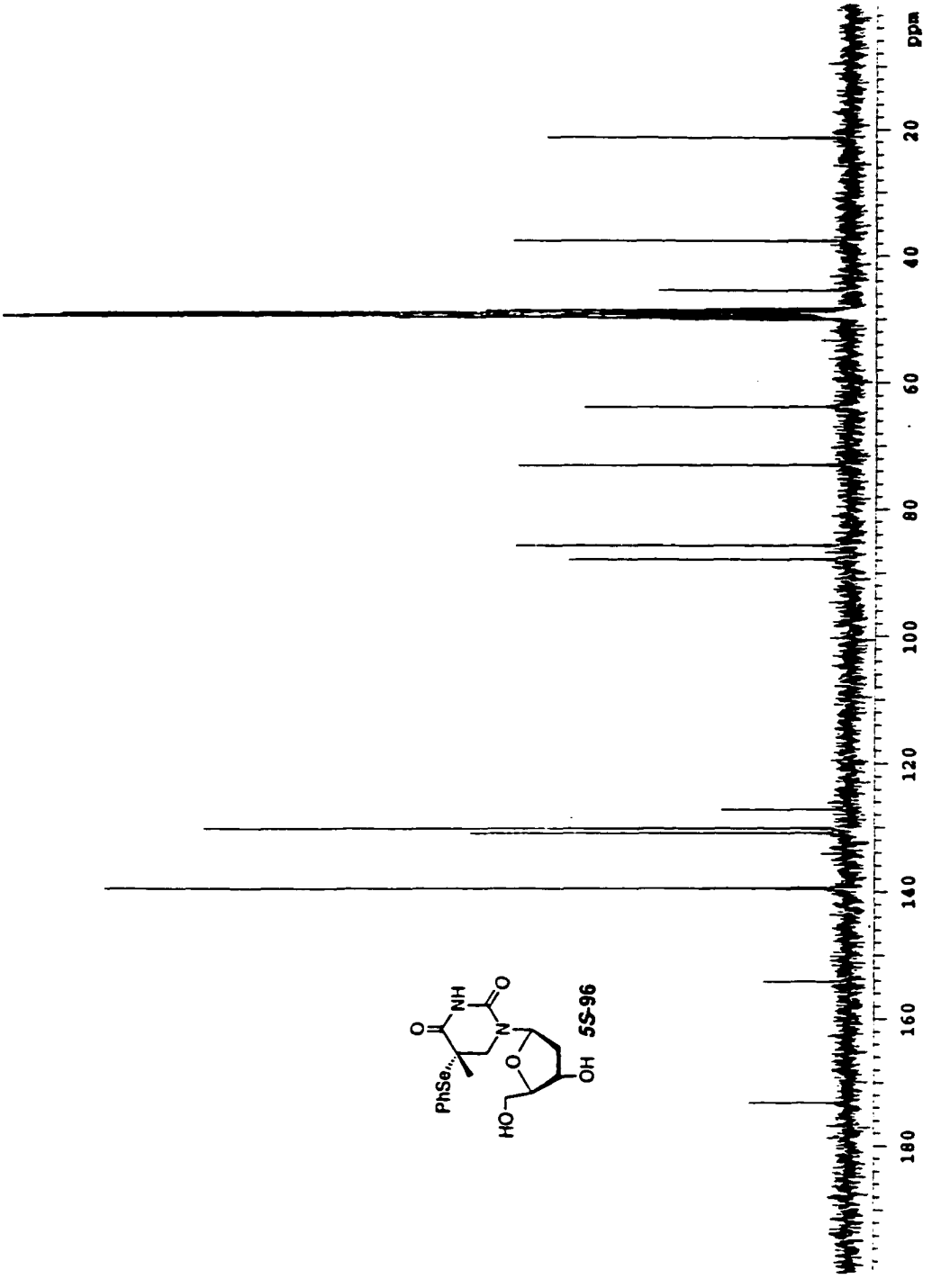

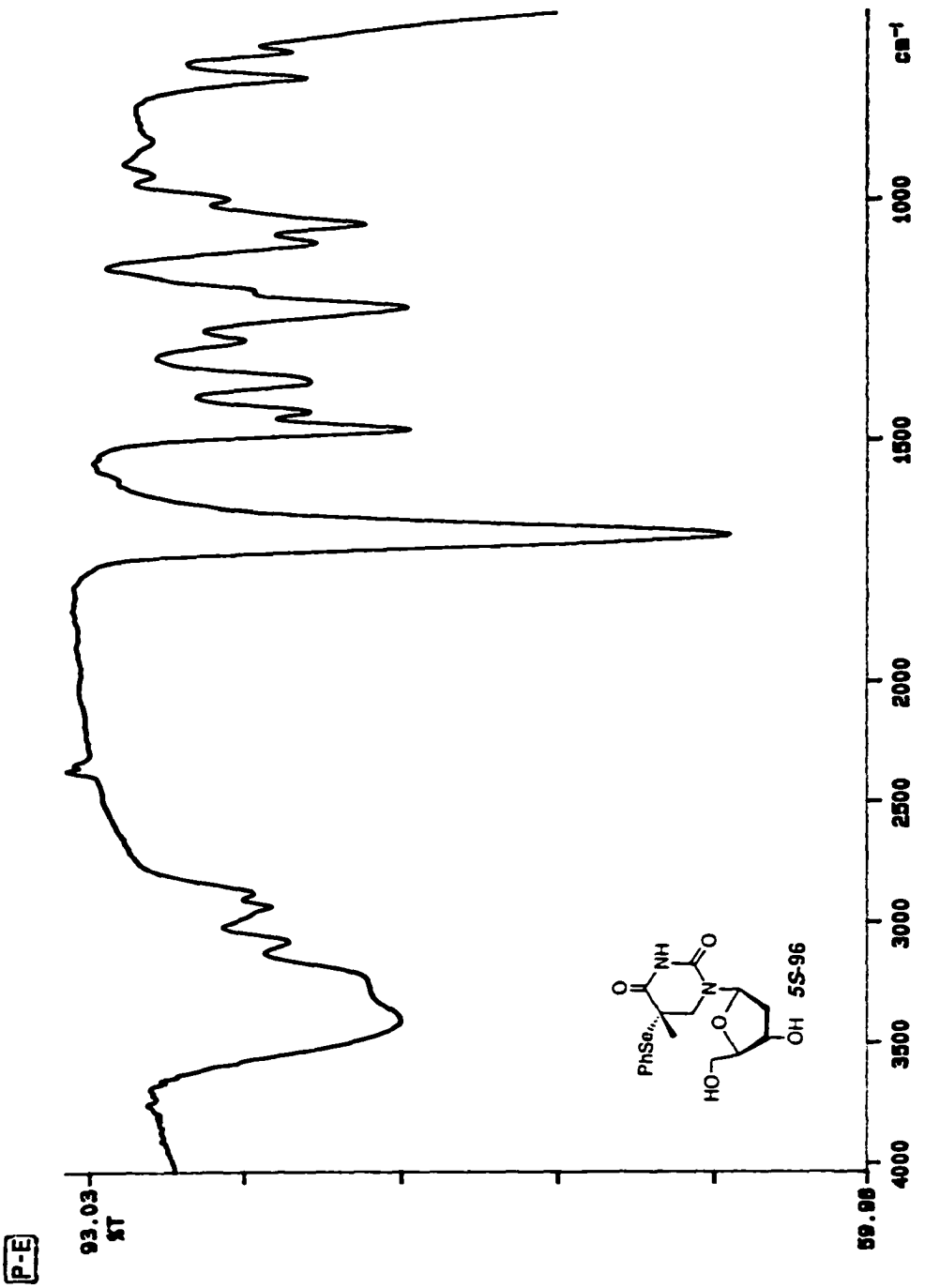

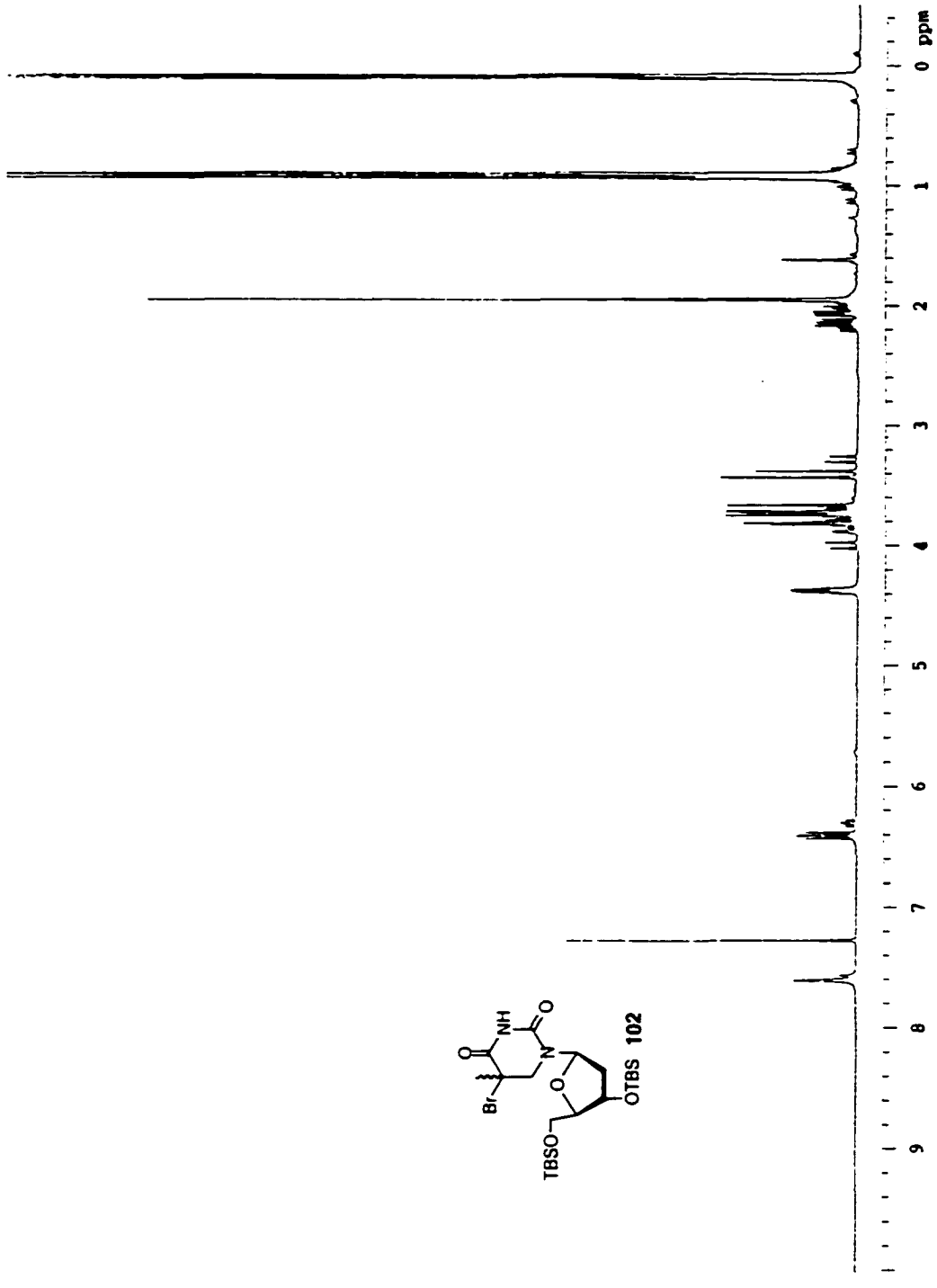

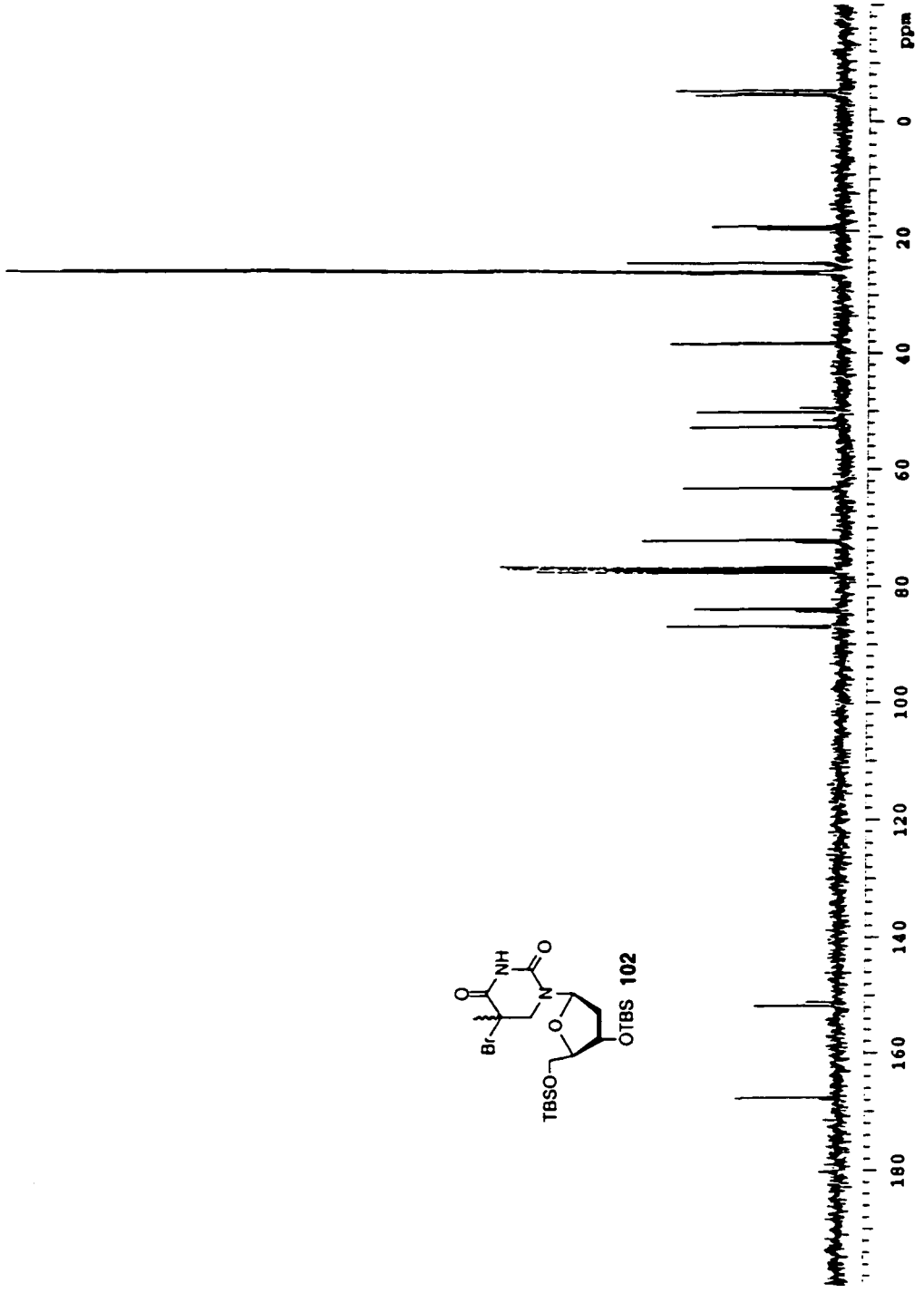

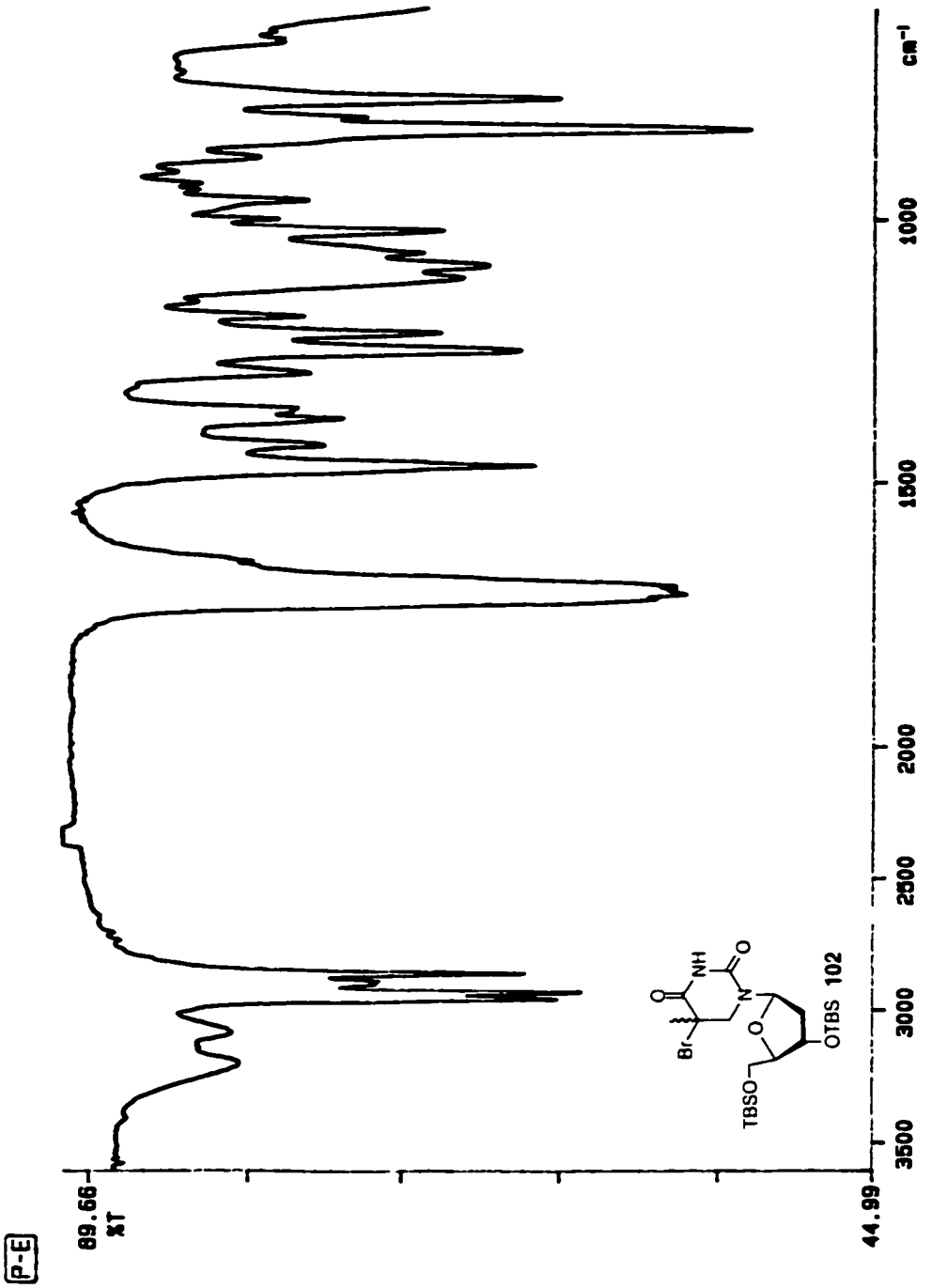

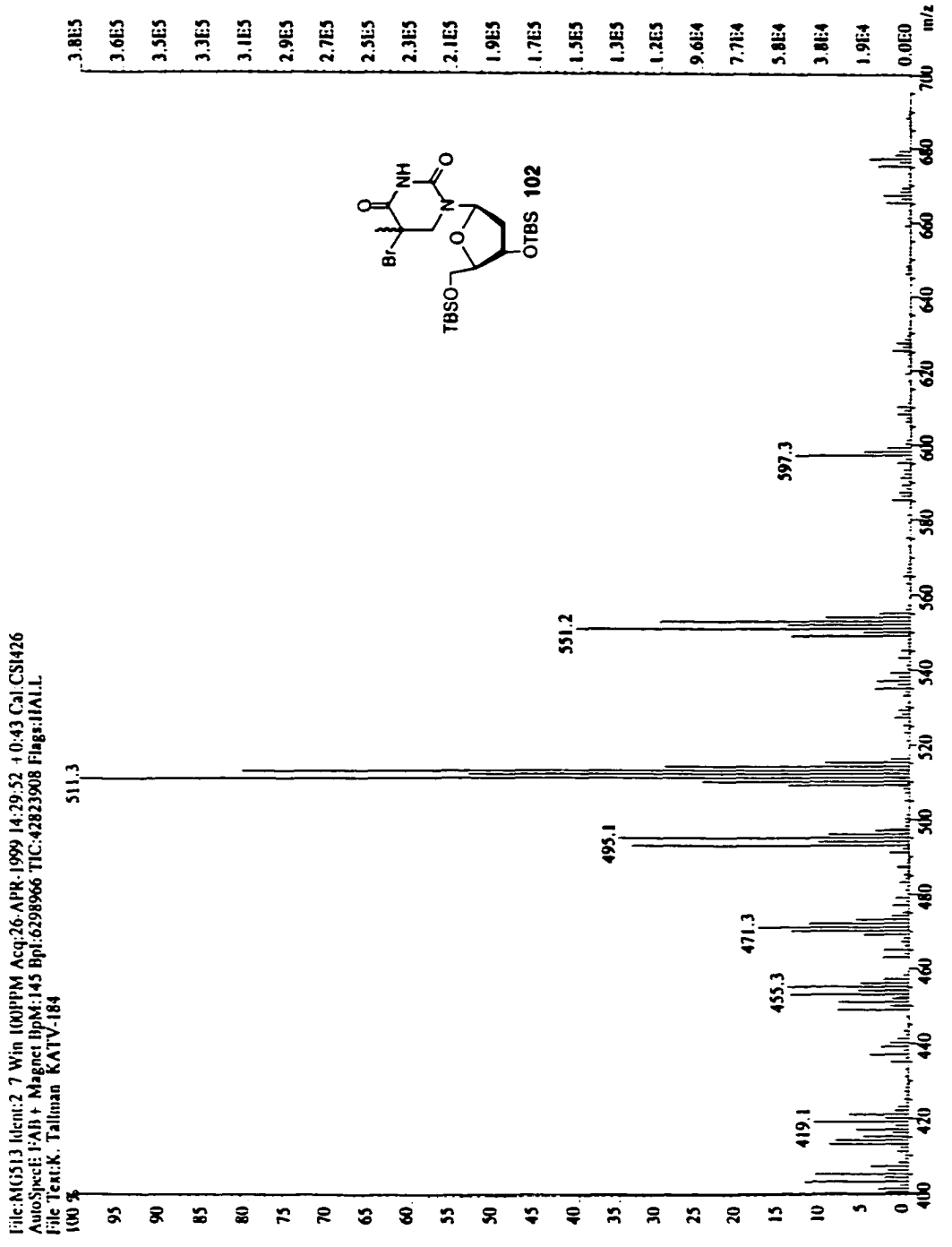

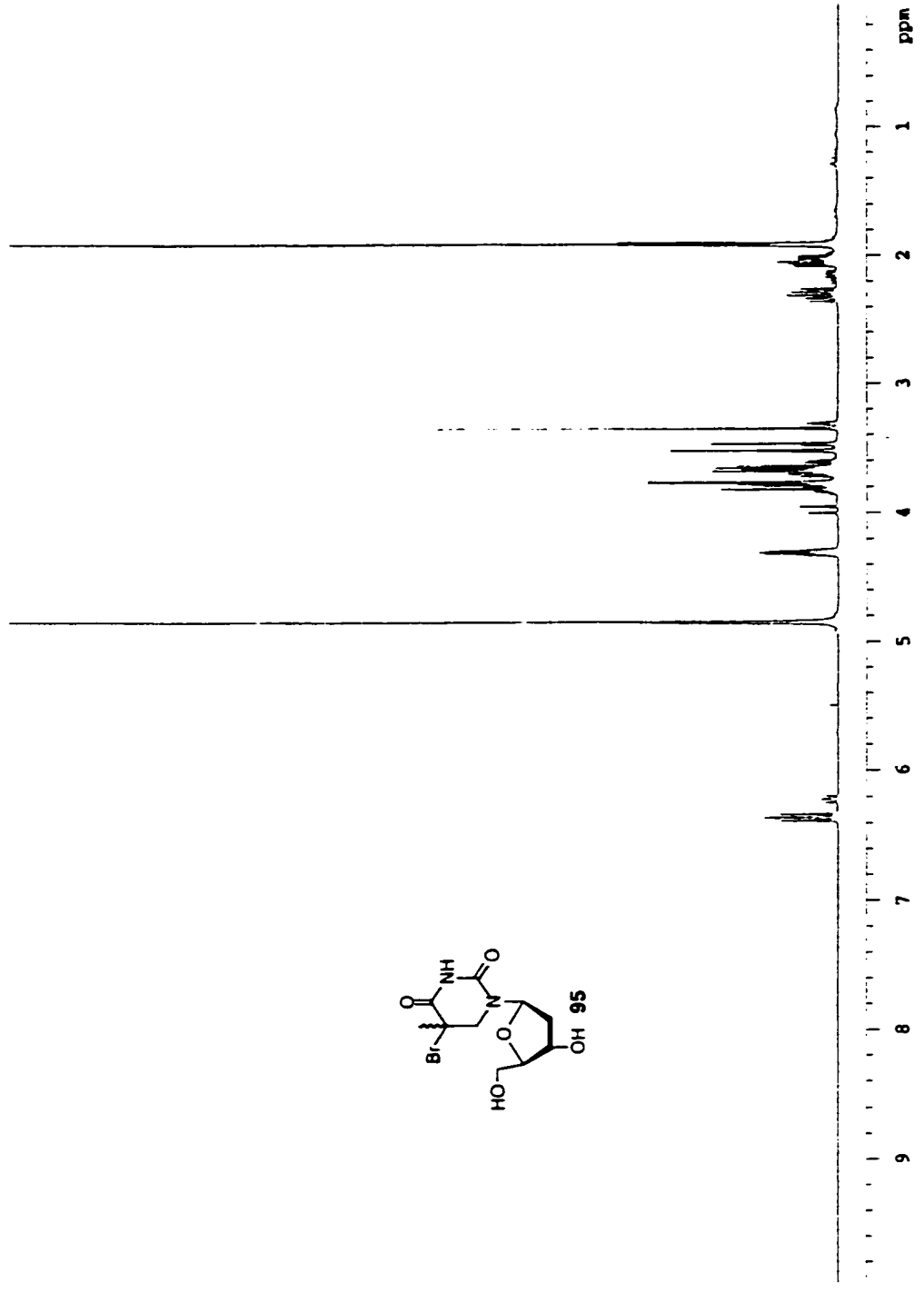

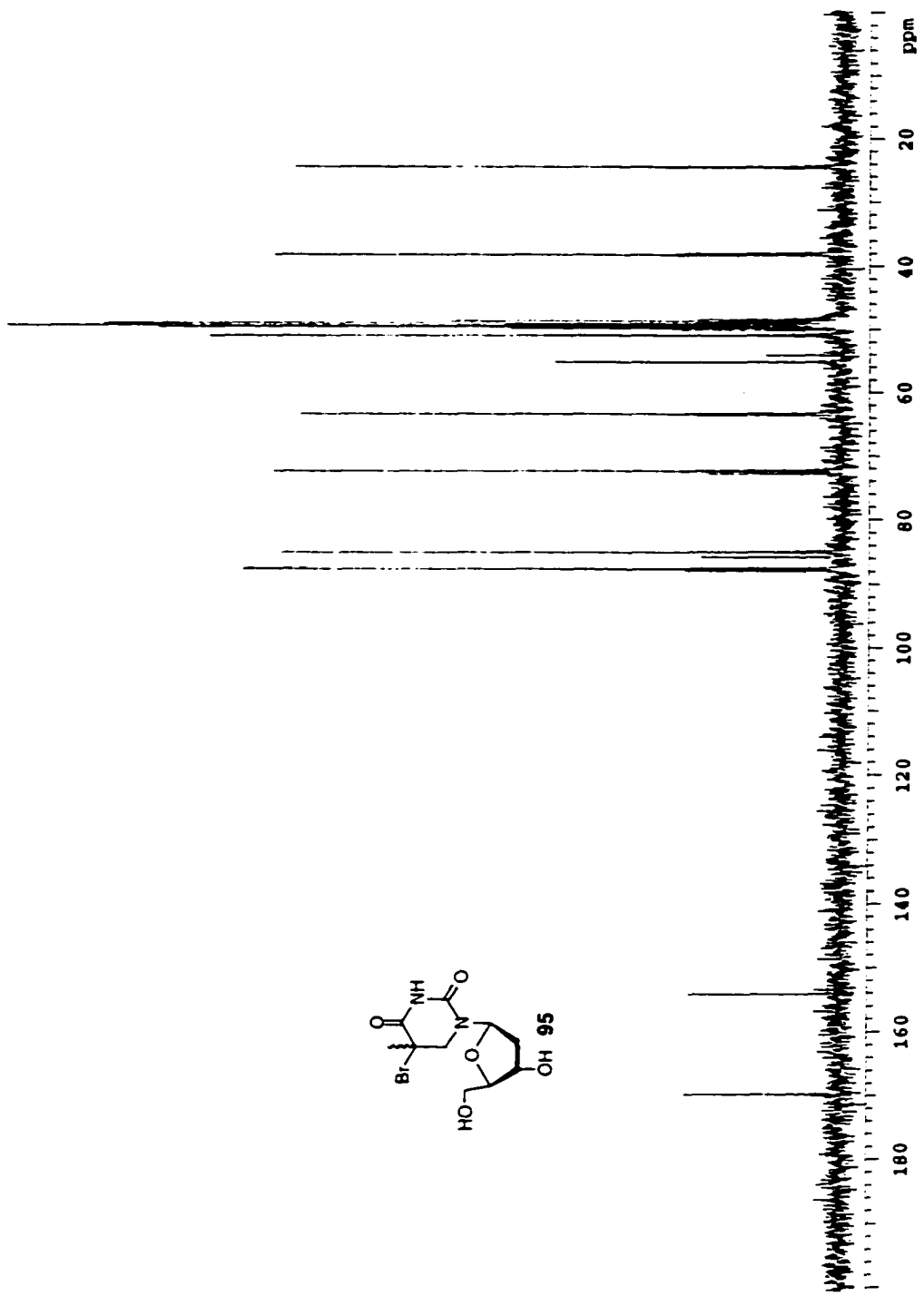

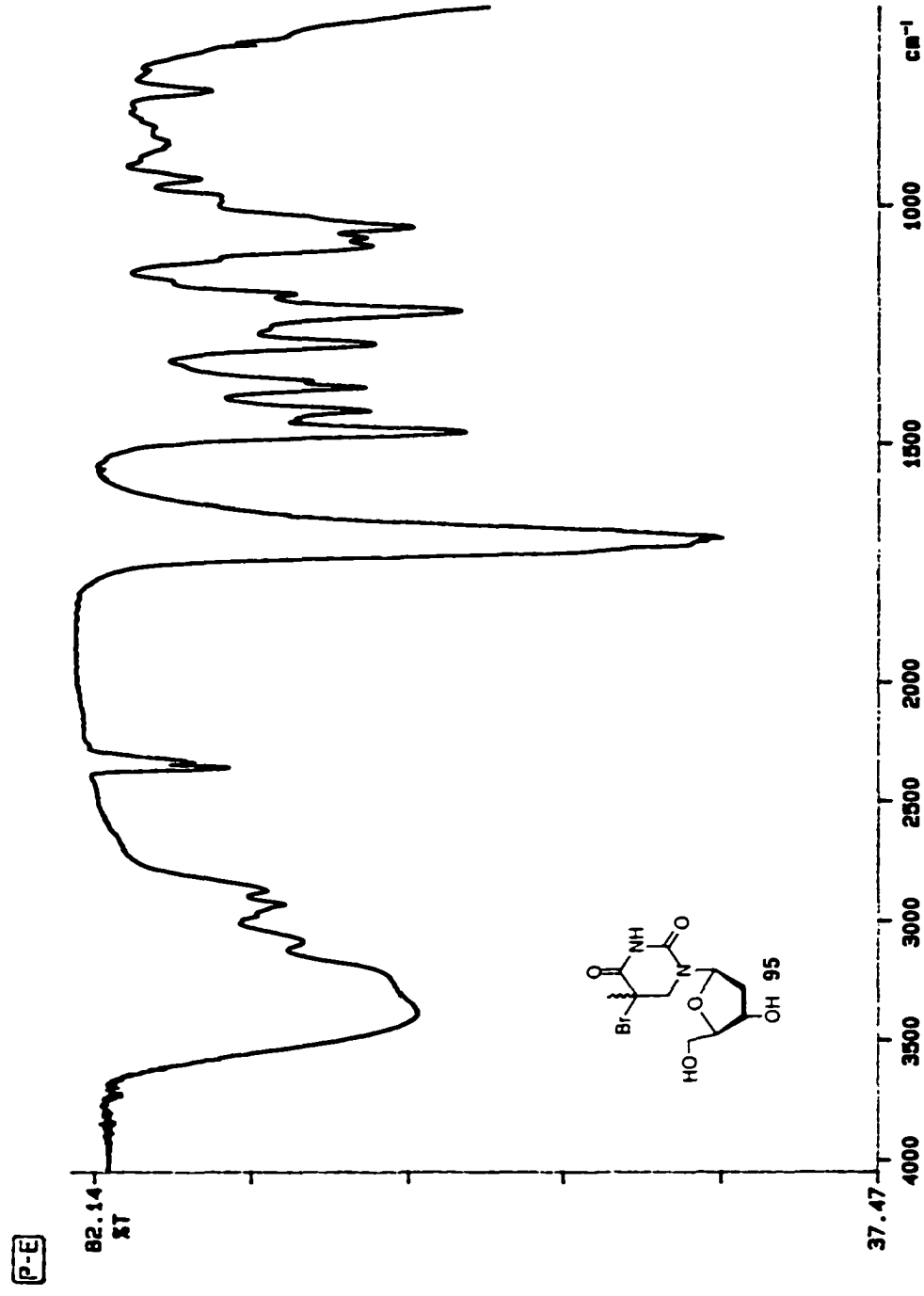

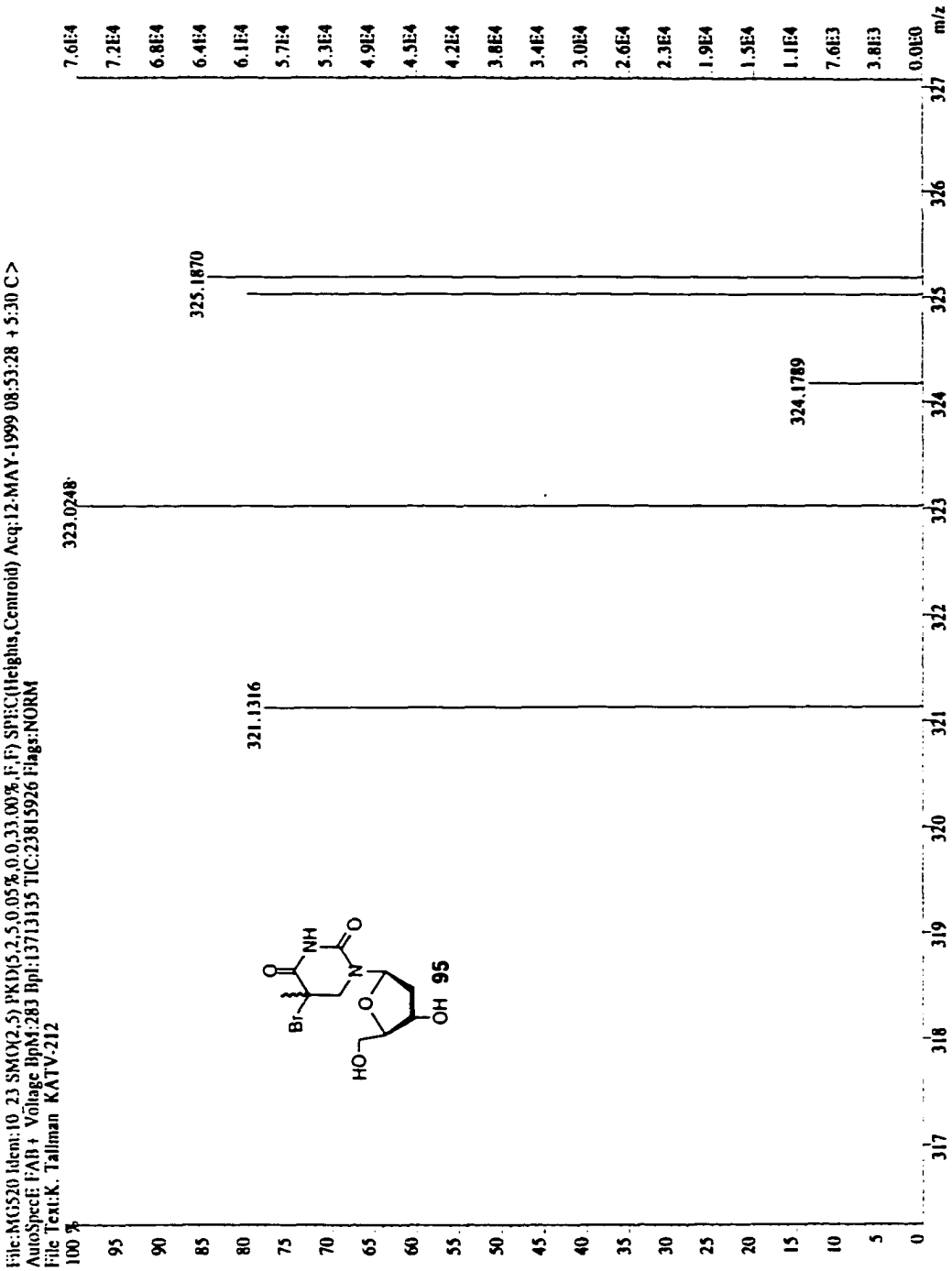

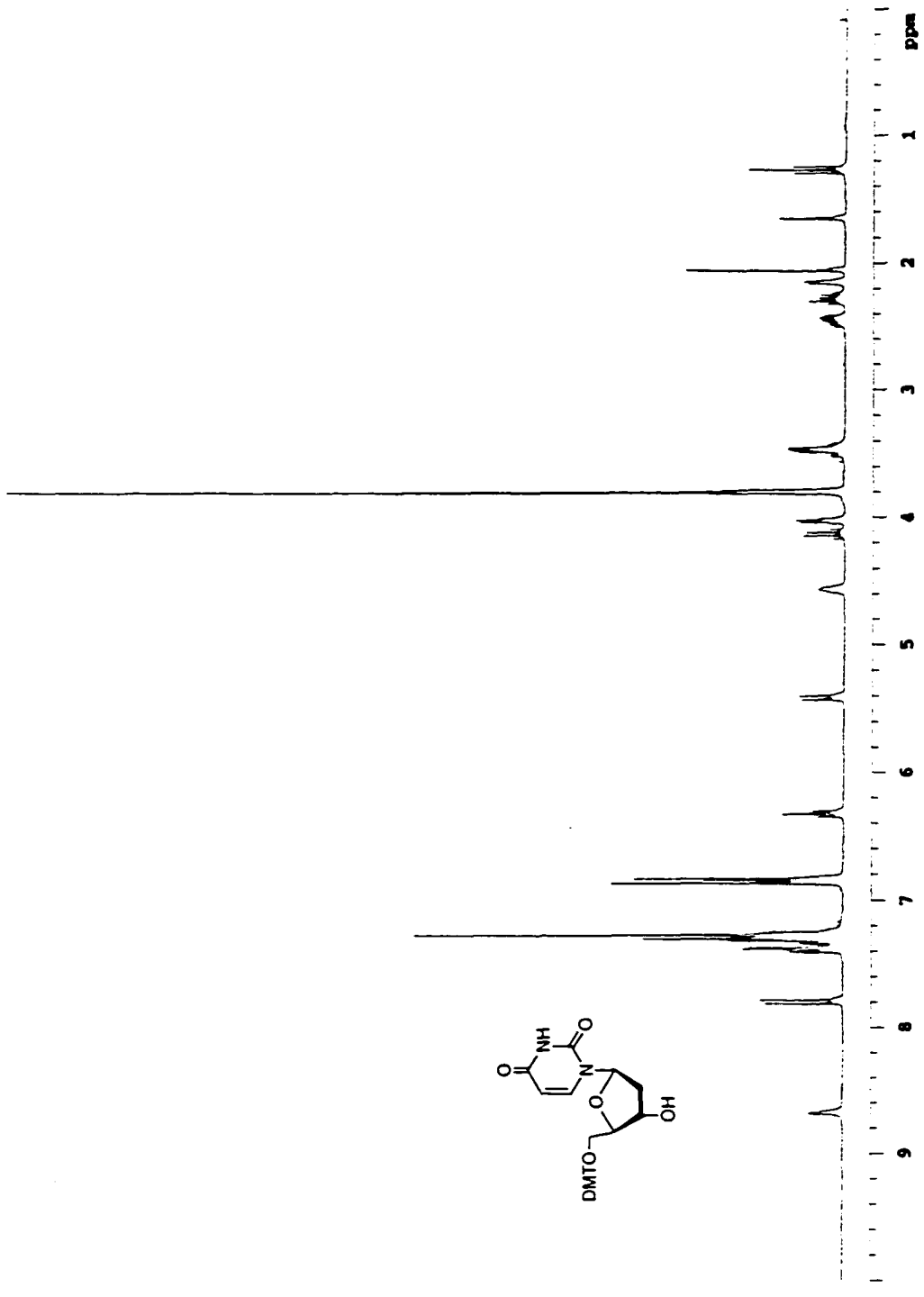

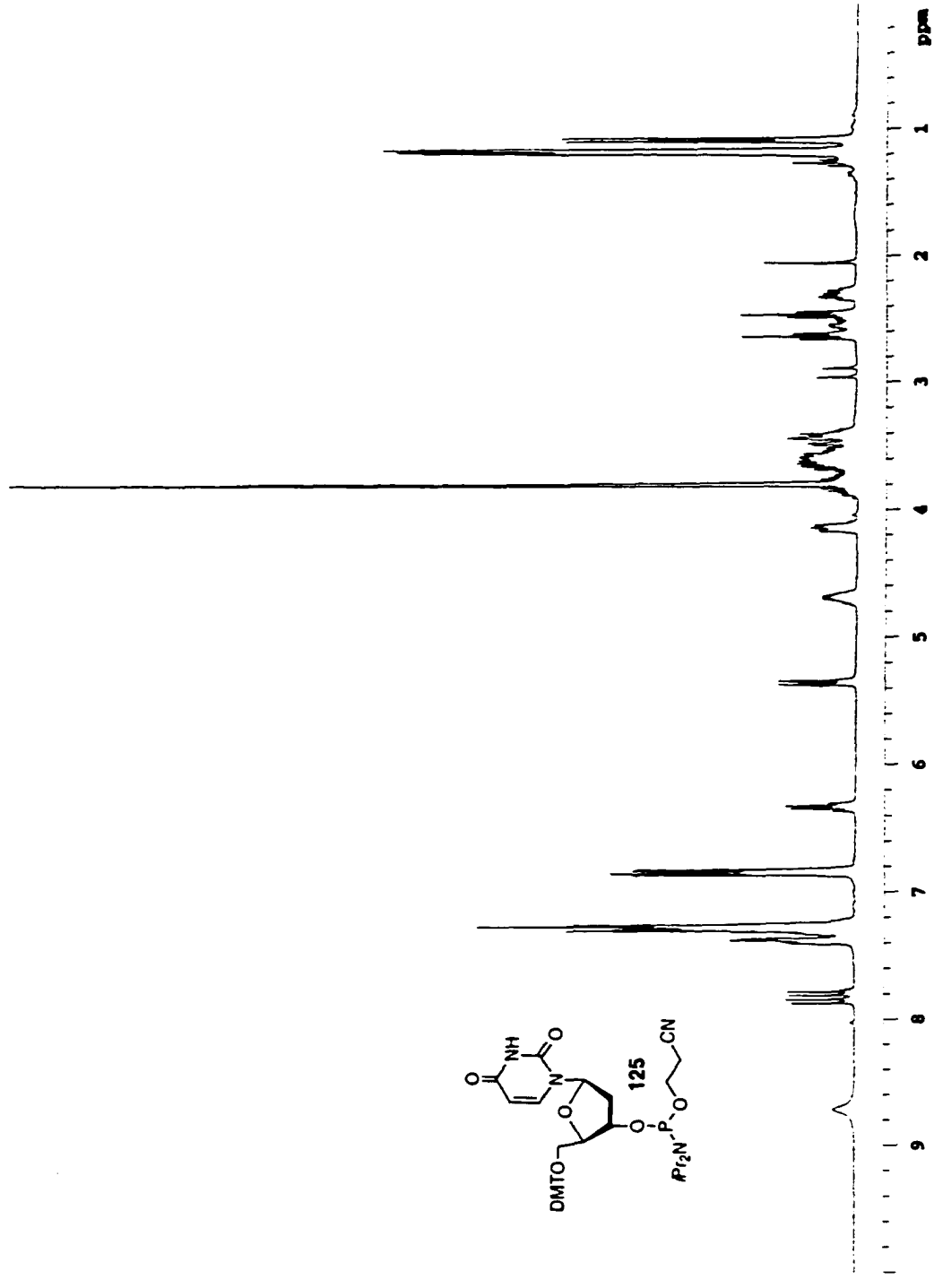

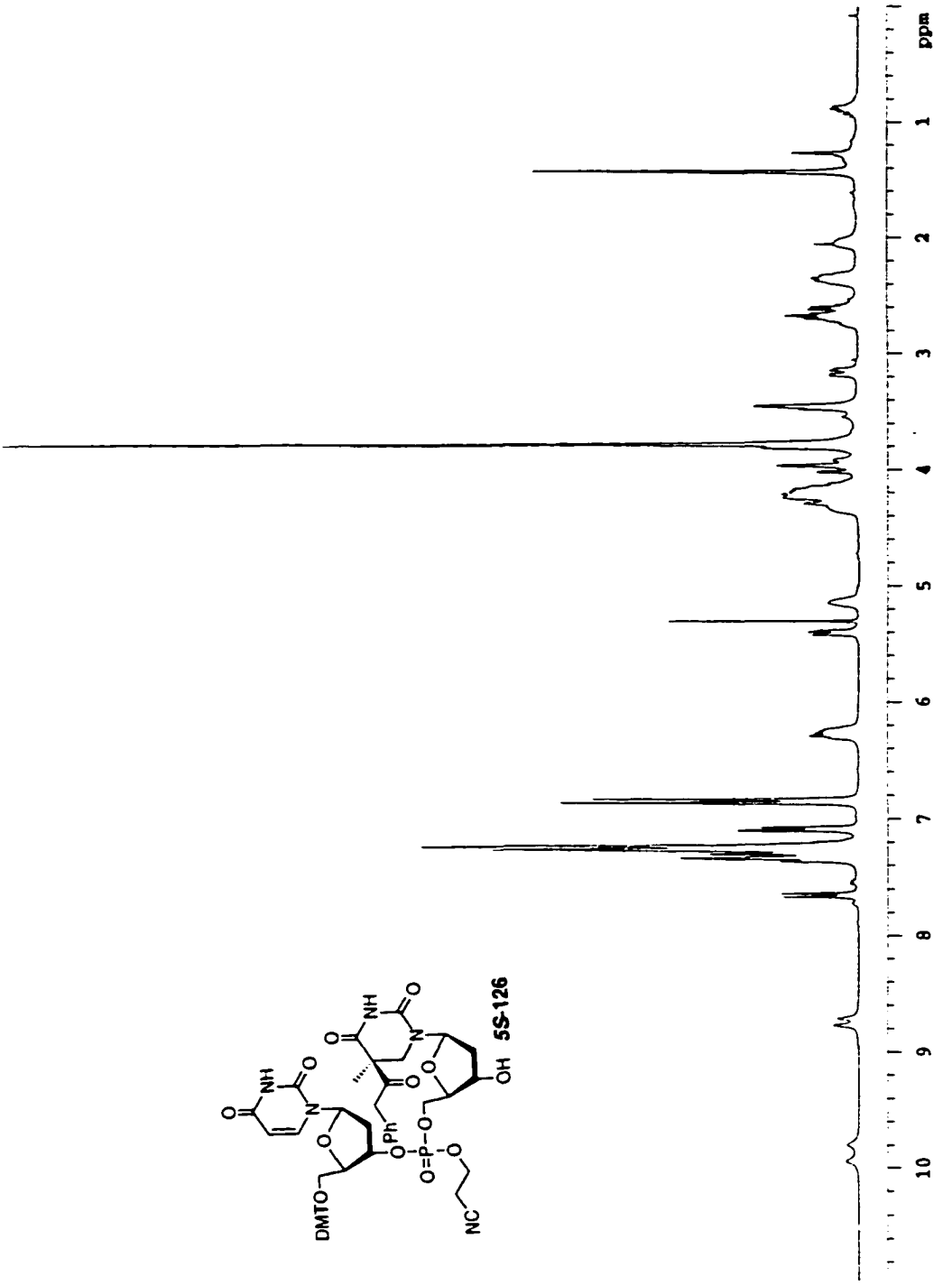

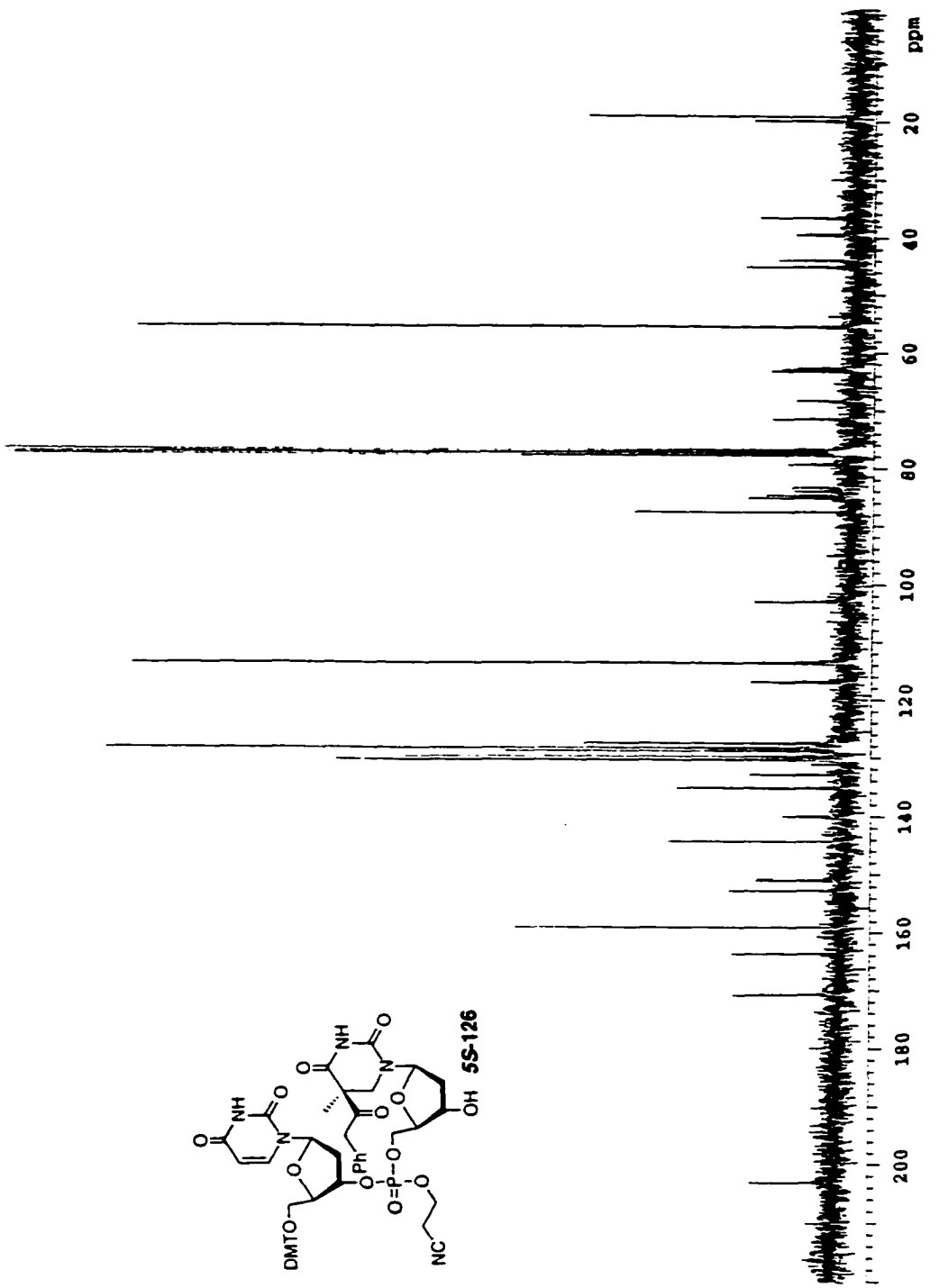

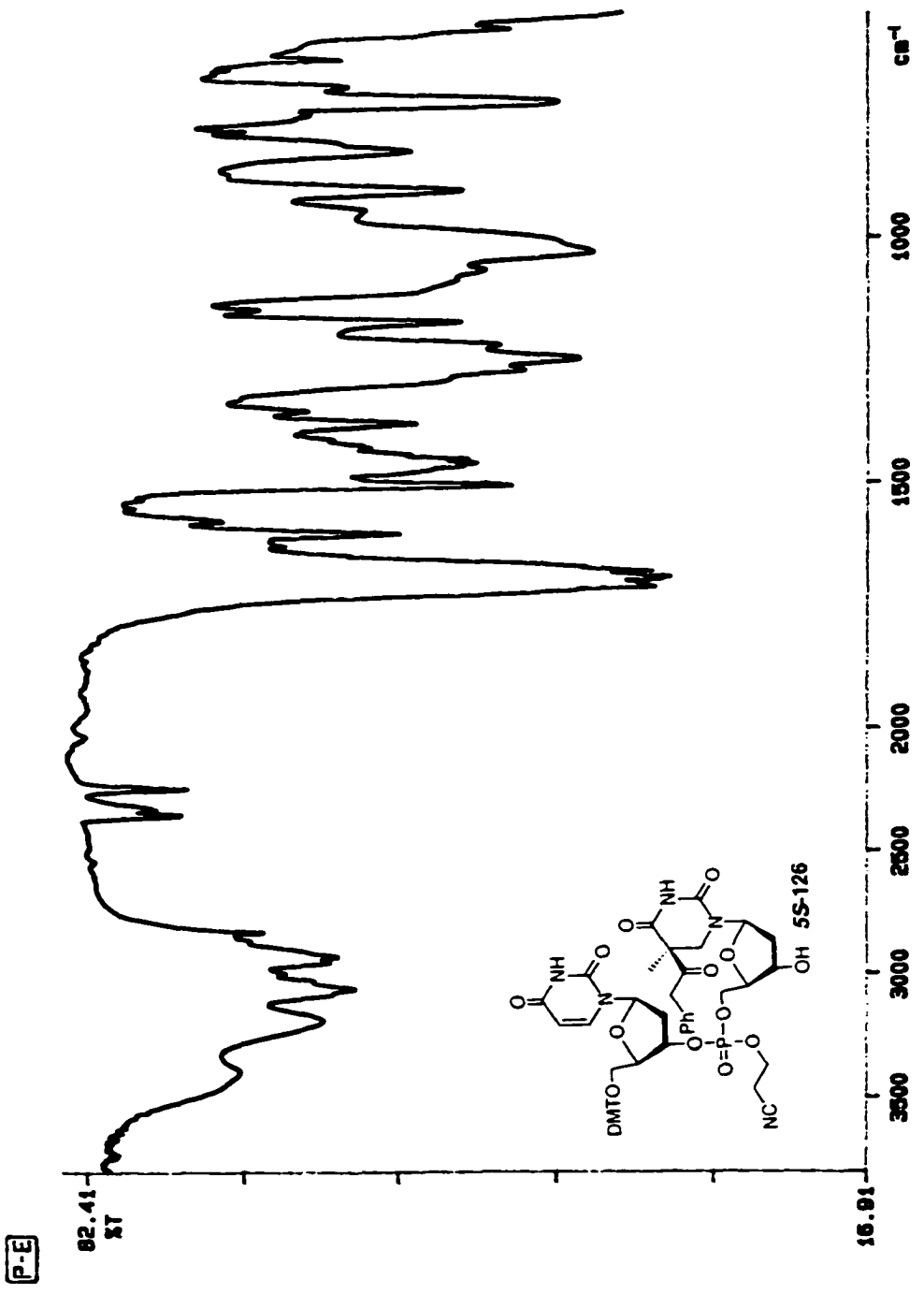

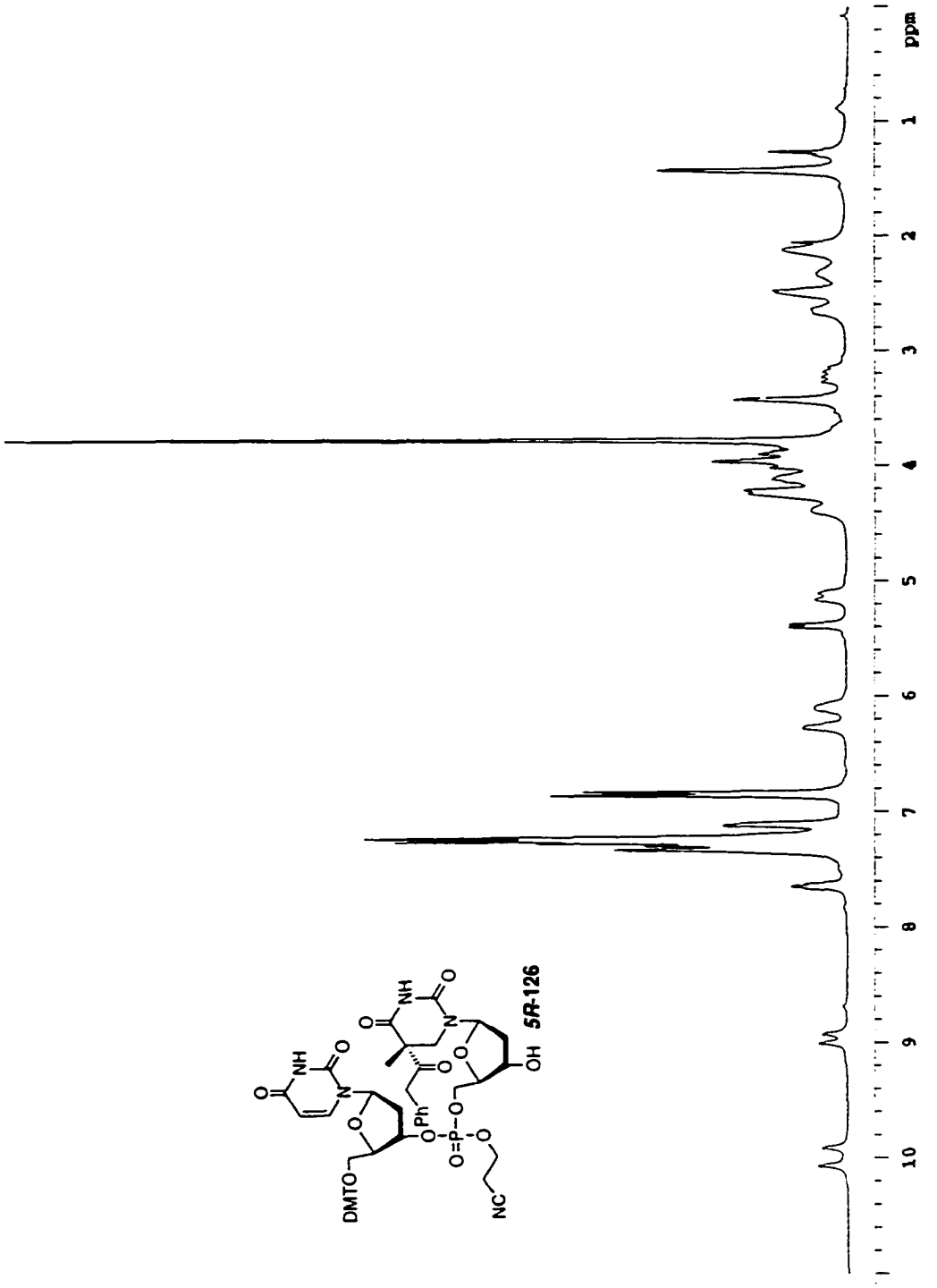

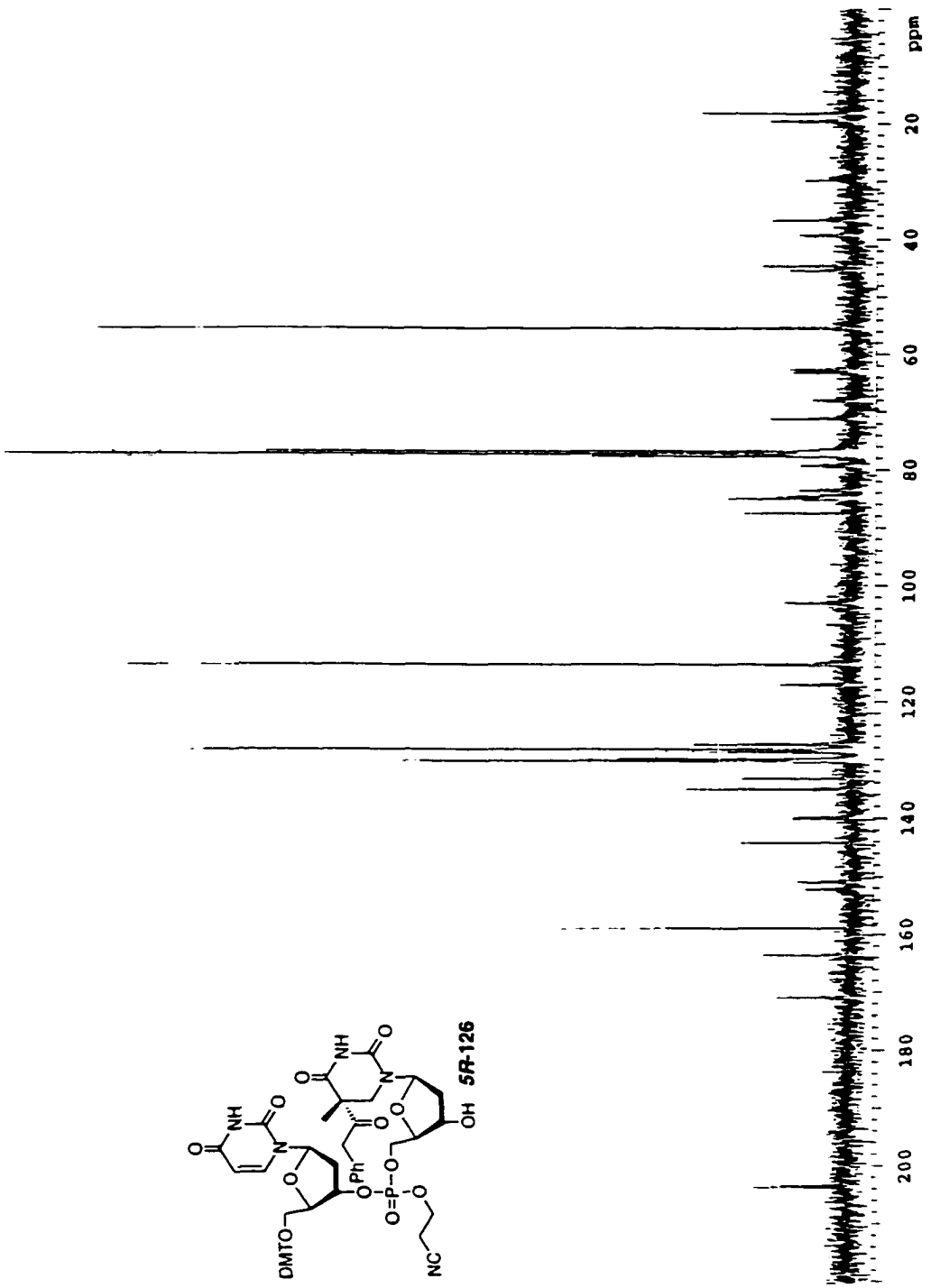

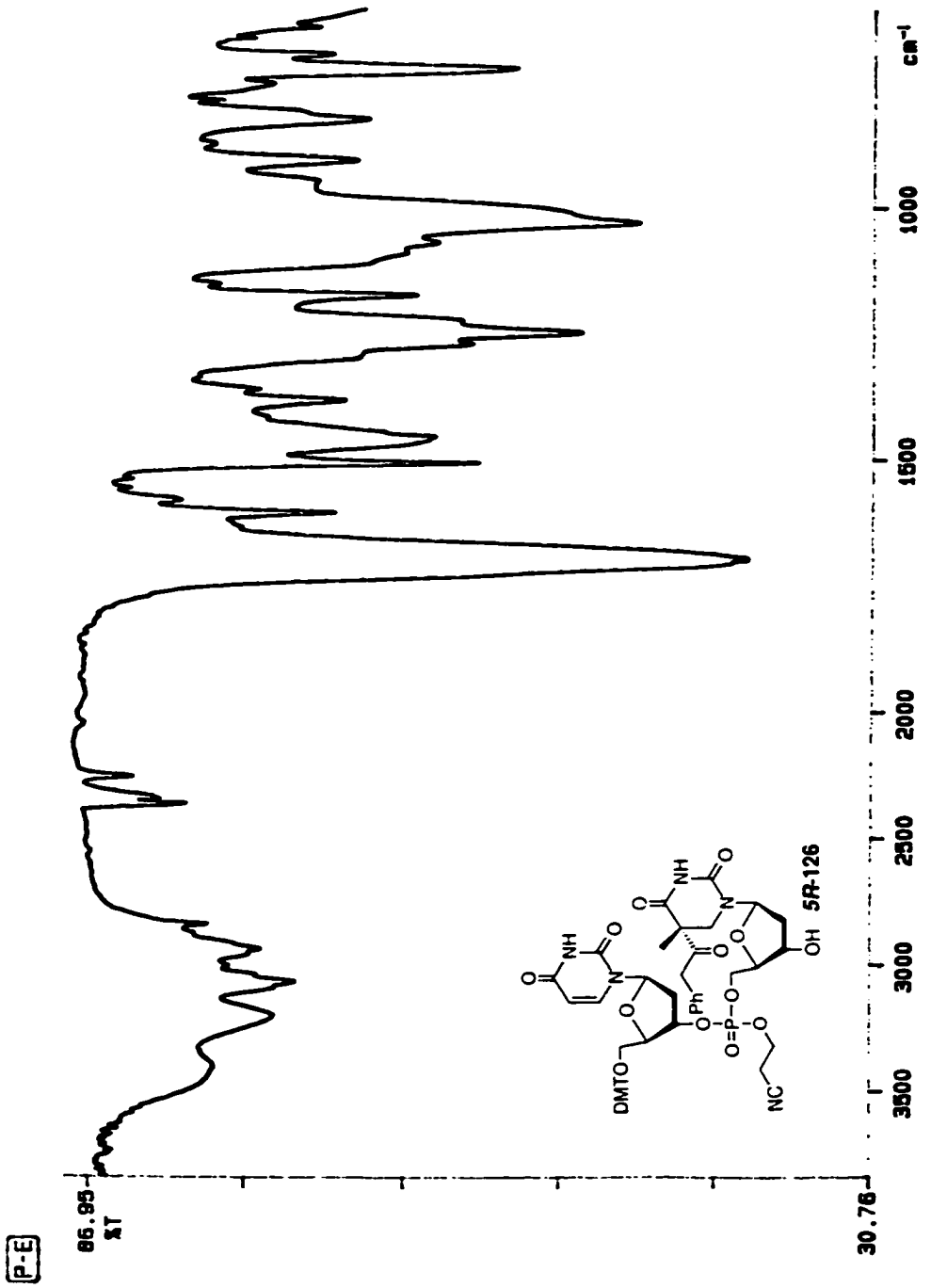

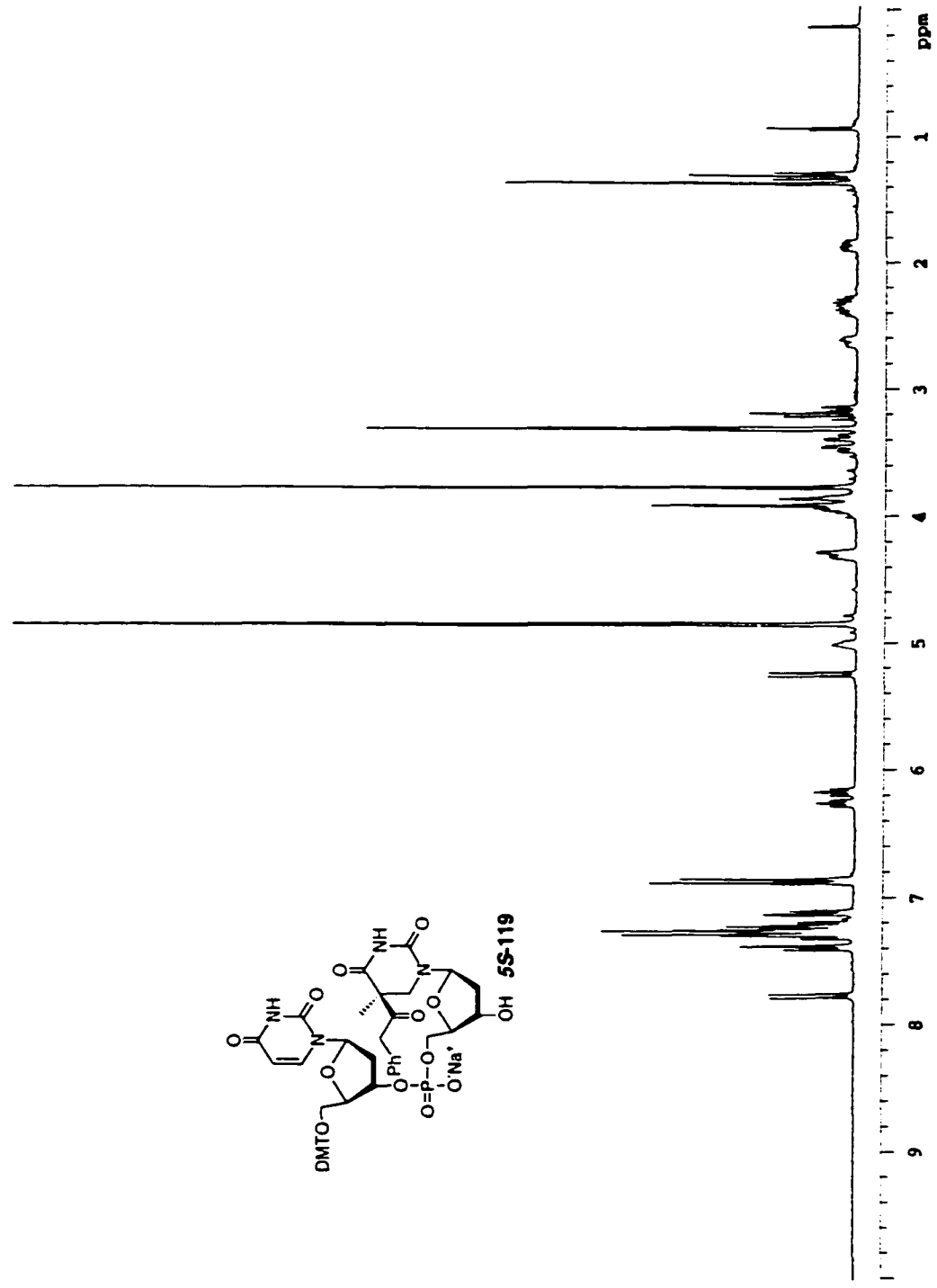

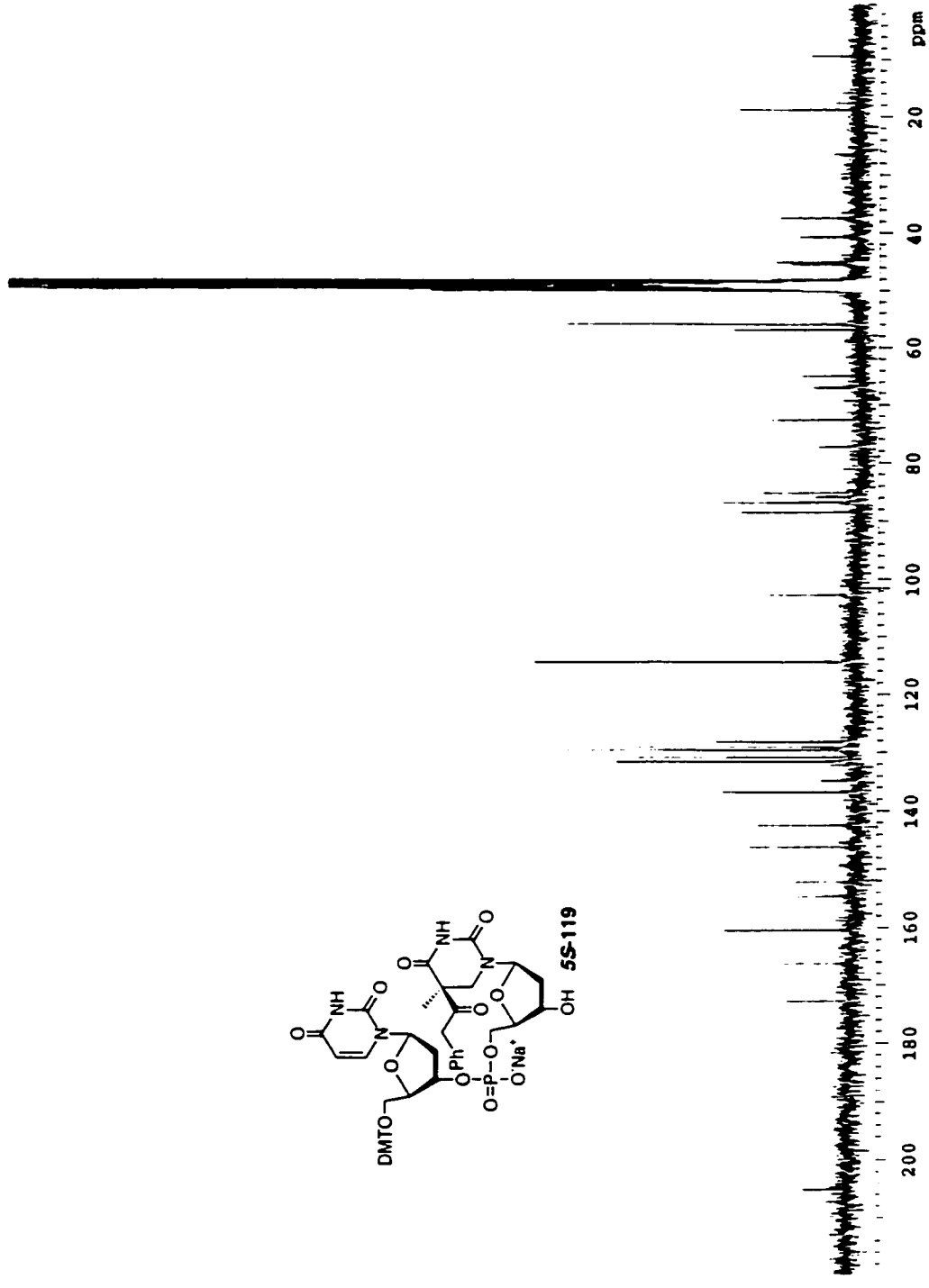

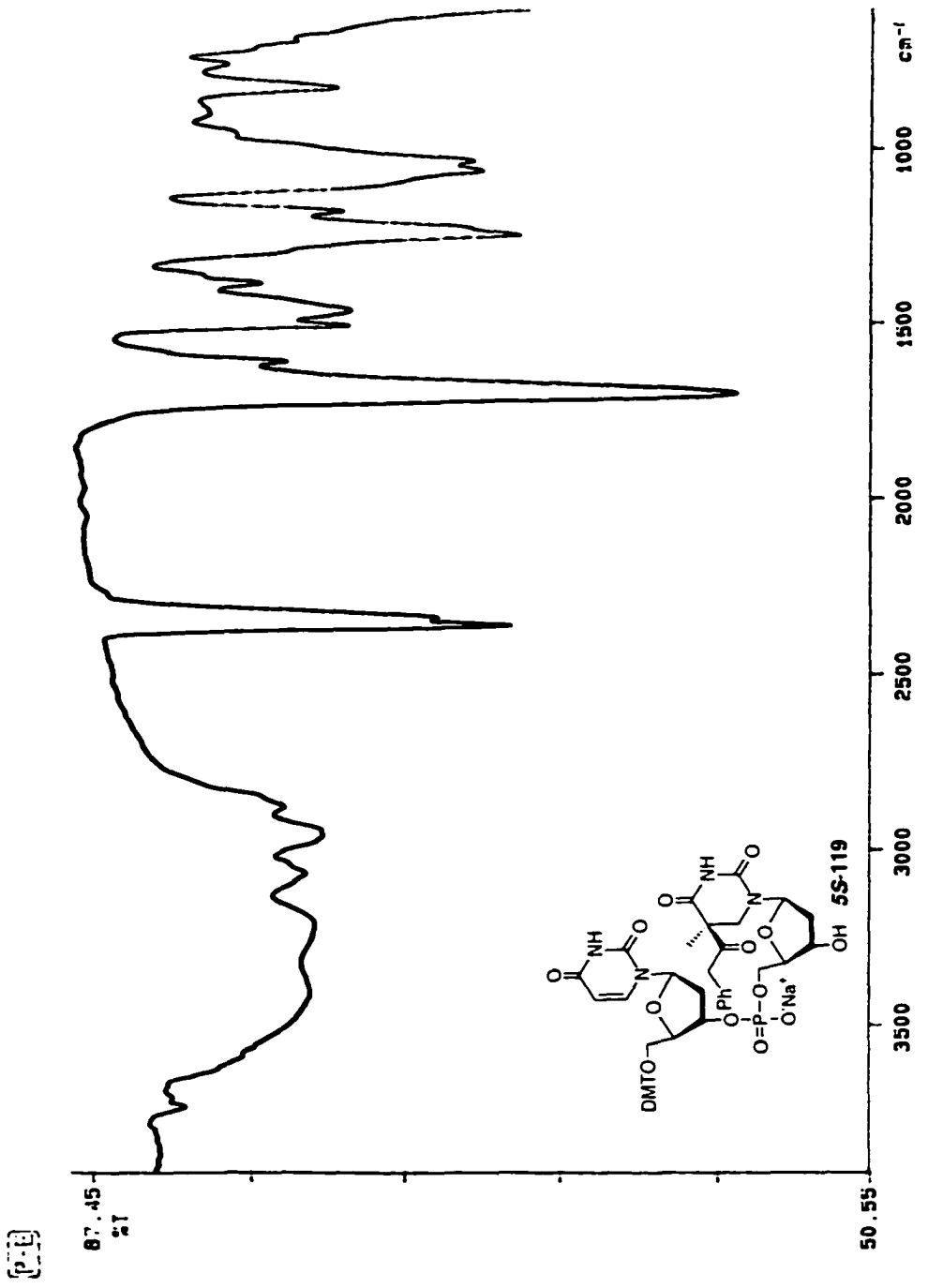

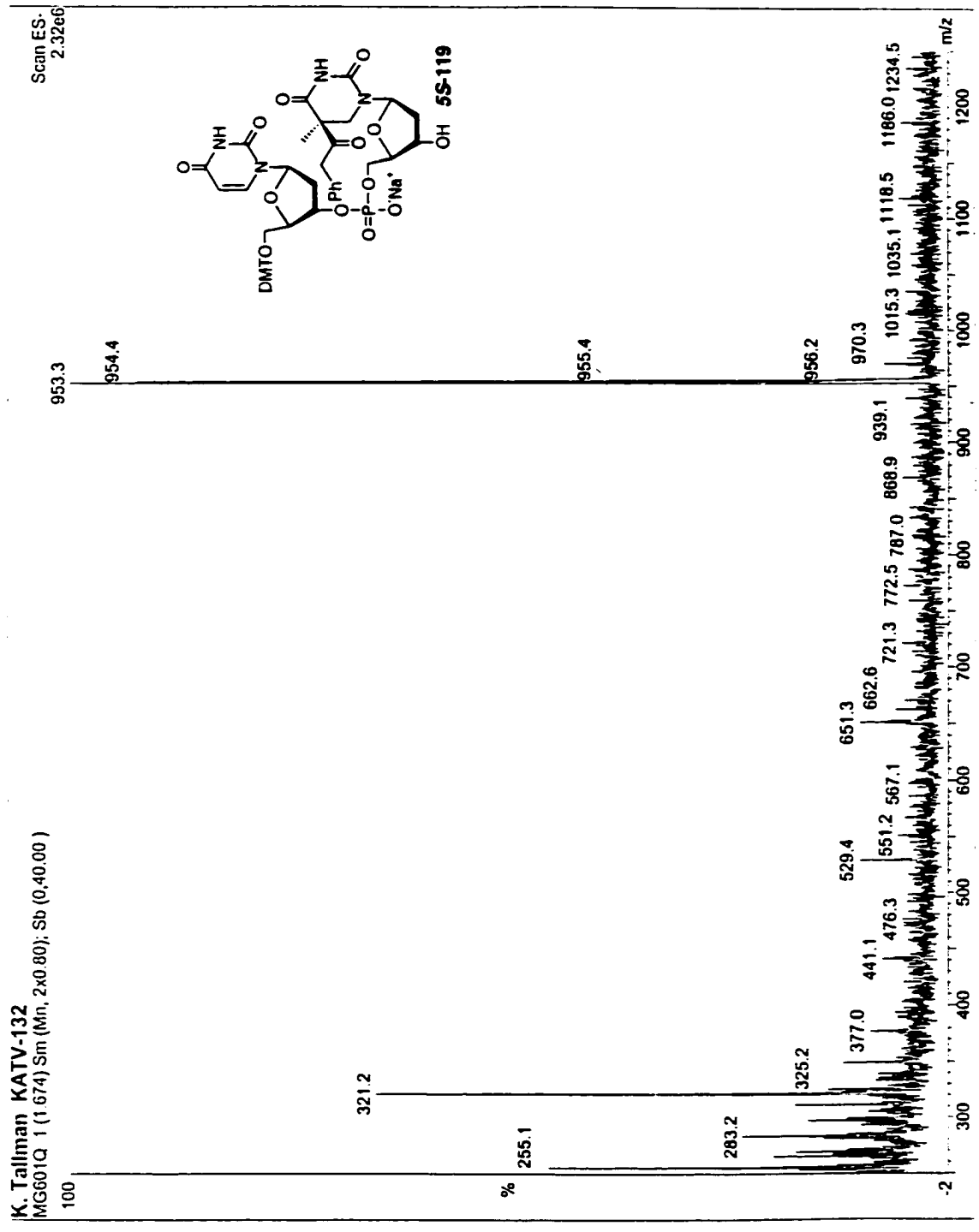

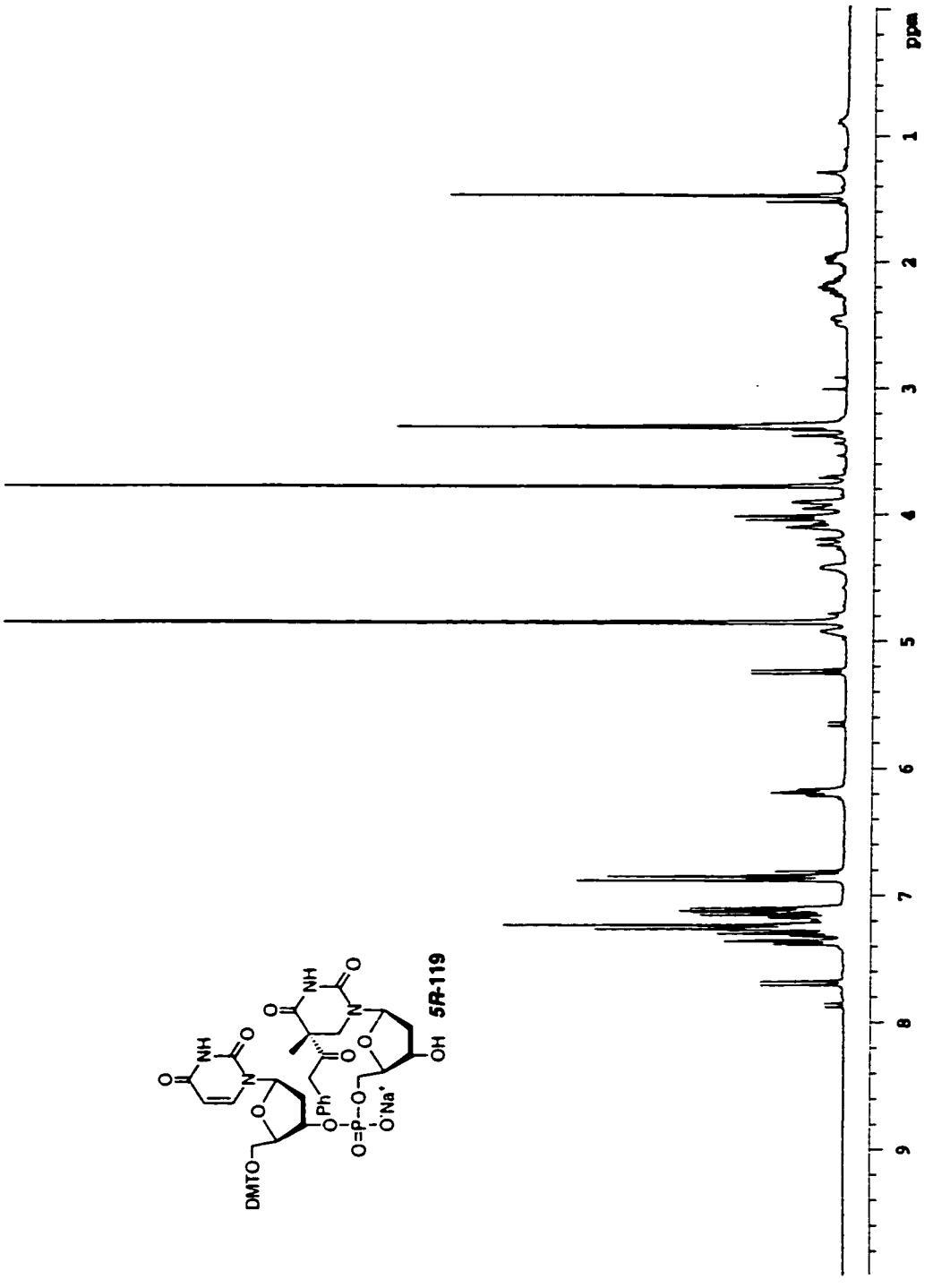

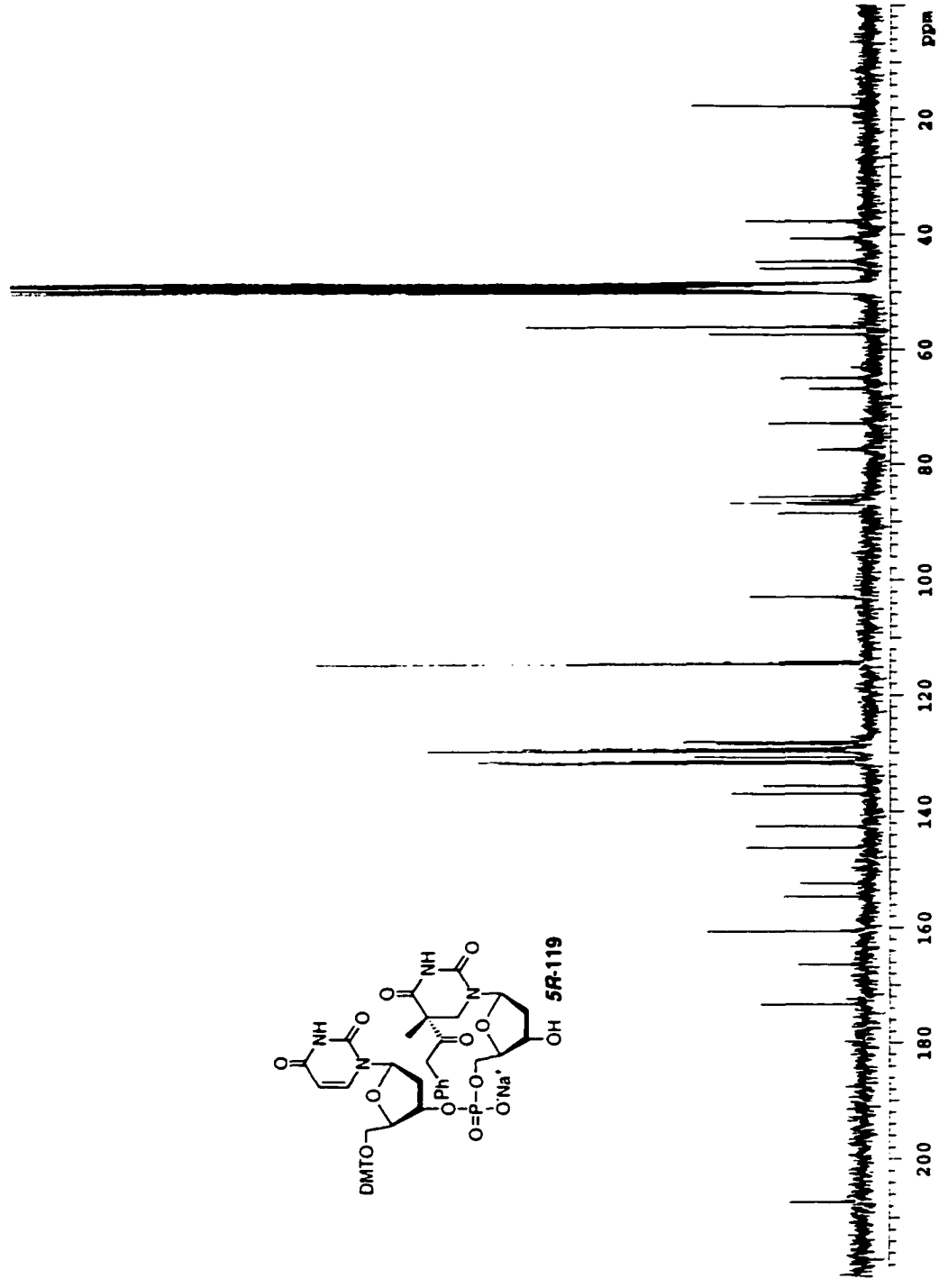

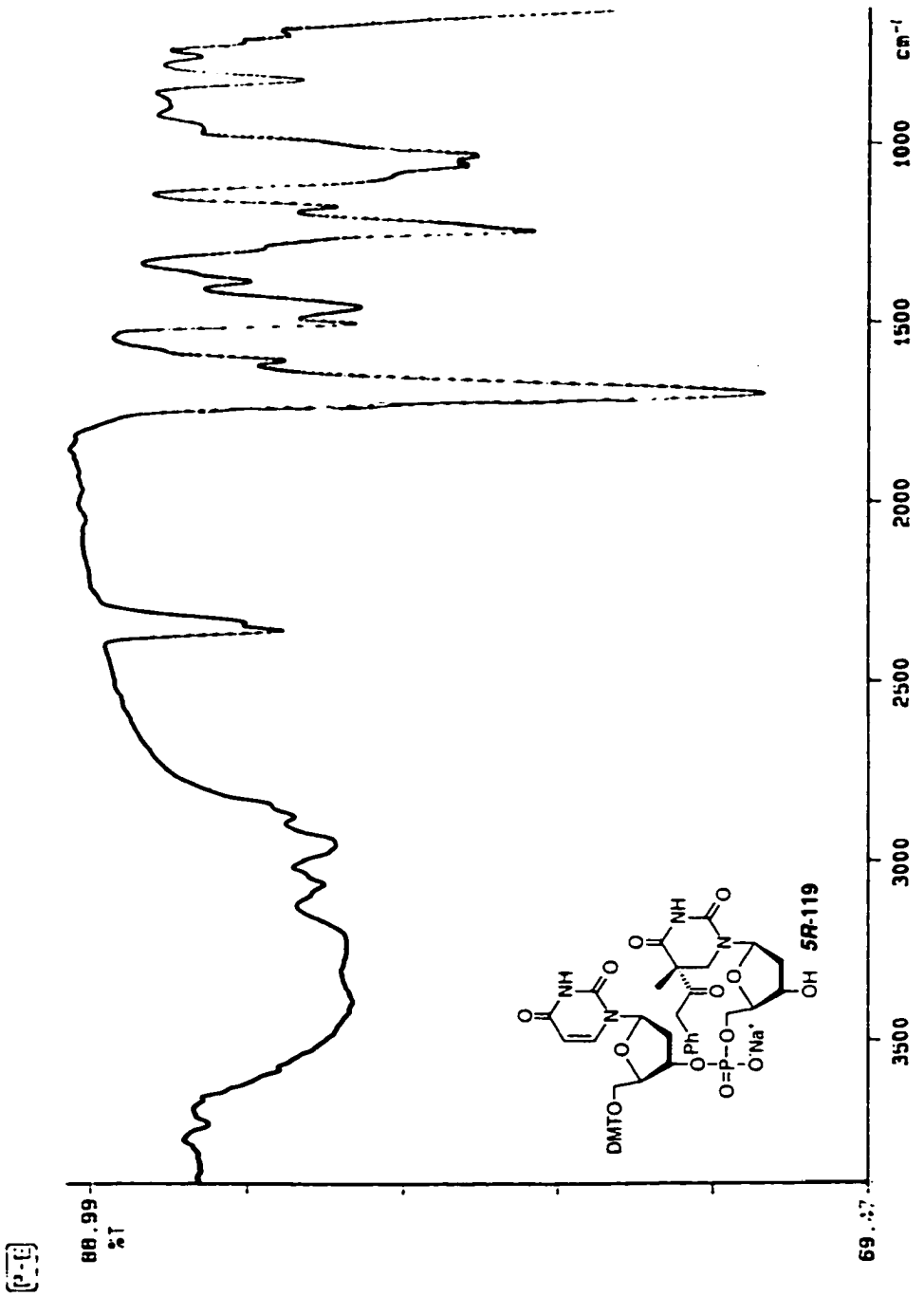

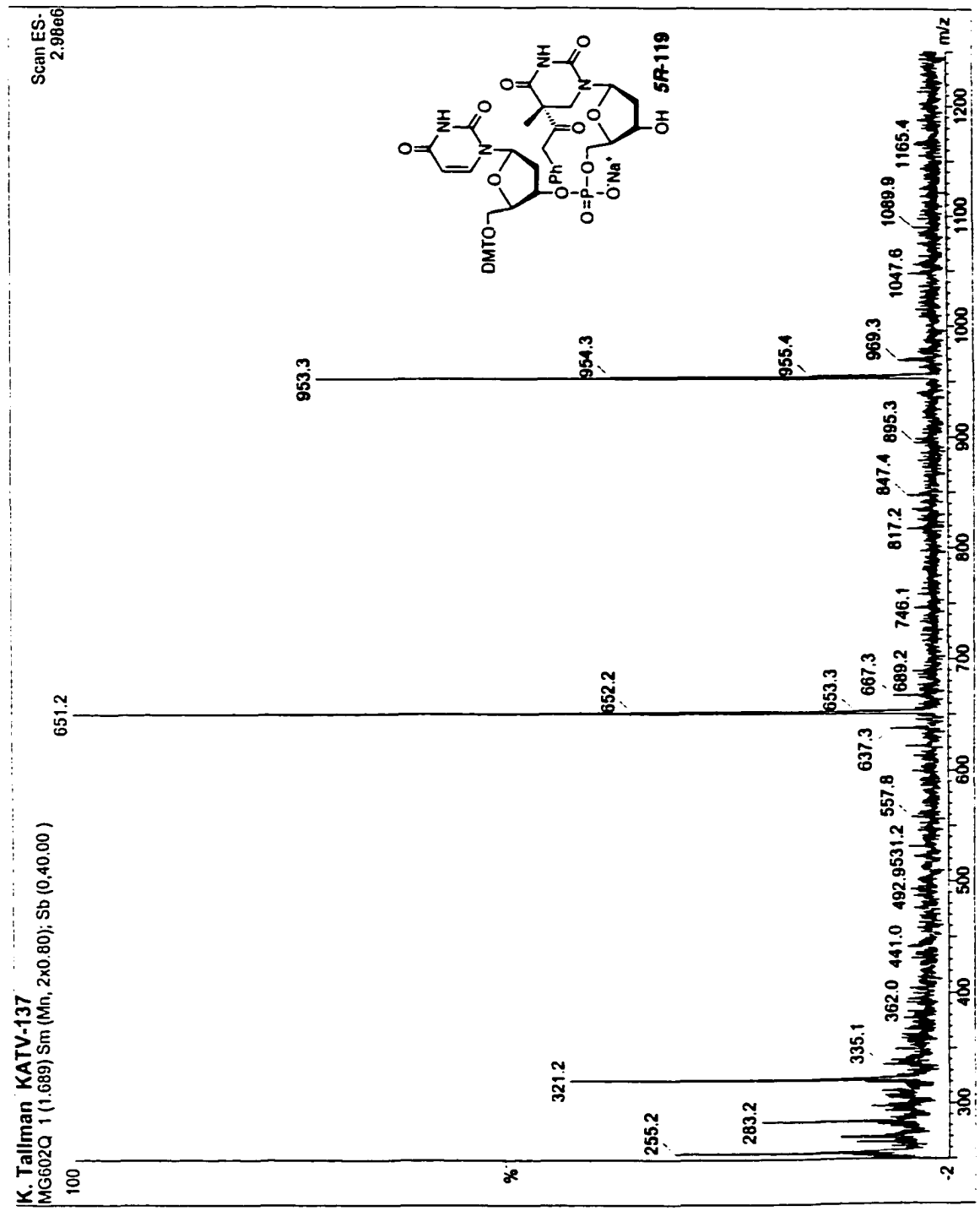

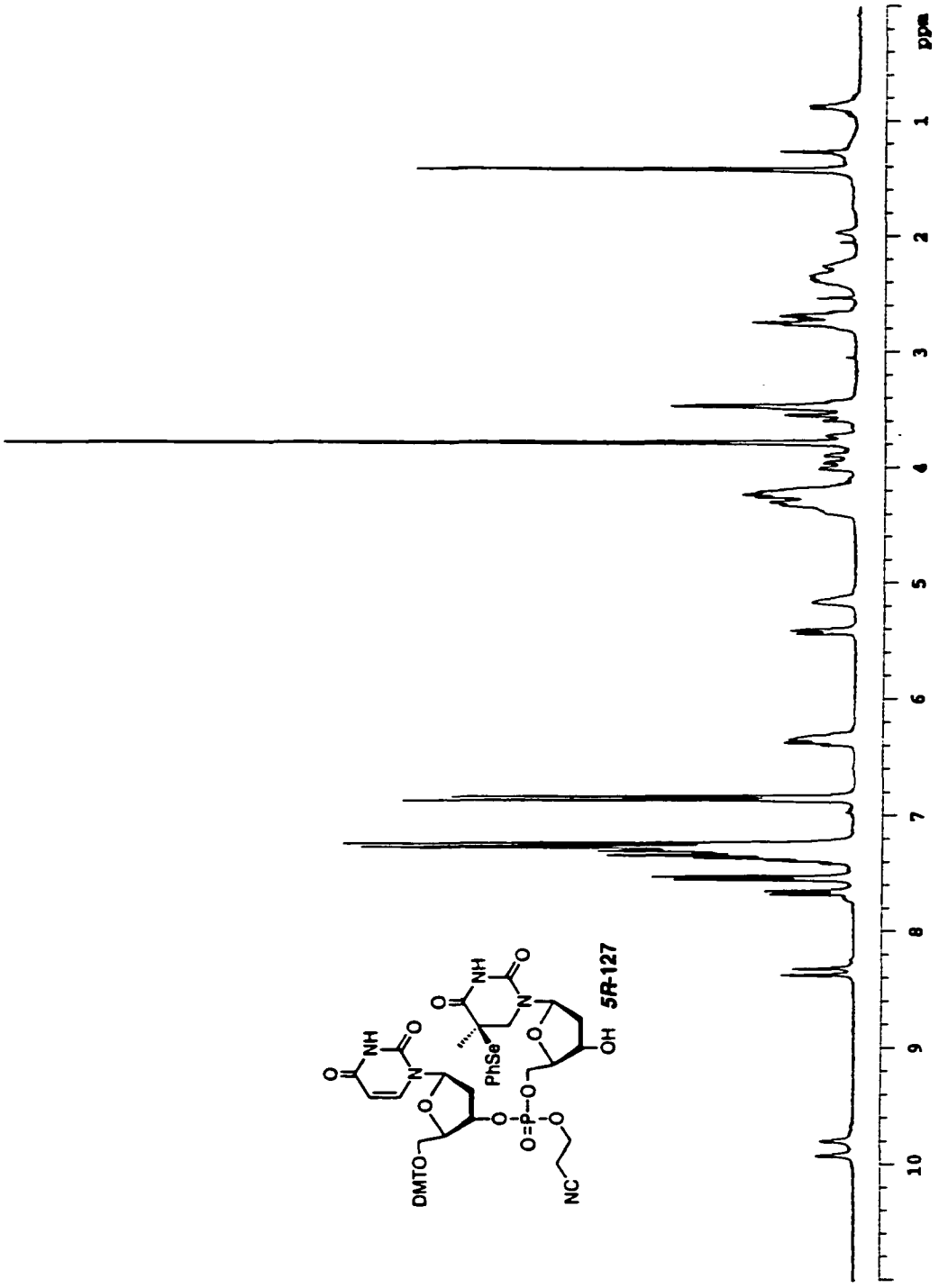

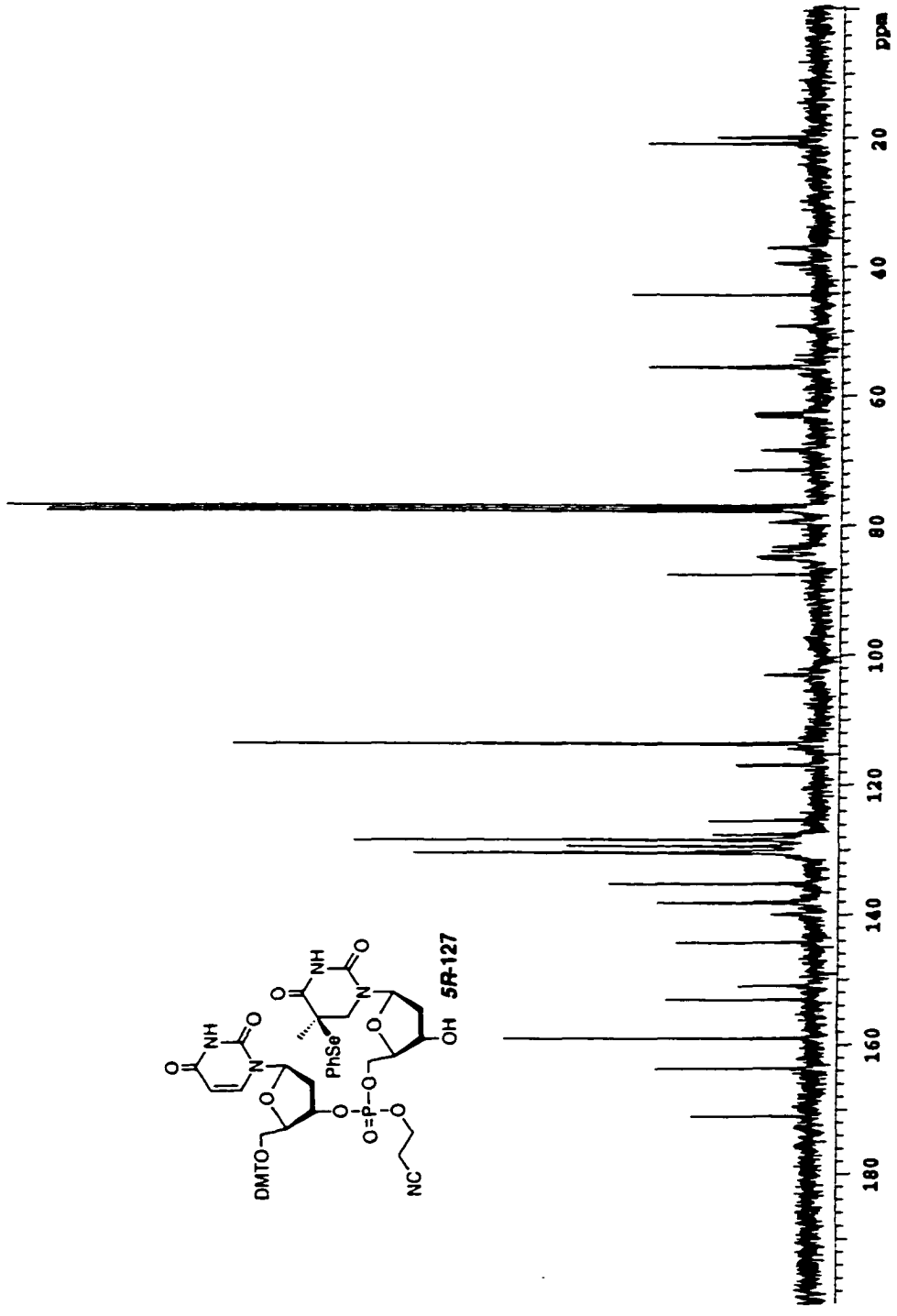

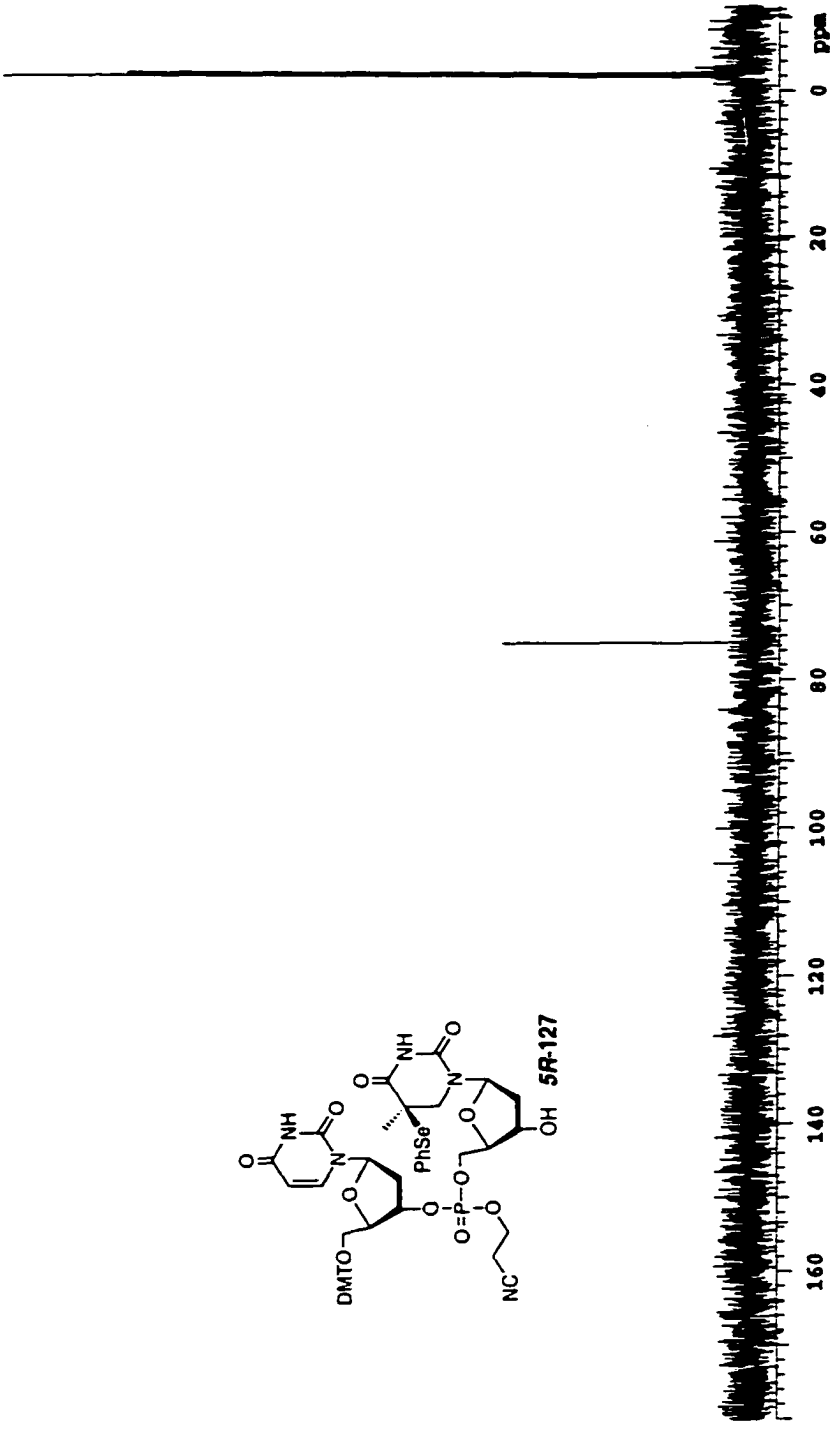

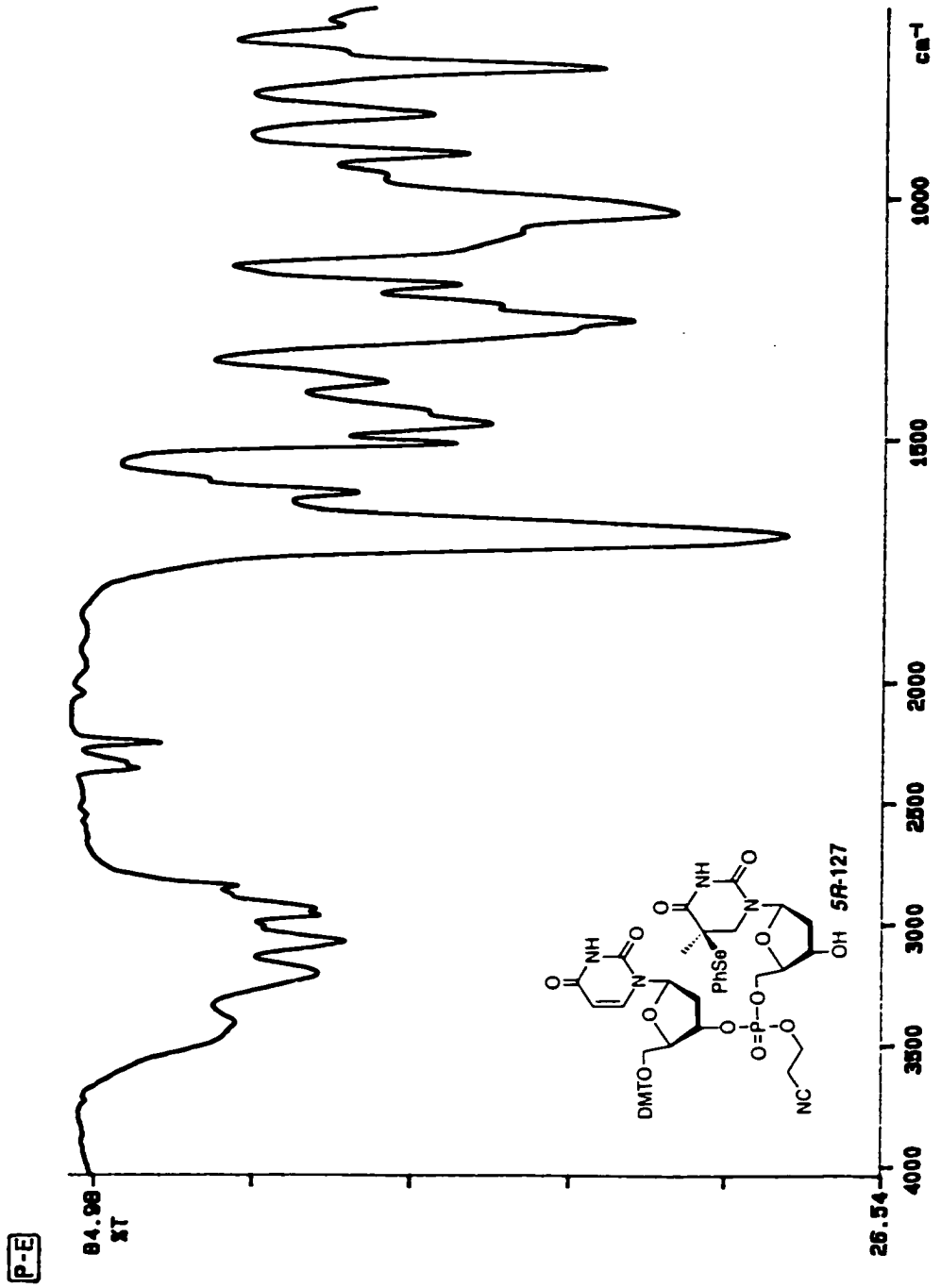

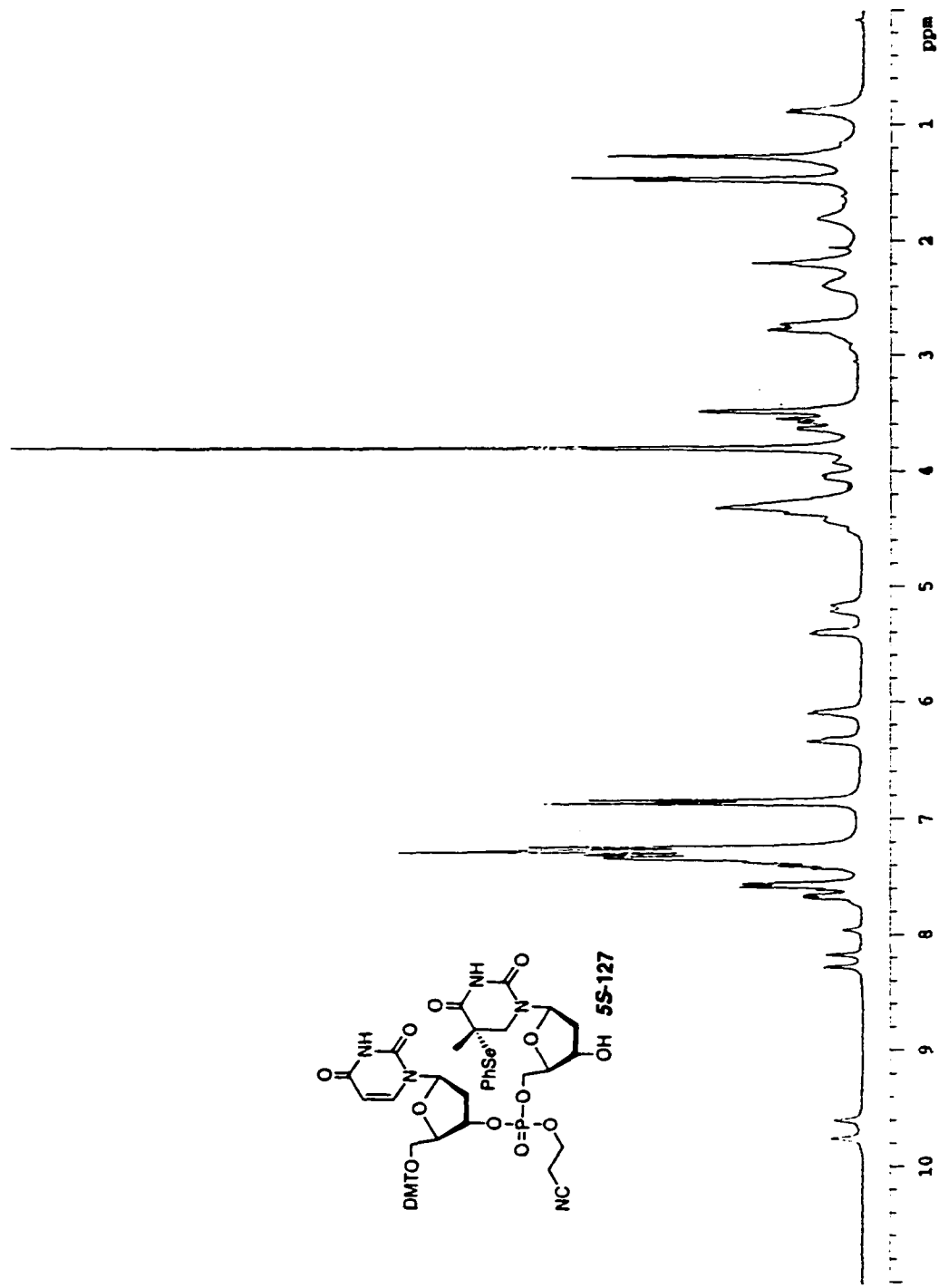

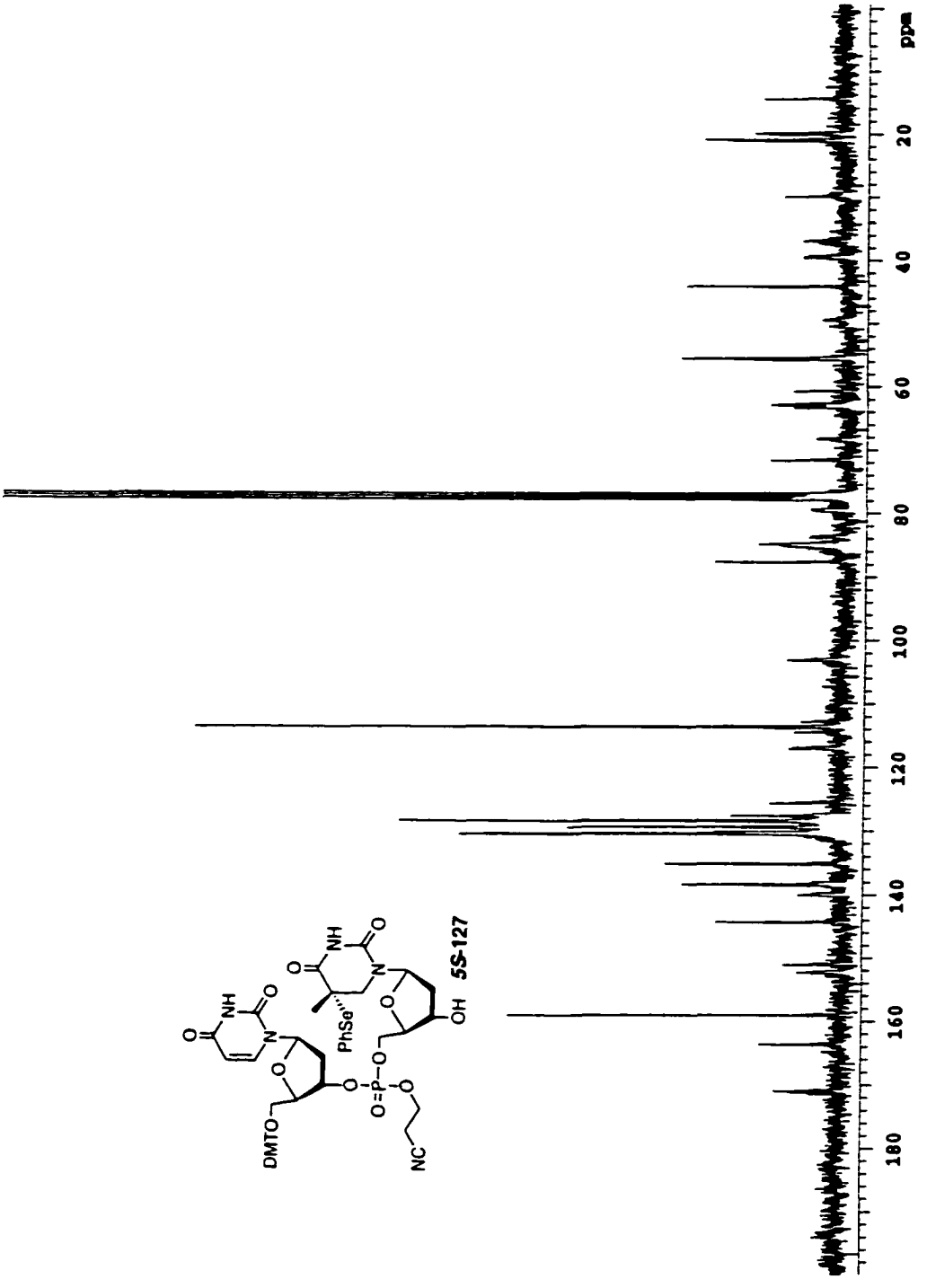

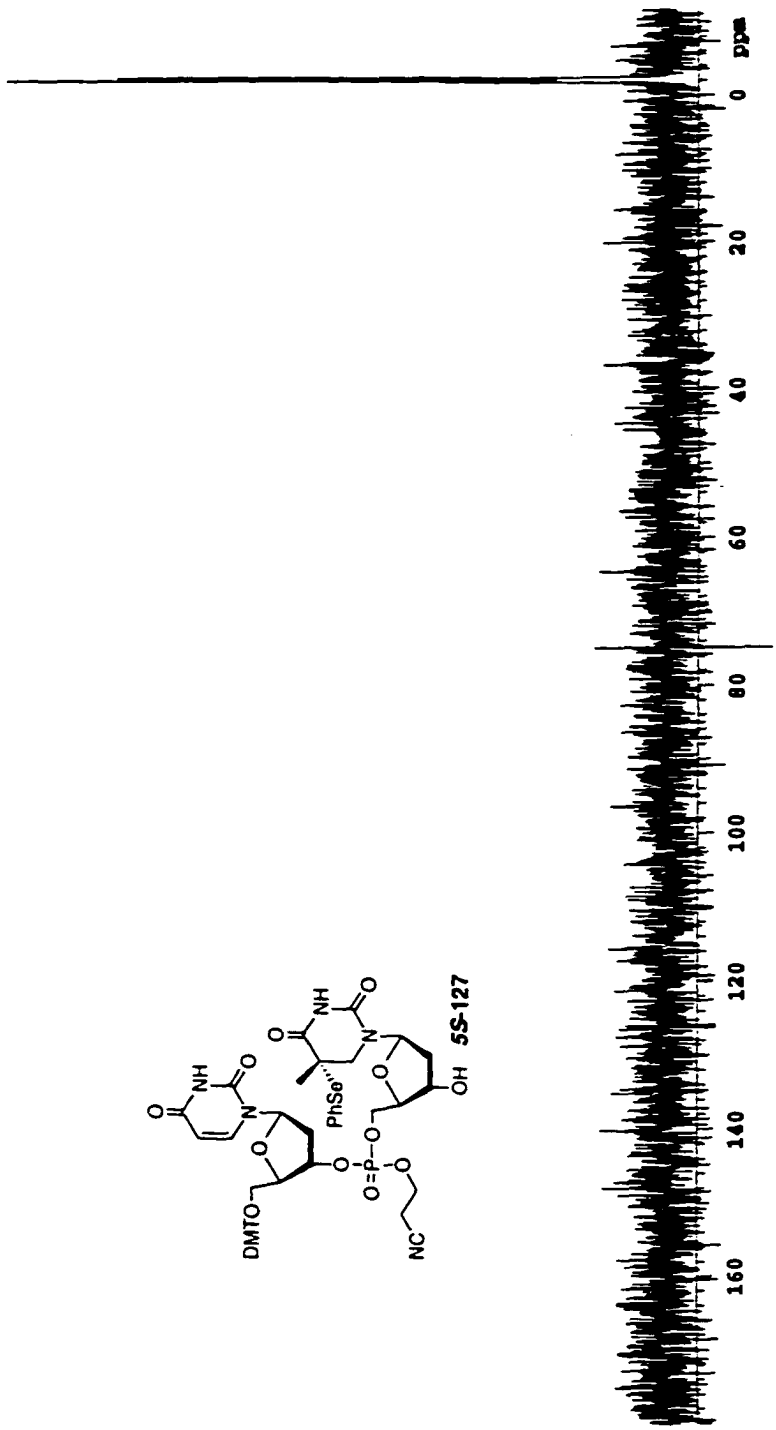

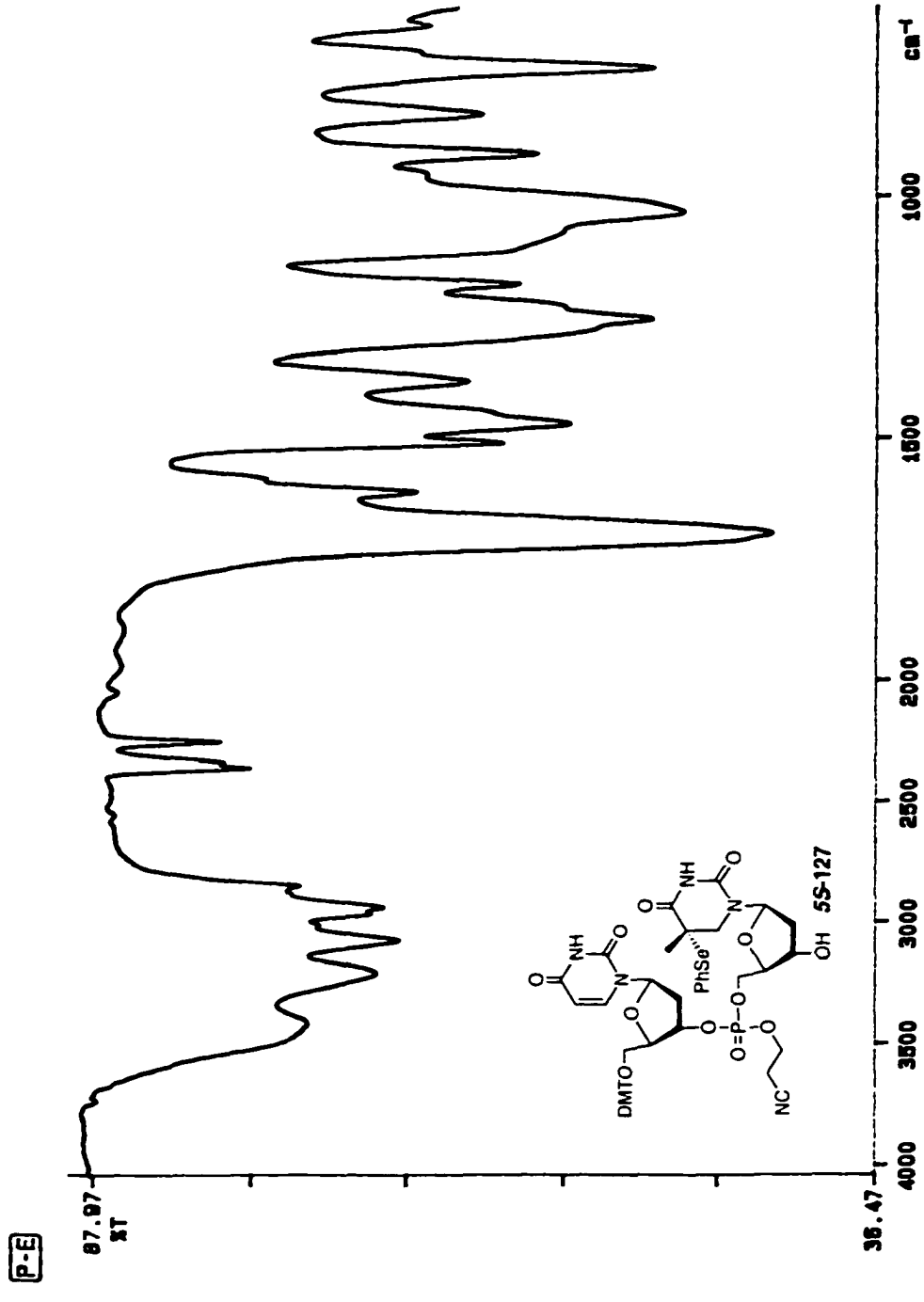

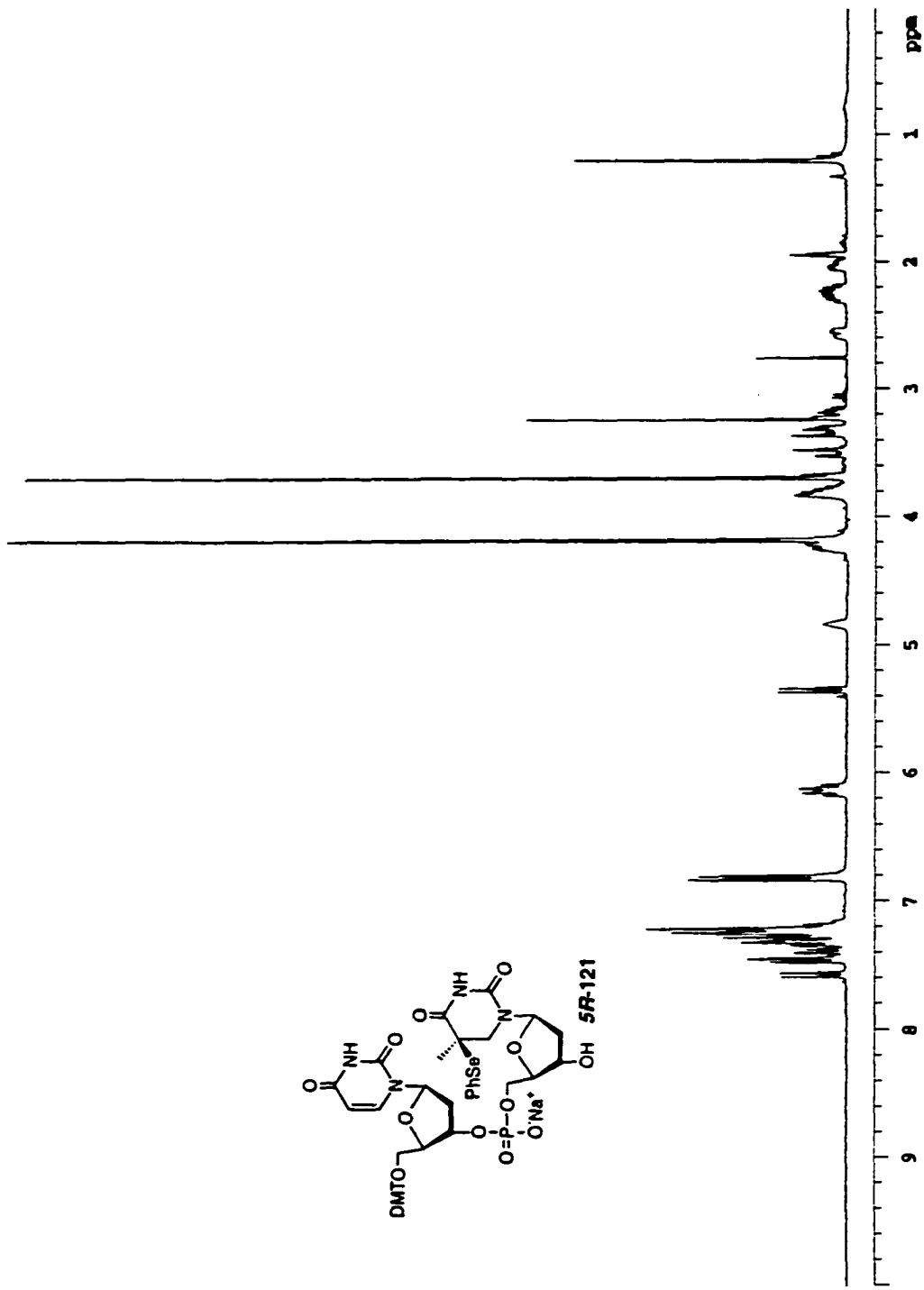

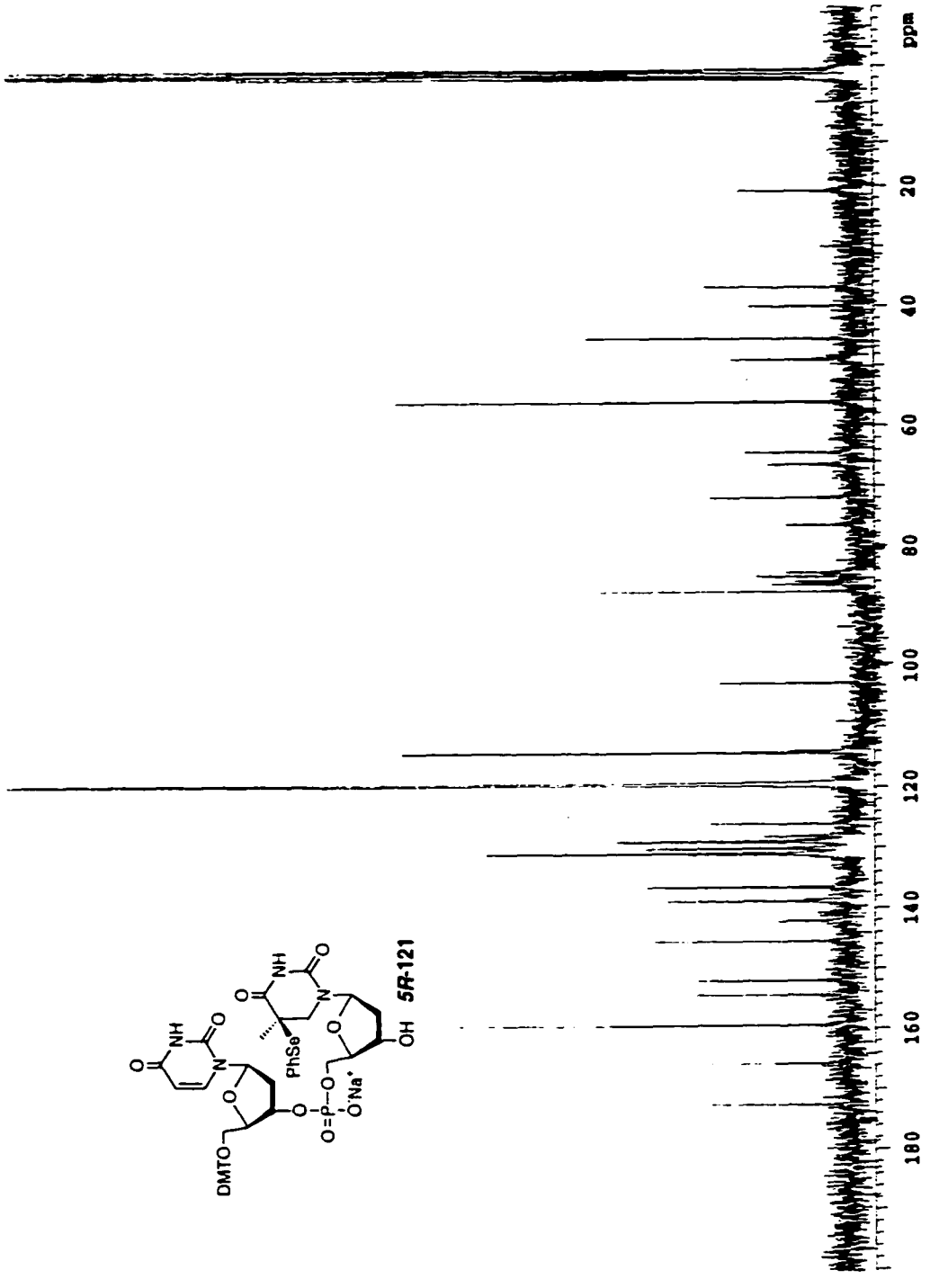

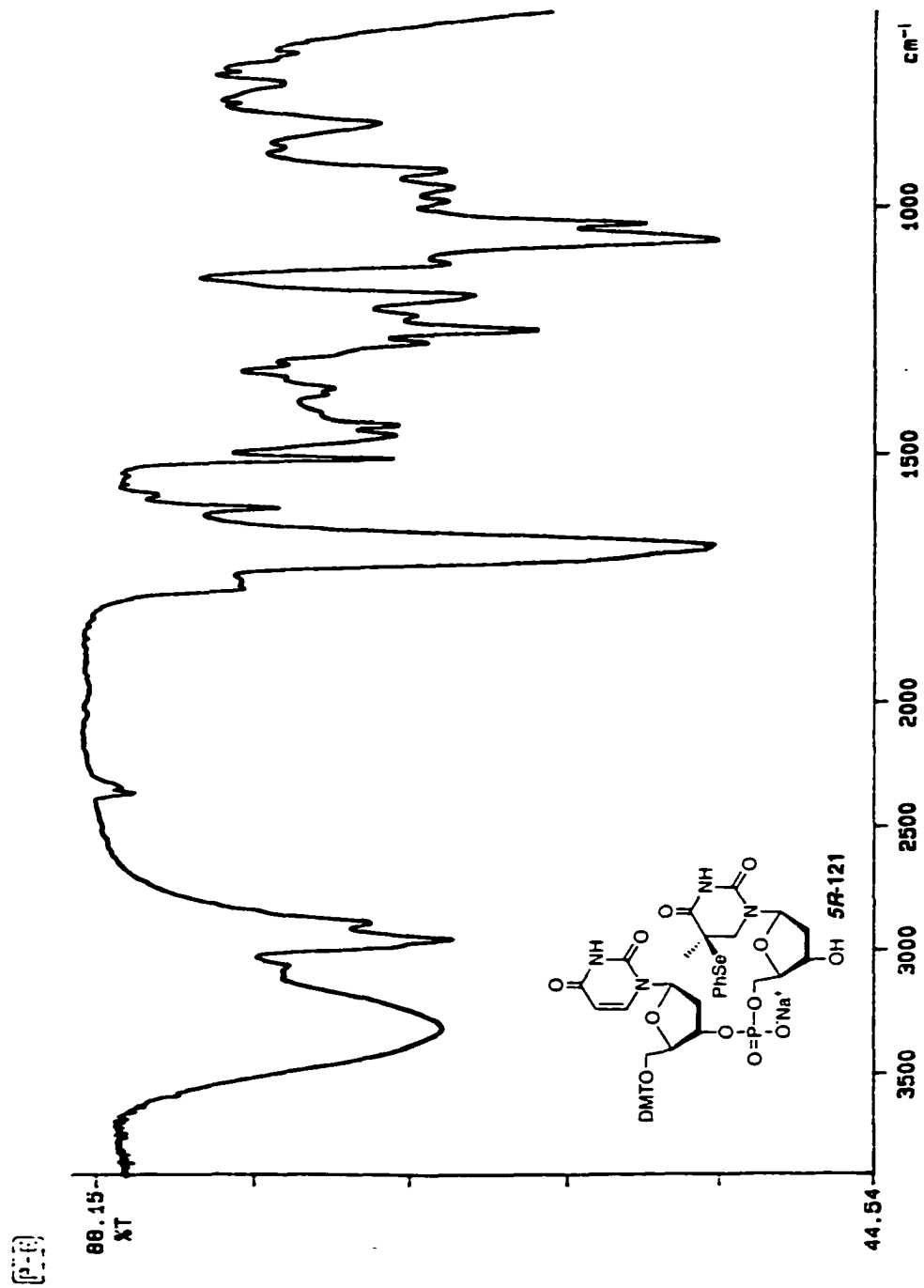

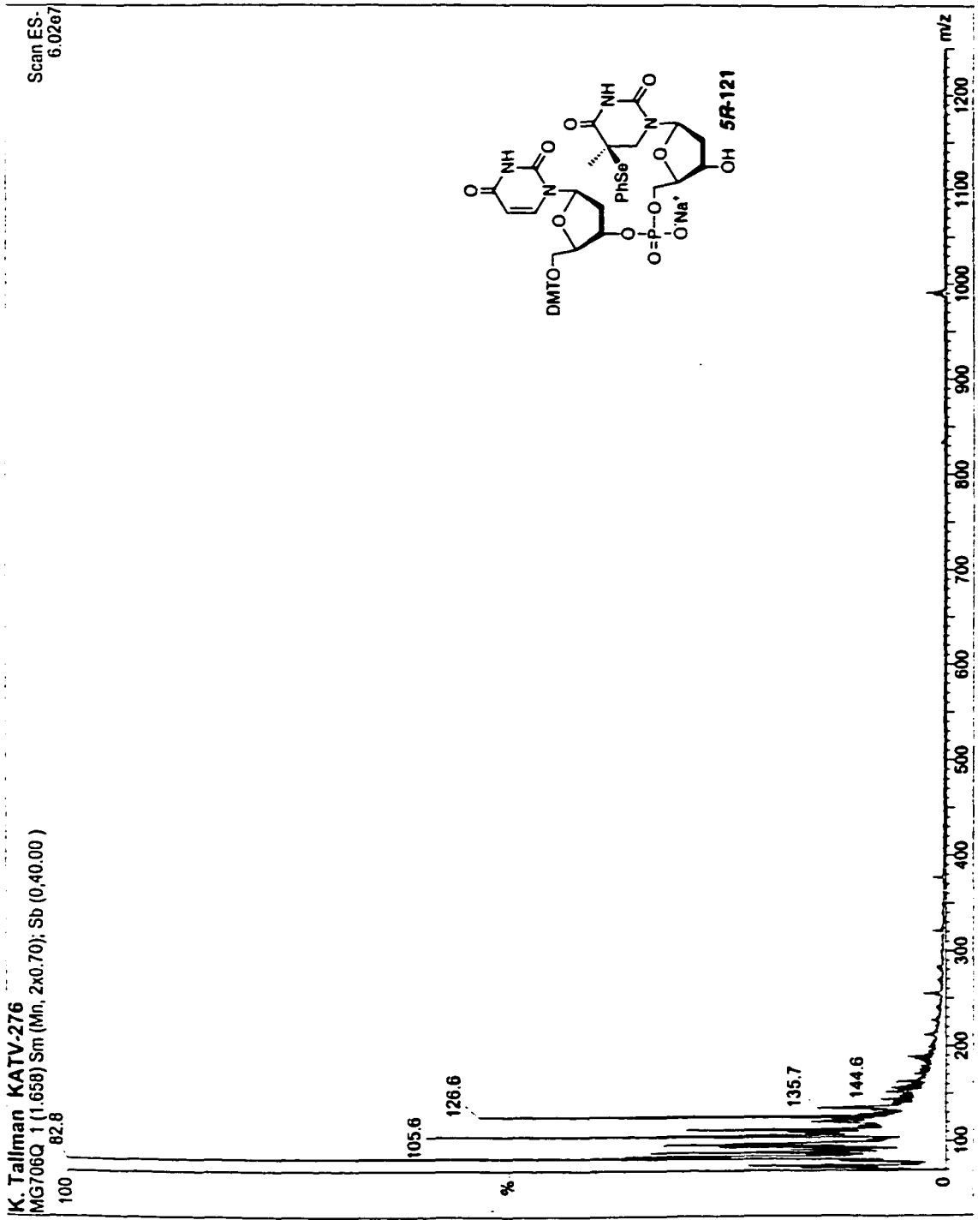

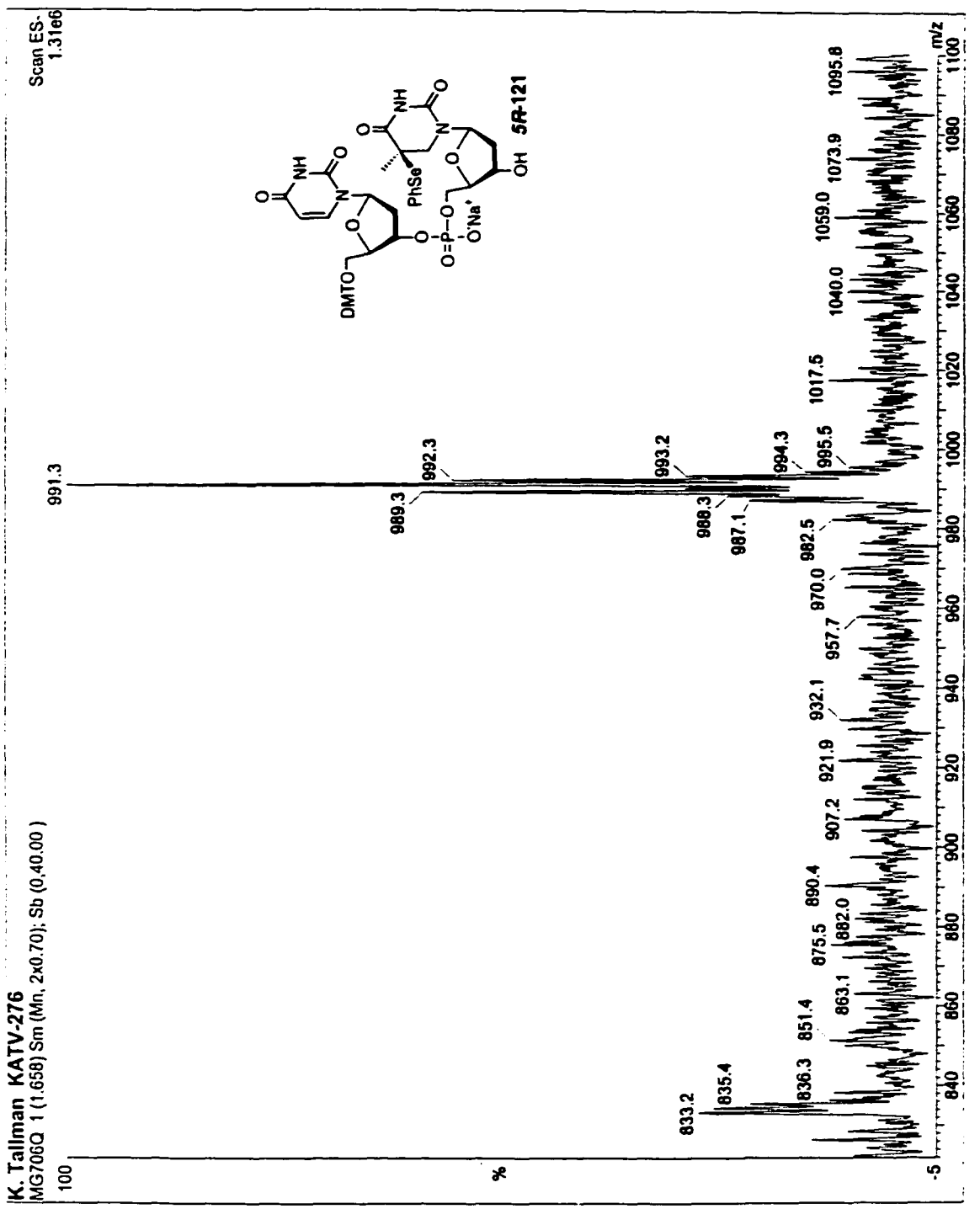

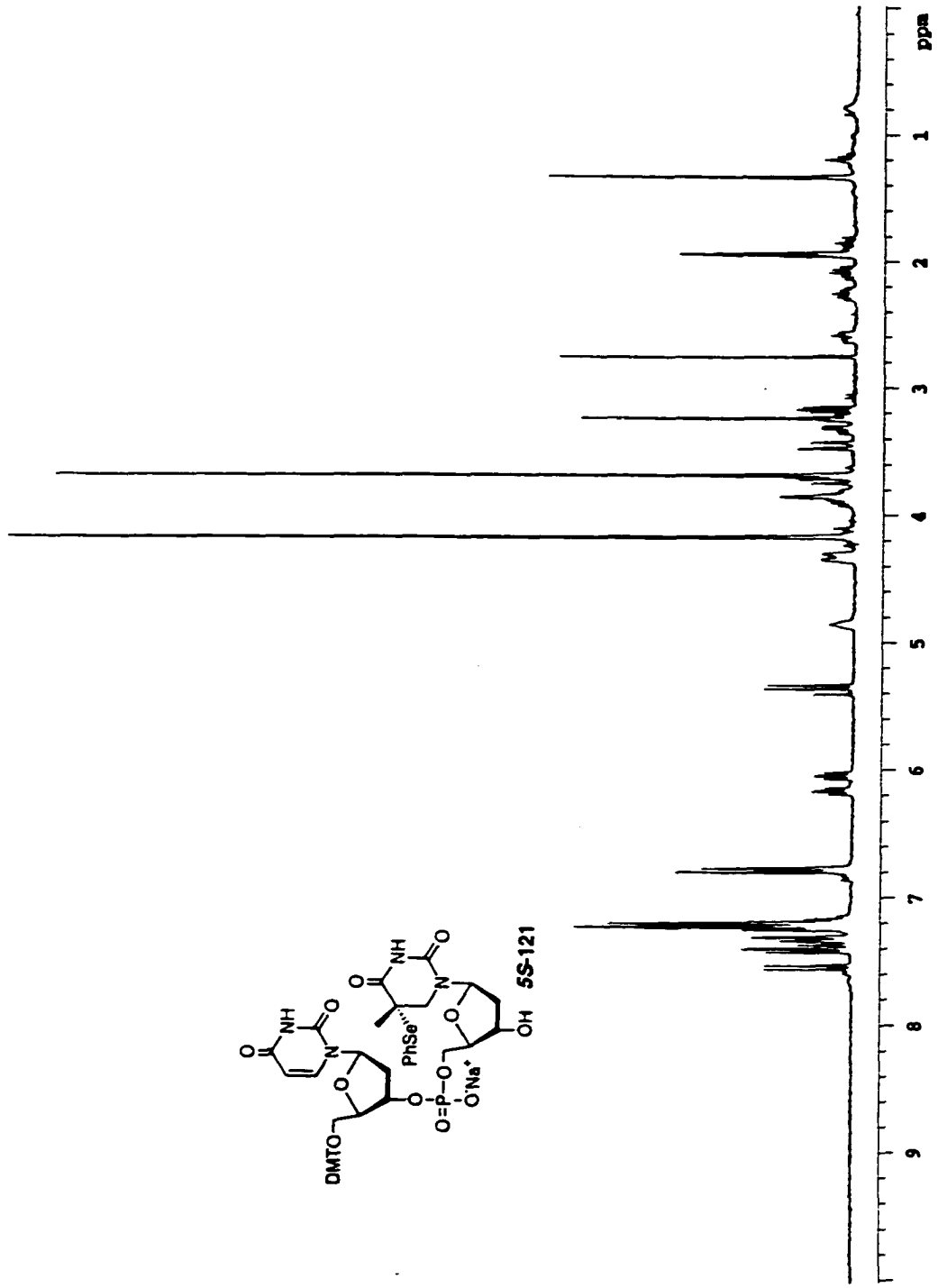

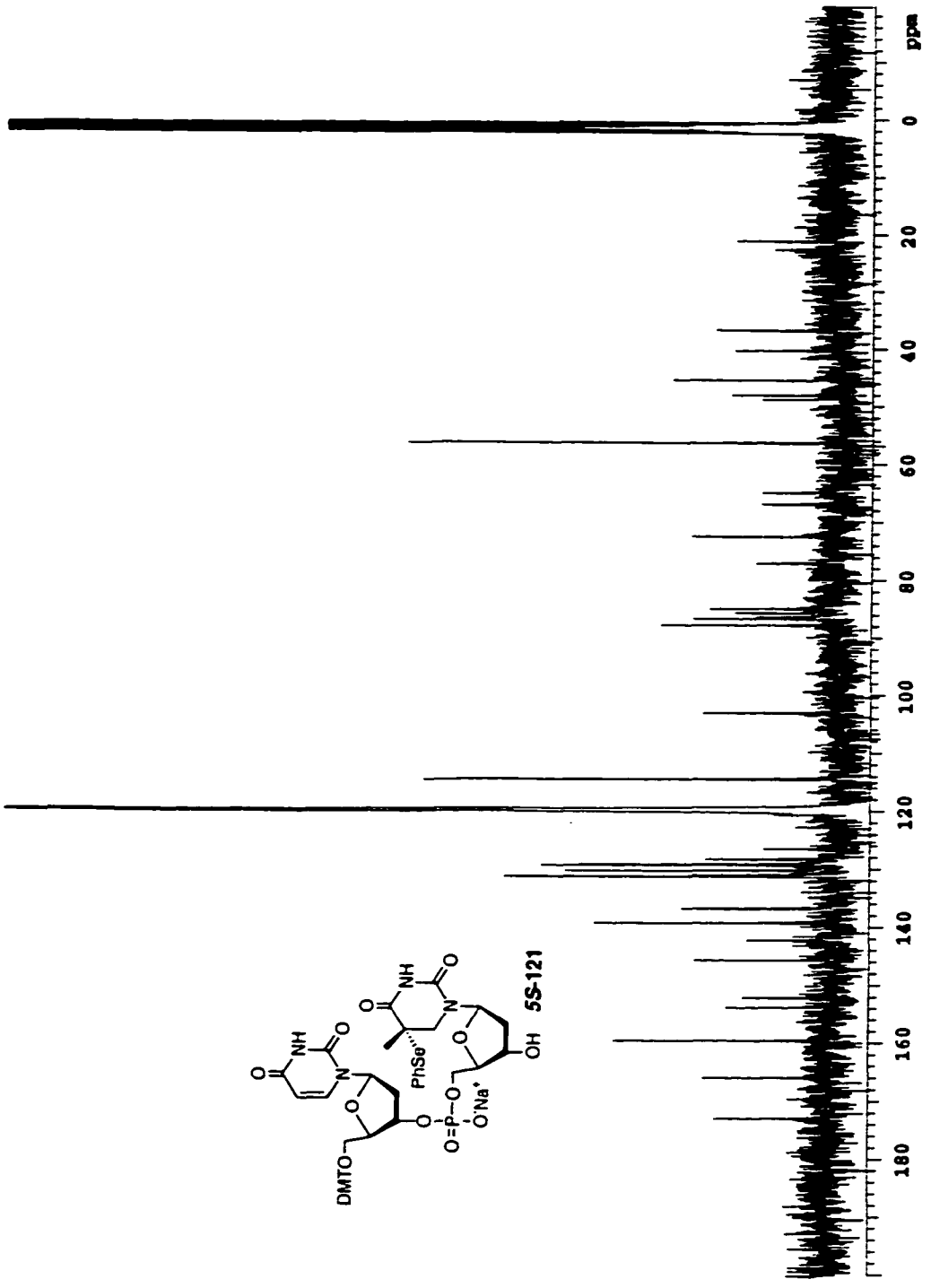

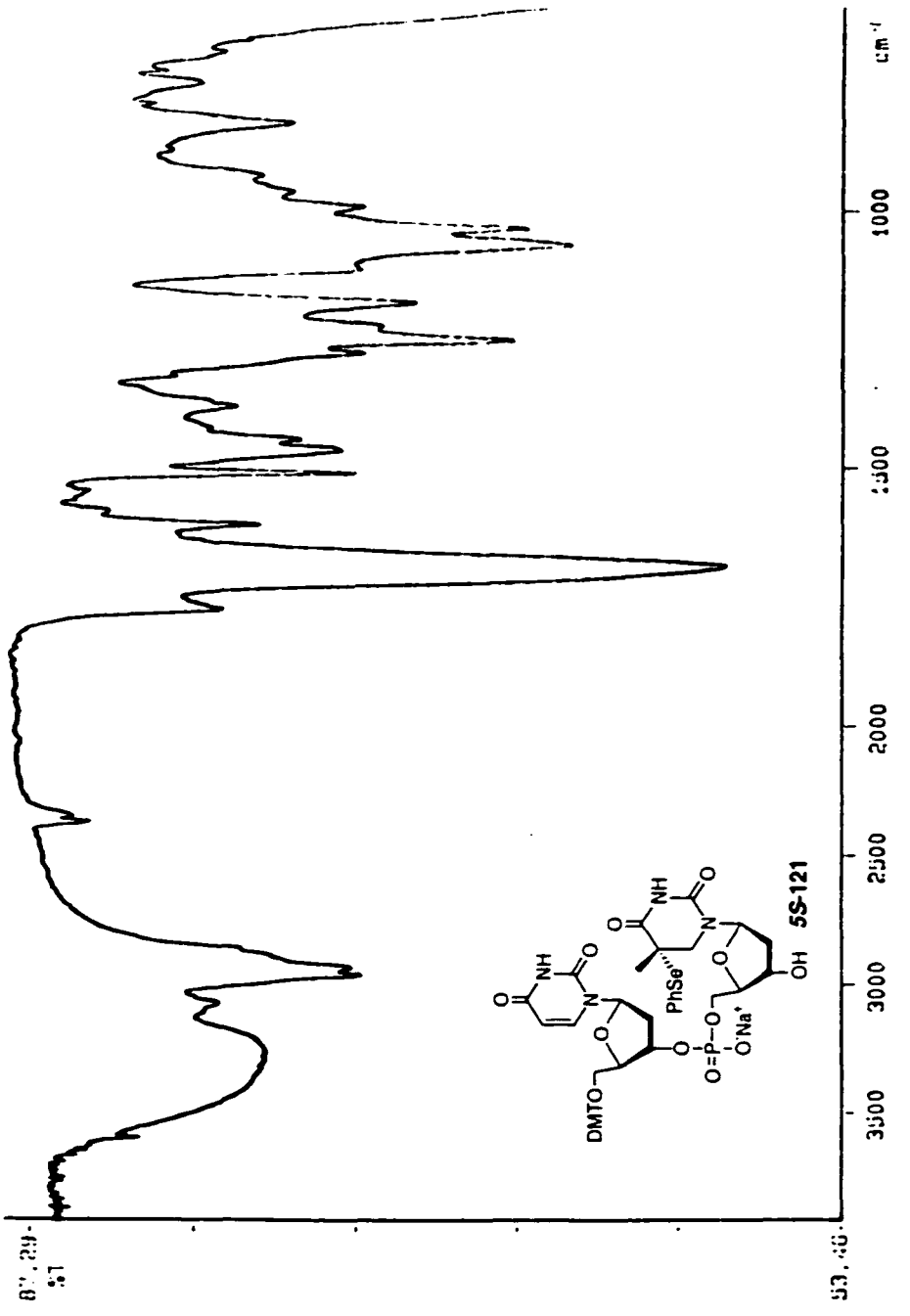

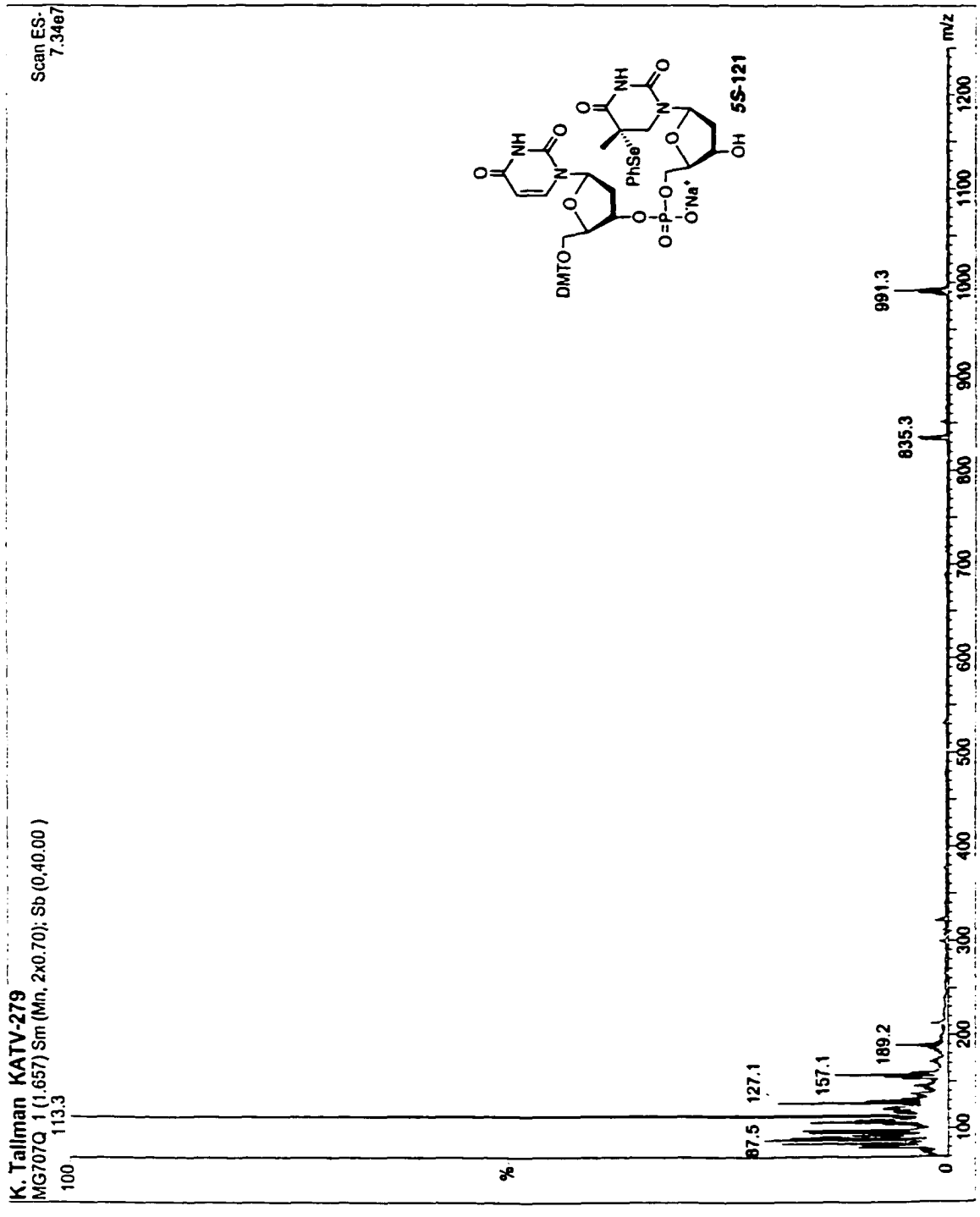

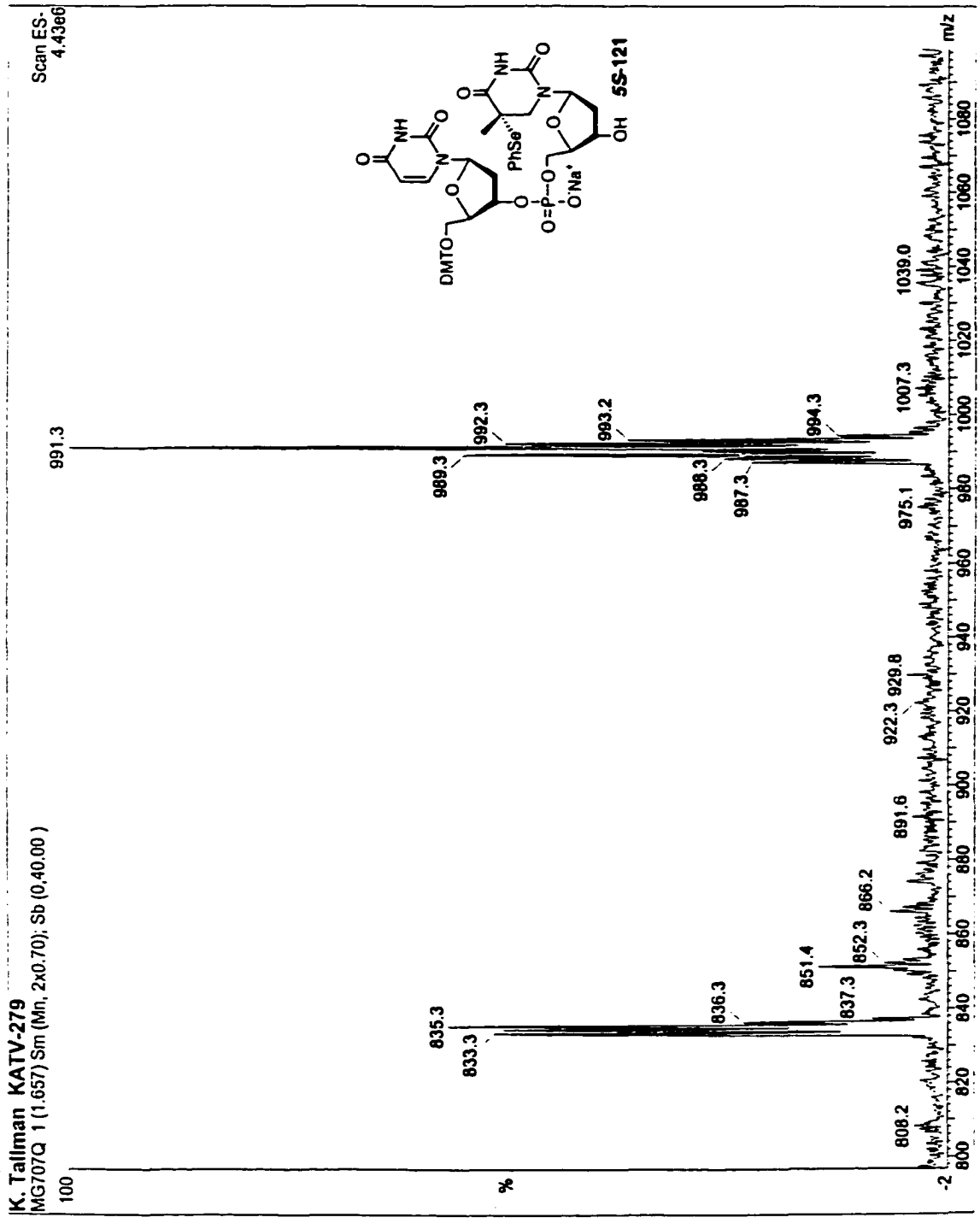

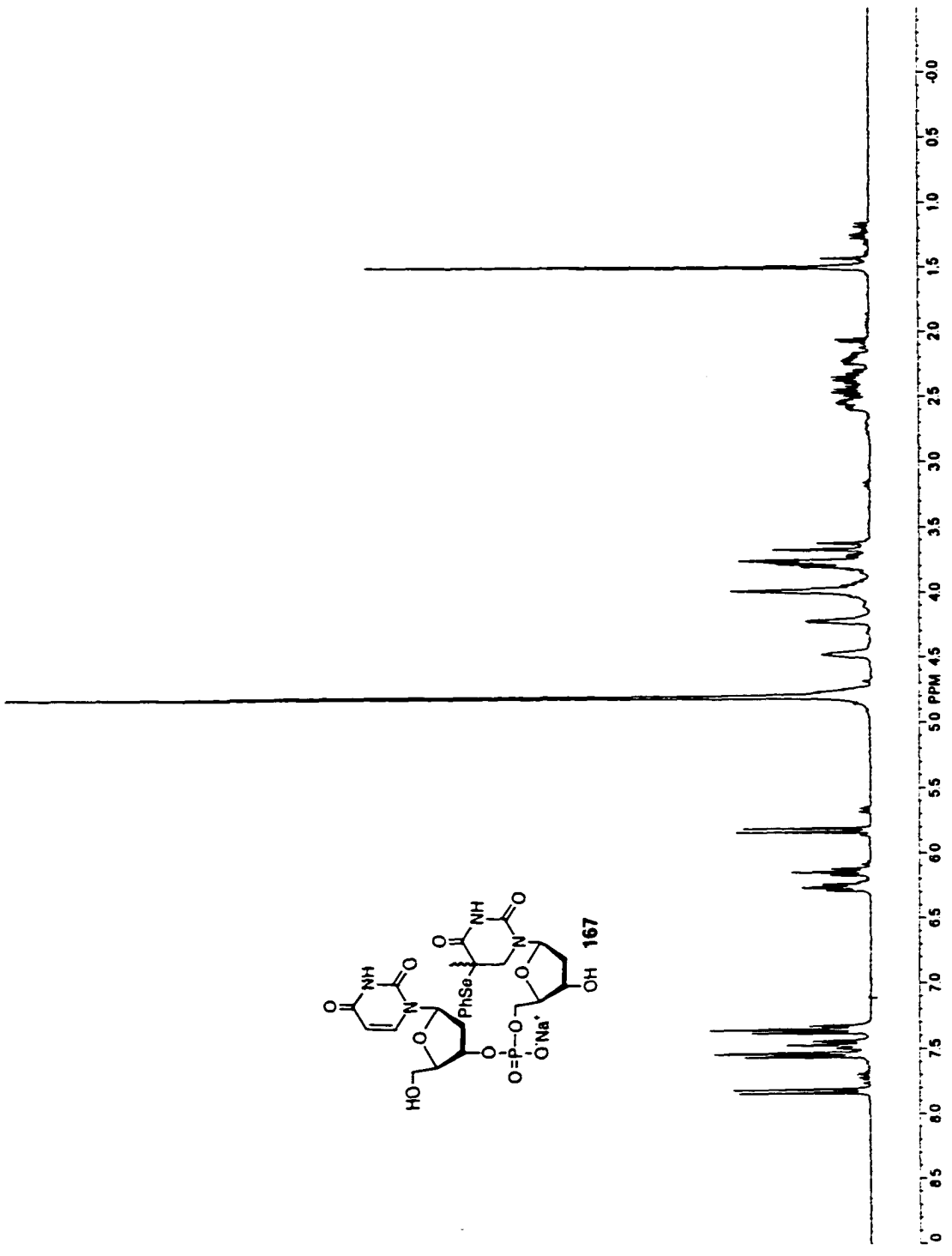

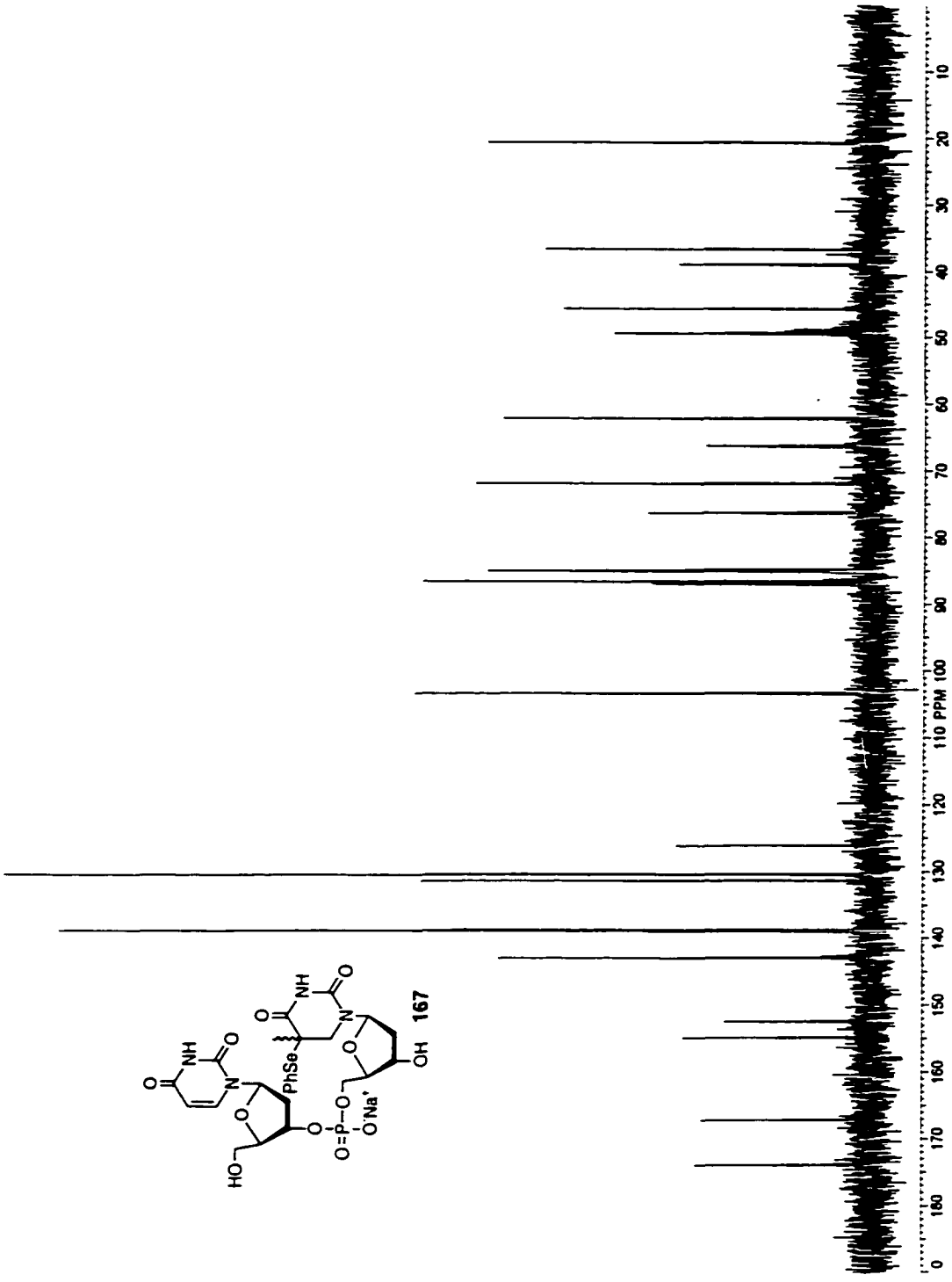

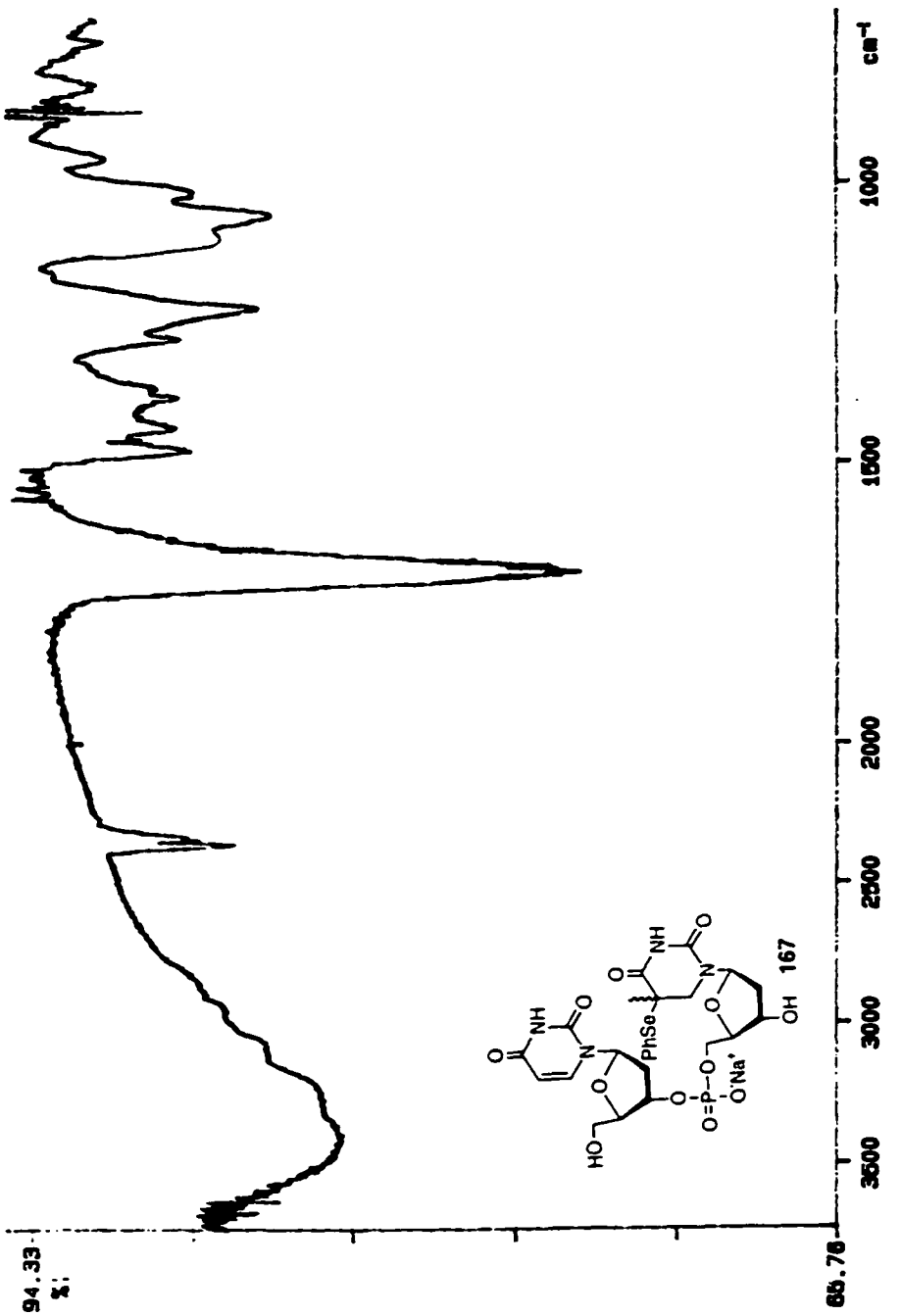

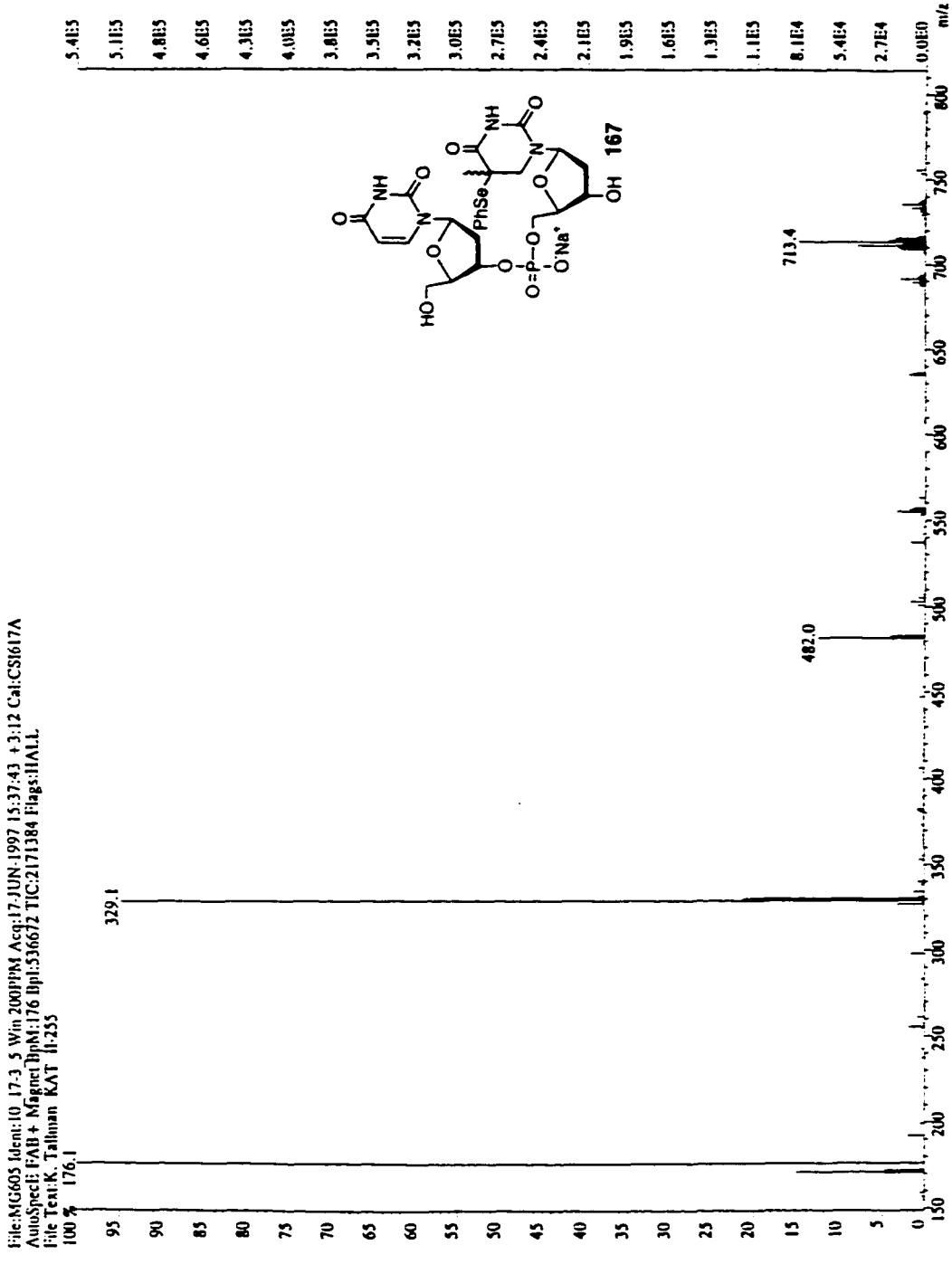

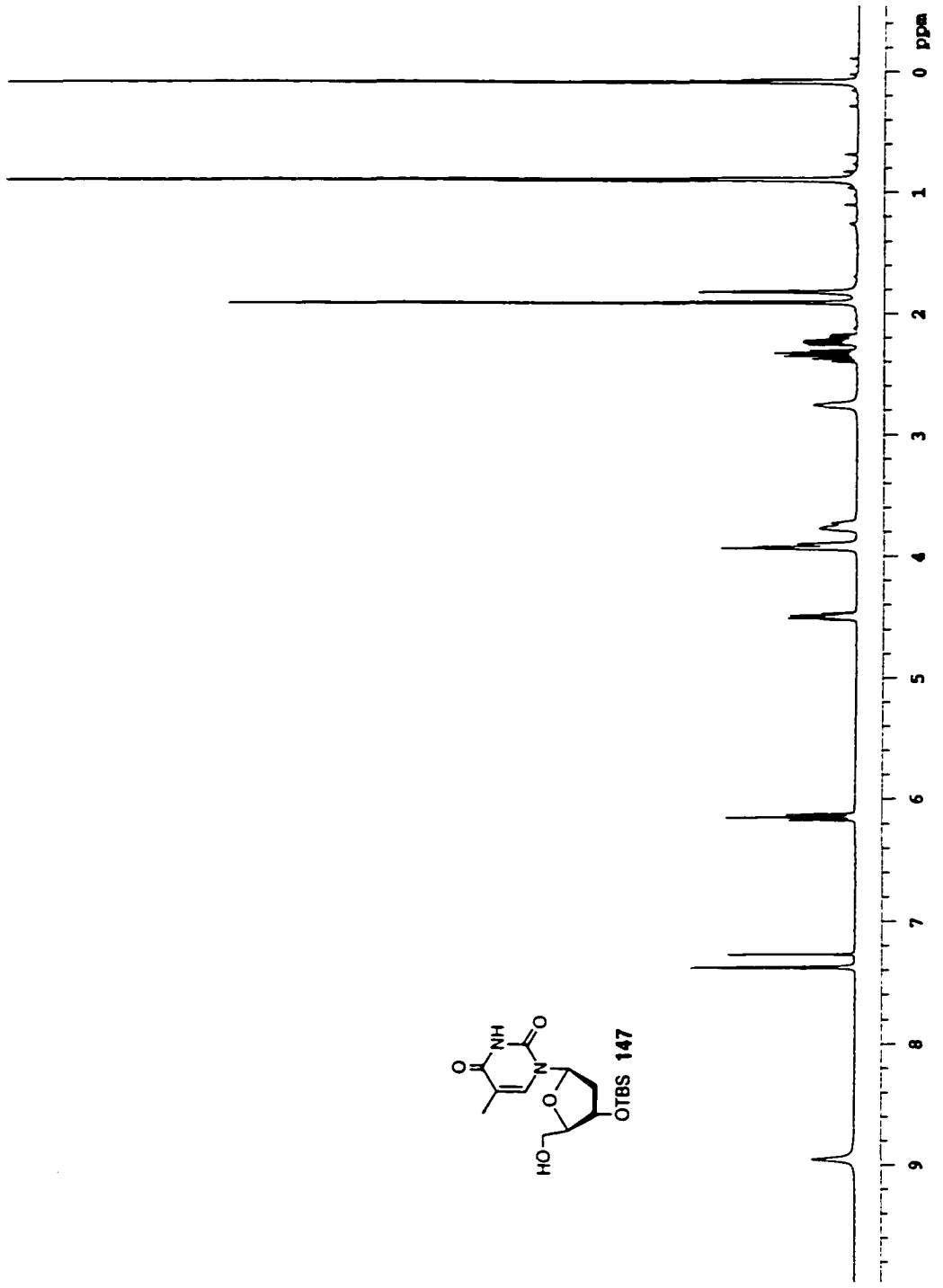

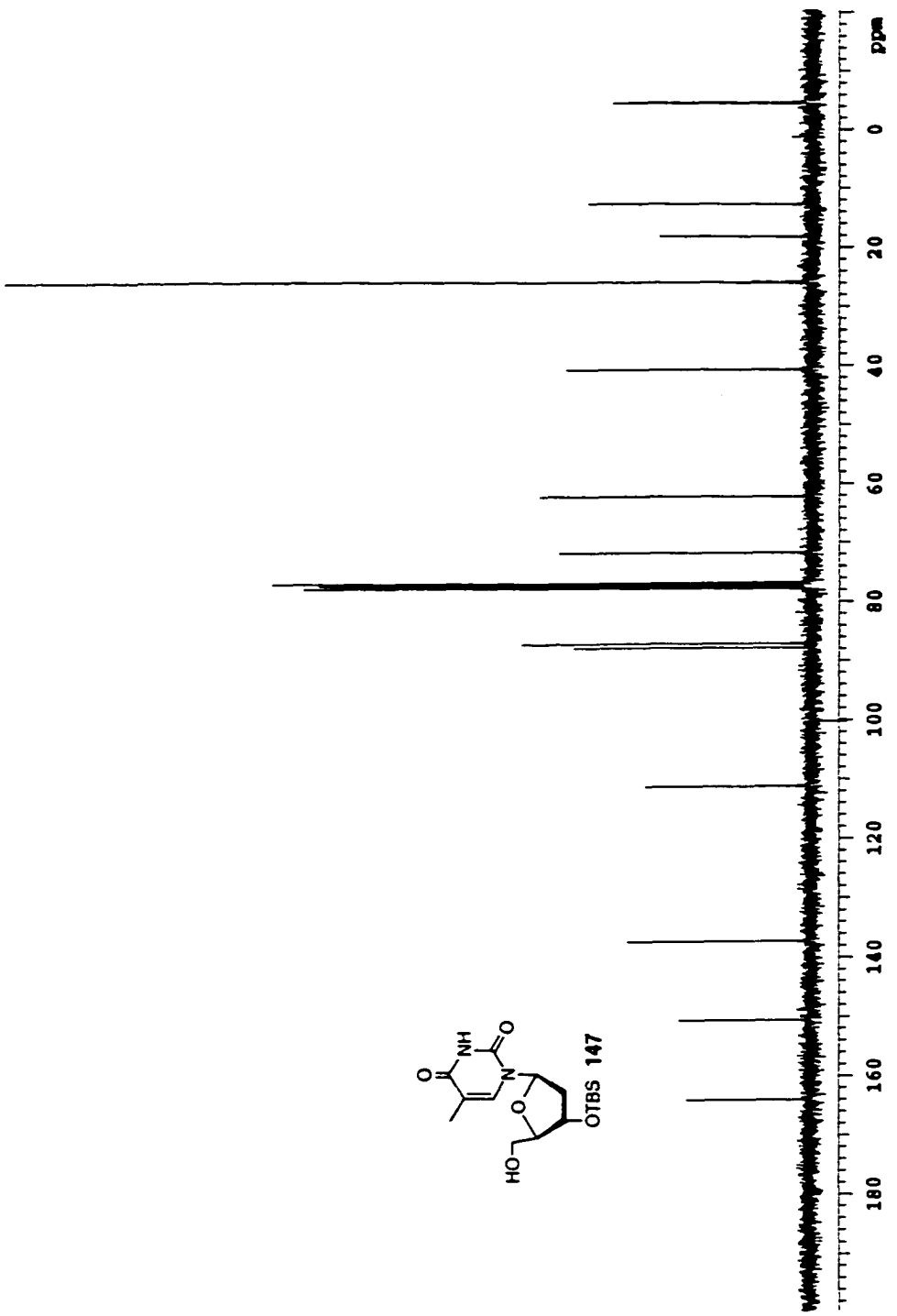

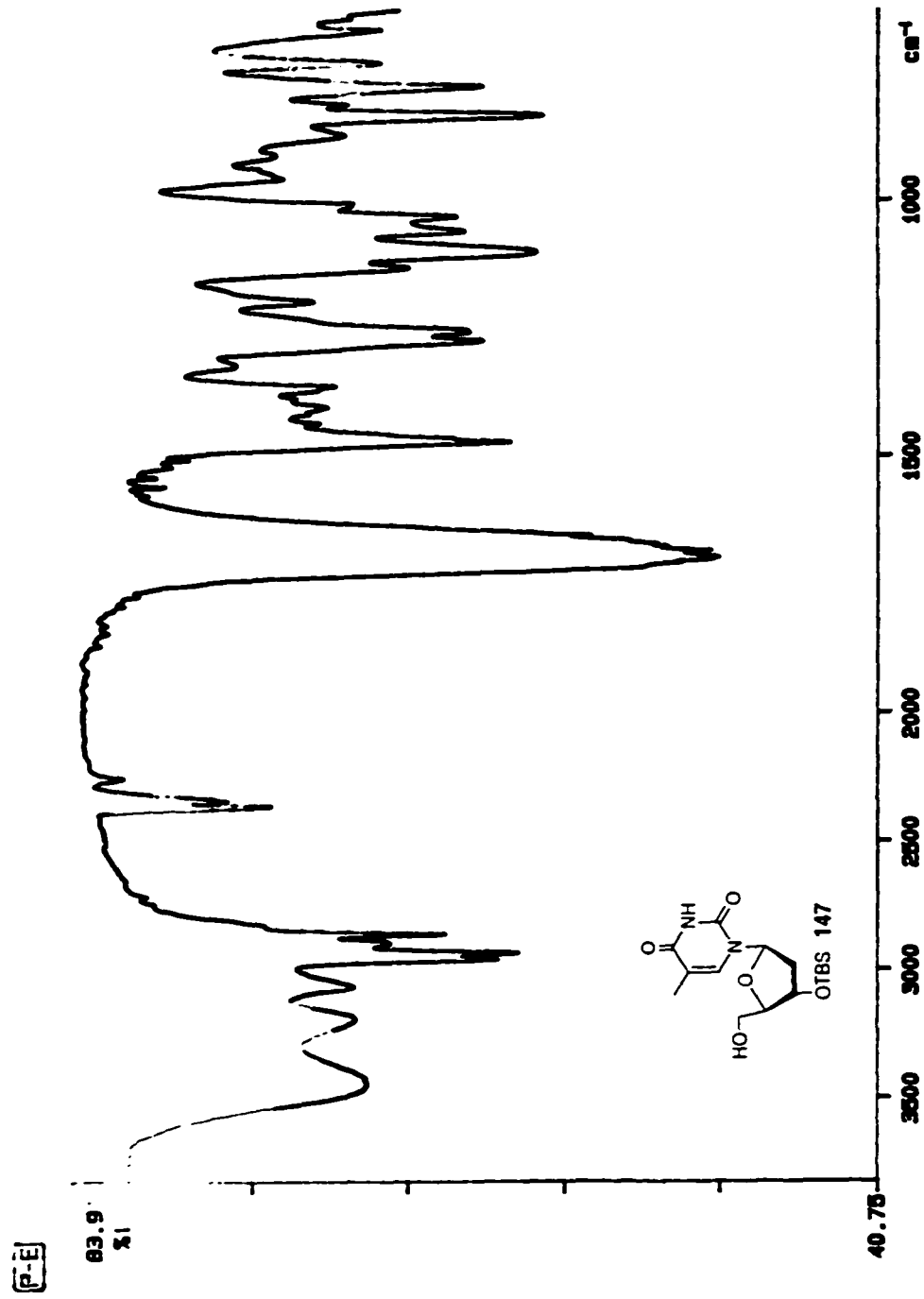

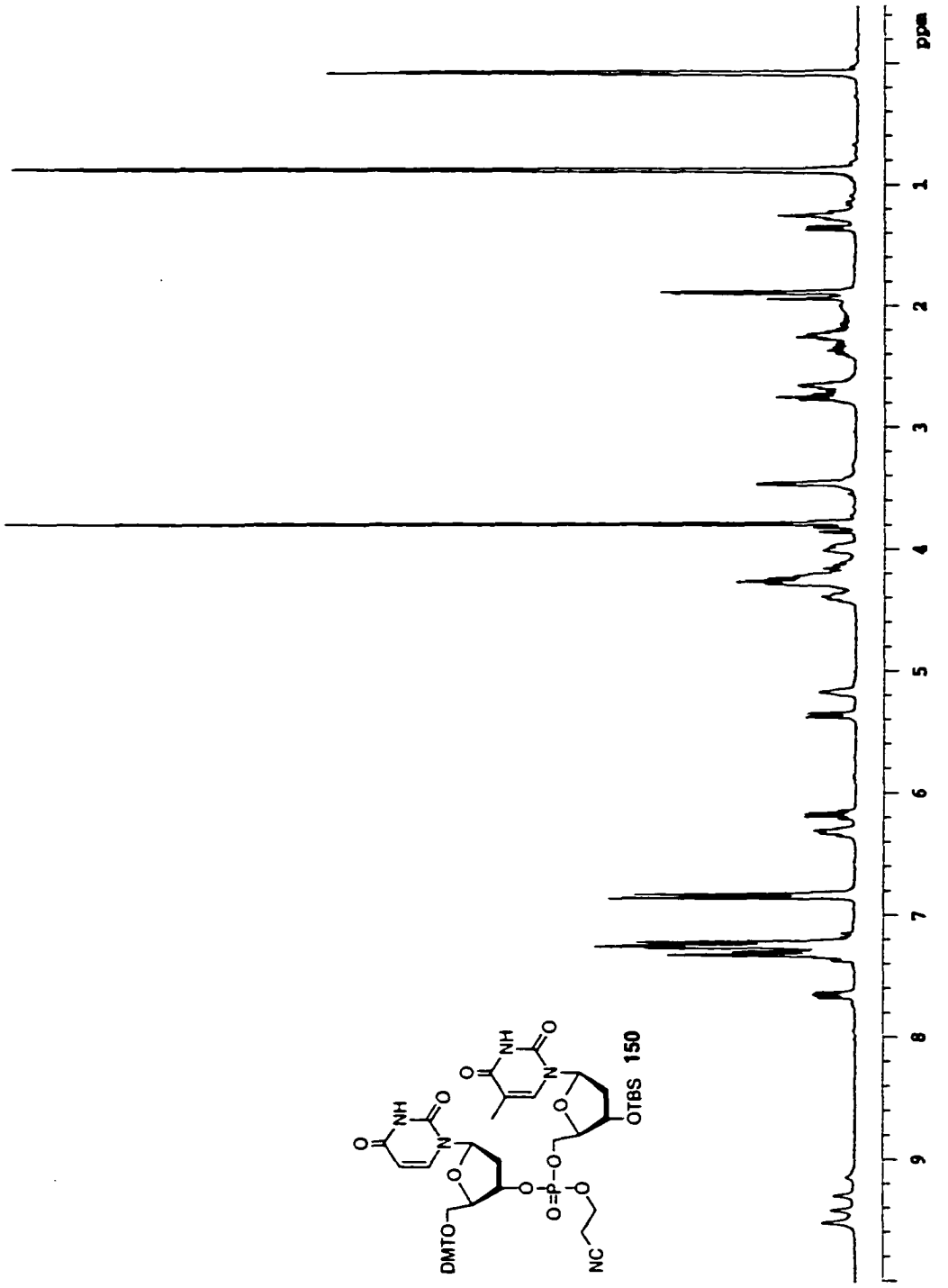

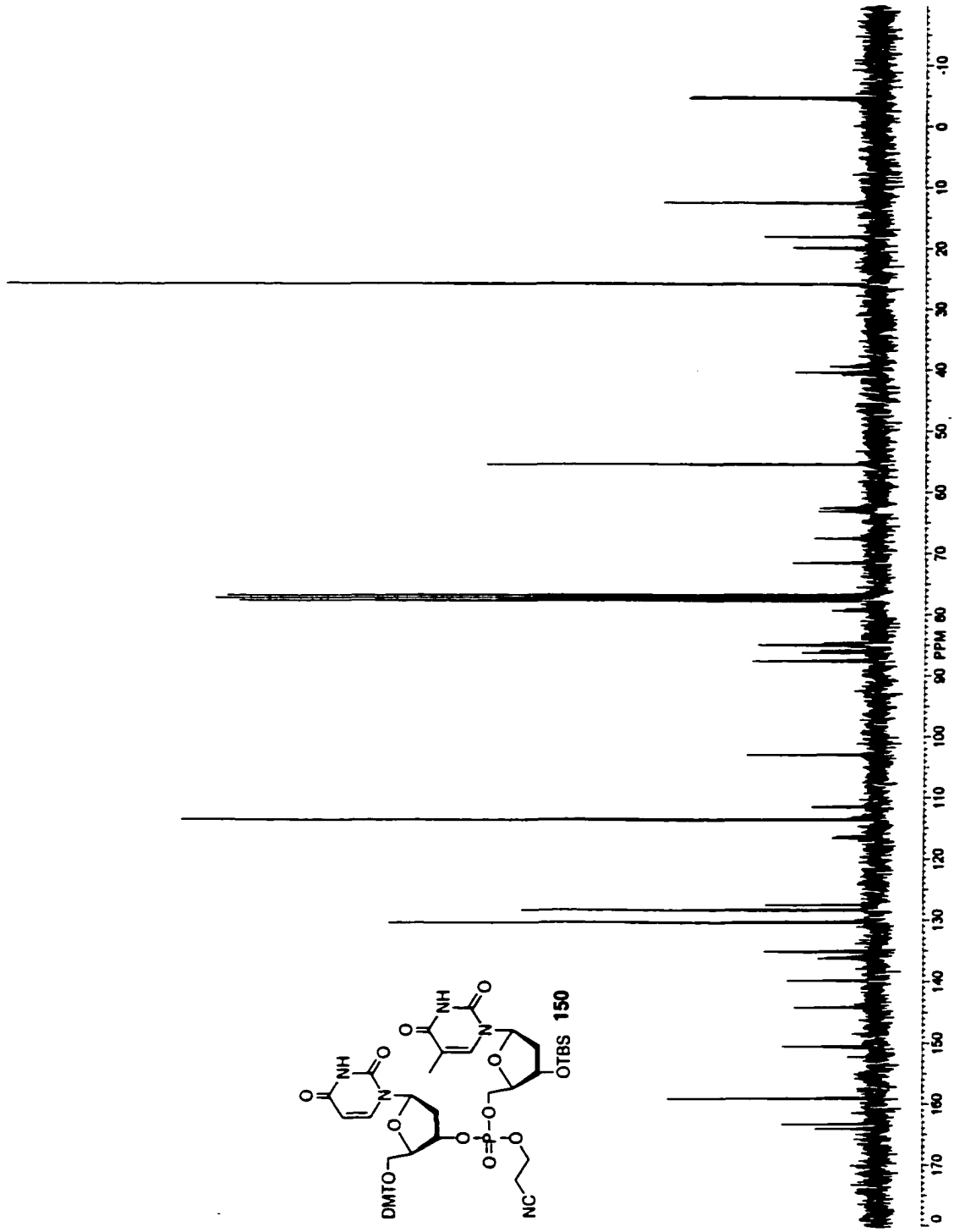

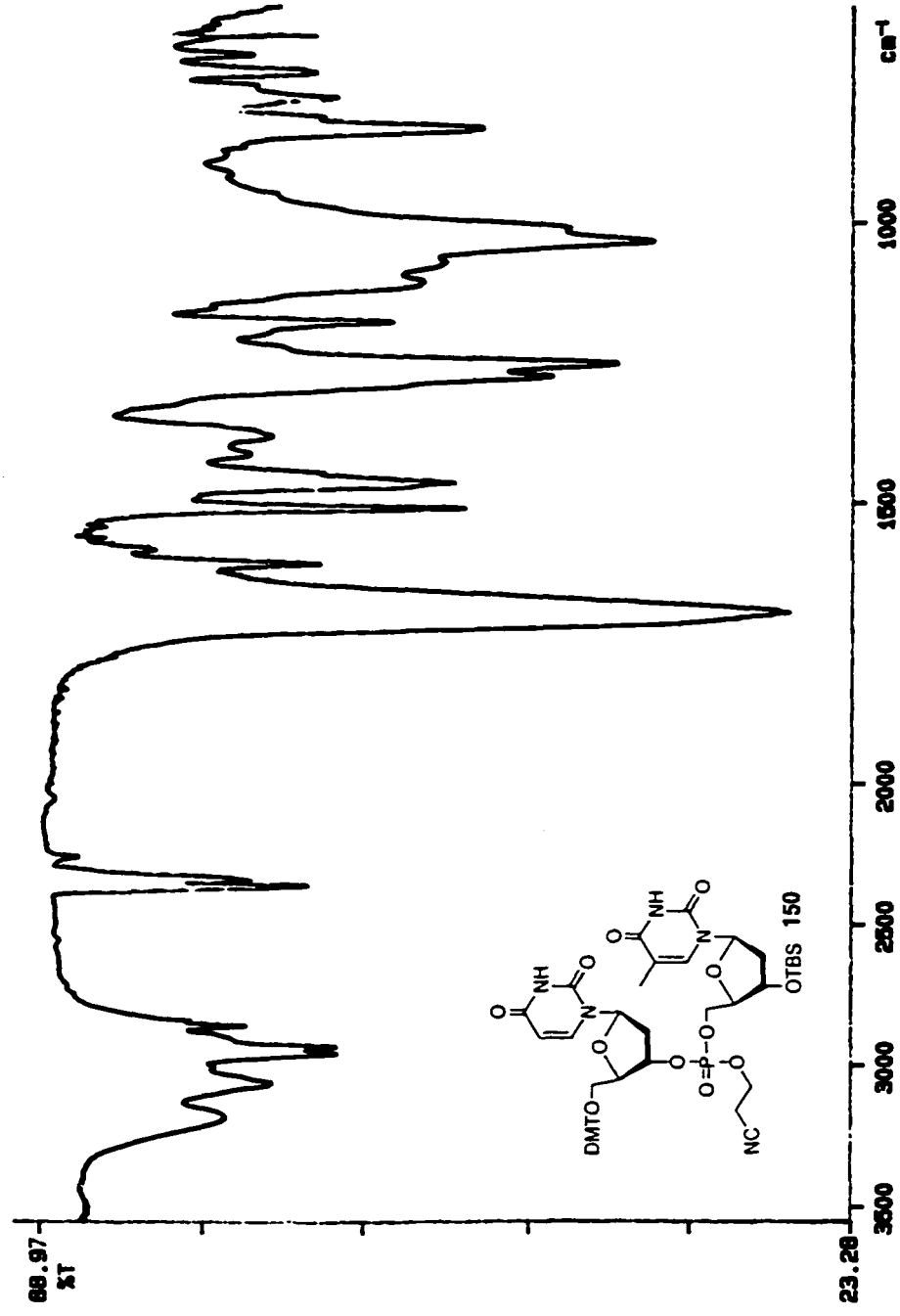

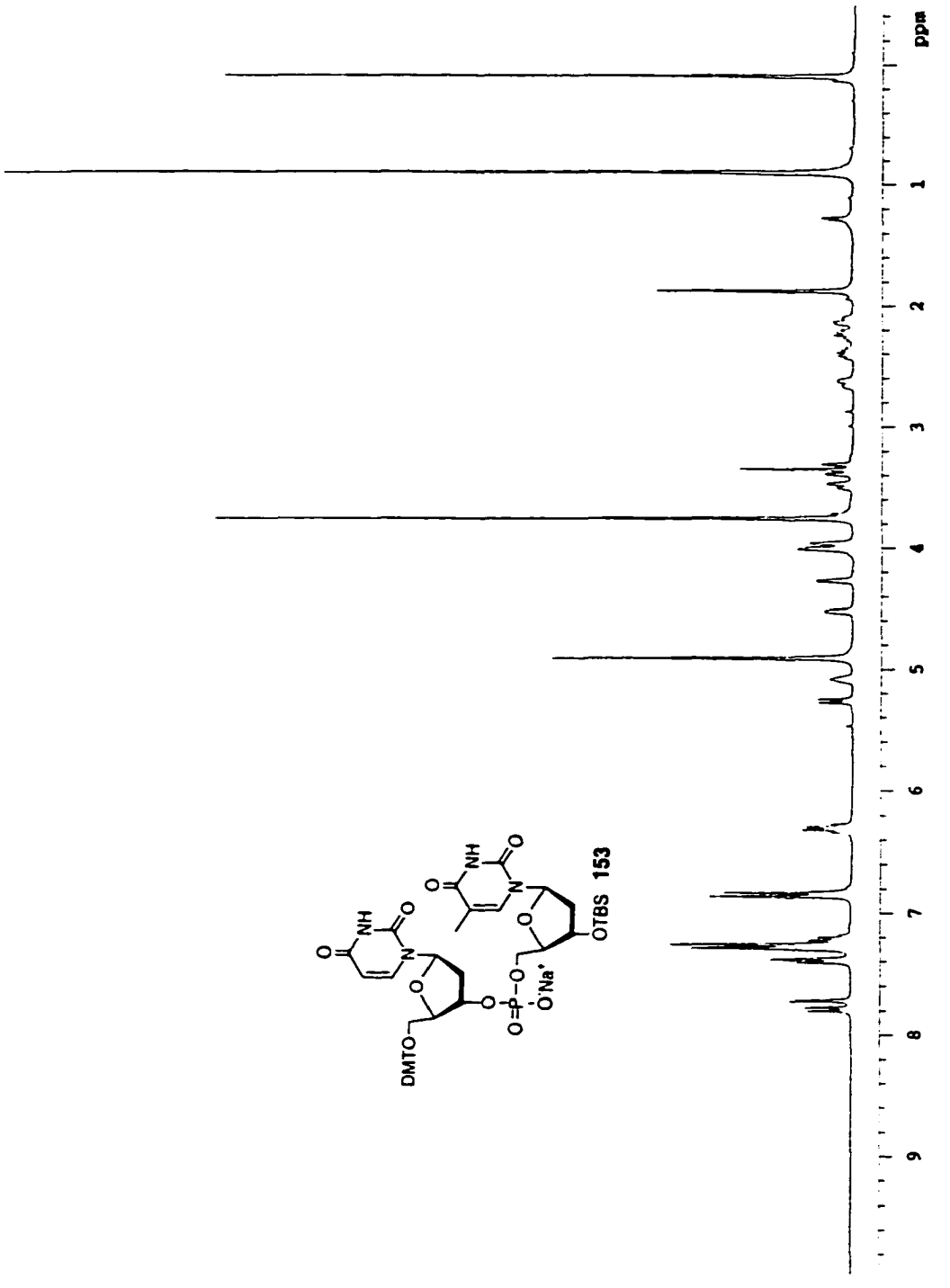

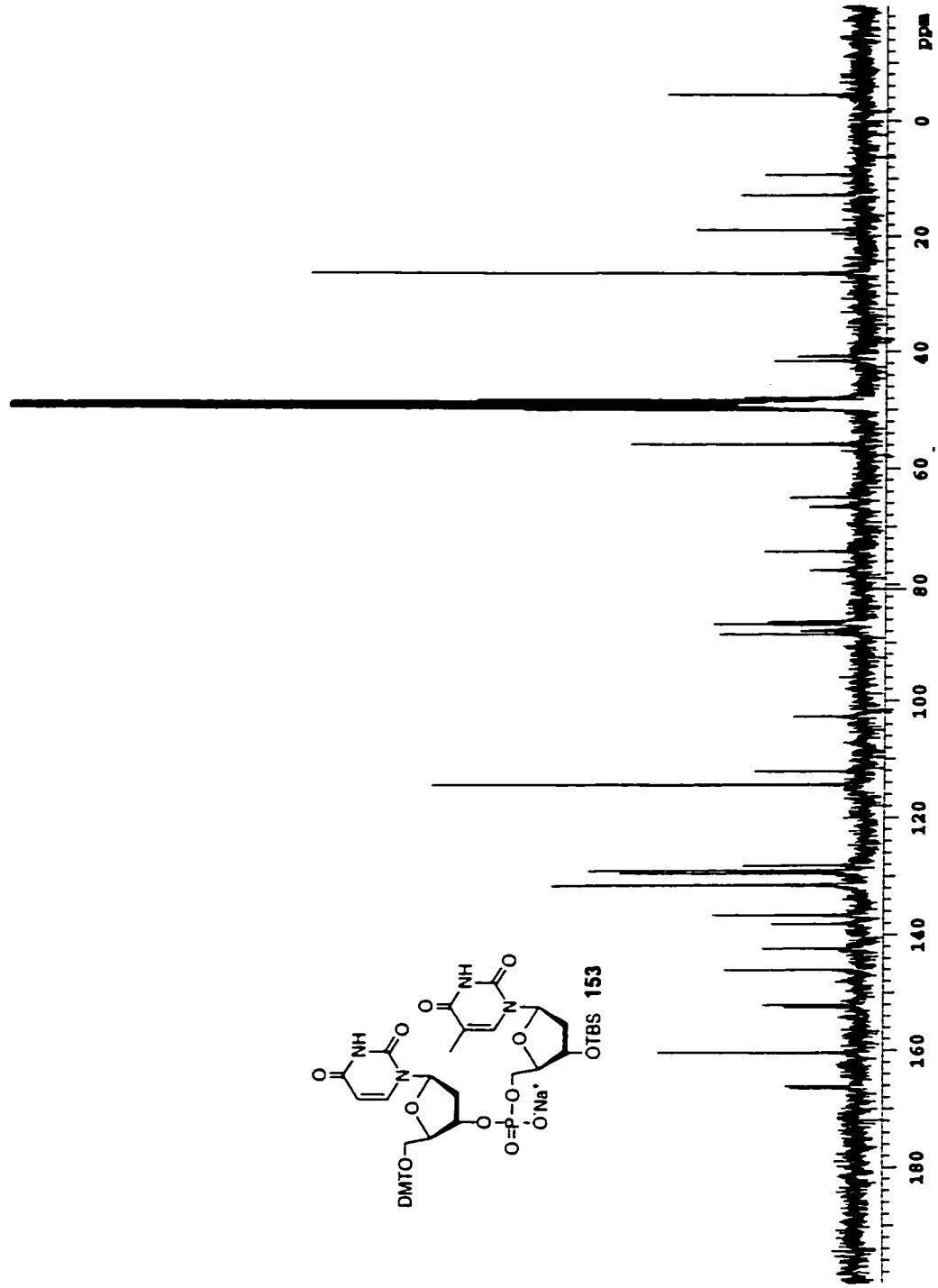

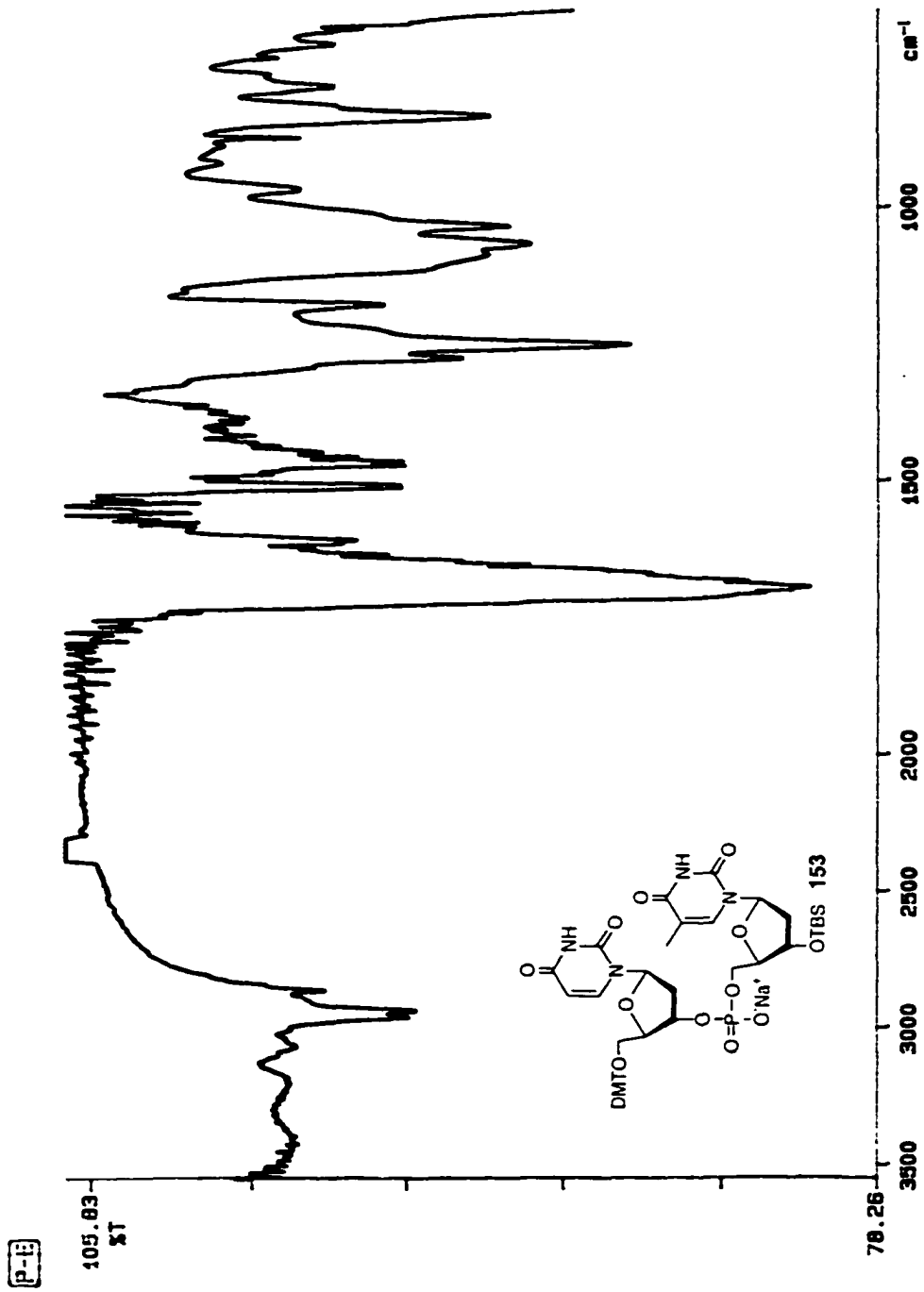

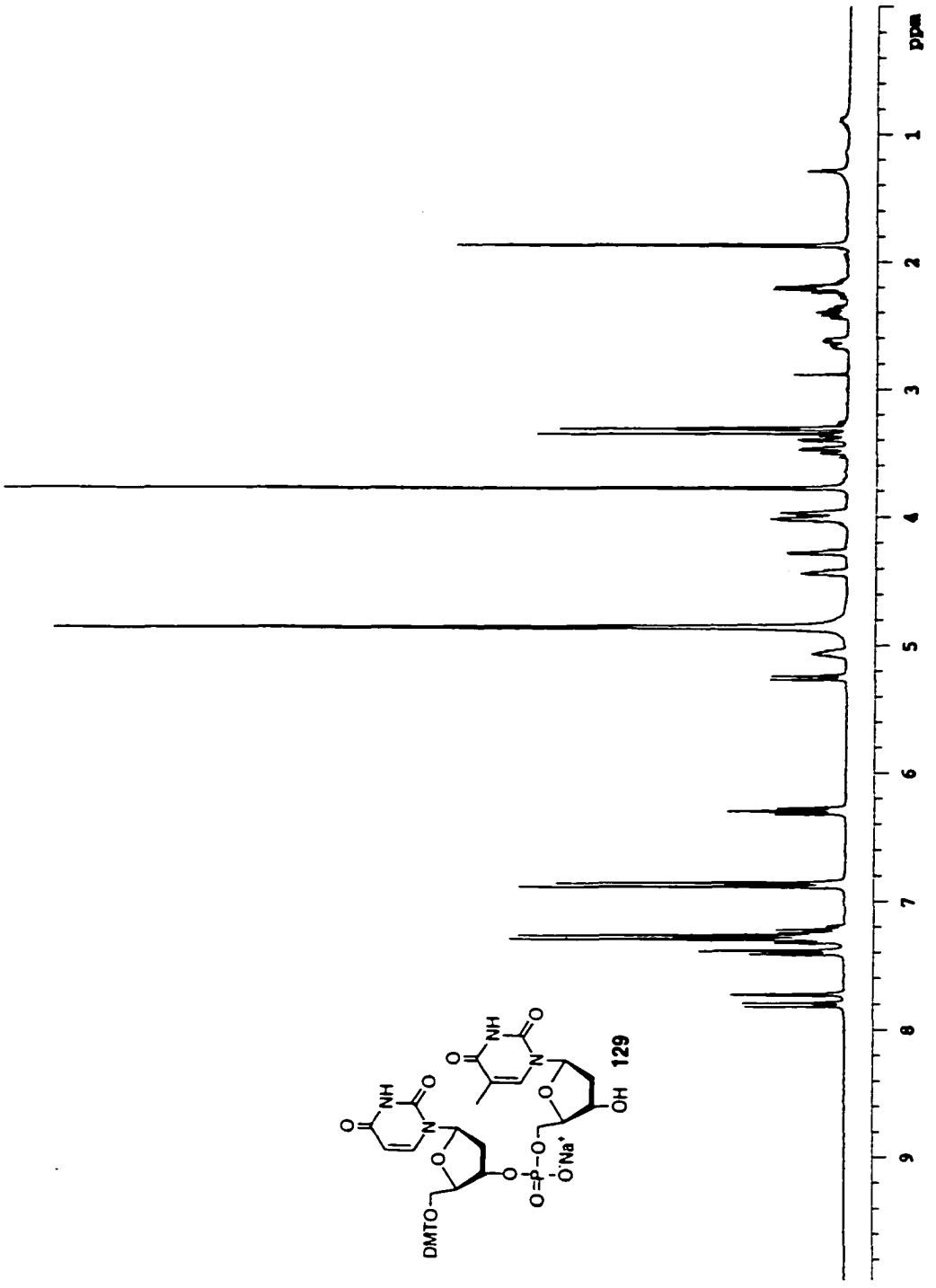

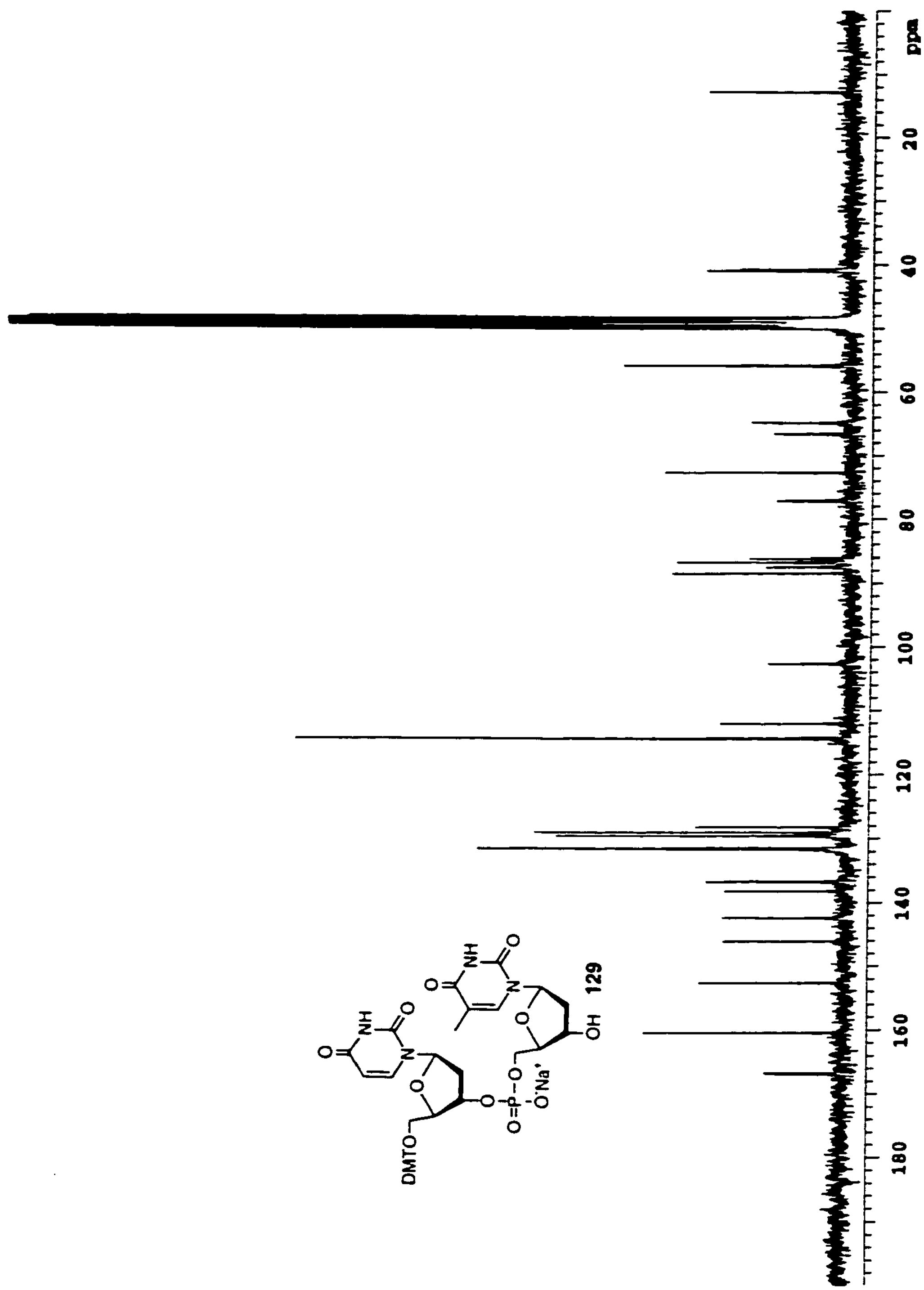

129